GASTROINTESTINAL TUMOR HETEROGENEITY AND RELATED ANTI-CANCER STRATEGIES

EDITED BY: Rui Liao, Yujun Shi and Ju Cao
PUBLISHED IN: Frontiers in Oncology

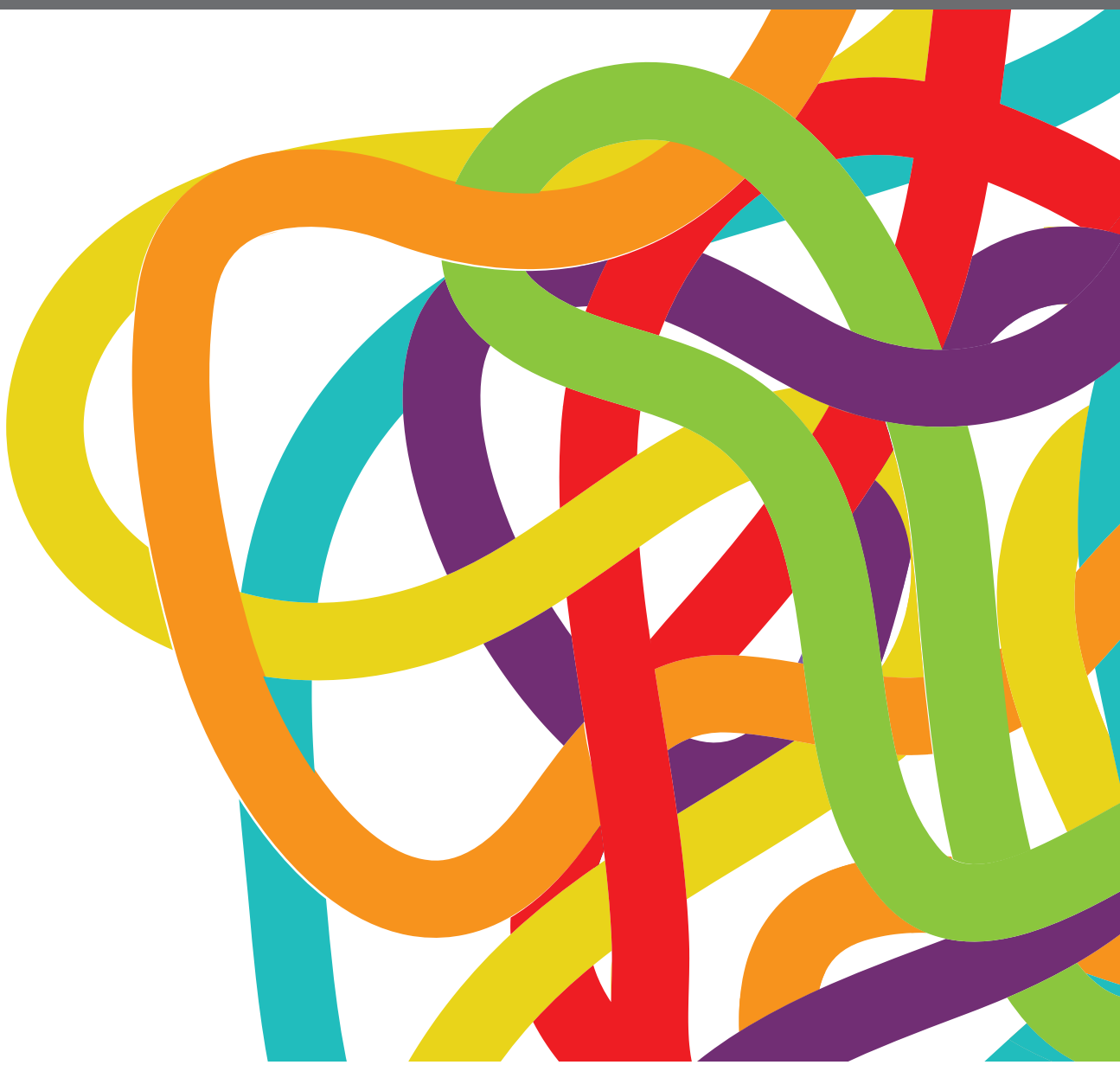

frontiers Research Topics

ISSN 1664-8714
ISBN 978-2-88976-379-5
DOI 10.3389/978-2-88976-379-5

About Frontiers

Frontiers is more than just an open-access publisher of scholarly articles: it is a pioneering approach to the world of academia, radically improving the way scholarly research is managed. The grand vision of Frontiers is a world where all people have an equal opportunity to seek, share and generate knowledge. Frontiers provides immediate and permanent online open access to all its publications, but this alone is not enough to realize our grand goals.

Frontiers Journal Series

The Frontiers Journal Series is a multi-tier and interdisciplinary set of open-access, online journals, promising a paradigm shift from the current review, selection and dissemination processes in academic publishing. All Frontiers journals are driven by researchers for researchers; therefore, they constitute a service to the scholarly community. At the same time, the Frontiers Journal Series operates on a revolutionary invention, the tiered publishing system, initially addressing specific communities of scholars, and gradually climbing up to broader public understanding, thus serving the interests of the lay society, too.

Dedication to Quality

Each Frontiers article is a landmark of the highest quality, thanks to genuinely collaborative interactions between authors and review editors, who include some of the world's best academicians. Research must be certified by peers before entering a stream of knowledge that may eventually reach the public - and shape society; therefore, Frontiers only applies the most rigorous and unbiased reviews.
Frontiers revolutionizes research publishing by freely delivering the most outstanding research, evaluated with no bias from both the academic and social point of view. By applying the most advanced information technologies, Frontiers is catapulting scholarly publishing into a new generation.

What are Frontiers Research Topics?

Frontiers Research Topics are very popular trademarks of the Frontiers Journals Series: they are collections of at least ten articles, all centered on a particular subject. With their unique mix of varied contributions from Original Research to Review Articles, Frontiers Research Topics unify the most influential researchers, the latest key findings and historical advances in a hot research area! Find out more on how to host your own Frontiers Research Topic or contribute to one as an author by contacting the Frontiers Editorial Office: frontiersin.org/about/contact

GASTROINTESTINAL TUMOR HETEROGENEITY AND RELATED ANTI-CANCER STRATEGIES

Topic Editors:
Rui Liao, First Affiliated Hospital of Chongqing Medical University, China
Yujun Shi, Sichuan University, China
Ju Cao, First Affiliated Hospital of Chongqing Medical University, China

Citation: Liao, R., Shi, Y., Cao, J., eds. (2022). Gastrointestinal Tumor Heterogeneity and Related Anti-Cancer Strategies. Lausanne: Frontiers Media SA. doi: 10.3389/978-2-88976-379-5

Table of Contents

frontiers | Frontiers in Oncology

EDITORIAL
published: 11 April 2022
doi: 10.3389/fonc.2022.873240

Editorial: Gastrointestinal Tumor Heterogeneity and Related Anti-Cancer Strategies

Rui Liao[1]*, *Yu-Jun Shi*[2], *Michael D. Chuong*[3,4] and *Ju Cao*[5]

[1] Department of Hepatobiliary Surgery, The First Affiliated Hospital of Chongqing Medical University, Chongqing, China, [2] Institute of Clinical Pathology, Key Laboratory of Transplant Engineering and Immunology, National Health Commission (NHC), West China Hospital, Sichuan University, Chengdu, China, [3] Department of Radiation Oncology, Miami Cancer Institute, Baptist Health South Florida, Miami, FL, United States, [4] Herbert Wertheim College of Medicine, Florida International University, Miami, FL, United States, [5] Department of Laboratory Medicine, The First Affiliated Hospital of Chongqing Medical University, Chongqing, China

Keywords: gastrointestinal tumor, tumor microenvironment, inter-patient heterogeneity, intra-tumor heterogeneity, phenotypic plasticity, targeted therapy

Editorial on the Research Topic

Gastrointestinal Tumor Heterogeneity and Related Anti-Cancer Strategies

The significance of tumor microenvironment (TME) heterogeneity is increasingly becoming recognized as playing an essential role in tumorigenesis and malignant biological behaviors. Dr. Hanahan D (1) presents several prospective new cancer hallmarks and its enabling characteristics closely associated with tumor heterogeneity: 1) unlocking phenotypic plasticity, 2) non-mutational epigenetic reprogramming, 3) polymorphic microbiomes, and 4) senescent cells. The new facets of the conceptualization of cancer have a heuristic value in paving the way for the development of precision therapies and new targeted therapies. A growing knowledge base has revealed that the heterogeneity of gastrointestinal tumors, including inter-patient heterogeneity (IPH) and intra-tumor heterogeneity (ITH) of gastric cancer, colorectal cancer, hepatocellular carcinoma (HCC), cholangiocarcinoma, pancreatic cancer, gallbladder carcinoma, and esophageal adenocarcinoma, is a determining factor of tumor development (2, 3). Therefore, based on molecular heterogeneity in TME, more novel and effective anti-cancer therapeutic algorithms have been discussed to selected subsets of gastrointestinal tumors.

Of note, inter-patient molecular heterogeneity has hampered the clinical practice of an expanding variety of targeted therapies and personalizing their prescriptions. An inter-patient molecular heterogeneity investigation using genomic and transcriptomic data for 4890 tumors from The Cancer Genome Atlas database showed that the repertoires of molecular targets of the clinical recommendations for accepted drugs were not congruent with the gene mutation patterns of different cancer types (4). Due to IPH, gastrointestinal tumors between individual patients frequently exhibit distinct clinical behaviors and treatment response produced by high levels of transcriptomic and (epi)genomic variation. A comprehensive single-cell profile of gastric cancer across clinical stages and histological subtypes identified 34 distinct cell-lineage states, and highlighted inter- and intra-lineage similarities and differences between patient-derived organoids and primary tumors (5). Enhancer variation has been identified as a major cause of IPH in cancer. Histone modification and functional assay data may be one of the options contributing genetic (e.g. ING1, ARL4C) and regulatory trans-acting factor (e.g. HNF4α) mechanisms to gastric cancer enhancer functional heterogeneity (6).

OPEN ACCESS

Edited and reviewed by:
Liang Qiao,
Westmead Institute for Medical Research, Australia

***Correspondence:**
Rui Liao
liaorui99@163.com

Specialty section:
This article was submitted to Gastrointestinal Cancers, a section of the journal Frontiers in Oncology

Received: *10 February 2022*
Accepted: *09 March 2022*
Published: *11 April 2022*

Citation:
Liao R, Shi Y-J, Chuong MD and Cao J (2022) Editorial: Gastrointestinal Tumor Heterogeneity and Related Anti-Cancer Strategies. Front. Oncol. 12:873240. doi: 10.3389/fonc.2022.873240

Also, ITH poses an important clinical challenge in therapeutic resistance. To better address the origin and drivers of ITH across cancer types, a robust consensus strategy has been developed to assess ITH and its origin, drivers, and recurrent changes in mutation signature activity *via* copy number and cluster mutations (7). This study underlined the importance of ITH and also provided detailed insight into tumor evolutionary dynamics. In HCC, the heterogeneous genomic landscape may facilitate effective anti-cancer therapeutic algorithms of personalized management. For instance, the molecular profile of the original tumor revealed that patients with intra-hepatic metastases should receive targeted therapy, whereas patients with multicentric tumors patients sharing the same genetic and environmental backgrounds could benefit from treating the underlying liver disease (8). An atlas of inter- and intra-tumor heterogeneity of apoptosis competency in colorectal cancer suggested that ITH may represent an intrinsic, non-genomic property instead of increase with the process of malignant transformation (9).

Therefore, further in-depth analyses of IPH and ITH in larger patient cohorts with gastrointestinal tumors are required. This Research Topic collection embodies 16 multidisciplinary articles focused on "gastrointestinal tumor heterogeneity and related anti-cancer strategies". Overall, the 16 papers in this Research Topic discussed gastrointestinal IPH and ITH deepening mechanistic insights, involved with basic experimental research, and clinical outcome predictive model and bioinformatics analysis for early diagnosis and targeted therapies of tumors. Specifically in this Research Topic, Kim et al. reported that dynamic changes in serum $KRAS^{G12/13}$ mutation heterogeneous status in serum cell-free DNA represented a potential source for monitoring recurrence of colorectal adenocarcinoma. Moreover, Gao et al. found the HCC patients from distinct immune subclasses with various heterogeneous statuses had different clinical prognoses and responses to personalized treatment through tumor transcriptome data analysis. In a review article, Li et al. summarized current advances concerning the reciprocal crosstalk of malignant cells and mesenchymal stem cells in the progression of gastric cancer, stressed the complexity and heterogeneity of tumor-stroma connections, and discussed their underlying therapeutic implications.

We sincerely thank all the authors, various reviewers/editors of the respective manuscripts, and the editorial team at Frontiers for their assistance and support in the process of reviewing and publishing this Research Topic, "Gastrointestinal Tumor Heterogeneity and Related Anti-Cancer Strategies". The next decade promises to illuminate more in-depth aspects of tumor heterogeneity contributing to gastrointestinal cancer prevention and treatments.

AUTHOR CONTRIBUTIONS

RL wrote this manuscript. YJ, MC, and JC reviewed it. All authors listed have made a direct and intellectual contribution to the work, and approved the submitted version.

FUNDING

This research was supported by the National Natural Science Foundation of China (No. 82072689), Science and Health Joint Research Project of Chongqing Municipality (2020GDRC013).

REFERENCES

1. Hanahan D. Hallmarks of Cancer: New Dimensions. *Cancer Discov* (2022) 12 (1):31–46. doi: 10.1158/2159-8290.CD-21-1059
2. Xue R, Li R, Wang J, Tong W, Hao J. Horizons on the Therapy of Biliary Tract Cancers: A State-Of-the-Art Review. *J Clin Transl Hepatol* (2021) 9(4):559–67. doi: 10.14218/JCTH.2021.00007
3. Hong WF, Gu YJ, Wang N, Xia J, Zhou HY, Zhan K, et al. Integrative Characterization of Immune-Relevant Genes in Hepatocellular Carcinoma. *J Clin Transl Hepatol* (2021) 9(3):301–14. doi: 10.14218/JCTH.2020.00132
4. Zolotovskaia MA, Sorokin MI, Petrov IV, Poddubskaya EV, Moiseev AA, Sekacheva MI, et al. Disparity Between Inter-Patient Molecular Heterogeneity and Repertoires of Target Drugs Used for Different Types of Cancer in Clinical Oncology. *Int J Mol Sci* (2020) 21(5):1580. doi: 10.3390/ijms21051580
5. Kumar V, Ramnarayanan K, Sundar R, Padmanbahan N, Srivastava S, Koiwa M, et al. Single-Cell Atlas of Lineage States, Tumor Microenvironment and Subtype-Specific Expression Programs in Gastric Cancer. *Cancer Discov* (2022) 12(3):670-91. doi: 10.1158/2159-8290.CD-21-0683
6. Sheng T, Ho SWT, Ooi WF, Xu C, Xing M, Padmanabhan N, et al. Integrative Epigenomic and High-Throughput Functional Enhancer Profiling Reveals Determinants of Enhancer Heterogeneity in Gastric Cancer. *Genome Med* (2021) 13(1):158. doi: 10.1186/s13073-021-00970-3
7. Dentro SC, Leshchiner I, Haase K, Tarabichi M, Wintersinger J, Deshwar AG, et al. Characterizing Genetic Intra-Tumor Heterogeneity Across 2,658 Human Cancer Genomes. *Cell* (2021) 184(8):2239–54.e2239. doi: 10.1016/j.cell.2021.03.009
8. Dong LQ, Peng LH, Ma LJ, Liu DB, Zhang S, Luo SZ, et al. Heterogeneous Immunogenomic Features and Distinct Escape Mechanisms in Multifocal Hepatocellular Carcinoma. *J Hepatol* (2020) 72(5):896–908. doi: 10.1016/j.jhep.2019.12.014
9. Lindner AU, Salvucci M, McDonough E, Cho S, Stachtea X, O'Connell EP, et al. An Atlas of Inter- and Intra-Tumor Heterogeneity of Apoptosis Competency in Colorectal Cancer Tissue at Single-Cell Resolution. *Cell Death Differ* (2021). doi: 10.1038/s41418-021-00895-9

Conflict of Interest: The authors declare that the research was conducted in the absence of any commercial or financial relationships that could be construed as a potential conflict of interest.

frontiers in Oncology

ORIGINAL RESEARCH
published: 11 January 2021
doi: 10.3389/fonc.2020.604772

Serum-Based KRAS$^{G12/G13}$ Mutation Detection Using Droplet Digital PCR: Clinical Implications and Limitations in Colorectal Adenocarcinoma With Tumor Heterogeneity

Ju Seok Kim[1†], Go Eun Bae[2†], Seok-Hwan Kim[3], Min Kyung Choi[2] and Min-Kyung Yeo[2]*

[1] Department of Internal Medicine, Chungnam National University School of Medicine, Daejeon, South Korea, [2] Department of Pathology, Chungnam National University School of Medicine, Daejeon, South Korea, [3] Department of Surgery, Chungnam National University School of Medicine, Daejeon, South Korea

OPEN ACCESS

Edited by:
Yujun Shi,
Sichuan University, China

Reviewed by:
Ji Yun Jeong,
Kyungpook National University Chilgok Hospital, South Korea
Nara Yoon,
Catholic University of Korea, South Korea

***Correspondence:**
Min-Kyung Yeo
mkyeo83@gmail.com

†These authors share co-first authorship

Specialty section:
This article was submitted to Gastrointestinal Cancers, a section of the journal Frontiers in Oncology

Received: *10 September 2020*
Accepted: *27 November 2020*
Published: *11 January 2021*

Citation:
Kim JS, Bae GE, Kim S-H, Choi MK and Yeo M-K (2021) Serum-Based KRAS$^{G12/G13}$ Mutation Detection Using Droplet Digital PCR: Clinical Implications and Limitations in Colorectal Adenocarcinoma With Tumor Heterogeneity. Front. Oncol. 10:604772. doi: 10.3389/fonc.2020.604772

Background: Cell-free DNA (cfDNA) has arisen as an alternative target for evaluating somatic mutations in cancer. KRAS mutation status is critical for targeted therapy in colorectal adenocarcinoma (CRAC). We evaluated KRAS$^{G12/G13}$ mutations in cfDNA extracted from serum and compared the results with KRAS$^{G12/G13}$ mutations detected in tissue samples. We assessed the clinical significance of KRAS$^{G12/G13}$ mutation in serum in regard to recurrence and metastasis of CRAC.

Methods: A total of 146 CRAC patients were enrolled, and KRAS$^{G12/G13}$ mutations were evaluated in 146 pairs of serum and tissue samples. In addition, 35 pairs of primary and metastatic CRAC tissue samples were evaluated for KRAS$^{G12/G13}$ mutational status.

Results:
Detection of KRAS$^{G12/13}$ mutation from serum and tissue had a 55% concordance rate, and serum detection had a sensitivity of 39.8%. Detection of the KRAS$^{G12/13}$ mutation yielded a 14% discordance rate between primary and metastatic tissue. CRAC patients with mutant KRAS$^{G12/13}$ mutation in serum but wild-type KRAS$^{G12/13}$ in tissue had concurrent KRAS$^{G12/13}$-mutant metastatic tumors, indicating spatial genetic heterogeneity. Changes in serum KRAS$^{G12/G13}$ mutation status during postoperative follow-up were associated with recurrence. Conclusion: Although serum detection of the KRAS$^{G12/13}$ mutation cannot substitute for detection in tissue, serum testing can support the interpretation of a CRAC patient's status in regard to concurrent metastasis. Dynamic changes in serum KRAS$^{G12/13}$ mutation status during follow-up indicated that cfDNA from serum represents a potential source for monitoring recurrence in CRAC patients.

Keywords: colorectal adenocarcinoma, cell free DNA, serum, KRAS, heterogeneity

INTRODUCTION

Identification of genetic mutations in solid cancer is important for targeted therapy. For genotyping, a certain amount of tumor tissue acquired by biopsy or surgical resection is required. However, biopsy or excision of tumors can be difficult in some patients due to an unreachable tumor location, the risk of tumor spread, or potential clinical complications. Consequently, a more effective and non-invasive means of detecting genetic mutations is needed. To address this issue, cell-free DNA (cfDNA) has arisen as an alternative target for evaluating somatic mutations in cancer. Detection of mutations using cfDNA extracted from liquid samples, such as blood, urine, and saliva, is easily repeated and much less invasive than biopsy. In addition, the mutational status of cfDNA can be used to assess a cancer patient's current status (1). Genetic mutation analysis using liquid samples has advanced rapidly in accordance with recently developed sensitive sequencing techniques (2). One such sequencing technique is droplet digital PCR (ddPCR), which is capable of sensitive detection of target DNA and quantification of mutations in small amounts of target DNA (3). ddPCR can be used to evaluate somatic mutations in liquid samples, including blood (4).

In colorectal cancer (CRC), KRAS mutational status is critical for targeted therapy (5) because it can predict the therapeutic response to anti-epidermal growth factor receptor (EGFR) treatment; consequently, KRAS genotyping is routine in patients with metastatic CRC. Tissue samples are commonly used for genotyping in CRC patients, but several studies have tried to establish the presence of KRAS mutations in cfDNA (6–8). Evaluation of mutation status using cfDNA is used primarily for genotyping; in addition, cfDNA has the advantage that it reflects tumor dynamics more closely than tissue samples. On the other hand, cfDNA also has drawbacks, including the fact that it is easily degraded and cannot be detected at low levels in samples (4). Clinical meaning of serum KRAS mutation has shown to have its own clinical implication apart from tissue KRAS related to prognosis (7).

Detection of KRAS mutations in cfDNA from CRC patient serum has been proposed, but the clinical implications and limitations of serum detection of KRAS mutations have not yet been clarified. This study sought to evaluate i) the concordance of detection of KRAS mutation between serum and tissue: can serum substitute for tissue in evaluation of KRAS mutation in CRC patients? ii) clinical implications of KRAS mutation status in serum: does the presence of KRAS mutation in serum, or the KRAS mutation fraction, have clinical implications in CRC patients? and iii) the change in KRAS status during follow-up: does KRAS status predict patient metastasis or recurrence in CRC? We evaluated KRAS mutation by ddPCR using serum and tissue samples from CRC patients and assessed the clinical significance of serum detection of the KRAS$^{G12/G13}$ mutation.

MATERIALS AND METHODS

KRAS$^{G12/G13}$ Mutation Detection in Colorectal Adenocarcinoma Patients

This retrospective study included 146 colorectal adenocarcinoma (CRAC) patients who underwent surgical resection of primary colorectal tumors. Patients were diagnosed at the Chungnam National University Hospital (Daejeon, Korea) between January 2014 and December 2017; mean follow-up was 54 months. Pre-operative blood samples (within 1 week prior to the operation) from all patients were collected at the time of the first surgery, and 146 pairs of primary tumor samples were obtained from formalin-fixed, paraffin-embedded (FFPE) tissue blocks. Thirty-nine of the 146 patients exhibited concurrent liver metastases at the time of the first surgery; liver tissue samples were obtained by surgical tumorectomy from seven of the 39. Forty-seven patients had CRAC recurrence during follow-up, and follow-up blood samples were collected from 12 of the 47 patients (within a week prior to the second recurrent tumor operation) along with paired recurrent tumor samples. Clinical data of CRAC patients were available from the archives of the same institution. At the time of collection of pre-operative serum samples, no patients had received pre-operative chemo- or radiotherapy. Patients with stage III or higher CRAC who underwent curative resections received adjuvant FOLFOX (5-fluorouracil (FU) + oxaliplatin + leucovorin) with cetuximab (anti-epidermal growth factor receptor monoclonal antibody for tissue KRAS wild type) chemotherapy. An additional 35 CRAC patients with distant metastasis were evaluated for KRAS$^{G12/G13}$ mutation. Thirty-five primary and metastatic tumor FFPE tissue samples were used to evaluate KRAS$^{G12/G13}$ mutational status.

Serum and tumor tissue samples of CRAC patients were provided by the Biobank of Chungnam National University Hospital, a member of the Korea Biobank Network. This study was approved by the institutional review board of Chungnam National University Hospital (IRB file no. 2018-10-012-001). Because the study was retrospective, a waiver of consent was approved by the IRB.

Serum KRAS$^{G12/G13}$ Mutation Detection Using Droplet Digital Polymerase Chain Reaction

A total of 146 peripheral blood samples were collected, centrifuged to isolate serum, and stored in liquid nitrogen. cfDNA was extracted from 200 µl of stored serum using the QIAamp Circulating Nucleic Acid kit (Qiagen). Extracted cfDNA was eluted in 100 µl of Tris-EDTA buffer and diluted to 10 ng/µl. Sixteen serum samples from healthy people were used as negative controls. DNA extracted from CRAC serum was tested by ddPCR (QX200; Bio-Rad, Hercules, CA, USA) using the ddPCR Bio-Rad KRAS G12/G13 multiplex kit (#1863506). Reaction mixtures (final volume, 20 µl) consisted of extracted DNA (1 µl), 2× SuperMix for probe (10 µl), KRAS screening probe (1 µl), and distilled water (8 µl). The mixture was loaded into a disposable droplet generator cartridge (Bio-Rad), and 70 µl of droplet generation oil for primers (Bio-Rad) was loaded into each of the eight oil wells (**Figure 1**). The cartridge was then placed inside the QX200 droplet generator (Bio-Rad), which partitioned each tissue sample into ~22,000 droplets per tissue sample. When droplet generation was complete, the droplets were transferred to a 96-well PCR plate. The plate was heat-sealed with foil and placed in a conventional thermal cycler (T100, Bio-Rad) using the following reaction conditions: 95°C for 10 min (1 cycle); 94°C for 30 s and 55°C for 1 min (40 cycles); 98°C for 10 min (1 cycle); and 4°C (hold). Cycled droplets were read

individually on a QX200 droplet-reader (Bio-Rad). Samples were transferred to the QX200 for fluorescence measurement of a mutant probe labeled with 6-fluorescein amidite (FAM) and wild-type probe labeled with hexachlorofluorescein (HEX) (**Figure 1**). DNA from SW480 cells, which harbor the KRAS G12V mutation, served as a positive control; DNA from the leukocytes of heathy persons, DNA from HEK cells, and distilled water were used as negative controls.

The ddPCR platform used the QuantaSoft software (version 1.7; Bio-Rad) to calculate the number of positive and negative fluorescence signals in droplets. Mutant allele frequency (MAF) was measured as the percentage of mutant droplets relative to the total (mutant + wild type). Samples from healthy volunteers contained no KRAS$^{G12/G13}$ mutant droplets.

Detection of KRAS$^{G12/G13}$ in Tissue by Sanger Sequencing

A total of 146 primary tumor tissue slides were reviewed by two pathologists (M-KY and GEB), and representative tissue FFPE blocks were selected. FFPE tissue samples with minimum 1.0 x 1.0 x 0.3 cm tumor size at least 70% of tumor cell content were macro-dissected and sectioned. Four sections (5-mm thickness) of each qualifying tumor tissue sample were used for DNA extraction. Tumor tissue DNA was isolated from FFPE slides using he QIAamp DNA FFPE Tissue Kit (QIAGEN Korea, Seoul, Korea). Extracted DNA (20 ng) from CRAC tissue samples were subjected to Sanger sequencing (performed by Macrogen, Seoul, Korea). For detection of mutations in codons 12 and 13 of the *KRAS* gene, primer sequences were as follows: exon 2, 50-GTAAAACGACGGC CAGTGTGTGACATGTTCTAATATAGTCA-30 (forward) and 50-GCGGATAA CAATTTCACACAGGGAATGGTCCTG CACCAGTAA-30 (reverse); exon 3, 50-TAATACGACTCAC TATAGGGGTGCTTAGTGGCCATTTGTC-30 (forward) and 50-GCTAGTTATTGC TCAGCGGTATGCATGGCATT AGCAAAG-30 (reverse). PCR amplification conditions were as follows: 95°C for 5 min (1 cycle); 95°C for 30 s, 60°C for 30 s, and 72°C for 1 min (35 cycles); and 72°C for 7 min. PCR products were purified using MultiScreen-PCR$_{96}$ filter plates (Millipore SAS, Molsheim, France). The purified PCR products were then Sanger sequenced on a 3730xl automated sequencer (Applied Biosystems, Foster City, CA, USA) using the BigDye terminator v3.1 sequencing kit. Nucleotide sequence data were analyzed using the Variant reporter software version 1.1 (Applied Biosystems).

An additional 35 CRAC patients with distant metastasis were evaluated for the KRAS$^{G12/G13}$ mutation by Sanger sequencing. Thirty-five pairs of primary and metastatic tumor FFPE tissue samples were used to evaluate KRAS$^{G12/G13}$ mutation status. Concordance and discordance in KRAS$^{G12/G13}$ mutation status between primary and metastatic tumors were evaluated.

Statistical Analysis

Detection of the KRAS$^{G12/G13}$ mutation was compared between serum and tissue, and correlation was assessed by κ statistics (0.00–0.19, slight; 0.21–0.39, fair; 0.40–0.59; moderate agreement). Diagnostic value of the serum KRAS$^{G12/G13}$ mutation (sensitivity, specificity, positive predictive value, and negative predictive value) were calculated for the detection of tissue KRAS$^{G12/G13}$ mutation. The associations of serum KRAS$^{G12/G13}$ detection with clinicopathological variables were examined using Spearman's rank correlation, Mann-Whitney U-test, and Fisher's exact test. All statistical analyses were performed using SPSS version 26.0 for Windows (SPSS Inc., Chicago, IL, USA) and MedCalc version 19.2.0 for Windows (MedCalc Software Ltd, Belgium).

RESULTS

Comparison of KRAS$^{G12/G13}$ Mutation Detection in Serum and Tissue

Paired pre-operative serum and tissue samples from a total of 146 CRAC patients were evaluated for detection of KRAS$^{G12/G13}$

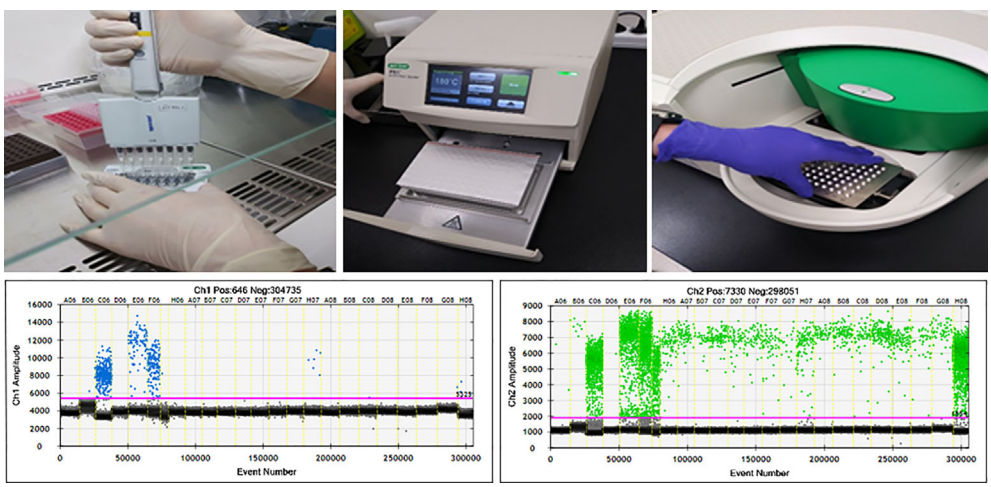

FIGURE 1 | ddPCR workflow and results of ddPCR for detection of KRAS$^{G12/13}$. Channel 1: fluorescence measurement of mutant probe labeled with 6-fluorescein amidite (FAM) (lower left). Channel 2; wild-type probe labeled with hexachlorofluorescein (HEX) (lower right).

mutation (**Table 1**). We detected KRAS$^{G12/G13}$ mutations in 46 of 146 (32%) serum samples and 98 of 146 (67%) tissue samples. Serum KRAS$^{G12/G13}$ mutation were matched with tissue KRAS$^{G12/G13}$ mutation in 39/98 (40%) of CRAC patients. Sixty six patients yielded discrepant KRAS$^{G12/G13}$ status, with mutant KRAS$^{G12/G13}$ in serum and wild-type KRAS$^{G12/G13}$ in tissue; 59 patients had wild-type KRAS$^{G12/G13}$ in serum and mutant KRAS$^{12/G13}$ in tissue; and 7 patients (* in **Table 1**) had serum KRAS$^{G12/G13}$ mutation without KRAS$^{G12/G13}$ mutation in tissue. The κ agreement of serum and tissue KRAS$^{G12/G13}$ detection was 0.198 (p = 0.002) and the concordance rate was 55%.

Next, we calculated the diagnostic value of serum KRAS$^{G12/G13}$ mutation (detected by ddPCR) for prediction of tissue KRAS$^{G12/13}$ mutation in the same patient (**Supplementary Table 1**). The sensitivity and specificity of the serum KRAS$^{G12/G13}$ mutation were 39.8 and 85.44% for the detection of tissue KRAS$^{G12/G13}$ mutation. The positive and negative predictive values of serum KRAS$^{G12/13}$ mutation detection using ddPCR were 84.8 and 41.0%, respectively (**Supplementary Table 1**).

TABLE 1 | Comparison of pre-operative serum and tissue KRAS$^{G12/13}$ detection in CRAC patients (n = 146).

Tissue KRAS$^{G12/13}$	Pre-operative serum KRAS$^{G12/13}$ ddPCR	
Sanger sequencing	**Mutant**	**Wild-type**
Mutant	39 (85%)	59 (59%)
Wild	*7 (15%)	41 (41%)
Total	46 (32%)	100 (69%)

**Cases yielded discrepant KRAS$^{G12/G13}$ status: mutant KRAS in serum and wild-type KRAS in tissue.*

Clinical Significance of Serum KRAS$^{G12/G13}$ Mutation Detection

The clinical significance of serum KRAS$^{G12/G13}$ detection was evaluated separately in CRAC patients with wild-type and mutant KRAS$^{G12/G13}$ in tissue. The clinical significance of serum KRAS$^{G12/G13}$ detection was then evaluated in CRAC patients with wild-type KRAS$^{G12/13}$ in tissue (n = 48); clinico-pathological parameters are shown in **Table 2**. Detection of serum KRAS$^{G12/13}$ was significantly related to concurrent metastasis (M1) (p = 0.004); seven patients with mutant KRAS$^{G12/13}$ in serum but wild-type KRAS$^{G12/13}$ in tissue had a distant metastasis at the time of primary colon cancer surgery. Serum KRAS$^{G12/G13}$ detection was not correlated with tumor size, stage (T, N), or differentiation (p = 0.963, p = 0.329, p = 0.813, and p = 538, respectively).

The clinical significance of serum KRAS$^{G12/G13}$ detection was evaluated in patients with mutant KRAS$^{G12/13}$ in tissue (n = 98); clinico-pathological parameters are shown in **Supplementary Table 2**. Serum KRAS$^{G12/G13}$ detection was not correlated with tumor size, stage (T, N, M), or differentiation (p = 0.334, p = 0.451, p = 1.000, p = 0.07, and p = 1.000, respectively). Serum KRAS$^{G12/G13}$ MAF was not related to clinico-pathological parameters.

Cases With Discordant KRASG12/13 Results: Mutant in Preoperative Serum and Wild Type in Primary Tissue

Seven CRAC patients had mutant KRAS$^{G12/13}$ in serum but wild-type KRAS$^{G12/13}$ in primary tissue. All seven had simultaneous liver metastases (**Table 3**). Five of the seven had KRAS$^{G12/13}$ mutation in the metastatic tumor (liver) without mutation in primary tissue. The MAF of serum KRAS ranged from 0.53% to 10%.

TABLE 2 | Clinical significance of preoperative Serum KRAS$^{G12/13}$ status detected by ddPCR in CRAC patients with wild-type KRAS$^{G12/13}$ in tissue (n = 48).

Characteristics inpatients with wild-type KRAS in tissue	Patients	Serum KRAS$^{G12/13}$ status of patients with wild-type KRAS$^{G12/13}$ in tissue		
	No. (%)	**Mutant**	**Wild-type**	**P**
Age (mean)	62 (100)	62 (15)	62 (85)	0.263
Sex				0.295
Male	33 (69)	6 (86)	27 (66)	
Female	15 (31)	1 (14)	14 (34)	
Size (cm)	5.0 (100)	5.3 (15)	5.0 (85)	0.963
T stage				0.329
T1+T2	5 (10)	0 (0)	5 (12)	
T3+T4	43 (90)	7 (100)	36 (88)	
N stage				0.813
N0	12 (25)	2 (29)	10 (24)	
N1+N2	36 (75)	5 (71)	31 (76)	
M stage				0.004
M0	24 (50)	0 (0)	24 (59)	
M1	24 (50)	*7 (100)	17 (42)	
Differentiation				0.538
WD+MD	44 (92)	6 (86)	38 (93)	
PD	4 (8)	1 (14)	3 (7)	
Postop Recurrence				0.597
Absent	23 (48)	4 (57)	19 (46)	
Present	25 (52)	3 (43)	22 (54)	

Postop, Post-operative; WD, well differentiated; MD, moderately differentiated; PD, poorly differentiated.
7 cases described in **Table 3.*

TABLE 3 | Seven discordant KRAS$^{G12/13}$ (*Table 1) cases: pre-operative serum, matched primary and concurrent metastatic tissue.

Patient	Pre-operative serum KRAS MAF	Primary tumor (colon) KRAS Sanger sequencing	Concurrent tumor (liver) KRAS Sanger sequencing
D1	10	Wild-type	Codon 12
D2	4.88	Wild-type	Codon 12
D3	3.85	Wild-type	Codon 12
D4	2.53	Wild-type	Wild-type
D5	1.23	Wild-type	Codon 12/13
D6	1.19	Wild-type	Wild-type
D7	0.53	Wild-type	Wild-type

MAF, mutant allele frequency.

Dynamics of KRAS$^{G12/13}$ Detection in Serum and in Matched Primary and Recurrent Tissue

Pre- and post-operative serum samples from 12 patients were evaluated for KRAS$^{G12/13}$ by ddPCR. Detection of tissue KRAS$^{G12/13}$ status in matched primary (colon and rectum) and recurrent (as distant metastasis) tissue was assessed as shown in **Figure 2**. All patients received postoperative adjuvant chemotherapy, and patients with wild-type KRAS$^{G12/13}$ (B3–B12) received additional cetuximab treatment. Patients B1 and B2 had a preoperative serum KRAS$^{G12/13}$ MAF of 0 but were positive for tissue KRAS$^{G12/13}$ mutation. In the follow-up period, all 12 patients had recurrence and underwent radical or palliative resection of recurrent tumors with distant metastasis. Post-operative serum KRAS$^{G12/13}$ status was altered in several patients: three (B1, B3, and B4) became positive for serum KRAS$^{G12/13}$ mutation, and two of those three (B1 and B3) were positive for tissue KRAS$^{G12/13}$ mutation. The MAF of serum KRAS exhibited a recurrent tumor tissue KRAS$^{G12/13}$ mutation (B1, B3) showed 3.12 and 2.06% MAF. The MAF of serum KRAS showed recurrent tumor tissue KRAS$^{G12/13}$ wild type (B4) showed 0.32% MAF.

Discordance in Detection of KRAS$^{G12/13}$ Mutation Between Primary and Metastatic Colorectal Adenocarcinoma Tissue Samples

An additional 35 CRAC patients with distant metastasis were evaluated for KRAS$^{G12/G13}$ mutation by Sanger sequencing. Pairs of 35 FFPE tissue samples from primary and metastatic tumors were used to evaluate KRAS$^{G12/G13}$ mutation status (**Supplementary Table 1**). Twelve of 35 (34%) were KRAS$^{G12/13}$ mutant, and 18 of 35 (51%) were KRAS$^{G12/G13}$ wild type in both primary and metastatic tumor tissue. Five (T13–T17, * in **Supplementary Table 3**) out of 35 (14%) patients exhibited discordant KRAS$^{G12/13}$ mutation status between primary and metastatic tissue. Of the five discordant cases, four (T14–T17) acquired KRAS$^{G12/G13}$ mutation in distant tumor tissue samples (liver, lung bone, and ovary), whereas the primary tissue was wild type. The other patient (T13) was KRAS$^{G12/G13}$ mutant in primary colon tissue but lost the mutation in distant tumor tissue (liver).

DISCUSSION

DNA fragments released by tumor cells can be detected in blood. Blood can be obtained easily and repeatably in the clinic. Hence, mutational analysis of cfDNA from blood represents an excellent alternative to tumor tissue samples. In this study, we evaluated the possibility of detecting KRAS$^{G12/G13}$ mutation in serum samples from CRAC patients. KRAS$^{G12/G13}$ mutation could be detected in 40% of serum samples from CRAC patients with KRAS$^{G12/G13}$ mutation in tissue. Concordance between serum and tissue was limited (55%). Serum KRAS$^{G12/13}$ mutation could detect tissue KRAS$^{G12/13}$ mutation with a sensitivity of 39.8%, which is quite low. Previous studies reported concordance rates of 24.3% (7) and 50% when using DNA from circulating tumor cell samples (9). The serum samples could be used for genotyping but due to the low concordance rate were not an adequate substitute for tissue samples.

Mutational assessment of cfDNA in blood has prognostic significance (10, 11). The KRAS$^{G12/G13}$ mutational status of CRAC patients had a different clinical impact depending on whether the mutation was detected in tissue or serum. Simultaneous KRAS mutation in both tumor and serum is associated with worse prognosis than when the mutation is only detected in tissue (8, 11). In this study, neither the presence of KRAS$^{G12/G13}$ mutation in serum nor the MAF of KRAS$^{G12/G13}$ had prognostic implications. Notably, serum KRAS$^{G12/13}$ mutation was detected in 15% in patients who had

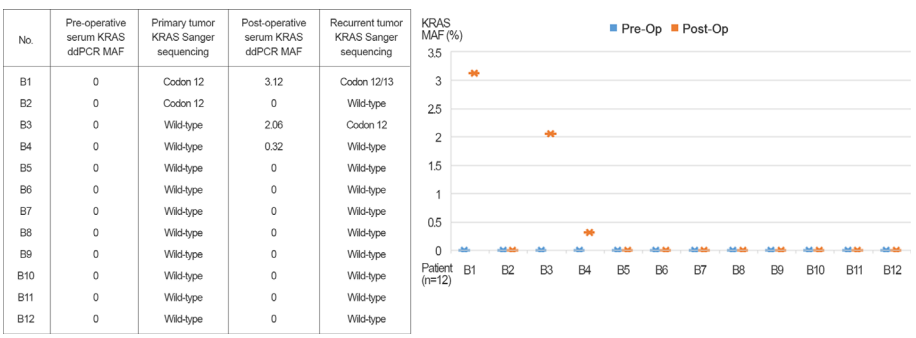

No.	Pre-operative serum KRAS ddPCR MAF	Primary tumor KRAS Sanger sequencing	Post-operative serum KRAS ddPCR MAF	Recurrent tumor KRAS Sanger sequencing
B1	0	Codon 12	3.12	Codon 12/13
B2	0	Codon 12	0	Wild-type
B3	0	Wild-type	2.06	Codon 12
B4	0	Wild-type	0.32	Wild-type
B5	0	Wild-type	0	Wild-type
B6	0	Wild-type	0	Wild-type
B7	0	Wild-type	0	Wild-type
B8	0	Wild-type	0	Wild-type
B9	0	Wild-type	0	Wild-type
B10	0	Wild-type	0	Wild-type
B11	0	Wild-type	0	Wild-type
B12	0	Wild-type	0	Wild-type

FIGURE 2 | Pre- and post-operative serum KRAS$^{G12/13}$ detected by ddPCR and primary and recurrent (as distant metastasis) tissue.

wild-type KRAS$^{G12/13}$ in tissue, and these patients was significantly related to M1 stage (concurrent metastasis).

We observed that KRAS$^{G12/G13}$ mutation status was heterogeneous in serum and tissue, and considered to be related to concurrent metastasis. Tumor heterogeneity can be detected between different tumor regions, e.g., between primary and metastatic tumors (spatial heterogeneity) and within the primary tumor (intratumoral heterogeneity) (12, 13). Genetic discordance existed between primary and metastatic tumor that previous studies reported discordance of KRAS mutation status between primary colon and liver were approximately 5% (14, 15). We observed 86% concordance in KRAS$^{G12/13}$ mutation status between primary and metastatic (liver, lung, bone, etc.) Two possibility of genetic discordancy in serum and tissue in our study has to be considered that intra-tumoral heterogeneity came from the primary tumor (we evaluated the representative section of tumor tissue) or spatial genetic heterogeneity between primary and metastatic tumor existed. All patients with mutant KRAS$^{G12/13}$ in serum and wild-type KRAS$^{G12/13}$ in tissue exhibited concurrent metastasis; accordingly, the metastatic tumor could be considered to be the source of the KRAS$^{G12/G13}$ mutation. Patients with discordance between serum and tissue should be carefully monitored that patients need to be evaluated unidentified or hidden concurrent metastasis.

Mutational assessment of cfDNA in blood has the potential to predict recurrence or patient metastasis. KRAS mutations is acquired after chemotherapy as a resistance mechanism (16, 17). In the pre- and postoperative serum monitoring performed in this study, three patients exhibited conversion of post-operative serum KRAS$^{G12/13}$ mutation status from preoperative wild type to postoperative mutant. Two of the three also had tissue KRAS$^{G12/13}$ mutations. Changes in serum KRAS$^{G12/G13}$ mutation status during postoperative follow-ups were related to recurrence. Dynamic changes in serum KRAS$^{G12/13}$ mutation status during follow-up indicated that cfDNA from serum represents a potential source for monitoring recurrence in CRAC patients.

The present study had several limitations. Due to the small number of patients, the results provide less definitive conclusions regarding the effectiveness of ddPCR-based detection of serum KRAS$^{G12/G13}$ status in CRAC patients. In our retrospective study, frozen stored serum samples could affect mutational output due to archiving status and time interval. Moreover, because changes in KRAS$^{G12/G13}$ mutation occurred in only 3 of 12 patients, the ability to predict recurrence was limited. Serum KRAS$^{G12/G13}$ status can give additional supportive information for the interpretation of CRAC patient status but must be considered along with other clinical and radiologic findings.

We compared the performance of KRAS$^{G12/G13}$ somatic alterations in cfDNA with that of tissue samples. The use of ddPCR enables tracking of the appearance and disappearance of somatic alterations in serum-derived cfDNA. cfDNA mutational analysis captures tumor molecular heterogeneity, providing different view of a patient's disease status. Because of the lack of follow-up samples, we cannot say whether KRAS$^{G12/G13}$ mutations in cfDNA can be detected before radiological relapse. Hence, further studies involving larger numbers of patients and a prospective design are required.

DATA AVAILABILITY STATEMENT

The raw data supporting the conclusions of this article will be made available by the authors, without undue reservation.

ETHICS STATEMENT

The studies involving human participants were reviewed and approved by the institutional review board of Chungnam National University Hospital (IRB file no. 2018-10-012-001). Because the study was retrospective, a waiver of consent was approved by the IRB.

AUTHOR CONTRIBUTIONS

JK provided the resources and contributed to the data curation. GB conceptualized and wrote, reviewed, and edited the manuscript. S-HK conceptualized and validated the study. MC conducted the formal analysis. M-KY supervised, wrote the original draft, and wrote, reviewed, and edited the manuscript. All authors have read and agreed to the published version of the manuscript. All authors contributed to the article and approved the submitted version.

FUNDING

This study was supported by the research fund of Chungnam National University, grants from the Basic Science Research Program through the National Research Foundation of Korea (NRF) funded by the Ministry of Education (2017R1D1A1B04031187), and the Bio and Medical Technology Development Program of the National Research Foundation (NRF) funded by the Korean government (MSIT) (2019M3E5D1A02068558).

SUPPLEMENTARY MATERIAL

The Supplementary Material for this article can be found online at: https://www.frontiersin.org/articles/10.3389/fonc.2020.604772/full#supplementary-material

REFERENCES

1. Levy B, Hu ZI, Cordova KN, Close S, Lee K, Becker D. Clinical Utility of Liquid Diagnostic Platforms in Non-Small Cell Lung Cancer. *Oncologist* (2016) 21(9):1121–30. doi: 10.1634/theoncologist.2016-0082
2. Vaidyanathan R, Soon RH, Zhang P, Jiang K, Lim CT. Cancer diagnosis: from tumor to liquid biopsy and beyond. *Lab Chip* (2019) 19(1):11–34. doi: 10.1039/c8lc00684a
3. Lee K, Lee T, Choi M, Kwon I, Bae G, Yeo M-K. Identification of a Clinical Cutoff Value for Multiplex KRASG12/G13 Mutation Detection in Colorectal Adenocarcinoma Patients Using Digital Droplet PCR, and Comparison with Sanger Sequencing and PNA Clamping Assay. *J Clin Med* (2020) 9:2283. doi: 10.3390/jcm9072283
4. Olmedillas-López S, García-Arranz M, García-Olmo D. Current and Emerging Applications of droplet Digital PCR in Oncology. *Mol Diagn Ther* (2017) 21(5):493–510. doi: 10.1007/s40291-017-0278-8
5. Feng Q-Y, Wei Y, Chen J-W, Chang W-J, Ye L-C, Zhu D-X, et al. Anti-EGFR and anti-VEGF agents: important targeted therapies of colorectal liver metastases. *World J Gastroenterol* (2014) 20(15):4263. doi: 10.3748/wjg.v20.i15.4263
6. Kloten V, Rüchel N, Brüchle NO, Gasthaus J, Freudenmacher N, Steib F, et al. Liquid biopsy in colon cancer: comparison of different circulating DNA extraction systems following absolute quantification of KRAS mutations using Intplex allele-specific PCR. *Oncotarget* (2017) 8(49):86253–63. doi: 10.18632/oncotarget.21134
7. Pu X, Pan Z, Huang Y, Tian Y, Guo H, Wu L, et al. Comparison of KRAS/BRAF mutations between primary tumors and serum in colorectal cancer: biological and clinical implications. *Oncol Lett* (2013) 5(1):249–54. doi: 10.3892/ol.2012.963
8. Thomsen CEB, Appelt AL, Andersen RF, Lindebjerg J, Jensen LH, Jakobsen A. The prognostic value of simultaneous tumor and serum RAS/RAF mutations in localized colon cancer. *Cancer Med* (2017) 6(5):928–36. doi: 10.1002/cam4.1051
9. Fabbri F, Carloni S, Zoli W, Ulivi P, Gallerani G, Fici P, et al. Detection and recovery of circulating colon cancer cells using a dielectrophoresis-based device: KRAS mutation status in pure CTCs. *Cancer Lett* (2013) 335(1):225–31. doi: 10.1016/j.canlet.2013.02.015
10. Alcaide M, Cheung M, Bushell K, Arthur SE, Wong HL, Karasinska J, et al. A Novel Multiplex Droplet Digital PCR Assay to Identify and Quantify KRAS Mutations in Clinical Specimens. *J Mol Diagn* (2019) 21(2):214–27. doi: 10.1016/j.jmoldx.2018.09.007
11. Xu J-M, Liu X-J, Ge F-J, Lin L, Wang Y, Sharma MR, et al. KRAS mutations in tumor tissue and plasma by different assays predict survival of patients with metastatic colorectal cancer. *J Exp Clin Cancer Res* (2014) 33(1):104. doi: 10.1186/s13046-014-0104-7
12. Li SC, Tachiki LML, Kabeer MH, Dethlefs BA, Anthony MJ, Loudon WG. Cancer genomic research at the crossroads: realizing the changing genetic landscape as intratumoral spatial and temporal heterogeneity becomes a confounding factor. *Cancer Cell Int* (2014) 14(1):115. doi: 10.1186/s12935-014-0115-7
13. Blank A, Roberts DEI, Dawson H, Zlobec I, Lugli A. Tumor heterogeneity in primary colorectal cancer and corresponding metastases. Does the apple fall far from the tree? *Front Med* (2018) 5:234. doi: 10.3389/fmed.2018.00234
14. Lee KH, Kim JS, Kim JY. Necessity of Genetic Evaluation of Metachronous Metastases of Colorectal Cancer: Quantitative Analysis of Genetic Discordance Between Metachronous Metastases and Radically Resected Primary Colorectal Cancers Using Next-Generation Sequencing. *Dis Colon Rectum* (2019) 62(7):832–9. doi: 10.1097/DCR.0000000000001386
15. Knijn N, Mekenkamp L, Klomp M, Vink-Börger M, Tol J, Teerenstra S, et al. KRAS mutation analysis: a comparison between primary tumours and matched liver metastases in 305 colorectal cancer patients. *Br J Cancer* (2011) 104(6):1020–6. doi: 10.1038/bjc.2011.26
16. Bray SM, Lee J, Kim ST, Hur JY, Ebert PJ, Calley JN, et al. Genomic characterization of intrinsic and acquired resistance to cetuximab in colorectal cancer patients. *Sci Rep* (2019) 9(1):1–13. doi: 10.1038/s41598-019-51981-5
17. Pietrantonio F, Vernieri C, Siravegna G, Mennitto A, Berenato R, Perrone F, et al. Heterogeneity of acquired resistance to anti-EGFR monoclonal antibodies in patients with metastatic colorectal cancer. *Clin Cancer Res* (2017) 23(10):2414–22. doi: 10.1158/1078-0432.CCR-16-1863

Conflict of Interest: The authors declare that the research was conducted in the absence of any commercial or financial relationships that could be construed as a potential conflict of interest.

frontiers in Oncology

ORIGINAL RESEARCH
published: 21 January 2021
doi: 10.3389/fonc.2020.606790

LETM1 Knockdown Promotes Autophagy and Apoptosis Through AMP-Activated Protein Kinase Phosphorylation-Mediated Beclin-1/Bcl-2 Complex Dissociation in Hepatocellular Carcinoma

Baoyong Zhou[1], Changhong Yang[2], Xiong Yan[1], Zhengrong Shi[1], Heng Xiao[1], Xufu Wei[1], Ning Jiang[3] and Zhongjun Wu[1]**

[1] Department of Hepatobiliary Surgery, the First Affiliated Hospital of Chongqing Medical University, Chongqing, China, [2] Department of Bioinformatics, Chongqing Medical University, Chongqing, China, [3] Department of Pathology, Chongqing Medical University, Chongqing, China

OPEN ACCESS

Edited by:
Yujun Shi,
Sichuan University, China

Reviewed by:
Helen He Zhu,
Shanghai Jiao Tong University, China
Peizhi Li,
Chongqing Medical University, China
Yongjie Zhou,
Sichuan University, China

***Correspondence:**
Ning Jiang
jiangning@cqmu.edu.cn
Zhongjun Wu
wzjtcy@126.com

Specialty section:
This article was submitted to Gastrointestinal Cancers, a section of the journal Frontiers in Oncology

Received: 15 September 2020
Accepted: 04 December 2020
Published: 21 January 2021

Citation:
Zhou B, Yang C, Yan X, Shi Z, Xiao H, Wei X, Jiang N and Wu Z (2021) LETM1 Knockdown Promotes Autophagy and Apoptosis Through AMP-Activated Protein Kinase Phosphorylation-Mediated Beclin-1/Bcl-2 Complex Dissociation in Hepatocellular Carcinoma. Front. Oncol. 10:606790. doi: 10.3389/fonc.2020.606790

Leucine zipper/EF hand-containing transmembrane-1 (LETM1) is an inner mitochondrial membrane protein that has been reported to be involved in many primary tumors and may regulate many biological processes. However, the biological role and molecular mechanism of LETM1 in the progression of hepatocellular carcinoma (HCC) remain largely unknown. In this study, we found that LETM1 was highly expressed in HCC tissues and cell lines and that higher LETM1 expression was associated with a lower overall survival rate in HCC patients. In addition, knockdown of LETM1 inhibited proliferation and enhanced apoptosis and autophagy in the Huh 7 and QGY-7701 liver cancer cell lines. Mechanistically, knockdown of LETM1 dissociated the Beclin-1/Bcl-2 complex through phosphorylation of AMPK and Bcl-2. These results demonstrated that LETM1 is involved in the development of HCC and could be a novel therapeutic target in HCC.

Keywords: hepatocellular carcinoma, LETM1, apoptosis, autophagy, AMP-activated protein kinase (AMPK), beclin-1/Bcl-2 complex

INTRODUCTION

Hepatocellular carcinoma (HCC) is the sixth most common malignant tumor worldwide and is particularly prevalent in China, where approximately half of new cases and deaths occur (1, 2). Due to the high invasiveness and high mortality rate of HCC, the survival time of most patients with advanced HCC is only approximately 2–3 months (3). Given the advances in some novel therapeutic strategies against HCC such as resection, chemotherapy, and transplantation, the survival of HCC patients has improved. Unfortunately, because there are no obvious clinical symptoms at an early stage, most patients are diagnosed at an advanced stage, and the 5-year recurrence rate after surgery is greater than 70%; moreover, recurrence often results in death (4, 5).

Therefore, further studies on diagnostic and prognostic markers for HCC are key to developing more effective treatments.

Autophagy is an important lysosomal process for removing damaged organelles/proteins and limiting genomic instability (6). Autophagy can regulate cellular processes such as proliferation and apoptosis in liver cells (7). Autophagy plays a variety of roles in maintaining the stability of the internal environment of the liver, maintains the genomic stability of liver cells and prevents malignant transformation (8, 9). Researchers have found that autophagy plays a key role in the adaptation of HCC cells and that dysregulation of autophagy is connected with the occurrence of liver cancer (10). Low expression of Beclin1 in human HCC tissues is associated with tumor recurrence (11). Beclin1 is an important autophagy protein that has been shown to be related to HCC tumors. Recently, a study suggested that disruption of the Beclin1/Bcl-2 complex is an effective mechanism for increasing mammalian autophagy, thus preventing premature aging (12). Both Bcl-2 and Bcl-2L1 directly bind to Beclin-1 through their BH3 domains (13). Dissociation of Bcl-2 or Bcl-2 L1 from Beclin-1 may be a necessary condition for upregulating autophagy both *in vitro* and *in vivo* (14). In addition, posttranslational modification of Beclin-1 can promote its dissociation from the Bcl-2 or Bcl-2 L1 complex (15). AMP-activated protein kinase (AMPK) has been implicated in cell growth and proliferation (16). It has been demonstrated that AMPK promotes autophagy and apoptosis, and AMPK may be upstream of Beclin1 and Bcl-2 (17). Therefore, we speculated that AMPK may regulate autophagy and apoptosis through the Beclin-1/Bcl-2 complex.

Leucine zipper/EF hand-containing transmembrane-1 (LETM1), which is a transporter protein localized to the inner mitochondrial membrane, is reported to be conserved between yeast and humans (18). Studies have shown that LETM1 has important roles in mitochondrial morphology and mitochondrial K^+ and Ca^{2+} homeostasis (19, 20). Accumulating evidence indicates that LETM1 expression is markedly increased in various tumors and may be a potential marker for tumorigenesis (21–24). In addition, it has been demonstrated that knockdown of LETM1 can cause a significant decrease in ATP levels, after which the ADP or AMP/ATP ratio can be changed, and activated AMPK, which is a bioenergy sensor that leads to the formation of autophagosomes, is then activated (25). These findings provide a theoretical basis for the hypothesis that LETM1 may regulate AMPK-mediated autophagy. However, there are only a few studies about LETM1 in autophagy and apoptosis in HCC, and greater insight into the mechanisms linking LETM1 with HCC is needed.

Based on the findings to date, we hypothesized that LETM1 regulates autophagy and apoptosis through activation of AMPK-mediated Beclin-1/Bcl-2 complex dissociation in hepatocellular carcinoma. In this research, LETM1 was found to be highly expressed in HCC tissues, and the overall survival time of patients with high LETM1 expression was found to be significantly shorter than that of patients with low LETM1 expression. We also found that the level of LETM1 was higher in HCC cell lines than in the normal hepatocyte line LO2. Furthermore, silencing LETM1 inhibited HCC growth and promoted autophagy and apoptosis *in vitro* and *in vivo*. More importantly, we discovered for the first time that LETM1 may regulate the dissociation of the Beclin-1/Bcl-2 complex through activation of AMPK to influence autophagy and apoptosis in HCC.

MATERIALS AND METHODS

Oncomine Data Extraction

Oncomine data were processed to assess the expression of LETM1 in tumor tissues and normal liver tissues. Then, we plotted survival curves to assess the diagnostic significance of LETM1.

Clinical Specimen Collection

Tumor tissues and adjacent tissues from 90 HCC patients who underwent hepatic resection were obtained from the First Affiliated Hospital of Chongqing Medical University from 2012 to 2018. All patients agreed to provide informed consent, and the experimental protocols were approved by the local ethics committee. The relationships between the level of LETM1 and clinical features such as age, sex, tumor size, tumor, node, and metastasis (TNM) stage, death, or time of last follow-up were evaluated, as shown in **Table 1**. Next, we performed Pearson correlation analysis to evaluate the correlations between the LETM1 expression level and the clinical variables of HCC patients. In addition, we performed univariate and multivariate Cox regression analyses to evaluate the relative risk associated with LETM1 for the prognosis of HCC. Kaplan-Meier analysis was used to evaluate the overall survival of HCC patients with high LETM1 expression.

Cell Line Culture

HCC cell lines, including SMMC-7721, HCC-LM3, Huh7, HepG2, QGY-7701, and Hep3B, and the normal human liver cell line LO-2 were obtained from the Department of Hepatobiliary Surgery of the First Affiliated Hospital of Chongqing Medical University. All cells were maintained in RPMI-1640 medium (Gibco, USA) supplemented with 10% fetal bovine serum (Gibco, USA), 1% penicillin, and 1% streptomycin at 37°C in 5% CO_2.

Real-Time Quantitative PCR

Total RNA was extracted from tissues or cells with TRIzol reagent (Takara, Japan) according to the instructions and was then reverse transcribed into complementary DNA (cDNA), which was used as the template for PCR amplification. The 20 μl reaction system contained 1 μl of cDNA template, 0.5 μl of each primer, 10 μl of 2 × PCR mix, and 8 μl of diethylpyrocarbonate (DEPC) water. The PCR conditions were as follows: predenaturation at 95°C for 5 min, followed by 35 cycles of denaturation at 95°C for 30 s, annealing at 55°C for 30 s, and extension at 72°C for 60 s. The method was used to analyze the data.

Western Blotting

Radioimmunoprecipitation assay buffer (RIPA) buffer purchased from Beyotime Biotechnology (China) was used to extract total

TABLE 1 | Relationship between LETM1 expression and clinicopathologic features in patients with hepatocellular carcinoma.

Variable	LETM1 expression		p-value
	High-LETM1	Low-LETM1	
In general			
Adjacent tissue	30	60	0.000
Tumor tissue	53	37	
Gender			
Male	28	17	0.520
Female	25	20	
Age, years			
≤60	39	30	0.408
≤60	14	7	
Tumor size, cm			
≤5	18	27	0.000
≤5	35	10	
AFP, ng/ml			
≤400	18	19	0.099
≤400	35	18	
HBsAg			
Positive	24	16	0.848
Negative	29	21	
Liver cirrhosis			
Yes	21	12	0.486
No	32	25	
Portal vein emboli and metastasis			
Yes	32	12	0.009
No	21	25	
TNM stage (AJCC)			
I–II	19	23	0.014
III–IV	34	14	
Tumor differentiation			
I–II	34	25	0.737
III–IV	19	12	

protein from tissues and cultured cells, and the supernatant was collected after centrifugation (12,000×g, 10 min, 4°C). After blocking with 5% skim milk, the membrane was incubated with primary antibodies against LETM1 (1:500, Santa Cruz, USA), AMPK (1:500, ABclonal, China), p-AMPK (1:500, ABclonal, China), Bcl-2 (1:500, ABclonal, China), p-Bcl-2 (1:500, Proteintech, USA), Bax (1:500, ABclonal, China), caspase-3 (1:500, Proteintech, USA), Beclin-1 (1:500, Proteintech, USA), p62 (1:500, Proteintech, China), LC3 (1:500, Proteintech, USA), and β-actin (1:2000, ABclonal, China) overnight. The membrane was then incubated with secondary antibodies (1:2,000, Proteintech, China) for 2 h the next day. The protein bands on the blot were analyzed.

Immunohistochemistry and Determination of Staining Results

All specimens were fixed with 4% neutral formaldehyde, embedded in paraffin, and sectioned at 4 μm. Sections were baked at 60°C for 1 h and were then dewaxed, rehydrated through a gradient alcohol series and washed. Sections were boiled in antigen repair solution for 10 min for antigen repair, and the remaining steps were carried out in accordance with the instructions. After DAB staining, the sections were counterstained with hematoxylin and sealed. The percentage of positive tumor cells was scored as follows: 1–25%, 1; 26–50%, 2; 51–75%, 3; and 76–100%, 4. The intensity of LETM1 staining was scored as follows: no staining, 0; weak staining, 1; and strong staining, 2. These two scores were multiplied to obtain the final score, and the expression of LETM1 was determined as low expression (score <4) or high expression (score ≥ 4).

Immunofluorescence Analysis

Sterile coverslips were placed in a 24-well plate, and HCC cells were seeded on the coverslips. When the HCC cells had grown to approximately 40% confluence, they were washed with cold PBS, fixed with 4% paraformaldehyde, permeabilized with 0.3% Triton X-100 for 20 min, sealed at room temperature with 3% BSA for 1 h, and incubated with a primary antibody against LC3 (1:500, Proteintech, USA) at 4°C overnight. The next day, the plate was reheated for half an hour, washed with PBS, and incubated with secondary antibodies. Nuclei were stained with DAPI (ABclonal, China). Finally, the fluorescence staining in the cells was observed under an Olympus confocal fluorescence microscope.

Establishment of Stable LETM1-Knockdown Cell Lines

LETM1 short hairpin RNA (shRNA) and control shRNA constructs were designed and synthesized by GenePharma Corporation (Shanghai, China). Huh7 and QGY-7701 HCC cells were transfected with LETM1-lentivirus shRNA (sh-LETM1) and control-lentivirus shRNA (sh-NC) using siLentFect™ Lipid Reagent (Bio-Rad, USA) according to the manufacturer's protocol. Stable cell lines were established and selected with 2 μg/ml puromycin (Vicmed, China) for 8–12 days. The expression levels in the stably transfected and control HCC cells were determined by RT-qPCR and Western blotting.

Cell Proliferation Assay

A Cell Counting Kit (CCK)-8 (Beyotime Biotechnology, China) was used to assess the effect of LETM1 on cell proliferation. Cells in different groups were seeded into 96-well plates. According to the protocol, CCK-8 solution in serum-free medium (10 μl/100 μl) was added to each well and incubated at 37°C for 2 h. The absorbance at 450 nm was measured to assess cell proliferation.

Flow Cytometric Analysis of Apoptosis

An Annexin V-FITC/PI Apoptosis Detection Kit (Beyotime, China) was used to assess apoptosis. Cells were washed with cold PBS and resuspended in buffer. Annexin V-FITC solution was added to the cells and incubated for approximately 15 min at room temperature. Next, 5 μl of propidium iodide (PI) solution was mixed with the cells for 5 min in the dark, and the ratio of apoptotic cells was determined by flow cytometry.

Coimmunoprecipitation

Total protein was harvested from cultured HCC cells. According to the manufacturer's instructions, coimmunoprecipitation (Co-IP) was conducted, and an anti-Bcl-2 antibody (1:500, ABclonal, China), an anti-Beclin-1 antibody (1:500, Proteintech, USA), and protein A/G agarose (MedChemExpress, USA) were used. Immunoprecipitated proteins were collected and then used for Western blot analysis to evaluate the interaction between Beclin-1 and Bcl-2.

Tumorigenicity Assay *In Vivo*

All animal experimental procedures were approved by the Laboratory Animal Ethics Committee of Chongqing Medical University. Cells transfected with shRNAs (2×10^7 cells/ml) were injected subcutaneously into the left dorsal region of each immunodeficient mouse. The nude mice (18~22 g, 4~6 weeks old) were randomized into four groups: the sh-LETM1- Huh7 group, sh-NC- Huh7 group, sh-LETM1- QGY-7701 group, and sh-NC-QGY-7701 group (n=6 mice per group). The tumor volume (V) was calculated using the following formula: V (cm^3) = 0.5×width^2 (cm^2)×length (cm). The volumes of tumors in the nude mice were recorded, and tissues were collected after 4 weeks.

Statistical Analysis

All quantitative experimental data are shown as the means ± SEMs and were analyzed with SPSS 22 (IBM, USA) and GraphPad Prism 7.0 (CA, USA). The chi-square test and Pearson correlation analysis were used to evaluate the correlations between LETM1 expression and clinical variables of HCC patients. A Cox regression model was used for statistical analysis of survival-related factors in univariate analysis and multivariate analysis. The Kaplan-Meier method was used to generate survival curves, and the log-rank test was used to calculate differences in overall survival times. Comparisons between two groups were analyzed by t tests, and comparisons among multiple groups were analyzed by one-way ANOVA. Differences with $p < 0.05$ were considered significant.

RESULTS

LETM1 Was Significantly Upregulated in Hepatocellular Carcinoma Tissues

The messenger RNA (mRNA) levels of LETM1 in HCC tissues and normal liver tissues from the Oncomine database are shown in **Figure 1A**, and Kaplan-Meier survival analysis indicated that upregulated LETM1 expression predicted poor prognosis (**Figure 1B**) ($p < 0.05$). Then, the mRNA and protein levels of LETM1 in six HCC patient tissues and paired adjacent tumor tissues from the First Affiliated Hospital of Chongqing Medical University were determined by RT-qPCR and Western blotting. The results revealed that both the relative mRNA level ($p < 0.01$, **Figure 1C**) and the protein expression level ($p < 0.01$, **Figures 1D, E**) of LETM1 in HCC tissues were significantly higher than those in adjacent tumor tissues. Our results demonstrated that LETM1 overexpression may be related to HCC development.

High LETM1 Expression Was Associated With Poor Prognosis in Hepatocellular Carcinoma Patients

Then, to illustrate the relationships between LETM1 expression and clinicopathological features as well as overall survival time in HCC patients, immunohistochemistry was conducted to detect the expression of LETM1 in 82 HCC patients (eight patients' clinical data and follow-up data were unavailable). The data revealed that the expression of LETM1 in HCC tissues was higher than that in the corresponding adjacent tissues and that LETM1 was mainly localized in the cytoplasm, as shown in **Figures 1F, G**. Moreover, the chi-square test and Pearson correlation analysis showed that LETM1 overexpression was significantly correlated with tumor size ($p<0.001$), portal vein emboli, metastasis (both $p<0.01$), and TNM stage of HCC ($p<0.05$) (**Tables 1** and **2**). In addition, we performed univariate and multivariate Cox regression analyses to identify whether LETM1 is a risk factor in HCC patients. As shown in **Table 3**, univariate Cox regression analysis illustrated that high LETM1 expression was associated with a significantly increased risk of death in HCC patients ($p<0.001$) compared to that of patients with low LETM1 expression, and multivariate Cox regression analysis demonstrated that LETM1 expression could be a factor related to poor survival. Kaplan-Meier analysis also indicated that HCC patients with high levels of LETM1 were more likely to have a poor prognosis ($p < 0.05$, **Figure 1H**). Collectively, these results indicated a significant correlation of LETM1 expression with prognosis.

Knockdown of LETM1 Inhibits the Proliferation and Promotes the Apoptosis of Huh7 and QGY-7701 Cells

The level of LETM1 in LO2 normal liver cells and HCC cell lines, including SMMC-7721, HCC-LM3, Huh7, HepG2, QGY-7701, and Hep3B, was further explored by RT-qPCR and Western blotting. Compared with that in LO2 cells, the relative mRNA level of LETM1 (**Figure 2A**) was increased in SMMC-7721 ($p<0.01$), HCCLM3 ($p<0.05$), Huh7 ($p<0.001$), HepG2 ($p<0.01$), and QGY-7701 ($p<0.001$) cells, but the difference was not obvious in Hep3B cells. The Western blot results also indicated a consistent conclusion (**Figures 2B, C**). As a result, the Huh7 and QGY-7701 HCC cell lines were selected for the following experiments. Here, we used shRNA lentivirus to establish stable Huh7 and QGY-7701 LETM1-knockdown cell lines, and RT-qPCR and Western blotting were used to detect the transfection efficiency (**Figures 2D–F**). Next, the effects of LETM1 knockdown on the proliferation and apoptosis of HCC cells were explored. The CCK-8 assay revealed that proliferation was significantly decreased in the sh-LETM1 group compared with the NC group in both Huh7 and QGY-7701 cells (**Figures 2G, H**). In addition, the flow cytometry results showed that the apoptosis rate of Huh7 and QGY-7701 cells was significantly increased in the sh-LETM1 groups compared with the sh-NC groups (**Figure 2I**). The Western blot results revealed that the p-Bcl-2/Bcl-2 ratio and the expression levels of Bax and Caspase-3 were increased in the sh-LETM1 group compared with the NC group in both Huh7 and QGY-7701 cells (**Figures 2E, F**). These results indicated that knockdown of LETM1 inhibits the proliferation and promotes the apoptosis of Huh7 and QGY-7701 cells.

Knockdown of LETM1 Triggers Autophagy in Huh7 and QGY-7701 Cells

Then, Western blotting and immunofluorescence were used to test whether LETM1 is involved in autophagy *in vitro*. Beclin1,

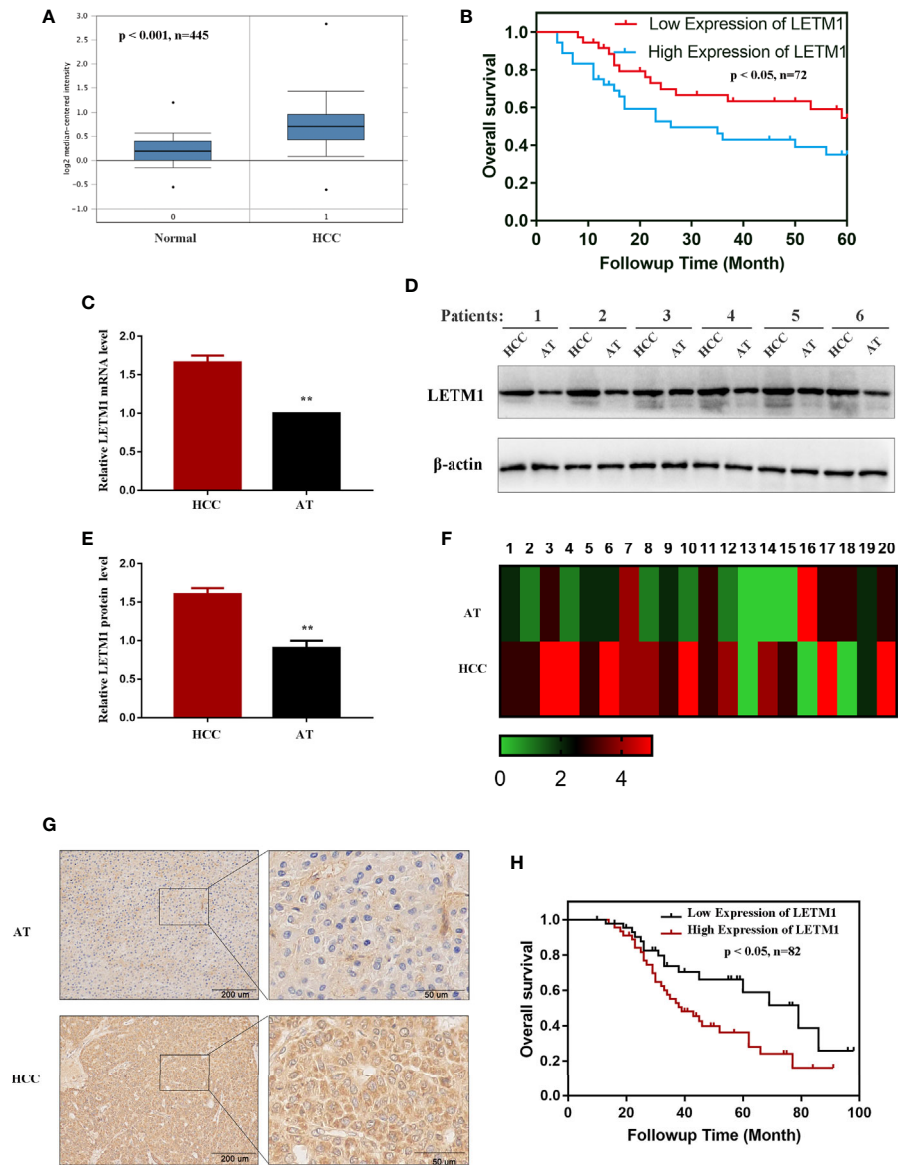

FIGURE 1 | LETM1 was significantly upregulated in hepatocellular carcinoma (HCC) tissues. **(A)** Expression of LETM1 was significantly upregulated in HCC tumor tissues compared with normal liver tissue samples in the Oncomine database ($p < 0.001$, n=445). **(B)** Kaplan-Meier overall survival curves for patients with HCC stratified by high and low expression of LETM1 from the Oncomine database ($p < 0.05$, n=72). **(C)** Relative mRNA level of LETM1 in HCC tissues and adjacent tumor tissues collected from First Affiliated Hospital of Chongqing Medical University. **(D, E)** Western blot of LETM1 expression in HCC tissues and adjacent tumor tissues from First Affiliated Hospital of Chongqing Medical University. **(F)** LETM1 expression was markedly increased in 20 paired HCC tissues and their adjacent tumor tissues. **(G)** Representative images of LETM1 expression in HCC tissues and their adjacent normal tissues. **(H)** Kaplan-Meier overall survival curves for patients with HCC stratified by high and low expression of LETM1 from clinical specimens ($p < 0.05$, n=82). Data are presented as means ± SEM, $^{**}p < 0.01$ *versus* HCC group. HCC, hepatocellular carcinoma tissue; AT, adjacent tumor tissue.

p62, and LC3II/I ratio are effective markers of autophagy, and the Western blot results shown in **Figures 3A, B** revealed that the level of Beclin1 and LC3II/I were increased in the sh-LETM1 group compared with the NC group (**Figures 3A, B**), while the level of p62 was decreased in the sh-LETM1 group compared with the NC group. The immunofluorescence assay demonstrated that the fluorescence intensity of LC3 was significantly higher in the sh-LETM1 group than in the NC group in both Huh7 and QGY-7701 cells (**Figure 3C**).

Knockdown of LETM1 Regulates Autophagy and Apoptosis by Activating AMPK

It has been reported that LETM1 can inhibit the activation of AMPK, and AMPK has been reported to be associated with autophagy and apoptosis. Therefore, we attempted to determine whether LETM1 can regulate autophagy and apoptosis by activating AMPK in HCC cell lines. Here, an AMPK inhibitor, dorsomorphin, together with LETM1 shRNA, was used in Huh7 and QGY-7701 cells to investigate the possible

mechanism. As shown in **Figure 4**, the expression of LETM1 did not differ significantly between the sh-LETM1 group and the sh-LETM1+dorsomorphin group, while the expression of p-AMPK was increased in the sh-LETM1 group compared with the NC group, and the effect of sh-LETM1 on p-AMPK was reversed by dorsomorphin. These results indicated that LETM1 may be upstream of AMPK and that knockdown of LETM1 can promote the phosphorylation of AMPK. In addition, dorsomorphin reversed the effect of LETM1 shRNA on the expression of Beclin1, p62, and LC3II/I (LETM1 shRNA group *vs*. LETM1 shRNA+dorsomorphin group). These results demonstrated that LETM1 may regulate autophagy through AMPK phosphorylation in HCC cells.

LETM1 Knockdown Promotes Autophagy and Apoptosis Through AMPK-Mediated Beclin-1/Bcl-2 Complex Dissociation in Hepatocellular Carcinoma Cells

AMPK has been reported to be located upstream of Beclin-1 and Bcl-2, and Beclin-1 and Bcl-2 may exist as a complex. In addition, LETM1 can regulate the phosphorylation of AMPK. Therefore, we proposed that LETM1 regulates the dissociation of the Beclin-1/Bcl-2 complex through phosphorylation of AMPK, thus affecting autophagy and apoptosis. To verify this hypothesis, coimmunoprecipitation experiments were conducted. As shown in **Figure 5**, the interaction of Beclin-1 and Bcl-2 was decreased in the sh-LETM1 group but increased in the dorsomorphin group, indicating that LETM1 knockdown promoted the dissociation of the Beclin-1/Bcl-2 complex and that inhibition of AMPK suppressed this dissociation. Moreover, inhibition of AMPK reversed the effect of LETM1 shRNA on Beclin-1/Bcl-2 complex dissociation (LETM1 shRNA group *vs*. LETM1 shRNA+dorsomorphin group).

TABLE 2 | Spearman analysis of correlation between LETM1 and clinicopathological.

Variables	LETM1 expression level	
	Spearman correlation	*p*-Value
Gender	-0.068	0.526
Age, years	0.087	0.414
Tumor size, cm	0.384	0.000
AFP, ng/ml	0.174	0.101
HBsAg	0.020	0.850
Liver cirrhosis	0.073	0.492
Portal vein emboli and metastasis	0.275	0.009
TMN stage (AJCC)	0.260	0.014
Tumor differentiation	0.035	0.741

LETM1 Knockdown Suppressed the Tumorigenicity of Transfected Hepatocellular Carcinoma Cell Lines *In Vivo*

Eventually, we further explored the effect of LETM1 knockdown on HCC growth in nude mice. Stable Huh7 and QGY-7701 LETM1-knockdown cells were injected subcutaneously into nude mice. The volume and weight of tumors were recorded; as shown in **Figure 6**, tumor growth in the sh-LETM1 group was slower than that in the NC group ($p < 0.01$) (**Figure 6A**), and the tumor weights and volumes were significantly lower in the sh-LETM1 group than in the NC group (**Figures 6B, C**). Tumor tissues were assessed by Western blotting, which revealed that the levels of Beclin1, LC3II/I, p-Bcl-2/Bcl-2, Bax, and caspase-3 were increased in sh-LETM1 tumor tissues compared with NC tumor tissues (**Figures 6D–F**). In contrast, the level of p62 was decreased in sh-LETM1 tumor tissues (**Figures 6D, E**). Taken together, these results in this tumor formation experiment indicated that LETM1 may play an important role in the tumorigenicity of HCC cells.

DISCUSSION

In this study, high LETM1 expression in HCC was associated with poor patient outcome. The findings of this study indicated that LETM1 is involved in HCC tumor cell aggressiveness by promoting cell proliferation and inhibiting autophagy and apoptosis. Mechanistically, this study suggested that LETM1 regulates the dissociation of the Beclin-1/Bcl-2 complex through AMPK in HCC.

The LETM1 protein has been identified as a mitochondrial membrane protein that may regulate mitochondrial morphology and cell proliferation (19, 20). There is accumulating evidence that LETM1 expression is significantly increased in several kinds of cancers and is associated with poor prognosis (22–24). Doonan et al. (20). found that downregulation of LETM1 caused the accumulation of S-phase cells and that re-expression of LETM1 reversed the accumulation of S-phase cells, suggesting that inhibiting LETM1 may suppress cell proliferation by disrupting cell cycle progression (23). Piao et al. (21). found that overexpression of LETM1 could cause the necrosis and death of HeLa cells by reducing ATP production and mitochondrial biogenesis (21). This finding was consistent with our results, which revealed that the expression of LETM1 was increased in HCC tissues and cell lines and that high expression of LETM1 was associated with tumor size, portal vein emboli, metastasis, and

TABLE 3 | Univariate and multivariate analyses of various prognostic parameters in patients with hepatocellular carcinoma (HCC) Cox-regression analysis.

LETM1	Univariate analysis			Multivariate analysis		
	p	Hazard ratio	95% confidence	*p*	Hazard ratio	95% confidence
Tumor size	0.000	5.110	2.570–10.160	0.008	2.742	1.303–5.768
Portal vein emboli and metastasis	0.000	6.656	3.321–13.341	0.001	3.676	1.711–7.898
TNM stage (AJCC)	0.000	4.092	2.124–7.883	0.009	2.523	1.258–5.059

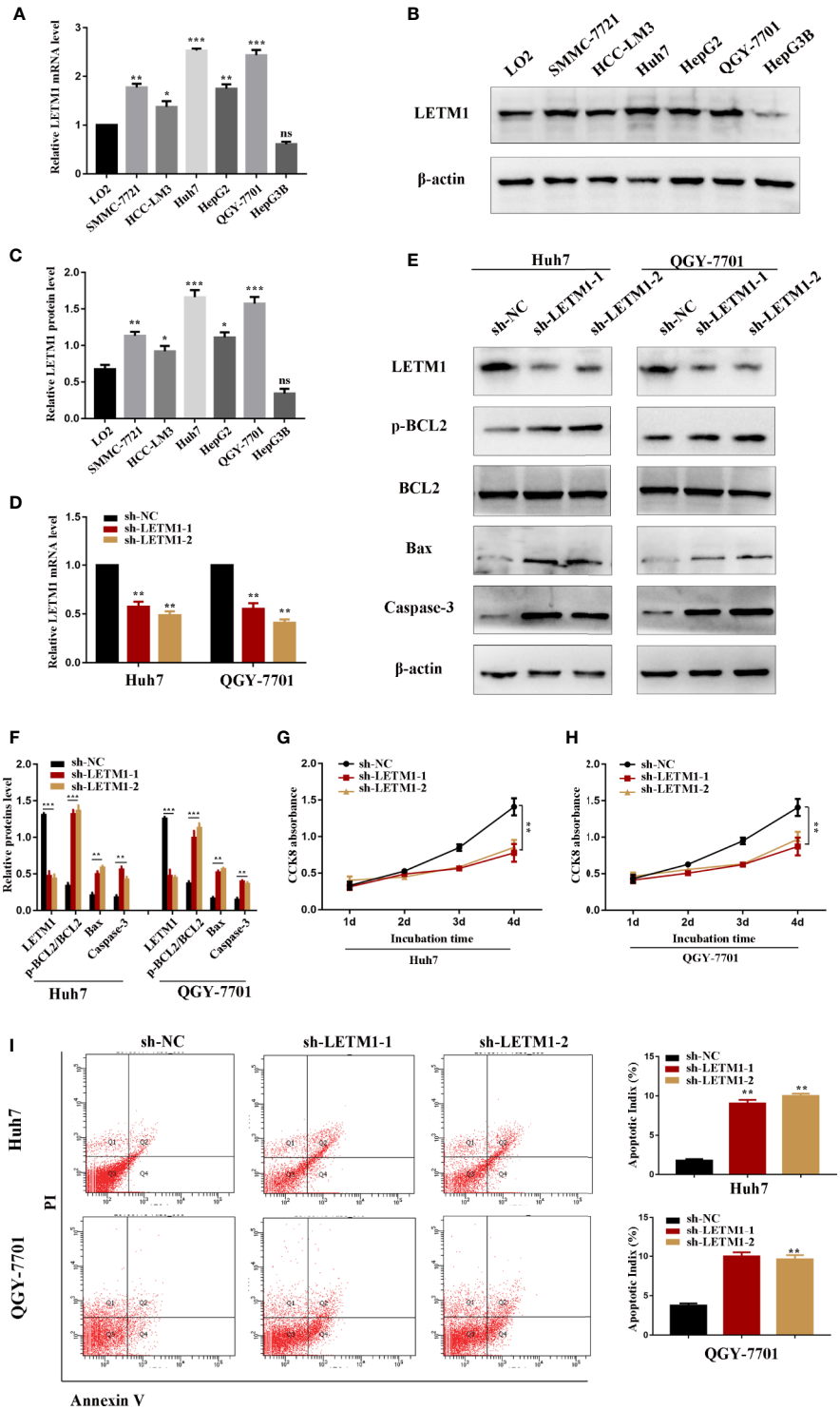

FIGURE 2 | Knockdown of LETM1 inhibits cell proliferation and promotes apoptosis in hepatocellular carcinoma (HCC) cell lines. **(A)** RT-qPCR analysis of LETM1 expression in LO2 and HCC cell lines. **(B, C)** Western blotting of LETM1 expression in LO2 and HCC cell lines. **(D)** RT-qPCR analysis to estimate the transfection effect of LETM1 shRNA lentivirus. **(E, F)** Western blotting of LETM1 and apoptotic-related proteins (p-Bcl-2, Bcl-2, Bax, caspase-3) in Huh7 and QGY-7701 cell lines. **(G, H)** CCK8 assays to detect the growth rate of LEMT1 knockdown in Huh7 and QGY-7701 cell lines. **(I)** Flow cytometry to test the apoptotic index in LETM1-knockdown Huh7 and QGY-7701 cells. $^{*}p < 0.05$, $^{**}p < 0.01$, $^{***}p < 0.001$ *versus* sh-NC group. ns, no significance.

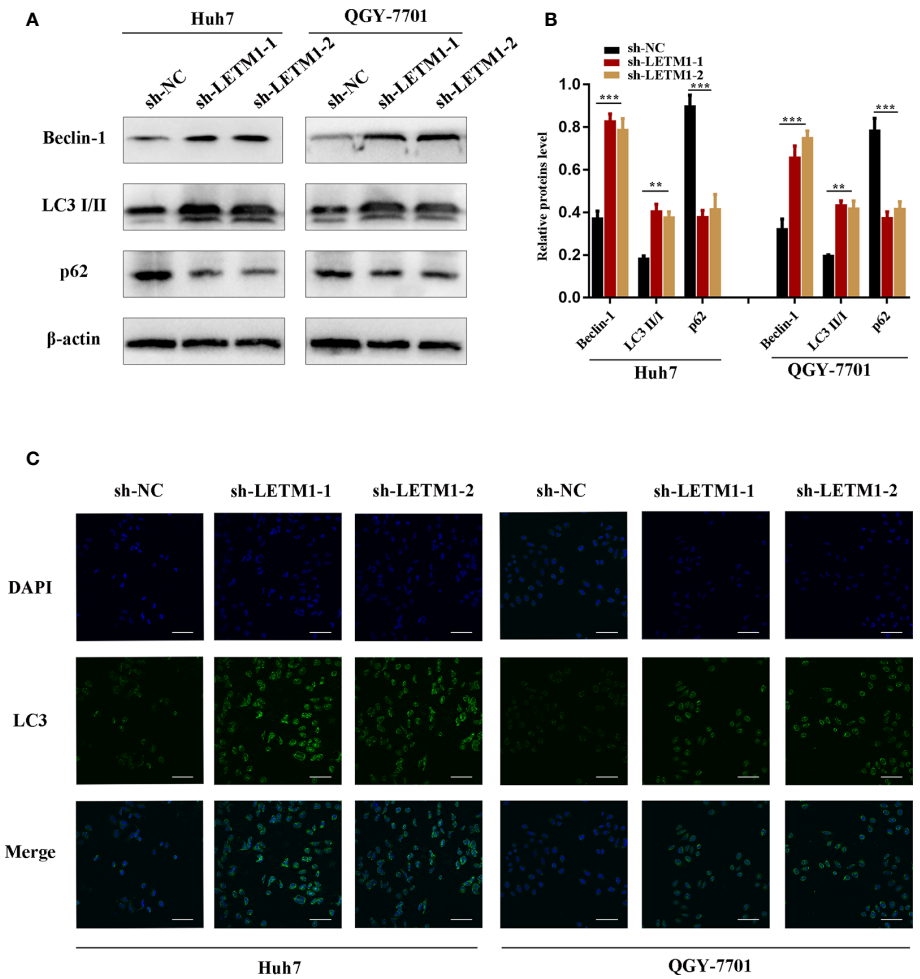

FIGURE 3 | Knockdown of LETM1 triggers autophagy in Huh7 and QGY-7701 cell lines. **(A, B)** Western blotting of LETM1 and auto-related proteins in LETM1-knockdown Huh7 and QGY-7701 cell lines. **(C)** Immunofluorescence assay of LC3 to reflect autophagy level (× 400). $^{**}p < 0.01$, $^{***}p < 0.001$.

TNM stage in HCC patients. Therefore, these results provide evidence that LETM1 may act as a biomarker in HCC.

Autophagy has been reported to play important roles in the occurrence and development of HCC, but this possibility remains controversial (26). The conventional view is that in the early stage of liver cancer, when liver cells are stressed and DNA is damaged, autophagy can function as a tumor-suppressive mechanism by removing damaged mitochondria or liver cells with genetic mutations to maintain the genomic stability of liver cells (27, 28). After the formation of liver cancer, the system regulating autophagy is also disrupted (29). Therefore, autophagy plays a more important role in promoting the survival of liver cancer cells during tumor development than prior to tumor formation. Apoptosis resistance is considered to be another major factor affecting the occurrence of cancer (30). During hepatocarcinogenesis, the balance between cell growth and apoptosis is disrupted (31). It has been reported that LETM1 could be related to autophagy (20). In this study, we found that the levels of autophagy and apoptosis were both increased in Huh7 and QGY-7701 cells with LETM1 silencing, indicating that LETM1 knockdown promoted autophagy and apoptosis. However, further studies on the underlying mechanisms of LETM1 need to be conducted.

It has been proven that knockdown of LETM1 can lead to a significant decrease in the ATP level, resulting in changes in the ADP/ATP and AMP/ATP ratios. An abnormal AMP/ATP ratio may affect the activation of AMPK, leading to abnormal autophagosome formation (25). AMPK has been shown to be involved in mitochondrial biogenesis (32) and lysosome biogenesis (33). Studies have shown that AMPK acts as either a tumor suppressor gene or an oncogene in different cancer cells (34). Other studies have shown that AMPK-mediated signal transduction induces cancer cell death through autophagy and/or apoptosis (35). Research has confirmed that AMPK plays an important role in the activation of autophagy in HCC cells (36). In addition, it has been demonstrated that AMPK is upstream of Beclin1 and Bcl-2 and regulates autophagy and apoptosis (17), and the Beclin1/Bcl-2 complex is a key player in

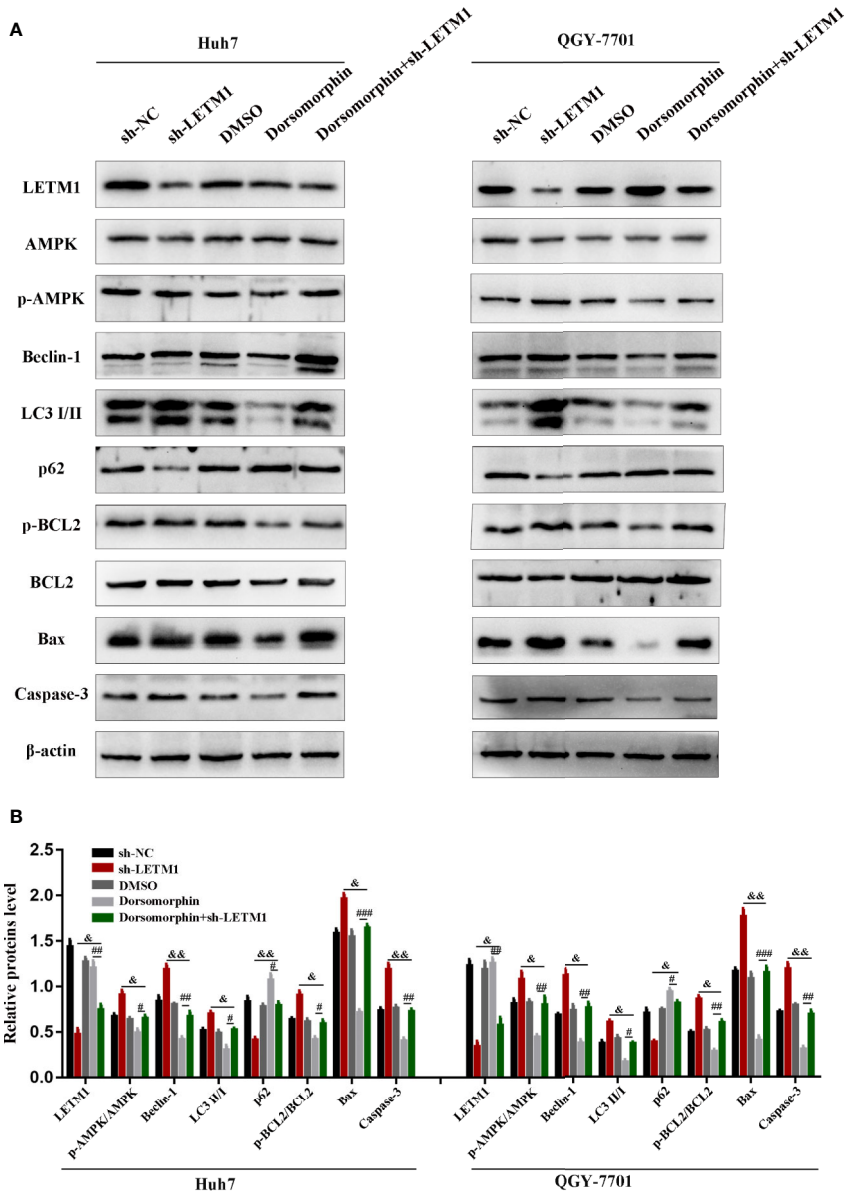

FIGURE 4 | Knockdown of LETM1 regulates autophagy and apoptosis through activating AMPK. **(A, B)** Western blot analysis of the expressions of autophagic associated proteins (Beclin1, p62, and LC3), apoptotic-related proteins (p-Bcl-2, Bcl-2, Bax, caspase-3), LETM1, and AMPK in LETM1-knockdown along with AMPK inhibitor Huh7 and QGY-7701 cell lines. $^{\#}p < 0.05$, $^{\#\#}p < 0.01$, $^{\#\#\#}p < 0.001$ means dorsomorphin *versus* LETM1 shRNA+dorsomorphin group; $^{\&}p < 0.05$, $^{\&\&}p < 0.01$, means LETM1 shRNA group *versus* LETM1 shRNA+dorsomorphin group.

mammalian autophagy and apoptosis (12). Beclin-1 and Bcl-2 interact *via* their common BH3 domains (13). Conditions such as phosphorylation of Bcl-2 can cause Beclin1 and Bcl-2 to dissociate from Beclin1/Bcl-2 complex, thus regulating autophagy and apoptosis (37). The results of our study suggested that LETM1 knockdown led to dissociation of Beclin1 and Bcl-2 from the complex through phosphorylation of AMPK as well as phosphorylation of Bcl-2 and then promoted autophagy and apoptosis, respectively.

In conclusion, this is the first study to find that high expression of LETM1 is significantly associated with tumor size, portal vein emboli, metastasis, TNM stage, and overall survival time in HCC patients. *In vitro* experiments demonstrated that high expression of LETM1 promoted the proliferation of HCC cells. More importantly, this is the first study to discover that high LETM1 expression inhibits autophagy and apoptosis in HCC cells. Mechanistically, LETM1 regulates autophagy and apoptosis *via* AMPK activation-mediated Beclin-1/Bcl-2 complex dissociation in HCC cells (**Figure 7**). These findings suggest that LETM1 could be a potentially valuable biomarker for the diagnosis and prognosis of HCC.

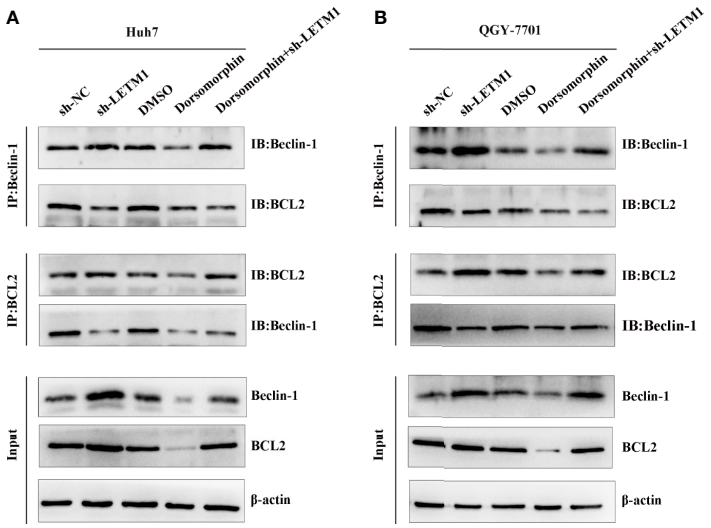

FIGURE 5 | LETM1 knockdown promotes autophagy and apoptosis through AMPK mediated Beclin-1/Bcl-2 complex dissociating in hepatocellular carcinoma cell. **(A)** Co-immunoprecipitation experiment of the interation of Beclin-1 and Bcl-2 in in LETM1-knockdown along with AMPK inhibitor Huh7 cell line. **(B)** Co-immunoprecipitation experiment of the combination of Beclin-1 and Bcl-2 in in LETM1-knockdown along with AMPK inhibitor QGY-7701 cell line.

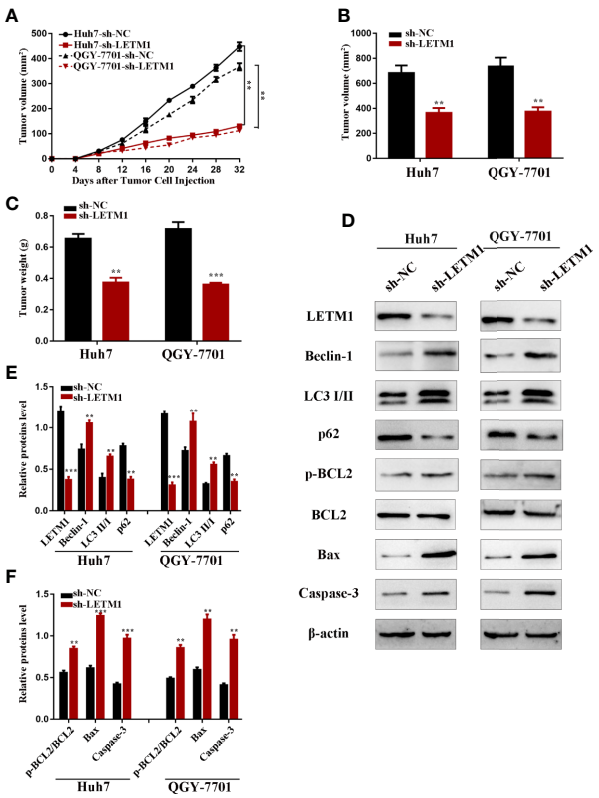

FIGURE 6 | LETM1 knockdown suppressed tumorigenicity of Huh7 and QGY-7701 cells *in vivo*. **(A)** The growth curve of the *in vivo* tumorigenicity assa in LETM1 knockdown Huh7 and QGY-7701 cells transfected nude mice (N=6/per group). **(B)** The weight of tumors in LETM1 knockdown Huh7 and QGY-7701 cells transfected nude mice (N=6/per group). **(C)** The volume of tumors in LETM1 knockdown Huh7 and QGY-7701 cells transfected nude mice (N=6/per group). **(D–F)** The protein level of autophagic associated proteins (Beclin1, p62, and LC3), apoptotic-related proteins (p-Bcl-2, Bcl-2, Bax, caspase-3) and LETM1 in tumor tissues of mice. $^{**}p < 0.01$, $^{***}p < 0.001$ *versus* sh-NC group.

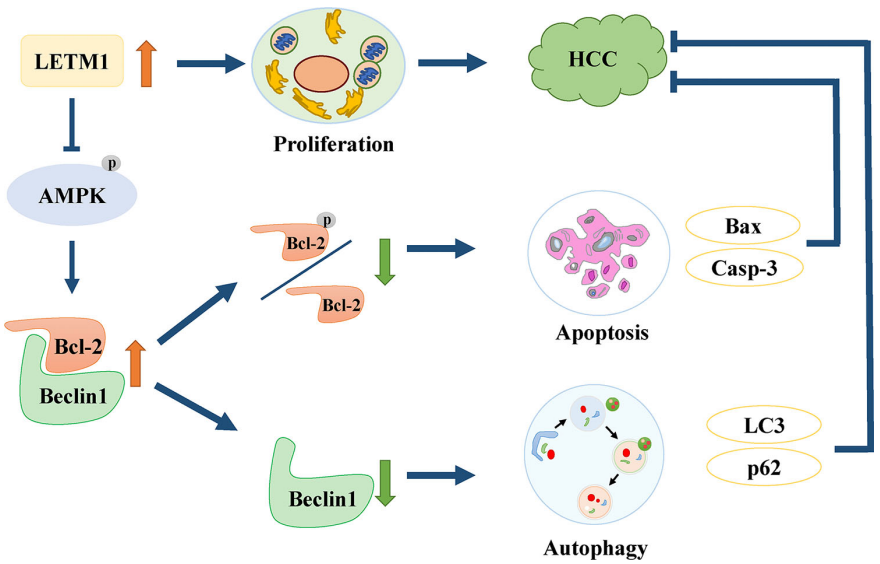

FIGURE 7 | Schematic of oncogenic role of LETM1 in hepatocellular carcinoma (HCC). LETM1 promotes HCC progression through enhancing cell proliferation and suppressing autophagy and cell apoptosis *via* inhibiting AMPK activation mediated-Beclin-1/Bcl-2 complex dissociation.

DATA AVAILABILITY STATEMENT

The raw data supporting the conclusions of this article will be made available by the authors, without undue reservation.

ETHICS STATEMENT

The studies involving human participants were reviewed and approved by Ethics Committee of Chongqing Medical University. The patients/participants provided their written informed consent to participate in this study. The animal study was reviewed and approved by Laboratory Animal Ethics Committee of Chongqing Medical University of China.

AUTHOR CONTRIBUTIONS

BZ and ZW conceived and designed the experiments. CY and XY analyzed the data and processed them. HX and XW performed the experiments. NJ and ZS wrote the paper. All authors read and approved the manuscript. All authors contributed to the article and approved the submitted version.

FUNDING

This work was supported by The National Natural Science Foundation of China (No. 81873592 and No. 81703063).

REFERENCES

1. Heimbach JK, Kulik LM, Finn RS, Sirlin CB, Abecassis MM, Roberts LR, et al. AASLD guidelines for the treatment of hepatocellular carcinoma. *Hepatology* (2018) 67(1):358–80. doi: 10.1002/hep.29086
2. Bray F, Ferlay J, Soerjomataram I, Siegel RL, Torre LA, Jemal A. Global cancer statistics 2018: GLOBOCAN estimates of incidence and mortality worldwide for 36 cancers in 185 countries. *CA Cancer J Clin* (2018) 68(6):394–424. doi: 10.3322/caac.21492
3. Ganten TM, Stauber RE, Schott E, Malfertheiner P, Buder R, Galle PR, et al. Sorafenib in Patients with Hepatocellular Carcinoma—Results of the Observational INSIGHT Study. *Clin Cancer Res* (2017) 23(19):5720–8. doi: 10.1158/1078-0432.CCR-16-0919
4. Hernaez R, El-Serag HB. How We Approach it: Treatment Options For Hepatocellular Carcinoma. *Am J Gastroenterol* (2018) 113(6):791–4. doi: 10.1038/s41395-018-0008-9
5. Forner A, Reig M, Bruix J. Hepatocellular carcinoma. *Lancet* (2018) 391 (10127):1301–14. doi: 10.1016/S0140-6736(18)30010-2
6. Czaja MJ, Ding WX, Donohue TM Jr, Friedman SL, Kim JS, Komatsu M, et al. Functions of autophagy in normal and diseased liver. *Autophagy* (2013) 9 (8):1131–58. doi: 10.4161/auto.25063
7. Wu SY, Lan SH, Wu SR, Chiu YC, Lin XZ, Su IJ, et al. Hepatocellular carcinoma-related cyclin D1 is selectively regulated by autophagy degradation system. *Hepatology* (2018) 68(1):141–54. doi: 10.1002/hep.29781
8. Ordoñez R, Fernández A, Prieto-Domínguez N, Martínez L, García-Ruiz C, Fernández-Checa JC, et al. Ceramide metabolism regulates autophagy and apoptotic cell death induced by melatonin in liver cancer cells. *J Pineal Res* (2015) 59(2):178–89. doi: 10.1111/jpi.12249
9. Liu L, Liao J-Z, He X-X, Li P-Y. The role of autophagy in hepatocellular carcinoma: friend or foe. *Oncotarget* (2017) 8(34):57707–22. doi: 10.18632/oncotarget.17202
10. Owada S, Endo H, Shida Y, Okada C, Ito K, Nezu T, et al. Autophagy–mediated adaptation of hepatocellular carcinoma cells to hypoxia–mimicking conditions constitutes an attractive therapeutic target. *Oncol Rep* (2018) 39(4):1805–12. doi: 10.3892/or.2018.6279
11. Yazdani H, Huang H, Tsung A. Autophagy: Dual Response in the Development of Hepatocellular Carcinoma. *Cells* (2019) 8(2):91. doi: 10.3390/cells8020091
12. Fernández ÁF, Sebti S, Wei Y, Zou Z, Shi M, McMillan KL, et al. Disruption of the beclin 1–BCL2 autophagy regulatory complex promotes longevity in mice. *Nature* (2018) 558(7708):136–40. doi: 10.1038/s41586-018-0162-7

13. Malik SA, Orhon I, Morselli E, Criollo A, Shen S, Mariño G, et al. BH3 mimetics activate multiple pro-autophagic pathways. *Oncogene* (2011) 30 (37):3918–29. doi: 10.1038/onc.2011.104
14. Zalckvar E, Berissi H, Mizrachy L, Idelchuk Y, Koren I, Eisenstein M, et al. DAP-kinase-mediated phosphorylation on the BH3 domain of beclin 1 promotes dissociation of beclin 1 from Bcl-XL and induction of autophagy. *EMBO Rep* (2009) 10(3):285–92. doi: 10.1038/embor.2008.246
15. Gurkar AU, Chu K, Raj L, Bouley R, Lee SH, Kim YB, et al. Identification of ROCK1 kinase as a critical regulator of Beclin1-mediated autophagy during metabolic stress. *Nat Commun* (2013) 4(1):2189. doi: 10.1038/ncomms3189
16. Garcia D, Shaw RJ. AMPK: Mechanisms of Cellular Energy Sensing and Restoration of Metabolic Balance. *Mol Cell* (2017) 66(6):789–800. doi: 10.1016/j.molcel.2017.05.032
17. Wang L, Li H, Zhen Z, Ma X, Yu W, Zeng H, et al. CXCL17 promotes cell metastasis and inhibits autophagy via the LKB1-AMPK pathway in hepatocellular carcinoma. *Gene* (2019) 690:129–36. doi: 10.1016/j.gene.2018.12.043
18. Frazier AE, Taylor RD, Mick DU, Warscheid B, Stoepel N, Meyer HE, et al. Mdm38 interacts with ribosomes and is a component of the mitochondrial protein export machinery. *J Cell Biol* (2006) 172(4):553–64. doi: 10.1083/jcb.200505060
19. Jiang D, Zhao L, Clapham DE. Genome-Wide RNAi Screen Identifies Letm1 as a Mitochondrial Ca2+/H+ Antiporter. *Sci (80-)* (2009) 326(5949):144–7. doi: 10.1126/science.1175145
20. Doonan PJ, Chandramoorthy HC, Hoffman NE, Zhang X, Cárdenas C, Shanmughapriya S, et al. LETM1-dependent mitochondrial Ca $^{2+}$ flux modulates cellular bioenergetics and proliferation. *FASEB J* (2014) 28 (11):4936–49. doi: 10.1096/fj.14-256453
21. Piao L, Li Y, Kim SJ, Byun HS, Huang SM, Hwang SK, et al. Association of LETM1 and MRPL36 Contributes to the Regulation of Mitochondrial ATP Production and Necrotic Cell Death. *Cancer Res* (2009) 69(8):3397–404. doi: 10.1158/0008-5472.CAN-08-3235
22. Li N, Zheng Y, Xuan C, Lin Z, Piao L, Liu S. LETM1 overexpression is correlated with the clinical features and survival outcome of breast cancer. *Int J Clin Exp Pathol* (2015) 8(10):12893–900.
23. Huang B, Zhang J, Zhang X, Huang C, Hu G, Li S, et al. Suppression of LETM1 by siRNA inhibits cell proliferation and invasion of bladder cancer cells. *Oncol Rep* (2017) 38(5):2935–40. doi: 10.3892/or.2017.5959
24. Piao L, Yang Z, Feng Y, Zhang C, Cui C, Xuan Y. LETM1 is a potential biomarker of prognosis in lung non-small cell carcinoma. *BMC Cancer* (2019) 19(1):898. doi: 10.1186/s12885-019-6128-9
25. Cárdenas C, Miller RA, Smith I, Bui T, Molgó J, Müller M, et al. Essential Regulation of Cell Bioenergetics by Constitutive InsP3 Receptor Ca2+ Transfer to Mitochondria. *Cell* (2010) 142(2):270–83. doi: 10.1016/j.cell.2010.06.007
26. Kim KM, Kim SG. Autophagy and microRNA dysregulation in liver diseases. *Arch Pharm Res* (2014) 37(9):1097–116. doi: 10.1007/s12272-014-0439-9
27. Sun K, Guo XL, Zhao QD, Jing YY, Kou XR, Xie XQ, et al. Paradoxical role of autophagy in the dysplastic and tumor-forming stages of hepatocarcinoma development in rats. *Cell Death Dis* (2013) 4(2):e501–1. doi: 10.1038/cddis.2013.35
28. Peng WX, Wan YY, Gong AH, Ge L, Jin J, Xu M, et al. Egr-1 regulates irradiation-induced autophagy through Atg4B to promote radioresistance in hepatocellular carcinoma cells. *Oncogenesis* (2017) 6(1):e292–2. doi: 10.1038/oncsis.2016.91
29. Tian Y, Kuo CF, Sir D, Wang L, Govindarajan S, Petrovic LM, et al. Autophagy inhibits oxidative stress and tumor suppressors to exert its dual effect on hepatocarcinogenesis. *Cell Death Differ* (2015) 22(6):1025–34. doi: 10.1038/cdd.2014.201
30. Mortezaee K. Human hepatocellular carcinoma: Protection by melatonin. *J Cell Physiol* (2018) 233(10):6486–508. doi: 10.1002/jcp.26586
31. Lin S, Hoffmann K, Gao C, Petrulionis M, Herr I, Schemmer P. Melatonin promotes sorafenib-induced apoptosis through synergistic activation of JNK/c-jun pathway in human hepatocellular carcinoma. *J Pineal Res* (2017) 62(3): e12398. doi: 10.1111/jpi.12398
32. Herzig S, Shaw RJ. AMPK: guardian of metabolism and mitochondrial homeostasis. *Nat Rev Mol Cell Biol* (2018) 19(2):121–35. doi: 10.1038/nrm.2017.95
33. Eichner LJ, Brun SN, Herzig S, Young NP, Curtis SD, Shackelford DB, et al. Genetic Analysis Reveals AMPK Is Required to Support Tumor Growth in Murine Kras-Dependent Lung Cancer Models. *Cell Metab* (2019) 29(2):285–302.e7. doi: 10.1016/j.cmet.2018.10.005
34. Liang J, Mills GB. AMPK: A Contextual Oncogene or Tumor Suppressor? *Cancer Res* (2013) 73(10):2929–35. doi: 10.1158/0008-5472.CAN-12-3876
35. Mihaylova MM, Shaw RJ. The AMPK signalling pathway coordinates cell growth, autophagy and metabolism. *Nat Cell Biol* (2011) 13(9):1016–23. doi: 10.1038/ncb2329
36. Carroll B, Dunlop EA. The lysosome: a crucial hub for AMPK and mTORC1 signalling. *Biochem J* (2017) 474(9):1453–66. doi: 10.1042/BCJ20160780
37. Li P, Shi M, Maique J, Shaffer J, Yan S, Moe OW, et al. Beclin 1/Bcl2 complex-dependent autophagy activity modulates renal susceptibility to ischemia-reperfusion injury and mediates renoprotection by Klotho. *Am J Physiol Physiol* (2020) 318(3):F772–92. doi: 10.1152/ajprenal.00504.2019

Conflict of Interest: The authors declare that the research was conducted in the absence of any commercial or financial relationships that could be construed as a potential conflict of interest.

The reviewer PL declared a shared affiliation, with no collaboration, with the authors to the handling editor at the time of the review.

frontiers in Oncology

ORIGINAL RESEARCH
published: 10 February 2021
doi: 10.3389/fonc.2020.607742

Re-Clustering and Profiling of Digestive System Tumors According to Microenvironment Components

Yongwei Wang[1], *Sen Guo*[1], *Zhihong Chen*[1], *Bing Bai*[2], *Shuo Wang*[2] *and Yaxian Gao*[2]*

[1] Department of Anatomy, Basic Medical Institute, Chengde Medical College, Chengde, China, [2] Department of Immunology, Basic Medical Institute, Chengde Medical College, Chengde, China

OPEN ACCESS

Edited by:
Rui Liao,
First Affiliated Hospital of Chongqing Medical University, China

Reviewed by:
Louise Catherine Connell,
Cornell University, United States
An-hua Wu,
China Medical University, China

***Correspondence:**
Yaxian Gao
yaxiangao@163.com

Specialty section:
This article was submitted to Gastrointestinal Cancers, a section of the journal Frontiers in Oncology

Received: 18 September 2020
Accepted: 17 December 2020
Published: 10 February 2021

Citation:
Wang Y, Guo S, Chen Z, Bai B, Wang S and Gao Y (2021) Re-Clustering and Profiling of Digestive System Tumors According to Microenvironment Components. Front. Oncol. 10:607742. doi: 10.3389/fonc.2020.607742

Background: Immunotherapy has become the most promising therapy in digestive system tumors besides conventional chemotherapy and radiotherapy. But only a few patients can benefit from different types of immunotherapies, such as immune checkpoint blockade (ICB). To identify these ICB-susceptible patients, methods are urgently needed to screen and profile subgroups of patients with different responsiveness to ICB.

Methods: This study carried out analysis on patients with digestive system tumors that were obtained from Cancer Genome Atlas (TCGA) cohorts. The analyses were mainly performed using GraphPad Prism 7 and R language.

Results: We have quantified the microenvironmental components of eight digestive system tumor patients in TCGA cohorts and evaluated their clinical value. We re-clustered patients based on their microenvironment composition and divided these patients into six clusters. The differences between these six clusters were profiled, including survival conditions, enriched biological processes, genomic mutations, and microenvironment traits. Cluster 3 was the most immune-related cluster, exhibiting a high infiltration of non-tumor components and poor survival status, along with an inhibitory immune status, and we found that patients with high stromal score indicated a poor response in ICB cohort.

Conclusions: Our research provides a new strategy based on the microenvironment components for the reclassification of digestive system tumors, which could provide guidance for prognosis judgment and treatment response prediction like ICB.

Keywords: The Cancer Genome Atlas (TCGA), digestive system tumors, immune, stromal, microenvironment

INTRODUCTION

Digestive system tumors are the most common tumor type and are associated with rapid malignant progression (1). Even after patients receive standard radiotherapy and chemotherapy treatment, the prognosis remains poor (2, 3). This unsatisfactory prognosis is in part due to the hidden nature of digestive system tumors, making them difficult to detect early. These tumors are often found at advanced and malignant stages, where symptoms are obvious. But the metastatic and recurrent traits of digestive system tumors make them difficult for conventional treatment programs to handle (4–8).

In recent years, more and more research has focused on the importance of the tumor microenvironment in driving malignancy, including in digestive system tumors (9–12). Most of the previous studies have only focused on tumor cells themselves and their internal mechanisms, but mutual communication and regulation exist between tumor cells and other components of their microenvironment (13–15). Through paracrine mechanisms, tumor cells could reprogram their surrounding immune and stromal microenvironments into a "pro-tumor" microenvironment. The reprogrammed microenvironment could facilitate the malignant phenotype of tumor cells, such as proliferation, invasion, migration, and pro-vasculogenic effects (16). Meanwhile, increasing evidence suggested that the disorganized microenvironment may contribute to tumor cells' abilities to escape the effects of conventional treatments, such as chemotherapy, radiotherapy, and anti-vasculogenic therapy, as well as some classical molecular targeting therapies (17–19).

In recent years, studies have begun to focus on immunotherapy, which is considered as a promising and upcoming therapy that has been extensively used in basic and preclinical research. Among the different forms of immunotherapy, immune checkpoint blockade (ICB) has achieved significant effects in inhibiting the malignant progression of tumors, including digestive system tumors. But, results from clinical trials show that only a selection of tumor patients respond well to ICB (20). The difference and complexity of microenvironmental components may partially explain the heterogeneity of the ICB response among tumor patients (18). It is urgent to re-cluster digestive system tumors according to individual trait of microenvironment composition, and profile relevant clinical transformation significance in corresponding cluster.

In this study, we quantified ten major non-tumor cells and evaluated the clinical value of corresponding cell components in individual cancers, where we found that some cell components are often accompanied with poor prognosis, such as neutrophils, fibroblasts, and endothelial cells. Subsequently, we re-clustered patients with digestive system tumors based on microenvironmental components and conducted in-depth analysis including clinical prognostic difference, genomic's level, enriched biological processes and microenvironmental component characteristics. In addition, we found that the stromal score robustly enhanced in cluster 3 subgroup, which was consistently correlated with multiple negative immune cell components. We proposed that the inhibitory immune status may be characterized by high stromal scores. In the IMvigor210 database, the response rate of ICB immunotherapy for patients with high stromal scores was significantly limited, which confirmed the relationship between stromal components and the inhibitory immune microenvironment.

Abbreviations: ICB, Immune checkpoint blockade; TCGA, The Cancer Genome Atlas; SCNA, Somatic copy number variation; GSVA, Gene set variation analysis; ROC, Receiver operating characteristic; STAD, Stomach adenocarcinoma; LIHC, Liver hepatocellular carcinoma; PAAD, Pancreatic adenocarcinoma; READ, Rectum adenocarcinoma; COAD, Colon adenocarcinoma; ESCA, Esophageal adenocarcinoma; SNP, Single Nucleotide Polymorphisms.

MATERIALS AND METHODS

Data Acquisition

The normalized RNA sequencing and clinical information of 1,526 patients were downloaded from the UCSC website (https://genome.ucsc.edu/). For genomic level analyses, we downloaded these six types of tumors' mutation data (MAF file) from https://portal.gdc.cancer.gov/ and Firehose (http://gdac.broadinstitute.org/). Two immunotherapy cohorts were the IMvigor210 cohort and GSE78220 respectively; the former was downloaded from http://research-pub.Gene.com/IMvigor210CoreBiologies, and the latter was obtained from https://www.ncbi.nlm.nih.gov/geo/query/acc.cgi?acc=GSE78220 (21, 22).

The Quantification of Microenvironment Components and K-Means Clustering Analysis

The ESTIMATE R package was used to calculate stromal and immune scores, and tumor purity was calculated according to the formula from Yoshihara and colleagues (23). The relative immune cell proportions were calculated based on the CIBERSORT algorithm (24). MCP counter was conducted to calculate the enrichment of several critical immune and stromal cell components (25). The cluster analyses based on the MCP counter results were performed by consensus unsupervised analysis according to the ClusterProfiler R package, which was used to identify the most proper category from the scale of microenvironment components (26).

Differential Enriched Biological Process and Driver Mutations

Limma R package was used to calculate the differentially expressed genes among different groups. We quantified tumor related biological process by using Gene set variation analysis (GSVA), which was further conducted to explore differential signaling pathways among different groups (27). Maftools R package and Pheatmap package were performed to illustrate significant differential driver mutations between different groups.

Statistical Analysis

R 3.6.1 (https://www.r-project.org/) and GraphPad Prism 7 were used for statistical analysis. Kaplan–Meier survival analysis was

used to evaluate the prognostic value. The receiver operating characteristic (ROC) curve was made using GraphPad Prism 7 software. A Student's t-test was performed to analyze differential expressed expression. Chi-square test is used to evaluate the difference in treatment response between two groups. Survival curves were exported by GraphPad Prism 7. Two-tail p-value <0.05 was termed as significant.

RESULTS

Overall Profiling of the Digestive System Tumor Microenvironment Components and Their Clinical Value

We first calculated the microenvironmental components of each digestive system of tumor patient through the MCP counter package and performed a visual exhibition (**Figure 1A**); we found that the content of fibroblasts is the most enriched, and the content of NK cells is less enriched. Similarly, by drawing a heatmap, we can clearly see that in the microenvironment of digestive system tumors, stromal components like fibroblast and endothelial cells were more enriched in environment, where monocytes are the main immune component (**Figure 1B**). Next, we calculated the impact of each microenvironment component on the survival prognosis of tumor patients through univariate Cox regression analysis in each type of tumor. There were several survival-related microenvironment component of stomach adenocarcinoma (STAD) (**Figure 1C**). We used the log-rank test method to draw survival curves of the microenvironment components, aiming to identify survival-related components in different tumors. We found that the survival-related microenvironment components in liver hepatocellular carcinoma (LIHC), pancreatic adenocarcinoma (PAAD), and rectum adenocarcinoma (READ) are not well predicted under the log-rank test (**Figures 1D–F**). While in STAD, Cox results suggested that neutrophils, fibroblasts, and endothelial cells are associated with poor prognosis, which were also significantly related to the prognosis under the log-rank test (**Figures 1G–I**).

Re-Clustering Patients With Digestive System Tumors Based on Microenvironmental Components

We performed K means unsupervised clustering of patients with digestive system tumors based on the characteristics of the microenvironmental components calculated by MCP (**Figures 2A, B**), and the results showed that the six types of discrimination were the best. We analyzed the proportions of the six categories in each type of digestive system tumor. The results showed that the COAD and READ had a relative average distribution among these six clusters, while cluster 4 in ESCA was relatively enriched and cluster 6 in LIHC was the main component. Cluster 1 was dominant in PAAD, and cluster 3 had the highest proportion in STAD (**Figure 2C**). We further performed a Sankey diagram to depict the correspondence between cancer species and clusters (**Figure 2D**). Moreover, we described the main non-tumor cell components in different clusters and found that cluster 3 contains the highest content of immune and stromal cells, while cluster 6 has relatively low numbers of immune and stromal cells (**Figure 2E**). Survival analysis suggests that cluster 1 and cluster 3 have a relatively poor prognosis, where both have a high proportion of microenvironmental components, while cluster 6 has a relatively good prognosis, displaying a low proportion of non-tumor cells (**Figures 2F–H**).

Profiling of Cluster-Related Mutations at the Genome Level

In order to compare the differences between different clusters at the genome level, we obtained the Single Nucleotide Polymorphisms (SNP) mutation data of these six digestive system tumors. Since the cluster 3 subgroup is accompanied by a high level of non-tumor microenvironment components and tends to be distributed in STAD, we have analyzed the classic tumor driver gene mutations in the cluster 3 and non-cluster 3 subgroups of STAD to exclude the influence of the tumor type. The results showed that the cluster 3 subgroup of STAD patients was accompanied by a low TP53 mutation rate and a high LRP1B mutation rate, suggesting a potential upstream mechanism for the poor prognosis and increased infiltration of non-tumor components of cluster 3 (**Figures 3A, B**). Similarly, due to the relatively large proportion of cluster 6 in LIHC, we analyzed the classic driver gene mutations of cluster 6 and non-cluster 6 subgroups of LIHC patients. We found that the cluster 6 subgroups of LIHC patients were accompanied by higher CTNNB1 and TTN mutations (**Figures 3C, D**). As PAAD occupied a large proportion of cluster 1, we compared the genomic differences between the cluster 1 subgroup and the non-cluster 1 subgroup, we found that the C1 subgroup of PAAD was accompanied by a higher mutation rate of KRAS and SMAD4, suggesting a potential mechanism for the poor prognosis of cluster 1 patients (**Figures 3E, F**).

Differential Function Enrichment Analysis Among Clusters

In order to explore the underlying mechanism of differences in clinical and survival characteristics of patients in different clusters, we selected more than 70 classical tumor-related pathways or critical biological processes and calculated the corresponding ssGSEA score for each tumor patient. Then, we displayed the results using a heatmap and found that some pathways that regulate the malignant behavior of tumor cells and immune-related pathways are significantly enriched in cluster 3, which is characterized by a high infiltration of non-tumor cells (**Figure 4A**). Subsequently, we conducted a series of comparisons of cancer hallmarks. In terms of several classical metabolic pathways like glucose and lipid metabolism, *etc*. The enrichment of cluster 6 was significantly higher than that of other clusters. This may be because cluster 6 is mainly composed

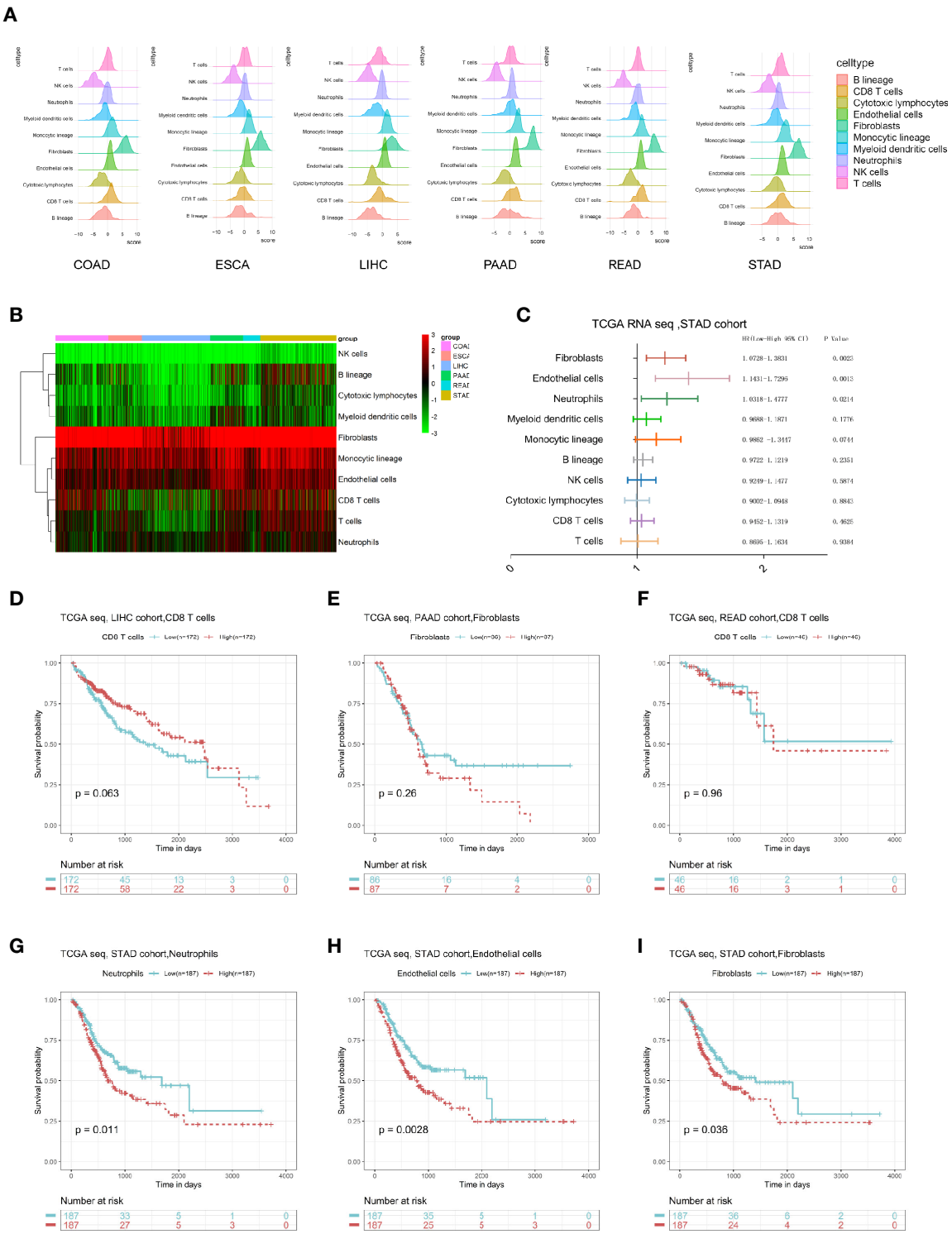

FIGURE 1 | Overall description of the digestive system tumor microenvironment components and clinical value. **(A)** The landscape of microenvironmental components in digestive system cancers. **(B)** A heatmap of the MCP-counter results in these six cancers. **(C)** Univariate Cox results of each cell component in the STAD cohort. **(D–I)** The log-rank survival curve of some type of cells in specific cancer with prognostic value.

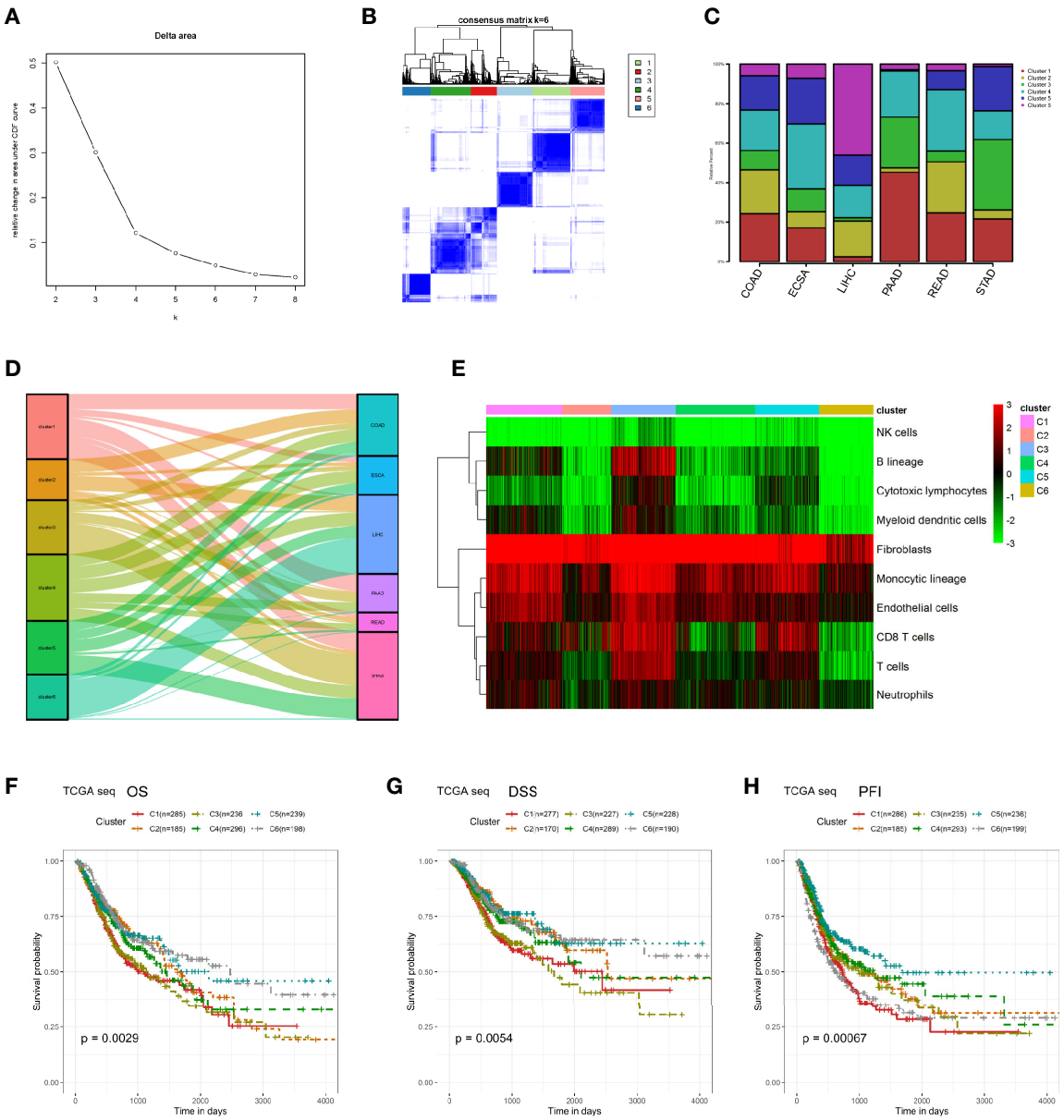

FIGURE 2 | Re-clustering digestive system tumor patients based on microenvironmental components. **(A, B)** K means unsupervised clustering of patients with digestive system tumors based on the characteristics of their microenvironmental components. **(C)** The proportions of the six kinds of clusters in each type of digestive system tumor. **(D)** Sankey diagram was performed to depict the correspondence between cancer species and clusters. **(E)** The heatmap of the microenvironmental components in these six clusters. **(F–H)** Survival analyses between these six clusters in OS, DSS, and PFI.

of tumor cells (**Figures 4B–F**). The level of DNA replication and mismatch repair of cluster 2 was significantly higher than that of the other clusters (**Figures 4G, H**). Cluster 3 focused on the interaction of cytokines and receptors, chemokines, TGFβ pathway, VEGF pathway, and focal adhesion pathway, which further suggested that microenvironmental factors may lead to the unique clinical characteristics of cluster 3 patients (**Figures 4I–M**).

Cluster 3 Is Closely Related to the Characteristics of an Immunosuppressive Microenvironment

In order to further evaluate the microenvironment characteristics of patients in cluster 3, we performed X-cell analysis and displayed the results of each cluster subgroup using a heatmap. The results showed that the immune cell and stromal cell components in cluster 3 were robustly enriched,

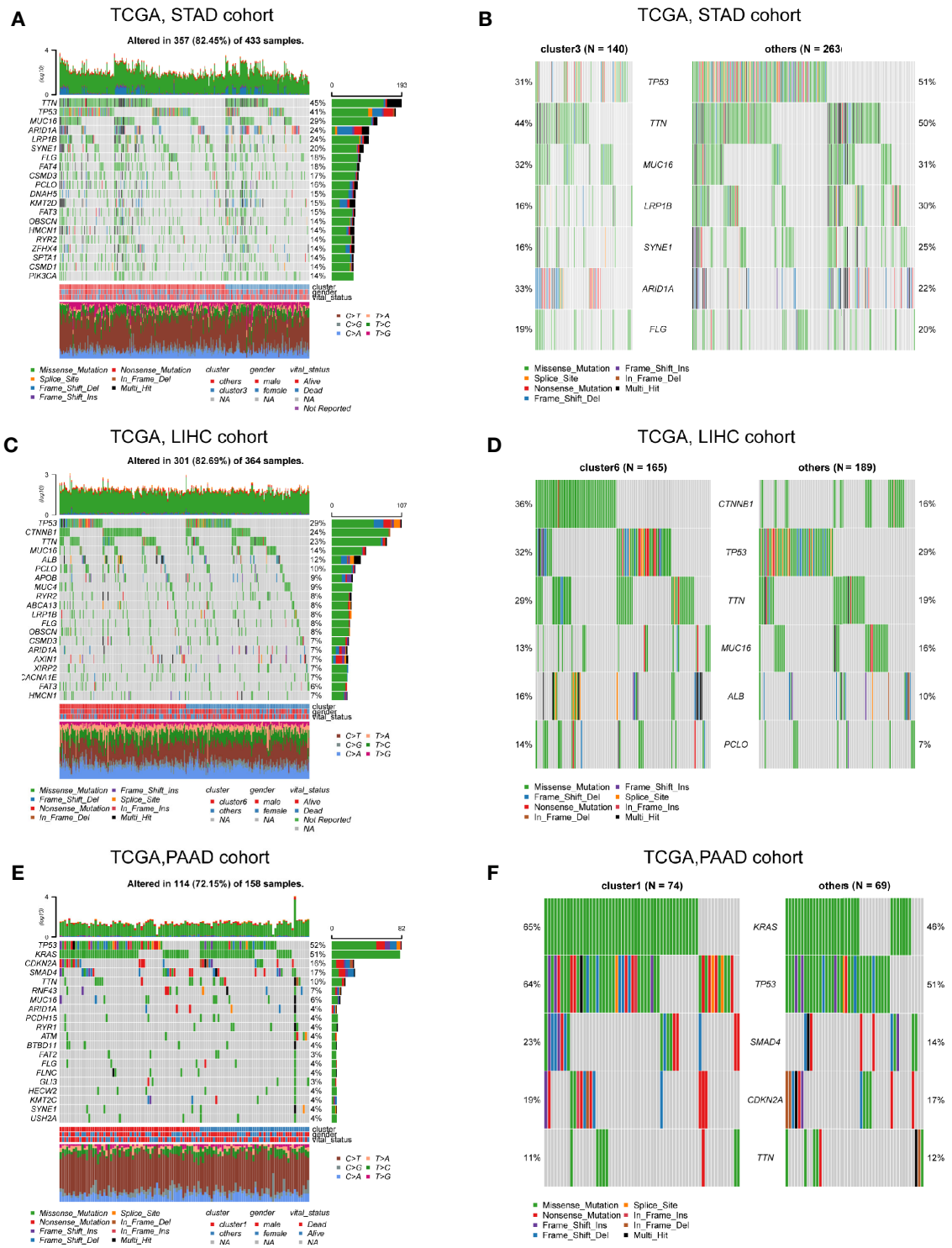

FIGURE 3 | Profiling of cluster-related mutations at the genome level. **(A)** The landscape of classical driver gene mutations in the C3 and non-C3 clusters of the STAD cohort. **(B)** The most different driver mutations between C3 and non-C3 clusters of STAD cohort. **(C)** The landscape of classical driver gene mutations in the C6 and non-C6 clusters of the LIHC cohort. **(D)** The most different driver mutations between C6 and non-C6 clusters of the LIHC cohort. **(E)** The landscape of classical driver gene mutations in the C1 and non-C1 clusters of the PAAD cohort. **(F)** The most different driver mutations between C1 and non-C1 clusters of the PAAD cohort.

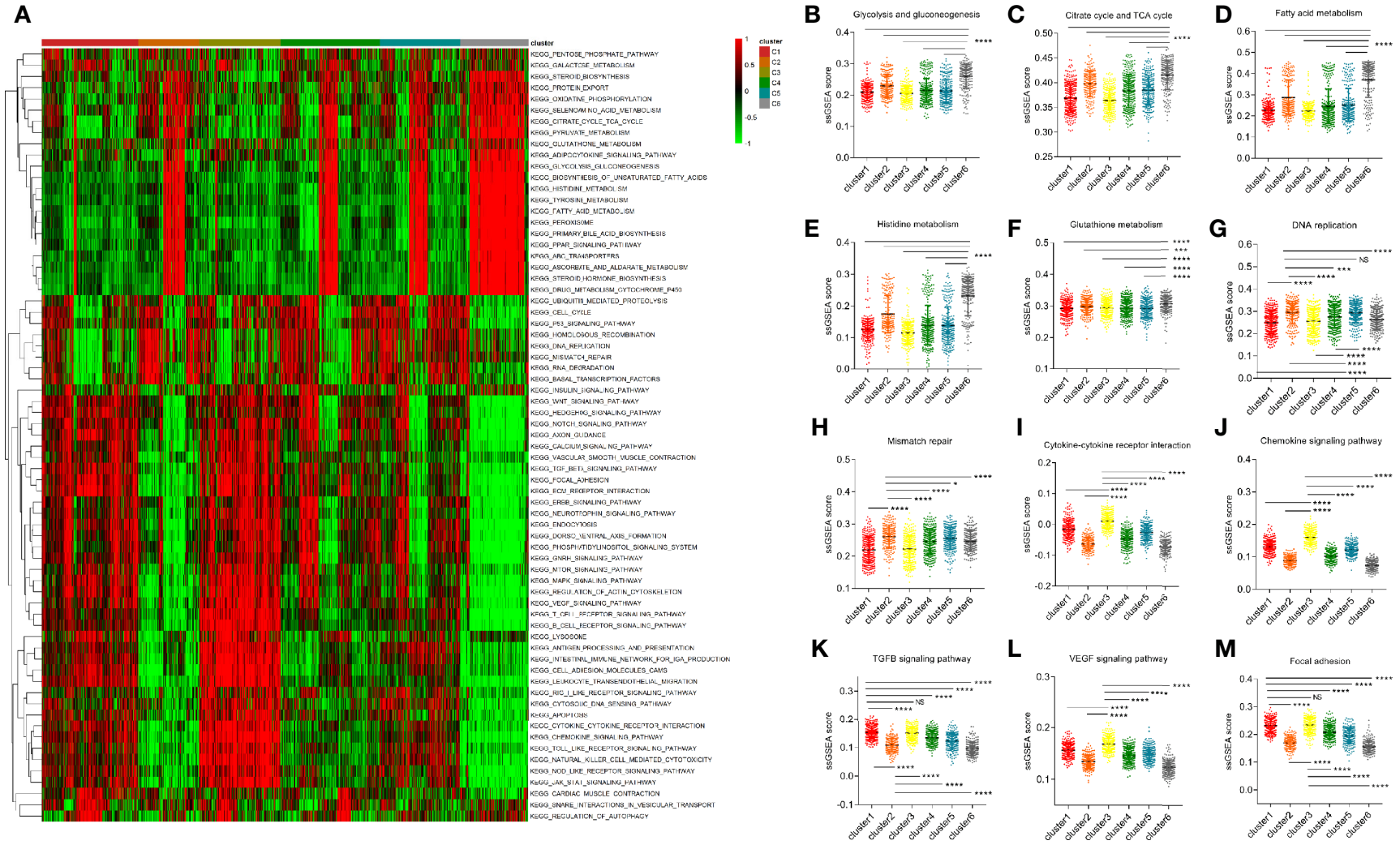

FIGURE 4 | Differential function enrichment analysis among clusters. **(A)** More than 70 classical tumor-related pathways were quantified by ssGSEA method and exhibited in a heatmap. **(B–F)** Several metabolic pathways enhanced in cluster 6. **(G, H)** The level of DNA replication and mismatch repair of cluster 2 is significantly higher than that of other subgroups. **(I–M)** Cluster 3 was enriched with immune microenvironmental related terms such as the interaction of cytokines and receptors, chemokines, TGFB pathway, VEGF pathway, and focal adhesion pathway. (NS means no significance, * means $P < 0.05$, *** means $P < 0.001$, **** means $P < 0.0001$).

including both activated and suppressed immune cell components (**Figure 5A**). Moreover, the microenvironmental, immune and stromal scores in cluster 3 were significantly higher than other clusters (**Figures 5B–D**). As for the classical inhibitory immune checkpoints, we found that PD1, PDL1, and CTLA4 molecules in cluster 3 and cluster 5 were significantly increased compared to other clusters (**Figures 5E–G**).

Stromal Score Could Be Used to Predict the Response of Anti-PD1/PDL1 Treatment

Based on the robustly enhanced microenvironmental components and suppressive immune status of cluster 3, we proposed that tumor patients with cluster 3 traits may be insensitive to immunotherapy. We represented the characteristics of cluster 3 by microenvironment, immune and

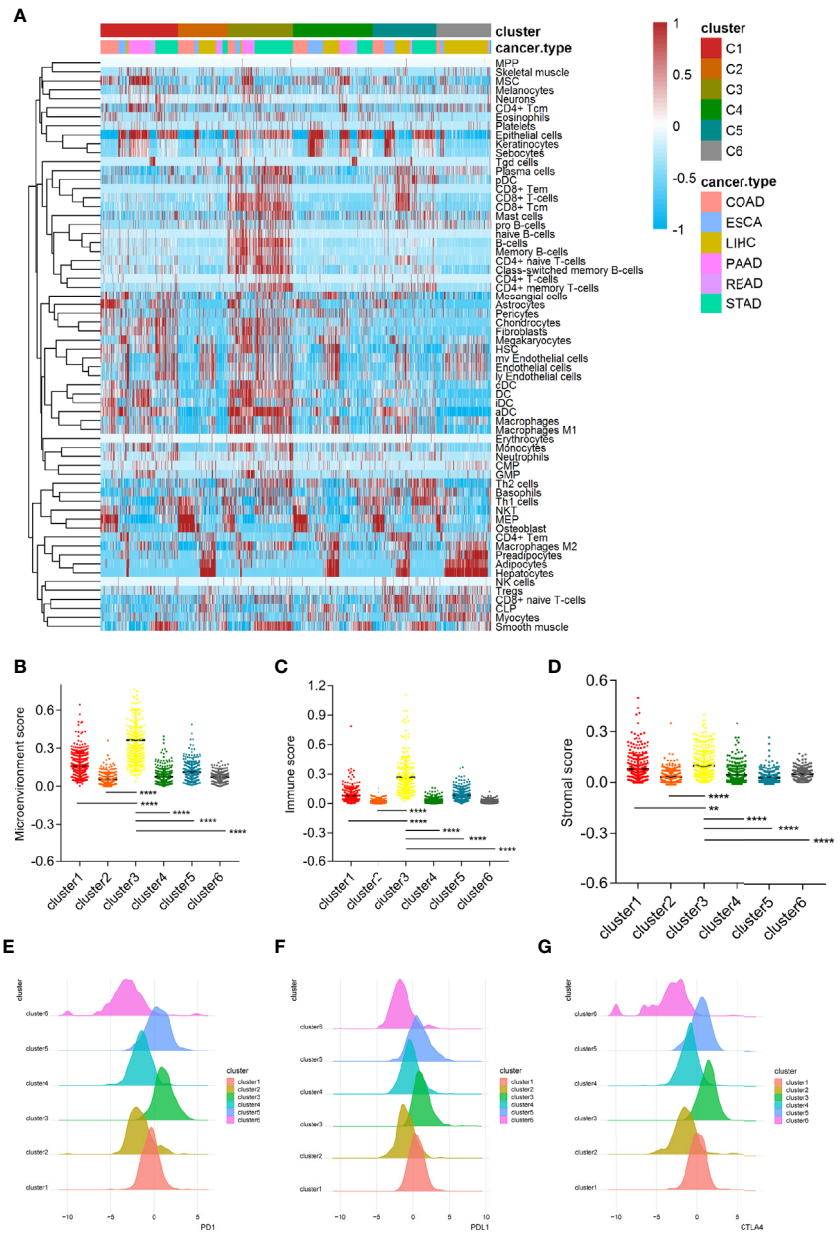

FIGURE 5 | Cluster 3 is closely related to the characteristics of the immunosuppressive microenvironment. **(A)** The microenvironmental components of the six clusters conducted by X cell method. **(B–D)** The microenvironment score, immune score and stromal score in cluster 3 are significantly higher than other subgroups. **(E–G)** Classical immune checkpoints such as PD1, PDL1, and CTLA4 in cluster 3 and cluster 5 subgroups were significantly increased. (** means $P < 0.01$, **** means $P < 0.0001$).

stromal scores, and then evaluated the effective response rate of different groups in the ICB immunotherapy cohorts. In the Imvigor210 anti-PDL1 immunotherapy cohort, we found that there is no significant difference in the immunotherapy response rate between the high and low score groups when the microenvironment score and immune score were used as the stratified criteria (**Figures 6A, B**). When the stromal score was used as the distinction criteria, we found that the immunotherapy response rate in the high score group was significantly lower than that in the low scoring group (**Figure 6C**). Moreover, the ROC curve showed that the stromal score had a predictive effect on the positive response rate (**Figure 6D**).

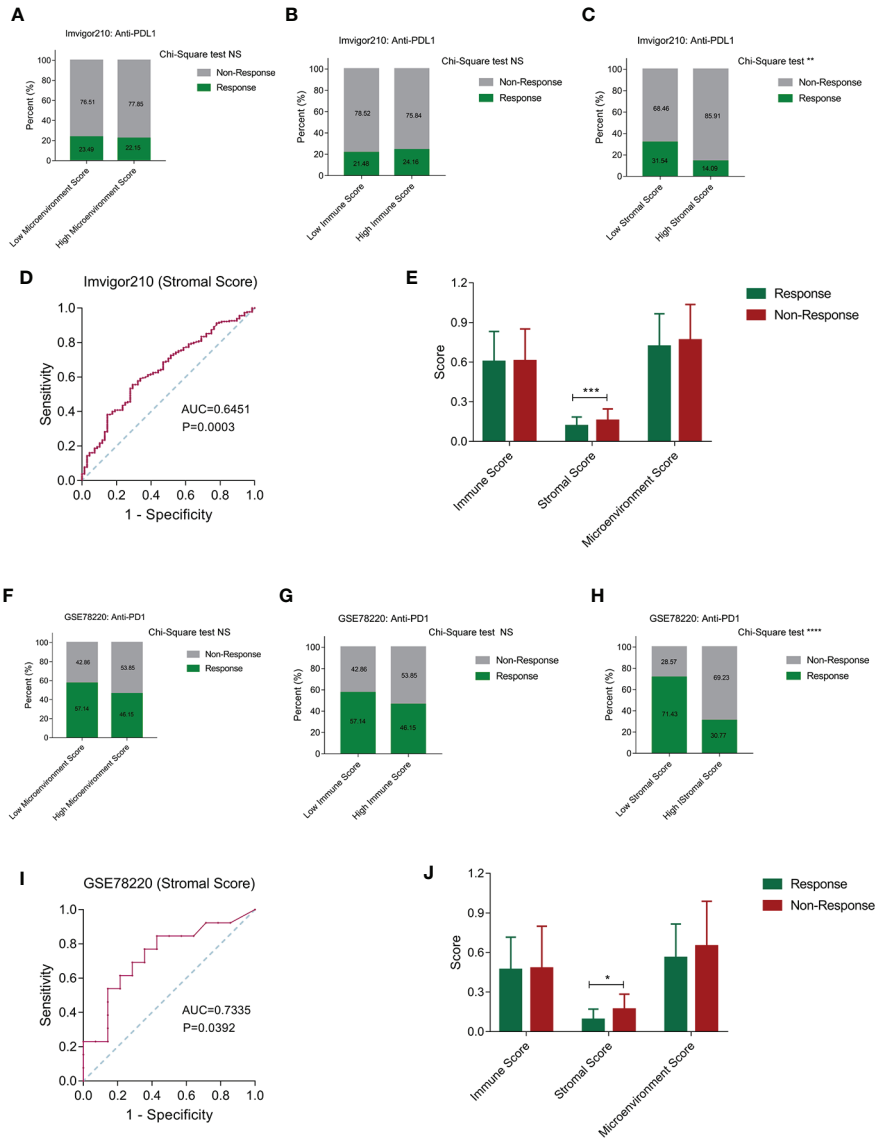

FIGURE 6 | Stromal score can be used to predict the effect of anti-PD1/PDL1 treatment. **(A, B)** Patients were stratified by the microenvironment score and immune score, while there is no significant difference in the immunotherapy response rate between the high and low score groups. **(C)** The immunotherapy response rate in the high stromal score group was significantly lower than that in the low stromal score group. **(D)** The ROC curve showed that the stromal score had a well predictive effect on the positive response rate. **(E)** The stromal score in the positive response group was significantly lower than non-response group. **(F–H)** Among microenvironmental score, immune score and stromal score, only stromal score has the value in distinguishing patients with positive treatment response in GSE78220 cohort. **(I)** The ROC curve showed that the stromal score had a well predictive effect on the positive response rate in GSE78220 cohort. **(J)** The stromal score in the positive response group was significantly lower than non-response group in GSE78220 cohort. (NS means Chi-Square test no significance, * means $P < 0.05$, ** means $P < 0.01$, *** means $P < 0.001$, **** means $P < 0.0001$).

In addition, the stromal score in the response group was also significantly lower than in the no response group (**Figure 6E**). Similarly, we observed a similar conclusion in the GSE78220 anti-PD1 immunotherapy cohort, where the stromal score is more effective in distinguishing patients with positive treatment response than the microenvironment and immune scores (**Figures 6F–H**). In addition, the stromal score has a good predictive effect on the positive response to ICB treatment. The stromal score of the response group was significantly lower than that of unresponsive group (**Figures 6I, J**).

DISCUSSION

Increasing studies have shown that the microenvironmental components of malignant tumors are important factors affecting the poor prognosis and low response to treatment (28, 29). The non-tumor cell components and tumor cell components in the microenvironment can mutually regulate and transform each other to accelerate the malignant progress of tumors (16). There were a few studies that tried to enhance the immunotherapy efficiency by remodeling the microenvironment (30–32). Analyzing the microenvironment composition mode of different tumor patients can provide a certain guidance value for the selection of the next treatment strategy such as immunotherapy. Thus it is urgent to identify the subgroups of patients with different responsiveness to ICB treatment from the scale of microenvironment factors. This study first quantified eight key microenvironment components of patients with digestive system tumors and found that the two main stromal components of fibroblasts and vascular endothelial cells were prefer enriched, and the most enriched immune components were monocytes. We further evaluated the clinical value of these key microenvironmental components and found that fibroblasts, vascular endothelial cells, and neutrophils are closely related to poor prognosis.

While classification of digestive system tumors is mainly based on clinical parameters, such as tissue source, TNM stage, and grade, this study clustered patients based on characteristics of their microenvironment composition. We believe that tumors that share similar microenvironment compositions may have similar clinical characteristics. Based on the characteristics of the microenvironmental components calculated by MCP-Counter, we performed K means unsupervised clustering on patients with digestive system tumors and divided these patients into six clusters. We quantified the main non-tumor cell components in different clusters and found that cluster 3 has the highest content of immune and stromal cells, and cluster 6 has a relatively low content of immune and stromal cells. Survival analysis suggested that the prognosis of cluster 1 and cluster 3 was relatively poor, which have a high proportion of microenvironmental components, while cluster 6 has a lower proportion of non-tumor cells but exhibits a relatively good prognosis.

In addition, in order to explore the underlying mechanism of the differences between patients in different clusters, we quantified classical tumor driven biological processes. We found that in cluster 3, some pathways that regulate the malignant behavior of tumor cells and immune-related pathways were significantly enriched. In addition, cluster 3 was significantly enriched in microenvironment-related functions, such as cytokine–receptor interactions, chemokines, TGFB pathway, VEGF pathway, and focal adhesion pathway; those were all involved with microenvironment remodeling and could be termed as targeted signaling in the immunotherapy (33–37), which further suggested that microenvironmental factors may contribute to the unique clinical features of cluster 3. Based on the significantly enriched microenvironmental components and suppressive immune status of cluster 3, we speculate that tumor patients with cluster 3 characteristics may be insensitive to immunotherapy. We replaced the characteristics of cluster 3 with microenvironmental score, immune score and stromal score respectively, and then tested the treatment response rate of different groups in the ICB immunotherapy cohorts. First of all, in the Imvigor210 anti-PDL1 immunotherapy cohort, we found that when the stromal score was used as the distinguishing standard, the immunotherapy response rate in the high score group was significantly lower than that in the low score group (22). The ROC curve showed that the stromal score had a good predictive effect on the positive response rate. The stromal score in the positive response group was also significantly lower than that in the non-response group. We also reached a similar conclusion in the GSE78220 anti-PD1 immunotherapy cohort (21), where stromal score was more effective in distinguishing patients with positive response to ICB treatment.

In summary, the composition of the microenvironmental components of various tumors in the digestive system is heterogeneous. There is a subgroup of patients characterized with high stromal and immune components that are accompanied with a poor prognosis and insensitivity to ICB therapy. Our research provides a new approach for precise diagnosis and treatment of digestive system tumor patients.

DATA AVAILABILITY STATEMENT

Publicly available datasets were analyzed in this study. These data can be found here: http://genome.ucsc.edu/, https://portal.gdc.cancer.gov/, http://gdac.broadinstitute.org/, http://research-pub.Gene.com/IMvigor210CoreBiologies, https://www.ncbi.nlm.nih.gov/geo/query/acc.cgi?acc=GSE78220.

AUTHOR CONTRIBUTIONS

WY and GY conceptualized and designed the study. BB and WS downloaded the data and contributed to the data curation. CZ developed the methodology. WY and GS analyzed and interpreted the data. WY and GY wrote and revised the manuscript. All authors contributed to the article and approved the submitted version.

FUNDING

This work was supported by the Science and Technology Research Project for Colleges and Universities in Hebei Province (grant number: QN2016060, QN2015044), Launch Fund for High-Level Talents Scientific Research of Chengde Medical College (grant number: 202002), and Medical Scientific Research Project for Hebei Provincial Health and Family Planning Commission (grant number: 20160313, 20160310).

REFERENCES

1. Bray F, Ferlay J, Soerjomataram I, Siegel R, Torre L, Jemal A. Global cancer statistics 2018: GLOBOCAN estimates of incidence and mortality worldwide for 36 cancers in 185 countries. *CA Cancer J Clin* (2018) 68:394–424. doi: 10.3322/caac.21492
2. Kawaguchi Y, Vauthey J. The Landmark Series: Randomized Control Trials Examining Perioperative Chemotherapy and Postoperative Adjuvant Chemotherapy for Resectable Colorectal Liver Metastasis. *Ann Surg Oncol* (2020) 27(11):4263–70. doi: 10.1245/s10434-020-08777-z
3. St James S, Bednarz B, Benedict S, Buchsbaum J, Dewaraja Y, Frey E, et al. Current Status of Radiopharmaceutical Therapy. *Int J Radiat Oncol Biol Phys* (2020) S0360-3016(20)34125-0. doi: 10.1016/j.ijrobp.2020.08.035
4. Dai W, Wang Y, Yang T, Wang J, Wu W, Gu J. Downregulation of exosomal CLEC3B in hepatocellular carcinoma promotes metastasis and angiogenesis via AMPK and VEGF signals. *Cell Commun Signal* (2019) 17:113. doi: 10.1186/s12964-019-0423-6
5. Ye K, Ouyang X, Wang Z, Yao L, Zhang G. SEMA3F Promotes Liver Hepatocellular Carcinoma Metastasis by Activating Focal Adhesion Pathway. *DNA Cell Biol* (2020) 39:474–83. doi: 10.1089/dna.2019.4904
6. Gu L, Liu Y, Jiang C, Sun L, Zhou H. Identification and clinical validation of metastasis-associated biomarkers based on large-scale samples in colon-adenocarcinoma. *Pharmacol Res* (2020) 160:105087. doi: 10.1016/j.phrs.2020.105087
7. Liu J, Zhu Y, Ge C. LncRNA ZFAS1 promotes pancreatic adenocarcinoma metastasis via the RHOA/ROCK2 pathway by sponging miR-3924. *Cancer Cell Int* (2020) 20:249. doi: 10.1186/s12935-020-01322-8
8. Zang D, Zhang C, Li C, Fan Y, Li Z, Hou K, et al. LPPR4 promotes peritoneal metastasis via Sp1/integrin α/FAK signaling in gastric cancer. *Am J Cancer Res* (2020) 10:1026–44.
9. Cao D, Chen M, Zhang Q, Zhou Y, Zhang M, Mai S, et al. Identification of immunological subtypes of hepatocellular carcinoma with expression profiling of immune-modulating genes. *Aging* (2020) 12:12187–205. doi: 10.18632/aging.103395
10. Liu H, Ni S, Wang H, Zhang Q, Weng W. Charactering tumor microenvironment reveals stromal-related transcription factors promote tumor carcinogenesis in gastric cancer. *Cancer Med* (2020) 9:5247–57. doi: 10.1002/cam4.3133
11. Yang S, Liu T, Cheng Y, Bai Y, Liang G. Immune cell infiltration as a biomarker for the diagnosis and prognosis of digestive system cancer. *Cancer Sci* (2019) 110:3639–49. doi: 10.1111/cas.14216
12. Zhu X, Xie X, Zhao Q, Zhang L, Li C, Zhao D. Potential Prognostic Value and Mechanism of Stromal-Immune Signature in Tumor Microenvironment for Stomach Adenocarcinoma. *BioMed Res Int* (2020) 2020:4673153. doi: 10.1155/2020/4673153
13. Navarro R, Tapia-Galisteo A, Martín-García L, Tarín C, Corbacho C, Gómez-López G, et al. TGF-β-induced IGFBP-3 is a key paracrine factor from activated pericytes that promotes colorectal cancer cell migration and invasion. *Mol Oncol* (2020) 14(10):2609–28. doi: 10.1002/1878-0261.12779
14. Sperb N, Tsesmelis M, Wirth T. Crosstalk between Tumor and Stromal Cells in Pancreatic Ductal Adenocarcinoma. *Int J Mol Sci* (2020) 21(15):5486. doi: 10.3390/ijms21155486
15. Mroweh M, Decaens T, Marche P, Macek Jilkova Z, Clément F. Modulating the Crosstalk between the Tumor and Its Microenvironment Using RNA Interference: A Treatment Strategy for Hepatocellular Carcinoma. *Int J Mol Sci* (2020) 21(15):5250. doi: 10.3390/ijms21155250
16. Zhao W, Ajani J, Sushovan G, Ochi N, Hwang R, Hafley M, et al. Galectin-3 Mediates Tumor Cell-Stroma Interactions by Activating Pancreatic Stellate Cells to Produce Cytokines via Integrin Signaling. *Gastroenterology* (2018) 154:1524–37.e6. doi: 10.1053/j.gastro.2017.12.014
17. Aronovich A, Moyal L, Gorovitz B, Amitay-Laish I, Naveh H, Forer Y, et al. Cancer-Associated Fibroblasts in Mycosis Fungoides Promote Tumor Cell Migration and Drug Resistance via CXCL12/CXCR4. *J Invest Dermatol* (2020) S0022-202X(20)31966-7. doi: 10.1016/j.jid.2020.06.034
18. Wang S, Li Y, Xing C, Ding C, Zhang H, Chen L, et al. Tumor microenvironment in chemoresistance, metastasis and immunotherapy of pancreatic cancer. *Am J Cancer Res* (2020) 10:1937–53.
19. Orme J, Huang H. Microenvironment-Mediated Resistance to Anti-Androgen Therapy. *Cancer Cell* (2020) 38:155–7. doi: 10.1016/j.ccell.2020.07.007
20. Lei Q, Wang D, Sun K, Wang L, Zhang Y. Resistance Mechanisms of Anti-PD1/PDL1 Therapy in Solid Tumors. *Front Cell Dev Biol* (2020) 8:672. doi: 10.3389/fcell.2020.00672
21. Cloughesy TF, Mochizuki AY. Neoadjuvant anti-PD-1 immunotherapy promotes a survival benefit with intratumoral and systemic immune responses in recurrent glioblastoma. *Nat Med* (2019) 25:477–86. doi: 10.1038/s41591-018-0337-7
22. Mariathasan S, Turley SJ, Nickles D, Castiglioni A, Yuen K, Wang Y, et al. TGFβ attenuates tumour response to PD-L1 blockade by contributing to exclusion of T cells. *Nature* (2018) 554:544–8. doi: 10.1038/nature25501
23. Bindea G, Mlecnik B, Tosolini M, Kirilovsky A, Waldner M, Obenauf A, et al. Spatiotemporal dynamics of intratumoral immune cells reveal the immune landscape in human cancer. *Immunity* (2013) 39:782–95. doi: 10.1016/j.immuni.2013.10.003
24. Newman A, Liu C, Green M, Gentles A, Feng W, Xu Y, et al. Robust enumeration of cell subsets from tissue expression profiles. *Nat Methods* (2015) 12:453–7. doi: 10.1038/nmeth.3337
25. Becht E, Giraldo N, Lacroix L, Buttard B, Elarouci N, Petitprez F, et al. Estimating the population abundance of tissue-infiltrating immune and stromal cell populations using gene expression. *Genome Biol* (2016) 17:218. doi: 10.1186/s13059-016-1070-5
26. Yu G, Wang L, Han Y, He Q. clusterProfiler: an R package for comparing biological themes among gene clusters. *Omics J Integr Biol* (2012) 16:284–7. doi: 10.1089/omi.2011.0118
27. Hänzelmann S, Castelo R, Guinney J. GSVA: gene set variation analysis for microarray and RNA-seq data. *BMC Bioinformatics* (2013) 14:7. doi: 10.1186/1471-2105-14-7
28. Lazăr DC, Avram MF, Romoăan I, Cornianu M, Tăban S, Goldiă A. Prognostic significance of tumor immune microenvironment and immunotherapy: Novel insights and future perspectives in gastric cancer. *World J Gastroenterol* (2018) 24:3583–616. doi: 10.3748/wjg.v24.i32.3583
29. Öjlert Å K, Halvorsen AR, Nebdal D, Lund-Iversen M, Solberg S, Brustugun OT, et al. The immune microenvironment in non-small cell lung cancer is predictive of prognosis after surgery. *Mol Oncol* (2019) 13:1166–79. doi: 10.1002/1878-0261.12475
30. Musetti S, Huang L. Nanoparticle-Mediated Remodeling of the Tumor Microenvironment to Enhance Immunotherapy. *ACS Nano* (2018) 12:11740–55. doi: 10.1021/acsnano.8b05893
31. Newton JM, Hanoteau A, Liu HC, Gaspero A, Parikh F, Gartrell-Corrado RD, et al. Immune microenvironment modulation unmasks therapeutic benefit of radiotherapy and checkpoint inhibition. *J Immunother Cancer* (2019) 7:216. doi: 10.1186/s40425-019-0698-6
32. Pitt JM, Marabelle A, Eggermont A, Soria JC, Kroemer G, Zitvogel L. Targeting the tumor microenvironment: removing obstruction to anticancer immune responses and immunotherapy. *Ann Oncol* (2016) 27:1482–92. doi: 10.1093/annonc/mdw168
33. Berraondo P, Sanmamed MF, Ochoa MC, Etxeberria I, Aznar MA, Pérez-Gracia JL, et al. Cytokines in clinical cancer immunotherapy. *Br J Cancer* (2019) 120:6–15. doi: 10.1038/s41416-018-0328-y

34. Jiang H, Hegde S. Targeting focal adhesion kinase renders pancreatic cancers responsive to checkpoint immunotherapy. *Nat Med* (2016) 22:851–60. doi: 10.1038/nm.4123
35. Murphy JM, Rodriguez YAR, Jeong K, Ahn EE. Targeting focal adhesion kinase in cancer cells and the tumor microenvironment. *Exp Mol Med* (2020) 52:877–86. doi: 10.1038/s12276-020-0447-4
36. Nagarsheth N, Wicha MS, Zou W. Chemokines in the cancer microenvironment and their relevance in cancer immunotherapy. *Nat Rev Immunol* (2017) 17:559–72. doi: 10.1038/nri.2017.49
37. Palazon A, Tyrakis PA, Macias D, Veliça P, Rundqvist H, Fitzpatrick S, et al. An HIF-1α/VEGF-A Axis in Cytotoxic T Cells Regulates Tumor Progression. *Cancer Cell* (2017) 32:669–83.e5. doi: 10.1016/j.ccell.2017.10.003

Conflict of Interest: The authors declare that the research was conducted in the absence of any commercial or financial relationships that could be construed as a potential conflict of interest.

frontiers in Oncology

ORIGINAL RESEARCH
published: 19 February 2021
doi: 10.3389/fonc.2020.605801

Vacuolar Membrane ATPase Activity 21 Predicts a Favorable Outcome and Acts as a Suppressor in Colorectal Cancer

Fan Zhang[1†], *Hao Shen*[2,3†], *Yating Fu*[1†], *Guanyu Yu*[4], *Fuao Cao*[4], *Wenjun Chang*[1*] *and Zhongdong Xie*[3,5*]

[1] Department of Environmental and Occupational Health, Second Military Medical University, Shanghai, China, [2] School of Medicine, Yunnan University, Kunming, China, [3] Department of Gastrointestinal Surgery, First Affiliated Hospital of Wenzhou Medical University, Zhejiang, China, [4] Department of Colorectal Surgery, Changhai Hospital, Second Military Medical University, Shanghai, China, [5] Department of Colorectal Surgery, Union Hospital, Fujian Medical University, Fuzhou, China

Extracellular and/or intracellular manipulation of pH in tumor may have noticeable potential in cancer treatment. Although the assembly factor genes of V_0 domain of the V-ATPase complex are required for intracellular pH homeostasis, their significance in colorectal cancer (CRC) remains largely unknown. Here, we used bioinformatics to identify the candidates from known assembly factor genes of the V_0 domain, which were further evaluated by immunohistochemistry (IHC) in CRC and adjacent normal specimens from 661 patients. Univariate and multivariate Cox analyses were used to evaluate factors contributing to prognosis. The effects of variations in the expression of VMA21 on tumor growth were assessed *in vitro* and *in vivo*. Of five known assembly factors, only VMA21 showed differential expression between CRC and adjacent normal tissues at both mRNA and protein levels. Patients with high VMA21 expression had higher differentiation grade and longer disease-specific survival (DSS) at stages I–III disease. High VMA21 expression in tumors was also an independent predictor of DSS (hazard ratio, 0.345; 95% confidence interval, 0.123–0.976), with covariates included TNM stage and differentiation grade. VMA21 overexpression decreased CRC growth, whereas VMA21 knockdown increased CRC growth *in vitro* and *in vivo*. VMA21 expression suppresses CRC growth and predicts a favorable DSS in patients with stage I-III disease.

Keywords: vacuolar membrane ATPase activity 21 (VMA21), vacuolar ATPases, prognosis, tumor suppressor, colorectal carcinoma

OPEN ACCESS

Edited by:
Yujun Shi
Sichuan University, China

Reviewed by:
Hui Guo,
First Affiliated Hospital of Xi'an Jiaotong University, China
Fei Fei,
Peking University Third Hospital, China
Diao He,
Sichuan University, China

***Correspondence:**
Wenjun Chang
cwjcwj1976@smmu.edu.cn
Zhongdong Xie
m15868503931@163.com

[†]These authors have contributed equally to this work and share first authorship

Specialty section:
This article was submitted to Gastrointestinal Cancers, a section of the journal Frontiers in Oncology

Received: *13 September 2020*
Accepted: *31 December 2020*
Published: *19 February 2021*

Citation:
Zhang F, Shen H, Fu Y, Yu G, Cao F, Chang W and Xie Z (2021) Vacuolar Membrane ATPase Activity 21 Predicts a Favorable Outcome and Acts as a Suppressor in Colorectal Cancer. Front. Oncol. 10:605801. doi: 10.3389/fonc.2020.605801

INTRODUCTION

Colorectal cancer (CRC) is one of the most common malignances worldwide, and surgical resection supplemented with chemotherapy remains the most effective treatment in patients without distant metastasis (1, 2). However, 30–50% of patients experience relapse or metachronous metastases after surgery (1, 2). Post-surgical chemotherapy and extensive surveillance are beneficial for patients who are more likely to show disease exacerbation. However, identifying patients who would benefit from these treatments is challenging because tumors are heterogenous, even among patients with the same tumor-node-metastasis (TNM) stage (1–3). The only validated marker for prognosis stratification and for selecting the appropriate chemotherapy in CRC is microsatellite instability (MSI) (3, 4), although many biomarkers have been investigated. Therefore, additional effective biomarkers are urgently required (5).

The vacuolar H+-ATPase complexes (V-ATPases) are large multisubunit protein complexes that are required to maintain the pH homeostasis of intracellular compartments (6). The complex consists of two domains, a membrane-integral V_0 domain for proton translocation and a cytosolic V1 domain for ATP hydrolysis, which are assembled separately in the endoplasmic reticulum and cytosol, respectively (7, 8). The assembly of the V_0 domain depends on a set of endoplasmic reticulum (ER)-resident chaperones, including TMEM199, VMA21, CCDC115, ATP6AP1, and ATP6AP2 (8). Loss-of-function mutations of the assembly factor genes are associated with a spectrum of disease symptoms (8–13), and the normal function of CCDC115, ATP6AP1, and ATP6AP2 is associated with favorable phenotypes in several cancer types (14, 15). However, the clinical significance and biological role of assembly factor genes in CRC is largely unknown.

To address these challenges, in the study we aimed to evaluate whether the five assembly factor genes of V_0 domain associated with the development and progression of CRC and further to investigate the biological function of the candidate. We showed that among five V_0 domain assembly factors genes, VMA21 was the only differentially expressed gene between CRC and neighboring normal tissues. Tumors with high VMA21 expression had higher differentiation grade and were associated with longer disease-specific survival (DSS) than VMA21-low tumors. Ectopic expression of VMA21 reduced the growth of CRC cells *in vitro* and *in vivo*. The present data suggest that VMA21 acts as a tumor suppressor and predicts a favorable prognosis, although VMA21 expression is elevated in CRC tissues.

MATERIALS AND METHODS

Bioinformatics Analysis

The expression of five genes (TMEM199, VMA21, CCDC115, ATP6AP1, and ATP6AP2) in CRC and corresponding normal tissue specimens was firstly analyzed on the Expression Profiling Interactive Analysis (GEPIA) website based on the dataset of The Cancer Genome Atlas (TCGA) (16). Co-expression of the genes was analyzed using the Pearson Correlation Coefficient (PCC). Candidate genes showing a 1.5-fold difference between CRC and adjacent normal tissues were further investigated in other cancer types using TCGA data and in our CRC cohort by immunochemistry (IHC).

Patients and Tissues

Formalin-fixed, paraffin-embedded (FFPE) specimens from 661 cancerous tissues, 26 adenoma, and 65 para-carcinoma tissues were obtained from 661 patients treated at Changhai Hospital, Second Military Medical University, Shanghai, between 2001 and 2011. None of the patients received chemotherapy or radiation therapy before surgery. All tissue samples were tested histologically by the pathologists to verify the diagnosis. Outdo Biotech Co., Ltd (Shanghai, China) constructed the tissue microarrays (TMAs) containing the FFPE specimens as previously described (17). The baseline information of each specimen donors, including age, tumor location, differentiation grade, number of examined lymph nodes, TNM stage (determined according to the American Joint Committee on Cancer Staging Manual, seventh edition), adjuvant chemotherapy, serum carcinoembryonic antigen (CEA), and carbohydrate antigen 199 (CA199) levels, were documented. The follow-up of patients was performed regularly as previously described (17). The disease-specific survival (DSS) and disease-free survival (DFS) were defined as the time from surgery to death caused by CRC and the time from surgery to relapse, respectively. Written informed consent was obtained from all patients and approved by the Ethics Committees of Changhai Hospital.

Immunohistochemistry

The slides of TMAs (4-μm thick) were prepared for IHC examination of the detection of VMA21 immunstaining. Each slide was deparaffinized using xylene and rehydrated in graded alcohol, and endogenous peroxidase activity was blocked using 3% H_2O_2. After antigen retrieval of VMA21 for 30 minutes in 10 mmol/L sodium citrate buffer (pH 6.0), slides were blocked with 5% normal goat serum for 10 min at room temperature. Then, the slides were incubated with anti-human VMA21 polyclonal antibody (PA5-42630, 1:150 dilution; Invitrogen, Carlsbad, California, USA) overnight at 4°C, followed by incubation with a secondary antibody from the ElivisionTMsuper HRP (Mouse/Rabbit) for 30 min. Then, the sections were reacted with 3-3-aminobenzidine (DAB) solution for 45 seconds and counterstained with hematoxylin for 25 seconds.

Immunohistochemistry Scoring

Two authors (F.Z. and H.S.) who were blinded to the clinicopathological information, evaluated the VMA21 immunostaining data independently. The intensity level of each specimen dot was evaluated using the H-score method as described previously (18, 19). H-score was evaluated by multiplying the average percentage of positive cells (0–100%) by the staining intensity (0, negative; 1, weakly positive; 2,

moderately positive; and 3, strongly positive staining). The IHC scores of each specimen provided by the two observers were averaged for further studies.

Cell Culture, qRT-PCR, and Western Blotting

Four human CRC cell lines (RKO, SW620, LoVo, and CACO2) were maintained in RPMI-1640 or DEME medium with 10% heat-inactivated fetal bovine serum (FBS) (GIBCO, Grand Island, NY, USA) and 2% penicillin/streptomycin (GIBCO). All cells were obtained commercially from the Cell Bank affiliated to the Chinese Academy of Sciences (Shanghai, China). The LightCycler 480 II system (Roche, Basel, Switzerland) with SYBR Green reagent (Takara, Bio, Dalian, China) was used to detect the relative expression of *VMA21* mRNA using the following primers: 5′-TGG AGC GCC CGG ATA AGG-3′ (forward) and 5′-CTG TTT GCC TTC ACG CCA C-3′ (reverse). Human GAPDH served as an internal control with the primers 5′-GGA GCG AGA TCC CTC CAA AAT-3′ (forward) and 5′-GGC TGT TGT CAT ACT TCT CAT GG-3' (reverse). Western blot analysis of CRC cells and specimens was performed using routine protocols with antibodies against human VMA21 (1:150, PA5-42630, Invitrogen) or human GAPDH (1:1000, AP0063, Bioworld Technology, St. Louis Park, MN, USA)

cDNA Expression Constructs

Invitrogen Co., Ltd (Shanghai, China) synthesized and validated the cDNA sequence of the VMA21 transcript (NM_001017980). The products were subcloned into the pENTRTM3C vector, and the recombinant VMA21 was Gateway-recombined into the pInducer 20 vector (Addgene) (20). A Lenti-XTM HTX Packaging System (Clontech Laboratories, Inc., CA, USA) was used to produce lentiviral particles in HEK293T cells, which were titrated onto SW620 or LoVo cells cultured in media containing 1 μg/mL puromycin to reach the optimal expression of the target protein using the minimum viral load. G418 (2 mg/ml) was added to induce *VMA21* gene expression, which was confirmed by qRT-PCR and western blotting.

Construction of Stable Cells With Inducible *V*acuolar *M*embrane ATPase *A*ctivity 21 Knockdown

A microRNA (miR)-30 loop and appropriate flanking sequences were added to the different miR-30-mediated shRNAs to specifically target VMA21 as described previously (21). The sequence was as followed: 5′-CAU CUA CAC UGA AGA CGC UTT AGC GUC UUC AGU GUA GAU GTT-3′. After the synthesis of single-stranded DNA templates for shRNAs, the templates were amplified with primers including Xho1 or BamH1 restriction enzymes sites. The target DNA was purified and subcloned into the Pinducer10 vector (20). Lentiviral particles were produced as described above and titrated onto RKO cells. Expression of VMA21 was induced using 1 μg/mL doxycycline (dox) and confirmed by qRT-PCR and western blotting.

Colony Formation Assay

CRC cells (LoVo and SW480) were seeded into 6-well plates (Corning, NY, USA) at a density of 1.5×10^3 cells/well. The cell medium was replaced every 72 h during growth. After 7–14 days of incubation, the supernatant was removed, cells were fixed with methanol, and then dyed with crystal violet. Images were captured, and colonies were counted when they contained more than 50 cells.

In Vivo Tumor Growth

Male nude mice (BALB/c, 5–6 weeks old) were purchased from SLAC Laboratory Animal Co. (Shanghai, China) and were accustomed to a pathogen-free environment for 1 week. For setting up the xenograft implant tumor models, the stable inducible CRC cells (VMA21-LoVo, VMA21-SW620, and shRNA-VMA21 RKO) were subcutaneously injected into test (treated with G418 or Dox) and control groups. Tumor formation was continuously monitored using calipers every 3–4 days. The tumor volume was calculated using the formula (length × width^2)/2. The mice were euthanized after 19–30 days depending on tumor size, and the tumor xenografts were removed and tested. All procedures were performed according to the National Research Council's Guide for the Care and Use of Laboratory Animals.

Statistical Analysis

Differences in VMA21 expression between CRC and adjacent non-tumorous tissues were analyzed using the Student's *t* test and we used independent-sample t-tests for the differences of mRNA expression in different CRC cells. The $\chi 2$ test and Student's *t* test were used to compare categorical data and continuous data separately. The R package of maxstat (22) was used to determine the optimal value for the classification of patients into subgroups according to the expression of VMA21 determined by immunostaining. The subgroups were further compared using the Kaplan-Meier method and Cox proportional hazards models. All statistical tests were performed with R 3.6.1 and SPSS (Version 23.0 for Windows), and two-tailed tests with a $P < 0.05$ were considered significant.

RESULTS

Vacuolar Membrane ATPase Activity 21 is Upregulated in Colorectal Cancer Epithelial Cells

To identify V-ATPase assembly factor gene candidates associated with the progression of CRC, the expression of five genes required for the V_0 domain of V-ATPase (TMEM199, VMA21, CCDC115, ATP6AP1, and ATP6AP2) (8) were analyzed using TCGA-CRC cohort. Three (CCDC115, ATP6AP1 and ATP6AP2) of the five assembly factor genes are associated with several cancers (14, 15). We found that VMA21 was the only gene showing significantly higher mRNA expression in colon and rectal cancerous tissues than in adjacent normal tissues (all $P < 0.05$), as shown in **Figure 1A**.

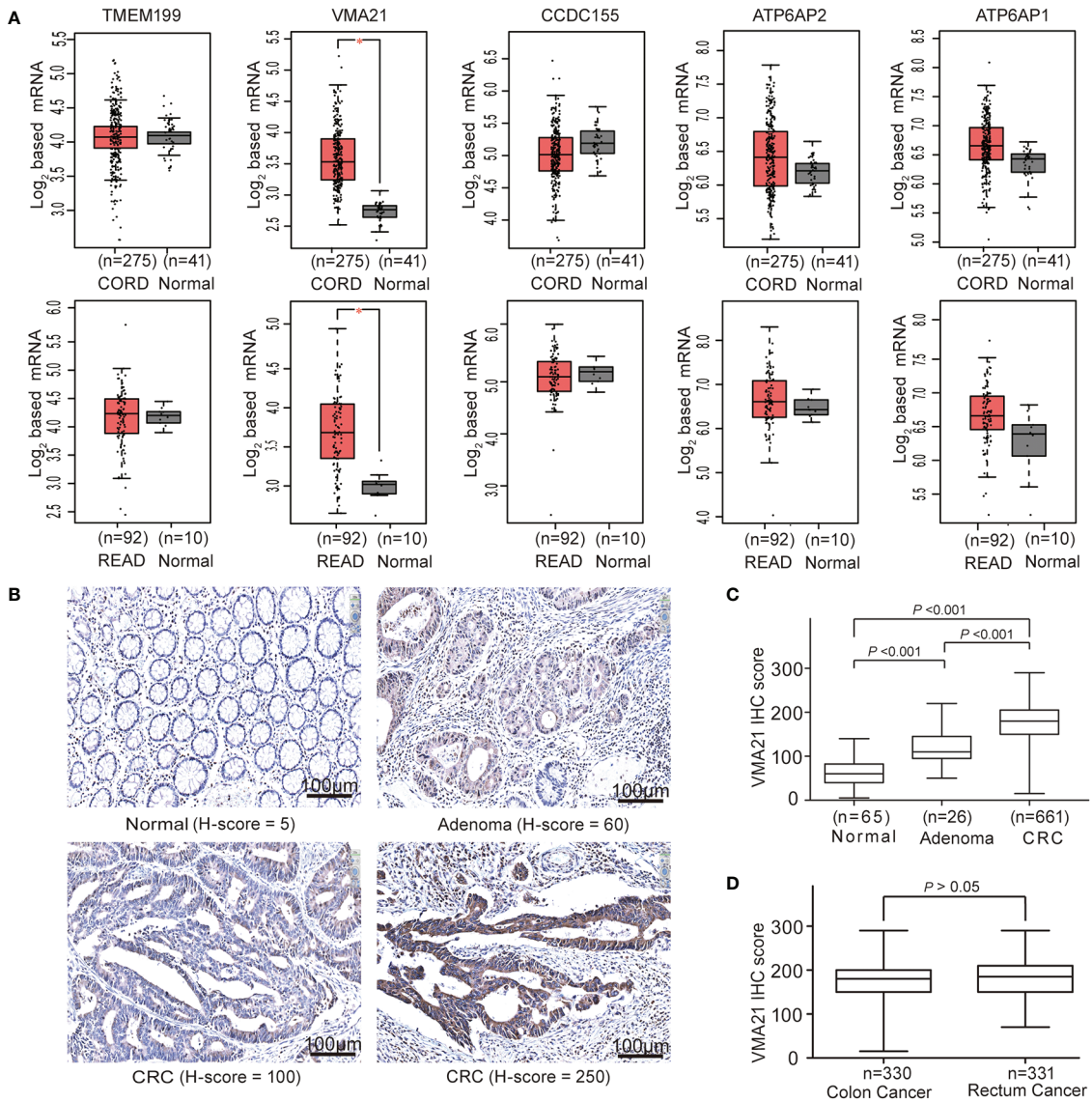

FIGURE 1 | VMA21 is elevated in colorectal cancer. **(A)** Expression patterns of five assembly factor genes of the V_0 domain of V-ATPase based on TCGA-CRC mRNA data. **(B)** Immunostaining of VMA21 in CRC and noncancerous tissues. **(C)** VMA21 protein expression in normal, adenoma, and CRC tissue specimens. **(D)** Expression pattern of the VMA21 protein in colon cancer and rectal cancer. CORD, colon cancer; READ, rectum cancer.

The associations between VMA21 and ATP6AP1 (r = 0.56, $P < 0.001$) and ATP6AP2 (r = 0.52, $P < 0.001$) were significant, as indicated by Pearson correlation coefficients (**Supplementary Figure 1**). Therefore, VMA21 was identified as a new candidate gene involved in the development of CRC.

VMA21 expression in CRC epithelial cells may be affected by the expression profiles of whole tissues because of the potential mixture of transcripts from different cell populations (23, 24). We therefore investigated the expression pattern of VMA21 in our specimens using IHC. VMA21 protein expression was primarily detected in the cytoplasm of colorectal epithelial cells (**Figure 1B**). The immunostaining marks of VMA21 increased gradually in adjacent normal tissues, adenoma, and primary CRC (*P trend* < 0.001), as shown in **Figure 1C**. There was no difference in VMA21 protein expression between colon and rectal cancerous tissues (**Figure 1D**, $P > 0.05$). Taken together, these results indicate that VMA21 is upregulated in CRC at the mRNA and protein levels, suggesting that it plays a role in CRC.

Associations Between *Vacuolar Membrane ATPase Activity 21* Expression and Clinical Variables of *Colorectal Cancer* Patients

Based on the 97.5% quantile (175) of VMA21 in the IHC scores from noncancerous specimens, the 661 patients were classified into two groups, the VMA21-high group (score >175) and the

VMA21-low group (score ≤ 175). The associations between VMA21 expression and the clinical features of CRC patients are shown in **Table 1**. There were no significant associations between VMA21 protein expression and several clinical factors (all P >0.05), including age, gender, TNM stage, tumor location, and serum CEA and CA199 levels. However, VMA21-high expression was significantly associated with higher differentiation grade (P = 0.011) compared with VMA21-low expression, indicating that the expression of VMA21 may be negatively related to the progression of CRC.

High Vacuolar Membrane ATPase Activity 21 Expression Tends to Indicate a Favorable Outcome

The associations between the expression of VMA21 and clinical outcomes were further investigated in 639 patients with stage I-III CRC. According to the optimal IHC-score cut-off value (215) determined by maxstat software, which could most efficiently distinguish differences in clinical outcomes (**Supplementary Figure 2**), patients were classified into two subgroups: patients with VMA21-high (>215) and those with VMA21-low (≤215) tumors. As shown in **Figure 2A**, VMA21-high tumors were strongly correlated with a favorable DSS (P = 0.035) but not DFS (P = 0.390). Next, the associations between VMA21 expression and DFS and DSS in patients with stage I and II disease were estimated. The results showed a significant association between VMA21 expression and DSS (P = 0.034), but not DFS, in stage I-II CRC patients (**Figure 2B**). VMA21 expression was not significantly associated with DFS or DSS in patients with stage III disease (P > 0.05) (**Figure 2C**). Multivariate Cox analysis (**Table 2**) showed that VMA21 expression was associated with DSS [hazard ratio (HR), 0.345; 95% confidence interval (CI), 0.123–0.976] in patients with stage I–III disease, with the covariates including stage, lymph nodes, grade, and serum CEA levels. In patients receiving chemotherapy, the expression of VMA21 in CRC was marginally (P = 0.062) associated with DSS in stage II disease, whereas the association was not significant in patients who did not receive chemotherapy (P = 0.52) (**Supplementary Figure 3**).

Vacuolar Membrane ATPase Activity 21 Inhibits the Growth of Colorectal Cancer Cells

The effect of VMA21 expression on the growth of CRC cells was tested to explore. As shown in **Figure 3A**, VMA21 expression is relatively low in LoVo and SW620 cells, and VMA21 was overexpressed in these cell lines for further evaluation (**Figure 3B**). In the colony formation assays, VMA21 overexpression decreased the number of CRC cell colonies compared with those in the control groups in both SW620 and LoVo cell models (**Figure 3C**). The data suggest that VMA21 is involved in the negative regulation of CRC cell proliferation.

TABLE 1 | Characteristics of patient with CRC dichotomized by VMA21 expression.

Characteristics	Expression of VMA21 protein		*P* Value*
	Low(n = 289)	High(n = 372)	
Age (years)	61.47 ± 12.77	60.19 ± 13.02	0.208**
Differentiation grade, n (%)			**0.011**
Well+ Moderately	214 (74.0)	308 (82.8)	
Poor	65 (22.5)	56 (15.1)	
Missing	10 (3.5)	8 (2.1)	
Lymph nodes, n (%)			0.677
≤ 12	89 (30.8)	109 (29.3)	
>12	200 (69.2)	263 (70.7)	
TNM stage, n (%)			0.211
I+II	187 (64.7)	223 (59.9)	
III+ IV	102 (35.3)	149 (40.1)	
Chemotherapy, n (%)			0.369
Yes	226 (78.2)	281 (75.6)	
No	49 (17.0)	50 (13.4)	
Missing	14 (4.8)	41 (11.0)	
Serum CEA, n (%)			0.684
< 5ng/ml	177 (61.2)	224 (60.2)	
≥ 5ng/ml	108 (37.4)	145 (39.0)	
Missing	4 (1.4)	3 (0.8)	
Serum CA199, n (%)			0.960
< 37U/ml	242 (83.7)	313 (84.1)	
≥ 37U/ml	43 (14.9)	55 (14.8)	
Missing	4 (1.4)	4 (1.1)	

*Pearson's chi-squared test.

**Student's t test.

Missing values are excluded for all statistic tests.

CRC, colorectal cancer; CEA, carcinoembryonic antigen; CA199, carbohydrate antigen 199.

Bold number represents statistically p value < 0.05.

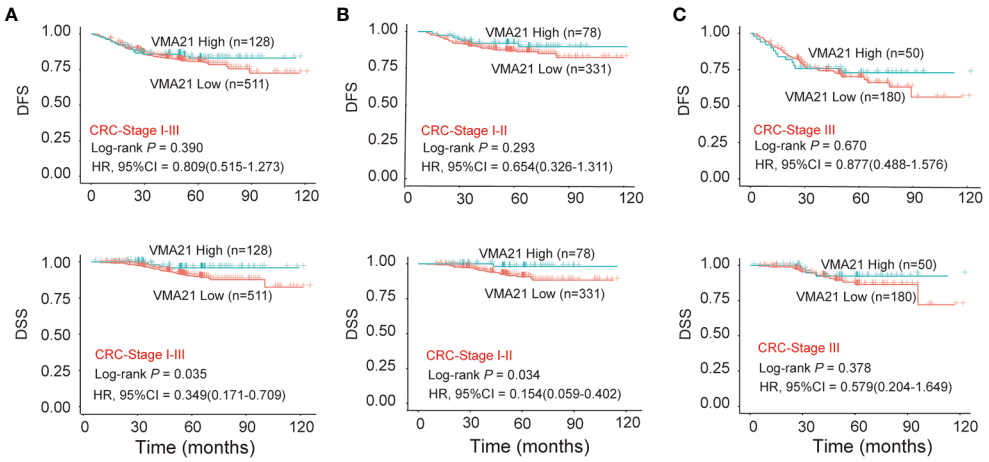

FIGURE 2 | Relationship between VMA21 expression and patient survival. **(A–C)** DFS and DSS analysis in patient subgroups with high or low VMA21 protein expression in stage I-III, stage I-II, and stage III disease. DFS, disease free survival; DSS, disease specific survival.

TABLE 2 | Cox regression analysis of prognostic factors for DSS in 639 CRC patients.

Variables	Univariate analysis		Multivariate analysis*	
	HR (95% CI)	*P* value	HR (95% CI)	*P* value
VMA21 scores				
High vs. Low	0.340 (0.122–0.950)	**0.039**	0.345 (0.123–0.976)	**0.043**
Gender				
Male vs. Female	1.202 (0.662–2.184)	0.545		
Tumor location				
Colon vs. Rectum	1.058 (0.589–1.903)	0.850		
Differential grade				
Per increase in grade	1.904 (1.007–3.597)	**0.047**	1.649 (0.847–3.210)	0.142
Lymph nodes				
>12 vs. ≤12	1.916 (0.969–3.785)	0.061	2.075 (1.046–4.117)	**0.037**
TNM stage				
Per increase in stage	1.511 (0.939–2.431)	0.089	1.385 (0.848–2.262)	0.193
Chemotherapy				
Yes vs. No	1.766 (0.627–4.977)	0.282		
Serum CEA (ng/mL)				
< 5 vs. ≥ 5	0.542 (0.302–0.973)	**0.040**	0.603 (0.333–1.090)	0.094
Serum CA199 (U/mL)				
< 37 vs. ≥37	0.692 (0.322–1.486)	0.345		

**Variates with a p value of <0.1 in univariate analysis were included in the multivariate analysis.*
CRC, colorectal cancer; DSS, disease specific survival; CA199, carbohydrate antigen 199; CEA, carcinoembryonic antigen; TNM, tumor to node to metastasis.
Bold number represents statistically p value < 0.05.

Vacuolar Membrane ATPase Activity 21 Suppresses Colorectal Cancer Growth in Animal Models

VMA21-SW620 or VMA21-LoVo cells were subcutaneously injected into BALB/c nude mice (supplemented with or without G418 in drinking water) to determine whether VMA21 overexpression reduces CRC growth in animal models. In the first 10 days for VMA21-SW620 and the first 25 days for VMA21-LoVo models, tumor size did not differ significantly between the test (G418+) and control (G418-) groups in both cell models (**Figure 4A**). However, xenograft tumors were significantly smaller in the test groups than in the control groups after the indicated days (**Figure 4A**). By the end of the observation period, both the size (**Figure 4B**) and weight (**Figure 4C**) of isolated tumors were significantly lower in the test animals than in the control animals for both cell models. In xenograft tumors from RKO cells, knockdown of VMA21 promoted the development of CRC, as shown in **Figure 5**. Therefore, high VMA21 expression suppresses tumor growth *in vivo*, indicating that VMA21 is a negative regulator of CRC tumorigenicity.

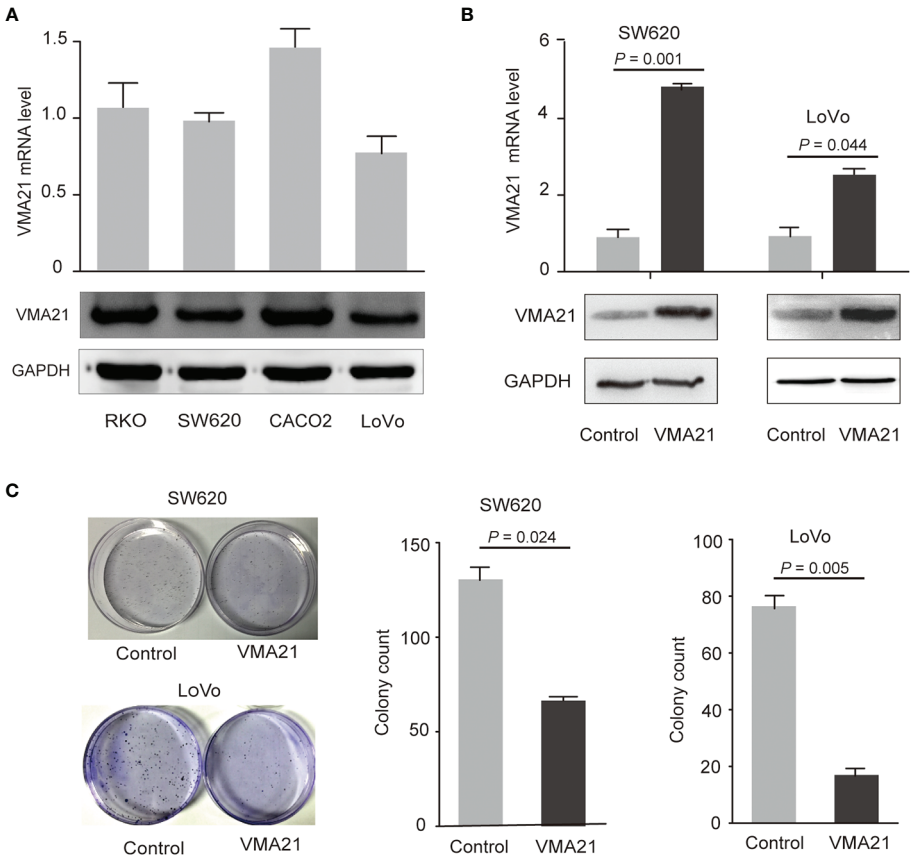

FIGURE 3 | VMA21 overexpression suppresses colony formation of CRC cells. **(A)** Baseline mRNA and protein expression of VMA21 (lower panel) in four CRC cell lines. **(B)** The efficiency of VMA21 overexpression in the indicated CRC cells at the mRNA and protein levels (lower panel). **(C)** The colony formation abilities are affected by overexpressed VMA21 in CRC cells.

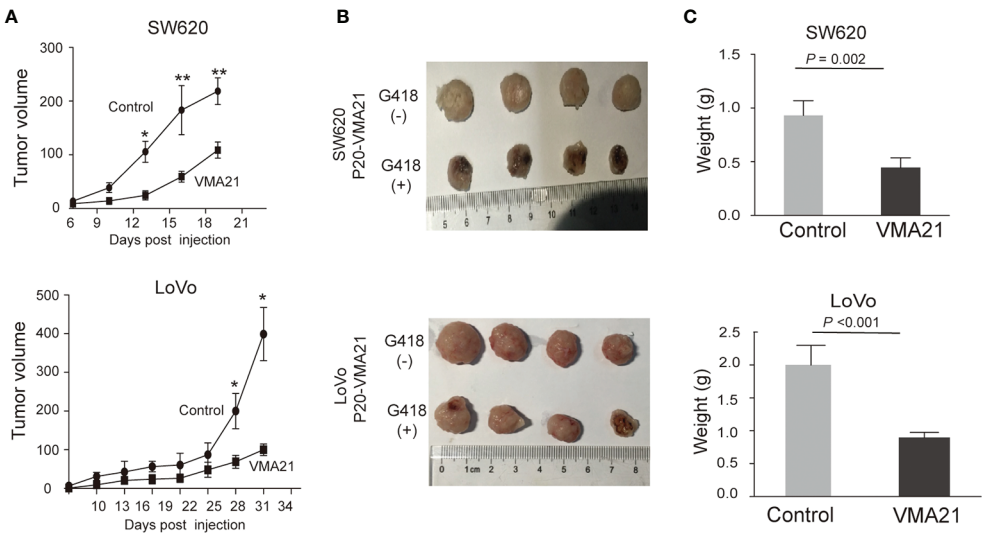

FIGURE 4 | Effects of VMA21 overexpression on xenograft tumor growth. **(A)** Dynamic effect of VMA21 overexpression on the volume of xenograft CRC models. **(B)** Isolated tumors after surgical excision. **(C)** Comparison of the weights of isolated tumors between the subgroups of VMA21 overexpression and the control. (*$P < 0.05$; **$P < 0.01$; ***$P < 0.001$).

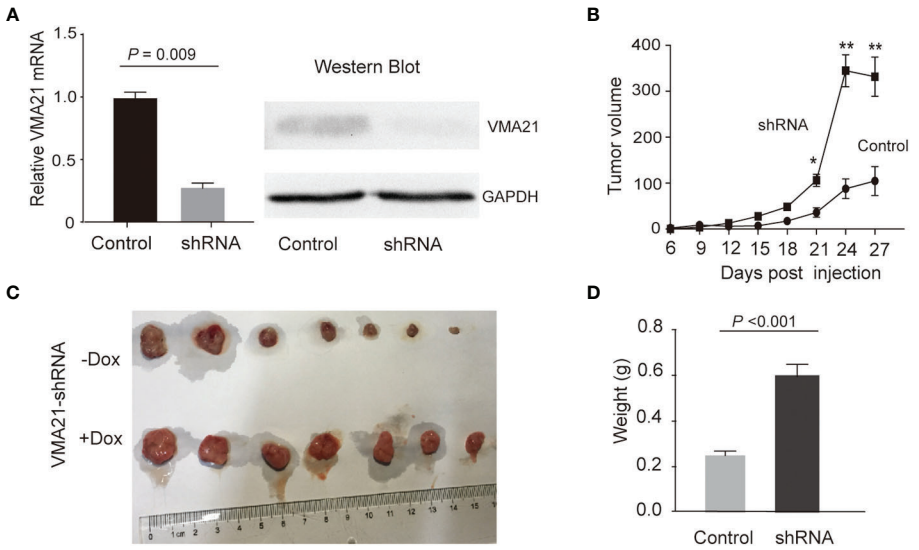

FIGURE 5 | Effects of VMA21 knockdown on xenograft tumor growth. **(A)** The efficiency of VMA21 knockdown in RKO cells at the mRNA and protein levels. **(B)** Dynamic effect of VMA21 knockdown on the volume of CRC xenograft models. **(C)** Isolated tumors after surgical excision. **(C)** Comparison of the isolated tumor weights from the subgroups with VMA21 knockdown or not. (*$P < 0.05$; **$P < 0.01$; ***$P < 0.001$).

DISCUSSION

The lysosome mediates the degradation and recycling of macromolecules and signals to the cytosol and nucleus by releasing metabolites and ions; it is implicated in several malignancies (25). These lysosomal behaviors depend on a low intraluminal pH. Although the V_0 domain of V-ATPases is required for proton translocation and lysosome acidification (6–8), the role of the assembly factor genes of the domain in cancer remains largely unknown. In this study, we identified VMA21 as the only candidate gene showing differential expression between cancer and noncancerous colorectal tissues among five known assembly factor genes (TMEM199, VMA21, CCDC115, ATP6AP1, and ATP6AP2) of the V_0 domain. IHC data confirmed that VMA21 expression is higher in CRC than in adjacent normal tissues. The data consistently suggested that VMA21 plays a critical role in the development of CRC.

The genes encoding CCDC115, ATP6AP1, and ATP6AP2 may play a tumor suppressor role in different cancer types (14, 15). In this study, the expression of VMA21 was correlated with the expression of ATP6AP1 and ATP6AP2, although which were not differentially expressed between cancer and noncancer tissues. These data suggest that VMA21 plays a negative role in CRC development. Similar findings were reported for the gene encoding GUCY2C, which is elevated in CRC but serves as a tumor suppressor (26). Further, we observed that high expression of VMA21 was associated with the well differentiation of CRC. Survival analysis showed that high expression of VMA21 was associated with longer DSS in stage I–III disease and served as an independent risk factor, and this observation was similar in patients with early CRC and in those receiving chemotherapy for stage II disease. Although we observed no associations between DFS and the expression of VMA21 in the subgroups with different disease stages or chemotherapy regimens, the evidence indicated that elevated VMA21 may be a important factor involved in controlling the progression of CRC.

To further elucidate the biological role of VMA21 in CRC, we modulated the expression of VMA21 in different CRC cells and evaluated its function. Overexpression of VMA21 in human colon cancer LoVo and SW620 cells significantly suppressed colony formation ability. Consistently, ectopic expression or knockdown of VMA21 significantly inhibited or increased CRC development in animal models, confirming the clinical data and *in vitro* results, as well as the suppressive effect of VMA21 on CRC growth. Previous investigation of the underlying molecular mechanism showed that VMA21 deficiency decreases lysosomal-mediated degradation and blocks autophagy (27), and increased autophagy inhibits tumor progression (28, 29). However, the recent evidence also shows that VMA21 may have a positive role to promote the growth of ovarian cancer and lung cancer cells (30, 31). Therefore, tumorigenesis is an extremely complex process involving several factors and many biological phenomena, and it reflects a competition between carcinogens and tumor suppressors (32). Defining the exact role of VMA21 in CRC requires further investigation.

The present study had several limitations. First, the inconsistencies in the prognostic role of VMA21 in DFS and DSS cannot be explained. Second, other critical prognostic factors, such as MSI (4) were not included in our studies because the information was difficult to obtain. Finally, the potential mechanism about the role VMA21 as a tumor suppressor was not explored in the present study. In summary, we showed that VMA21 is upregulated in CRC and associated with a high differentiation grade and favorable DFS. Ectopic

expression of VMA21 in CRC significantly inhibited the growth of CRC in cell culture models and animal models. Although the mechanisms involved in VMA21-mediated tumor suppression remain unclear, the current study provides the first evidence of the clinical and biological significance of VMA21 in CRC, as well as their application in the targeted drugs and chemotherapy will be further explored based on mechanism research. The expression of VMA21 may represent a potential diagnostic and prognostic marker for CRC, especially for patients with early-stage CRC.

DATA AVAILABILITY STATEMENT

The raw data supporting the conclusions of this article will be made available by the authors, without undue reservation.

ETHICS STATEMENT

The studies involving human participants were reviewed and approved by the Ethics Committees of the Changhai Hospital. The patients/participants provided their written informed consent to participate in this study. The animal study was reviewed and approved by the Ethics Committees of the Changhai Hospital.

AUTHOR CONTRIBUTIONS

As for the authorship, FZ, HS, and YF analyzed whole data independently and presented the same results. GY and FC were responsible for the follow-up of CRC patients. FZ, HS, and YF were responsible for pathological analysis. GY, FC, and ZX were involved in the pathological diagnosis and recruitment of the patients in the hospital. FZ, WC, and ZX were responsible for the statistical analysis. WC, FZ, and ZX designed and organized the study and wrote the manuscript. All authors contributed to the article and approved the submitted version.

FUNDING

This work was supported by grants from the National Natural Science Foundation of China (81972302 and 81572451 to WC) and the Wenzhou Science & technological Project (Y2020927 to ZX).

SUPPLEMENTARY MATERIAL

The Supplementary Material for this article can be found online at: https://www.frontiersin.org/articles/10.3389/fonc.2020.605801/full#supplementary-material

REFERENCES

1. Torre LA, Bray F, Siegel RL, Ferlay J, Lortet-Tieulent J, Jemal A. Global cancer statistics, 2012. *CA Cancer J Clin* (2015) 65:87–108. doi: 10.3322/caac.21262
2. Schmoll HJ, Van Cutsem E, Stein A, Valentini V, Glimelius B, Haustermans K, et al. ESMO Consensus Guidelines for management of patients with colon and rectal cancer :a personalized approach to clinical decision making. *Ann Oncol* (2012) 23:2479–516. doi: 10.1093/annonc/mds236
3. Van Schaeybroeck S, Allen WL, Turkington RC, Johnston PG. Implementing prognostic and predictive biomarkers in CRC clinical trials. *Nat Rev Clin Oncol* (2011) 8:222–32. doi: 10.1038/nrclinonc.2011.15
4. Popat S, Hubner R, Houlston RS. Systematic review of microsatellite instability and colorectal cancer prognosis. *J Clin Oncol* (2005) 23:609–18. doi: 10.1200/JCO.2005.01.086
5. Brown K, Solomon MJ, Mahon K, O'Shannassy S. Management of colorectal cancer. *BMJ* (2019) 366:l4561. doi: 10.1136/bmj.l4561
6. Breton S, Brown D. Regulation of Luminal Acidification by the V-ATPase. *Physiology* (2013) 28:318–29. doi: 10.1152/physiol.00007.2013
7. Cotter K, Stransky L, McGuire C, Forgac M. Recent Insights into the Structure, Regulation, and Function of the V-ATPases. *Trends Biochem Sci* (2015) 40:611–22. doi: 10.1016/j.tibs.2015.08.005
8. Whitton B, Okamoto H, Packham G, Crabb SJ. Vacuolar ATPase as a potential therapeutic target and mediator of treatment resistance in cancer. *Cancer Med* (2018) 7:3800–11. doi: 10.1002/cam4.1594
9. Cannata Serio M, Graham LA, Ashikov A, Larsen LE, Raymond K, Timal S, et al. sMutations in the V-ATPase assembly factor VMA21 cause a congenital disorder of glycosylation with autophagic liver disease. *Hepatology* (2020) 72:1968–86. doi: 10.1002/hep.31218
10. Jansen EJR, Timal S, Ryan M, Ashikov A, van Scherpenzeel M, Graham LA, et al. ATP6AP1 deficiency causes an immunodeficiency with hepatopathy, cognitive impairment and abnormal protein glycosylation. *Nat Commun* (2016) 7:11600. doi: 10.1038/ncomms11600
11. Rujano MA, Cannata Serio M, Panasyuk G, Péanne R, Reunert J, Rymen D, et al. Mutations in the X-linked ATP6AP2 cause a glycosylation disorder with autophagic defects. *J Exp Med* (2017) 214:3707–29. doi: 10.1084/jem.20170453
12. Guida MC, Hermle T, Graham LA, Hauser V, Ryan M, Stevens TH, et al. ATP6AP2 functions as a V-ATPase assembly factor in the endoplasmic reticulum. *Mol Biol Cell* (2018) 29:2156–64. doi: 10.1091/mbc.E18-04-0234
13. Stransky L, Cotter K, Forgac M. The Function of V-ATPases in Cancer. *Physiol Rev* (2016) 96:1071–91. doi: 10.1152/physrev.00035.2015
14. Winter JM, Curry NL, Gildea DM, Williams KA, Lee M, Hu Y, et al. Modifier locus mapping of a transgenic F2 mouse population identifies CCDC115 as a novel aggressive prostate cancer modifier gene in humans. *BMC Genomics* (2018) 19:450. doi: 10.1186/s12864-018-4827-2
15. Pareja F, Brandes AH, Basili T, Selenica P, Geyer FC, Fan D, et al. Loss-of-function mutations in ATP6AP1 and ATP6AP2 in granular cell tumors. *Nat Commun* (2018) 9:3533. doi: 10.1038/s41467-018-05886-y
16. Tang Z, Li C, Kang B, Gao G, Li C, Zhang Z. GEPIA: a web server for cancer and normal gene expression profiling and interactive analyses. *Nucleic Acids Res* (2017) 45:W98–W102. doi: 10.1093/nar/gkx247
17. Chang W, Gao X, Han Y, Du Y, Liu Q, Wang L, et al. Gene expression profiling-derived immunohistochemistry signature with high prognostic value in colorectal carcinoma. *Gut* (2014) 63:1457–67. doi: 10.1136/gutjnl-2013-305475
18. Finn RS, Press MF, Dering J, Arbushites M, Koehler M, Oliva C, et al. Estrogen receptor, progesterone receptor, human epidermal growth factor receptor 2 (HER2), and epidermal growth factor receptor expression and benefit from lapatinib in a randomized trial of paclitaxel with lapatinib or placebo as first-line treatment in HER2-negative or unknown metastatic breast cancer. *J Clin Oncol* (2009) 27:3908–15. doi: 10.1200/JCO.2008.18.1925
19. Dziadziuszko R, Merrick DT, Witta SE, Mendoza AD, Szostakiewicz B, Szymanowska A, et al. Insulin-like growth factor receptor 1 (IGF1R) gene copy number is associated with survival in operable non-small-cell lung cancer: a comparison between IGF1R fluorescent in situ hybridization, protein expression, and mRNA expression. *J Clin Oncol* (2010) 28:2174–80. doi: 10.1200/JCO.2009.24.6611
20. Meerbrey KL, Hu G, Kessler JD, Roarty K, Li MZ, Fang JE, et al. The pINDUCER lentiviral toolkit for inducible RNA interference in vitro and in

vivo. *Proc Natl Acad Sci USA* (2011) 108:3665–70. doi: 10.1073/pnas.1019736108
21. Dow LE, Premsrirut PK, Zuber J, Fellmann C, McJunkin K, Miething C, et al. A pipeline for the generation of shRNA transgenic mice. *Nat Protoc* (2012) 7:374–93. doi: 10.1038/nprot.2011.446
22. Choi YH, Lee JW, Lee SH, Choi JH, Kang J, Lee BS, et al. A High Monocyte-to-Lymphocyte Ratio Predicts Poor Prognosis in Patients with Advanced Gallbladder Cancer Receiving Chemotherapy. *Cancer Epidemiol Biomarkers Prev* (2019) 28:1045–51. doi: 10.1158/1055-9965.EPI-18-1066
23. Shen-Orr SS, Tibshirani R, Khatri P, Bodian DL, Staedtler F, Perry NM, et al. Cell type-specific gene expression differences in complex tissues. *Nat Methods* (2010) 7:287–9. doi: 10.1038/nmeth.1439
24. Zhong Y, Wan YW, Pang K, Chow LM, Liu Z. Digital sorting of complex tissues for cell type-specific gene expression profiles. *BMC Bioinf* (2013) 14:89. doi: 10.1186/1471-2105-14-89
25. McCarty MF, Whitaker J. Manipulating tumor acidification as a cancer treatment strategy. *Altern Med Rev* (2010) 15:264–72.
26. Bashir B, Merlino DJ, Rappaport JA, Gnass E, Palazzo JP, Feng Y, et al. Silencing the GUCA2A-GUCY2C tumor suppressor axis in CIN, serrated, and MSI colorectal neoplasia. *Hum Pathol* (2019) 87:103–14. doi: 10.1016/j.humpath.2018.11.032
27. Ramachandran N, Munteanu I, Wang P, Ruggieri A, Rilstone JJ, Israelian N, et al. VMA21 deficiency prevents vacuolar ATPase assembly and causes autophagic vacuolar myopathy. *Acta Neuropathol* (2013) 125:439–57. doi: 10.1007/s00401-012-1073-6
28. Nassour J, Radford R, Correia A, Fusté JM, Schoell B, Jauch A, et al. Autophagic cell death restricts chromosomal instability during replicative crisis. *Nature* (2019) 565:659–63. doi: 10.1038/s41586-019-0885-0
29. Delaney JR, Patel CB, Bapat J, Jones CM, Ramos-Zapatero M, Ortell KK, et al. Autophagy gene haploinsufficiency drives chromosome instability, increases migration, and promotes early ovarian tumors. *PloS Genet* (2020) 16: e1008558. doi: 10.1371/journal.pgen.1008558
30. Xue M, Tao W, Yu S, Yan Z, Peng Q, Jiang F, et al. LncRNA ZFPM2-AS1 promotes proliferation via miR-18b-5p/VMA21 axia in lung adenocarcinoma. *J Cell Biochem* (2020) 121:313–21. doi: 10.1002/jcb.29176
31. Xue F, Xu YH, Shen CC, Qin ZL, Zhou HB. Non-coding RNA LOXL1-AS1 exhibits oncogenic activity in ovarian cancer via regulation of miR-18b-5p/VMA21 axia. *BioMed Pharmacother* (2020) 125:109568. doi: 10.1016/j.biopha.2019.109568
32. Zhang J, Zhu Y, Xie K, Peng Y, Tao J, Tang J, et al. Yin Yang-1 suppresses invasion and metastasis of pancreatic ductal adenocarcinoma by downregulating MMP10 in a MUC4/ErbB2/p38/MEF2C-dependent mechanism. *Mol. Cancer* (2014) 13:130. doi: 10.1186/1476-4598-13-130

Conflict of Interest: The authors declare that the research was conducted in the absence of any commercial or financial relationships that could be construed as a potential conflict of interest.

frontiers in Oncology

ORIGINAL RESEARCH
published: 19 February 2021
doi: 10.3389/fonc.2020.610513

Tumor Immune Microenvironment Characterization in Hepatocellular Carcinoma Identifies Four Prognostic and Immunotherapeutically Relevant Subclasses

Xingxing Gao[1,2,3†], *Hechen Huang*[1,2,3†], *Yubo Wang*[1,2,3], *Caixu Pan*[1,2,3], *Shengyong Yin*[1,2,3], *Lin Zhou*[1,2,3*] *and Shusen Zheng*[1,2,3*]

[1] Division of Hepatobiliary and Pancreatic Surgery, Department of Surgery, The First Affiliated Hospital, Zhejiang University School of Medicine, Hangzhou, China, [2] NHC Key Laboratory of Combined Multi-organ Transplantation, Hangzhou, China, [3] Key Laboratory of Organ Transplantation, Research Center for Diagnosis and Treatment of Hepatobiliary Diseases, Hangzhou, China

Purpose: The tumor microenvironment (TME) plays a critical role in the pathogenesis of hepatocellular carcinoma (HCC). However, underlying compositions and functions that drive the establishment and maintenance of the TME classifications are less-well understood.

Methods: A total of 766 HCC patients from three public cohorts were clustered into four immune-related subclasses based on 13 TME signatures (11 immune-related cells and 2 immune-related pathways) calculated by MCP-counter. After analyzing the landscapes of functional annotation, methylation, somatic mutation, and clinical characteristics, we built a TME-based Support Vector Machine of 365 patients (discovery phase) and 401 patients (validation phase). We applied this SVM model on another two independent cohorts of patients who received sorafenib/pembrolizumab treatment.

Results: About 33% of patients displayed an immune desert pattern. The other subclasses were different in abundance of tumor infiltrating cells. The Immunogenic subclass (17%) associated with the best prognosis presented a massive T cell infiltration and an activation of immune checkpoint pathway. The 13 TME signatures showed a good potential to predict the TME classification (average AUC = 88%). Molecular characteristics of immunohistochemistry from Zhejiang cohort supported our SVM classification. The optimum response to pembrolizumab (78%) and sorafenib (81%) was observed in patients belonging to the Immunogenic subclass.

Conclusions: The HCC patients from distinct immune subclass showed significant differences in clinical prognosis and response to personalized treatment. Based on tumor transcriptome data, our workflow can help to predict the clinical outcomes and to find appropriate treatment strategies for HCC patients.

Keywords: tumor microenvironment, carcinoma, hepatocellular, cancer immunology, classification, machine learning

OPEN ACCESS

Edited by:
Rui Liao,
First Affiliated Hospital of Chongqing Medical University, China

Reviewed by:
Bin-Yan Zhong,
The First Affiliated Hospital of Soochow University, China
Limin Zheng,
Sun Yat-Sen University, China

****Correspondence:***
Lin Zhou
linzhou19@163.com
Shusen Zheng
shusenzheng@zju.edu.cn

†These authors have contributed equally to this work

Specialty section:
This article was submitted to Gastrointestinal Cancers, a section of the journal Frontiers in Oncology

Received: *26 September 2020*
Accepted: *24 December 2020*
Published: *19 February 2021*

Citation:
Gao X, Huang H, Wang Y, Pan C, Yin S, Zhou L and Zheng S (2021) Tumor Immune Microenvironment Characterization in Hepatocellular Carcinoma Identifies Four Prognostic and Immunotherapeutically Relevant Subclasses. Front. Oncol. 10:610513. doi: 10.3389/fonc.2020.610513

INTRODUCTION

Hepatocellular carcinoma (HCC), the predominant type of primary liver cancer, is the fourth leading cause of cancer mortality worldwide with about 782,000 deaths annually (1). HCC is strongly influenced by the tumor microenvironment (TME), as well as reported to benefit from the immune-checkpoint blockade treatment. As an inflammation-related tumor, the specific TME of HCC can influence the immune tolerance and evasion by mixed mechanisms. Numerous studies have been reported that the TME plays a critical role in tumor initiation, progression, and outcome (2, 3). The TME is an intricate system, which coexists and interacts with cancer cells, immune cell subsets, extracellular matrix, various cytokine, and other unknown components to maintain the tumorigenesis of HCC (4). The complexity of the TME relies on the immune infiltration, as tumors could be classified into the tumor immunity continuum (5). Hegde et al. suggested that human tumors could be categorized as inflamed, immune desert, or immune-excluded phenotypes correspond to different mechanisms of immune response and escape (6). Thorsson et al. proposed a classification of six immune subclasses (wound healing, lymphocyte depleted, TGF-β dominant, inflammatory, immunologically quiet, IFN-γ dominant), based on extensive immunogenomic analysis of 33 cancer types compiled by TCGA (7).

Meanwhile, estimating the cellular composition of the TME requires accurate and robust methods. Fluorescence-activated cell sorting (FACS) operates only a small number of cell type-specific markers and requires large amounts of fresh tumor tissues, which limit the applications on tumor biopsies (8). Single-cell sequencing has a high precision, but currently it is too expensive for large-scale clinical application (9). In order to overcome the above shortcomings, we turn to the methods for high-throughput technologies applied in clinical settings, which TME are inferred using computational algorithms. High throughput technologies, such as RNA-Seq and microarray, provide large-scaled transcriptome data and offer opportunity for estimation of the abundance of tumor infiltrated immune cells. Several methods like Microenvironment Cell Population-counter (MCP-counter), CIBERSORT and TIMER have been developed to robustly and precisely quantify immune cells using transcriptome data obtained from bulk tissue specimens (10–12).

After exploring the distinct compositions and functions of the TME by MCP-counter, a total of 766 HCC patients from three public cohorts were clustered into four subclasses (namely Immune desert, Immunogenic, Innate immune and Mesenchymal) based on 13 TME signatures. Furthermore, a Support Vector Machine (SVM) was constructed to predict the HCC classification (average AUC = 88%). Finally, by applying our SVM model on another two independent cohorts of patients who received sorafenib/pembrolizumab treatment, we found that patients classified into Immunogenic subclass showed the highest response rate to sorafenib (81%) and pembrolizumab (78%). Thus, we suggested that HCC patients may benefit from identifying the immune subclass which infer clinical outcomes and guide personalized treatment strategies (**Supplementary Figure 1**).

MATERIALS AND METHODS

Ethics Statement and Consent for Publication

The studies involving human participants were reviewed and approved by Clinical Research Ethics Committee of the First Affiliated Hospital College of Medicine, Zhejiang University (2014-334). Operation informed consents and Informed consent form for scientific research were obtained from all participants for the publication of any potentially identifiable images or data included in this article.

Clinical Cohorts and Preprocessing

Three public transcriptome data sets were enrolled in our study, including the TCGA-LIHC cohort of the Cancer Genome Atlas (n = 365), the CHCC-HBV cohort of Gao et al. (n = 159) and the GSE14520 cohort of Roessler et al. (n = 242) (13, 14). Among above data sets, any case with null value of survival information had been excluded. As to TCGA-LIHC and CHCC-HBV cohort, the fragments per kilobase per million (FPKM) data and clinic information were downloaded from the UCSC Xena (xenabrowser.net) and The National Omics Data Encycolpedia (www.biosino.org/node), respectively. The "CEL" files of GSE14520 were downloaded and normalized by the "frma" function using frma (R package). Besides, GSE78220 (28 melanoma patients received pembrolizumab) and GSE109211 (67 HCC patients received sorafenib) were also included in our study (15, 16). All FPKM values were transformed into transcripts per kilobase million (TPM) values. Raw data files of GSE109211 were normalized by lumi (R package). cBioPortal (www.cbioportal.org) was used to download the beta value of DNA methylation status of checkpoint genes from TCGA-LIHC cohort. Gene mutation data (MAF files) of TCGA-LIHC cohort was achieved from TCGA database.

In our previous study, liver tumor tissues from 32 patients in First Affiliated Hospital, School of Medicine, Zhejiang University were collected from November 2013 to July 2014 (GSE138485/PRJNA576155) (17). Only a few of the 32 patients have the available Formalin Fixed Paraffin Embedded (FFPE) specimens. Detailed information of patients is described in **Supplementary Tables S7, S8**.

Quantification of TME Infiltration

The abundances of immune and stromal cells in TME were quantified by MCP-counter based on cell-type specific transcriptome signatures (10). According to Sylvie's study (18), a total of 13 TME signatures, which contained 11 stromal and immune cell populations (Lymphoid, B_derived, T_adaptive, Cytotoxic, Monocyte_derived, Myeloid, NK_or_T, Fibroblast, HSCactivated, HSCquiescent, and Myofibroblast) and two functional signatures representing the immune checkpoints (named Checkpoint) and the immunosuppression pathways (named Immunosuppression), were included (**Supplementary Table S1**). In addition, we used the CIBERSORT to validate the immune characterization (11).

Evaluation of the Immune Score and Stromal Score

The immune score and stromal score of each patient were calculated by ESTIMATE algorithm based on transcriptomic data (19). The R code of ESTIMATE was downloaded from the public source website (https://sourceforge.net/projects/estimateproject).

Unsupervised Clustering Based on 13 TME Signatures

Based on above 13 signatures, consensus clustering method was used to classify HCC patients into distinct immune subclasses by ConsensusClusterPlus (R package) (20). Detailed settings were as followed: repetitions = 500 times; pItem = 0.8; pFeature = 0.8. The number of the clusters was determined by consensus cumulative distribution function (CDF) curve and the delta area (relative change in CDF area). Because the CDF curve and delta area plot showed that the delta area increased slightly for k = 5 compared to k = 4, we finally selected k = 4 (four immune subclasses) as the best solution (**Supplementary Figure 2**).

Functional Characterization of Immune Subclass

For pathway analysis of transcriptomic data among immune subclasses, we performed Gene Set Variation Analysis (GSVA) analysis with the "GSVA" R package (21). The gene sets of "c2.cp.kegg.v7.1.symbols", "c2.cp.bp.v7.1.symbols", "c2.cp.biocarta.v7.1.symbols", and "c2.cp.pid.v7.1.symbols" were downloaded from Molecular Signatures Database (MSigDB). Adjusted ANOVA model q value <0.05 was considered as statistically significance.

Classifier Model Construction and Validation

Based on the 13 TME signatures, we developed a classifier model using Support Vector Machine, as implemented in python package "scikit-learn" (version 0.21.3). The TCGA-LIHC cohort was used as discovery phase, as well as the CHCC-HBV and GSE14520 cohort were validation phases. Detailed information for model construction is described in Supplementary Methods. The efficiency of the classifier model was evaluated by receiver operating characteristic (ROC) curve and the area under the curve (AUC).

Statistical Analysis

Continuous variables conforming to normal distribution were compared with Student t test, otherwise the Wilcoxon rank sum test was used. One-way ANOVA models and Kruskal-Wallis tests were used for multigroup comparison. The association between immune subclasses and the clinical parameters were evaluated by chi-squared test or Fisher-exact test. Overall survival (OS) curves were calculated according to the Kaplan-Meier method (R package survival) and differences between curves were assessed using the log-rank test. Statistical analyses were performed on R 3.6.2 software and SPSS V26.0 for Windows.

RESULTS

Identified Four Immune Subclasses Based on TME of HCC

Three public HCC data sets with clinical information (TCGA, CHCC-HBV, GSE14520) were enrolled in this study. According to Sylvie's study (18), a total of 13 TME signatures represented the major infiltrated cell composition and several components of tumor-stroma interaction were included (**Supplementary Table S1**). First, we performed spearman correlation analysis on the 11 cell-type signatures to find the interdependent relationship. **Figure 1A** and **Supplementary Figure 3A** showed that these 11 cell-type signatures were clustered into three distinct clusters (named ACTIVATED_FIBROBLASTS, INNATE_IMMUNITY, and ADAPTIVE_IMMUNITY). In addition, two functional pathways were added, namely, a signature of immune checkpoint related to immune therapy and a signature of genes involved in immunosuppression. Then consensus clustering was performed on the three data sets based on above 13 signatures, and four distinct immune patterns were finally identified, named C1 to C4 (**Figure 1B**, **Supplementary Figure 3B**). Subclass C1 showed an immune desert pattern distinguished by low abundances of all the TME signatures. Subclass C2 displayed an immunogenic pattern distinguished by high abundances of both INNATE_IMMUNITY and ADAPTIVE_IMMUNITY, activation of immune checkpoint pathway and low abundances of ACTIVATED_FIBROBLASTS. Subclass C3 showed an innate immune pattern distinguished by moderate to high abundances of INNATE_IMMUNITY and immunosuppression pathway, rather low abundances of ADAPTIVE_IMMUNITY. Subclass C4 displayed a mesenchymal pattern which was characterized by high abundances of ACTIVATED_FIBROBLASTS and immunosuppression pathway. Principal component analysis (PCA) also showed a significant spatial separation among these four subclasses in TCGA cohort (**Figure 1C**).

Next, we investigated the association between clinical outcomes and immune subclass. In all cohorts, significant differences of prognosis were existed among four immune subclasses, indicating that they could be clinically relevant subclasses (TCGA cohort: log-rank test P = 0.0005; CHCC-HBV cohort: log-rank test P = 0.0052; GSE14520 cohort: log-rank test P = 0.0073) (**Figures 1D, E**, **Supplementary Figure 3C**). In TCGA cohort, C2 Immunogenic subclass showed the longest median survival time (MST) (MST = 82.8 months), followed by C1 Immune desert subclass (MST = 71.0 months), thirdly C4 Mesenchymal subclass (MST = 52.0 months), lastly C3 Innate immune subclass (MST = 21.3 months). Similar results were found in other two data sets. In summary, subclass C2 showed a survival advantage with respect to the other subclasses.

Immune Functional Characteristics of the Immune Subclasses

To refine the immune characterization, we performed both ESTIMATE and CIBERSORT to calculate the Immune/Stromal scores and the proportion of 22 tumor infiltrating immune cells. C1 Immune desert subclass showed the lower Immune score and

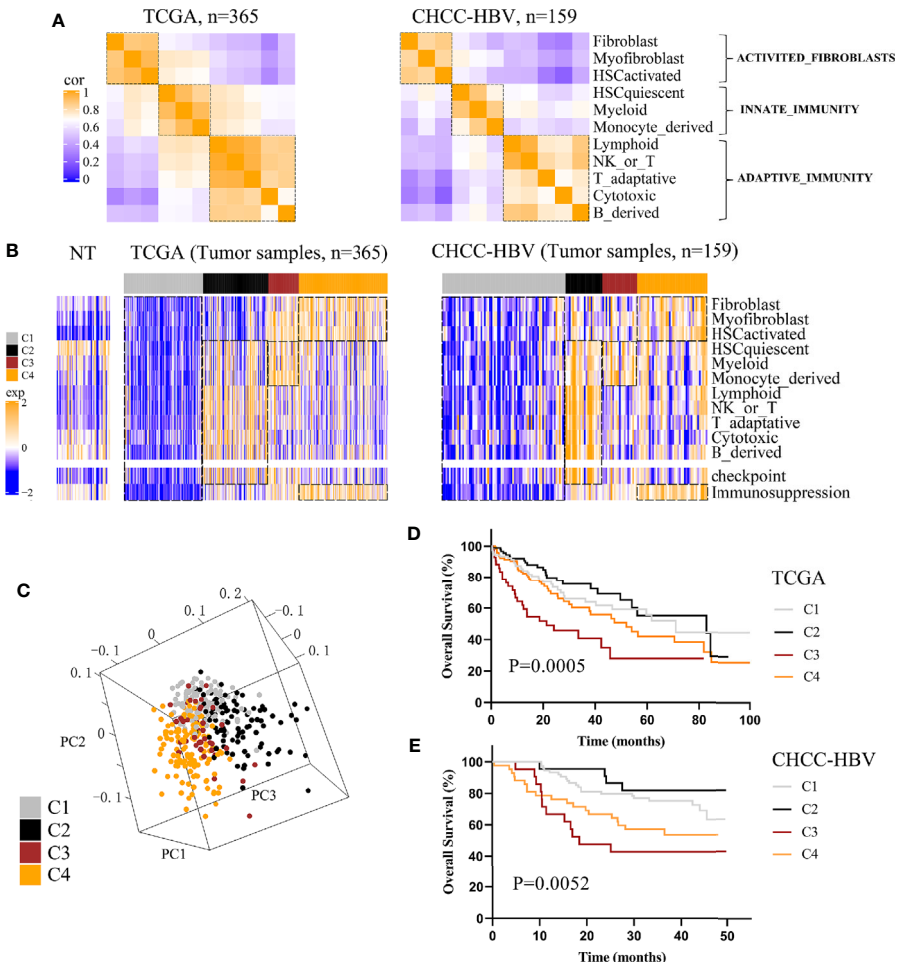

FIGURE 1 | Classification based on tumor microenvironment stratifies HCCs into four subclasses. **(A)** Correlation heatmap of 11 TME cell signatures in two data sets. Color scale: Spearman correlation coefficient from 0 (blue) to 1 (orange). **(B)** Consensus clustering analysis of two data sets revealed four HCC subclasses based on 13 TME signatures. Color scale: Z score from -2 (blue) to +2 (orange). **(C)** Principal-component analysis based on 13 TME signatures separated different subclasses in TCGA cohort. Kaplan-Meier curves of overall survival for TCGA cohort **(D)** and CHCC-HBV cohort **(E)** based on immune subclasses (log-rank test).

Stromal score, while C2 Immunogenic subclass and C4 Mesenchymal subclass showed the highest Immune score and Stromal score, respectively (**Supplementary Figure 4**). CIBERSORT analysis revealed significant difference in 16 out of 22 tumor-infiltrating immune cells, especially an enrichment of $CD4^+$ and $CD8^+$ T cells in C2, as well as an enrichment of M2 macrophages in C3 (**Supplementary Table S2**). The results of ESTIMATE and CIBERSORT further confirmed the characteristics of the four subclasses defined by MCP-counter.

To explore the functional differences among these four subclasses, we performed GSVA enrichment analysis on TCGA cohort (**Figure 2A**, **Supplementary Table S3**). C1 Immune desert subclass showed a highly attenuation of stromal and immune pathways. C2 Immunogenic subclass showed an enrichment of immune response, such as major histocompatibility complex (MHC) class I and class II biosynthesis, B cell mediated immunity and chemotaxis, T cell cytotoxicity, $CD8^+$ T cell activation and differentiation, T cell survival, and immune checkpoint pathway (CTLA4 and PD-1). C3 Innate immune subclass was enriched in macrophage activation, M2 macrophage polarization, TLR3 and LPS signaling. C3 subclass also showed an enrichment of T cell activation and cytotoxicity pathway, but not of T cell survival (different with C2 subclass). These results may account for the lack of adaptive immunity in C3 subclass. C4 subclass was remarkably enriched in activated HSC and stromal pathways such as ECM assembly, EMT, angiogenesis, TGF beta, integrin signaling pathway. The expressions of genes belonging to several immune pathways confirmed the differences among the four subclasses (**Figure 2B**). Markers of macrophage chemotaxis were increased in both C2 and C3, while C3 showed higher expression of macrophage activation. Moreover, the increases in markers of T cell survival, T cell chemotaxis and activation were observed in C2. Markers of all the pathways were low expressed in C1. Specially, compared to the other subclass, C2 subclass showed the both higher

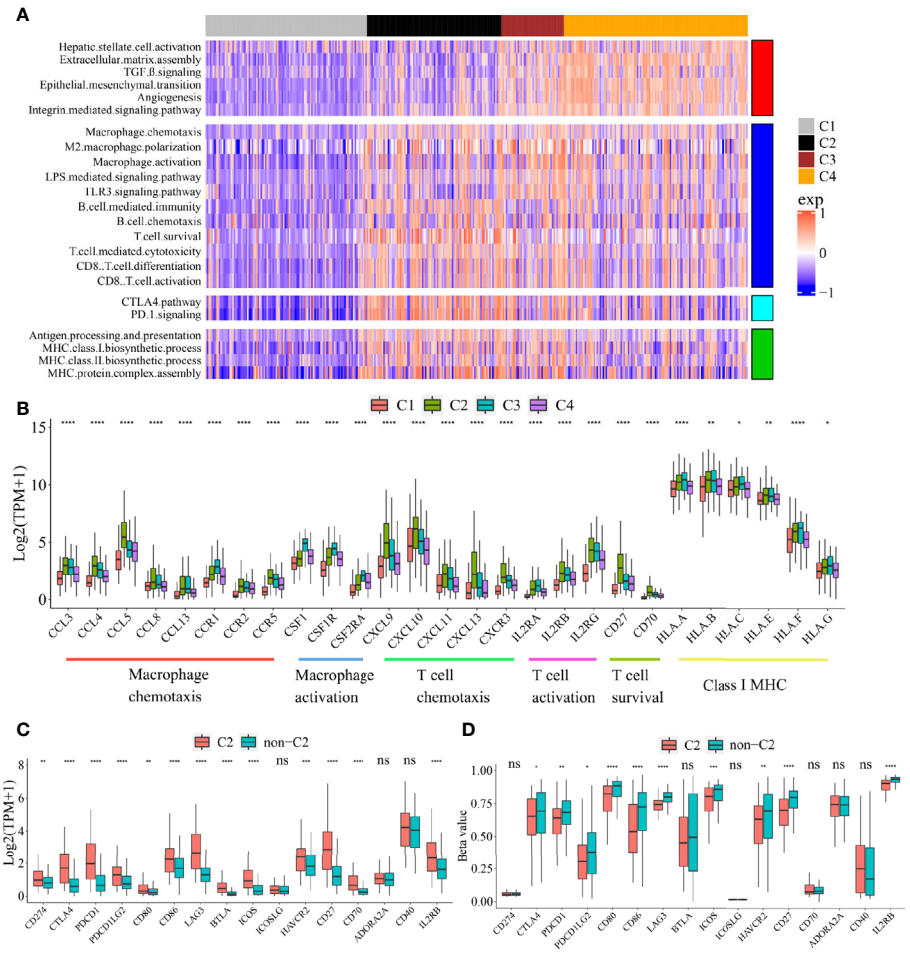

FIGURE 2 | Functional characteristics of four immune subclasses. **(A)** Heatmap of GSVA scores for indicated functional signatures. Color scale: GSVA score from −1 (blue) to +1(red). **(B)** Boxplot plot of the expression levels for selected immune-related pathways. (One-way ANOVA test). Boxplot of the expression **(C)** and methylation **(D)** levels of immune checkpoint-related genes between C2 and non-C2 subclass. (Student's t test). All P values labels: ns P > 0.05, *P < 0.05, **P < 0.01, ***P < 0.001, ****P < 0.0001). Error bars are presented as the standard deviation (SD).

expressions and methylation levels of checkpoint-related genes obtained from bulk tumor tissues, which indicated that the overexpression of checkpoints in C2 subclass was potentially triggered by hypomethylation of these genes (**Figures 2C, D**) (22).

Mutational Landscape of the Immune Subclasses

Somatic alterations have been proven to be correlated with TME (23). We analyzed somatic mutation data from the whole tumor of several genes with high frequency of mutation and in specific pathways, such as P53-pathway, Wnt-pathway, Chromatin modifiers pathway, and hepatic differentiation from TCGA-LIHC cohort (**Figure 3A**, **Supplementary Table S4**) (24). C1 subclass showed the highest mutation frequency of CTNNB1 ($P < 0.0001$), while the highest mutation frequency of ARID2 ($P = 0.049$) was observed in C2 subclass (**Figure 3B**, **Supplementary Table S4**). The highest mutation frequency of TP53 was observed in C3 subclass ($P = 0.015$). Then, we compared the tumor mutation burden and predicted neoantigens among these four subclasses (**Figures 3C, D**). The lowest tumor mutation burden and numbers of predicted neoantigens were detected in C4 subclass. Moreover, in CHCC-HBV cohort, Gao et al. found that signature for aristolochic acids (AA signature) was correlated to tumor mutation burden and response to immunotherapy. In CHCC-HBV cohort, C4 subclass also showed a lower proportion of AA signature than other three subclasses, which indicated a lower benefit from checkpoint blockade therapy (**Figure 3E**).

Associations Between Immune Subclass and Clinical Characteristic in TCGA and CHCC-HBV Cohort

Next, we discovered the associations between clinical characteristics and immune subclass in TCGA and CHCC-HBV cohort (**Figure 4**, **Supplementary Table S5, S6**). The patients from C2 subclass had a higher proportion of

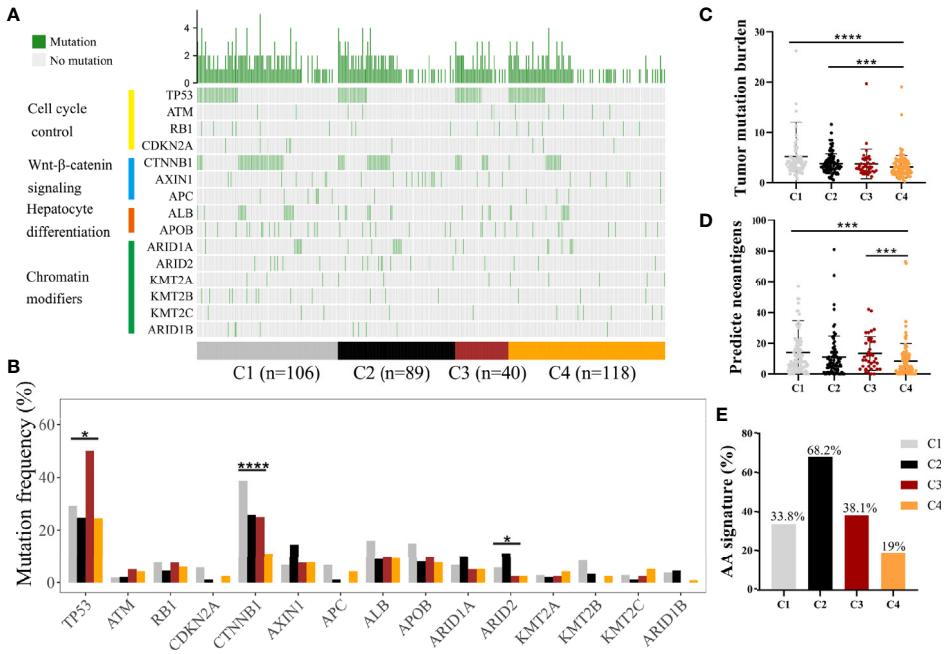

FIGURE 3 | Differences in the mutational landscape among distinct immune subclasses. **(A)** Oncoplot of tumor somatic mutation of genes in P53 pathway, Wnt/beta-catenin pathway, Chromatin modifiers pathway and hepatic differentiation based on TCGA cohort. **(B)** Comparisons of the frequently mutated genes among four immune subclasses based on TCGA cohort. (Fisher's exact test). Comparison of tumor mutation burden **(C)** and predicted neoantigens **(D)** among four immune subclasses. (Wilcoxon rank sum test). **(E)** The proportion of patients with AA signature among distinct subclasses in CHCC-HBV cohort. *P < 0.05, **P < 0.01, ***P < 0.001, ****P < 0.0001.

pathologic stage I/II (TCGA: P = 0.002, CHCC-HBV: P = 0.011). Patients from C3 subclass showed a higher proportion of HBV infection (P = 0.048). Most of the clinicopathological characteristics did not show significant differences, which suggested that the main factors distinguishing distinct immune subclass were the TME signatures, rather than the above-mentioned clinical features.

Furthermore, we compared our classification with several previous reported classifications based on transcriptomic, including Lee's classification (High/Low survival), Boyault's classification (G1 to G6), Chiang's classification (five classes), Hoshida's classification (S1 to S3), and Lachenmayer's classification (CTNNB1 class/Wnt-TGF-beta class) (25–29). In TCGA and CHCC-HBV cohort, C1 subclass was co-clustered with the better-prognosis subclasses (Lee's High survival, Boyault's G5&6, Chiang's CTNNB1 class, Hoshida's S3, Lachenmayer's CTNNB1-class). C3 subclass was largely co-clustered with poor-prognosis subclasses (Lee's Low survival, Boyault's G3, Chiang's Proliferation class, Hoshida's S1, Lachenmayer's Wnt-TGF-beta class). C2 subclass was linked to both better-prognosis subclass (Lee's High survival, Hoshida's S3) and poor-prognosis subclasses (Boyault's G1&G2, Chiang's Proliferation, Wnt-TGF beta class). C4 subclass was co-clustered with Lee's Low survival, Boyault's G1&G2, Chiang's Proliferation and Interferon class, Hoshida's S3, Lachenmayer's Wnt-TGF-beta class.

Construction and Validation of a Classifier Based on TME

Characteristics of the clinical traits and biological behaviors among four immune subclasses supported our classification. To apply this classification on clinical use, we developed a Support Vector Machine model to classify HCC patients into above four immune subclasses. The input was the 13 TME signatures of each case from the above data sets, and the output was the immune subclass of each case calculated by this model. The ROC curve represents the accuracy between the subclass clustered in **Figure 1B** and **Supplementary Figure 3B** and the subclass predicted by this SVM model. As **Figures 5A–C** showed, these 13 TME signatures revealed a great classification performance in both discovery phase (TCGA cohort: AUC = 0.98) and validation phases (CHCC-HBV cohort: AUC = 0.91; GSE14520 cohort: AUC = 0.85). Furthermore, we applied this classifier model on 32 HBV-related HCC patients (Zhejiang cohort) to divide these patients into four subclasses. We selected a random sample from each subclass to perform immunohistochemical staining for verifying the accuracy of our classifier model (**Figure 5D**, **Supplementary Figure 5**). Several markers of immune and stromal cells were selected, specifically, CD4 and CD8 for T-lymphocytes, CD20 for B-lymphocytes, CD68 for macrophages, αSMA for fibroblastic cells and Vimentin for mesenchymal cells. These markers varied markedly among four subclasses. The expression of Vimentin and αSMA was low

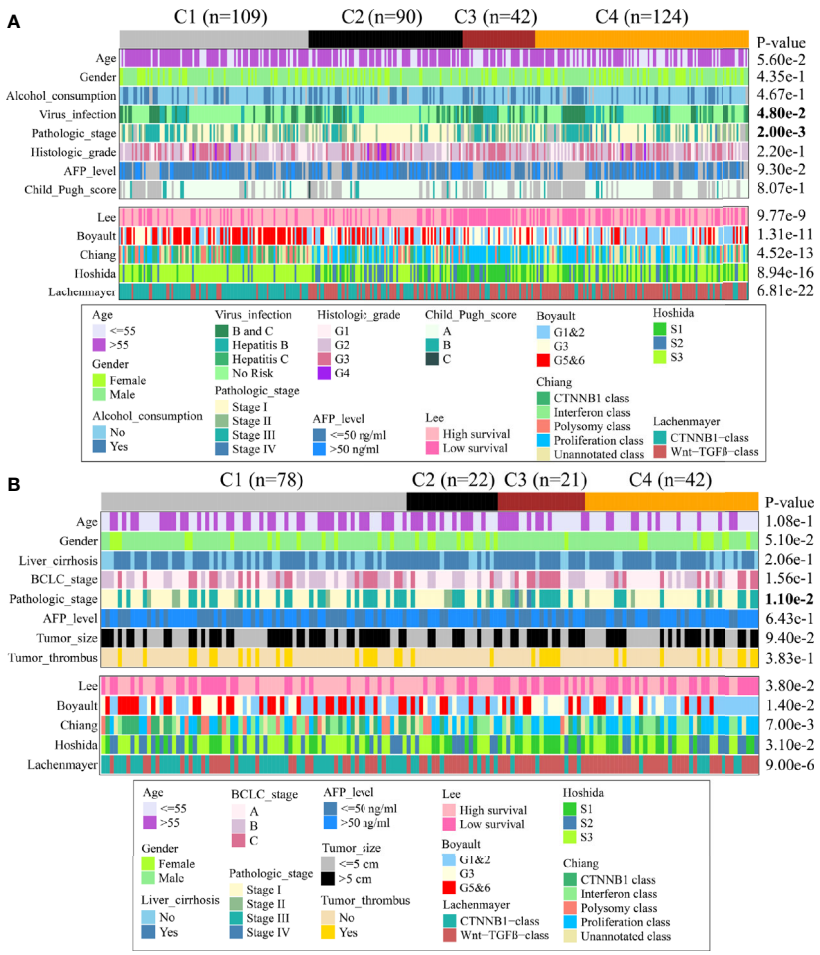

FIGURE 4 | Clinical characteristics of four immune subclasses. Correlation of the immune subclass with clinical characteristics and previously reported HCC classification in TCGA cohort **(A)** and CHCC-HBV cohort **(B)**.

in the patient classified into subclass C1, moderate in subclass C2 and C3, high in subclass C4. The patient classified into subclass C2 was characterized by the massive infiltration $CD4^+$, $CD8^+$ and $CD20^+$ lymphocytes. Innate immune cells (macrophages) were also observed in subclass C2. Subclass C3 displayed a high infiltration of macrophages. Subclass C4 contained a low density of macrophages and $CD4^+$ T cells. Thus, based on immunohistochemistry, the phenotypic features of HCC tumors were consistent with the classification of our SVM model. The results of immunohistochemistry not only partially proved the accuracy of our model, but also supported the rationality of the classification of four immune-related subclasses.

Different Sensitivity to Personalized Treatment Among Four Immune Subclasses

In HCC patients with Child-Pugh Class A or B, the multi-kinase inhibitor sorafenib has become the first-line systemic therapy (30). However, there were still no effective clinical characteristics to predict the response to sorafenib so far. Several recent studies suggested that sorafenib may exert the anti-tumor effect by regulating the TME of HCC (31, 32). By our SVM classifier, 67 patients from GSE109211 were divided into four subclasses to explore the associations between the immune subclass and the response to sorafenib. We found that 81% cases of C2 subclass showed a significant response to sorafenib, indicating that patients from Immunogenic subclass were more likely to benefit from sorafenib treatment (**Figure 6A**). As Pinyol and colleagues divided these 67 patients into Good/Poor Prognosis subgroups, C2 subclass was also coclustered with the Good Prognosis subgroup (95%) (**Figure 6B**).

In recent years, some immunotherapies like PD-1 blockade have achieved success in HCC (33). Different immune cell infiltrations and expressions of checkpoint-related genes suggested that four immune subclasses could have the distinct response to immunotherapy (34). We tried to apply our model on another pembrolizumab-treated cohort (GSE78220). The highest response rate (77.8%) to pembrolizumab was observed

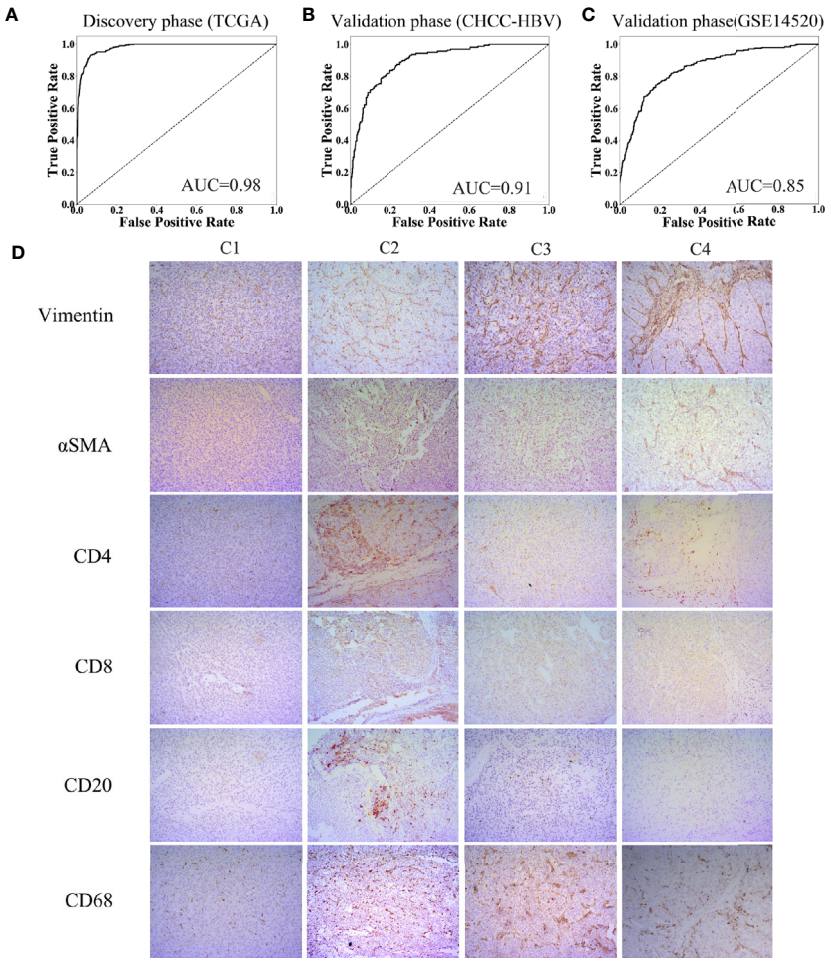

FIGURE 5 | Construction of support vector machine model and performance validation. ROC curves for classifiers designed to predict the immune subclass for TCGA **(A)**, CHCC-HBV **(B)**, and GSE14520 **(C)**. **(D)** Representative immunohistochemical pictures of HCC samples belonging to each subclass (100X) (Zhejiang cohort).

in patients belonging to C2 subclass with the best outcome (**Figures 6C, D**). The results indicated that HCC patients belonging to immunogenic subclass may benefit from anti-PD-1 therapy inferentially.

DISCUSSION

Although there is a strong heterogeneity in the tumor immune microenvironment of each HCC patient, a clinical benefit could be made from classifying a patient into a specific immune subclass. After analyzing the landscapes of transcriptome, methylation, somatic mutation, and clinical characteristics, we found that these four subclasses may correspond to different mechanisms of immune escape (**Figure 6E**). Immune desert subclass (C1) is characterized by immune ignorance and a lack of priming T cell, corresponding to immune-desert phenotype. The activation of the β-catenin caused by CTNNB1 mutation might account for the low immune infiltration represented in C1 (35). Immunogenic subclass (C2) is characterized by a massive immune cell ($CD4^+$ T cell, $CD8^+$ T cell, B cell, and macrophage) infiltration in tumor corresponding to immune-inflamed phenotype. Negative regulators of the immune response (PD-L1, CTLA4, etc.) might be involved in counteraction of anti-tumor immune response (36). A mount of patients belonging to C2 subclass showed a low pathological stage (TNM stage). In line with our study, several studies demonstrated that the tumors in low pathologic stage usually infiltrated with numerous immune cells. The patients belonging to C2 subclass showed the highest mutation frequency of ARID2 which was related to the efficacy of checkpoint blockade immunotherapy in clear cell renal cell carcinoma (37). Innate immune subclass (C3) is characterized by the activation of M2 macrophages (related to innate immunity). M2 macrophage, which exerts the anti-inflammatory and immunosuppressive effects, might promote the immune escape represented in C3 subclass through inhibiting the infiltration of adaptive immune cells (38). Mesenchymal subclass (C4) shows a large number of

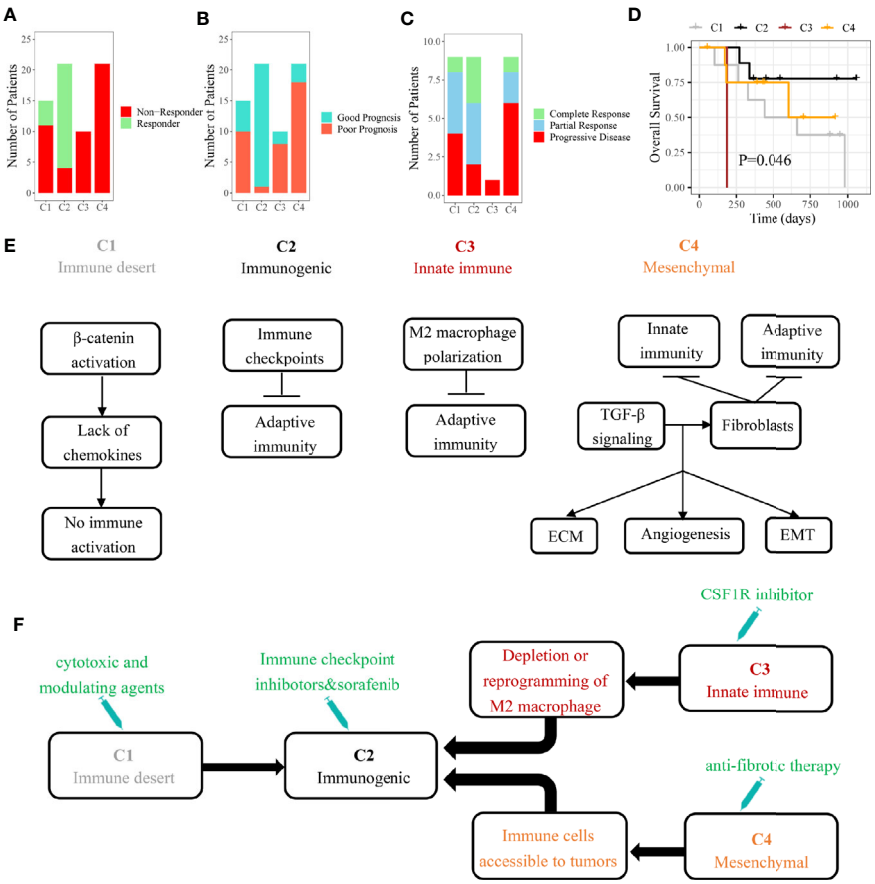

FIGURE 6 | The role of immune subclass in personalized treatment and schematic summary of each immune subclass. **(A)** The number of patients with response to sorafenib. **(B)** The number of patients belonged to good or poor prognosis subgroup. **(C)** The number of patients with response to anti-PD-1 therapy. **(D)** Kaplan-Meier curves of overall survival for GSE78220 cohort (log-rank test, P = 0.046). **(E)** The mechanisms of immune escape for each immune subclass. **(F)** Potential therapeutic strategies for each immune subclass.

activated fibroblasts (including HSC and myofibroblast) which influence EMT and the sensitivity of drug treatment through synthesizing growth factors, chemokines and adhesion molecules (39).

Kaplan-Meier analysis based on 766 participants showed that significant differences in overall survival were discovered to exist among our four immune subclasses. Immunogenic subclass (C2) represented the best clinical outcome, while innate immune subclass (C3) have the worst. This suggested that the different TME continuously and chronically affects the progression of HCC, which is ultimately reflected in the different clinical outcome. Based on the RNA-seq data from bulk tumor tissues, our convenient classification dividing the patients into four subclasses may infer the prognosis. What is more, the conversions of the immune subclasses by external interventions may benefit the long-term clinical results and outcomes of HCC patients.

Additionally, we established an SVM model based on the 13 TME signatures (11 immune-related cells and 2 immune-related pathways) and confirmed its predictive value (CHCC-HBV cohort: AUC = 0.91; GSE14520 cohort: AUC = 0.85). The input (13 TME signatures) of the SVM model were calculated by MCP-counter based on transcriptomic data, while giving a specific output (which immune subclass). Thanks to the wide applications of RNA-seq, our workflow only required frozen/fresh tissue samples (< 100 mg), as well the model constructed on python was convenient and efficient. The immunohistochemistry from each subclass proved not only the rationality of the TME classification but also the accuracy of the SVM model (**Figure 5D**). Accordingly, this suggested that for any HCC patient undergoing liver biopsy or liver resection, our SVM model can be used to infer the prognosis and guide the follow-up treatment.

HCC patients may benefit from identifying immune subclass which may guide personalized treatment strategies (**Figure 6F**). In our study, we found that the patients belonging to C2 subclass might be more suitable for sorafenib and anti-PD-1 therapy. According to the reported study, the patients belonging to C3 subclass could be treated with colony-stimulating factor-1 inhibitor which improved the efficacy of immunotherapy through inhibiting the intertumoral accumulation of M2 macrophages (40, 41). For the abundant fibrous stroma

observed in C4 subclass, anti-fibrosis drugs (like NOX4 inhibitor) suppressed the activation of cancer-associated fibroblasts and promoted the infiltration of $CD8^+$ T cells, ultimately improving the efficacy of immunotherapy (42). As for C1 subclass, the application of cytotoxic and modulating agents which can convert cold tumors to inflamed tumors was a potential strategy (43).

Our workflow is limited by the HCC patients obtained specimens for the first time, as well as the influences of confounding variables such as HBV/HCV infection, alcoholic fatty liver, non-alcoholic fatty liver, and cirrhosis were not considered. We will improve them in the future work.

In conclusion, our study dementated a new landscape for the composition of HCC tumor microenvironment. We identified four immune subclasses with distinct mechanisms of immune escape. The patients from distinct subclasses showed a significant difference in clinical prognosis and response to personalized treatment. Based on transcriptome data, our workflow might help to predict the clinical outcome and to find appropriate treatment strategies for HCC patients.

DATA AVAILABILITY STATEMENT

The data sets presented in this study can be found in online repositories. The names of the repository/repositories and accession number(s) can be found in the article/**Supplementary Material**.

ETHICS STATEMENT

The studies involving human participants were reviewed and approved by the Clinical Research Ethics Committee of the First Affiliated Hospital College of Medicine, Zhejiang University (2014-334). The patients/participants provided written informed consent to participate in this study. Written informed consent was obtained from the individuals for the publication of any potentially identifiable images or data included in this article.

AUTHOR CONTRIBUTIONS

Study concept and design: SZ, LZ, and XG. Analysis and interpretation of data: XG. Technical and material support: SY, YW, and CP. Drafting of the manuscript: SZ, LZ, and HH. All authors contributed to the article and approved the submitted version.

FUNDING

This study was supported by Zhejiang Provincial Public Welfare Technology Research Program (LGF18C100001). This study was also supported by Innovative Research Groups of National Natural Science Foundation of China (no. 81721091), National S&T Major Project of China (no. 2017ZX100203205) and Research Unit Project of Chinese Academy of Medical Sciences (2019-I2M-5-030). This study was also supported by Zhejiang International Science and Technology Cooperation Project (no. 2016C04003).

SUPPLEMENTARY MATERIAL

The Supplementary Material for this article can be found online at: https://www.frontiersin.org/articles/10.3389/fonc.2020.610513/full#supplementary-material

REFERENCES

1. Bray F, Ferlay J, Soerjomataram I, Siegel RL, Torre LA, Jemal A. Global cancer statistics 2018: GLOBOCAN estimates of incidence and mortality worldwide for 36 cancers in 185 countries. *CA Cancer J Clin* (2018) 68:394–424. doi: 10.3322/caac.21492
2. Hou J, Zhang H, Sun B, Karin M. The immunobiology of hepatocellular carcinoma in humans and mice: Basic concepts and therapeutic implications. *J Hepatol* (2020) 72:167–82. doi: 10.1016/j.jhep.2019.08.014
3. Prieto J, Melero I, Sangro B. Immunological landscape and immunotherapy of hepatocellular carcinoma. *Nat Rev Gastroenterol Hepatol* (2015) 12:681–700. doi: 10.1038/nrgastro.2015.173
4. Lu C, Rong D, Zhang B, Zheng W, Wang X, Chen Z, et al. Current perspectives on the immunosuppressive tumor microenvironment in hepatocellular carcinoma: challenges and opportunities. *Mol Cancer* (2019) 18:130. doi: 10.1186/s12943-019-1047-6
5. Hegde PS, Chen DS. Top 10 Challenges in Cancer Immunotherapy. *Immunity* (2020) 52:17–35. doi: 10.1016/j.immuni.2019.12.011
6. Hegde PS, Karanikas V, Evers S. The Where, the When, and the How of Immune Monitoring for Cancer Immunotherapies in the Era of Checkpoint Inhibition. *Clin Cancer Res* (2016) 22:1865–74. doi: 10.1158/1078-0432.CCR-15-1507
7. Thorsson V, Gibbs DL, Brown SD, Wolf D, Bortone DS, Ou Yang TH, et al. The Immune Landscape of Cancer. *Immunity* (2018) 48:812–30.e14. doi: 10.1016/j.immuni
8. Sturm G, Finotello F, Petitprez F, Zhang JD, Baumbach J, Fridman WH, et al. Comprehensive evaluation of transcriptome-based cell-type quantification methods for immuno-oncology. *Bioinformatics* (2019) 35:i436–45. doi: 10.1093/bioinformatics/btz363
9. Zhang Q, He Y, Luo N, Patel SJ, Han Y, Gao R, et al. Landscape and Dynamics of Single Immune Cells in Hepatocellular Carcinoma. *Cell* (2019) 179:829–45.e20. doi: 10.1016/j.cell.2019.10.003
10. Becht E, Giraldo NA, Lacroix L, Buttard B, Elarouci N, Petitprez F, et al. Estimating the population abundance of tissue-infiltrating immune and stromal cell populations using gene expression. *Genome Biol* (2016) 17:218. doi: 10.1186/s13059-016-1070-5
11. Newman AM, Liu CL, Green MR, Gentles AJ, Feng W, Xu Y, et al. Robust enumeration of cell subsets from tissue expression profiles. *Nat Methods* (2015) 12:453–7. doi: 10.1038/nmeth.3337
12. Li T, Fan J, Wang B, Traugh N, Chen Q, Liu JS, et al. TIMER: A Web Server for Comprehensive Analysis of Tumor-Infiltrating Immune Cells. *Cancer Res* (2017) 77:e108–10. doi: 10.1158/0008-5472.CAN-17-0307
13. Gao Q, Zhu H, Dong L, Shi W, Chen R, Song Z, et al. Integrated Proteogenomic Characterization of HBV-Related Hepatocellular Carcinoma. *Cell* (2019) 179:561–77.e22. doi: 10.1016/j.cell.2019.08.052
14. Roessler S, Jia HL, Budhu A, Forgues M, Ye QH, Lee JS, et al. A unique metastasis gene signature enables prediction of tumor relapse in early-stage hepatocellular carcinoma patients. *Cancer Res* (2010) 70:10202–12. doi: 10.1158/0008-5472.CAN-10-2607

15. Hugo W, Zaretsky JM, Sun L, Song C, Moreno BH, Hu-Lieskovan S, et al. Genomic and Transcriptomic Features of Response to Anti-PD-1 Therapy in Metastatic Melanoma. *Cell* (2016) 165:35–44. doi: 10.1016/j.cell.2016.02.065
16. Pinyol R, Montal R, Bassaganyas L, Sia D, Takayama T, Chau GY, et al. Molecular predictors of prevention of recurrence in HCC with sorafenib as adjuvant treatment and prognostic factors in the phase 3 STORM trial. *Gut* (2019) 68:1065–75. doi: 10.1136/gutjnl-2018-316408
17. Huang H, Ren Z, Gao X, Hu X, Zhou Y, Jiang J, et al. Integrated analysis of microbiome and host transcriptome reveals correlations between gut microbiota and clinical outcomes in HBV-related hepatocellular carcinoma. *Genome Med* (2020) 12:102. doi: 10.1186/s13073-020-00796-5
18. Job S, Rapoud D, Dos Santos A, Gonzalez P, Desterke C, Pascal G, et al. Identification of Four Immune Subtypes Characterized by Distinct Composition and Functions of Tumor Microenvironment in Intrahepatic Cholangiocarcinoma. *Hepatology* (2020) 72:965–81. doi: 10.1002/hep.31092
19. Yoshihara K, Shahmoradgoli M, Martínez E, Vegesna R, Kim H, Torres-Garcia W, et al. Inferring tumour purity and stromal and immune cell admixture from expression data. *Nat Commun* (2013) 4:2612. doi: 10.1038/ncomms3612
20. Wilkerson MD, Hayes DN. ConsensusClusterPlus: a class discovery tool with confidence assessments and item tracking. *Bioinformatics* (2010) 26:1572–3. doi: 10.1093/bioinformatics/btq170
21. Hanzelmann S, Castelo R, Guinney J. GSVA: gene set variation analysis for microarray and RNA-seq data. *BMC Bioinf* (2013) 14:7. doi: 10.1186/1471-2105-14-7
22. Emran AA, Chatterjee A, Rodger EJ, Tiffen JC, Gallagher SJ, Eccles MR, et al. Targeting DNA Methylation and EZH2 Activity to Overcome Melanoma Resistance to Immunotherapy. *Trends Immunol* (2019) 40:328–44. doi: 10.1016/j.it.2019.02.004
23. Rooney MS, Shukla SA, Wu CJ, Getz G, Hacohen N. Molecular and genetic properties of tumors associated with local immune cytolytic activity. *Cell* (2015) 160:48–61. doi: 10.1016/j.cell.2014.12.033
24. Llovet JM, Montal R, Sia D, Finn RS. Molecular therapies and precision medicine for hepatocellular carcinoma. *Nat Rev Clin Oncol* (2018) 15:599–616. doi: 10.1038/s41571-018-0073-4
25. Lee JS, Chu IS, Heo J, Calvisi DF, Sun Z, Roskams T, et al. Classification and prediction of survival in hepatocellular carcinoma by gene expression profiling. *Hepatology* (2004) 40:667–76. doi: 10.1002/hep.20375
26. Boyault S, Rickman DS, de Reyniès A, Balabaud C, Rebouissou S, Jeannot E, et al. Transcriptome classification of HCC is related to gene alterations and to new therapeutic targets. *Hepatology* (2007) 45:42–52. doi: 10.1002/hep.21467
27. Chiang DY, Villanueva A, Hoshida Y, Peix J, Newell P, Minguez B, et al. Focal gains of VEGFA and molecular classification of hepatocellular carcinoma. *Cancer Res* (2008) 68:6779–88. doi: 10.1158/0008-5472.CAN-08-0742
28. Hoshida Y, Nijman SM, Kobayashi M, Chan JA, Brunet JP, Chiang DY, et al. Integrative transcriptome analysis reveals common molecular subclasses of human hepatocellular carcinoma. *Cancer Res* (2009) 69:7385–92. doi: 10.1158/0008-5472.CAN-09-1089
29. Lachenmayer A, Alsinet C, Savic R, Cabellos L, Toffanin S, Hoshida Y, et al. Wnt-pathway activation in two molecular classes of hepatocellular carcinoma and experimental modulation by sorafenib. *Clin Cancer Res* (2012) 18:4997–5007. doi: 10.1158/1078-0432.CCR-11-2322
30. Benson AB3, D'Angelica MI, Abbott DE, Abrams TA, Alberts SR, Saenz DA, et al. NCCN Guidelines Insights: Hepatobiliary Cancers, Version 1.2017. *J Natl Compr Canc Netw* (2017) 15:563–73. doi: 10.6004/jnccn.2017.0059
31. Sprinzl MF, Reisinger F, Puschnik A, Ringelhan M, Ackermann K, Hartmann D, et al. Sorafenib perpetuates cellular anticancer effector functions by modulating the crosstalk between macrophages and natural killer cells. *Hepatology* (2013) 57:2358–68. doi: 10.1002/hep.26328
32. Chen ML, Yan BS, Lu WC, Chen MH, Yu SL, Yang PC, et al. Sorafenib relieves cell-intrinsic and cell-extrinsic inhibitions of effector T cells in tumor microenvironment to augment antitumor immunity. *Int J Cancer* (2014) 134:319–31. doi: 10.1002/ijc.28362
33. El-Khoueiry AB, Sangro B, Yau T, Crocenzi TS, Kudo M, Hsu C, et al. Nivolumab in patients with advanced hepatocellular carcinoma (CheckMate 040): an open-label, non-comparative, phase 1/2 dose escalation and expansion trial. *Lancet* (2017) 389:2492–502. doi: 10.1016/S0140-6736(17)31046-2
34. Gibney GT, Weiner LM, Atkins MB. Predictive biomarkers for checkpoint inhibitor-based immunotherapy. *Lancet Oncol* (2016) 17:e542–51. doi: 10.1016/S1470-2045(16)30406-5
35. Berraondo P, Ochoa MC, Olivera I, Melero I. Immune Desertic Landscapes in Hepatocellular Carcinoma Shaped by β-Catenin Activation. *Cancer Discovery* (2019) 9:1003–5. doi: 10.1158/2159-8290.CD-19-0696
36. Pardoll DM. The blockade of immune checkpoints in cancer immunotherapy. *Nat Rev Cancer* (2012) 12:252–64. doi: 10.1038/nrc3239
37. Miao D, Margolis CA, Gao W, Voss MH, Li W, Martini DJ, et al. Genomic correlates of response to immune checkpoint therapies in clear cell renal cell carcinoma. *Science* (2018) 359:801–6. doi: 10.1126/science.aan5951
38. Noy R, Pollard JW. Tumor-associated macrophages: from mechanisms to therapy. *Immunity* (2014) 41:49–61. doi: 10.1016/j.immuni.2014.06.010
39. Trédan O, Galmarini CM, Patel K, Tannock IF. Drug resistance and the solid tumor microenvironment. *J Natl Cancer Inst* (2007) 99:1441–54. doi: 10.1093/jnci/djm135
40. Mok S, Koya RC, Tsui C, Xu J, Robert L, Wu L, et al. Inhibition of CSF-1 receptor improves the antitumor efficacy of adoptive cell transfer immunotherapy. *Cancer Res* (2014) 74:153–61. doi: 10.1158/0008-5472.CAN-13-1816
41. Paulus P, Stanley ER, Schäfer R, Abraham D, Aharinejad S. Colony-stimulating factor-1 antibody reverses chemoresistance in human MCF-7 breast cancer xenografts. *Cancer Res* (2006) 66:4349–56. doi: 10.1158/0008-5472.CAN-05-3523
42. Ford K, Hanley CJ, Mellone M, Szyndralewiez C, Heitz F, Wiesel P, et al. NOX4 Inhibition Potentiates Immunotherapy by Overcoming Cancer-Associated Fibroblast-Mediated CD8 T-cell Exclusion from Tumors. *Cancer Res* (2020) 80:1846–60. doi: 10.1158/0008-5472.CAN-19-3158
43. Galon J, Bruni D. Approaches to treat immune hot, altered and cold tumours with combination immunotherapies. *Nat Rev Drug Discovery* (2019) 18:197–218. doi: 10.1038/s41573-018-0007-y

Conflict of Interest: The authors declare that the research was conducted in the absence of any commercial or financial relationships that could be construed as a potential conflict of interest.

frontiers in Oncology

ORIGINAL RESEARCH
published: 25 February 2021
doi: 10.3389/fonc.2021.605234

Evaluation of the Therapeutic Effect of Adjuvant Transcatheter Arterial Chemoembolization Based on Ki67 After Hepatocellular Carcinoma Surgery

Yu-Fei Zhao†, Xiu Xiong†, Kai Chen†, Wei Tang†, Xu Yang† and Zheng-Rong Shi†*

Department of Hepatobiliary Surgery, The First Affiliated Hospital of Chongqing Medical University, Chongqing, China

OPEN ACCESS

Edited by:
Michael David Chuong, Baptist Health South Florida, United States

Reviewed by:
Jiwei Huang, Sichuan University, China
Yun-Fan Sun, Fudan University, China

***Correspondence:**
Zheng-Rong Shi
shizhengrongcqmu@163.com

†ORCID:
Yu-Fei Zhao
orcid.org/0000-0001-7451-2138
Xiu Xiong
orcid.org/0000-0003-4086-7664
Kai Chen
orcid.org/0000-0003-1083-073X
Wei Tang
orcid.org/0000-0001-7411-3268
Xu Yang
orcid.org/0000-0001-9650-1878
Zheng-Rong Shi
orcid.org/0000-0003-4252-768X

Specialty section:
This article was submitted to Gastrointestinal Cancers, a section of the journal Frontiers in Oncology

Received: *11 September 2020*
Accepted: *20 January 2021*
Published: *25 February 2021*

Citation:
Zhao Y-F, Xiong X, Chen K, Tang W, Yang X and Shi Z-R (2021) Evaluation of the Therapeutic Effect of Adjuvant Transcatheter Arterial Chemoembolization Based on Ki67 After Hepatocellular Carcinoma Surgery. Front. Oncol. 11:605234. doi: 10.3389/fonc.2021.605234

Background and aims: This study aimed to determine the relationship between Ki67 expression and the efficacy of postoperative adjuvant transcatheter arterial chemoembolization (PA-TACE) in patients with hepatocellular carcinoma.

Methods: The Kaplan-Meier method was used to analyze the recurrence-free survival (RFS) and overall survival (OS) rates between the sub-groups in the ki67 low expression group and the ki67 high expression group and analyze the relationship between the expression of Ki67 and the efficacy of TACE.

Results: After PSM, there was no significant difference in the RFS and OS between the surgery + TACE and surgery subgroups after 1, 2, or 3 years (RFS: 63.9%, 55.6%, and 42.9% vs. 83.3%, 63.9%, and 55.6%, respectively, P = 0.279; OS: 91.7%, 83.3%, and 74.3% vs. 91.7%, 88.9%, and 71.4%, respectively, P = 0.890) in the Ki67 low-expression group. The RFS and OS were higher in the surgery + TACE subgroup than the surgery subgroup after 1, 2, and 3 years (RFS: 80.0%, 77.5%, and 69.2% vs. 53.5%, 39.5%, and 32.6%, respectively, P<0.001; OS: 97.5%, 85.0%, and 79.5% vs. 79.1%, 48.8%, and 42.9%, respectively, P = 0.001) in the Ki67 high expression group. The RFS was higher in the Ki67 high-expression subgroup than the low-expression subgroup after 1, 2, and 3 years, and OS had no significant difference (RFS: 80.0%, 79.5%, and 69.2% vs. 67.4%, 56.5%, and 46.7%, respectively, P = 0.035; OS: 97.5%, 85.0%, and 79.5% vs. 93.5%, 82.6%, and 75.6%, respectively, P = 0.665) in the surgery + TACE group.

Conclusions: For patients with hepatocellular carcinoma and high expression of Ki67 (Ki67≥20%), adjuvant hepatic artery chemoembolization after radical liver tumor resection effectively reduced the probability of tumor recurrence after surgery and prolonged the OS of patients. High Ki67 expression during the post-operative follow-up evaluation of hepatocellular carcinoma patients is an indicator for adjuvant TACE therapy.

Keywords: hepatocellular carcinoma (HCC), ki67, postoperative adjuvant transcatheter arterial chemoembolization (PA-TACE), propensity score matching (PSM), prognosis

Abbreviations: PA-TACE, post-operative adjuvant transcatheter arterial chemoembolization; PSM, propensity score matching; RFS, recurrence-free survival; OS, overall survival; TACE, transcatheter arterial chemoembolization; DFS, disease-free survival; HCC, hepatocellular carcinoma.

INTRODUCTION

A radical liver resection is currently the most effective way to treat patients with hepatocellular carcinoma (HCC) (1), and studies have shown that the recurrence rate of patients undergoing radical liver resection alone is approximately 70% 5 years after surgery, while the 5-year survival rate is decreased by 24% in patients with a HCC recurrence compared to patients without a recurrence (2). Indeed, the median survival time is decreased by 54 months in patients with a HCC recurrent (2). Postoperative adjuvant treatment can effectively delay tumor recurrence and prolong the survival of patients. Specifically, transcatheter arterial chemoembolization (TACE) is currently the most widely used adjuvant treatment program for patients with HCC (3). A large number of studies in China and abroad have confirmed that for patients with tumors >5 cm in diameter, multinodular tumors, or MVI-positive HCC, post-operative adjuvant transcatheter arterial chemoembolization (PA-TACE) can effectively improve the overall survival (OS) and disease-free survival (DFS) (4); however, a clear standard for patients who will benefit from PA-TACE has not been established. Therefore, further research is needed to determine the selection criteria for patients who are candidates for TACE after radical liver resection. The development of a precise standard will facilitate clinical decision-making and treat patients in a timely fashion, thus improving the postoperative tumor recurrence and survival rates.

Ki67 is an antigen that reflects the active status of cell proliferation and is closely related to the prognosis of malignant tumors (5). Studies have shown that Ki67 is an independent risk factor for disease-free survival (DFS) and overall survival (OS) in HCC patients (6). Studies have shown that the expression of Ki67 in HCC patients is of considerable value in predicting the postoperative recurrence of HCC (7). The liver cancer blood supply is mainly provided by the hepatic artery, and TACE embolizes the main blood vessel supplying the tumor, resulting in ischemia and necrosis of the tumor tissue in the embolized area. TACE commonly uses chemotherapy drugs, such as oxaliplatin (8) and irinotecan (9), and epirubicin (10), which all have the main effect of inhibiting tumor cell proliferation and inhibiting DNA replication. We speculate that HCC patients with high expression of Ki67 have more active cell proliferation, and the therapeutic effect of postoperative adjuvant TACE will be better. If so, this approach can serve as a guide to determine if PA-TACE should be performed. At present, there are few studies involving Ki67 and PA-TACE in China and abroad (11). The current study will determine the relationship between the expression of Ki67 and the prognosis of patients undergoing radical liver resection and PA-TACE and to guide the use of adjuvant therapy.

MATERIALS AND METHODS

General Information

This study was performed under a human investigational protocol that was approved and monitored by the Institutional Review Board of The First Affiliated Hospital of Chongqing Medical University (the ethical approval number:2019-021). The Ethics Committee also approved the retrospective analysis of existing patient data without informed consent because of the low risk for breaching confidentiality. A retrospective analysis was conducted using the clinical data of patients with liver cancer who underwent radical liver resection in the Department of Hepatobiliary Surgery at the First Affiliated Hospital of Chongqing Medical University from January 2013 to June 2017. The inclusion criteria were as follows: 1) preoperative liver function Child-Pugh score A/B, and liver reserve function indicating sufficient residual liver volume; 2) radical liver tumor resection, and postoperative medical examination confirming that no cancer cells are involved in the resection margin; 3) hepatocellular carcinoma confirmed by postoperative medical examination and immunohistochemical analysis; 4) no portal vein or other large blood vessel invasion or distant metastasis; and 5) patients in the interventional group who received 1–2 TACE treatments after surgery. The exclusion criteria were as follows: 1) tumor recurrence demonstrated within 2 month after surgery or during TACE therapy; 2) co-existing tumors; 3) adjuvant treatments other than TACE performed during the interval between the first diagnosis of recurrence or metastasis after surgery; and 4) loss to follow-up in <1 year. A total of 180 patients with HCC after liver resection were enrolled; 94 patients underwent radical liver resection and 86 patients received adjuvant TACE treatment after liver resection. The clinical data (gender, age, hepatitis B history, co-existing liver cirrhosis, preoperative liver function, and preoperative AFP level) and related data (maximum diameter of lesions, MVI, the degree of tumor differentiation and expression of Ki67) were collected. The preoperative liver function was determined by the Child-Pugh score. The number and maximum diameter of the lesions in the surgically-resected specimens were measured. MVI, Liver cirrhosis, the degree of tumor differentiation and the Ki67 level was determined by a pathologist in the Pathology Department.

Tissue samples from non-necrotic areas were selected from HCC specimens obtained by surgery and fixed in 10% paraformaldehyde for 24 hours. They were then treated with tissue processor, dehydrated and embedded in paraffin. After sections, they were washed with phosphate buffer saline (PBS) for 5 min and added with 3% H_2O_2 at room temperature for 10 min. A primary antibodies raised against Ki67 was then added for immunohistochemical detection. Results were interpreted from active cancer tissues and phosphate buffer was used as negative control. Several high-magnification microscopic fields were observed randomly, the percentage of positive cells was calculated and the average value was calculated. All tissue specimens were examined and reported by a qualified pathologist in the Department of Pathology of our hospital. (Interpretation criteria: Ki67 positive cells with thick brown yellow particles in the nucleus were randomly selected from 5 different high-power fields to calculate the percentage of the number of Ki67 positive cells in the total number of observed cells).

Therapeutic Conditions

Preoperative liver function for all patients was rated as grade A/B and the imaging examinations showed no large vessel invasion or distant metastasis. Liver reserve function suggested that the

residual liver volume was sufficient postoperatively. When the tumor was confined locally or occupied one-half of the liver, an anatomic liver resection was performed. When multiple tumors occupied the two half-livers, tumor enucleations were performed separately. All postoperative adjuvant TACE patients were included in a multidisciplinary discussion (including hepatobiliary and pancreatic surgery, oncology, pathology, and radiology), and the patients at high risk of recurrences, such as maximum diameter of lesions >5 cm, MVI>M1 and less differentiated tumor after curative hepatectomy, TACE was indicated. Within 1 month after liver resection, the Seldinger technique was used to puncture the catheter through the femoral artery, and chemotherapy embolization was performed with injection of oxaliplatin, irinotecan, pirarubicin, or epirubicin and lipiodol in the proper hepatic artery. The dosage was determined based on body surface area and liver function. A total of 1–2 TACE treatments were given, with an interval of at least 3 weeks, and liver function was assessed before surgery to confirm the ability to withstand interventional therapy. None of the patients with HCC enrolled in the group received other types of adjuvant therapy, such as targeted therapy, immunotherapy, or absolute alcohol injection, from the time of surgery to the first diagnosis of a recurrence or metastasis.

Follow-Up

All patients were followed regularly in the outpatient clinics (every 3 months for 1 year after surgery, then every 6 months for 1 year). The outpatient follow-up evaluations included liver and kidney function tests, HBV-DNA quantification, tumor marker profile, abdominal color Doppler ultrasound or abdominal enhanced CT, and a chest CT scan. The endpoint of follow-up was June 20, 2020. The median duration of follow-up was 47 months (95% CI: 43.2–50.7 months). The diagnostic criteria for tumor recurrence were consistent with the initial diagnostic criteria for HCC. The follow-up endpoint of this study was tumor recurrence or metastasis, as indicated by imaging.

Statistics

SPSS 22.0 software was used for statistical analysis. The endpoint of the study was overall survival (OS). The OS was the time from the first operation to the death from any causes. Propensity score matching (PSM) was used to reduce the bias in clinical and medical examination data between the groups. The two groups were matched according to the 1:1 nearest neighbor matching method, and the standard deviation was <0.2. A $\chi 2$ test was used for comparisons between groups. The Kaplan-Meier method was used for survival analysis, and a log-rank test was used for comparisons between groups. The Cox risk ratio model was used to analyze independent risk factors affecting prognosis. A $P < 0.05$ was considered statistically significant.

RESULTS

Basic Information of Patients

From January 2013 to June 2017, a total of 180 patients with HCC underwent surgical treatment; 94 patients underwent radical liver resection alone (operating group) and 86 patients received adjuvant TACE treatment after liver resection (operation + TACE group). There was no statistical difference between the two groups with respect to clinical data (age, sex, hepatitis B history, preoperative liver function, and pre-operative AFP level) and disease examination-related data (number of lesions, maximum diameter of lesions, and expression of Ki67). The proportion of patients with liver cirrhosis in the pre-PSM surgery group was higher. After propensity matching eliminated the difference variables, 83 pairs of HCC patients were assigned. There was no statistical difference between the two covariates (P value >0.05, **Table 1**). The patients were divided into the Ki67 low- and high-expression subgroups. There was no statistical difference between the two groups with respect to clinical data and disease examination-related data (P value >0.05, **Table 2**).

We divided the 180 patients with HCC into 97 patients with low expression of Ki67 and 83 patients with high expression of Ki67 [a Ki67 < 20% was considered low expression and a Ki67 ≥ 20% was considered high expression (12)]. The two groups of patients were further divided into surgery and surgery + TACE sub-groups. In the Ki67 low expression group, the proportion of patients >55 years of age in the pre-PSM subgroup was higher than the surgery + TACE subgroup. After propensity score

TABLE 1 | Basic information of all patients in terms of treatment options[cases(%)].

Clinical data	Pre-PSM			After PSM		
	Operating group (n=94)	operation + TACE group (n=86)	P	Operating group (n=83)	operation + TACE group (n=83)	P
Age(>55)	51(54.3)	35(40.7)	0.069	43(51.8)	33(39.8)	0.119
Gender(male)	83(88.3)	74(86.0)	0.651	72(86.7)	71(85.5)	0.822
Hepatitis B history	81(86.2)	78(90.7)	0.345	73(88.0)	75(90.4)	0.618
Liver cirrhosis	66(70.2)	48(55.8)	0.045	55(66.3)	48(57.8)	0.263
Pre-operative liver function(A)	93(98.9)	83(96.5)	0.270	82(98.8)	80(96.4)	0.311
AFP(>200 μg/liter)	28(29.8)	26(30.2)	0.948	24(28.9)	24(28.9)	1.000
Number of lesions(single)	82(87.2)	66(76.7)	0.066	71(85.5)	65(78.3)	0.226
Maximum diameter of lesions(>5 cm)	50(53.2)	44(51.2)	0.785	40(48.2)	43(51.8)	0.641
Ki67 (high expression)	43(45.7)	40(46.5)	0.918	37(44.6)	38(45.8)	0.876

The proportion of patients with liver cirrhosis in the pre-PSM surgery group was higher.

TABLE 2 | Basic information of all patients in the expression of Ki67[cases(%)].

Clinical data	Pre-PSM		
	Ki67 high expression(n=83)	Ki67 low expression(n=97)	P
Age(>55)	41(49.4)	45(46.4)	0.687
Hepatitis B history	76(91.6)	83(85.6)	0.211
Liver cirrhosis	58(69.9)	56(64.4)	0.092
Pre-operative liver function(A)	82(98.8)	94(96.9)	0.392
AFP(>200 μg/liter)	29(34.9)	25(25.8)	0.181
Diameter of tumor (Poorly differentiated, undifferentiated)	28(33.7)	25(25.8)	0.243
MVI(>M1)	29(34.9)	35(36.1)	0.873
Number of lesions(single)	69(83.1)	79(81.4)	0.768
Maximum diameter of lesions (>5 cm)	45(54.2)	49(50.5)	0.620

There was no statistical difference in the covariates.

matching eliminated the different variables, 36 pairs of liver cancer patients were created. There was no statistical difference between the two covariates (P value >0.05, **Table 3**). In the Ki67 high expression group, there was no statistical difference in the covariates between the surgery and surgery + TACE subgroups (P value >0.05, **Table 4**). In all surgery + TACE patients, there was no statistical difference in the covariates between the Ki67 high- and low-expression subgroups (P value >0.05, **Table 5**).

Effect of PA-TACE on Tumor Recurrence and OS in HCC Patients

After PSM, there was no statistical difference in the 1-, 2-, or 3-year RFS between the surgery + TACE and surgery subgroups, while the OS in the surgery + TACE subgroup was significantly higher than the surgery subgroup (RFS: 72.3%, 64.6%, and 56.8% vs. 69.9%, 53.0%, and 43.4%, respectively, P = 0.086; OS: 95.2%, 82.9%, and 76.5% vs. 88.0%, 71.1%, and 58.0%, respectively, P = 0.017; **Figure 1**).

Effect of PA-TACE on Tumor Recurrence and OS in the Ki67 Low Expression Group

After PSM, there was no statistically significant difference in the 1-, 2-, or 3-year RFS and OS between the surgery + TACE and surgery subgroups (RFS: 63.9%, 55.6%, and 42.9% vs. 83.3%, 63.9%, and 55.6%, respectively, P = 0.279; OS: 91.7%, 83.3%, and 74.3% vs. 91.7%, 88.9%, and 71.4%, respectively, P = 0.890; **Figure 2**).

TABLE 4 | Basic information of the Ki67 high expression subgroup[cases(%)].

Clinical data	Pre-PSM		
	Operating group (n=43)	operation + TACEGroup (n=40)	P
Age(>55)	22(51.2)	16(40.0)	0.739
Gender (male)	41(95.3)	36(90.0)	0.347
Hepatitis B history	40(93.0)	36(90.0)	0.620
Liver cirrhosis	32(74.4)	26(65.0)	0.350
Preoperative liver function(A)	42(97.7)	40(100.0)	0.332
AFP(>200 μg/liter)	15(34.9)	14(35.0)	0.991
Number of lesions (single)	38(88.4)	31(77.5)	0.186

There was no statistical difference in the covariates.

TABLE 5 | Basic information of the operation + TACE group[cases(%)].

Clinical data	Pre-PSM		
	Ki67 high expression(n=40)	Ki67 low expression(n=46)	P
Age(>55)	19(47.5)	16(34.8)	0.231
Hepatitis B history	36(90.0)	42(91.3)	0.835
Liver cirrhosis	26(65.0)	22(47.8)	0.110
Preoperative liver function(A)	40(100.0)	43(93.5)	0.100
AFP(>200 μg/liter)	14(35.0)	12(26.1)	0.369
Diameter of tumor (Poorly differentiated, undifferentiated)	15(37.5)	10(21.7)	0.108
MVI(>M1)	29(72.5)	35(76.1)	0.704
Number of lesions(single)	31(77.5)	35(76.1)	0.877
Maximum diameter of lesions (>5 cm)	22(55.0)	22(47.8)	0.507

There was no statistical difference in the covariates.

Effect of PA-TACE on Tumor Recurrence and OS in the Ki67 High Expression Group

The 1-, 2-, and 3-year RFS and OS in the surgery + TACE subgroup were higher than the surgery subgroup (RFS: 80.0%, 77.5%, and 69.2% vs. 53.5%, 39.5%, and 32.6%, respectively, P<0.001; OS: 97.5%, 85.0%, and 79.5% vs. 79.1%, 48.8%, and

TABLE 3 | Basic information of the Ki67 low-expression group[cases(%)].

Clinical data	Pre-PSM			After PSM		
	Operating group (n=51)	operation + TACEgroup (n=46)	P	Operating group (n=36)	operation + TACEgroup (n=36)	P
Age(>55)	29(56.9)	16(34.8)	0.029	15(41.7)	13(36.1)	0.629
Gender(male)	42(82.4)	38(82.6)	0.974	30(83.3)	30(83.3)	1.000
Hepatitis B history	41(80.4)	42(91.3)	0.127	32(88.9)	33(91.2)	0.691
liver cirrhosis	34(66.7)	22(47.8)	0.061	20(55.6)	17(47.2)	0.479
Preoperative liver function (A)	51(100.0)	43(93.5)	0.064	36(100.0)	36(100.0)	1.000
AFP(>200 μg/liter)	13(25.5)	12(26.1)	0.947	9(25.0)	10(27.8)	0.789
Number of lesions(single)	44(86.3)	35(76.1)	0.197	29(80.1)	28(77.8)	0.772

The proportion of patients >55 years of age in the pre-PSM subgroup was higher than the surgery + TACE subgroup.

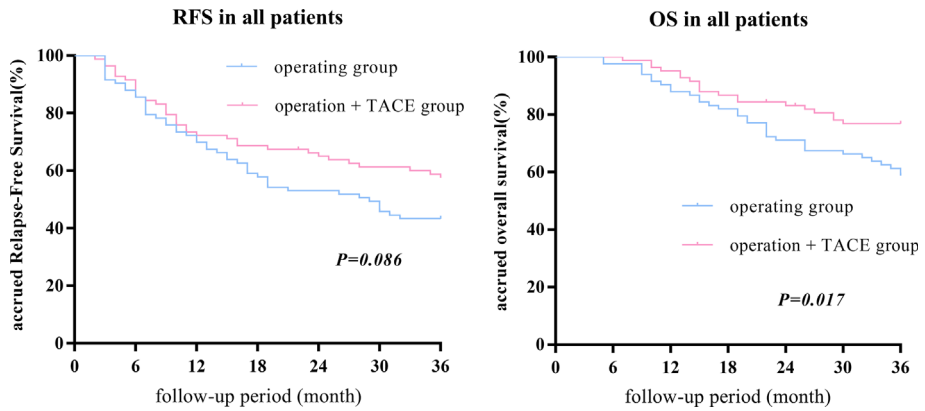

FIGURE 1 | After PSM, there was no statistical difference between the 1-, 2-, or 3-year RFS between the surgery + TACE and surgery subgroups, while the OS in the surgery + TACE subgroup was significantly higher than the surgery subgroup.

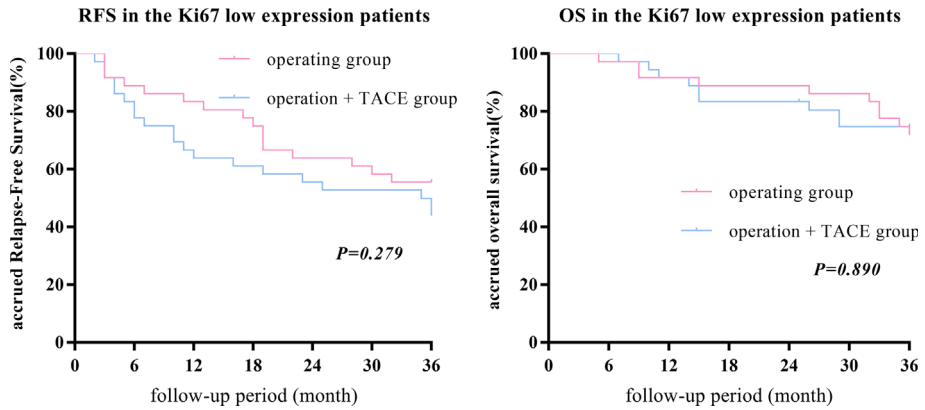

FIGURE 2 | After PSM, there was no statistically significant difference in the 1-, 2-, or 3-year RFS and OS between the surgery + TACE and surgery subgroups in the Ki67 low-expression group.

42.9%, respectively, P = 0.001). The differences in RFS and OS between the two groups were statistically significant (**Figure 3**).

Effect of PA-TACE on Tumor Recurrence and OS in the Surgery + TACE Group

After PSM, there was no statistical difference in the 1-, 2-, or 3-year OS between low- and high-expression subgroups, while the RFS in the high-expression subgroup was significantly higher than the low-expression subgroup (RFS: 80.0%, 79.5%, and 69.2% vs. 67.4%, 56.5%, and 46.7%, respectively, P = 0.035; OS: 97.5%, 85.0%, and 79.5% vs. 93.5%, 82.6%, and 75.6%, respectively, P = 0.665; **Figure 4**).

Multivariate Analysis on Recurrence and Survival of Patients With HCC After Surgery

After PSM, multivariate analysis in the Ki67 low expression group showed that a preoperative AFP level >200μg/liter (13) and a tumor maximum diameter ≥5 cm (14) were independent risk factors for RFS and OS rates in patients post-operatively, and liver cirrhosis was an independent risk factor for RFS (HR = 3.50 and 2.58, P = 0.001 and 0.015, respectively; and HR = 4.10 and 2.79, P = 0.006 and 0.041, respectively; and HR = 2.39, P = 0.02). Multivariate analysis in the Ki67 high expression group showed that postoperative adjuvant TACE treatment was an independent protective factor for RFS and OS after surgery (HR = 0.27, P < 0.001 and HR = 0.21, P < 0.001, respectively; **Table 6**).

DISCUSSION

HCC is the third most common cause of cancer-related deaths worldwide (15). If a radical liver resection is performed on patients with HCC, the 5-year recurrence rate is approximately 70%. The 5-year survival rate of patients with recurrent HCC decreases by 24% compared to patients without relapse, and the median survival time decreases by 54 months, which has a significant

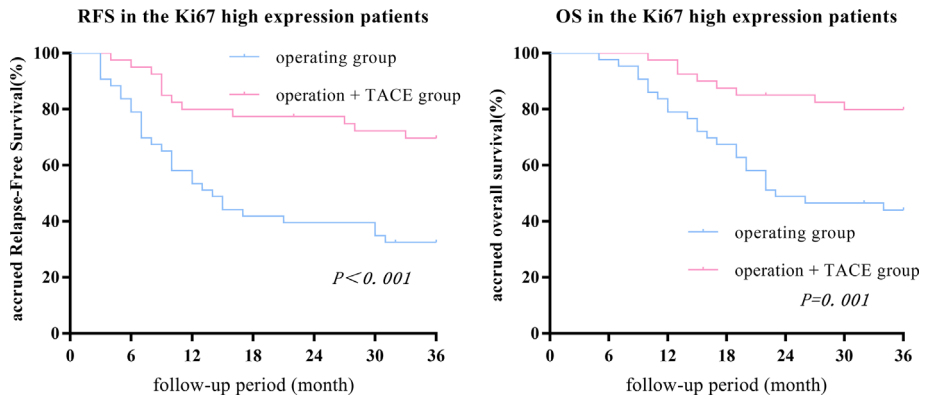

FIGURE 3 | The 1-, 2-, and 3-year RFS and OS in the surgery + TACE subgroup were higher than the surgery subgroup in the Ki67 high-expression group. The differences in RFS and OS between the two groups were statistically significant.

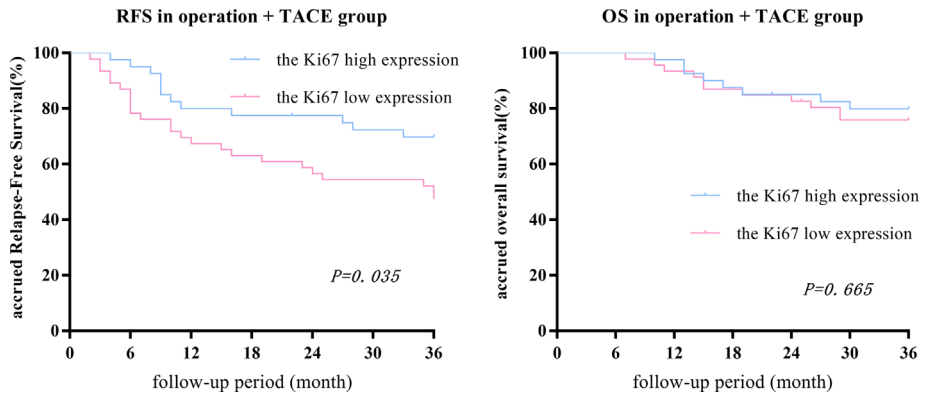

FIGURE 4 | In the surgery + TACE group, there was no statistical difference between the 1-, 2-, or 3-year OS between the Ki67 low- and high-expression subgroups, while the RFS in the high-expression subgroup was significantly higher than the low-expression subgroup.

TABLE 6 | Multivariate analysis on recurrence and survival of patients with HCC after surgery.

Factors	the Ki67 low-expression subgroup				the Ki67 high-expression subgroup			
	RFS		OS		RFS		OS	
	HR(95%CI)	P	HR(95%CI)	P	HR(95%CI)	P	HR(95%CI)	P
Hepatitis B history	–	–	–	–	–	–	–	–
Liver cirrhosis	2.39(1.15–4.95)	0.02	–	–	–	–	–	–
AFP(>200 μg/liter)	3.50(1.62–7.56)	0.001	4.10(1.49–11.3)	0.06	–	–	–	–
Number of lesions(multiple)	–	–	–	–	–	–	–	–
Maximum diameter of lesions (>5 cm)	2.58(1.20–5.54)	0.015	2.79(1.04–7.43)	0.041	–	–	–	–
PA-TACE	–	–	–	–	0.27(0.13–0.55)	<0.001	0.21(0.89–0.49)	<0.001

effect on prognosis (2). Postoperative adjuvant treatments, such as TACE, targeted therapy, and immunotherapy, can effectively delay tumor recurrence and prolong patient survival. Among the postoperative adjuvant treatments, PA-TACE is currently the most widely used (3).

The curative effects of PA-TACE are as follows: 1) TACE can increase the local drug concentration, which inhibits tumor proliferation and reduces the probability of recurrence (15); and 2) residual liver postoperatively can trigger the rapid regeneration phase, and proliferation of the residual tumor

cells is apparent, which is more susceptible to chemotherapy drugs. Ki67 is an antigen related to cell proliferation, thus reflecting the activity of cell proliferation (5). Therefore, we speculated that HCC patients with high expression of Ki67 have more active cell proliferation, and the effect of adjuvant TACE after surgery will be superior. There are very few studies, however, involving the relationship between Ki67 and PA-TACE (11).

This study conducted a retrospective analysis involving 180 patients with HCC who underwent radical liver resections. There was no significant difference in the 1-, 2-, and 3-year RFS between the surgery + TACE and surgery subgroups, while the OS of the surgery + TACE subgroup were significantly greater compared with the surgery subgroup, which is in agreement with previous studies (16–18). A further stratified subgroup analysis showed that in the Ki67 low expression group, there was no significant difference in the 1-, 2-, and 3-year RFS and OS between the surgery + TACE and surgery subgroup. In the Ki67 high expression group, the 1-, 2-, and 3-year RFS and OS of the surgery + TACE subgroups were greater than the surgery group. The RFS was higher in the Ki67 high-than low-expression subgroup after 1, 2, and 3 years, and OS was no significant difference in all surgery + TACE patients. Multivariate analysis in the Ki67 high expression group showed that postoperative adjuvant TACE treatment was an independent protective factor for postoperative RFS and OS postoperatively.

Although TACE is currently widely used in the treatment of HCC, the indications for postoperative adjuvant TACE treatment are still controversial. Multi-center studies have shown that postoperative adjuvant TACE therapy can significantly improve the RFS but does not significantly improve the OS. Further stratification studies have shown that for patients at high risk for a post-operative recurrence with tumors >5 cm in diameter, MVI-positive tumors, and poorly differentiated HCC, PA-TACE can significantly improve the prognosis of patients (4). Studies have also shown that postoperative adjuvant TACE have shown a survival rate advantage in the case of vascular invasion or large HCC (diameter >5 cm) (19). In addition, studies have suggested that postoperative adjuvant TACE has a positive effect on patients with HCC that are prone to early recurrence and can be used as an empirical active intervention measure to prevent tumor recurrence (20). Studies have shown that PA-TACE can prolong the OS and DFS of MVI-positive patients, but is unrelated to the OS and DFS of MVI-negative patients (21). The current study showed that the RFS and OS in the surgery + TACE subgroup in the Ki67 high expression group were greater than the surgery subgroup, while there was no statistical difference between the two subgroups in the Ki67 low expression group, suggesting that the tumor Ki67 level can be used as a criterion for performing PA-TACE after radical liver tumor resection and screen suitable patients for effective anti-relapse treatment. There was no statistical difference between the Ki67 low- and high-expression subgroups at high risk for recurrence (number of lesions, maximum diameter of lesions, MVI,and the degree of tumor differentiation). This finding suggests that the tumor Ki67 level is an independent influencing factor unrelated to these factors. In addition, there was no statistical difference in the OS between the Ki67 low- and high-expression subgroups in all surgery + TACE patients, while the RFS in the high- was significantly greater than the low-expression subgroup. There was a greater balance between the two subgroups in terms of risk factors for recurrence. Ki67 is internationally recognized as the tumor proliferation index, and the higher the value, the worse the prognosis, which is in contrast to our results. This discrepancy may be related to the line of PA-TACE, which also demonstrates our conclusion that patients with high Ki67 expression have survival benefit from PA-TACE.

Studies have shown that After TACE treatment, the tumor Ki67 level and percentage of necrotic cells in tumor tissues were significantly higher than before treatment, and the level of Ki67 was positively correlated with the percentage of necrosis (22, 23), which is in agreement with our conclusions; however, we showed that some patients exist with high expression of Ki67 and non-poorly differentiated tumors who have a better prognosis after adjuvant TACE treatment. This finding suggests that post-operative TACE treatment based on the Ki67 level may be more accurate, and further stratified analysis needs to be carried out. The nuclear Ki-67 protein is related to cell proliferation activity and highly expressed in the G2/M phase, while physical factors, such as hypoxia and lack of a blood supply, have a greater impact on cells with vigorous replication in the G2/M phase (22), which may explain why TACE is more effective in patients with high Ki67 expression. In addition, the pharmacologic effects of chemotherapeutic drugs, such as doxorubicin, enter the nucleus to interfere with the transcription process, prevent mRNA synthesis, block the cell cycle, and inhibit tumor growth in the G2 phase of cell division (24), which is more effective in the Ki67 high expression group.

The current study showed that the 1-, 2-, and 3-year RFS and OS of the surgery + TACE subgroup in the Ki67 low expression group were less than the surgery subgroup. This may be related to the activation of related signaling pathways after embolization and the induction of neoangiogenesis, forming a microenvironment conducive to tumor proliferation (25). In addition, the serum concentrations of vascular endothelial and fibroblast growth factors increase after TACE, and the serum levels are positively correlated with tumor progression (26). Tumor cells with low Ki67 expression are less sensitive to chemotherapeutic drugs, and the therapeutic effect of the drugs is less than the proliferation induced by hypoxia. As a result, patients with low Ki67 expression will have a worse prognosis after TACE treatment; however, there is no statistical difference between the two sub-groups, which may be related to the small sample size. Thus, a corollary with a larger sample size is warranted. Studies have shown that the tumor Ki67 is not static. After TACE treatment, the expression of Ki67 in HCC tissues is higher than untreated HCC tissues, which may be related to the cell cycle of tumor induced by local treatment (27). This finding also indicates that TACE treatment in patients with low expression of Ki67 may lead to a poor prognosis.

This study had several limitations. First, our clinical data only represented a single research center, the sample size was small, and the conclusion was based on a retrospective analysis. Thus, a prospective, multi-center, large-sample random clinical trial should be conducted to further verify the relationship between Ki67 expression and PA-TACE with survival benefits. Second, the results of this study were from East Asia, and most of the patients had HCC caused by hepatitis B, which may not be applicable to hepatitis C or alcohol-related HCC. Third, the medications used in all TACE treatments in the current study were basically the same, and whether different medications led to different survival benefits remains to be further studied. Fourth, the current study was stratified according to a Ki67 ≥20% and <20%, but other studies have shown different stratification parameters (28); the precise cut-off value needs to be established. In addition, the prognosis of patients with early post-operative recurrence was extremely poor, which may represent the true recurrence of the primary cancer spread *via* the portal vein before HCC resection (2). The extensive clinical application of immunotherapy and targeted therapy in recent years has prolonged the survival time of patients with distant metastases of HCC after a recurrence; however, the time span of data collection in our center was relatively long. These factors may have an impact on the conclusions in the current study.

This study analyzed the relationship between the expression of Ki67 and the efficacy of postoperative adjuvant TACE in patients with HCC, and confirmed that when Ki67 was highly expressed, adjuvant TACE after liver resection could effectively reduce postoperative tumor recurrence and significantly improve the long-term survival rate, while when the expression of Ki67 was low, PA-TACE may result in a poor prognosis. Therefore, for HCC patients with high expression of Ki67, TACE treatment is recommended to improve the prognosis after liver resection.

DATA AVAILABILITY STATEMENT

The raw data supporting the conclusions of this article will be made available by the authors, without undue reservation.

ETHICS STATEMENT

The studies involving human participants were reviewed and approved by the Institutional Review Board of The First Affiliated Hospital of Chongqing Medical University. Written informed consent for participation was not required for this study in accordance with the national legislation and the institutional requirements.

AUTHOR CONTRIBUTIONS

Y-FZ performed the study and wrote the paper. WT, KC, and XY collected and analyzed the data and made the tables and figures. Z-RS and XX designed the study, edited the manuscript, and offered suggestions for this study. Y-FZ and XX contributed equally to this work. All authors contributed to the article and approved the submitted version.

FUNDING

In vitro high-throughput drug sensitivity screening with patient-derived primary cells as a guide for clinical practice in hepatocellular carcinoma (2019GDRC002); Differentiation of adipose mesenchymal stem cells into hepatocytes induced by HNF-4α combined with HNF-3γ (cstc2019jcyj-msxmX0837).

REFERENCES

1. Jean-Luc R, Julien E. Systemic treatment of hepatocellular carcinoma: standard of care in China and elsewhere. *Lancet Oncol* (2020) 21(4):479–81. doi: 10.1016/S1470-2045(20)30082-6
2. Parissa T, Ghalib J, Brian S, Myron S, Sasan R. Recurrence of hepatocellular cancer after resection: patterns, treatments, and prognosis. *Ann Surg* (2015) 261(5):947–55. doi: 10.1097/SLA.0000000000000710
3. Bruix J, Gores GJ, Mazzaferro V. Hepatocellular carcinoma: clinical frontiers and perspectives. *Gut* (2014) 63(5):844–55. doi: 10.1136/gutjnl-2013-306627
4. Chen W, Ma T, Zhang J, Zhang XZ, Chen W, Bai XL, et al. A systematic review and meta-analysis of adjuvant transarterial chemoembolization after curative resection for patients with hepatocellular carcinoma. *HPB (Oxford)* (2020) 22(6):795–808. doi: 10.1016/j.hpb.2019.12.013
5. Yerushalmi R, Woods R, Ravdin PM, Hayes MM, Gelmon KA. Ki67 in breast cancer: prognostic and predictive potential. *Lancet Oncol* (2010) 11(2):174–83. doi: 10.1016/S1470-2045(09)70262-1
6. Cao Y, Ke R, Wang S, Zhu X, Chen J, Huang C, et al. DNA topoisomerase IIalpha and Ki67 are prognostic factors in patients with hepatocellular carcinoma. *Oncol Lett* (2017) 13(6):4109–16. doi: 10.3892/ol.2017.5999
7. Zhang HM, Li S-P, Yu Y, Wang Z, He JD, Xu Y-J, et al. Bi-directional roles of IRF-1 on autophagy diminish its prognostic value as compared with Ki67 in liver transplantation for hepatocellular carcinoma. *Oncotarget* (2016) 7 (25):37979–92. doi: 10.18632/oncotarget.9365
8. He M, Li Q, Zou R, Shen J, Fang W, Tan G, et al. Sorafenib Plus Hepatic Arterial Infusion of Oxaliplatin, Fluorouracil, and Leucovorin vs Sorafenib Alone for Hepatocellular Carcinoma With Portal Vein Invasion: A Randomized Clinical Trial. *JAMA Oncol* (2019) 5(7):953–60. doi: 10.1001/jamaoncol.2019.0250
9. Gruber-Rouh T, Kamal A, Eichler K, Beeres M, Langenbach M, Naguib N, et al. Transarterial Chemoembolization (TACE) Using Mitomycin with or without Irinotecan for Hepatocellular Carcinoma in European Patients. *Oncol Res Treat* (2018) 41(7-8):438–42. doi: 10.1159/000488644
10. NIOSH List of Antineoplastic and Other Hazardous Drugs in Healthcare Settings: Proposed Additions to the NIOSH Hazardous Drug List 2018. *Federal Register/FIND* (2018) 83(31):174–36.
11. Singla S, LeVea C, Pokuri V, Attwood K, Wach M, Kuvshinoff B, et al. Ki67 score as a potential predictor in the selection of liver-directed therapies for metastatic neuroendocrine tumors: a single institutional experience. *J Gastrointest Oncol* (2016) 7(3):441–8. doi: 10.21037/jgo.2016.02.02
12. Chen Y, Qin X, Long L, Zhang L, Huang Z, Jiang Z, et al. Diagnostic Value of Gd-EOB-DTPA-Enhanced MRI for the Expression of Ki67 and Microvascular Density in Hepatocellular Carcinoma. *J Magn Reson Imaging* (2020) 51 (6):1755–63. doi: 10.1002/jmri.26974
13. Mishra G, Dev A, Paul E, Cheung W, Koukounaras J, Jhamb A, et al. Prognostic role of alpha-fetoprotein in patients with hepatocellular carcinoma treated with repeat transarterial chemoembolisation. *BMC Cancer* (2020) 20(1):483. doi: 10.1186/s12885-020-06806-4
14. Liu S, Li H, Guo L, Zhang B, Zhou BH, Zhang WT, et al. Tumor Size Affects Efficacy of Adjuvant Transarterial Chemoembolization in Patients with Hepatocellular Carcinoma and Microvascular Invasion. *Oncologist* (2019) 24(4):513–20. doi: 10.1634/theoncologist.2018-0305

15. Kew MC. Hepatocellular carcinoma: epidemiology and risk factors. *J Hepatocell Carcinoma* (2014) 13(1):115–25. doi: 10.2147/JHC.S44381
16. Bai T, Chen J, Xie ZB, Wu FX, Wang SD, Li LQ, et al. The efficacy and safety of postoperative adjuvant transarterial embolization and radiotherapy in hepatocellular carcinoma patients with portal vein tumor thrombus. *Onco Targets Ther* (2016) 27(9):3841–8. doi: 10.2147/OTT.S104307
17. Sun JJ, Wang K, Zhang CZ, Guo WX, Shi J, Cong WM, et al. Postoperative Adjuvant Transcatheter Arterial Chemoembolization After R0 Hepatectomy Improves Outcomes of Patients Who have Hepatocellular Carcinoma with Microvascular Invasion. *Ann Surg Oncol* (2016) 23(4):1344–51. doi: 10.1245/s10434-015-5008-z
18. Jiang JH, Guo Z, Lu H-F, Wang X-B, Yang H-J, Yang F-Q, et al. Adjuvant transarterial chemoembolization after curative resection of hepatocellular carcinoma: propensity score analysis. *World J Gastroenterol* (2015) 21 (15):4627–34. doi: 10.3748/wjg.v21.i15.4627
19. Qi X, Liu L, Wang D, Li H, Su C, Guo X. Hepatic resection alone versus in combination with pre- and post-operative transarterial chemoembolization for the treatment of hepatocellular carcinoma: A systematic review and meta-analysis. *Oncotarget* (2015) 6(34):36838–59. doi: 10.18632/oncotarget.5426
20. Peng BG, He Q, Li J-P, Zhou F. Adjuvant transcatheter arterial chemoembolization improves efficacy of hepatectomy for patients with hepatocellular carcinoma and portal vein tumor thrombus. *Am J Surg* (2009) 198(3):313–8. doi: 10.1016/j.amjsurg.2008.09.026
21. Wang H, Du P-C, Wu M-C, Cong W-M. Postoperative adjuvant transarterial chemoembolization for multinodular hepatocellular carcinoma within the Barcelona Clinic Liver Cancer early stage and microvascular invasion. *Hepatobiliary Surg Nutr* (2018) 7(6):418–28. doi: 10.21037/hbsn.2018.09.05
22. Huang Z, Xu X, Meng X, Hou Z, Liu F, Hua Q, et al. Correlations between ADC values and molecular markers of Ki-67 and HIF-1alpha in hepatocellular carcinoma. *Eur J Radiol* (2015) 84(12):2464–9. doi: 10.1016/j.ejrad.2015.09.013
23. Li Y, Yana C, Weng S, Shia Z, Suna H, Chen J, et al. Texture analysis of multi-phase MRI images to detect expression of Ki67 in hepatocellular carcinoma. *Clin Radiol* (2019) 74(10):813.e19–27. doi: 10.1016/j.crad.2019.06.024
24. Kunimoto S, Miura K, Takahashi Y, Takeuchi T, Umezawa Hd. Rapid uptake by cultured tumor cells and intracellular behavior of 4'-O-tetrahydropyranyladriamycin. *J Antibiot (Tokyo)* (1983) 36(3):312–7. doi: 10.7164/antibiotics.36.312
25. Ader I, Brizuela L, Bouquerel P, Malavaud B, Cuvillier O. Sphingosine kinase 1: a new modulator of hypoxia inducible factor 1alpha during hypoxia in human cancer cells. *Cancer Res* (2008) 68(20):8635–42. doi: 10.1158/0008-5472.CAN-08-0917
26. Jang JH, Lee J-W, Hong JT, Jin Y-J. Transarterial chemoembolization for hepatocellular carcinoma: an evidence-based review of its place in therapy. *J Hepatocell Carcinoma* (2015) 2(2):123–9. doi: 10.2147/JHC.S44380
27. Farris AR, Dursun N, Dhanasekaran R, Coban I, McIntosh EB, Adsay NV, et al. Tumoral and angiogenesis factors in hepatocellular carcinoma after locoregional therapy. *Pathol Res Pract* (2012) 208(1):15–21. doi: 10.1016/j.prp.2011.10.005
28. Li HH, Qi LN, Ma L, Chen ZS, Xiang BD, Li LQ. Effect of KI-67 positive cellular index on prognosis after hepatectomy in Barcelona Clinic Liver Cancer stage A and B hepatocellular carcinoma with microvascular invasion. *Onco Targets Ther* (2018) 10(11):4747–54. doi: 10.2147/OTT.S165244

Conflict of Interest: The authors declare that the research was conducted in the absence of any commercial or financial relationships that could be construed as a potential conflict of interest.

frontiers in Oncology

ORIGINAL RESEARCH
published: 25 February 2021
doi: 10.3389/fonc.2021.621806

Mining of RNA Methylation-Related Genes and Elucidation of Their Molecular Biology in Gallbladder Carcinoma

Changhong Yang[1], Jialei Chen[2], Zhe Yu[3], Jing Luo[4], Xuemei Li[4], Baoyong Zhou[5] and Ning Jiang[4]**

[1] Department of Bioinformatics, Chongqing Medical University, Chongqing, China, [2] Department of Otolaryngology, The First Affiliated Hospital of Chongqing Medical University, Chongqing, China, [3] School of Life Sciences, Peking University, Beijing, China, [4] Department of Pathology, Chongqing Medical University, Chongqing, China, [5] Department of Hepatobiliary Surgery, The First Affiliated Hospital of Chongqing Medical University, Chongqing, China

OPEN ACCESS

Edited by:
Yujun Shi,
Sichuan University, China

Reviewed by:
Zhengjun Zhou,
Fudan University, China
Chuang Zhou,
First Affiliated Hospital of Zhengzhou University, China

***Correspondence:**
Baoyong Zhou
sdlytczhzh@163.com
Ning Jiang
jiangning@cqmu.edu.cn

Specialty section:
This article was submitted to Gastrointestinal Cancers, a section of the journal Frontiers in Oncology

Received: 27 October 2020
Accepted: 11 January 2021
Published: 25 February 2021

Citation:
Yang C, Chen J, Yu Z, Luo J, Li X, Zhou B and Jiang N (2021) Mining of RNA Methylation-Related Genes and Elucidation of Their Molecular Biology in Gallbladder Carcinoma. Front. Oncol. 11:621806. doi: 10.3389/fonc.2021.621806

Gallbladder carcinoma (GBC), which has high invasion and metastasis risks, remains the most common biliary tract malignancy. Surgical resection for GBC is the only effective treatment, but most patients miss the opportunity for curative surgery because of a lack of timely diagnosis. The aim of this study was to identify and verify early candidate diagnostic and prognostic RNA methylation related genes for GBC *via* integrated transcriptome bioinformatics analysis. Lists of GBC-related genes and methylation-related genes were collected from public databases to screen differentially expressed genes (DEGs) by using the limma package and the RobustRankAggreg (RRA) package. The core genes were collected with batch effects corrected by the RRA algorithm through protein interaction network analysis, signaling pathway enrichment analysis and gene ranking. Four modules obtained from four public microarray datasets were found to be related to GBC, and *FGA*, *F2*, *HAO1*, *CFH*, *PIPOX*, *ITIH4*, *GNMT*, *MAT1A*, *MTHFD1*, *HPX*, *CTH*, *EPHX2*, *HSD17B6*, *AKR1C4*, *CFHR3*, *ENNP1*, and *NAT2* were revealed to be potential hub genes involved in methylation-related pathways and bile metabolism-related pathways. Among these, *FGA*, *CFH*, *F2*, *HPX*, and *PIPOX* were predicted to be methylated genes in GBC, but *POPIX* had no modification sites for RNA methylation. Furthermore, survival analysis of TCGA (the Cancer Genome Atlas) database showed that six genes among the hub genes, *FGA*, *CFH*, *ENPP1*, *CFHR3*, *ITIH4*, and *NAT2*, were highly expressed and significantly correlated with worse prognosis. Gene correlation analysis revealed that the *FGA* was positively correlated with the *ENPP1*, *NAT2*, and *CFHR3*, while *CFH* was positively correlated with the *NAT2*, *CFHR3*, and *FGA*. In addition, the results of immunohistochemistry (IHC) showed that the expressions of FGA, F2, CFH, PIPOX, ITIH4, GNMT, MAT1A, MTHFD1, HPX, CFHR3, NAT2, and ENPP1 were higher in GBC tissues than that in control tissues. In conclusion, two genes, *FGA* and *CFH*, were

identified as RNA methylation-related genes also involved in bile metabolism in GBC, which may be novel biomarkers to early diagnose and evaluate prognosis for GBC.

Keywords: gallbladder carcinoma, bioinformatics, biomarkers, differentially expressed genes, RNA methylation, bile metabolism

INTRODUCTION

Gallbladder carcinoma (GBC), which originates from the epithelia of bile ducts and the gallbladder, is the most common malignancy of the biliary tract and has a high possibility of metastasis (1). At present, the 5-year survival rate of patients with unresectable GBC is less than 5%, and complete surgical resection is still an effective curative therapy (2). However, due to a lack of specific signs and symptoms, it is very difficult to diagnose GBC at the early stage; thus, many patients miss the opportunity for surgery (3). A more in-depth understanding of the molecular mechanisms underlying the progression of gallbladder carcinoma will be advantageous for the development of treatment options. Thus, further exploration of GBC pathological development and identification of effective early prognostic biomarkers are important for GBC treatment.

RNA methylation is the most common modification of mRNAs (4) and is dynamic and reversible in mammalian cells (5). The dynamic regulation of RNA methylation has been indicated to be closely associated with gene expression (6, 7). Growing evidence has demonstrated that RNA methylation is involved in regulating RNA transcription (8), processing events (9), RNA stability (10), and translation (11). In addition, the clinical value of RNA methylation in cancers has become increasingly obvious. RNA methylation modification is reported to be associated with proliferation (12), tumorigenesis (13), invasion (13), and metastasis (14) in various cancers. In addition, RNA methylation not only affects the cleavage, transport, stability, and degradation of non-coding RNAs such as miRNAs, lncRNAs, and circRNAs but also regulates the biological functions of cells by regulating the levels of these non-coding RNAs (15). More importantly, non-coding RNAs can influence RNA-RNA or RNA-protein interactions to regulate particular biological functions (16). As a promising biomarker, RNA methylation has been increasingly utilized to detect and predict the occurrence of cancer, and its prognostic significance has been determined (17). Increasing numbers of studies have illustrated that RNA methylation may have potential clinical value as a therapeutic target for cancer patients (18). However, research on RNA methylation in GBC is still very scarce.

Previous studies on GBC have seemed to be limited and have focused mostly on either a single gene or a single omics data type (19, 20). However, the occurrence and development of GBC is a multifactorial and multistep process involving molecular changes at the transcriptional, posttranscriptional, and translational levels. Thus, there is an urgent need to comprehensively illustrate the gene interactions and molecular modulation network of GBC. With the rapid development of high-throughput technologies, bioinformatics has been widely applied to analyze massive amounts of biological data. Transcriptomics techniques include mainly microarrays and RNA sequencing, and microarrays include expression profile chips, lncRNA chips, miRNA chips, and methylation chips. Ma et al. (19) identified differentially expressed lncRNAs and mRNAs between GBC tissues and control tissues with chips and found that the lncRNA GCASPC could bind to miRNA-17-3 to negatively regulate the proliferation of GBC cells. Liang et al. (20) used a microRNA chip with high-throughput screening to discover that miRNA-143-3p inhibited the proliferation of GBC cells by binding to its target gene *MYBL2*. Currently, the most-studied pathways involved in GBC are the hedgehog pathway (21) and the PI3K/Akt pathway (22). Studies on RNA methylation in gallbladder carcinoma have not been reported, and integrated bioinformatics analysis using multiple public databases in gallbladder cancer is quite scarce.

In this study, we employed integrated transcriptome bioinformatics analysis based on four RNA microarray datasets (GSE45001, GSE31370, GSE26566, and GSE76633) to identify differentially expressed genes and RNA methylation-related genes in GBC. In addition, the core genes were collected through protein-protein interaction network analysis, signaling pathway enrichment analysis, and gene ranking. Moreover, the core genes were verified with the TCGA database, and posttranscriptional modifications, survival, a coexpression network, and the tumor microenvironment were predicted. Then, immunohistochemistry was used to detect the differences in the expression of the hub genes between the clinical GBC samples and control samples. The final screened genes could be novel biomarkers to early diagnose and evaluate prognosis for GBC.

METHODS

GBC-related gene lists and related genetic data were collected from public databases. Methylation-related genes were also obtained to screen the differentially expressed genes. The core genes were collected through protein interaction network analysis, signaling

Abbreviation: GBC, gallbladder carcinoma; DEGs, differentially expressed genes; RRA, RobustRankAggreg; PPI, protein-protein interaction; IHC, immunohistochemistry; TCGA, the Cancer Genome Atlas; GEO, gene expression omnibus; NCBI, national coalition building institute; KEGG, Kyoto encyclopedia of genes and genomes; EBI, European bioinformatics institute; limma, the linear models for microarray data; GO, gene ontology; FDR, false discovery rate; CHOL, cholangio carcinoma; SNP, single nucleotide polymorphisms; OS, overall survival; HR, hazard ratio; TISCH, the Tumor Immune Single-cell Hub database; FGA, fibrinogen alpha chain; F2, coagulation factor II; HAO1, the enzyme hydroxyacid oxidase 1; CFH, complement factor H; PIPOX, pipecolic acid and sarcosine oxidase; ITIH4, inter-alpha-trypsin inhibitor heavy chain 4; GNMT, glycine N-methyltransferase; MAT1A, methionine adenosyl transferase 1A; MTHFD1, methylenetetrahydrofolate dehydrogenase, cyclohydrolase, and formyltetrahydrofolate synthetase 1; HPX, hemagglutinin; CTH, cystathionine gamma-Lyase; EPHX2, epoxide hydrolase 2; HSD17B6, hydroxysteroid 17-Beta Dehydrogenase 6; AKR1C4, Aldo-Keto reductase family 1 member C4; CFHR3, complement factor H related 3; ENNP1, ectonucleotide pyrophosphatase/phosphodiesterase 1; NAT2, N-acetyltransferase 2; NSUN2, NOP2/Sun domain family member 2.

pathway enrichment analysis, and gene ranking. They were verified with the TCGA database, and posttranscriptional modifications, survival, and a coexpression network were predicted. Then, immunohistochemistry was used to detect the expression of the core genes between the clinical GBC samples and control samples. The flow chart is shown in **Figure 1**.

Data Sources

GBC-related genes were collected with the search terms "((gallbladder cancer) OR (gallbladder carcinoma) OR (gallbladder neoplasms) OR (cholecystic carcinoma) OR (biliary tract cancer)) AND (Homo sapiens[Organism])" from the NCBI Gene database, the GeneCards database, the KEGG DISEASE database, cBioPortal database and the National Gene Bank. In addition, GBC-related genes were obtained from the literature with the keywords "(gallbladder cancer[Title/Abstract]) OR (gallbladder carcinoma[Title/Abstract])) OR (gallbladder neoplasms[Title/Abstract]) OR (cholecystic carcinoma[Title/Abstract])) OR (biliary tract cancer[Title/Abstract])) AND (biomarker[Title/Abstract])" from NCBI PubMed. Next, GBC-related microarray data were collected with the search terms "((gallbladder cancer) OR (gallbladder carcinoma) OR (gallbladder neoplasms) OR (cholecystic carcinoma) OR (biliary tract cancer)) AND (Homo sapiens[Organism])" from the GEO (Gene Expression Omnibus) database, PubMed, ArrayExpress of the EBI, the National Gene Bank, the National Genomics Science Data Center, OmicsDI, and Integrated Proteome Resources. Finally, all differentially methylated genes in GBC were obtained from the RMBase v2.0 database and the m6AVar database.

Methods for Identification of Differentially Expressed Genes

The Linear Models for Microarray Data (limma) package, which is a Bioconductor package of the R statistical language, was used to identify differentially expressed genes in six main steps. First, the expression matrix, grouping matrix and differential expression matrix were constructed. Second, the data were fitted to a linear model with the lmFit function. Third, the differences were calculated according to the contrast model with the contrasts.fit function. Fourth, the Bayesian test was conducted with the eBayes function. Fifth, test results were generated for all genes with the topTable function, and Benjamini and Hochberg test method was used to correct the *P* value. Finally, the results of differential analysis were screened according to a threshold of a corrected *P* value <0.050. RobustRankAggreg, another R package, is a tool that integrates differential expression analysis results from different platforms mainly with the RobustRank Aggregation (RRA) algorithm to obtain a comprehensive ranking list (23). To identify differentially expressed genes in this study, data were first downloaded from the GEO database. Limma software was then used to analyze the differentially expressed genes in each microarray dataset. The differentially expressed genes according to the fold change value were sorted. Finally, RobustRankAggreg software was used to integrate and analyze these results with the RRA algorithm.

Protein-Protein Interaction Network and Module Analysis

To better mine the core regulatory genes, protein-protein interaction analysis was used in this study. First, STRING (version 11, https://string-db.org/) software was used to analyze the protein interactions of the differentially expressed genes. Next, the CytoHubba plugin of Cytoscape software (version 3.7.2, https://cytoscape.org/) was used to rank the genes in the network with the Degree algorithm, and the top 25 ranked genes were considered the hub gene set. Simultaneously, the MCODE plugin was used to extract the core module from the protein interaction results with the following parameters: degree cutoff >=2, K -score >=2.

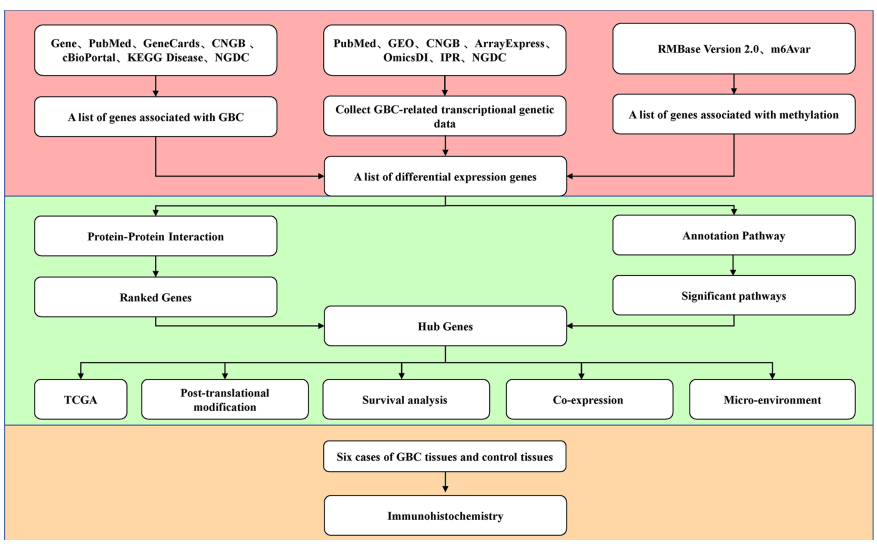

FIGURE 1 | Workflow chart of mining of RNA methylation-related genes in gallbladder carcinoma.

Functional Enrichment Analysis

ShinyGO V0.60 software was used to analyze the signaling pathways of the core module obtained from protein interaction analysis (24). ShinyGO software, a gene set enrichment analysis software program, is based on 55 kinds of databases, such as the Gene Ontology (GO), KEGG, Reactome, Panther, Biocarta, GeneSetDB EHMN, HumanCyc, NetPath, and MSigDB databases. ShinyGO software was used to functionally annotate genes or proteins with pathway databases, and the FDR (false discovery rate) values of the corresponding enriched pathways were obtained. The ggplot2 package was used to visualize the enrichment analysis results.

Annotation of Core Genes

The core genes in the hub module of the protein-protein interaction network that overlapped with genes involved in significant biological processes were annotated. An RNA sequencing dataset for CHOL including data on 36 patients with GBC and 9 controls were downloaded from the TCGA (25), and the limma package of the R language was used to analyze differentially expressed genes in order to verify the hub genes. In addition, the RMBase v2.0 database (26), which is a database of epigenetic modifications at the RNA level, and the m6AVar database (27), which predicts the impact of SNPs on RNA methylation modification, were used to predict the sites of RNA methylation modification of the core genes.

Survival Analysis of Hub Genes

Different endpoints that were stratified by mean and median, such as overall survival (OS), were used to analyze the prognosis of survival. Survival curves were assessed by the Kaplan-Meier method and Cox proportional hazards model. The hazard ratios (HRs) with 95% confidence intervals were determined.

Coexpression Network and Microenvironment Prediction

The GeneMANIA plug-in of Cytoscape software (version 3.7.2) was applied to analyze the gene coexpression network. The strength of regulation among genes was represented in the coexpression network through a weight value ranging from 0 to 1. The Tumor Immune Single-cell Hub (TISCH) database (http://tisch.comp-genomics.org/home/) (28) was used to analyze the tumor microenvironment.

Clinical Specimen Collection

Six samples of tumor tissues from patients with GBC and six samples of gallbladder tissues from patients with gallstones were obtained from the First Affiliated Hospital of Chongqing Medical University from 2019 to 2020, and all tissues were fixed with 4% paraformaldehyde. All patients agreed to provide informed consent, and the experimental protocols were approved by the local ethics committee.

Immunohistochemistry and Staining Result Determination

All specimens were paraffin-embedded and sectioned at 4 μm. The sections were baked at 60°C for 1 h, dewaxed, rehydrated in a graded alcohol series, and washed. The sections were boiled for 10 min antigen repair solution for antigen repair, and the remaining steps were carried out in accordance with the instructions. Primary antibodies against the following proteins were purchased: FGA (1:50, Boster, China), F2 (1:50, Boster, China), CFH (1:50, Boster, China), PIPOX (1:50, Absin, China), ITIH4 (1:50, Proteintech, USA), GNMT (1:50, Proteintech, USA), MAT1A (1:50, Fine Biotech, China), MTHFD1 (1:50, Proteintech, USA), HPX (1:50, Boster, China), CTH (1:50, Boster, China), CFHR3 (1:50, Fine Biotech, China), ENNP1 (1:50, Abcam, USA), and NAT2 (1:50, Abclonal, China). After DAB staining, the tablets were redyed with hematoxylin and sealed. The proportion of positive tumor cells was scored as follows: 1, 1–25%; 2, 26–50%; 3, 51–75%; and 4, 76–100%. The intensity of methylated protein staining in GBC was scored as follows: 0, no staining; 1, weak staining; and 2, strong staining. These two kinks of scores were multiplied to obtain a final score, and the expression of protein was determined to be low for scores <4 or high for scores ≥4.

Statistical Analysis

All statistical analyses were performed with R software (version 3.6.3). The threshold for screening of differentially expressed genes was an adjusted P value <0.05, an absolute fold change >1, and an RRA score <0.05. The methods of statistical analysis in this study included the hypergeometric test and Fisher's exact test, and the false discovery rate method was used with Benjamini and Hochberg correction. Correlations were assessed using Pearson's correlation coefficient.

RESULTS

Construction of Lists of Related Genes

GBC-related genes were collected from the following sources: 415 from the Gene database of NCBI, 415 from the GeneCards database, 4 from the KEGG DISEASE database, 1,637 from the cBioPortal gene database, 100 from the National Gene Bank, and 151 from related literature in the PubMed database. After merging these gene sets and removing the redundancies, we obtained 6,026 genes related to GBC. Next, 9,569 RNA methylation-related genes were collected from the RMBase v2.0 database, while 3,472 RNA methylation-related genes were collected from the m6AVar database. Together, 11,581 RNA methylation-related genes were collected. The overlap of the above GBC-related genes and the RNA methylation-related genes was examined, and 3,072 GBC-related genes involved in RNA methylation were ultimately obtained, as shown in **Figure 2**. RNA microarray datasets (GSE45001, GSE31370, GSE26566, and GSE76633) were downloaded from GEO database (29), as shown in **Table 1**. There were 159 samples with transcriptomic data, including 129 GBC samples and 30 control samples.

Collection of Differentially Expressed Genes (DEGs) in GBC

Four microarray datasets with group correction and normalization were used to analyze the differentially expressed

genes. The specific numbers of upregulated and downregulated genes for each set are shown in **Supplementary Table 1**. The four datasets were intersected, and the genes were ranked according to the fold change value and integrated with the RRA algorithm of the RobustRankAggreg package to obtain 81 DEGs (score <0.050), including 13 upregulated genes and 68 downregulated genes (control *vs* GBC) (shown in **Figure 2B**).

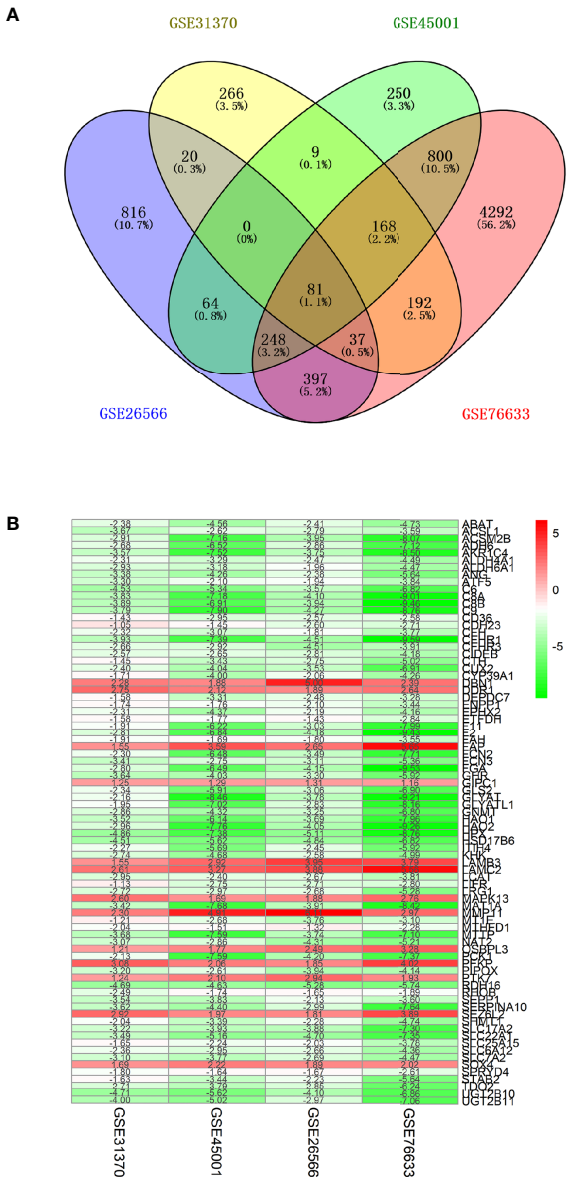

FIGURE 2 | Collection of differentially expressed genes (DEGs) in GBC. **(A)** Venn diagram of four RNA microarray datasets (GSE45001, GSE31370, GSE26566, and GSE76633). **(B)** heat map of differentially expressed genes. Each column represents one dataset and each row represents one gene. Green represents a lower expression level, red represents higher expression levels, and white represents that there is no different expression amongst the genes. The number in each rectangle represents the normalized gene expression level.

TABLE 1 | Information of the four microarray datasets from GEO.

GEO ID	Sample_Case	Sample_Control	Sample Total
GSE26566	104	6	110
GSE31370	6	5	11
GSE45001	10	10	20
GSE76633	9	9	18

GEO, Gene Expression Omnibus.

Establishment of the PPI Network

Based on the STRING database, a PPI network of the above 81 DEGs was constructed and ranked with topological analysis on nodes. The top 25 genes were clustered with MCODE to finally obtain four modules, as shown in **Table 2**.

GO, KEGG, and Reactome Enrichment Analysis

Almost 2.30~48.28% of the gene products were found to be associated with 33 biological process terms, such as the extracellular, cell surface, and mitochondria terms (enrichment FDR: 2.683E-10 ~ 3.348E-02). Approximately 2.30~35.63% of the genes were found to be associated with 87 molecular biology terms, including the REDOX enzyme activity, drug binding, and signal receptor binding terms (enrichment FDR: 6.936E-06 ~ 4.886E-02). Nearly 2.30~42.53% of the genes were associated with 400 biological process terms, such as the cholic acid biosynthesis, cholic acid metabolism, JAK-stat cascade, vascular development, inflammatory response, and cell adhesion terms (enrichment FDR: 1.022E-16 ~ 4.950E-02), as shown in **Figures 3A, B**. Overall, we obtained 23 genes involved in biological processes related to RNA methylation, and 12 of

TABLE 2 | Top 25 hub genes identified in PPI network for DEGs.

Rank	Name	Score	MCODE_Cluster	MCODE_Score
1	FGA	15	Cluster 1	6.000
2	F2	14	Cluster 1	6.000
3	C8A	13	Cluster 1	6.000
4	C8B	11	Cluster 1	6.000
5	C9	10	Cluster 3	4.464
6	C6	9	Cluster 1	6.000
6	HAO1	9	Cluster 1	5.000
6	UGT2B10	9	Cluster 1	5.000
9	SERPINA10	8	Cluster 1	6.000
9	HAO2	8	Cluster 2	4.000
12	ANG	7	Cluster 1	5.000
12	CFH	7	Cluster 1	5.000
12	F11	7	Cluster 1	6.000
12	PIPOX	7	Cluster 2	4.000
12	ITIH4	7	Cluster 3	4.000
17	SLC17A2	5	Cluster 1	5.000
17	GNMT	5	Cluster 2	4.000
17	MAT1A	5	Cluster 2	4.000
17	MTHFD1	5	Cluster 2	4.000
17	HPX	5	Cluster 3	4.000
22	CTH	4	Cluster 2	4.000
22	EPHX2	4	Cluster 2	4.000
22	UGT2B11	4	Cluster 4	3.000
25	AKR1C4	3	Cluster 4	3.000
25	HSD17B6	3	Cluster 4	3.000

PPI, protein-protein interaction; DEG, differentially expressed genes.

those genes were involved in biological processes related to bile metabolism.

Annotation of Core Genes

Seventeen core genes were obtained *via* intersection of the PPI network, methylation-related signaling pathways, and bile-related biological processes, including *FGA*, *F2*, *HAO1*, *CFH*, *PIPOX*, *ITIH4*, *GNMT*, *MAT1A*, *MTHFD1*, *HPX*, *CTH*, *EPHX2*, *HSD17B6*, *AKR1C4*, *CFHR3*, *ENNP1*, and *NAT2*. The 17 core genes were verified in TCGA's CHOL RNA-seq dataset, and all were significantly expressed. The fold change range of these 17 genes in the TCGA dataset was −184.580~−43.240, and the corrected *P* value range was 1.40E-04~1.24E-03, illustrating that the 17 core genes were all downregulated genes in control

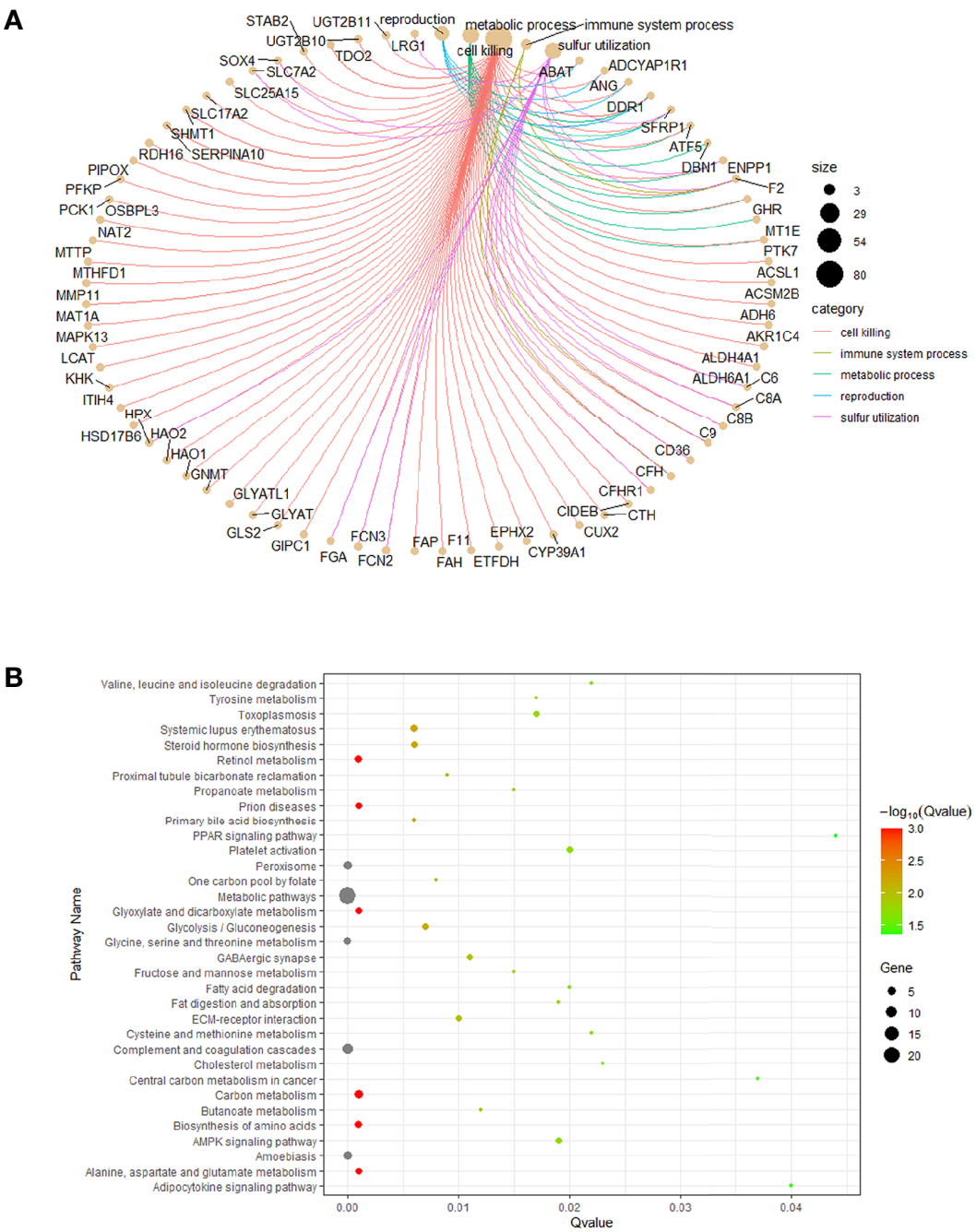

FIGURE 3 | Functional enrichment analysis. **(A)** co-expression of the DEGs. **(B)** the DEGs enriched pathway analysis.

vs GBC samples, as shown in **Figure 4A**. Then, Spearman correlation coefficients and Spearman *P* value were used to analyze the correlations of the levels of methylation of hub genes between the control and GBC cases. The results showed that the genes *CFH*, *F2*, *FGA*, *HPX*, and *PIPOX* were highly methylated in GBC cases compared with control cases (**Figure 4B**). Next, the RMBase database was used to analyze the RNA methylation sites of core genes (as shown in **Table 3**). The results showed that the genes *FGA*, *F2*, *HAO1*, *CFH*, *ITIH4*, *GNMT*, *MTHFD1*, *HPX*, *CTH*, *HSD17B6*, and *AKR1C4* had RNA methylation modification sites, but *EPHX2*, *MAT1A*, and *PIPOX* had no RNA methylation modification sites. Combining the above results, we came to the conclusion that the genes *CFH*, *F2*, *FGA*, and *HPX* are methylated genes in GBC.

Survival Analysis

To illustrate whether any core genes affect the overall survival of GBC patients, survival analysis was used to assess prognostic markers in the TCGA database. The results demonstrated that highly expressed *FGA*, *CFH*, *ENPP1*, *CFHR3*, *ITIH4*, and *NAT2* were associated with poor prognosis. Specifically, *FGA* was highly expressed in 14 samples but expressed at low levels in 22 samples. The 5-year overall survival HR was 2.680, and the log-rank *P* value was 0.037 (**Figure 5A**). *CFH* was highly expressed in 14 samples but expressed at low levels in 22 samples, and the 5-year overall survival HR was 3.490, with a log-rank *P* value of 0.007 (**Figure 5B**). *ENPP1* was highly expressed in 18 samples but expressed at low levels in 18 samples, and the 5-year overall survival HR was 3.250, with a log-rank *P* value of 0.020 (**Figure 5C**). *CFHR3* was highly expressed in 18 samples but expressed at low levels in 18 samples, and the 5-year overall survival HR was 4.660, with a log-rank *P* value of 0.003 (**Figure 5D**). *ITIH4* was highly expressed in 18 samples but expressed at low levels in 18 samples; the 5-year overall survival HR was 3.520, and the log-rank *P* value was 0.004 (**Figure 5E**). *NAT2* was highly expressed in 18 samples but expressed at low levels in 18 samples; the 5-year overall survival HR was 3.250, and the log-rank *P* value was 0.020 (**Figure 5F**). Moreover, survival analysis of the other 12 hub genes showed no significant differences (shown in **Supplementary Figure 1**). In addition, *Pearson* statistical analysis was performed to calculate the correlation coefficients among 17 core genes from the TCGA CHOL dataset, and the range of correlation coefficients between hub genes was −0.067~0.950, with a *P* value range of 4.8E-11~0.900 (details shown in **Supplementary Table 2** and **Figure 6A**). The results showed that the FGA gene was positively correlated with *ENPP1*, *NAT2*, and *CFHR3*, while the CFH gene was positively correlated with *FGA*, *NAT2*, and *CFHR3* (as shown in **Figure 6B**). Our results provide evidence for further research on RNA methylation in GBC.

Coexpression Network and Tumor Microenvironment Prediction

Coexpression network analysis of six genes (*FGA*, *CFH*, *CFHR3*, *NAT2*, *ENPP1*, and *ITIH4*) was carried out through GeneMANIA, and the results are shown in **Supplementary Figure 2A**. A weighted network was constructed with the following weight values: *FGA*, 0.003~0.108; *CFH*, 0.005~0.012; *CFHR3*, 0.003~0.027; *NAT2*, 0.006~0.020; *ENPP1*, 0.004~0.021; and *ITIH4*, 0.003~0.008. These results indicated that *FGA*, *CFH*, *CFHR3*, *NAT2*, *ENPP1*, and *ITIH4* had coexpression patterns. The TISCH database was used to predict the tumor microenvironment of these six genes, and the results revealed that the five genes other than *NAT2* were specifically expressed in cells, as shown in **Supplementary Figure 2A**. *FGA*, *CFH*, and *ITIH4* were expressed mainly in immune cells, malignant cells, and stromal cells, while *CFHR3* and *ENPP1* were expressed mainly in malignant cells and stromal cells. Our results further illustrated that these genes are closely associated and should be further studied.

Clinical Specimen Verification by Immunohistochemistry

To further verify the expression of hub genes in clinical samples, immunohistochemistry was used. According to the above findings, we screened 13 of the 17 hub genes for immunohistochemistry, including FGA, F2, CFH, PIPOX, ITIH4, GNMT, MAT1A, MTHFD1, HPX, CTH, CFHR3, ENNP1, and NAT2. As shown in **Figure 7**, the results showed that the expressions of FGA, CFH, PIPOX, GNMT, MAT1A, CFHR3, NAT2, and ENPP1 were higher in GBC tissues than in control tissues, and these proteins were mainly located in the cytoplasm of tumor cells. It is interesting to find that F2, ITIH4, and HPX proteins were mainly expressed in tumor cells of GBC tissues, but these proteins were located mainly in inflammatory cells of control tissues not normal gallbladder epithelium. Besides, MTHFD1 was expressed in both GBC tissues and control tissues, and there was no significant difference between tissue types. In addition, our results showed that CTH was not expressed in either GBC tissues or control tissues.

DISCUSSION

Although some advances in GBC research have been made, effective methods for the early diagnosis of GBC are still very scarce. In this study, 81 differentially expressed genes were identified from four array datasets from the GEO database through bioinformatics analysis and protein-protein interaction analysis. Among the ranked genes, 17 hub genes (*FGA*, *F2*, *HAO1*, *CFH*, *PIPOX*, *ITIH4*, *GNMT*, *MAT1A*, *MTHFD1*, *HPX*, *CTH*, *EPHX2*, *HSD17B6*, *AKR1C4*, *CFHR3*, *ENNP1*, and *NAT2*) involved in methylation signaling pathways and bile-related biological processes were confirmed. We performed pathway annotation, TCGA verification, posttranslational modification analysis, survival analysis, and IHC of these hub genes to finally obtain six candidates, including *FGA*, *CFH*, *ENPP1*, *ITIH4*, *CFHR3*, and *NAT2*, associated with GBC prognosis. Among these, *FGA* and *CFH* were identified as RNA methylation-related biomarkers in GBC, which may be novel biomarkers to early diagnose and evaluate prognosis for GBC.

The occurrence and progression of GBC is influenced by heredity and the environment, and epigenetic mechanisms, including histone modification (acetylation, methylation, and phosphorylation), have been reported to play important roles in the pathology of GBC (30). RNA methylation, which is one of the most common posttranscriptional modifications of RNAs, has recently been found to participate in tumorigenesis, invasion,

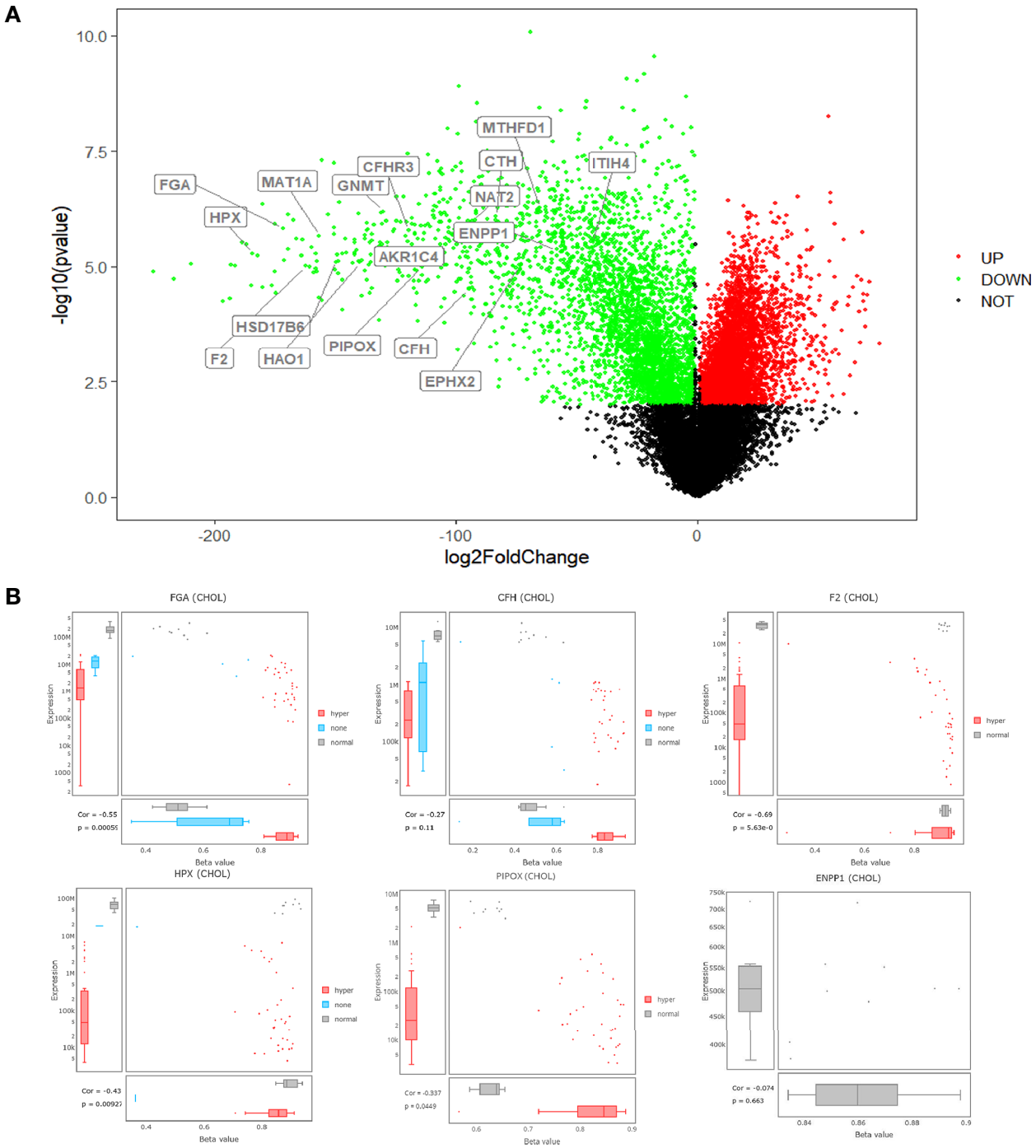

FIGURE 4 | Annotation of core genes. **(A)** volcano plots for DECs in GBC based on the four microarray datasets from GEO. **(B)** the levels of methylation of hub genes between the control and GBC cases from TCGA database.

metastasis, and drug resistance and could be a new diagnostic biomarker and therapeutic target (5). One study recently illustrated that NOP2/Sun domain family member 2 (*NSUN2*), a nuclear RNA methyltransferase catalyzing 5-methylcytosine formation, closely interacts with RPL6 to participate in GBC (31). However, research on the role of RNA methylation in gallbladder cancer is still very rare. In our present study, we finally identified 17 hub genes, among which *FGA*, *CFH*, *F2*, *HPX*, and *PIPOX* were highly methylated in GBC tissues. Surprisingly, our bioinformatics results showed that *PIPOX* has no methylation modification site. Next, we used clinical samples for verification and discovered that *FGA*, *CFH*, *F2*, *HPX*, and

TABLE 3 | RNA methylation sites of hub genes form RMBase database.

Gene_Symbol	RNA methylation_ Site_Number	Motif_Score	Location
AKR1C4	2	226.96~301.91	cds,5'-UTR
CFH	38	226.96~ 419.59	cds,5'-UTR,3'-UTR, intron
CTH	9	224.83~371.87	cds,5'-UTR,3'-UTR
F2	6	274.68~419.59	cds,5'-UTR,3'-UTR, intron
FGA	60	224.83~419.59	cds,5'-UTR,3'-UTR, intron
GNMT	2	344.64~369.74	3'-UTR
HAO1	3	226.96~349.63	cds,5'-UTR
HPX	4	274.68~371.87	cds,3'-UTR
HSD17B6	8	301.91~ 419.59	cds,5'-UTR, intron
ITIH4	45	224.83~ 419.59	cds,5'-UTR,3'-UTR, intron
MTHFD1	53	224.83~ 419.59	cds,5'-UTR,3'-UTR, intron

PIPOX were more highly expressed in GBC tissues than in control tissues but that expression was not significantly different. *FGA* encodes the alpha subunit of the coagulation factor fibrinogen, and downregulation of *FGA* seems to be associated with poor prognosis in human lung cancer (32). However, in our study, we found that *FGA* was highly expressed in GBC tissues from patients with a poor prognosis. Thus, it will be interesting to further explore the effect and underlying mechanism of *FGA* in GBC and whether *FGA* could be an indicator of the specific diagnosis of GBC. Complement factor H (*CFH*) was recently found to regulate complement activation in the liver, which is associated with hepatocellular injury (33), but our results demonstrated that there was no significant difference in *CFH* expression between GBC and control tissues. *F2*, known as coagulation factor II, encoding the prothrombin protein, was recently reported to be aberrantly methylated in old Chinese rhesus macaques, which is similar to our findings (34). *HPX* (hemagglutinin) is a plasma acute-phase glycoprotein produced by the liver that binds with high affinity to equimolar heme, and it can counteract cardiac heme toxicity such as that caused by oxidative stress, disruption of cardiac Ca^{2+} homeostasis and contractile dysfunction (35). *PIPOX*, which is a sarcosine-metabolizing enzyme, is highly expressed in HER-2 type cancer (36) but expressed at low levels in prostate cancer (33). We found that PIPOX was more highly expressed in GBC tissues than in control gallbladder tissues but that it has no methylation site. Differences in PIPOX expression in different tumors may be related to sarcosine metabolism, which also needs further study.

Aside from the above five methylation-related genes, other genes involved in bile-related biological processes, including *CTH*, *GNMT*, *HAO1*, *TIH4*, *MAT1A*, and *MTHFD1*, were identified. Abnormalities in bile metabolism, including increased biliary secretion (37) and hyposecretion of biliary bile acids (38), are closely related to gallstones, which are known risk factors for GBC (39). Therefore, we believe that these hub genes may have important clinical significance in the pathogenesis, diagnosis, and treatment of GBC. Increased *CTH* (Cystathionine Gamma-Lyase) expression in patients with

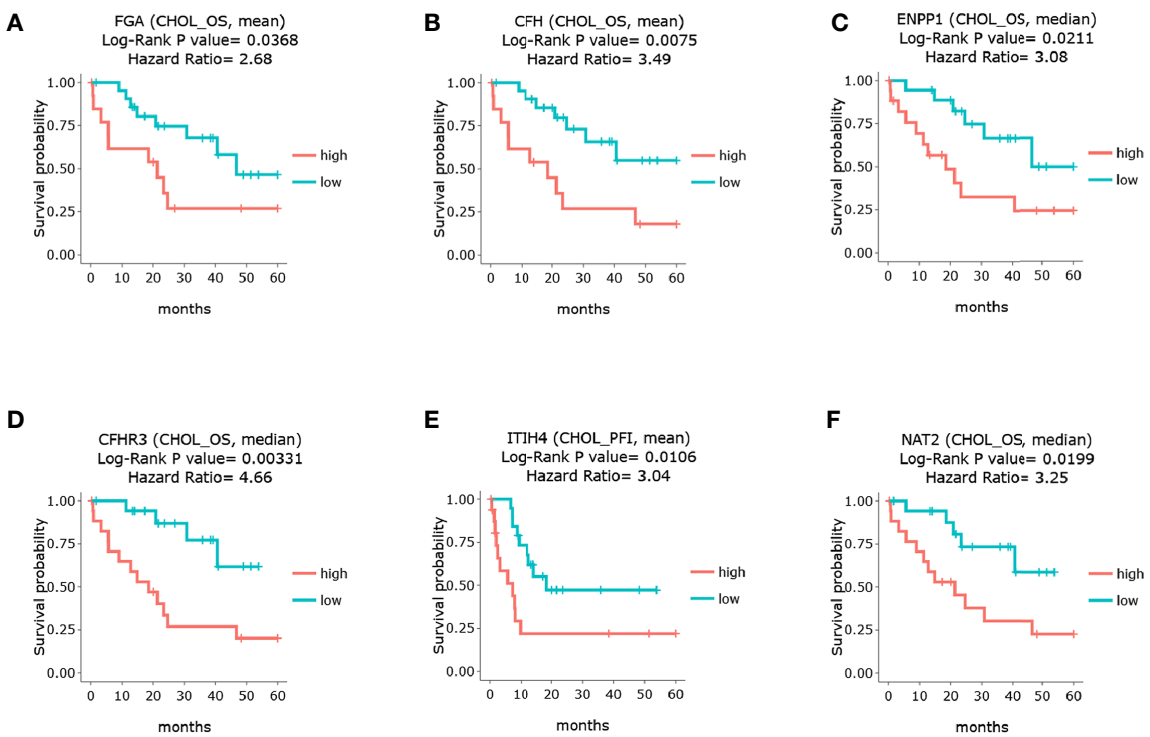

FIGURE 5 | Survival analysis of the core genes in GBC patients through TCGA database. **(A)** survival analysis of FGA. **(B)** survival analysis of CFH. **(C)** survival analysis of ENPP1. **(D)** survival analysis of CFHR3. **(E)** survival analysis of ITIH4. **(F)** survival analysis of NAT2.

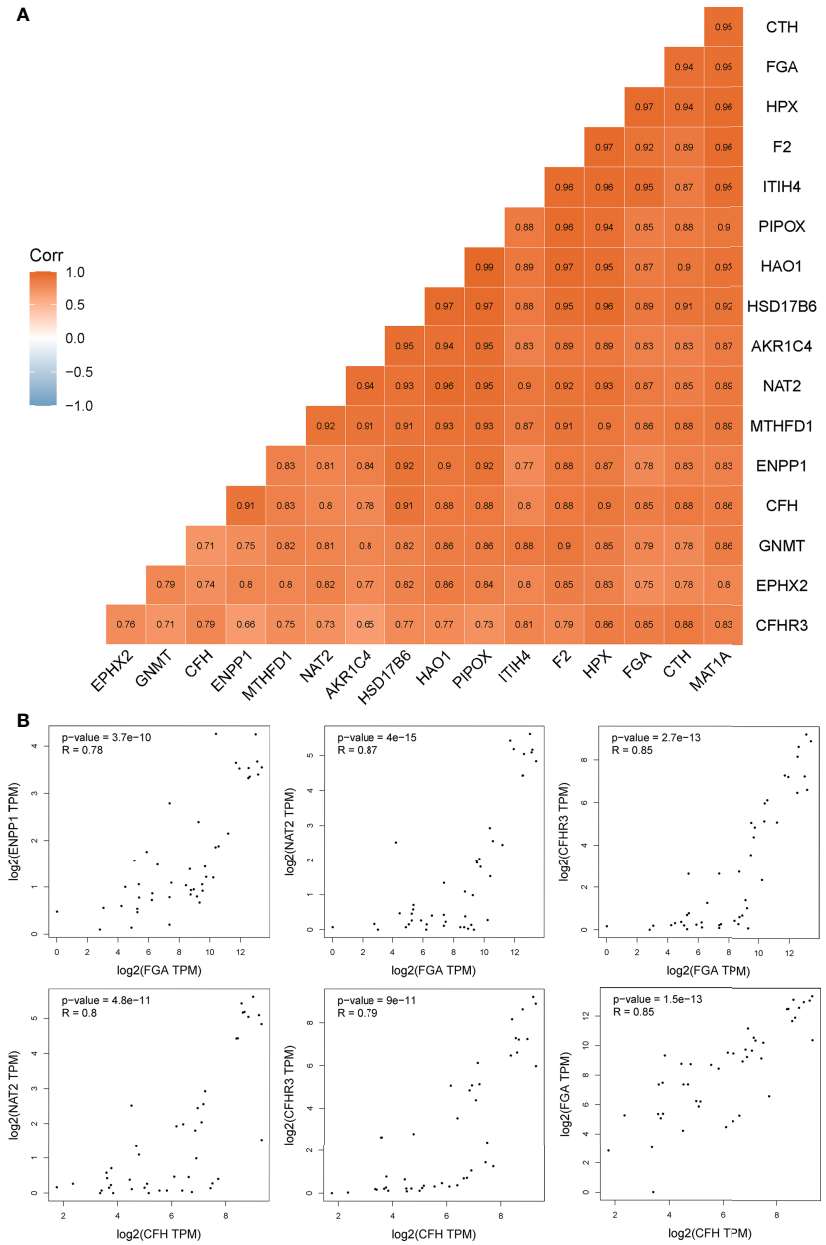

FIGURE 6 | The correlation coefficients among 17 core genes from the TCGA CHOL dataset. **(A)** the details of correlation coefficients by Pearson statistical analysis among 17 core genes. **(B)** the genes positively correlated with *FGA* and *CFH*.

advanced prostate cancer is associated with poor survival, and H2S produced by *CTH* promotes the progression and metastasis of prostate cancer through the IL-1β/NF-κB signaling pathway (40). *GNMT* (Glycine N-Methyltransferase) catalyzes the methylation of glycine to form sarcosine, but in this study, we found that it mainly participates in bile metabolism and has little to do with the methylation of hub genes in the development of gallbladder cancer (41). HAO1, encoding the enzyme hydroxyacid oxidase 1, is expressed primarily in the liver and is related to primary hyperoxaluria type 1 (42). *ITIH4*, inter-alpha-trypsin inhibitor heavy chain 4, is an acute response protein that is secreted primarily by the liver and associated with hepatocellular carcinoma (43). It has been found that crosstalk between FOXM1/NF-κB and MAT1A (methionine adenosyl transferase 1A) may affect tumorigenesis in liver cancer, but little is known about *MAT1A* in GBC (44). *MTHFD1*, methylenetetrahydrofolate dehydrogenase, cyclohydrolase, and formyltetrahydrofolate synthetase 1, has also been reported to be overexpressed in hepatocellular carcinoma and to predict poor survival and recurrence (45).

On account of the results above, *FGA*, *CFH*, *ENPP1*, *ITIH4*, *CFHR3*, and *NAT2* were highly expressed in GBC tissues than

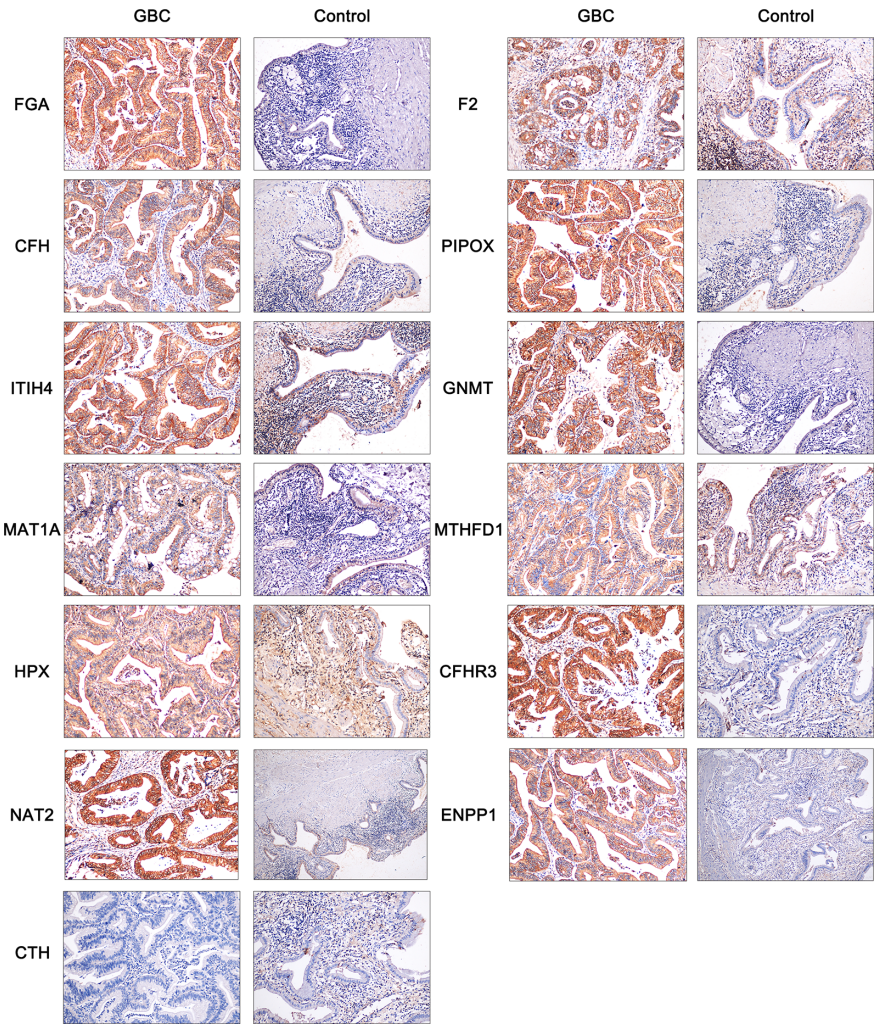

FIGURE 7 | Immunohistochemistry of FGA, F2, CFH, PIPOX, ITIH4, GNMT, MAT1A, MTHFD1, HPX, CTH, CFHR3, ENNP1, and NAT2 in clinical GBC and control specimens.

control tissues, and associated with GBC prognosis. In addition, *FGA* and *CFH* were identified as RNA methylation-related biomarkers in GBC, which may be novel biomarkers to early diagnose and evaluate prognosis for GBC.

CONCLUSION

In conclusion, by utilizing a comprehensive strategy of big data mining and computational biology, we constructed a protein-protein interaction network and ranked genes, ultimately finding that the core genes *FGA*, *F2*, *HAO1*, *CFH*, *PIPOX*, *ITIH4*, *GNMT*, *MAT1A*, *MTHFD1*, *HPX*, *CTH*, *EPHX2*, *HSD17B6*, *AKR1C4*, *CFHR3*, *ENNP1*, and *NAT2* are involved in methylation signaling pathways and bile-related biological processes in GBC. We performed pathway annotation, TCGA verification, posttranslational modification analysis, survival analysis, and IHC on these core genes to finally obtain six candidates, including *FGA*, *CFH*, *ENPP1*, *ITIH4*, *CFHR3* and *NAT2*, associated with prognosis in GBC, and *FGA* and *CFH* were identified as RNA methylation-related biomarkers in GBC. Focusing on development and epigenetic changes such as RNA methylation may be helpful for early diagnosis of GBC, and we have reason to believe that detection of the RNA methylation levels of *FGA* and *CFH* could be used as a potential diagnostic and prognostic evaluation strategy. Moreover, whether the detection of circulating cell-free RNA of *FGA* and *CFH* is effective to diagnose the early stage of GBC will be further studied in our subsequent experiments.

DATA AVAILABILITY STATEMENT

The original contributions presented in the study are included in the article/**Supplementary Material**. Further inquiries can be directed to the corresponding authors.

ETHICS STATEMENT

The studies involving human participants were reviewed and approved by the ethics committee of Chongqing Medical University. The patients/participants provided their written informed consent to participate in this study. Written informed consent was obtained from the individual(s) for the publication of any potentially identifiable images or data included in this article.

AUTHOR CONTRIBUTIONS

CY and NJ conceived and designed this research. ZY, JL, and XL collected and downloaded the relative data. CY and JC analyzed the data and processed them. BZ collected clinical samples and performed histochemistry. NJ wrote the paper. All authors contributed to the article and approved the submitted version.

FUNDING

This work was supported by The National Natural Science Foundation of Chongqing of China (No. cstc2020jcyj-bshX0069).

SUPPLEMENTARY MATERIAL

The Supplementary Material for this article can be found online at: https://www.frontiersin.org/articles/10.3389/fonc.2021.621806/full#supplementary-material

REFERENCES

1. Montalvo-Jave EE, Rahnemai-Azar AA, Papaconstantinou D, Deloiza ME, Tsilimigras DI, Moris D, et al. Molecular pathways and potential biomarkers in gallbladder cancer: A comprehensive review. *Surg Oncol* (2019) 31:83–9. doi: 10.1016/j.suronc.2019.09.006
2. Ashai N, Prasad P, Rajdev L. Multimodality Management of Localized Biliary Cancer. *Curr Treat Options Oncol* (2019) 20(7):58. doi: 10.1007/s11864-019-0655-0
3. Miller G, Jarnagin WR. Gallbladder carcinoma. *Eur J Surg Oncol* (2008) 34 (3):306–12. doi: 10.1016/j.ejso.2007.07.206
4. Ma S, Chen C, Ji X, Liu J, Zhou Q, Wang G, et al. The interplay between m6A RNA methylation and noncoding RNA in cancer. *J Hematol Oncol* (2019) 12 (1):121. doi: 10.1186/s13045-019-0805-7
5. Pan Y, Ma P, Liu Y, Li W, Shu Y. Multiple functions of m 6 A RNA methylation in cancer. *J Hematol Oncol* (2018) 11(1):48. doi: 10.1186/s13045-018-0590-8
6. Wang Y, Li Y, Yue M, Wang J, Kumar S, Wechsler-Reya RJ, et al. N 6-methyladenosine RNA modification regulates embryonic neural stem cell self-renewal through histone modifications. *Nat Neurosci* (2018) 21(2):195–206. doi: 10.1038/s41593-017-0057-1
7. Lichinchi G, Gao S, Saletore Y, Gonzalez GM, Bansal V, Wang Y, et al. Dynamics of the human and viral m(6)A RNA methylomes during HIV-1 infection of T cells. *Nat Microbiol* (2016) 1:16011. doi: 10.1038/nmicrobiol.2016.11
8. Barbieri I, Tzelepis K, Pandolfini L, Shi J, Millán-Zambrano G, Robson SC, et al. Promoter-bound METTL3 maintains myeloid leukaemia by m6A-dependent translation control. *Nature* (2017) 552(7683):126–31. doi: 10.1038/nature24678
9. Kasowitz SD, Ma J, Anderson SJ, Leu NA, Xu Y, Gregory BD, et al. Nuclear m6A reader YTHDC1 regulates alternative polyadenylation and splicing during mouse oocyte development. *PloS Genet* (2018) 14(5):e1007412. doi: 10.1371/journal.pgen.1007412
10. Shi H, Wang X, Lu Z, Zhao BS, Ma H, Hsu PJ, et al. YTHDF3 facilitates translation and decay of N6-methyladenosine-modified RNA. *Cell Res* (2017) 27(3):315–28. doi: 10.1038/cr.2017.15
11. Cheng M, Sheng L, Gao Q, Xiong Q, Zhang H, Wu M, et al. The m6A methyltransferase METTL3 promotes bladder cancer progression via AFF4/NF-κB/MYC signaling network. *Oncogene* (2019) 38(19):3667–80. doi: 10.1038/s41388-019-0683-z
12. Liu J, Eckert MA, Harada BT, Liu SM, Lu Z, Yu K, et al. m6A mRNA methylation regulates AKT activity to promote the proliferation and tumorigenicity of endometrial cancer. *Nat Cell Biol* (2018) 20(9):1074–83. doi: 10.1038/s41556-018-0174-4
13. Lin S, Choe J, Du P, Triboulet R, Gregory RI. The m6A methyltransferase METTL3 promotes translation in human cancer cells. *Mol Cell* (2016) 62 (3):335–45. doi: 10.1016/j.molcel.2016.03.021
14. Ma JZ, Yang F, Zhou CC, Liu F, Yuan JH, Wang F, et al. METTL14 suppresses the metastatic potential of hepatocellular carcinoma by modulating N6-methyladenosine-dependent primary MicroRNA processing. *Hepatology* (2017) 65(2):529–43. doi: 10.1002/hep.28885
15. Dai D, Wang H, Zhu L, Jin H, Wang X. N6-methyladenosine links RNA metabolism to cancer progression. *Cell Death Dis* (2018) 9(2):124. doi: 10.1038/s41419-017-0129-x
16. Patil DP, Chen CK, Pickering BF, Chow A, Jackson C, Guttman M, et al. m(6)A RNA methylation promotes XIST-mediated transcriptional repression. *Nature* (2016) 537(7620):369–73. doi: 10.1038/nature19342
17. Chen M, Wei L, Law CT, Tsang FH, Shen J, Cheng CL, et al. RNA N6-methyladenosine methyltransferase-like 3 promotes liver cancer progression through YTHDF2-dependent posttranscriptional silencing of SOCS2. *Hepatology* (2018) 67(6):2254–70. doi: 10.1002/hep.29683
18. Zhou S, Bai ZL, Xia D, Zhao ZJ, Zhao R, Wang YY, et al. FTO regulates the chemo-radiotherapy resistance of cervical squamous cell carcinoma (CSCC) by targeting β-catenin through mRNA demethylation. *Mol Carcinog* (2018) 57(5):590–7. doi: 10.1002/mc.22782
19. Ma MZ, Zhang Y, Weng MZ, Wang SH, Hu Y, Hou ZY, et al. Long noncoding RNA GCASPC, a target of miR-17-3p, negatively regulates pyruvate carboxylase-dependent cell proliferation in gallbladder cancer. *Cancer Res* (2016) 76(18):5361–71. doi: 10.1158/0008-5472.CAN-15-3047
20. Liang HB, Cao Y, Ma Q, Shu YJ, Wang Z, Zhang F, et al. MYBL2 is a potential prognostic marker that promotes cell proliferation in gallbladder cancer. *Cell Physiol Biochem* (2017) 41(5):2117–31. doi: 10.1159/000475454
21. Matsushita S, Onishi H, Nakano K, Nagamatsu I, Imaizumi A, Hattori M, et al. Hedgehog signaling pathway is a potential therapeutic target for gallbladder cancer. *Cancer Sci* (2014) 105(3):272–80. doi: 10.1111/cas.12354
22. Li M, Liu F, Zhang F, Zhou W, Jiang X, Yang Y, et al. Genomic ERBB2/ERBB3 mutations promote PD-L1-mediated immune escape in gallbladder cancer: a whole-exome sequencing analysis. *Gut* (2019) 68(6):1024–33. doi: 10.1136/gutjnl-2018-316039
23. Kolde R, Laur S, Adler P, Vilo J. Robust rank aggregation for gene list integration and meta-analysis. *Bioinformatics* (2012) 28(4):573–80. doi: 10.1093/bioinformatics/btr709
24. Ge SX, Jung D, Jung D, Yao R. ShinyGO: A graphical gene-set enrichment tool for animals and plants. *Bioinformatics* (2020) 36(8):2628–9. doi: 10.1093/bioinformatics/btz931
25. Deng M, Brägelmann J, Schultze JL, Perner S. Web-TCGA: an online platform for integrated analysis of molecular cancer data sets. *BMC Bioinformatics* (2016) 17:72. doi: 10.1186/s12859-016-0917-9
26. Xuan JJ, Sun WJ, Lin PH, Zhou KR, Liu S, Zheng LL, et al. RMBase v2.0: deciphering the map of RNA modifications from epitranscriptome sequencing data. *Nucleic Acids Res* (2018) 46(D1):D327–34. doi: 10.1093/nar/gkx934
27. Zheng Y, Nie P, Peng D, He Z, Liu M, Xie Y, et al. m6AVar: a database of functional variants involved in m6A modification. *Nucleic Acids Res* (2018) 46 (D1):D139–45. doi: 10.1093/nar/gkx895

28. Sun D, Wang J, Han Y, Dong X, Ge J, Zheng, et al. TISCH: a comprehensive web resource enabling interactive single-cell transcriptome visualization of tumor microenvironment. *Nucleic Acids Res* (2021) 49(D1):D1420–30. doi: 10.1093/nar/gkaa1020
29. Clough E, Barrett T. The gene expression omnibus database. *Methods Mol Biol*. Springer (2016) 1418:93–110. doi: 10.1007/978-1-4939-3578-9_5
30. Tiwari PK. Epigenetic Biomarkers in Gallbladder Cancer. *Trends Cancer* (2020) 6(7):540–3. doi: 10.1016/j.trecan.2020.03.003
31. Gao Y, Wang Z, Zhu Y, Zhu Q, Yang Y, Jin Y, et al. NOP2/Sun RNA methyltransferase 2 promotes tumor progression via its interacting partner RPL6 in gallbladder carcinoma. *Cancer Sci* (2019) 110(11):3510–9. doi: 10.1111/cas.14190
32. Wang M, Zhang G, Zhang Y, Cui X, Wang S, Gao S, et al. Fibrinogen Alpha Chain Knockout Promotes Tumor Growth and Metastasis through Integrin-AKT Signaling Pathway in Lung Cancer. *Mol Cancer Res* (2020) 18(7):943–54. doi: 10.1158/1541-7786.MCR-19-1033
33. Khan AP, Rajendiran TM, Ateeq B, Asangani IA, Athanikar JN, Yocum AK, et al. The role of sarcosine metabolism in prostate cancer progression. *Neoplasia* (2013) 15(5):491–501. doi: 10.1593/neo.13314
34. Zhou M, Zhang L, Yang Q, Yan C, Jiang P, Lan Y, et al. Age-related gene expression and DNA methylation changes in rhesus macaque. *Genomics* (2020) 112(6):5147–56. doi: 10.1016/j.ygeno.2020.09.021
35. Ingoglia G, Sag CM, Rex N, De Franceschi L, Vinchi F, Cimino J, et al. Hemopexin counteracts systolic dysfunction induced by heme-driven oxidative stress. *Free Radic Biol Med* (2017) 108:452–64. doi: 10.1016/j.freeradbiomed.2017.04.003
36. Yoon JK, Kim DH, Koo JS. Implications of differences in expression of sarcosine metabolism-related proteins according to the molecular subtype of breast cancer. *J Transl Med* (2014) 7(11):7824–33. doi: 10.1186/1479-5876-12-149
37. Nepokroeff CM, Lakshmanan MR, Ness GC, Dugan RE, Porter JW. Regulation of the diurnal rhythm of rat liver beta-hydroxy-beta-methylglutaryl coenzmye A reductase activity by insulin, glucagon, cyclic AMP and hydrocortisone. *Arch Biochem Biophys* (1974) 160(2):387–96. doi: 10.1016/0003-9861(74)90412-3
38. Subbiah MT, Yunker RL. Cholesterol 7 alpha-hydroxylase of rat liver: an insulin sensitive enzyme. *Biochem Biophys Res Commun* (1984) 124(3):896–902. doi: 10.1016/0006-291X(84)91042-8
39. Lee DK, Jang SI. Pathogenesis and treatment of gallbladder stone. *Diseases of the Gallbladder*. (2020). p. 85–100. doi: 10.1007/978-981-15-6010-1_8
40. Wang YH, Huang JT, Chen WL, Wang RH, Kao MC, Pan YR, et al. Dysregulation of cystathionine γ-lyase promotes prostate cancer progression and metastasis. *EMBO Rep* (2019) 20(10):e45986. doi: 10.15252/embr.201845986
41. Chen M, Yang M-H, Chang M-M, Tyan Y-C, Chen Y-MA. Tumor suppressor gene glycine N-methyltransferase and its potential in liver disorders and hepatocellular carcinoma. *Toxicol Appl Pharmacol* (2019) 378:114607. doi: 10.1016/j.taap.2019.114607
42. Querbes W, Fitzgerald K, Bettencourt B, Liebow A, Erbe DV. *Compositions and methods for inhibition of HAO1 (Hydroxyacid Oxidase 1 (Glycolate Oxidase)) gene expression*. U.S. Patent and Trademark Office (2019) U.S. Patent 10,478,500.
43. Nakamura N, Hatano E, Iguchi K, Sato M, Kawaguchi H, Ohtsu I, et al. Elevated levels of circulating ITIH4 are associated with hepatocellular carcinoma with nonalcoholic fatty liver disease: from pig model to human study. *BMC Cancer* (2019) 19(1):621. doi: 10.1186/s12885-019-5825-8
44. Li Y, Lu L, Tu J, Zhang J, Xiong T, Fan W, et al. Reciprocal Regulation Between Forkhead Box M1/NF-κB and Methionine Adenosyltransferase 1A Drives Liver Cancer. *Hepatology* (2020) 72(5):1682–700. doi: 10.1002/hep.31196
45. Yu H, Wang H, Xu HR, Zhang YC, Yu XB, Wu MC, et al. Overexpression of MTHFD1 in hepatocellular carcinoma predicts poorer survival and recurrence. *Future Oncol* (2019) 15(15):1771–80. doi: 10.2217/fon-2018-0606

Conflict of Interest: The authors declare that the research was conducted in the absence of any commercial or financial relationships that could be construed as a potential conflict of interest.

frontiers in Oncology

ORIGINAL RESEARCH
published: 11 March 2021
doi: 10.3389/fonc.2021.646536

Grade G2 Rectal Neuroendocrine Tumor Is Much More Invasive Compared With G1 Tumor

Yi-Wei Li[1,2†], *Yi-Ping He*[2,3†], *Fang-Qi Liu*[1,2], *Jun-Jie Peng*[1,2], *San-Jun Cai*[1,2], *Ye Xu*[1,2*] *and Ming-He Wang*[1,2*]

[1] Department of Colorectal Surgery, Fudan University Shanghai Cancer Center, Shanghai, China, [2] Department of Oncology, Shanghai Medical College, Fudan University, Shanghai, China, [3] Department of Endoscopy, Fudan University Shanghai Cancer Center, Shanghai, China

OPEN ACCESS

Edited by:
Rui Liao,
First Affiliated Hospital of Chongqing Medical University, China

Reviewed by:
Guiyu Wang,
The Second Affiliated Hospital of Harbin Medical University, China
Jian Li,
Beijing Cancer Hospital, China

***Correspondence:**
Ming-He Wang
wangminghe250@sina.com
Ye Xu
xu_shirley021@163.com

[†]These authors have contributed equally to this work and share first authorship

Specialty section:
This article was submitted to Gastrointestinal Cancers, a section of the journal Frontiers in Oncology

Received: 27 December 2020
Accepted: 28 January 2021
Published: 11 March 2021

Citation:
Li Y-W, He Y-P, Liu F-Q, Peng J-J, Cai S-J, Xu Y and Wang M-H (2021) Grade G2 Rectal Neuroendocrine Tumor Is Much More Invasive Compared With G1 Tumor. Front. Oncol. 11:646536. doi: 10.3389/fonc.2021.646536

Background: To compare clinicopathologic feature of rectal neuroendocrine tumor (NET) grade G1 with G2 NET.

Methods: Six hundred-one cases of rectal G1 and G2 NETs diagnosed in our center were analyzed.

Results: Of 601 cases of rectal NET, 515 cases were with grade G1 and 86 cases were with grade G2. Median tumor size was 0.7 cm. Compared with G1 NET, G2 tumors were with significantly larger tumor size (0.8 vs 2.2 cm, $p < 0.001$), less percentages of patients with tumors confined to submucosa (92.6 vs 42.8%, $p < 0.001$), more frequent presence of microvascular invasion (MVI) (3.6 vs 16.9%, $p < 0.001$) or peri-neural invasion (PNI) (2.0 vs 24.1%, $p < 0.001$). Incidence of lymph node and distant metastasis was 5.2 and 2.1% in G1 NET compared with 44.2 and 31.4% in G2 tumor, respectively ($p < 0.001$). For tumors sized 1–2 cm and confined to submucosa, incidence of lymph node metastasis was 6.1% for G1 NET compared with 21.1% for G2 NET. Status of MVI/PNI was predictive of lymph node metastasis for G2 tumor rather than G1 NET in this subgroup.

Conclusions: Rectal G2 NET was much more invasive with significantly elevated prevalence of lymph node metastasis compared with G1 tumor.

Keywords: neuroendocrine tumor (NET), neuroendocrine *neoplasm* (NEN), carcinoid, metastasis, treatment

INTRODUCTION

Neuroendocrine tumor (NET) of the rectum includes three subgroups of tumors with great heterogeneity. According to mitotic count or Ki-67 index, NET is divided into three subgroups: well-differentiated G1 NET with indolent nature and favorable prognosis, moderately-differentiated G2 NET with intermediate risk of metastasis, and poorly-differentiated G3 NET (also termed as neuroendocrine carcinoma, NEC) with frequent metastasis and dismal outcome (1, 2). Evidence from the Surveillance, Epidemiology, and End Results (SEER) registries has indicated that the median survival for localized, regional, and distant disease is 223/111/33 months in well- and moderately-differentiated NET compared with 34/14/5 months in poorly-differentiated NET, respectively (3, 4). Grade is a dominant predictor for metastasis of rectal NET (5). Therefore,

precise classification of tumor grade is important for management of rectal NET. However, due to low prevalence of rectal NET, diagnosis and evaluation of tumor grade is sometimes difficult in some hospitals without large sample size of patients. Information about tumor grade is frequently missing in most reported literature from nationwide or multi-center database (6, 7). Data from National Cancer Database of the America included 16,531 cases of rectal NET from 2004 to 2015, of which tumor grade was unknown in 59.9% of patients (4). Besides, most reports have included G1 NET and G2 NET together, termed as carcinoid. Since G1 tumor accounts for approximately 80–90% of rectal NET. This would underestimate the metastatic risk of this disease. Up to now, few studies have focused on detailed information about clinicopathologic feature, treatment modality and prognosis of rectal NETs based on different grades (G1/G2/G3). Direct comparison of rectal NET G1 with G2 tumor is necessary regarding more precise therapy.

Prediction of lymph node metastasis plays crucial role for management of rectal carcinoid according to consensus guidelines (1, 2). For rectal carcinoid sized smaller than 10 mm and confined to submucosa, local excision is suggested to be enough due to rare incidence of lymph node metastasis. A report enrolling 788 cases with T1 rectal carcinoid tumors from The Surveillance Epidemiology and End Results (SEER) database indicated that prevalence of metastasis was 1.1% for tumors ≤ 10 mm compared with 6.6% in lesions 11 to 19 mm (8). Another national cohort study from National Cancer Database (NCDB) enrolled 17,448 cases of rectal NET, of which 4.2% of cases were moderate-differentiated tumors (G2). The results indicated that prevalence of lymph node metastasis was 2.5% for tumors ≤ 10 mm compared with 12.8% for tumors sized 11–20 mm (4). By contrast, evidence from multi-institutional studies of European and North American centers (9) or Japan (7) indicated much higher prevalence of lymph node metastasis: 7–8% for tumors sized ≤10 mm and 31–40% for tumors sized 11–20 mm, respectively. For rectal carcinoid larger than 20 mm, prevalence of lymph node metastasis increased as high as 24.1–58% (4, 7). Therefore, radical resection with regional lymphadenectomy was recommended.

Treatment of rectal carcinoid tumors sized 10 to 20 mm is still controversial. For patients with high risk of lymph node metastasis including presence of lymphovascular invasion (LVI) or peri-neural invasion (PNI), radical resection with regional lymphadenectomy is recommended. Data from NCDB of the America indicated that about three quarters (755/1,013, 263/342) of rectal carcinoid sized 11–20 mm or 10–20 mm received local excision (4, 10). By contrast, a nationwide cohort in Japan from 1984 to 1998 enrolled 345 cases of colorectal carcinoids (rectum: 92%), of which only 19% of cases received endoscopic resection and 80% of cases received surgery (7). Several reasons might contribute to the difference between western and eastern countries. First, percentage of cases with tumors smaller than 10 mm was 79.8% in the cohort from NCDB of the America compared with 63% in the cohort from Japan. Second, the cohort from Japan was in the earlier era when endoscopic resection was not widely used. More importantly, moderately differentiated G2 NET consisted only 4.2% of the cohort from NCDB, which was much lower than that reported from other countries (11). Information about tumor differentiation grade was unknown in 59.9% of cases from NCDB cohort and not mentioned in the Japan cohort. Due to frequent loss of information about tumor grade (12), comparison of results from different institutions seemed difficult. Comparison of G1 with G2 rectal NET is therefore necessary for better understanding of the disease and optimal choice of treatment.

In the present study, we analyzed 601 cases of rectal G1 and G2 NETs diagnosed in our center. Our results demonstrated that, compared with G1 NET, G2 tumors were with significantly larger tumor size, deeper invading depth, more frequent presence of microvascular invasion or peri-neural invasion, which were associated with elevated incidence of lymph node metastasis and distant metastasis. For tumors sized 1–2 cm and confined to submucosa, local excision might be appropriate, for which evaluation of MVI/PNI was useless. By contrast, for G2 tumors, radical resection was recommended especially for those with presence of MVI/PNI. Our results would help discriminate the metastatic potential as well as treatment modalities for indolent G1 NET compared with moderately-invasive G2 tumor.

MATERIALS AND METHODS

From 1981 to 2018, 656 cases of rectal neuroendocrine tumors (NET) were diagnosed and treated in Shanghai Cancer Center Fudan University (FUSCC). 55 cases were excluded from analysis, of which 40 cases were with accompanied malignancy of other origin, 5 cases were with indeterminate tumor size, 6 cases were with unknown tumor invading depth and 4 cases were with uncertain pathology (**Figure 1**). All the cases were pathologically confirmed. Tumor grade was determined by cell mitoses or Ki-67 index (2) as well as histology: <2 mitoses/HPF or <3% Ki-67 index for G1, 2-20 mitoses/HPF or 3–20% Ki-67 index for G2, respectively (13). Tumor staging was conducted according to European Neuroendocrine Tumor Society (ENETS) TNM classification for NET of the colon and rectum (2), in which T stage was combination of tumor invading depth and tumor size. Tumors invaded mucosa or submucosa and sized ≤ 2 cm were defined as stage T1, tumors invaded muscularis propria or sized >2 cm were defined as stage T2. Clinicopathologic data was recorded from hospital database. This study was approved by the Research Ethics Committee of FUSCC. Informed consent was obtained from all participants. The last follow-up time was June 2019. Data analysis was performed using IBM SPSS statistics version 23. Chi-square analysis was used to test differences among subgroups. A two-sided $p < 0.05$ was considered as statistically significant.

RESULTS

Clinicopathologic Feature of the Cohort

Of 601 cases of rectal neuroendocrine tumors (**Table 1**), 346 (57.6%) cases were male. Median values for patient age, distance

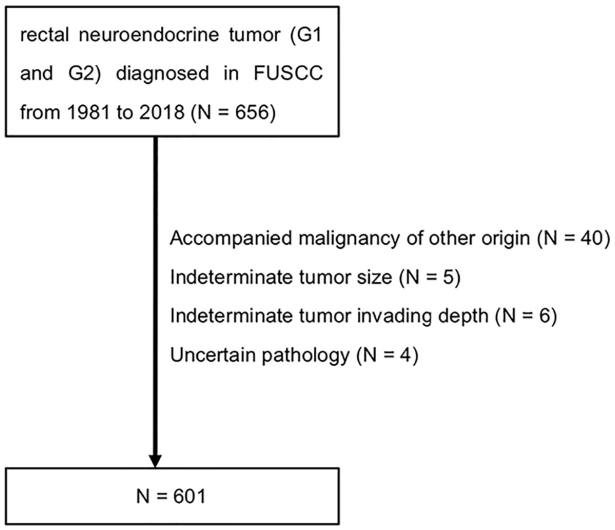

FIGURE 1 | Flowchart of the study population. FUSCC, Fudan University Shanghai Cancer Center.

TABLE 1 | Clinicopathologic Features of 601 cases of G1/G2 rectal NET.

Gender	Male	346 (57.6%)
	Female	255 (42.4%)
Age (year)	Median 50 (18–83)	
Distance from anal verge (cm)	Median 5 (1–15)	
Tumor size (cm)	Median 0.7 (0.2-13.0)	
Tumor grade	G1	515 (85.7%)
	G2	86 (14.3%)
Invading depth	T0	399 (66.4%)
	T1	114 (19.0%)
	T2	34 (5.7%)
	T3	31 (5.2%)
	T4	21 (3.5%)
N stage	N0	536 (89.2%)
	N1	65 (10.8%)
M stage	M0	563 (93.7%)
	M1	38 (6.3%)
ENETS TNM stage	Ia	392 (65.2%)
	Ib	108 (18.0%)
	II	21 (3.5%)
	III	42 (7.0%)
	IV	38 (6.3%)
Microvascular invasion	no	293 (48.8%)
	yes	19 (3.2%)
	unknown	289 (48.1%)
Perineural invasion	no	288 (47.9%)
	yes	19 (3.2%)
	unknown	294 (48.9%)
Surgical modality	none	13 (2.1%)
	EMR	49 (8.2%)
	ESD	196 (32.6%)
	TEM	266 (44.3%)
	AR/APR/hartman	77 (12.8%)

EMR, Endoscopic Mucosal Resection; ESD, Endoscopic Submucosal Dissection; TEM, Transanal Endoscopic Microsurgery; AR, Anterior Resection; APR, Abdomen Perineal Resection.

from anal verge and tumor diameter were 50 years old (range 18–83), 5 cm (range 1–15) and 0.7 cm (range 0.2–13.0), respectively. 515 (85.7%) cases were with grade G1 and 86 (14.3%) cases were with grade G2. 513 (85.4%) cases were with tumors confined to submucosa and 86 (14.3%) cases were with tumors invading deeper than muscularis propria. Sixty-five (10.8%) cases were with regional lymph node metastasis and 38 (6.3%) cases were with distant metastasis. Percentages of patients with ENETS TNM stage I, II, III, and IV were 83.2, 3.5, 7.0, and 6.3%, respectively. For evaluation of microvascular invasion (MVI), information was unknown for 289 (48.1%) cases. 19 patients were with presence of MVI and 293 cases were with absence of MVI. For evaluation of perineural invasion (PNI), information was indeterminate for 294 (48.9%) cases. Nineteen cases were with positive PNI and 288 cases were with negative PNI. Thirteen (2.1%) patients gave up for any treatment, 511 (85.0%) cases received local excision and 77 (12.8%) cases received radical resection.

Comparison of Rectal G1 NET With G2 Tumor

Using chi-square analysis, we tested the difference between rectal G1 NET with G2 tumor (**Table 2**). Distribution of patient gender ($p = 0.290$) as well as distance from anal verge ($p = 0.768$) was not significantly different between G1 and G2 NETs. Patients diagnosed with G1 NET were younger than patients with G2 disease (49 vs 52 years old, $p = 0.043$). Compared with G1 NET, patients with G2 tumor were with significantly larger tumor size (0.8 vs 2.2 cm, $p = 3.3E-10$), less percentages of cases with tumor confined to submucosa (92.6 vs 42.8%, $p = 4.5E-47$), elevated incidence of lymph node metastasis (5.2 vs 44.2%, $p = 5.0E-27$) as well as distant metastasis (2.1 vs 31.4%, $p = 5.6E-25$). Percentages of patients with ENETS TNM stage I disease were much fewer for patients with G2 NET compared with G1 tumor (36.0 vs 91.1%, $p = 3.2E-39$). Presence of microvascular invasion (16.9 vs 3.6%, $p = 1.0E-4$) or perineural invasion (24.1 vs 2.0%, $p = 2.9E-10$) was much more common for G2 NET compared with G1 disease. The 92.9% of cases received local excision for G1 NET, compared with 48.1% for G2 tumors ($p = 1.6E-27$).

Risk Factors Predicting Lymph Node Metastasis for Rectal NET

Management of rectal NET was decided by predicted risk of regional lymph node metastasis, which was mainly influenced by tumor size, invading depth and MVI/PNI positivity. For tumors sized <1cm, 1–2 cm and >2 cm subgroups, incidence of lymph node metastasis was 0.5, 11.6, and 57.1% for G1 NET ($p = 3.7E-31$) compared with 0, 43.2, and 68.8% for G2 NET ($P = 2.4E-5$), respectively. For tumors with invading depth of T0-1, T2, T3, and T4 subgroups, risk of lymph node metastasis was 1.4, 36.4, 66.7, and 80.0% for G1 NET ($p = 2.9E-46$) compared with 11.1, 58.3, 76.0, and 63.6% for G2 NET ($p = 2.0E-6$). Compared with patients without microvascular invasion (MVI), patients with presence of MVI were with higher incidence of lymph node metastasis for G1 NET (7.4 vs 33.3%, $p = 0.030$) as well as for G2 NET (42.9 vs 80.0%, $p = 0.042$). For G1 NET, presence of

TABLE 2 | Comparison of rectal G1 NET with G2 tumor (n = 601).

		G1	G2	p
Gender	male	292	54	0.290
	female	223	32	
Age	mean	49	52	0.043
Distance from anal verge (cm)	mean	5.9	5.8	0.768
Tumor size (cm)	mean	0.8	2.2	3.3E-10
Invading depth*	T0	394	5	4.5E-47
	T1	83	31	
	T2	22	12	
	T3	6	25	
	T4	10	11	
	T0-1/total, %	92.6	42.8	
N stage	N0	488	48	5.0E-27
	N1	27	38	
	N1/total, %	5.2	44.2	
M stage	M0	504	59	5.6E-25
	M1	11	27	
	M1/total, %	2.1	31.4	
TNM stage**	Ia	376	16	3.2E-39
	Ib	93	15	
	II	15	6	
	III	20	22	
	IV	11	27	
	I/total, %	91.1	36.0	
Microvascular invasion***	no	244	49	1.0E-4
	yes	9	10	
	yes/total	3.6	16.9	
Perineural invasion***	no	244	44	2.9E-10
	yes	5	14	
	yes/total, %	2.0	24.1	
Surgical modality******	EMR	48	1	1.6E-27
	ESD	179	17	
	TEM	246	20	
	AR/APR/hartman	36	41	
	local excision/total, %	92.9	48.1	

EMR, Endoscopic Mucosal Resection; ESD, Endoscopic Submucosal Dissection; TEM, Transanal Endoscopic Microsurgery; AR, Anterior Resection; APR, Abdomen Perineal Resection.

**T stage only indicates tumor invading depth without consideration of tumor diameter.*

***TNM stage is according to ENETS TNM staging system, in which T stage is determined by combination of invading depth and tumor size.*

****Information about microvascular invasion and perineural invasion is lost for 48.1% and 48.9% of cases.*

*****Local excision includes the sum of EMR, ESD, and TEM.*

perineural invasion (PNI) was not associated with elevated risk of lymph node metastasis (p = 0.359). Incidence of lymph node metastasis was significantly increased for G2 NET with presence of PNI compared with G2 tumor without presence of PNI (92.9 vs 34.1%, p = 1.3E-4).

Taking tumor size and invading depth together as recommended by consensus guideline for management of rectal NET, we further divided the cohort into three subgroups: tumors smaller than 1 cm and confined to submucosa, tumors sized 1–2 cm and confined to submucosa, tumor larger than 2 cm or invading deeper than muscularis propria. Incidence of lymph node metastasis in three subgroups was 0.3, 6.1, and 51.3% for G1 NET compared with 0, 21.1, and 68.8% for G2 NET, respectively. Of 149 cases with tumors sized 1–2 cm, 83 cases were with complete information of MVI and PNI for analysis. Presence of MVI/PNI was not significantly associated with increased risk of lymph node metastasis for G1 tumor (p = 0.546). For G2 tumor, presence of MVI/PNI was significantly associated with elevated incidence of lymph node metastasis (25.0 vs 100%, p = 0.014).

Treatment Modalities for Subgroups According to Consensus Guideline

We analyzed treatment modalities for subgroups according to consensus guideline for management of rectal NET (**Table 4**). Thirteen cases receiving no surgery were excluded from analysis. For patients with rectal G1 NET (n = 509), incidence of lymph node metastasis was 0.3% for tumors sized <1 cm and confined to submucosa, 98.1% of patients received local excision. For tumors sized >2 cm or invading through muscularis propria, incidence of lymph node metastasis was 55.9 and 61.8% of patients received radical resection. For tumors sized 1–2 cm and confined to submucosa, lymph node metastasis occurred in 8.2% of patients with negative microvascular invasion (MVI) or perineural invasion (PNI), of which 85.7% of patients received local excision. By contrast, no patient suffered from lymph node metastasis for patients with positive MVI or PNI, of which none received radical resection. Of 49 patients with unknown MVI/PNI status, lymph node metastasis rate was 4.1 and 98.0% (48/49) of patients received local excision.

For patients with G2 NET, 16 patients were with tumors sized <1 cm and confined to submucosa, of which incidence of lymph node metastasis was 0% and all the patients received local excision. 43 patients were with tumors larger than 2 cm or invading deeper than muscularis propria, of which lymph node metastasis rate was 72.1 and 86.0% of patients received radical resection. Of 19 patients with tumors sized 1–2 cm and confined to submucosa, 11 patients were with negative MVI/PNI. In 18.2% of patients, lymph node metastasis occurred and 90.9% of patients received local excision. One patient was with positive MVI/PNI, which suffered from lymph node metastasis and thus received radical resection. Information about MVI/PNI was unknown for seven patients, of which one patient suffered from lymph node metastasis and thus received radical resection.

Taking G1 and G2 NETs together into consideration, 392 patients were with tumors smaller than 1 cm and confined to submucosa, of which one patient suffered from lymph node metastasis and seven patients received radical resection. Seventy-seven patients were with tumors larger than 2 cm or invading deeper than muscularis propria, of which 50 patients suffered from lymph node metastasis and 58 patients received radical resection. One hundred-eighteen patients were with tumors sized 1–2 cm and confined to submucosa, of which 60 patients were with negative MVI/PNI. Six patients suffered from lymph node metastasis and eight patients received radical resection. Two patients were with positive MVI or PNI, of which one patient suffered from lymph node metastasis and received radical resection. Of 56 patients with unknown MVI/PNI status, three patients suffered from lymph node metastasis and two patients received radical resection.

DISCUSSION

Annual incidence of neuroendocrine tumor (NET) is steadily increasing from 1.09/100,000 (1973) to 5.25/100,000 (2004) in the United States, of which the rectum was the most common primary site in Asian/pacific Islander (3). A nation-wide retrospective epidemiological survey from 23 hospitals in China has also demonstrated a significantly increased incidence of gastroenteropancreatic NET from 2001 to 2010 and pancreas (31.5%) and the rectum (29.6%) are the most common primary sites (14). Most reported literature has enrolled rectal NET with G1 grade and G2 grade together as carcinoid, probably due to rare incidence of G2 tumor. Current consensus guideline for management of rectal carcinoid also takes indolent G1 tumor with moderately-invasive G2 tumor together into consideration. However, rectal G2 NET is with higher metastatic potential and poorer prognosis compared with G1 NET (11). Comparison of rectal G1 NET with G2 NET is necessary for more précising therapy of this disease.

Rectal NET grade G1 and grade G2 are with different metastatic potential and prognosis, of which the 5-year survival is 97.7 and 60.0%, respectively (11). However, G1 and G2 tumors are frequently included together for analysis in most reported literature. Information about tumor differentiation grade is commonly lost in majorities of reports. A report from National Cancer Database of the America including 17,448 cases of rectal NET indicated that tumor grade was unknown for 59.9% of patients (4). Therefore, comparison of results from different institutions will be difficult due to varied percentages that G1/G2 tumors accounted for. In our study, G2 tumors exhibited larger tumor size and deeper invading depth at diagnosis. The 92.6% of tumors were confined to submucora for G1 tumor compared with 42.8% for G2 tumor. The 44.2% of patients with G2 NET were with lymph node metastasis (**Table 2**), which means about half of G2 tumors can't be locally resected. By contrast, local excision is appropriate for approximately 80–90% of rectal G1 NET, as demonstrated by evidence from nation-wide database indicating that percentages of rectal NET receiving local excision is 79.4, 80, and 92.4% in America, Japan (7), and Korea (6), respectively.

Risk of lymph node metastasis is the most important determinant for deciding whether to receive local excision or radical resection, which was reported to be varied a lot from different countries. Evidence from national database indicated that prevalence of lymph node metastasis for rectal NET is 5.0% in Korea (6), 12.8% in America (6), and 15.1–31.0% in Japan (7, 15), respectively. In our study, prevalence of lymph node metastasis at initial presentation was 44.2% for G2 tumor compared with 5.2% for G1 tumor. Metastatic risk for G2 tumor was much higher than that in above-mentioned literature enrolling mixed population of G1 and G2 tumors together. Indeed, Juha Jernman reported that metastatic risk for G1, G2, and G3 rectal NETs were 0, 81.8, and 100%, respectively (16). In a cohort of 98 patients with rectal NET,

TABLE 3 | Risk factors associated with lymph node metastasis for rectal NET.

	G1 n = 515			G2 n = 86			G1+G2 n = 601		
metastasis	no	yes	%*	no	yes	%	no	yes	%
Tumor size (cm)		p = 3.7E-31			p = 2.4E-5			p = 9.8E-47	
<1	380	2	0.5	17	0	0	397	2	0.5
1-2	99	13	11.6	21	16	43.2	120	29	19.5
>2	9	12	57.1	10	22	68.8	19	34	64.1
Invading depth**		p = 2.9E-46			p = 2.0E-6			p = 7.8E-63	
T0-1	470	7	1.4	32	4	11.1	502	11	2.1
T2	14	8	36.4	5	7	58.3	19	15	44.1
T3	2	4	66.7	6	19	76.0	8	23	74.2
T4	2	8	80.0	4	7	63.6	6	15	71.4
MVI		p = 0.030			p = 0.042			p = 1.8E-5	
no	226	18	7.4	28	21	42.9	254	39	13.3
yes	6	3	33.3	2	8	80.0	8	11	57.9
PNI		p = 0.359			p = 1.3E-4			p = 7.7E-9	
no	224	20	8.2	29	15	34.1	253	35	12.1
yes	4	1	20.0	1	13	92.9	5	14	73.7
Size and depth		p = 5.7E-41			p = 4.2E-7			p = 1.4E-60	
<1cm and T1	376	1	0.3	17	0	0	393	1	0.3
1-2cm and T1	93	6	6.1	15	4	21.1	108	10	8.5
>2cm or T2	19	20	51.3	15	33	68.8	34	53	60.9
1-2cm and T1 subgroup***		p = 0.546			p = 0.014			p = 0.014	
MVI/PNI -	49	10	16.9	12	4	25.0	61	14	18.7
MVI/PNI +	3	1	25.0	0	4	100	3	5	62.5

MVI, Micro-Vascular Invasion; PNI, Peri-Neural Invasion.

Chi-square analysis was used.

**% = yes/(yes + no).*

***T stage only indicates tumor invading depth, without consideration of tumor size.*

****One hundred-eighteen cases were with tumors sized 1-2 cm in diameter and confined to submucosa, of which 83 cases were with complete information of MVI and PNI for analysis.*

TABLE 4 | Treatment modalities according to consensus guideline (n = 588).

Grade	Depth and size	MVI/PNI	LNM	Total	Local excision	Radical resection
G1	T0-1 and <1cm	/	1(0.3%)	376	369(98.1%)	7
	T0-1 and 1-2cm	–	4(8.2%)	49	42(85.7%)	7
		+	0(0%)	1	1	0(0%)
		unknown	2(4.1%)	49	48	1
	>2cm or T2-4	/	19(55.9%)	34	13	21(61.8%)
G2	T0-1 and <1cm	/	0(0%)	16	16(100%)	0
	T0-1 and 1-2cm	–	2(18.2%)	11	10(90.9%)	1
		+	1(100%)	1	0	1(100%)
		unknown	1(14.3%)	7	6	1
	>2cm or T2-4	/	31(72.1%)	43	6	37(86.0%)
G1+G2	T0-1 and <1cm	/	1(0.3%)	392	385(98.2%)	7
	T0-1 and 1-2cm	–	6(10.0%)	60	52(86.7%)	8
		+	1(50.0%)	2	1	1(50.0%)
		unknown	3(5.4%)	56	54	2
	>2cm or T2-4	/	50(64.9%)	77	19	58(75.3%)

MVI, Micro-Vascular Invasion; PNI, Peri-Neural Invasion, LNM, Lymph Node Metastasis.
Chi-square analysis was used.
Thirteen cases receiving no surgery were excluded from analysis.

diminutive tumor (< 1 cm) that metastasized were all G2 (5). Local excision should be done only in carefully selected patients with G2 rectal NET.

Management of rectal NET sized 1–2 cm is complicated. Patients with presence of microvascular invasion (MVI) or perineural invasion (PNI) are suggested to receive radical resection (1, 17). In our study, incidence of lymph node metastasis was 11.6% for G1 tumors sized 1–2 cm and 6.1% for G1 tumors sized 1–2 cm and confined to submucosa. Status of MVI/PNI was not predicted for lymph node metastasis risk for G1 tumors sized 1–2 cm and confined to submucosa (p = 0.546, **Table 3**). The 91.9% (91/99) of patients received local excision in our study (**Table 4**). Therefore, local excision might be enough for G1 tumors sized 1–2 cm and confined to submucosa. For G2 tumors, incidence of lymph node metastasis was 43.2% for tumors sized 1–2 cm and 21.1% for tumors sized 1–2 cm and confined to submucosa (**Table 3**). Presence of MVI or PNI was significantly associated with increased risk of lymph node metastasis. Therefore, local excision could only be done for carefully selected patients in this subgroup. Radical resection should be performed for patients with presence of MVI/PNI. What should be mentioned, information about MVI/PNI was frequently lost in reported literature. A multicenter study from Korea indicated that information about lymphovascular invasion was indeterminate for 43.2% of rectal NETs (18). In our study, information about MVI or PNI was unknown for 48.1 and 48.9% of patients (**Table 1**). Evaluation of MVI/PNI should be routinely done in clinical practice, which is especially important for rectal NETs sized 1–2 cm.

DATA AVAILABILITY STATEMENT

The raw data supporting the conclusions of this article will be made available by the authors, without undue reservation.

ETHICS STATEMENT

The studies involving human participants were reviewed and approved by the Ethical Committee of FUSCC (no.: 050432-4-1212B). The patients/participants provided their written informed consent to participate in this study.

AUTHOR CONTRIBUTIONS

Conception and design: Y-WL, Y-PH, and M-HW. Provision of study materials and patients: M-HW, YX, and S-JC. Data collection: J-JP and F-QL. Data analysis and interpretation: Y-WL and Y-PH. All authors contributed to the article and approved the submitted version.

FUNDING

This study was supported by National Natural Science Foundation of China (No. 81301761 and 81372646) and Research Fund for the Doctoral Program of Higher Education of China (No. 20130071120070).

REFERENCES

1. Ramage JK, Ahmed A, Ardill J, Bax N, Breen DJ, Caplin ME, et al. Guidelines for the management of gastroenteropancreatic neuroendocrine (including carcinoid) tumours (NETs). *Gut* (2012) 61(1):6–32. doi: 10.1136/gutjnl-2011-300831
2. Anthony LB, Strosberg JR, Klimstra DS, Maples WJ, O'Dorisio TM, Warner RR, et al. The NANETS consensus guidelines for the diagnosis and management of gastrointestinal neuroendocrine tumors (nets): well-differentiated nets of the distal colon and rectum. *Pancreas* (2010) 39 (6):767–74. doi: 10.1097/MPA.0b013e3181ec1261
3. Yao JC, Hassan M, Phan A, Dagohoy C, Leary C, Mares JE, et al. One hundred years after "carcinoid": epidemiology of and prognostic factors for neuroendocrine tumors in 35,825 cases in the United States. *J Clin Oncol* (2008) 26(18):3063–72. doi: 10.1200/JCO.2007.15.4377

4. Zhao B, Hollandsworth HM, Lopez NE, Parry LA, Abbadessa B, Cosman BC, et al. Outcomes for a Large Cohort of Patients with Rectal Neuroendocrine Tumors: an Analysis of the National Cancer Database. *J Gastrointest Surg* (2021) 25(2):489–91. doi: 10.1007/s11605-020-04525-6
5. Folkert IW, Sinnamon AJ, Concors SJ, Bennett BJ, Fraker DL, Mahmoud NN, et al. Grade is a Dominant Risk Factor for Metastasis in Patients with Rectal Neuroendocrine Tumors. *Ann Surg Oncol* (2020) 27(3):855–63. doi: 10.1245/s10434-019-07848-0
6. Colonoscopy Study Group of Korean Society of C. Clinical characteristics of colorectal carcinoid tumors. *J Korean Soc Coloproctol* (2011) 27(1):17–20. doi: 10.3393/jksc.2011.27.1.17
7. Konishi T, Watanabe T, Kishimoto J, Kotake K, Muto T, Nagawa H, et al. Prognosis and risk factors of metastasis in colorectal carcinoids: results of a nationwide registry over 15 years. *Gut* (2007) 56(6):863–8. doi: 10.1136/gut.2006.109157
8. Ngamruengphong S, Kamal A, Akshintala V, Hajiyeva G, Hanada Y, Chen YI, et al. Prevalence of metastasis and survival of 788 patients with T1 rectal carcinoid tumors. *Gastrointest Endosc* (2019) 89(3):602–6. doi: 10.1016/j.gie.2018.11.010
9. Shields CJ, Tiret E, Winter DC. International Rectal Carcinoid Study G. Carcinoid tumors of the rectum: a multi-institutional international collaboration. *Ann Surg* (2010) 252(5):750–5. doi: 10.1097/SLA.0b013e3181fb8df6
10. Concors SJ, Sinnamon AJ, Folkert IW, Mahmoud NN, Fraker DL, Paulson EC, et al. Predictors of Metastases in Rectal Neuroendocrine Tumors: Results of a National Cohort Study. *Dis Colon Rectum* (2018) 61(12):1372–9. doi: 10.1097/DCR.0000000000001243
11. Shen C, Yin Y, Chen H, Tang S, Yin X, Zhou Z, et al. Neuroendocrine tumors of colon and rectum: validation of clinical and prognostic values of the World Health Organization 2010 grading classifications and European Neuroendocrine Tumor Society staging systems. *Oncotarget* (2017) 8(13):22123–34. doi: 10.18632/oncotarget.13641
12. Ikeda K, Kojima M, Saito N, Sakuyama N, Koushi K, Watanabe T, et al. Current status of the histopathological assessment, diagnosis, and reporting of colorectal neuroendocrine tumors: A Web survey from the Japanese Society for Cancer of Colon and Rectum. *Pathol Int* (2016) 66(2):94–101. doi: 10.1111/pin.12388
13. Bosman FT, Carneiro F, Hruban RH, Theise ND. WHO classification of tumours of the digestive system. In: *International Agency for Research on Cancer Press, 4th edn* (2010).
14. Fan JH, Zhang YQ, Shi SS, Chen YJ, Yuan XH, Jiang LM, et al. A nation-wide retrospective epidemiological study of gastroenteropancreatic neuroendocrine neoplasms in china. *Oncotarget* (2017) 8(42):71699–708. doi: 10.18632/oncotarget.17599
15. Soga J. Early-stage carcinoids of the gastrointestinal tract: an analysis of 1914 reported cases. *Cancer* (2005) 103(8):1587–95. doi: 10.1002/cncr.20939
16. Jernman J, Valimaki MJ, Louhimo J, Haglund C, Arola J. The novel WHO 2010 classification for gastrointestinal neuroendocrine tumours correlates well with the metastatic potential of rectal neuroendocrine tumours. *Neuroendocrinology* (2012) 95(4):317–24. doi: 10.1159/000333035
17. Caplin M, Sundin A, Nillson O, Baum RP, Klose KJ, Kelestimur F, et al. ENETS Consensus Guidelines for the management of patients with digestive neuroendocrine neoplasms: colorectal neuroendocrine neoplasms. *Neuroendocrinology* (2012) 95(2):88–97. doi: 10.1159/000335594
18. Moon CM, Huh KC, Jung SA, Park DI, Kim WH, Jung HM, et al. Long-Term Clinical Outcomes of Rectal Neuroendocrine Tumors According to the Pathologic Status After Initial Endoscopic Resection: A KASID Multicenter Study. *Am J Gastroenterol* (2016) 111(9):1276–85. doi: 10.1038/ajg.2016.267

Conflict of Interest: The authors declare that the research was conducted in the absence of any commercial or financial relationships that could be construed as a potential conflict of interest.

frontiers in Oncology

ORIGINAL RESEARCH
published: 15 April 2021
doi: 10.3389/fonc.2021.607640

Prediction Model of Tumor Regression Grade for Advanced Gastric Cancer After Preoperative Chemotherapy

Wei Xu[1†], Qianchen Ma[2†], Lingquan Wang[1], Changyu He[1], Sheng Lu[1], Zhentian Ni[1], Zichen Hua[1], Zhenglun Zhu[1], Zhongyin Yang[1], Yanan Zheng[1], Runhua Feng[1], Chao Yan[1], Chen Li[1], Xuexin Yao[1], Mingmin Chen[1], Wentao Liu[1], Min Yan[1*] and Zhenggang Zhu[1*]*

[1] Department of General Surgery, Shanghai Key Laboratory of Gastric Neoplasms, Shanghai Institute of Digestive Surgery, Ruijin Hospital, Shanghai Jiao Tong University School of Medicine, Shanghai, China, [2] Department of Pathology, Ruijin Hospital, Shanghai Jiao Tong University School of Medicine, Shanghai, China

Background: Preoperative chemotherapy (PCT) has been considered an important treatment for advanced gastric cancer (AGC). The tumor regression grade (TRG) system is an effective tool for the assessment of patient responses to PCT. Pathological complete response (TRG = 0) of the primary tumor is an excellent predictor of better prognosis. However, which patients could achieve pathological complete response (TRG = 0) after chemotherapy is still unknown. The study aimed to find predictors of TRG = 0 in AGC.

Methods: A total of 304 patients with advanced gastric cancer from July 2009 to November 2018 were enrolled retrospectively. All patients were randomly assigned (2:1) to training and internal validation groups. In addition, 124 AGC patients receiving PCT from December 2018 to June 2020 were included prospectively in the external validation cohort. A prediction model for TRG = 0 was established based on four predictors in the training group and was validated in the internal and external validation groups.

Results: Through univariate and multivariate analyses, we found that CA199, CA724, tumor differentiation and short axis of the largest regional lymph node (LNmax) were independent predictors of TRG = 0. Based on the four predictors, we established a prediction model for TRG = 0. The AUC values of the prediction model in the training, internal and external validation groups were 0.84, 0.73 and 0.82, respectively.

Conclusions: We found that CA199, CA724, tumor differentiation and LNmax were associated with pathological response in advanced gastric cancer. The prediction model could provide guidance for clinical work.

Keywords: advanced gastric cancer, preoperative chemotherapy, tumor regression grade, prediction model, survival

OPEN ACCESS

Edited by:
Rui Liao,
First Affiliated Hospital of Chongqing Medical University, China

Reviewed by:
Shruti Rao,
Georgetown University Medical Center, United States
Jiankun Hu,
Sichuan University, China

***Correspondence:**
Wentao Liu
owenliu@sjtu.edu.cn
Min Yan
ym10299@163.com
Zhenggang Zhu
zzg1954@hotmail.com

[†]These authors have contributed equally to this work

Specialty section:
This article was submitted to Gastrointestinal Cancers, a section of the journal Frontiers in Oncology

Received: *17 September 2020*
Accepted: *19 March 2021*
Published: *15 April 2021*

Citation:
Xu W, Ma Q, Wang L, He C, Lu S, Ni Z, Hua Z, Zhu Z, Yang Z, Zheng Y, Feng R, Yan C, Li C, Yao X, Chen M, Liu W, Yan M and Zhu Z (2021) Prediction Model of Tumor Regression Grade for Advanced Gastric Cancer After Preoperative Chemotherapy. Front. Oncol. 11:607640. doi: 10.3389/fonc.2021.607640

INTRODUCTION

Gastric cancer (GC) causes enormous health and economic burdens worldwide. GC is the fifth most common cancer and the third leading cause of cancer-related deaths worldwide (1, 2). In China, GC is the second most common cancer and the second leading cause of cancer death (3). Despite the declining incidence of GC, patients still have poor prognosis. Gastric cancer is often either asymptomatic or may cause only nonspecific symptoms in its early stage. When patients experience symptoms, the cancer has often already reached an advanced stage with regional lymph node metastasis or distant metastasis. Surgery and chemotherapy are the main methods for the treatment of advanced gastric cancer (AGC). However, the prognosis of patients with AGC is still poor (4–6). Currently, preoperative chemotherapy (PCT) is considered a standard therapy for AGC (7–10). PCT has potential benefits, such as downstaging the tumor to increase the chance of curative resection while eliminating potential micrometastases to prevent or reduce tumor recurrence and metastasis and improving tumor-associated symptoms (11, 12). However, not all patients benefit from PCT. Patients respond to PCT differently. During preoperative chemotherapy, some patients do not respond, some have adverse events, and some progress and even lose the opportunity for radical surgery. The tumor regression grade (TRG) system is an effective histopathological evaluation method for assessing patient response to PCT. Based on the TRG system, some studies found that patients with a major pathologic response will have better overall survival than those with no response or minor pathologic changes after PCT in AGC (13–15). There are several TRG systems for the assessment of the tumor pathological response to PCT, including the Mandard, Ninomiya, Becker and Ryan classification systems (16–19). Different people have different TRG grades, and patients with pathological complete response postchemotherapy have a longer survival and better prognosis.

However, in East Asia, an area with a high incidence of gastric cancer, PCT has not become a routine treatment for AGC. Therefore, it is vital to select patients who would most likely benefit from PCT and find the most suitable patients to receive PCT. Thus, the purpose of this study is to explore predictors for pathological complete response and establish a prediction model for pathological complete response in AGC. Based on the prediction model, patients who would most likely benefit from PCT can be identified, and physicians can be more confident in recommending PCT to these patients. For this purpose, we conducted this retrospective-prospective study to explore potential predictors for pathological complete response in AGC and developed a prediction model to guide clinical application.

MATERIALS AND METHODS

Patient Selection and Study Design

This study was divided into two parts. In the first part, we used retrospective data to construct the prediction model and carried out internal validation. In the second part, after the prediction model was established, we collected data prospectively and then conducted an external validation of the prediction model.

Gastric cancer patient data from Shanghai Ruijin Hospital were retrospectively collected from July 2009 to November 2018. All gastric cancer patients were confirmed by endoscopic biopsy. The inclusion criteria were as follows: 1. patients were pathologically confirmed as having gastric adenocarcinoma; 2. patients had successfully undergone PCT before surgery; 3. gastrectomy was performed after PCT; 4. TRG can be assessed; and 5. pretreatment clinicopathological data can be collected. Samples were excluded if the patient did not meet the inclusion criteria. Patients in the retrospective cohort were randomly assigned (2:1) to a training group and an internal validation group. We developed a prediction model for TRG = 0 in the training group and then verified it in the internal validation group.

After the prediction model was established, we prospectively collected and recorded data from AGC patients from December 2018 to June 2020. The inclusion and exclusion criteria were the same as the criteria in the retrospective cohort mentioned above. The prediction model was verified in this prospective external validation group.

Assessment System for Tumor Regression Grade

This study applied the Ryan classification system, which is the most widely used and applied by the College of American Pathologists (CAP) and the Chinese Society of Clinical Oncology (CSCO), to assess the pathological response of tumors to PCT (10, 20). In the Ryan classification system, TRG is a semiquantitative parameter describing a relative proportion of residual tumor and stromal fibrosis. TRG of the primary tumor is divided into four categories: grade 0 (complete response: no viable cancer cells), grade 1 (moderate response: single cells or small groups of cancer cells), grade 2 (minimal response: residual cancer outgrown by fibrosis) and grade 3 (poor response: minimal or no tumor cells killed; extensive residual cancer). All histological slides were reexamined by the same pathologist to confirm the TRG grade.

Data Collection and Statistical Analysis

Pretreatment clinicopathological factors with potential prediction value were collected, including sex, age, body mass index (BMI), hemoglobin, leukocyte, neutrophil, lymphocyte, thrombocyte, prealbumin, total protein, albumin, CA125, CA199, CA724, CEA, AFP, tumor location, tumor differentiation, signet ring cell carcinoma component, Bormann type, chemotherapy regimen and short axis diameter of the largest regional lymph node (LNmax). Tumor location was classified into proximal, middle, distal 1/3 and whole stomach. LNmax was measured using multi-detector-row computed tomography (MDCT). The survival time after gastrectomy for every patient was also recorded by follow-up. The last follow-up time was 30, November 2019.

Univariate analysis was used to investigate whether any clinicopathological factors were correlated with TRG = 0. A

nonparametric Mann-Whitney rank test or t test was used for the analysis of quantitative data. The chi-square test was used to compare categorical data. For the potential predictors, which were originally continuous variables, we performed receiver operating characteristic (ROC) curve analysis using the observed outcomes (TRG = 0 vs TRG≠0) and identified an optimal cut-off value that maximized the area under the curve (AUC) of the ROC curve. Through multivariate stepwise logistic regression analysis, we further investigated independent predictors for TRG = 0. Based on the odds ratio (OR) of independent predictors, a prediction model for TRG = 0 was established. Thereafter, the prediction model was verified in the internal and external validation groups.

All statistical tests were two-tailed, and the differences were considered statistically significant at p values <0.05. Data analysis was conducted using SPSS software version 25 (IBM Statistical Product and Service Solutions, Armonk, USA). The ROC and K-M survival curves were constructed by GraphPad Prism Version 5 (GraphPad Software, USA).

RESULTS

Survival Analysis of Different TRG Groups

Previous studies showed that complete response (TRG = 0) after PCT was a predictor of good prognosis (13–15). To confirm the prognostic value of TRG, we conducted survival analysis of different TRG groups in the retrospective cohort. The last follow-up date for patients in the retrospective cohort was 30, November 2019, and the median follow-up time was 36.73 months (range 0.50 - 110 months). Of the 304 patients in the retrospective cohort, 90 patients (29.61%) had died of GC by the last follow-up day. A total of 26 (8.55%) patients were lost during the follow-up period.

Through the Kaplan-Meier (K-M) survival curve, we found that patients with TRG = 0 had significantly better survival than the others (P = 0.0011, **Figure 1A**). The estimated median survival of patients with TRG = 0, 1, 2, and 3 were undefined, 54.60, 24.40 and 14.64 months, respectively. The estimated 3-year survival rate of patients with TRG = 0 was significantly higher than that of patients with TRG≠0 (85.51% vs 54.13%, P=0.0077, **Figure 1B**).

For 156 patients who were followed up for more than 3 years in the retrospective cohort, we also the plotted the K-M survival curve. The patients with TRG = 0 also had better survival than the others (P = 0.0431, **Figure 2A**). The median survival of patients with TRG = 0, 1, 2, and 3 were undefined, 54.30, 35.70 and 14.65 months, respectively. The 3-year survival rate of patients with TRG = 0 was also significantly higher than that of patients with TRG≠0 (80% vs 56.70%, P=0.0329, **Figure 2B**). Therefore, TRG = 0 was the focus of our attention, and we developed a prediction model for it.

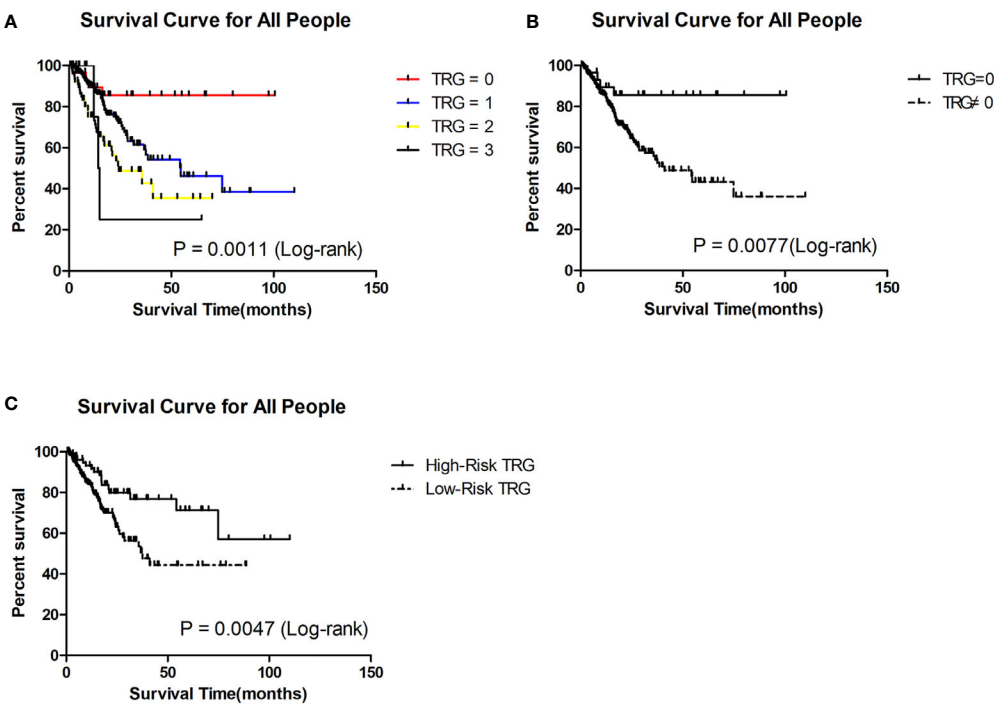

FIGURE 1 | Survival analysis of patients in different TRG group in the retrospective cohort. **(A)** Survival analysis of patients between 0, 1, 2 and 3 grade TRG group. **(B)** Survival analysis of patients between TRG = 0 and TRG ≠0 group. **(C)** Survival analysis of patients between low-risk and high-risk TRG group.

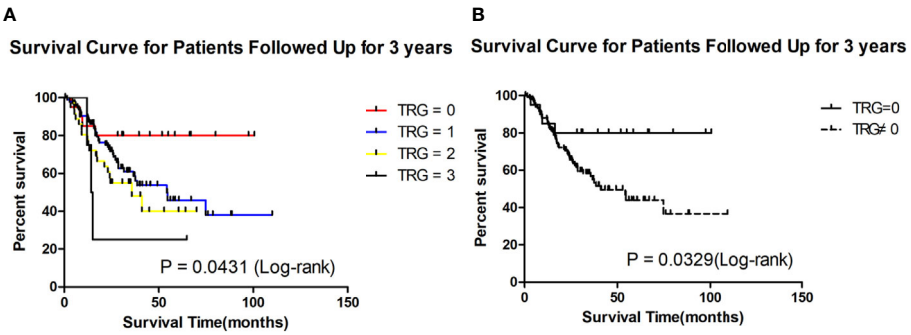

FIGURE 2 | Survival analysis of patients followed up for 3 years in different TRG group in the retrospective cohort. **(A)** Survival analysis of patients between 0, 1, 2 and 3 grade TRG group. **(B)** Survival analysis of patients between TRG = 0 and TRG ≠0 group.

Characteristics of the Study Population

A total of 304 gastric cancer patients were enrolled retrospectively, and 124 patients were enrolled prospectively. All patients' clinical stages at diagnosis were cT4N+Mx, which indicated that these tumors have invaded the serosal layer of the stomach and have regional lymph node metastasis, with or without distant metastasis. In the retrospective cohort, the study population comprised 224 male and 80 female patients. The median age was 61 years (range: 21-80 years). There were 281 patients without distant metastasis, 4 patients with single liver metastasis and 19 patients with retroperitoneal lymph node metastasis. All patients had received an average of three cycles of PCT before gastrectomy. The main regimens of PCT were EOX (Epirubicin plus Oxaliplatin and Capecitabine) and taxane-containing chemotherapy. There were 30 patients assessed with TRG = 0, including 6 patients with positive lymph nodes, which means that the primary tumor completely disappeared, but positive lymph nodes remained. Clinicopathological factors were compared between the different TRG groups (**Table 1**). We found that CA199, CA724, tumor differentiation, pathological type of signet ring cell carcinoma and LNmax were significantly different (P<0.05) between the different TRG groups. To develop a prediction model for TRG = 0, the study population was randomly assigned into the training set (202 patients) and the internal validation set (102 patients).

In the prospective cohort, there were 85 male and 39 female patients. The median age was 63 years (range: 27-79 years). There were 113 patients without distant metastasis, 4 patients with single liver metastasis, 5 patients with retroperitoneal lymph node metastasis, 1 patient with single pulmonary metastasis and 1 patient with ovarian metastasis. The main regimens of PCT were SOX (S-1 plus Oxaliplatin) and FLOT (Fluorouracil plus Leucovorin, Oxaliplatin, and Docetaxel). Nine patients were assessed with TRG = 0, including 1 patient with positive lymph nodes.

Derivation of a Prediction Model for TRG = 0

In the training group, the five factors (CA199, CA724, tumor differentiation, pathological type of signet ring cell carcinoma and LNmax) were also significantly different (P<0.05) between the different TRG groups (**Table 2**). To perform multivariate logistic regression analysis with the five factors, we performed ROC analysis for originally continuous variables, including CA199, CA724 and LNmax. The optimal cut-off values for CA199, CA724 and LNmax were 10.90 U/ml, 3.19 U/ml and 1.535 cm, respectively. The sensitivity, specificity and AUC values of CA199 were 51.74%, 85% and 0.67 ± 0.05, respectively (95% CI: 0.57–0.77; P = 0.002). For CA724, the sensitivity, specificity and AUC values were 56.14%, 80% and 0.65 ± 0.05, respectively (95% CI: 0.55–0.76; P = 0.002). For LNmax, the sensitivity, specificity and AUC values were 62.28%, 78.95% and 0.66 ± 0.07, respectively (95% CI: 0.52–0.81; P = 0.001).

In multivariate logistic regression analysis, we found that four factors were significantly different (**Table 3**). CA199 ≤10.90 U/ml, CA724 ≤3.19 U/ml, well differentiation and LNmax ≥1.535 cm were independent predictors for TRG=0 (P<0.05). A risk score was assigned to each predictor on the basis of the OR resulting from the logistic regression analysis. CA199 ≤10.90 U/mL, CA724 ≤3.19 U/mL, well differentiation and LNmax ≥1.535 cm were assigned 5, 4, 7, and 7 points, respectively (**Table 4**). The final scores ranged from 0 to 23 points. Based on the risk score, we established a prediction model for TRG = 0. According to the prediction model, we calculated the sum scores of the patients in the training group. The AUC of the prediction model was 0.84 (SD = 0.03; 95% CI: 0.77-0.91; P<0.0001) (**Figure 3A**). The optimal cut-off point for TRG in the prediction model was 13 points resulting from ROC curve analysis. The patients were divided into a low-risk (≤13 points) and a high-risk (>13 points) TRG group. TRG = 0 was discovered in 0% and 22.35% of the patients in the low-risk and high-risk TRG groups, respectively. The higher the score is, the more likely it indicates TRG = 0.

Validation of the Prediction Model for TRG = 0

To validate the prediction model for TRG = 0, we also performed ROC analysis in the internal and external validation groups. The AUC of the prediction model in the internal validation group was 0.73 (SD=0.09; 95% CI: 0.55-0.91; P=0.017) (**Figure 3B**).

TABLE 1 | Univariate analysis: Characteristics of the Whole Study Population.

Characteristics	Total (N = 304)	TRG = 0 (n = 30)	TRG ≠ 0 (n = 274)	P
Sex (n[%])				0.41 *
Male	224 (73.69)	24 (80.00)	200 (72.99)	
female	80 (26.31)	6 (20.00)	74 (27.01)	
Age (y)				0.51§
Median (range)	61(21-80)	61(31-75)	61(21-80)	
BMI (kg/m^2)				0.58§
Median (range)	22.65(14-36.33)	22.72(19.53-31.74)	22.54(14-36.33)	
Hemoglobin(g/L)				0.45§
Median (range)	121(44-166)	115.50(52-162)	121(44-166)	
Leukocyte(10^9/L)				0.42§
Median(range)	5.80(2.40-19.70)	6.30(3.10-11.20)	5.80(2.40-19.73)	
Neutrophil(10^9/L)				0.53§
Median (range)	3.57(1.14-17.22)	3.97(1.59-8.27)	3.55(1.14-17.22)	
Lymphocyte(10^9/L)				0.28§
Median (range)	1.47(0.59-7.51)	1.51(0.63-2.77)	1.44(0.59-7.51)	
Thrombocyte (10^9/L)				0.30§
Median (range)	233(82-924)	248(93-924)	231(82-875)	
Prealbumin (g/L)				0.92*
Median (range)	203(79-354)	207(145-280)	203(79-354)	
Total Protein(g/L)				0.57§
Median (range)	64(46-80)	63.5(51-72)	64(46-80)	
Albumin (g/L)				0.46§
Median (range)	36(20-46)	37.50(27-44)	36(20-46)	
CA125(U/mL)				0.80§
Median (range)	12.85(3.80-361.30)	11.70(3.90-160.7)	13(3.80-361.30)	
CA199(U/mL)				0.02§
Median (range)	9.7(0.80-7424.00)	6.5(1.40-109.70)	10.25(0.80-7424.00)	
CA724(U/mL)				0.002§
Median (range)	3.67(0.06-300.00)	1.68(0.06-61.23)	4.18(0.20-300.00)	
CEA(ng/mL)				0.66§
Median (range)	2.73(0.50-4996.88)	2.92(0.79-82.15)	2.71(0.50-4996.88)	
AFP(ng/mL)				0.92§
Median (range)	2.69(0.65-16965.09)	2.63(1.08-3103.14)	2.70(0.65-16965.09)	
Location (n[%])				0.73*
Cardia	87(28.62)	10(33.33)	77(28.10)	
Body	96(31.58)	10(33.33)	86(31.39)	
Antrum	113(37.17)	10(33.33)	103(37.59)	
Whole stomach	8(2.63)	0(0)	8(2.92)	
Differentiation (n[%])				0.000*
Well	87(28.62)	19(63.33)	68(24.82)	
poor	217(71.38)	11(36.67)	206(75.18)	
Signet ring cell (n[%])				0.02*
Yes	57(18.75)	1(3.33)	56(20.44)	
No	247(81.25)	29(96.67)	218(79.56)	
Borrmann (n[%])				0.17*
I	9(2.96)	2(6.67)	7(2.55)	
II	12(3.95)	3(10.00)	9(3.28)	
III	257(84.54)	23(76.67)	234(85.40)	
IV	26(8.55)	2(6.67)	24(8.76)	
Regimens (n[%])				
EOX	237(77.96)	25(83.33)	212(77.37)	0.46*
Non EOX	67(22.04)	5(16.67)	62(22.63)	
Taxane	34(11.18)	2(6.67)	32(11.68)	0.41*
Non Taxane	270(88.82)	28(93.33)	242(88.32)	
LNmax (cm)				0.002§
Median (range)	1.27(0.49-5.05)	1.84(0.49-5.00)	1.18(0.50-5.05)	

$\chi 2$ test (compares the counts of categorical responses between 2 or more independent groups).

§Mann-Whitney rank test (a nonparametric alternative to the 2 sample t test compares the means of 2 independent groups).

The sensitivity, specificity, negative predictive value (NPV), positive predictive value (PPV), and accuracy in the internal validation group were 60%, 77.11%, 94.12%, 24% and 75.27%, respectively. In the external validation group, the AUC of the prediction model was 0.82 (SD=0.05; 95% CI: 0.71-0.92; P=0.0016) (**Figure 3C**). The sensitivity, specificity, NPV, PPV, and accuracy in the external validation group were 55.56%, 82.61%, 95.96%, 20% and 80.65%, respectively.

TABLE 2 | Univariate analysis: Characteristics in the Training Set.

Characteristics	Total (N = 202)	TRG = 0 (n = 20)	TRG ≠ 0 (n =182)	P
Sex (n[%])				0.77 *
Male	147 (72.77)	14 (70.00)	133 (73.08)	
female	55 (27.23)	6 (30.00)	49 (26.92)	
Age (y)				0.81§
Median (range)	61(21-80)	61(40-75)	61(21-80)	
BMI (kg/m^2)				0.24§
Median (range)	22.23(15.70-31.74)	22.77(19.53-31.74)	22.09(15.70-31.30)	
Hemoglobin(g/L)				0.45§
Median (range)	119(44-166)	113.50(65-154)	120.50(44-166)	
Leukocyte(10^9/L)				0.63§
Median(range)	5.83(2.40-16.48)	6.20(3.10-11.20)	5.80(2.40-16.48)	
Neutrophil(10^9/L)				0.68§
Median (range)	3.60(1.14-8.31)	3.96(1.59-8.27)	3.57(1.14-8.31)	
Lymphocyte(10^9/L)				0.54§
Median (range)	1.43(0.63-2.77)	1.47(0.63-2.77)	1.43(0.69-2.65)	
Thrombocyte (10^9/L)				0.29§
Median (range)	233(86-875)	247(93-531)	231(86-875)	
Prealbumin (g/L)				0.92*
Median (range)	197.5(79-354)	207(151-249)	194.5(79-354)	
Total Protein(g/L)				0.57§
Median (range)	64(48-79)	63(51-72)	64(48-79)	
Albumin (g/L)				0.65§
Median (range)	36(20-46)	37(27-43)	36(20-46)	
CA125(U/mL)				0.64§
Median (range)	13.30(3.80-185.70)	13.85(3.90-160.7)	13.20(3.80-185.70)	
CA199(U/mL)				0.01§
Median (range)	10.15(0.80-7424.00)	5.80(1.40-109.70)	12.05(0.80-7424.00)	
CA724(U/mL)				0.02§
Median (range)	3.41(0.06-239.40)	1.90(0.06-61.23)	3.78(0.20-239.40)	
CEA(ng/mL)				0.71§
Median (range)	2.84(0.50-4996.88)	2.90(0.79-72.67)	2.78(0.50-4996.88)	
AFP(ng/mL)				0.51§
Median (range)	2.69(0.90-10783.52)	2.22(1.08-3103.14)	2.79(0.90-10783.52)	
Location (n[%])				0.43*
Cardia	62(30.69)	9(45.00)	53(29.12)	
Body	64(31.68)	6(30.00)	58(31.87)	
Antrum	70(34.65)	5(25.00)	65(35.71)	
Whole stomach	6(2.97)	0(0)	6(3.30)	
Differentiation (n[%])				0.000*
Well	54(26.73)	13(65.00)	41(22.53)	
poor	148(73.27)	7(35.00)	141(77.47)	
Signet ring cell (n[%])				0.03*
Yes	35(17.33)	0(0)	35(19.23)	
No	167(82.67)	20(100)	147(80.77)	
Borrmann (n[%])				0.12*
I	6(2.97)	2(10.00)	4(2.20)	
II	3(1.49)	1(5.00)	2(1.10)	
III	174(86.14)	15(75.00)	159(87.36)	
IV	19(9.40)	2(10.00)	17(9.34)	
Regimens (n[%])				
EOX	158(78.22)	16(80.00)	142(78.02)	0.84*
Non EOX	44(21.78)	4(20.00)	40(21.98)	
Taxane	23(11.39)	2(10.00)	21(11.54)	0.84*
Non Taxane	179(88.61)	18(90.00)	161(88.46)	
LNmax (cm)				0.02§
Median (range)	1.34(0.49-5.05)	2.07(0.49-5.00)	1.20(0.50-5.05)	

**χ2 test (compares the counts of categorical responses between 2 or more independent groups).*

§Mann-Whitney rank test (a nonparametric alternative to the 2 sample t test compares the means of 2 independent groups).

Prognostic Value of the Prediction Model

To evaluate whether the prediction model is useful for predicting prognosis, we plotted Kaplan-Meier (K-M) survival curves for the low-risk and high-risk TRG groups in the retrospective cohort. We found that patients in the high-risk TRG group had better survival than patients in the low-risk TRG group

TABLE 3 | Multivariate analysis: variables correlated with TRG in the training set.

Variables	B	P**	OR	95% CI
CA199, ≤/>10.90 U/mL	1.725	0.023	5.615	1.272-24.782
CA724, ≤/>3.19 U/mL	1.511	0.029	4.531	1.167-17.589
Differentiation, well/poor	2.005	0.002	7.426	2.143-25.725
Signet Ring cell Carcinoma, yes/no	17.341	0.998	33985914	0.000-0.000
LNmax, ≥/<1.535cm	2.073	0.002	7.945	2.085-30.279

B, beta coefficient; OR, odds ratio; 95% CI, 95% confidence interval.
***multivariable logistic regression analysis.*

TABLE 4 | Risk Score of Prediction Model for TRG.

Predictors	Score			
	0	**4**	**5**	**7**
CA199 (U/mL)	>10.90		≤10.90	
CA724 (U/mL)	>3.19	≤3.19		
Differentiation	poor			well
LNmax (cm)	<1.535			≥1.535

(P<0.05, **Figure 1C**). The estimated median survival times of patients in the high- and low-risk TRG groups were undefined and 37.50 months; the estimated 3-year survival rates were 76.75% and 53.45%, respectively. Therefore, this prediction model was also effective for prognosis.

DISCUSSION

Currently, PCT is considered a standard therapy for AGC. However, the risk of tumor progression is still worrisome. Despite enduring the side effects of PCT, patients may still experience tumor progression and lose the chance of radical surgery (21). The TRG system is an effective assessment method for pathological response and has been widely applied in clinical work. In the current study, we applied the Ryan classification system to assess tumor response after PCT. AGC patients have different responses to PCT. Complete response (TRG = 0) was considered the best response and a predictor of better prognosis. To explore which patients will benefit most from PCT, we conducted this current study. We found that four pretreatment factors were independent predictors for TRG=0 in AGC and established a prediction model for it. The four predictors were CA199 ≤10.90 U/mL, CA724 ≤3.19 U/mL, LNmax ≥1.535 cm, and well differentiation of the tumor. The four indicators used in this model are easy to obtain, which extends the model's range of applications.

Tumor markers (CA125, CA199, CA724, CEA and AFP) are widely used for the early diagnosis and prognostic evaluation of gastric cancer (22–24). However, the clinical value of tumor markers for predicting the response to PCT is still unclear (25, 26). A previous study showed that high preoperative CA724 and CA199 levels were associated with a higher risk of death, and a

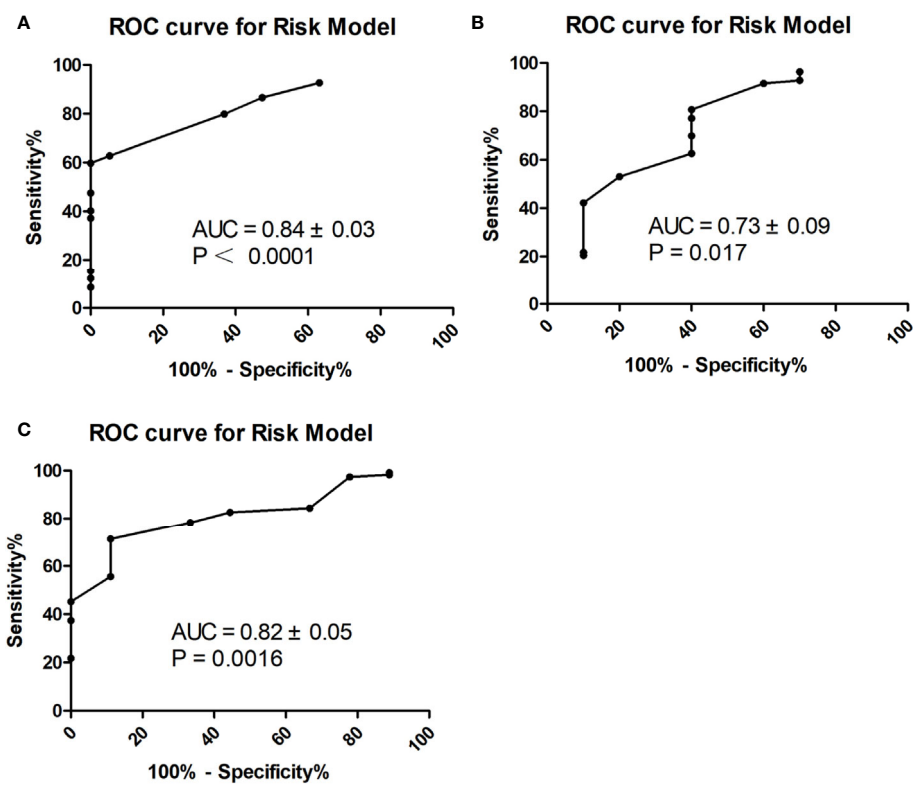

FIGURE 3 | ROC curve for prediction model in the training **(A)**, internal **(B)** and external **(C)** validation group.

decrease (>70%) in CA724 may predict the pathological response to PCT (26). In our study, we found that CA199 ≤10.90 U/mL and CA724 ≤3.19 U/mL were associated with TRG = 0 in GC patients after PCT. In other words, lower CA199 and CA724 levels are associated with a better response to PCT.

Patients with well-differentiated GC are regarded to have better survival than those with poorly differentiated GC (27, 28). In addition, a previous study showed that well differentiation is a vital predictor of pathologic response (29). In this study, we also found that well differentiation is an independent predictor of TRG = 0. This is consistent with previous studies.

In the current study, LNmax was significantly associated with TRG = 0. To our knowledge, this is the first report showing the value of LNmax for predicting TRG = 0 after PCT in gastric cancer. We speculate that patients with large regional lymph nodes have strong immunity against infection and tumor cell invasion. Patients with large regional lymph nodes have the chance to respond sooner to the tumor, with a stronger response. With stronger immunity, the effect of PCT is increasingly obvious. These patients will have a better pathological response and prognosis. However, further investigations are needed to identify the underlying physiological mechanism.

We established a prediction model for TRG = 0 after PCT in advanced gastric cancer with four independent predictors. The prediction model showed that patients with higher scores were more likely to obtain a better pathological response and prognosis. We found that the optimal cut-off value of the prediction model was 13 points. If patients received more than 13 points, we recommend that these patients receive PCT instead of direct surgery. On the other hand, if patients received very low points, we should be careful in choosing PCT for these patients.

This study had some limitations. This was a single-center clinical study, and the sample size was not very large. Patients in this study were enrolled over a large time span (2009-2018) and had different chemotherapy regimens. Besides, the model was based on common clinicopathological factors. Currently, the Cancer Genome Atlas (TCGA) Research Network conducted a comprehensive molecular characterization of GC, which proposed a molecular classification dividing GC into four subtypes: tumors positive for Epstein-Barr virus (EBV), microsatellite instability (MSI) tumors, genomically stable (GS) tumors and tumors with chromosomal instability (CIN) (30). Many studies had been carried out on the basis of TCGA classification. Several studies showed that patients with MSI-low GC could benefit from chemotherapy plus surgery, however those with MSI-high GC did not (31–33). Besides, several studies showed EBV positivity in GC patients was associated with better prognosis (34, 35).To improve this prediction model, we could integrate genetic factors according to the TCGA classification in future studies. Further investigation is needed to identify other predictors and optimize the prediction model for TRG = 0.

Despite the limitation of this study, we found that CA199, CA724, tumor differentiation and LNmax were associated with pathological response in AGC patients. We established a prediction model for TRG = 0 in AGC patients that could provide guidance for clinical work.

DATA AVAILABILITY STATEMENT

The raw data supporting the conclusions of this article will be made available by the authors, without undue reservation.

ETHICS STATEMENT

The studies involving human participants were reviewed and approved by the Human Ethics Committee of Shanghai Jiao Tong University School of Medicine Ruijin Hospital. The patients/participants provided their written informed consent to participate in this study.

AUTHOR CONTRIBUTIONS

WX conceived and designed the study, analyzed the data and wrote the paper. QM reexamined the tumor regression grade of all patients. LW, CH, SL, ZN, ZH, ZLZ, ZY and YZ collected the pretreatment clinicopathological factors of all patients. RF, CY, CL, XY and MC followed up the patient's survival status. WL revised the paper. MY and ZGZ gave professional guidance. All authors contributed to the article and approved the submitted version.

FUNDING

This work was supported by National Natural Science Foundation of China NO. 81772518 and clinical research project of Ruijin Hospital, Shanghai Jiao Tong University School of Medicine (DLY201602 and 2018CR003).

REFERENCES

1. Bray F, Ferlay J, Soerjomataram I, Siegel R, Torre L, Jemal A. Global cancer statistics 2018: GLOBOCAN estimates of incidence and mortality worldwide for 36 cancers in 185 countries. *CA: Cancer J Clin* (2018) 68(6):394–424. doi: 10.3322/caac.21492
2. Smyth E, Nilsson M, Grabsch H, van Grieken N, Lordick F. Gastric cancer. *Lancet (London England)* (2020) 396(10251):635–48. doi: 10.1016/S0140-6736(20)31288-5
3. Chen W, Zheng R, Baade P, Zhang S, Zeng H, Bray F, et al. Cancer statistics in China, 2015. *CA: Cancer J Clin* (2016) 66(2):115–32. doi: 10.3322/caac.21338
4. Katai H, Ishikawa T, Akazawa K, Isobe Y, Miyashiro I, Oda I, et al. Five-year survival analysis of surgically resected gastric cancer cases in Japan: a retrospective analysis of more than 100,000 patients from the nationwide registry of the Japanese Gastric Cancer Association (2001-2007). *Gastric Cancer Off J Int Gastric Cancer Assoc Jpn Gastric Cancer Assoc* (2018) 21 (1):144–54. doi: 10.1007/s10120-017-0716-7

5. van der Werf LR, Wijnhoven BPL, Fransen LFC, van Sandick JW, Nieuwenhuijzen GAP, Busweiler LAD, et al. A National Cohort Study Evaluating the Association Between Short-term Outcomes and Long-term Survival After Esophageal and Gastric Cancer Surgery. *Ann Surg* (2019) 270 (5):868–76. doi: 10.1097/SLA.0000000000003520
6. Yamaguchi K, Yoshida K, Tanahashi T, Takahashi T, Matsuhashi N, Tanaka Y, et al. The long-term survival of stage IV gastric cancer patients with conversion therapy. *Gastric Cancer* (2018) 21(2):315–23. doi: 10.1007/s10120-017-0738-1
7. Wang X, Zeng Z, Ye X, Sun J, Zhang Z, Kang W. Interpretation of the development of neoadjuvant therapy for gastric cancer based on the vicissitudes of the NCCN guidelines. *World J Gastrointestinal Oncol* (2020) 12(1):37–53. doi: 10.4251/wjgo.v12.i1.37
8. Smyth E, Verheij M, Allum W, Cunningham D, Cervantes A, Arnold D. Gastric cancer: ESMO Clinical Practice Guidelines for diagnosis, treatment and follow-up. *Ann Oncol Off J Eur Soc Med Oncol* (2016) 27:v38–49. doi: 10.1093/annonc/mdw350
9. Japanese Gastric Cancer A. Japanese gastric cancer treatment guidelines 2014 (ver. 4). *Gastric Cancer* (2017) 20(1):1–19. doi: 10.1007/s10120-016-0622-4
10. Wang FH, Shen L, Li J, Zhou ZW, Liang H, Zhang XT, et al. The Chinese Society of Clinical Oncology (CSCO): clinical guidelines for the diagnosis and treatment of gastric cancer. *Cancer Commun (Lond)* (2019) 39(1):10. doi: 10.1186/s40880-019-0349-9
11. Cunningham D, Allum W, Stenning S, Thompson J, Van de Velde C, Nicolson M, et al. Perioperative chemotherapy versus surgery alone for resectable gastroesophageal cancer. *New Engl J Med* (2006) 355(1):11–20. doi: 10.1056/NEJMoa055531
12. Xu A, Huang L, Liu W, Gao S, Han W, Wei Z. Neoadjuvant chemotherapy followed by surgery versus surgery alone for gastric carcinoma: systematic review and meta-analysis of randomized controlled trials. *PloS One* (2014) 9 (1):e86941. doi: 10.1371/journal.pone.0086941
13. Neves Filho E, de Sant'Ana R, Nunes L, Pires A, da Cunha M. Histopathological regression of gastric adenocarcinoma after neoadjuvant therapy: a critical review. *APMIS Acta Pathol Microbiol Immunol Scand* (2017) 125(2):79–84. doi: 10.1111/apm.12642
14. Tomasello G, Petrelli F, Ghidini M, Pezzica E, Passalacqua R, Steccanella F, et al. Tumor regression grade and survival after neoadjuvant treatment in gastro-esophageal cancer: A meta-analysis of 17 published studies. *Eur J Surg Oncol J Eur Soc Surg Oncol Br Assoc Surg Oncol* (2017) 43(9):1607–16. doi: 10.1016/j.ejso.2017.03.001
15. Derieux S, Svrcek M, Manela S, Lagorce-Pages C, Berger A, Andre T, et al. Evaluation of the prognostic impact of pathologic response to preoperative chemotherapy using Mandard's Tumor Regression Grade (TRG) in gastric adenocarcinoma. *Dig Liver Dis Off J Ital Soc Gastroenterol Ital Assoc Study Liver* (2020) 52(1):107–14. doi: 10.1016/j.dld.2019.07.010
16. Mandard A, Dalibard F, Mandard J, Marnay J, Henry-Amar M, Petiot J, et al. Pathologic assessment of tumor regression after preoperative chemoradiotherapy of esophageal carcinoma. Clinicopathologic correlations. *Cancer* (1994) 73(11):2680–6. doi: 10.1002/1097-0142(19940601)73:11<2680::AID-CNCR2820731105>3.0.CO;2-C
17. Ninomiya Y, Yanagisawa A, Kato Y, Kitagawa T, Ishihara S, Nakajima T. Histological indications of a favorable prognosis with far-advanced gastric carcinomas after preoperative chemotherapy. *J Cancer Res Clin Oncol* (1999) 125(12):699–706. doi: 10.1007/s004320050337
18. Becker K, Mueller J, Schulmacher C, Ott K, Fink U, Busch R, et al. Histomorphology and grading of regression in gastric carcinoma treated with neoadjuvant chemotherapy. *Cancer* (2003) 98(7):1521–30. doi: 10.1002/cncr.11660
19. Ryan R, Gibbons D, Hyland J, Treanor D, White A, Mulcahy H, et al. Pathological response following long-course neoadjuvant chemoradiotherapy for locally advanced rectal cancer. *Histopathology* (2005) 47(2):141–6. doi: 10.1111/j.1365-2559.2005.02176.x
20. Chanjuan Shi M, Berlin J, Branton PA, Fitzgibbons PL, Frankel WL, Hofstetter WL, et al. Protocol for the Examination of Specimens From Patients With Carcinoma of the Stomach. *College of American Pathologists* (2020).
21. Zhou J, Shen J, Seifer B, Jiang S, Wang J, Xiong H, et al. Approaches and genetic determinants in predicting response to neoadjuvant chemotherapy in locally advanced gastric cancer. *Oncotarget* (2017) 8(18):30477–94. doi: 10.18632/oncotarget.12955
22. Feng F, Tian Y, Xu G, Liu Z, Liu S, Zheng G, et al. Diagnostic and prognostic value of CEA, CA19–9, AFP and CA125 for early gastric cancer. *BMC Cancer* (2017) 17(1):737. doi: 10.1186/s12885-017-3738-y
23. Chen XZ, Zhang WK, Yang K, Wang LL, Liu J, Wang L, et al. Correlation between serum CA724 and gastric cancer: multiple analyses based on Chinese population. *Mol Biol Rep* (2012) 39(9):9031–9. doi: 10.1007/s11033-012-1774-x
24. Yang AP, Liu J, Lei HY, Zhang QW, Zhao L, Yang GH. CA72-4 combined with CEA, CA125 and CAl9-9 improves the sensitivity for the early diagnosis of gastric cancer. *Clin Chim Acta* (2014) 437:183–6. doi: 10.1016/j.cca.2014.07.034
25. Yamao T, Kai S, Kazami A, Koizumi K, Handa T, Takemoto N, et al. CA19-9 and CA125 in monitoring of response to systemic chemotherapy in patients with advanced gastric cancer. *Jpn J Clin Oncol* (1999) 29(11):550–5. doi: 10.1093/jjco/29.11.550
26. Sun Z, Zhang N. Clinical evaluation of CEA, CA19-9, CA72-4 and CA125 in gastric cancer patients with neoadjuvant chemotherapy. *World J Surg Oncol* (2014) 12:397. doi: 10.1186/1477-7819-12-397
27. Lazar D, Taban S, Sporea I, Dema A, Cornianu M, Lazar E, et al. Gastric cancer: correlation between clinicopathological factors and survival of patients (III). *Rom J Morphol Embryol Rev Rom Morphol Embryol* (2009) 50(3):369–79.
28. Kim S, Min B, Ahn J, Jung S, An J, Choi M, et al. Nomogram to predict lymph node metastasis in patients with early gastric cancer: a useful clinical tool to reduce gastrectomy after endoscopic resection. *Endoscopy* (2020) 52(6):435–43. doi: 10.1055/a-1117-3059
29. Wang L, Teng R, Jiang Z, Hu W, Dong M, Yuan X, et al. Clinicopathologic variables predicting tumor response to neoadjuvant chemotherapy in patients with locally advanced gastric cancer. *J Surg Oncol* (2012) 105(3):293–6. doi: 10.1002/jso.22085
30. Cancer Genome Atlas Research N. Comprehensive molecular characterization of gastric adenocarcinoma. *Nature* (2014) 513(7517):202–9. doi: 10.1038/nature13480
31. Pietrantonio F, Miceli R, Raimondi A, Kim Y, Kang W, Langley R, et al. Individual Patient Data Meta-Analysis of the Value of Microsatellite Instability As a Biomarker in Gastric Cancer. *J Clin Oncol Off J Am Soc Clin Oncol* (2019) 37(35):3392–400. doi: 10.1200/JCO.19.01124
32. Kohlruss M, Grosser B, Krenauer M, Slotta-Huspenina J, Jesinghaus M, Blank S, et al. Prognostic implication of molecular subtypes and response to neoadjuvant chemotherapy in 760 gastric carcinomas: role of Epstein-Barr virus infection and high- and low-microsatellite instability. *J Pathol Clin Res* (2019) 5(4):227–39. doi: 10.1002/cjp2.137
33. Hashimoto T, Kurokawa Y, Takahashi T, Miyazaki Y, Tanaka K, Makino T, et al. Predictive value of MLH1 and PD-L1 expression for prognosis and response to preoperative chemotherapy in gastric cancer. *Gastric Cancer* (2019) 22(4):785–92. doi: 10.1007/s10120-018-00918-4
34. Camargo MC, Kim WH, Chiaravalli AM, Kim KM, Corvalan AH, Matsuo K, et al. Improved survival of gastric cancer with tumour Epstein-Barr virus positivity: an international pooled analysis. *Gut* (2014) 63(2):236–43. doi: 10.1136/gutjnl-2013-304531
35. Hewitt LC, Inam IZ, Saito Y, Yoshikawa T, Quaas A, Hoelscher A, et al. Epstein-Barr virus and mismatch repair deficiency status differ between oesophageal and gastric cancer: A large multi-centre study. *Eur J Cancer* (2018) 94:104–14. doi: 10.1016/j.ejca.2018.02.014

Conflict of Interest: The authors declare that the research was conducted in the absence of any commercial or financial relationships that could be construed as a potential conflict of interest.

frontiers in Oncology

ORIGINAL RESEARCH
published: 16 April 2021
doi: 10.3389/fonc.2021.659676

Suppression of Heterogeneous Nuclear Ribonucleoprotein C Inhibit Hepatocellular Carcinoma Proliferation, Migration, and Invasion *via* Ras/MAPK Signaling Pathway

Jiejun Hu, Dong Cai, Zhibo Zhao, Guo-Chao Zhong†† and Jianping Gong*††

Department of Hepatobiliary Surgery, The Second Affiliated Hospital of Chongqing Medical University, Chongqing, China

OPEN ACCESS

Edited by:
Yujun Shi,
Sichuan University, China

Reviewed by:
Urbain Weyemi,
University of Texas at Austin, United States
Arun Upadhyay,
Northwestern University, United States

***Correspondence:**
Jianping Gong
gongjianping@cqmu.edu.cn
Guo-Chao Zhong
gczhong1991@stu.cqmu.edu.cn

†*These authors share senior authorship*

Specialty section:
This article was submitted to Gastrointestinal Cancers, a section of the journal Frontiers in Oncology

Received: *28 January 2021*
Accepted: *30 March 2021*
Published: *16 April 2021*

Citation:
Hu J, Cai D, Zhao Z, Zhong G-C and Gong J (2021) Suppression of Heterogeneous Nuclear Ribonucleoprotein C Inhibit Hepatocellular Carcinoma Proliferation, Migration, and Invasion via Ras/MAPK Signaling Pathway. Front. Oncol. 11:659676. doi: 10.3389/fonc.2021.659676

Hepatocellular carcinoma (HCC), the most common malignant tumor, has high fatality and recurrence rates. Accumulating evidence shows that heterogeneous nuclear ribonucleoprotein C (HNRNPC), which is mainly involved in RNA splicing, export, and translation, promotes progression and metastasis of multiple tumor types; however, the effects of HNRNPC in HCC are unknown. In the present study, high levels of HNRNPC were detected in tumor tissues compared with para-tumor tissues by immunohistochemical and western blot assays. Furthermore, Cox proportional hazards regression models, the Kaplan–Meier method, and clinicopathologic features analysis showed that HNRNPC was not only an independent prognostic factor for both overall and disease-free survival in HCC but also a predictor of large tumor size and advanced tumor stage. Functional experiments revealed that silencing of HNRNPC not only led to arrest of more HCC cells at G0/G1 phase to inhibit their proliferation, but also suppressed EMT process to block their invasion, and migration *in vitro*; this was related to the Ras/MAPK signaling pathway. In addition, blocking of HCC cell proliferation regulated by HNRNPC silencing was observed *in vivo*. Finally, rescue tests showed that after recovery of Ras/MAPK signaling pathway activity by treatment with Ras agonists, the proliferation, migration, and invasion suppression of Huh-7 and Hep 3B cell lines caused by HNRNPC knockdown was partially reversed. Taken together, these results indicate that HNRNPC knockdown inhibits HCC cell proliferation, migration and invasion, in part *via* the Ras/MAPK signaling pathway. Thus, HNRNPC may have an important role in the progression of HCC and represents a promising biomarker for evaluation of prognosis and a potential therapeutic target in HCC patients.

Keywords: HCC, HNRNPC, alternative splicing, Ras, MAPK

INTRODUCTION

Hepatocellular carcinoma (HCC) is the fifth most common cancer and the fourth leading cause of cancer-associated deaths worldwide, with a gradually increasing global burden (1, 2). For patients with early-stage tumors, liver resection and transplantation are the main treatment modes (3–5), whereas for patients with advanced-stage tumors, multimodal treatment is increasingly popular; this includes immunological therapy, molecular targeted treatments, microwave ablation, and transarterial chemoembolization (6–11). Although an increasing number of therapies are used to treat HCC, the prognosis of HCC patients remains poor (12–14), with a 5-year overall survival rate of less than 20% (15–17), primarily owing to the difficulty of early-stage diagnosis (18). For these reasons, there is a need to explore novel biomarkers that could be used as targets for HCC therapy and for predicting the prognosis of HCC patients.

Alternative splicing enables the generation of vast protein diversity by cutting out the introns and connecting the exons of heterogeneous nuclear RNAs (19). Increasing numbers of reports indicate that alternative splicing is intimately related to tumor occurrence, progression, and therapeutic resistance (20–23). A known RNA-binding protein, heterogeneous nuclear ribonucleoprotein C (HNRNPC) plays an important part in RNA splicing (24, 25), stability (26, 27), and expression (28). HNRNPC has been identified as an oncogene, enhancing deterioration in multiple tumor types, including gastric cancer (29), breast cancer (27), esophageal squamous cell carcinoma (26), and oral squamous cell carcinoma (30). According to previous reports, HNRNPC primarily regulates the biological activity of the IFNβ signaling pathway (27), p53 gene (31), and AKT signaling pathway (32), which are associated with tumor proliferation, invasion, and metastasis. Bioinformatic analysis has shown that HNRNPC, as a gene correlated with N6-methyladenosine RNA methylation, predicts poor prognosis of patients with glioblastoma multiforme (33), lung adenocarcinoma (34), and head and neck squamous cell carcinoma (35). Thus, HNRNPC is considered to be a tumor-related gene. Nevertheless, its impact on patient prognosis and the mechanism by which it regulates the biological characteristics of tumor cells in HCC remain unknown.

The mitogen-activated protein kinase (MAPK) cascade consists of serine/threonine kinases, which mainly participate in the transduction of cellular signals (36, 37). There are four important protein kinases, Ras, Raf, MEK, and Erk, in the MAPK signaling pathway (38). In response to signals from epidermal growth factor receptor, insulin like growth factor-1 receptor (IGF-1R), and calmodulin, the GDP combined with Ras is replaced by GTP. Then, the activated Ras cascade phosphorylates its downstream targets Raf, MEK, and Erk to regulate cell proliferation, differentiation, and cycling (39–41). Additionally, Ras/MAPK signaling pathway promoting epithelial-mesenchymal transition (EMT) to facilitate tumor migration and invasion have been reported in recent years (42–44). Abnormal activation of the MAPK pathway is involved in the progression of many malignancies, including gastric cancer (45), cervical carcinoma (46), and HCC (47). Hence, targeting Ras/Raf/MEk/Erk is regarded as a potential approach to treating HCC (36), esophageal carcinoma (48), acute lymphoblastic leukemia (49), and melanoma (50).

In the present study, we used western blotting, immunohistochemistry (IHC), and bioinformatics analysis to demonstrate that HNRNPC had significantly elevated expression in HCC tumor tissues compared with para-tumor tissues. In addition, high levels of HNRNPC protein were related to larger tumor size, advanced TNM stage, and poor prognosis. Subsequently, functional experiments revealed that silencing of HNRNPC expression could inhibit HCC cells' growth by G0/G1 arrest, in part *via* the Ras/MAPK signaling pathway. Meanwhile, *in vitro* tests, we also demonstrated that the inhibition of Ras/MAPK signaling pathway caused by HNRNPC suppression could negatively regulate EMT progress to hinder migration and invasion of HCC cells. In vivo, xenograft assays showed that HNRNPC knockdown could block the proliferation of HCC cells, with a statistically significant effect. Therefore, HNRNPC may be a promising biomarker for evaluating prognosis of HCC patients, as well as a potential therapeutic target.

MATERIALS AND METHODS

Sample Collection

In order to detect differences in HNRNPC protein levels between tumor tissues and para-tumor tissues, we collected 12 pairs of fresh tissues (tumor and matched para-tumor tissue) from patients diagnosed with HCC by a pathologist after undergoing hepatectomy between Dec 2018 and Jan 2019 in the Department of Hepatobiliary Surgery of the Second Affiliated Hospital of Chongqing Medical University. For analysis of prognosis and clinical information, our study enrolled 147 available cases from Jul 2014 to Nov 2016 from the same department who had not received chemotherapy, radiofrequency ablation, or molecular targeted therapy before liver resection. These 147 cases included 128 male and 19 female patients, with an average age of 53.67 years. Specific patient information is given in **Table 1**. The selection criteria were as follows. Inclusion criteria: HCC confirmed by biopsy after surgery; exclusion criteria: patients with other cancers, distant metastasis, or grade C Child–Pugh liver function. A total of 147 tumor tissues and 82 available corresponding para-tumor tissues were used to construct tissue microarrays (TMAs). This research was approved by the Ethics Committee at the Second Affiliated Hospital of Chongqing Medical University ((2017)36), and informed consent was obtained from all patients.

Abbreviations: HCC, hepatocellular carcinoma; HNRNPC, heterogeneous nuclear ribonucleoprotein C; IHC, immunohistochemical; MAPK, mitogen-activated protein kinase; AFP, alpha fetoprotein; EMT, epithelial-mesenchymal transition; HBV, hepatitis B virus; Lv-NC, hepatocellular carcinoma cell lines infected with negative control lentiviruses; Lv-HNRNPC, hepatocellular carcinoma cell lines infected with targeted HNRNPC lentiviruses; EMT, epithelial-mesenchymal transition.

TABLE 1 | Relationships of HNRNPC protein levels with clinicopathologic features in 147 HCC patients.

Clinicopathologic features	All patients (n=147)	High HNRNPC (n=80)	Low HNRNPC (n=67)	P-value
Gender				
Male	128	70 (54.7%)	58 (45.3%)	1.000
Female	19	10 (52.6%)	9 (47.4%)	
Age (M ± SD)	53.67 ± 10.21	53.94 ± 9.95	53.48 ± 10.49	0.784
<55 y	82	46 (56.1%)	36 (43.9%)	0.739
≥55 y	65	34 (52.3%)	31 (47.7%)	
HBV infection				
negative	25	16 (64.0%)	9 (36.0%)	0.379
positive	122	64 (52.5%)	58 (47.5%)	
Liver cirrhosis				
absent	55	33 (60.0%)	22 (40.0%)	0.310
present	92	47 (51.1%)	45 (48.9%)	
AFP				
<400 ng/ml	89	45 (50.6%)	44 (49.4%)	0.310
≥400 ng/ml	58	35 (60.3%)	23 (39.7%)	
Child–Pugh				
A	120	63 (52.5%)	57 (47.5%)	0.395
B	27	17 (63.0%)	10 (37.0%)	
Tumor number				
1	126	65 (51.6%)	61 (48.4%)	0.103
2–3	21	15 (71.4%)	6 (28.6%)	
Tumor size (M ± SD)	5.36 ± 3.09	5.99 ± 3.41	4.61 ± 2.48	**0.007**
< 5 cm	72	32 (44.4%)	40 (55.6%)	**0.021**
≥5 cm	75	48 (64.0%)	27 (36.0%)	
TNM stage				
I	88	41 (46.6%)	47 (53.4%)	**0.028**
II–III	59	39 (66.1%)	20 (33.9%)	
Tumor differentiation				
I–II	42	25 (59.5%)	17 (40.5%)	0.468
III–IV	105	55 (52.4%)	50 (47.6%)	

HNRNPC, heterogeneous nuclear ribonucleoprotein C; HBV, hepatitis B virus; AFP, alpha fetoprotein.
The bold values present statistical significance.

Follow-Up

Follow-up was carried out by phone, and alpha fetoprotein (AFP), liver function, and chest radiography were obtained at least every 2 months in the first 6 months after surgery, every 3 months for 6 months to 3 years following surgery, and every 6 months for 3–5 years after surgery. If necessary, magnetic resonance imaging or computed tomography was also used. Overall survival was defined as the time from liver resection to death or last follow-up; disease-free survival was defined as the time from liver resection to first recurrence or last follow-up.

IHC

Fresh tissues were immobilized with 4% formalin for 48 h at 37°C and subsequently washed with cool phosphate-buffered saline (PBS) three times for 5 min each time. Tissue samples were dehydrated using ethanol, embedded in paraffin, and then cut them into 4-μm-thick sections of 2 mm diameter to produce TMAs. The paraffin sections were dewaxed in an incubator at 65°C overnight, before being deparaffinized in xylene and rehydrated using a decreasing ethanol gradient. Sections were placed in ethylene diamine tetraacetic acid (cat.no. 0085; Beyotime) and heated in a microwave for 10 min for antigen repair. A 3% hydrogen peroxide was used to eliminate endogenous peroxidase at 37°C for 30 min. Sections were incubated with anti-HNRNPC (dilution 1:50, cat. no. ET1611-2; HUABIO), anti-ki67 (dilution 1:10000, cat. no. 27309; Proteintech), anti-CD34 (dilution 1:50, cat. no. ET1606-11; HUABIO), anti-Vimentin (dilution 1:100, cat. no. ET1610-39; HUABIO), and anti-E-Cadherin (dilution 1:50, cat. no. ET1607-75; HUABIO) antibodies at room temperature overnight, and then with secondary antibody (dilution: 1:1, cat.no. K5007; Dako) for 1 h at room temperature. Finally, sections were stained with an IHC kit (cat. no. K5007; Dako) according to the manufacturer's protocol.

IHC Scoring

The proportion of positive cells and staining strength were used to evaluate the expression of HNRNPC. Color intensity was ranked using four grades: no staining (score = 0), weak staining (score = 1), moderate staining (score = 2), and intense staining (score = 3); and the proportions of positive cells were divided into five classifications: < 5% (score = 0), 5–25% (score =1), 26–50% (score = 2), 51–75% (score = 3), and 76–100% (score = 4). These two values were multiplied to acquire the final score. All patients were divided into high and low HNRNPC expression groups according to the median score of 7. The IHC results were analyzed by two pathologists; uncertain results were judged by a third pathologist.

Western Blot Analysis

We collected total protein from cells or tissues using RIPA buffer with protease and phosphatase inhibitors. After separation by sodium dodecyl polyacrylamide gel electrophoresis, proteins were transferred onto polyvinylidene fluoride membranes. Subsequently, the membranes were blocked with 5% skim milk at room temperature for 1 h, then incubated with primary antibody at 4°C overnight. On the second day, the membranes were incubated with secondary antibody for 1 h at 37°C. The antibodies used were as follows: HNRNPC (dilution 1: 2000, cat. no. ET1611-2; HUABIO), Ras (dilution 1:1000, cat. no. 3339T; CST), c-Raf (1:1000, cat. no. 9422T; CST), P-c-Raf (dilution 1:1000, cat. no. 9427T; CST), MEK1/2 (dilution 1:1000, cat. no. 8727T; CST), P-MEK1/2 (Ser217/221) (dilution 1:1000, cat. no. 9154T; CST), Erk1/2 (dilution 1:1000, cat. no. 4695T; CST), P-Erk1/2 (Thr202/Tyr204) (dilution 1:1000, cat. no. 4377T; CST), c-Myc (dilution 1:1000, cat. no. 5605T; CST), CDK4 (dilution 1:2000, cat. no. ET1612-1; HUABIO), cyclin E1 (dilution 1:1000, cat. no. ET1612-16; HUABIO), Vimentin (dilution 1:2000, cat. no. ET1610-39; HUABIO), E-Cadherin (dilution 1:1000, cat. no. ET1607-75; HUABIO), β-actin, (dilution 1:2000, cat. no. BM0627; Boster), goat anti-mouse (dilution 1:5000, cat. no. ZB-2305; ZSGB-BIO), and goat-anti-rabbit (dilution 1:5000, cat. no. ZB-2301; ZSGB-BIO). Finally, the membranes were imaged using a chemiluminescent horseradish peroxidase substrate (cat. no. WBKL S0100; Millipore). β-actin was used as the internal reference, and the western blot analysis was performed using Image Lab 6.0. The tests mentioned above were operated three times respectively.

Quantitative Real-Time PCR (q-RT-PCR)

Total RNA was extracted from cells using an Animal Total RNA Isolation Kit (cat. no. RE-03011; Foregene) according to the

manufacturer's instructions. Total RNA was reverse transcribed to cDNA with an iScript cDNA synthesis kit (cat. no. 1708891; Bio-Rad), following the manufacturer's reaction protocol: 5 min at 25°C 20 min at 46°C, 1 min at 95°C, and holding at 4°C. Quantitation of cDNA was performed using a SYBR Green PCR kit (cat. no. 208054; QIAGEN). Relative HNRNPC expression was calculated by the $2^{-\triangle\triangle Cq}$ method, with GAPDH as an internal reference. The primers were designed as follows: GAPDH forward, 5′-GGAGTCCACTGGCGTCTTCA-3′, reverse, 5′-GTCATGAGTCCTTC CACGATACC-3′; HNRNPC forward, 5′-GCAGAGCCAAAAGTGAACCG-3′, reverse, 5′-ACGTTTCGAGGGCACTACAG-3′. The reaction protocol was given by the manufacturer as follows: 2 min at 95°C, 5 sec at 95°C, and 10 sec at 60°C, repeated for 35 cycles. Each test was repeated dividedly in triplicate.

Cell Lines and Culture

Huh-7 and Hep 3B HCC cell lines were purchased from the Chinese Academy of Sciences Stem Cell Bank (Shanghai, China) and identified with STR Profile. Both cell lines were cultured in DMEM (cat.no. SH30022.01; HyClone) or MEM (cat.no. SH30024.01; Hyclone) supplied with 10% fetal bovine serum (cat.no. 04-001-1ACS; BI) in an incubator containing 5% CO_2 at 37°C.

Cell Infection

Huh-7 and Hep 3B cells were cultured in six-well plates. When they reached 20–30% density, they were stably infected with HNRNPC lentivirus (Lv-HNRNPC) or a negative control lentivirus (Lv-NC) for 14 h (viral volume=MOI × cell number/viral titer; GeneChem, Shanghai, China). The lentiviral interference system was produced using a GV248 carrier loaded consecutively with the hU6 promoter, a multiple cloning site, the ubiquitin promoter, the EGFP gene, an IRES site, and the puromycin gene. A short hairpin RNA was designed to target the HNRNPC sequence (sh-HNRNPC): 5′-CTTCGTTCAGTATGTTAAT-3′; the negative sequence (sh-NC) was 5′-TTCTCCGAACGTGTCACGT-3′. After culture for 48 h, cells were filtrated with 2 μg/ml puromycin (cat. no. REVG1001; GeneChem, Shanghai, China) for 48 h; this was repeated twice. Infection and knockdown efficiency were detected by inverted fluorescence microscopy, and by western blotting and q-RT-PCR, respectively.

Colony Formation Assay

Approximately 500 cells were seeded in each well of the six-well plates and cultured in an incubator with 5% CO_2 at 37°C for 2 weeks. After washing with PBS, the cells were immobilized with 4% paraformaldehyde for 15 min at room temperature and then stained with 0.1% crystal violet solution (cat. no. G1062; Solarbio) for 30 min. Finally, the colony numbers were counted under a microscope. All experiments were operated independently three times.

Cell Viability Analysis

Approximately 3000 (Huh-7) or 8000 (Hep 3B) cells were seeded in each well of a 96-well plate and cultured for 72 h. After being seeded in a 96-well plate, cell viability was measured using a CCK-8 kit (cat. no. ZP328-3; ZOMANBIO) according to the manufacturer's instructions at 6, 24, 48 and 72h. Briefly, CCK-8 (10 μl) was added to each well, and the cells were incubated at 5% CO_2 and 37°C. The absorbance (optical density) was detected by enzyme-linked immunosorbent array at a wavelength of 450 nm. Each test was performed dividedly in triplicate.

Scratch Wound for Cell Migration Assay

When the cells had grown to a density of 90% in the six-well plates, we used a sterile 200-μl pipette tip to scratch a wound at the middle line of each well bottom. Subsequently, the suspended cells were removed by PBS, and the culture medium was replaced with serum-free medium. Cells were sequentially cultured for 48 h in an incubator containing 5% CO_2 at 37°C. The wound width was recorded under a light microscope at 0, 24 and 48h. The experiments mentioned above were operated three times respectively.

Cell Invasion Assay

To analyze the invasion ability of cells, a Corning BioCoat Matrigel Invasion Chamber (cat. no. 354480; Corning) was used according to the manufacturer's instructions. Specifically, cells (5×10^4/well) were cultured with serum-free medium in the upper chambers, while the lower chambers were loaded with DMEM or MEM supplied with 10% fetal bovine serum. After culture for 48 h, the cells were washed with PBS and fixed with 4% paraformaldehyde for 15 min at room temperature. Invading cells were captured with 0.1% crystal violet solution under a light microscope, and non-invading cells were eliminated with cotton swabs. Specifically, five fields in each chamber were randomly recorded, and average values were calculated. Each test was repeated independently in triplicate.

Cell Cycle Analysis

Approximately 25×10^4/well cells were seeded in six-well plates. Subsequently, the cells were collected in 1.5-ml EP tubes and then fixed with 70% ethanol at 4°C overnight. The next day, the cells were stained with propidium iodide with RNase A at 37°C for 30 min in the dark. Finally, the results were analyzed by flow cytometry. A total of 2×10^4 cells were recorded for each sample. All experiments were performed three times respectively.

Groups and Treatments

To verify the upstream and downstream relationships between HNRNPC and the MAPK signaling pathway, we used an agonist for Ras (ML-098) (cat. no. HY-19800; MCE). The specific treatments were as follows. To measure the efficiency of the activation of the MAPK signaling pathway by ML-098, the Lv-NC group was treated with dimethyl sulfoxide (DMSO) for 48 h, and the Lv-HNRNPC group was treated with ML-098 (20 nmol/l) and DMSO, for 48 h. CCK-8 tests, cell cycle analysis, scratch wound assay, and cell invasion tests were performed using the method described above. To detect the rescue efficiency of ML-098 for colony formation, we used ML-098 (20 nmol/l) to treat the Lv-HNRNPC group twice sequentially for 5 days each time. The Lv-NC group was treated with the same amount of DMSO as a control.

In Vivo Assay for Tumor Growth

A total of 12 5-week-old male BALB/c nude mice were purchased from Beijing Huafukang Biotechnology and randomly divided into two groups (six per group). Lv-HNRNPC- and Lv-NC-group Huh-7 cells were suspended in cool PBS and subsequently injected into the backs of mice subcutaneously (2.5×10^6/mice). The mice were fed at 23–25°C and 60% humidity with a 12-h light/dark cycle. Tumor size was measured with a caliper every 3 days; the formula for the size calculation was as follows: volume = (length × width^2)/2 cm^3. Twenty-seven days after implantation, the mice were killed by cervical dislocation and the tumors were removed. Finally, the tumor samples were fixed with 4% formalin for IHC analysis. All animal experiments were approved by the Ethics Committee of Chongqing Medical University.

Bioinformatic Analysis

The expression of HNRNPC in HCC tissues was analyzed by UALCAN (ualcan.path.uab.edu), using RNA sequencing data downloaded from The Cancer Genome Atlas for 50 normal liver tissues and 371 primary HCC tissues. HNRNPC-correlated genes were also acquired from UALCAN; we selected 3517 significantly correlated genes (Pearson correlation coefficient ≥ 0.5) for Kyoto Encyclopedia of Genes and Genomes (KEGG) analysis by WebGestalt 2013 (www.webgestalt.org/2013).

Statistical Analysis

IBM SPSS Statistics 23 was used for statistical analysis. Categorical data were analyzed by chi-square test, while continuous data between two groups were analyzed by t-test. Comparisons between multiple groups were performed by one-way analysis of variance (ANOVA), and the results were analyzed by LSD test and presented as mean ± standard deviation (SD). Univariate and multivariate Cox proportional hazards regression models were used to assess the risk factors associated with HCC. In addition, overall and disease-free survivals were computed by the Kaplan–Meier method and examined by log-rank test. Finally, a P-value less than 0.05 was considered to indicate a statistically significant difference.

RESULTS

HNRNPC Is Upregulated in Tumor Tissues and Predicts Large Tumor Size, Advanced TNM Stage, and Poor Prognosis in HCC

Using the UALCAN database, we found that HNRNPC mRNA levels were higher in 371 primary HCC tissues than in 50 normal liver tissues (P < 0.001, **Figure 1A**); in addition, the expression of HNRNPC mRNA was elevated in stage 2 (P = 0.033, **Figure 1B**) and stage 3 (P < 0.001, **Figure 1B**) HCC patients compared with stage 1 HCC patients. To compare HNRNPC protein expression in tumor and para-tumor tissues, western blotting and IHC were performed. HNRNPC protein levels were obviously higher in tumor tissues than in para-tumor tissues, based on western blot analysis of 12 HCC tumor tissues and their matched para-tumor tissues (P< 0.001, **Figures 1C, D**). The IHC results showed high expression of HNRNPC protein, mainly located in nuclei, in 80 of 147 tumor tissues (54.40%) and in 13 (15.90%) of 82 paired para-tumor tissues (P<0.001, **Figures 1E, F**). Correlations of HNRNPC protein levels with clinicopathological features in HCC were analyzed by chi-square test; this demonstrated that HNRNPC protein levels were significantly associated with tumor size (P = 0.007) and tumor TNM stage (P=0.028) (**Table 1**). To explore the effects of HNRNPC protein levels on survival of HCC patients, Kaplan–Meier survival curves were constructed, showing that patients with high HNRNPC protein expression had poorer overall survival (P = 0.001, **Figure 1G**) and disease-free survival (P < 0.001, **Figure 1H**) than those with low HNRNPC protein expression. Univariate and multivariate analysis were used to evaluate the risk factors associated with HCC patients' survival. According to our results, tumor size (P = 0.005, HR = 1.957), tumor TNM stage (P = 0.014, HR = 1.786), and high HNRNPC expression (P = 0.039, HR = 1.637) could be regarded as independent risk factors for overall survival of HCC patients (**Table 2**). Moreover, tumor TNM stage (P < 0.001, HR = 2.188) and high HNRNPC level (P = 0.002, HR = 1.883) could independently predict disease-free survival in HCC patients (**Table 2**).

Knockdown of HNRNPC Suppresses HCC Proliferation, Invasion, and Migration *In Vitro*

To observe the impact of HNRNPC on HCC proliferation, invasion, and migration, Lv-NC and Lv-HNRNPC lentiviruses were used to infect the Huh-7 and Hep 3B cell lines. After selection by puromycin, the infection efficiency of Huh-7 and Hep 3B cells was >90% (**Supplementary Figure 1A**), and lower HNRNPC expression was detected in Lv-HNRNPC Huh-7 and Hep 3B cells *via* western blotting and q-RT-PCR (**Supplementary Figures 1B, C**). CCK-8 and colony formation assays were used to analyze cell proliferation *in vitro*. The colony formation assay revealed that HNRNPC knockdown significantly inhibited proliferation of Huh-7 and Hep 3B cells (**Figure 2A**). In the CCK-8 test, the viability of Huh-7 and Hep 3B cells was also significantly suppressed by silencing of HNRNPC (**Figure 2B**). A transwell assay was performed to observe invasion; the results showed that inhibition of HNRNPC impaired the invasion activity of Huh-7 and Hep 3B cells (**Figure 2C**). The scratch wound assay showed decreased migration ability of Huh-7 and Hep 3B cells in the Lv-HNRNPC-group (**Figure 2D**).

Inhibition of HNRNPC Downregulates the Activity of the MAPK Signaling Pathway, Blocks Tumors at G0/G1 Phase, and Suppresses EMT Process *In Vitro*

To study the potential molecular mechanisms by which HNRNPC suppressed tumor growth, migration and invasion, we selected 3517 genes that were significantly correlated with HNRNPC (Pearson correlation coefficient ≥ 0.5) from the UALCAN database; these genes were subjected to KEGG

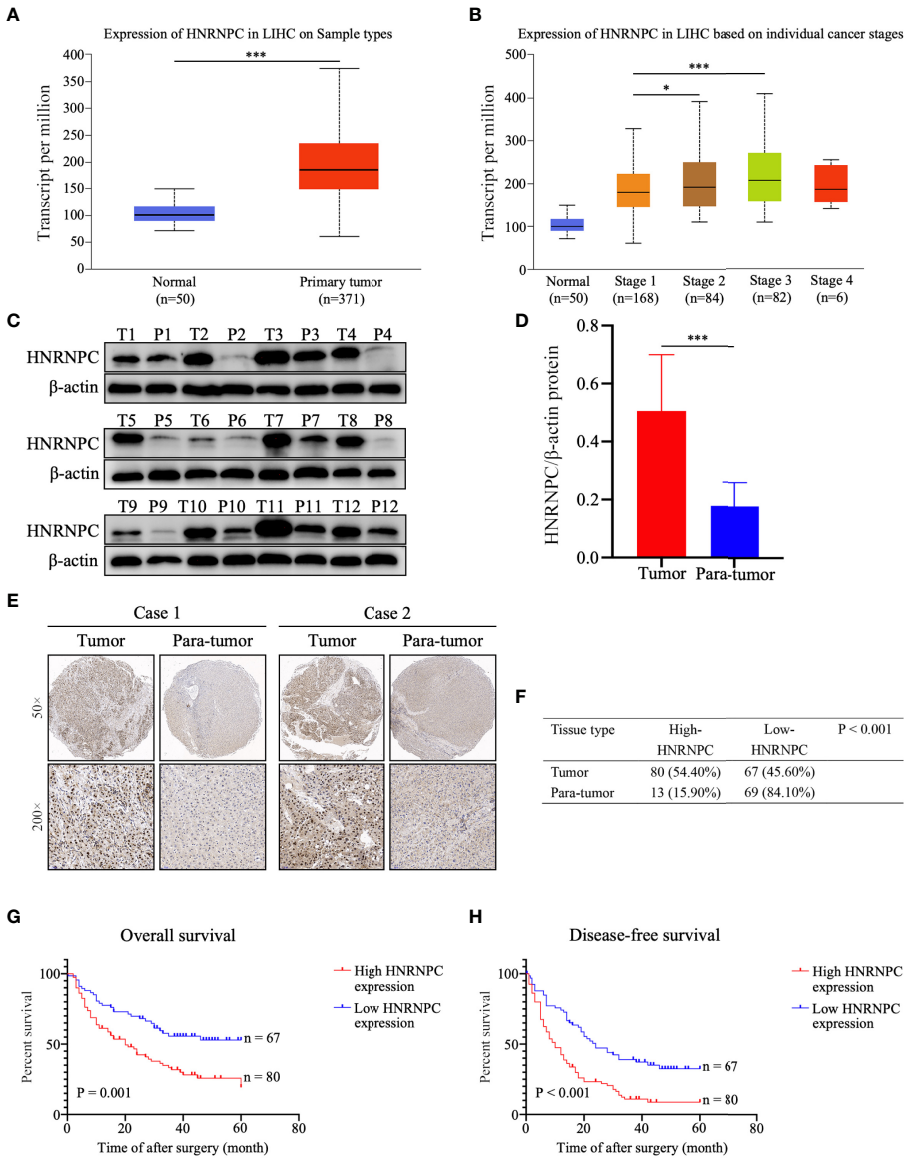

Tissue type	High-HNRNPC	Low-HNRNPC	P < 0.001
Tumor	80 (54.40%)	67 (45.60%)	
Para-tumor	13 (15.90%)	69 (84.10%)	

FIGURE 1 | High HNRNPC expression was detected in HCC tumor tissues, and predicts a poor survival in HCC patients. **(A)** HNRNPC mRNA expression in HCC tissues and normal liver tissues acquired from UALCAN analysis. **(B)** UALCAN analysis showing HNRNPC mRNA expression at different cancer stages. **(C, D)** Western blot showing protein expression of HNRNPC in HCC tumor tissues and matched para-tumor tissues. **(E)** Classical cases showing HNRNPC protein expression in HCC tumor tissues and paired para-tumor tissues. **(F)** The $\chi 2$ test was used to assess HNRNPC protein expression in HCC tissues and adjacent tissues. **(G)** Kaplan–Meier analysis showing the correlation of HNRNPC level with overall survival of HCC patients. **(H)** Kaplan–Meier analysis showing the association between HNRNPC level and disease-free survival. The final results were presented as mean ± standard deviation (SD). *P < 0.05, ***P < 0.001.

analysis using WebGestalt (2013). Among the enriched KEGG pathways, "Cell cycle" and "Pathways in cancer" were highly related to tumor growth (**Supplementary Figure 1D**), and "Pathways in cancer" mainly involved the MAPK and AKT signaling pathways (**Supplementary Figure 1E**). Subsequently, the activity of the MAPK signaling pathway was detected by western blotting. The results showed that HNRNPC knockdown statistically decreased the expression of Ras and the relative levels of p-Raf, p-MEK1/2, and p-Erk1/2 in Huh-7 and Hep 3B cells (**Figures 3A, B**). As the MAPK pathway activates a series of downstream genes to regulate the cell cycle, thereby regulating cell proliferation, we used flow cytometry for cell cycle analysis. The results showed that HNRNPC downregulation blocked more cells at G0/G1 phase and reduced the proportion of S-phase cells among both Huh-7 and Hep 3B cells (**Figures 3C, D**). CDK4, cyclin E1, and c-myc are well known as important

TABLE 2 | Univariate and multivariate analysis for survival of 147 HCC patients.

Clinical features	Univariate		Multivariate	
	HR (95% CI)	P-value	HR (95% CI)	P-value
Overall survival:				
Gender (female vs male)	0.938 (0.498–1.767)	0.843		
Age (≥55 y vs <55 y)	1.068 (0.698–1.636)	0.761		
HBV infection (negative vs positive)	0.717 (0.389–1.321)	0.286		
Liver cirrhosis (absent vs present)	0.675 (0.425–1.072)	0.095		
Child–Pugh (B vs A)	1.295 (0.761–2.205)	0.341		
Tumor number (2–3 vs 1)	1.392 (0.784–2.470)	0.259		
Tumor size (≥5 cm vs <5 cm)	2.501 (1.598–3.915)	**<0.001**	1.957 (1.224–3.135)	**0.005**
TNM stage (II–III vs I)	2.515 (1.634–3.871)	**<0.001**	1.786 (1.124–2.841)	**0.014**
Tumor differentiation (III–IV vs I–II)	1.017 (0.629–1.643)	0.946		
AFP (≥400 vs <400)	0.763 (0.496–1.173)	0.218		
HNRNPC (high vs low)	2.117 (1.349–3.322)	**0.001**	1.637 (1.025–2.611)	**0.039**
Disease-free survival:				
Gender (female vs male)	0.876 (0.501–1.536)	0.645		
Age (≥55 y vs <55 y)	1.090 (0.753–1.577)	0.649		
HBV infection (negative vs positive)	0.736 (0.439–1.233)	0.244		
Liver cirrhosis (absent vs present)	0.693 (0.466–1.028)	0.068		
Child–Pugh (B vs A)	1.170 (0.728–1.881)	0.516		
Tumor number (2–3 vs 1)	1.959 (1.184–3.241)	**0.009**	1.093 (0.620–1.927)	0.760
Tumor size (≥5 cm vs <5 cm)	1.830 (1.257–2.662)	**0.002**	1.348 (0.905–2.004)	0.142
TNM stage (II–III vs I)	2.572 (1.750–3.779)	**<0.001**	2.188 (1.471–3.257)	**<0.001**
Tumor differentiation (III–IV vs I–II)	1.099 (0.729–1.658)	0.652		
AFP (≥400 vs <400)	1.387 (0.954–2.012)	0.086		
HNRNPC (high vs low)	2.249 (1.525–3.317)	**<0.001**	1.883 (1.261–2.817)	**0.002**

HNRNPC, heterogeneous nuclear ribonucleoprotein C; HBV, hepatitis B virus; AFP, alpha fetoprotein.
The bold values present statistical significance.

molecules that positively regulate G1-S transition. In the present study, silencing of HNRNPC markedly downregulated CDK4, cyclin E1, and c-myc protein levels, as confirmed by western blotting (**Figures 3E, F**). Ras/MAPK signaling pathway not only positively regulate G1-S transition to promote tumor proliferation, but also accelerate EMT process to facilitate tumor migration and invasion. We also detected the marker of EMT by western blotting, our results indicated that HNRNPC silencing decreased Vimentin level, and upregulated E-cadherin expression statistically (**Figures 3G, H**).

HNRNPC Silencing Inhibits Tumor Growth *In Vivo*

To explore the impact of HNRNPC on tumor growth *in vivo*, Lv-NC and Lv-HNRNPC Huh-7 cells were implanted in nude mice subcutaneously. The tumors of the Lv-HNRNPC group showed obvious reductions in both size and weight compared with those of the Lv-NC group (**Figures 4A–C**). Subsequently, hematoxylin eosin (H&E) and IHC staining were performed to confirm the tumor tissues and HNRNPC knockdown efficiency, respectively (**Figure 4D**). In addition, Ki-67 was used to observe the proliferation of tumor cells *via* IHC; the Ki-67 staining intensity was stronger in the Lv-NC group than in the Lv-HNRNPC group (**Figure 4D**). Tumor migration and invasion are highly correlated with angiogenesis and EMT process, so Vimentin, E-cadherin, and CD34 were used to evaluate the ability of tumor invasion and migration by IHC. The results showed that Vimentin and CD34 staining intensity were weaker, and E-cadherin staining intensity was stronger in the Lv-HNRNPC group than in Lv-NC group (**Figure 4E**).

Ras Agonist Partly Recovers Growth, Migration, and Invasion Ability in Lv-HNRNPC Group

CDK4, cyclin E1, and c-myc are classical downstream genes of the MAPK signaling pathway. To confirm the upstream and downstream relationships between the MAPK signaling pathway and these cell cycle-related molecules, a Ras agonist (ML-098) was used to treat cells in the Lv-HNRNPC group. Details of this process are given in the Materials and Methods section. First, we performed western blotting to detect the recovery of MAPK pathway activity. After treatment with ML-098 for 48 h, the activity of the MAPK pathway was reversed completely in the Lv-HNRNPC group (**Figures 5A, B**). Moreover, colony formation and CCK-8 assays revealed that the proliferation ability of cells in the Lv-HNRNPC group was partly rescued by ML-098 (**Figures 5C–E**). Furthermore, the cell cycle assay showed that ML-098 treatment could partially reverse the G0/G1 arrest caused by HNRNPC knockdown in both Huh-7 and Hep 3B cells (**Figures 6A, B**). Finally, using western blotting, we showed that the effects of HNRNPC inhibition on CDK4, cyclin E1, and c-myc levels in HCC cells were reversed by ML-098 to some extent (**Figures 6C, D**). On the other hand, Ras/MAPK signaling pathway take part in EMT process. In present study, cell invasion and scratch wound assays showed that the invasion (**Figures 7A, B**) and migration (**Figures 7C, D**) abilities of the Lv-HNRNPC group

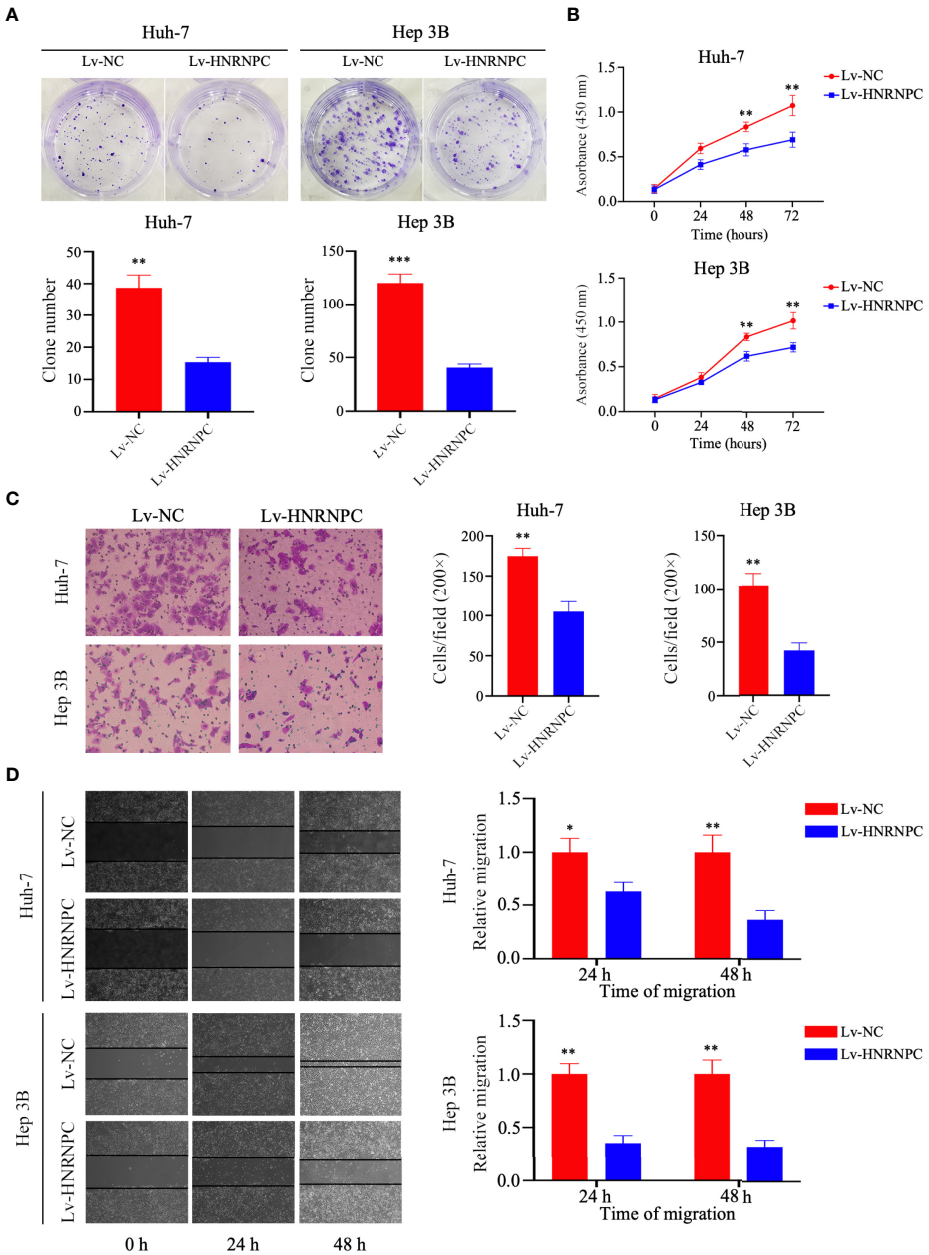

FIGURE 2 | Knockdown of HNRNPC suppressed proliferation, invasion, and migration of HCC cells *in vitro*. **(A)** Colony formation assay showing the impact of HNRNPC knockdown on HCC cell proliferation. **(B)** CCK-8 test showing the effects of HNRNPC downregulation on HCC cell viability. **(C)** Transwell assay showing the influence of HNRNPC inhibition on HCC cell invasion. **(D)** Scratch wound test showing the influence of HNRNPC suppression on HCC cell migration. All experiments were independently repeated three times, and the results were showed as mean ± standard deviation (SD). *P < 0.05, **P < 0.01, ***P < 0.001.

cells were recovered by ML-098 partly. Furthermore, the western blotting results demonstrated that after treatment with ML-098, the EMT process inhibition of cells in the Lv-HNRNPC group was reversed in part too (**Figures 7E, F**). Taken together, these results indicate that HNRNPC inhibition not only arrests HCC cells in G0/G1 phase to inhibit tumor proliferation, but also suppresses EMT process to block invasion and migration of HCC cells in part *via* the Ras/Raf/MEk/Erk signaling pathway.

DISCUSSION

With progress in medical treatment, molecular therapies are increasingly available for advanced HCC patients (51–53); however, the prognosis of these patients remains poor (1). This prompted us to explore novel pathogenetic mechanisms and therapeutic targets for HCC. According to present evidence, as a process fundamental to cancer (54), aberrant alternative splicing

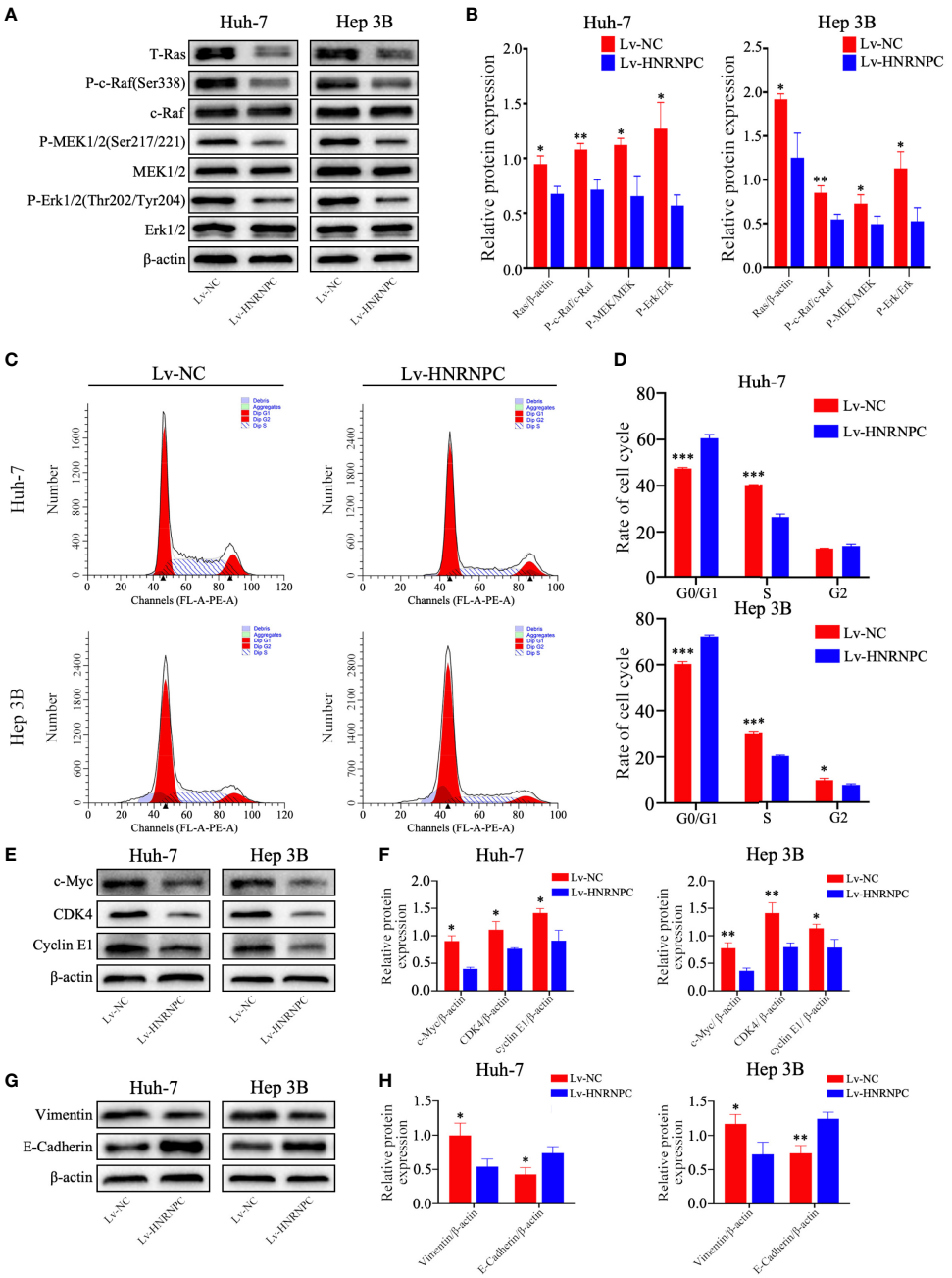

FIGURE 3 | HNRNPC suppression inhibited the Ras/MAPK signaling pathway, leading to arrest of more cells at S phase and blocking of EMT *in vitro*. **(A, B)** Western blot to detect activation of the Ras/MAPK signaling pathway in Lv-NC Huh-7, Lv-HNRNPC Huh-7, Lv-NC Hep 3B, and Lv-HNRNPC Hep 3B cells. **(C, D)** Cell cycle analysis for the various cell groups mentioned above. **(E, F)** Western blot to detect c-Myc, CDK4, and cyclin E1 levels in the various cell groups. **(G, H)** Western blot to analyze Vimentin and E-Cadherin expression in various cell groups. Each test was performed independently in triplicate, and the results were presented as mean ± standard deviation (SD). *P < 0.05, **P < 0.01, ***P < 0.001.

occurs more frequently in various malignant tumors, including renal cancer (55), lung cancer, and HCC (56); this makes it possible for cells with phenotypic variability to adapt to unfamiliar microenvironments, treatments, and immune responses (57). HNRNPs, which include HNRNP A2/B1, HNRNP L, HNRNP H, and HNRNPC, are primary factors for alternative splicing. HNRNPC is believed to be the founder of the HNRNP family (58), that is, it seems to be at the core of regulating alternative splicing. The relationships of HNRNP L (59), HNRNP A2/B1 (60), and HNRNP H (61) with HCC have

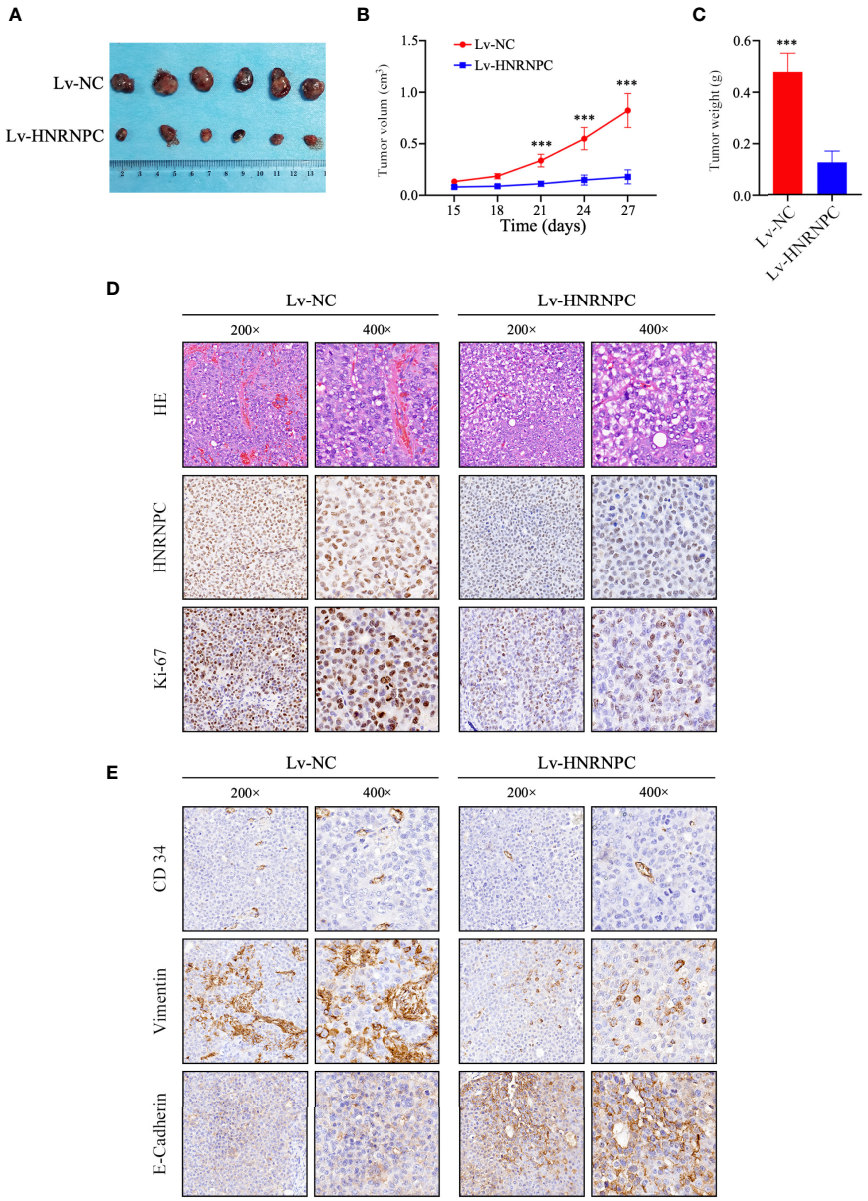

FIGURE 4 | HNRNPC knockdown blocked HCC cell proliferation *in vivo*. **(A)** Huh-7-cell xenograft tumors in Lv-HNRNPC and Lv-NC groups. **(B, C)** t-test analysis showing tumor weights and sizes in Lv-HNRNPC and Lv-NC Huh-7 cell groups. **(D)** H&E staining to confirm xenograft tumors (upper panel); IHC to detect HNRNPC levels in xenograft tumors (middle panel); proliferation of xenograft tumors as determined by Ki-67 staining (nether panel). **(E)** IHC staining to analyze CD34 (upper panel), Vimentin (middle panel), and E-Cadherin (nether panel) expression in xenograft tumors. The tumor size and weight were demonstrated as mean ± standard deviation (SD). ***P < 0.001.

been reported; however, any association of HNRNPC with HCC remained unknown.

Using two-dimensional difference electrophoresis, Sun et al. found that HNRNPC protein expression was higher in HCC tumor tissues than normal liver tissues (62). However, they did not further investigate any correlation of HNRNPC protein expression with prognosis or clinicopathologic characteristics in HCC. In the present study, we showed that HNRNPC protein levels were statistically higher in HCC tumor tissues than in para-tumor tissues by western blotting and IHC. Moreover, Kaplan–Meier analysis and Cox proportional hazards regression models were used to perform survival analysis; this demonstrated that a high HNRNPC protein level was an independent risk factor that could serve as a biomarker predicting poor overall survival and disease-free survival in HCC patients. By functional experiments, we showed that HNRNPC knockdown significantly inhibited proliferation, migration, and invasion of HCC cells *in vitro*. Finally, the

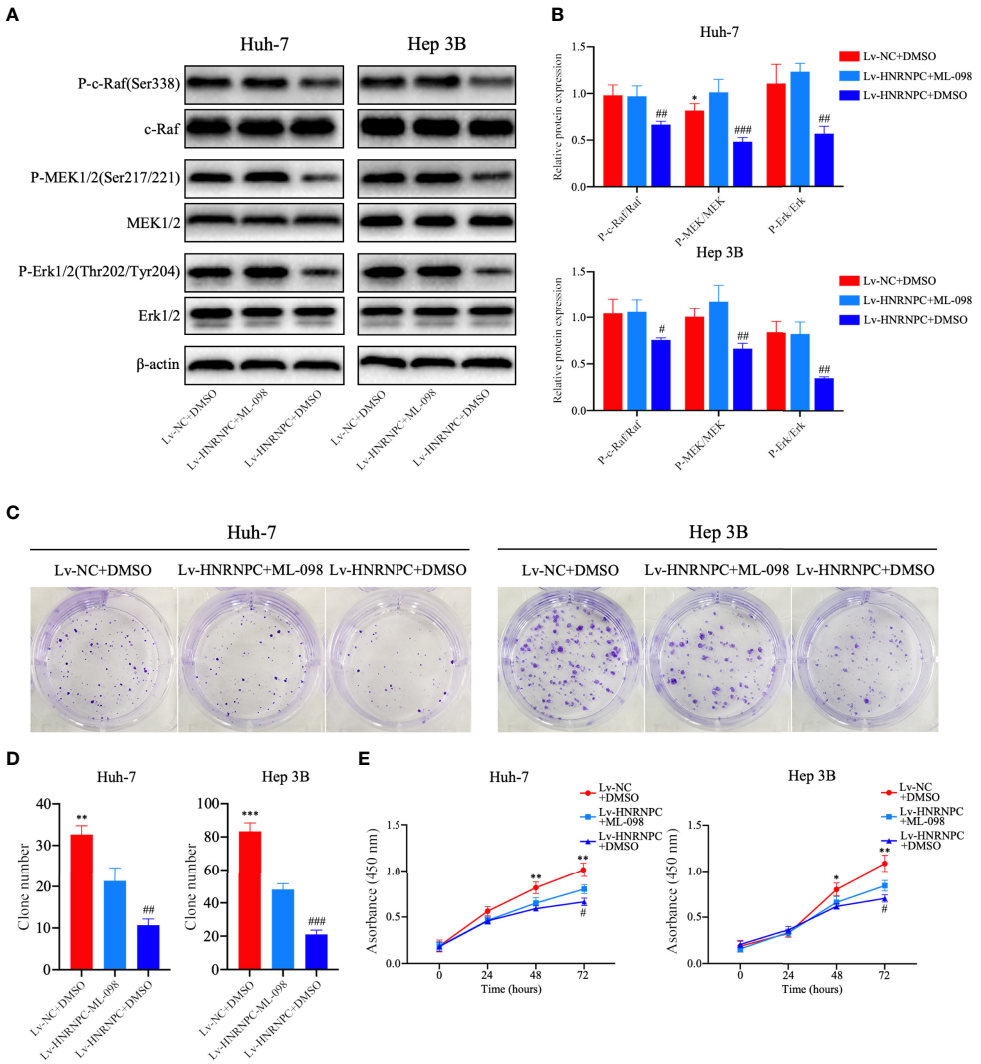

FIGURE 5 | After treatment with ML-098 (20 nmol/l), MAPK signaling pathway activation was recovered completely in Lv-HNRNPC-group cells, and proliferation ability was partially reversed. **(A, B)** Western blot to detect recovery of activation of the MAPK signaling pathway in Lv-HNRNPC groups after treatment with ML-098. **(C, D)** Colony formation assay showing the reversed efficiency of ML-098 in Lv-HNRNPC group cell proliferation. **(E)** CCK-8 test showing the rescue by ML-098 of cell viability in the Lv-HNRNPC group. The tests mentioned above were operated three times respectively, and the results were reported as mean ± standard deviation (SD). *P < 0.05, **P < 0.01, ***P < 0.001, for Lv-NC+DMSO group compared with Lv-HNRNPC+ML-098 group; #P < 0.05, ##P < 0.01, ###P < 0.001, for Lv-HNRNPC+DMSO group compared with Lv-HNRNPC+ML-098 group.

xenograft assay showed that suppressing HNRNPC significantly restrained tumor growth *in vivo*.

HNRNPC has an important role in RNA combination and alternative splicing. Fischl et al. reported that HNRNPC regulates alternative cleavage and polyadenylation (APA) profiles in colon cancer, and by coding region APA, HNRNPC mainly affected MTHFD1L protein levels, which are strongly linked to tumor progression (24). In addition, Wu et al. extended the function of HNRNPC to alternative splicing in breast cancer: by controlling endogenous double-stranded RNA, HNRNPC regulated the activation of the IFNβ signaling pathway to affect the progression of breast cancer (27). In the present study, we performed bioinformatic analysis of HNRNPC-correlated genes, which brought the Ras/Raf/MEK/Erk and AKT signaling pathways to our attention. HNRNPC has previously been reported to cause AKT phosphorylation in ovarian cancer (32). We used western blotting to detect the activation of the Ras/Raf/MEK/Erk signaling pathway; the results indicated that HNRNPC knockdown significantly inhibited the activation of the MAPK signaling pathway. Ras mutation has a very important role in many cancers (63–65), and HCC is no exception (66, 67). Both H-ras and K-ras have respective splice variants (68, 69), which could be regarded as Ras mutations at the mRNA level. Barbier et al. reported that H-ras splice variants including

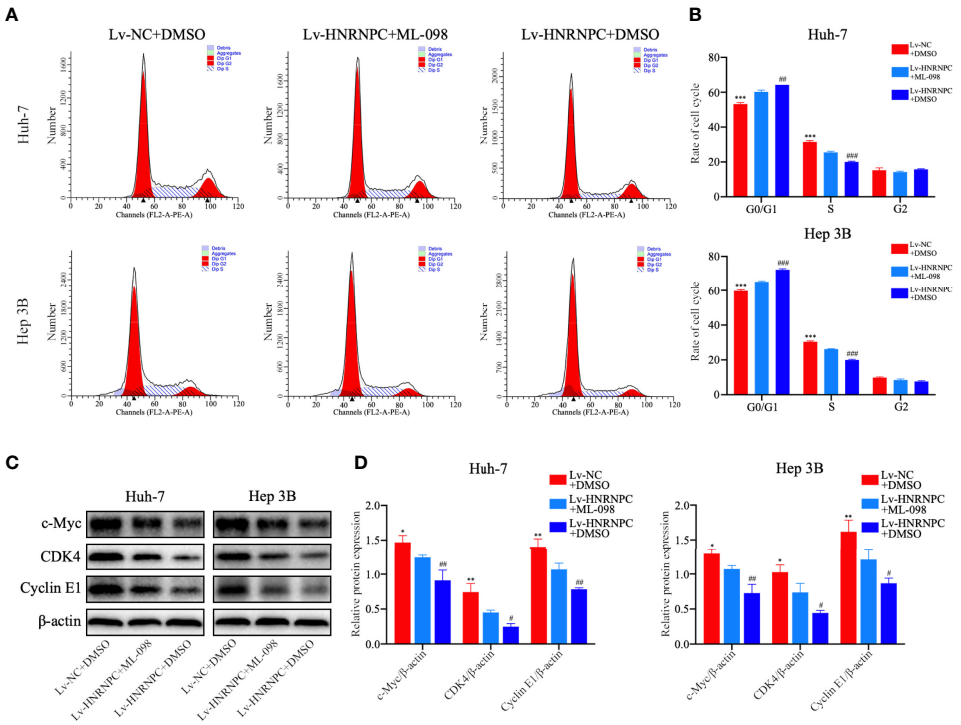

FIGURE 6 | ML-098 partly reversed the reduction in numbers of S phase cells in the Lv-HNRNPC group. **(A, B)** Cell cycle analysis to detect the recovery of numbers of S phase cells in the Lv-HNRNPC groups after treatment with ML-098. **(C, D)** Western blot to detect the recovery of c-Myc, CDK4, and cyclin E1 in Lv-HNRNPC cell groups after treatment with ML-098. All tests were repeated independently in triplicate, and the results were showed as mean ± standard deviation (SD). *P < 0.05, **P < 0.01, ***P < 0.001, for Lv-NC+DMSO group compared with Lv-HNRNPC+ML-098 group; $^{\#}$P < 0.05, $^{\#\#}$P < 0.01, $^{\#\#\#}$P < 0.001, for Lv-HNRNPC+DMSO group compared with Lv-HNRNPC+ML-098 group.

premature translation termination codons were selectively degraded by the nonsense-mediated mRNA decay pathway to regulate Ras expression (69). However, the mechanism by which Ras downregulation was caused by HNRNPC inhibition was not investigated in our study; this will be explored in the future. This novel means of Ras mutation may provide a new approach to HCC therapy.

The MAPK signaling pathway regulates the majority of cell functions, in particular, cell proliferation, apoptosis, and metabolism (70–72). After being activated, the Ras cascade phosphorylates Raf, Mek, and Erk to regulate cell proliferation and apoptosis by controlling G1-S transition (73, 74). In the present study, we prove that inhibition of the MAPK signaling pathway by HNRNPC suppression causes the arrest of more HCC cells at G0/G1 phase. CDK4 (75), cyclin E1 (76), and c-myc (77) play important parts in regulating G1-S transition. As G1-S transition overactivation occurs in the majority of malignant tumors, inhibitors of CDK4 and cyclin E1 have emerged as candidate drugs for tumor treatment (78, 79). In our study, we showed that HNRNPC knockdown statistically inhibited CDK4, cyclin E1, and c-myc expression. Subsequently, rescue experiments revealed that activation of the MAPK signaling pathway could partly recover CDK4, cyclin E1, and c-myc expression, demonstrating that knockdown of HNRNPC induced G0/G1 arrest in part *via* the MAPK signaling pathway. Epithelial-mesenchymal transition is an essential factor to initiate tumor migration and invasion (80). In recent years, more and more research indicated that Ras/MAPK signaling pathway play an important role in EMT process (43, 81, 82). In the present study, we proved that HNRNPC inhibition suppressed the EMT process of HCC cells. Additionally, after treatment with ML-098, the EMT process of HCC cells in Lv-HNRNPC group was recovered in part, which support the above point again. Ras is the second mutated gene driver in many malignant tumors (83), and Ras/MAPK have been shown to be activated in 50–100% of HCC patients (84). MAPK-associated inhibitors have been used to treat HCC (85), but very few HCC patients benefited from this treatment (86), largely owing to the compensatory activation of other Ras-related pathways such as the AKT (87) and IGF/FGF (88) signaling pathways. Thus, exploration of the mechanisms of Ras mutation may provide a novel approach for HCC therapy. In our study, we reported that HNRNPC knockdown inhibited Ras/MAPK activation to block proliferation of HCC cells, which may represent a new mutation mechanism for Ras. However, the present study did not consider how HNRNPC regulates Ras; this will be explored in our future studies to determine the mechanisms of novel Ras mutations and offer a new approach for HCC therapy.

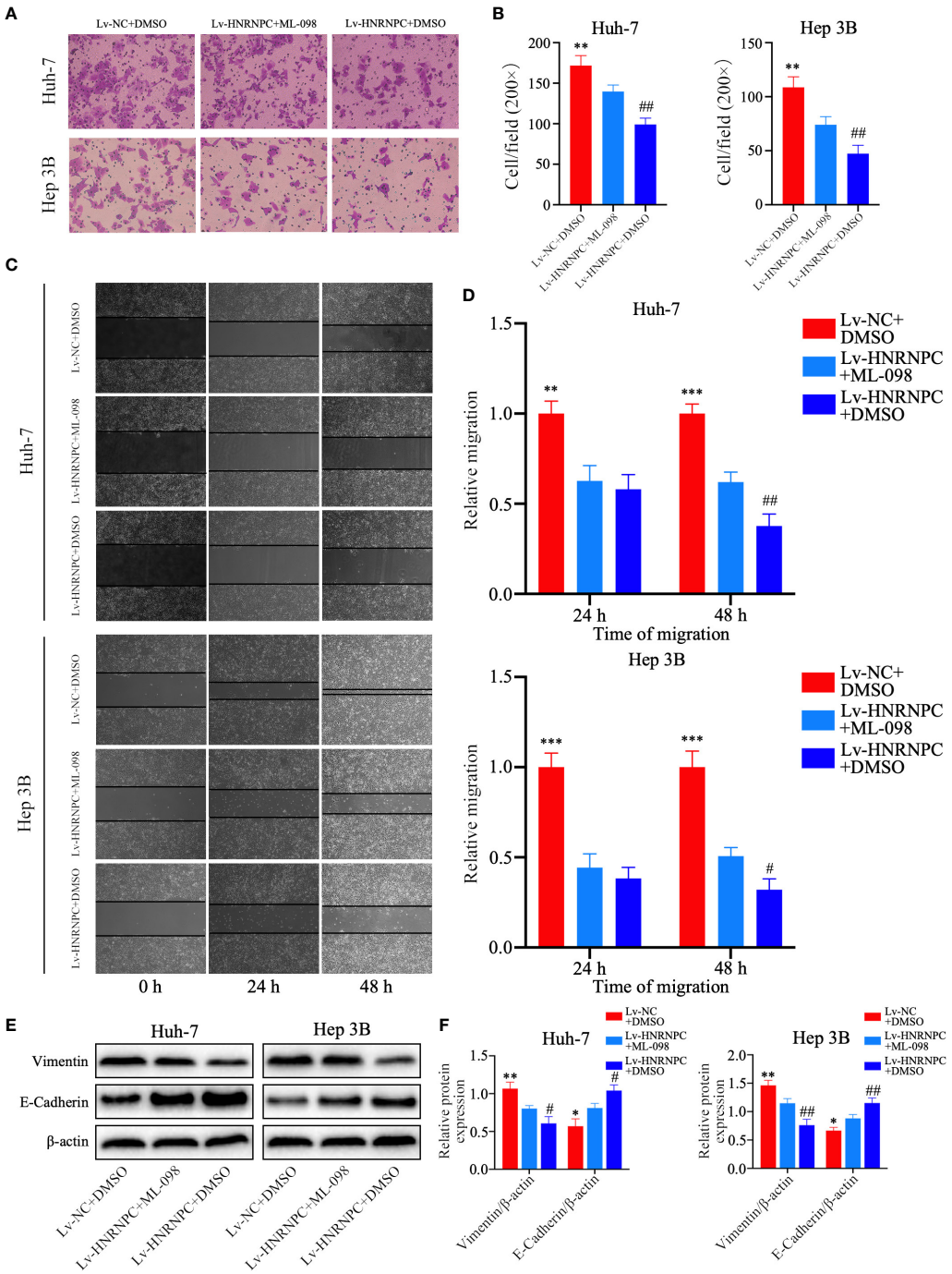

FIGURE 7 | ML-098 recovered the invasion and migration abilities of Lv-HNRNPC group cells in part. **(A, B)** Transwell assay demonstrating the recovered efficiency of ML-098 in Lv-HNRNPC group cell invasion. **(C, D)** Scratch wound test showing the rescue by ML-098 of cell migration in the Lv-HNRNPC group. **(E, F)** Western blot to detect the recovery of EMT process in Lv-HNRNPC cell groups after treatment with ML-098. Each test was repeated independently in triplicate, and the results were demonstrated as mean ± standard deviation (SD). *P < 0.05, **P < 0.01, ***P < 0.001, for Lv-NC+DMSO group compared with Lv-HNRNPC+ML-098 group; $^{\#}$P < 0.05, $^{\#\#}$P < 0.01, for Lv-HNRNPC+DMSO group compared with Lv-HNRNPC+ML-098 group.

DATA AVAILABILITY STATEMENT

The original contributions presented in the study are included in the article/**Supplementary Material**. Further inquiries can be directed to the corresponding authors.

ETHICS STATEMENT

The studies involving human participants were reviewed and approved by Ethics Committee at the Second Affiliated Hospital of Chongqing Medical University. The patients/participants provided their written informed consent to participate in this study. The animal study was reviewed and approved by Chongqing Municipal Committee of Science Technology.

AUTHOR CONTRIBUTIONS

The study was conceived and designed by JG. G-CZ, JH, and DC wrote the manuscript and performed the experiments. The statistical analysis was carried out by ZZ. All authors contributed to the article and approved the submitted version.

ACKNOWLEDGMENTS

We thank the Laboratory of Pathology, West China Medical College, and Sichuan University for supplying the experimental platform, and Charlesworth Author Services (https://www.cwauthors.com/) for editing a draft of this manuscript.

SUPPLEMENTARY MATERIAL

The Supplementary Material for this article can be found online at: https://www.frontiersin.org/articles/10.3389/fonc.2021.659676/full#supplementary-material

Supplementary Figure 1 | Knockdown efficiency of HNRNPC in Huh-7 and Hep 3B cells, and KEGG analysis. **(A)** EGFP expression showing the infective efficiency of the lentivirus. **(B)** Western blot to detect knockdown efficiency of HNRNPC in Huh-7 and Hep 3B cells. **(C)** q-RT-PCR to detect knockdown efficiency of HNRNPC in Huh-7 and Hep 3B cells. **(D, E)** KEGG analysis of 3517 HNRNPC-correlated genes by WebGestalt 2013. ***P<0.001.

REFERENCES

1. Akinyemiju T, Abera S, Ahmed M, Alam N, Alemayohu MA, Allen C, et al. The Burden of Primary Liver Cancer and Underlying Etiologies From 1990 to 2015 at the Global, Regional, and National Level: Results From the Global Burden of Disease Study 2015. *JAMA Oncol* (2017) 3(12):1683–91. doi: 10.1001/jamaoncol.2017.3055
2. Villanueva A. Hepatocellular Carcinoma. Reply. *N Engl J Med* (2019) 381(1): e2. doi: 10.1056/NEJMc1906565
3. Krenzien F, Schmelzle M, Struecker B, Raschzok N, Benzing C, Jara M, et al. Liver Transplantation and Liver Resection for Cirrhotic Patients with Hepatocellular Carcinoma: Comparison of Long-Term Survivals. *J Gastrointest Surg* (2018) 22(5):840–8. doi: 10.1007/s11605-018-3690-4
4. Lurje I, Czigany Z, Bednarsch J, Roderburg C, Isfort P, Neumann UP, et al. Treatment Strategies for Hepatocellular Carcinoma ‒ a Multidisciplinary Approach. *Int J Mol Sci* (2019) 20(6):1465. doi: 10.3390/ijms20061465
5. Sapisochin G, Bruix J. Liver transplantation for hepatocellular carcinoma: outcomes and novel surgical approaches. *Nat Rev Gastroenterol Hepatol* (2017) 14(4):203–17. doi: 10.1038/nrgastro.2016.193
6. Boland P, Wu J. Systemic therapy for hepatocellular carcinoma: beyond sorafenib. *Chin Clin Oncol* (2018) 7(5):50. doi: 10.21037/cco.2018.10.10
7. Facciorusso A, Di Maso M, Muscatiello N. Microwave ablation versus radiofrequency ablation for the treatment of hepatocellular carcinoma: A systematic review and meta-analysis. *Int J Hyperthermia* (2016) 32(3):339–44. doi: 10.3109/02656736.2015.1127434
8. Galle PR, Tovoli F, Foerster F, Wörns MA, Cucchetti A, Bolondi L. The treatment of intermediate stage tumours beyond TACE: From surgery to systemic therapy. *J Hepatol* (2017) 67(1):173–83. doi: 10.1016/j.jhep.2017.03.007
9. Johnston MP, Khakoo SI. Immunotherapy for hepatocellular carcinoma: Current and future. *World J Gastroenterol* (2019) 25(24):2977–89. doi: 10.3748/wjg.v25.i24.2977
10. Kirstein MM, Wirth TC. [Multimodal treatment of hepatocellular carcinoma]. *Internist (Berl)* (2020) 61(2):164–9. doi: 10.1007/s00108-019-00722-x
11. Liu Z, Lin Y, Zhang J, Zhang Y, Li Y, Liu Z, et al. Molecular targeted and immune checkpoint therapy for advanced hepatocellular carcinoma. *J Exp Clin Cancer Res* (2019) 38(1):447. doi: 10.1186/s13046-019-1412-8
12. Lee KF, Chong CCN, Fong AKW, Fung AKY, Lok HT, Cheung YS, et al. Pattern of disease recurrence and its implications for postoperative surveillance after curative hepatectomy for hepatocellular carcinoma: experience from a single center. *Hepatobiliary Surg Nutr* (2018) 7(5):320–30. doi: 10.21037/hbsn.2018.03.17
13. Llovet JM, Montal R, Villanueva A. Randomized trials and endpoints in advanced HCC: Role of PFS as a surrogate of survival. *J Hepatol* (2019) 70 (6):1262–77. doi: 10.1016/j.jhep.2019.01.028
14. Welling TH, Eddinger K, Carrier K, Zhu D, Kleaveland T, Moore DE, et al. Multicenter Study of Staging and Therapeutic Predictors of Hepatocellular Carcinoma Recurrence Following Transplantation. *Liver Transpl* (2018) 24 (9):1233–42. doi: 10.1002/lt.25194
15. Javadian P, Nezhat F. Endometrial Carcinoma and its Precursors. *Adv Exp Med Biol* (2020) 1242:59–72. doi: 10.1007/978-3-030-38474-6_4
16. Sarveazad A, Agah S, Babahajian A, Amini N, Bahardoust M. Predictors of 5 year survival rate in hepatocellular carcinoma patients. *J Res Med Sci* (2019) 24:86. doi: 10.4103/jrms.JRMS_1017_18
17. Wu G, Wu J, Wang B, Zhu X, Shi X, Ding Y. Importance of tumor size at diagnosis as a prognostic factor for hepatocellular carcinoma survival: a population-based study. *Cancer Manag Res* (2018) 10:4401–10. doi: 10.2147/cmar.S177663
18. Dimitroulis D, Damaskos C, Valsami S, Davakis S, Garmpis N, Spartalis E, et al. From diagnosis to treatment of hepatocellular carcinoma: An epidemic problem for both developed and developing world. *World J Gastroenterol* (2017) 23(29):5282–94. doi: 10.3748/wjg.v23.i29.5282
19. Baralle FE, Giudice J. Alternative splicing as a regulator of development and tissue identity. *Nat Rev Mol Cell Biol* (2017) 18(7):437–51. doi: 10.1038/nrm.2017.27
20. Du JX, Zhu GQ, Cai JL, Wang B, Luo YH, Chen C, et al. Splicing factors: Insights into their regulatory network in alternative splicing in cancer. *Cancer Lett* (2020) 501:83–104. doi: 10.1016/j.canlet.2020.11.043
21. Wan L, Yu W, Shen E, Sun W, Liu Y, Kong J, et al. SRSF6-regulated alternative splicing that promotes tumour progression offers a therapy target for colorectal cancer. *Gut* (2019) 68(1):118–29. doi: 10.1136/gutjnl-2017-314983
22. Zhan YT, Li L, Zeng TT, Zhou NN, Guan XY, Li Y. SNRPB-mediated RNA splicing drives tumor cell proliferation and stemness in hepatocellular carcinoma. *Aging (Albany NY)* (2020) 12:537–54. doi: 10.18632/aging.202164
23. Zhang F, Deng CK, Wang M, Deng B, Barber R, Huang G. Identification of novel alternative splicing biomarkers for breast cancer with LC/MS/MS and RNA-Seq. *BMC Bioinf* (2020) 21(Suppl 9):541. doi: 10.1186/s12859-020-03824-8

24. Fischl H, Neve J, Wang Z, Patel R, Louey A, Tian B, et al. hnRNPC regulates cancer-specific alternative cleavage and polyadenylation profiles. *Nucleic Acids Res* (2019) 47(14):7580–91. doi: 10.1093/nar/gkz461
25. Zarnack K, König J, Tajnik M, Martincorena I, Eustermann S, Stévant I, et al. Direct competition between hnRNP C and U2AF65 protects the transcriptome from the exonization of Alu elements. *Cell* (2013) 152 (3):453–66. doi: 10.1016/j.cell.2012.12.023
26. Zhang Y, Chen W, Pan T, Wang H, Zhang Y, Li C. LBX2-AS1 is activated by ZEB1 and promotes the development of esophageal squamous cell carcinoma by interacting with HNRNPC to enhance the stability of ZEB1 and ZEB2 mRNAs. *Biochem Biophys Res Commun* (2019) 511(3):566–72. doi: 10.1016/j.bbrc.2019.02.079
27. Wu Y, Zhao W, Liu Y, Tan X, Li X, Zou Q, et al. Function of HNRNPC in breast cancer cells by controlling the dsRNA-induced interferon response. *EMBO J* (2018) 37(23):e99017. doi: 10.15252/embj.201899017
28. Park YM, Hwang SJ, Masuda K, Choi KM, Jeong MR, Nam DH, et al. Heterogeneous nuclear ribonucleoprotein C1/C2 controls the metastatic potential of glioblastoma by regulating PDCD4. *Mol Cell Biol* (2012) 32 (20):4237–44. doi: 10.1128/mcb.00443-12
29. Huang H, Han Y, Zhang C, Wu J, Feng J, Qu L, et al. HNRNPC as a candidate biomarker for chemoresistance in gastric cancer. *Tumour Biol* (2016) 37 (3):3527–34. doi: 10.1007/s13277-015-4144-1
30. Chen Y, Bao C, Zhang X, Lin X, Fu Y. Knockdown of LINC00662 represses AK4 and attenuates radioresistance of oral squamous cell carcinoma. *Cancer Cell Int* (2020) 20:244. doi: 10.1186/s12935-020-01286-9
31. Shen Y, Liu S, Fan J, Jin Y, Tian B, Zheng X, et al. Nuclear retention of the lncRNA SNHG1 by doxorubicin attenuates hnRNPC-p53 protein interactions. *EMBO Rep* (2017) 18(4):536–48. doi: 10.15252/embr.201643139
32. Kleemann M, Schneider H, Unger K, Sander P, Schneider EM, Fischer-Posovszky P, et al. MiR-744-5p inducing cell death by directly targeting HNRNPC and NFIX in ovarian cancer cells. *Sci Rep* (2018) 8(1):9020. doi: 10.1038/s41598-018-27438-6
33. Wang LC, Chen SH, Shen XL, Li DC, Liu HY, Ji YL, et al. M6A RNA Methylation Regulator HNRNPC Contributes to Tumorigenesis and Predicts Prognosis in Glioblastoma Multiforme. *Front Oncol* (2020) 10:536875. doi: 10.3389/fonc.2020.536875
34. Zhuang Z, Chen L, Mao Y, Zheng Q, Li H, Huang Y, et al. Diagnostic, progressive and prognostic performance of m(6)A methylation RNA regulators in lung adenocarcinoma. *Int J Biol Sci* (2020) 16(11):1785–97. doi: 10.7150/ijbs.39046
35. Zhao X, Cui L. Development and validation of a m(6)A RNA methylation regulators-based signature for predicting the prognosis of head and neck squamous cell carcinoma. *Am J Cancer Res* (2019) 9(10):2156–69.
36. Yang S, Liu G. Targeting the Ras/Raf/MEK/ERK pathway in hepatocellular carcinoma. *Oncol Lett* (2017) 13(3):1041–7. doi: 10.3892/ol.2017.5557
37. Chang F, Steelman LS, Lee JT, Shelton JG, Navolanic PM, Blalock WL, et al. Signal transduction mediated by the Ras/Raf/MEK/ERK pathway from cytokine receptors to transcription factors: potential targeting for therapeutic intervention. *Leukemia* (2003) 17(7):1263–93. doi: 10.1038/sj.leu.2402945
38. Xu J, Pfarr N, Endris V, Mai EK, Md Hanafiah NH, Lehners N, et al. Molecular signaling in multiple myeloma: association of RAS/RAF mutations and MEK/ERK pathway activation. *Oncogenesis* (2017) 6(5):e337. doi: 10.1038/oncsis.2017.36
39. Wee P, Wang Z. Epidermal Growth Factor Receptor Cell Proliferation Signaling Pathways. *Cancers (Basel)* (2017) 9(5):52. doi: 10.3390/cancers9050052
40. Tang L, Yang J, Chen J, Yu J, Zhou Q, Lu X, et al. IGF-1R promotes the expression of cyclin D1 protein and accelerates the G1/S transition by activating Ras/Raf/MEK/ERK signaling pathway. *Int J Clin Exp Pathol* (2017) 10(12):11652–8.
41. Agell N, Bachs O, Rocamora N, Villalonga P. Modulation of the Ras/Raf/MEK/ERK pathway by Ca(2+), and calmodulin. *Cell Signal* (2002) 14(8):649–54. doi: 10.1016/s0898-6568(02)00007-4
42. Vuoriluoto K, Haugen H, Kiviluoto S, Mpindi JP, Nevo J, Gjerdrum C, et al. Vimentin regulates EMT induction by Slug and oncogenic H-Ras and migration by governing Axl expression in breast cancer. *Oncogene* (2011) 30(12):1436–48. doi: 10.1038/onc.2010.509
43. Mulholland DJ, Kobayashi N, Ruscetti M, Zhi A, Tran LM, Huang J, et al. Pten loss and RAS/MAPK activation cooperate to promote EMT and metastasis initiated from prostate cancer stem/progenitor cells. *Cancer Res* (2012) 72 (7):1878–89. doi: 10.1158/0008-5472.Can-11-3132
44. David CJ, Huang YH, Chen M, Su J, Zou Y, Bardeesy N, et al. TGF-β Tumor Suppression through a Lethal EMT. *Cell* (2016) 164(5):1015–30. doi: 10.1016/j.cell.2016.01.009
45. Gonzalez-Hormazabal P, Musleh M, Bustamante M, Stambuk J, Pisano R, Valladares H, et al. Polymorphisms in RAS/RAF/MEK/ERK Pathway Are Associated with Gastric Cancer. *Genes (Basel)* (2018) 10(1):20. doi: 10.3390/genes10010020
46. Zou Y, Liu FY, Wu J, Wan L, Fang SF, Zhang ZY, et al. Mutational analysis of the RAS/RAF/MEK/ERK signaling pathway in 260 Han Chinese patients with cervical carcinoma. *Oncol Lett* (2017) 14(2):2427–31. doi: 10.3892/ol.2017.6435
47. Li L, Zhao GD, Shi Z, Qi LL, Zhou LY, Fu ZX. The Ras/Raf/MEK/ERK signaling pathway and its role in the occurrence and development of HCC. *Oncol Lett* (2016) 12(5):3045–50. doi: 10.3892/ol.2016.5110
48. Chang YS, Liu JC, Fu HQ, Yu BT, Zou SB, Wu QC, et al. [Roles of targeting Ras/Raf/MEK/ERK signaling pathways in the treatment of esophageal carcinoma]. *Yao Xue Xue Bao* (2013) 48(5):635–41.
49. Knight T, Irving JA. Ras/Raf/MEK/ERK Pathway Activation in Childhood Acute Lymphoblastic Leukemia and Its Therapeutic Targeting. *Front Oncol* (2014) 4:160. doi: 10.3389/fonc.2014.00160
50. Wang AX, Qi XY. Targeting RAS/RAF/MEK/ERK signaling in metastatic melanoma. *IUBMB Life* (2013) 65(9):748–58. doi: 10.1002/iub.1193
51. Llovet JM, Montal R, Sia D, Finn RS. Molecular therapies and precision medicine for hepatocellular carcinoma. *Nat Rev Clin Oncol* (2018) 15 (10):599–616. doi: 10.1038/s41571-018-0073-4
52. Ikeda M, Morizane C, Ueno M, Okusaka T, Ishii H, Furuse J. Chemotherapy for hepatocellular carcinoma: current status and future perspectives. *Jpn J Clin Oncol* (2018) 48(2):103–14. doi: 10.1093/jjco/hyx180
53. Couri T, Pillai A. Goals and targets for personalized therapy for HCC. *Hepatol Int* (2019) 13(2):125–37. doi: 10.1007/s12072-018-9919-1
54. Urbanski LM, Leclair N, Anczuków O. Alternative-splicing defects in cancer: Splicing regulators and their downstream targets, guiding the way to novel cancer therapeutics. *Wiley Interdiscip Rev RNA* (2018) 9(4):e1476. doi: 10.1002/wrna.1476
55. Chen K, Xiao H, Zeng J, Yu G, Zhou H, Huang C, et al. Alternative Splicing of EZH2 pre-mRNA by SF3B3 Contributes to the Tumorigenic Potential of Renal Cancer. *Clin Cancer Res* (2017) 23(13):3428–41. doi: 10.1158/1078-0432.Ccr-16-2020
56. Li Y, Sun N, Lu Z, Sun S, Huang J, Chen Z, et al. Prognostic alternative mRNA splicing signature in non-small cell lung cancer. *Cancer Lett* (2017) 393:40–51. doi: 10.1016/j.canlet.2017.02.016
57. Marzese DM, Manughian-Peter AO, Orozco JIJ, Hoon DSB. Alternative splicing and cancer metastasis: prognostic and therapeutic applications. *Clin Exp Metastasis* (2018) 35(5-6):393–402. doi: 10.1007/s10585-018-9905-y
58. Geuens T, Bouhy D, Timmerman V. The hnRNP family: insights into their role in health and disease. *Hum Genet* (2016) 135(8):851–67. doi: 10.1007/s00439-016-1683-5
59. Klingenberg M, Groß M, Goyal A, Polycarpou-Schwarz M, Miersch T, Ernst AS, et al. The Long Noncoding RNA Cancer Susceptibility 9 and RNA Binding Protein Heterogeneous Nuclear Ribonucleoprotein L Form a Complex and Coregulate Genes Linked to AKT Signaling. *Hepatology* (2018) 68(5):1817–32. doi: 10.1002/hep.30102
60. Cui H, Wu F, Sun Y, Fan G, Wang Q. Up-regulation and subcellular localization of hnRNP A2/B1 in the development of hepatocellular carcinoma. *BMC Cancer* (2010) 10:356. doi: 10.1186/1471-2407-10-356
61. Xu H, Dong X, Chen Y, Wang X. Serum exosomal hnRNPH1 mRNA as a novel marker for hepatocellular carcinoma. *Clin Chem Lab Med* (2018) 56 (3):479–84. doi: 10.1515/cclm-2017-0327
62. Sun W, Xing B, Sun Y, Du X, Lu M, Hao C, et al. Proteome analysis of hepatocellular carcinoma by two-dimensional difference gel electrophoresis: novel protein markers in hepatocellular carcinoma tissues. *Mol Cell Proteomics* (2007) 6(10):1798–808. doi: 10.1074/mcp.M600449-MCP200

63. Wiesweg M, Kasper S, Worm K, Herold T, Reis H, Sara L, et al. Impact of RAS mutation subtype on clinical outcome-a cross-entity comparison of patients with advanced non-small cell lung cancer and colorectal cancer. *Oncogene* (2019) 38(16):2953–66. doi: 10.1038/s41388-018-0634-0
64. Huang Y, Wei J, Liu BR. [Research advances of K-ras mutation in the prognosis and targeted therapy of gastric cancer]. *Zhonghua Zhong Liu Za Zhi* (2016) 38(2):81–5. doi: 10.3760/cma.j.issn.0253-3766.2016.02.001
65. Hacioglu BM, Kodaz H, Erdogan B, Cinkaya A, Tastekin E, Hacibekiroglu I, et al. K-RAS and N-RAS mutations in testicular germ cell tumors. *Bosn J Basic Med Sci* (2017) 17(2):159–63. doi: 10.17305/bjbms.2017.1764
66. Luo D, Liu QF, Gove C, Naomov N, Su JJ, Williams R. Analysis of N-ras gene mutation and p53 gene expression in human hepatocellular carcinomas. *World J Gastroenterol* (1998) 4(2):97–9. doi: 10.3748/wjg.v4.i2.97
67. Cullen JM, Williams C, Zadrozny L, Otstot JT, Solomon GG, Sills RC, et al. H-ras consensus sequence and mutations in primary hepatocellular carcinomas of lemurs and lorises. *Vet Pathol* (2011) 48(4):868–74. doi: 10.1177/0300985810388526
68. Zolfaghari N, Shahbazi S, Torfeh M, Khorasani M, Hashemi M, Mahdian R. Identification of Differentially Expressed K-Ras Transcript Variants in Patients With Leiomyoma. *Reprod Sci* (2017) 24(10):1438–43. doi: 10.1177/1933719116689596
69. Barbier J, Dutertre M, Bittencourt D, Sanchez G, Gratadou L, de la Grange P, et al. Regulation of H-ras splice variant expression by cross talk between the p53 and nonsense-mediated mRNA decay pathways. *Mol Cell Biol* (2007) 27(20):7315–33. doi: 10.1128/mcb.00272-07
70. Wang C, Li P, Xuan J, Zhu C, Liu J, Shan L, et al. Cholesterol Enhances Colorectal Cancer Progression via ROS Elevation and MAPK Signaling Pathway Activation. *Cell Physiol Biochem* (2017) 42(2):729–42. doi: 10.1159/000477890
71. Sui X, Kong N, Ye L, Han W, Zhou J, Zhang Q, et al. p38 and JNK MAPK pathways control the balance of apoptosis and autophagy in response to chemotherapeutic agents. *Cancer Lett* (2014) 344(2):174–9. doi: 10.1016/j.canlet.2013.11.019
72. Cui X, Qian DW, Jiang S, Shang EX, Zhu ZH, Duan JA. Scutellariae Radix and Coptidis Rhizoma Improve Glucose and Lipid Metabolism in T2DM Rats via Regulation of the Metabolic Profiling and MAPK/PI3K/Akt Signaling Pathway. *Int J Mol Sci* (2018) 19(11)3634. doi: 10.3390/ijms19113634
73. Rodenak-Kladniew B, Castro A, Stärkel P, De Saeger C, García de Bravo M, Crespo R. Linalool induces cell cycle arrest and apoptosis in HepG2 cells through oxidative stress generation and modulation of Ras/MAPK and Akt/mTOR pathways. *Life Sci* (2018) 199:48–59. doi: 10.1016/j.lfs.2018.03.006
74. Guo N, Xiao Y, Chen D, Wang J. Antiproliferative effects of Norartocarpetin isoflavone in human lung carcinoma cells are mediated via targeting Ras/Raf/MAPK signalling pathway, mitochondrial mediated apoptosis, S-phase cell cycle arrest and suppression of cell migration and invasion. *J buon* (2020) 25(2):855–61.
75. Chen L, Wang X, Cheng H, Zhang W, Liu Y, Zeng W, et al. Cyclin Y binds and activates CDK4 to promote the G1/S phase transition in hepatocellular carcinoma cells via Rb signaling. *Biochem Biophys Res Commun* (2020) 533(4):1162–9. doi: 10.1016/j.bbrc.2020.09.127
76. Liu SL, Liu Z, Zhang LD, Zhu HQ, Guo JH, Zhao M, et al. GSK3β-dependent cyclin D1 and cyclin E1 degradation is indispensable for NVP-BEZ235 induced G0/G1 arrest in neuroblastoma cells. *Cell Cycle* (2017) 16(24):2386–95. doi: 10.1080/15384101.2017.1383577
77. Wang C, Yang Y, Zhang G, Li J, Wu X, Ma X, et al. Long noncoding RNA EMS connects c-Myc to cell cycle control and tumorigenesis. *Proc Natl Acad Sci USA* (2019) 116(29):14620–9. doi: 10.1073/pnas.1903432116
78. O'Leary B, Finn RS, Turner NC. Treating cancer with selective CDK4/6 inhibitors. *Nat Rev Clin Oncol* (2016) 13(7):417–30. doi: 10.1038/nrclinonc.2016.26
79. Milioli HH, Alexandrou S, Lim E, Caldon CE. Cyclin E1 and cyclin E2 in ER+ breast cancer: prospects as biomarkers and therapeutic targets. *Endocr Relat Cancer* (2020) 27(5):R93–r112. doi: 10.1530/erc-19-0501
80. De Craene B, Berx G. Regulatory networks defining EMT during cancer initiation and progression. *Nat Rev Cancer* (2013) 13(2):97–110. doi: 10.1038/nrc3447
81. Okada T, Sinha S, Esposito I, Schiavon G, López-Lago MA, Su W, et al. Author Correction: The Rho GTPase Rnd1 suppresses mammary tumorigenesis and EMT by restraining Ras-MAPK signalling. *Nat Cell Biol* (2019) 21(4):534. doi: 10.1038/s41556-019-0288-3
82. Fattet L, Yang J. RREB1 Integrates TGF-β and RAS Signals to Drive EMT. *Dev Cell* (2020) 52(3):259–60. doi: 10.1016/j.devcel.2020.01.020
83. Chen S, Li F, Xu D, Hou K, Fang W, Li Y. The Function of RAS Mutation in Cancer and Advances in its Drug Research. *Curr Pharm Des* (2019) 25(10):1105–14. doi: 10.2174/1381612825666190506122228
84. Delire B, Stärkel P. The Ras/MAPK pathway and hepatocarcinoma: pathogenesis and therapeutic implications. *Eur J Clin Invest* (2015) 45(6):609–23. doi: 10.1111/eci.12441
85. Sun S, He Z, Huang M, Wang N, He Z, Kong X, et al. Design and discovery of thioether and nicotinamide containing sorafenib analogues as multikinase inhibitors targeting B-Raf, B-Raf(V600E) and VEGFR-2. *Bioorg Med Chem* (2018) 26(9):2381–91. doi: 10.1016/j.bmc.2018.03.039
86. Takaya H, Namisaki T, Shimozato N, Kaji K, Kitade M, Moriya K, et al. ADAMTS13 and von Willebrand factor are useful biomarkers for sorafenib treatment efficiency in patients with hepatocellular carcinoma. *World J Gastrointest Oncol* (2019) 11(5):424–35. doi: 10.4251/wjgo.v11.i5.424
87. Li W, Dong X, He C, Tan G, Li Z, Zhai B, et al. LncRNA SNHG1 contributes to sorafenib resistance by activating the Akt pathway and is positively regulated by miR-21 in hepatocellular carcinoma cells. *J Exp Clin Cancer Res* (2019) 38(1):183. doi: 10.1186/s13046-019-1177-0
88. Tovar V, Cornella H, Moeini A, Vidal S, Hoshida Y, Sia D, et al. Tumour initiating cells and IGF/FGF signalling contribute to sorafenib resistance in hepatocellular carcinoma. *Gut* (2017) 66(3):530–40. doi: 10.1136/gutjnl-2015-309501

Conflict of Interest: The authors declare that the research was conducted in the absence of any commercial or financial relationships that could be construed as a potential conflict of interest.

frontiers in Oncology

ORIGINAL RESEARCH
published: 26 April 2021
doi: 10.3389/fonc.2021.628613

Clinical Use of Propranolol Reduces Biomarkers of Proliferation in Gastric Cancer

Qian Hu[1,2,3†], Ping Liao[1,2,3,4†], Wei Li[1,2,3], Jiali Hu[1,2,3], Cuiyu Chen[1,2,3], Yu Zhang[1,2,3], Yang Wang[1,2,3], Ling Chen[5], Kun Song[5], Jie Liu[1,2,3], Wei Zhang[1,2,3], Qing Li[1,2,3], Howard L. McLeod[1,2,3,6] and Yijing He[1,2,3*]*

[1] Department of Clinical Pharmacology, Xiangya Hospital, Central South University, Changsha, China, [2] Institute of Clinical Pharmacology, Central South University, Hunan Key Laboratory of Pharmacogenetics, Changsha, China, [3] National Clinical Research Center for Geriatric Disorders, Xiangya Hospital, Central South University, Changsha, China, [4] Department of Pharmacy, Affiliated Hospital of Nantong University, Nantong, China, [5] Department of Gastrointestinal Surgery, Xiangya Hospital, Central South University, Changsha, China, [6] USF Taneja College of Pharmacy, Tampa, FL, United States

OPEN ACCESS

Edited by:
Rui Liao,
First Affiliated Hospital of Chongqing Medical University, China

Reviewed by:
Ram Mohan Ram Kumar,
Rajiv Gandhi Centre for Biotechnology, India
Dong-Dong Wu,
Henan University, China

***Correspondence:**
Yijing He
heyijing@csu.edu.cn
Howard L. McLeod
hmcleod1965@gmail.com

†These authors have contributed equally to this work

Specialty section:
This article was submitted to Gastrointestinal Cancers, a section of the journal Frontiers in Oncology

Received: *12 November 2020*
Accepted: *29 March 2021*
Published: *26 April 2021*

Citation:
Hu Q, Liao P, Li W, Hu J, Chen C, Zhang Y, Wang Y, Chen L, Song K, Liu J, Zhang W, Li Q, McLeod HL and He Y (2021) Clinical Use of Propranolol Reduces Biomarkers of Proliferation in Gastric Cancer. Front. Oncol. 11:628613. doi: 10.3389/fonc.2021.628613

Gastric cancer has one of the highest mortality rate in the world, but the treatment is still limited. Building on previous studies, mechanistic studies on propranolol in gastric cancer mice models and gastric cancer patients were performed. Propranolol inhibited the *in vitro* proliferation of gastric cancer cells in a time- and concentration-dependent manner. Consistent findings were observed in MFC tumors engrafted 615 mice, which were treated with propranolol at 10 mg/kg daily for 14 days. Propranolol inhibited the phosphorylation of AKT, MEK, and ERK proteins than control in mice tumor tissues respectively (p-AKT 26.16 vs. 56.82, $P = 0.0196$, p-MEK 28.27 vs. 59.28, $P = 0.1102$, p-ERK 48.2 vs. 107.4, $P = 0.0062$). Propranolol had antiproliferative activity in gastric cancer patients receiving 60 mg daily for 7 days prior to surgery(ki67 44.8 vs 125.3 for placebo; $P = 0.02$). Phosphorylated AKT, MEK, and ERK did not differ between propranolol and placebo treatment in gastric cancer patients. The expression of molecules on $CD8^+$ T cells was not changed both in mice model and patients nor was there a statistically significant difference in $CD8^+$ T cell subsets in patients, although suggestion of an effect was evident. These results prove that propranolol may inhibit the growth of gastric cancer in mice model and patients and the possible mechanism was *via* inhibiting the AKT and MAPK pathways, but the frequency of tumor infiltration $CD8^+$ T cells did not increase significantly.

Keywords: gastric, propranolol, anti-proliferation, $CD8^+$ T cell, immunity, AKT/MAPK

INTRODUCTION

Propranolol is a non-selective β-adrenergic receptor (β-AR) blocker, which is mainly used for hypertension and is the first-line therapy for infantile hemangioma (1). In the past decade, many studies have proved that propranolol can induce apoptosis, inhibit proliferation, angiogenesis, and metastasis across solid tumors (2–6). Recent data suggested that propranolol suppressed colorectal cancer cell growth through simultaneously activating autologous $CD8^+$ T cells and decreasing the phosphorylation level of mitogen-activated protein kinase (MAPK)/(ATP-dependent tyrosine

kinases) AKT pathway (7). Several studies also observed that propranolol may exert an anti-tumor effect in melanoma and breast cancer by suppressing AKT and MAPK signaling pathways (8).

Propranolol-associated suppression of tumor growth has also been associated with enhanced intratumoral antitumor immune response in breast cancer (6) and colorectal cancer (7). However, if propranolol can suppress gastric tumor growth by elevating tumor infiltration of $CD8^+$ T cells is unclear. In this study, we hypothesized that propranolol may suppress the growth of gastric cancer by inhibiting the proliferation signaling *in vitro* and *in vivo*. The changes of T lymphocytes in tumor microenvironment were measured simultaneously.

MATERIALS AND METHODS

Cell Lines and Reagents

The AGS and MFC cell lines were purchased from the Cell Bank of the Chinese Academy of Sciences (Kunming, China). The HGC-27 cell line was purchased from Cell Bank of Typical Culture Preservation Committee, Chinese Academy of Sciences (Shanghai). AGS and HGC-27 were cultured in DMEM medium (Gibco, Life Technologies, China), MFC was cultured in 1640 medium (Gibco, Life Technologies, China) supplemented with 10% FBS (Gibco, Life Technologies Australia), 100 U/ml penicillin, and 100 μg/ml streptomycin at 37°C and 5% CO2 in tissue culture incubator.

Cell Viability Assays

The half-maximal inhibitory concentration (IC50) value was determined by CellTiter 96® AQueous One Solution Cell Proliferation Assay (MTS, Promega). Cells were plated in 96-well plates at a density of 2 to 4×10^3 and treated with 20 to 140 μM propranolol (propranolol hydrochloride, P0884, Sigma-Aldrich, USA) for 24, 48, and 72 h. Then, MTS assays were do according to the manufacturer's protocols. Each test was carried out in triplicate.

Animals and Treatments

Six weeks old 615 male mice (Institute of Transfusion and Hematology, Chinese Academy of Medical Sciences) were injected subcutaneously into the right flank with 10^6 living MFC cells in 100 μl PBS. Tumor volume was measured two times/week and tumor volume calculated = $W^2 \times L/2$ mm^3. After tumor volume reached 50 mm^3, the mice were randomly divided into control and propranolol groups. The propranolol group received 10 mg/kg propranolol in 100 μl of PBS and control group received 100 μl PBS by intraperitoneal injection every day. Treatment continued for the duration of the experiment. The mice were sacrificed at the end of treatment (around 2 weeks) and tumors were removed for further analysis.

Immunohistochemistry Assay

The paraffin-free tissue sections were treated with citrate antigen repair buffer (pH 6.0), and then the tissue sections were incubated with peroxidase blocking solution (S2023, Dako) for 15 min and blocked with protein (X0909, Dako) for 30 min. The corresponding specific primary antibodies were used: phosphor-ser221-MEK (rabbit, ab96379, Abcam), phospho-ERK1/2-Thr202/Tyr204 (rabbit, 4370, CST) and phospho-ser473-AKT (rabbit, 4060, CST). After treatment, the slides were incubated overnight at 4°C. Rabbit HRP conjugated secondary antibody (K4003, Dako) and hematoxylin (MHS32, Sigma) counterstain were used for treatment. The samples were observed with a digital microscope (Panoramic Viewer, 3D HISTECH), and protein expression was measured with a histochemical score (H-Score). Immunohistochemical results were scored with H-SCORE. The number of positive cells in each section H-SCORE = $\sum$ (PI × I) = (percentage of weak-strength cells × 1) + (percentage of medium-strength cells × 2) + percentage of cells. In this formula, PI represents the percentage of positive cells in the section, and I represents the staining intensity (9–11).

Flow Cytometry

The mouse tumor was cut into 2- to 3-mm pieces to make a single cell suspension. The tumor and spleen were mechanically macerated and passed directly through a 70-mm nylon cell filter (Corning). The cells were washed with flowing buffer (0.1% BSA in PBS) and incubated with Zombie NIRTM (Biolegend, 1:100) for 20 min at room temperature, and then cells were stained with extracellular antibodies: anti-mouse CD3 FITC, anti-mouse CD8a APC, anti-mouse CD4 PerCP/Cy5.5, anti-mouse Ly-6G/Ly-6C (Gr-1) PE/Cy7, anti-mouse CD11b PE, anti-mouse CD 279 (PD-1) Brilliant Violet 421TM or anti-mouse CD45 Brilliant Violet 510TM (Biolegend). For intracellular staining, cells were stained using the FoxP3/T-bet/IFN-γ/granzymeB (GrzmB) staining buffer set (Biolegend) for fixation and permeabilization after completion of extracellular staining according to the manufacturer's protocol. Cells were then stained with Biolegend's anti-mouse FoxP3 PE, anti-mouse T-bet PE/Cy7, anti-mouse GrzmB FITC or anti-mouse IFNr bright purple 510TM. All data were collected on a flow cytometer (BD Biosciences, Canto II) and analyzed using FlowJo v10 software (Tree Star, Inc.)

Immunofluorescence

Immunofluorescence uses color fluorescence channels to image specific target proteins through a fluorescence microscope. Deparaffinized tissue sections were treated with antigen recovery solution (made of citrate buffer, pH 6.0, T0050 Diapath). The tissue sections were then incubated with peroxidase blocking solution (S2023, Dako) for 15 min and with protein blocking (X0909, Dako) for 20 min. All sections were incubated with CD8 (ab4055, Abcam) antibody. The sections were incubated with GrzmB (NBP1-97525, Novus), IFN-γ (MAB285-sp, Novus) and T-bet (MAB5385, Novus) antibodies, respectively. The signal was counterstained using Cy3 conjugated goat anti-rabbit IgG (GB21303, Servicebio) and AlexaFluor® 488 conjugated AffiniPure goat anti-mouse IgG (GB25301, Servicebio). The slides were scanned with a fluorescence microscope (NIKON ECLIPSE TI-SR) at a magnification of 90 times.

Participants

Patients aged 18 to 70 years who were diagnosed with stage I–III gastric cancer were recruited and randomly divided into placebo group and propranolol group. In this trial, nine patients were assigned to propranolol and 20 to placebo. Patients were given propranolol or a placebo 1 week before surgery for gastric cancer, and tumor tissue was collected after surgery. Tumor proliferation, phosphorylation of the AKT/MAPK signaling pathway, and immunity levels were assessed using immunohistochemistry and immunofluorescence. The clinical trial was approved by the Ethics committee of Xiangya Hospital of Central South University (no. 201702049) and registered in the ClinicalTrial.gov (NCT03245554). All patients in this study signed informed consent, and strictly followed the clinical trial protocol.

Statistical Analysis

Student t test was used to compare data between two groups and tumor growth statistics were calculated using two-way ANOVA with Tukey analysis using Graphpad Prism software. One-way all data are depicted as mean ± SEM.

RESULTS

Propranolol Inhibits Tumor Growth in Mice

Propranolol significantly reduced *in vitro* cells viability of AGS and HGC in a concentration- and time-dependent manner (**Figures 1A, B**). In MFC cell, propranolol inhibited cell proliferation in a concentration- but not time-dependent manner (**Figure 1C**). The data showed that the IC50 of propranolol on AGS and HGC cell lines were lower than MFC cell line (**Figure 1D** and **Table 1**). And propranolol did not inhibited the cell viability of normal intestinal epithelial cell line NCM460 (**Figure S1**). The therapeutic effect of propranolol on gastric cancer was then assessed in MFC tumor engrafted 615 mice. The mean tumor size of propranolol-treated group was smaller than the PBS group on day 12 in MFC tumor model (937.9 ± 55.95 mm^3 vs. 1945 ± 70.38 mm^3, unpaired *t* test, $P < 0.0001$, **Figures 1E, F**). And there was no significant change in the body weight of the MFC mice before and after propranolol treatment (**Figure 1G**). Overall, these results indicated that propranolol can suppress the growth of gastric cancer.

Propranolol Inhibited Proliferation *In Vivo*

Compared with PBS treatment, the number of nuclei with karyorhexis and karyolysis was greatly increased in propranolol treated group, suggesting that propranolol could promote cell necrosis in tumor (**Figure 2A**). We detected the expression of Ki-67 as a cell proliferation marker in tumor sections. The Ki-67 index was significantly decreased in MFC tumor treated with propranolol (136.9 ± 3.56 vs. 103.2 ± 8.59, $P = 0.0067$, **Figure 2B**).

Propranolol Inhibited the AKT/MAPK Pathway *In Vivo*

As shown in **Figure 3**, the phosphorylation level of AKT (p-AKT) was reduced in the propranolol treated group compared with the PBS group in MFC tumor (56.82 ± 5.32 vs. 26.16 ± 9.1, $P = 0.0196$, **Figure 3B**). p-ERK was significantly reduced in the propranolol treated mice (107.4 ± 8.3 vs. 48.2 ± 13.77, $P = 0.0062$, **Figure 3C**). Furthermore, p-MEK was slightly reduced by propranolol (59.28 ± 14.48 vs. 28.27 ± 9.42, $P = 0.11$, **Figure 3D**), although this was not statistically different. We also detected the expression of AKT/MAPK pathway following treatment of propranolol (corresponding IC50 concentration) for 24 h in AGS and HGC cell lines, the expression were slight reduced (**Figure S2**). These data revealed that propranolol could inhibit the growth of gastric cancer *in vivo* by inhibiting the phosphorylation of the AKT and MAPK pathways.

Propranolol Did Not Change Tumor Infiltration of $CD8^+$/$CD4^+$ T Cells in MFC Mice

The frequency of $CD8^+$ and $CD4^+$ T cells in tumor microenvironment (TME) and spleen was assessed *via* flow cytometry. As shown in **Figures 4A–C**, the frequency of $CD8^+$ and $CD4^+$ T cells were not changed with propranolol treatment from tumor tissue and spleen in mice. We also found that the expression of the effector molecules on $CD8^+$ T cells in tumor tissue, including IFN-γ, GrzmB, T-bet, were all not significantly changed (**Figures 4D–F**). Similar result was reported for the ratio of $CD4^+FoxP3^+$ cells (**Figure 4G**). Data were shown in **Table 2**.

Propranolol Effects on the AKT/MAPK Pathway and $CD8^+$ T Cell in Gastric Cancer Patients

The basic characteristics for 29 gastric cancer patients are shown in **Table 3**. Patients received propranolol or placebo for 1 week before surgical resection. The expression of Ki-67 was reduced in patients receiving propranolol treatment than placebo (44.84 ± 15.60 vs 125.27 ± 14.76 in placebo; **Figure 5A**). However, the phosphorylated AKT, MEK, ERK were not significant different between two group (**Figures 5B, C**). Furthermore, the expression of IFN-γ, GrzmB, T-bet on $CD8^+$ T cell were numerically lower in the propranolol treated patients, although this did not reach statistical significance (**Figures 5D–G**). Specific data were shown in **Tables 4**, **5**.

DISCUSSION

This study elucidated that propranolol had antiproliferative activity in both mice model and gastric cancer patients although it could not increase tumor infiltration of $CD8^+$ T cells. Several lines of evidences have proved that β_2-ARs are abundantly expressed on the gastric cancer cells (12–15). Inhibition of β_2-ARs can reduce the concentration of cAMP and inhibit the activation of protein kinase A (PKA), thereby affecting the expression of downstream transcription factors, such as CREB and NF-KB, leading to inhibition of tumor cell proliferation. Zhou and colleagues found that propranolol can induce melanoma cell apoptosis and inhibit the proliferation *in vitro* and *in vivo* by inhibiting the phosphorylation of AKT,

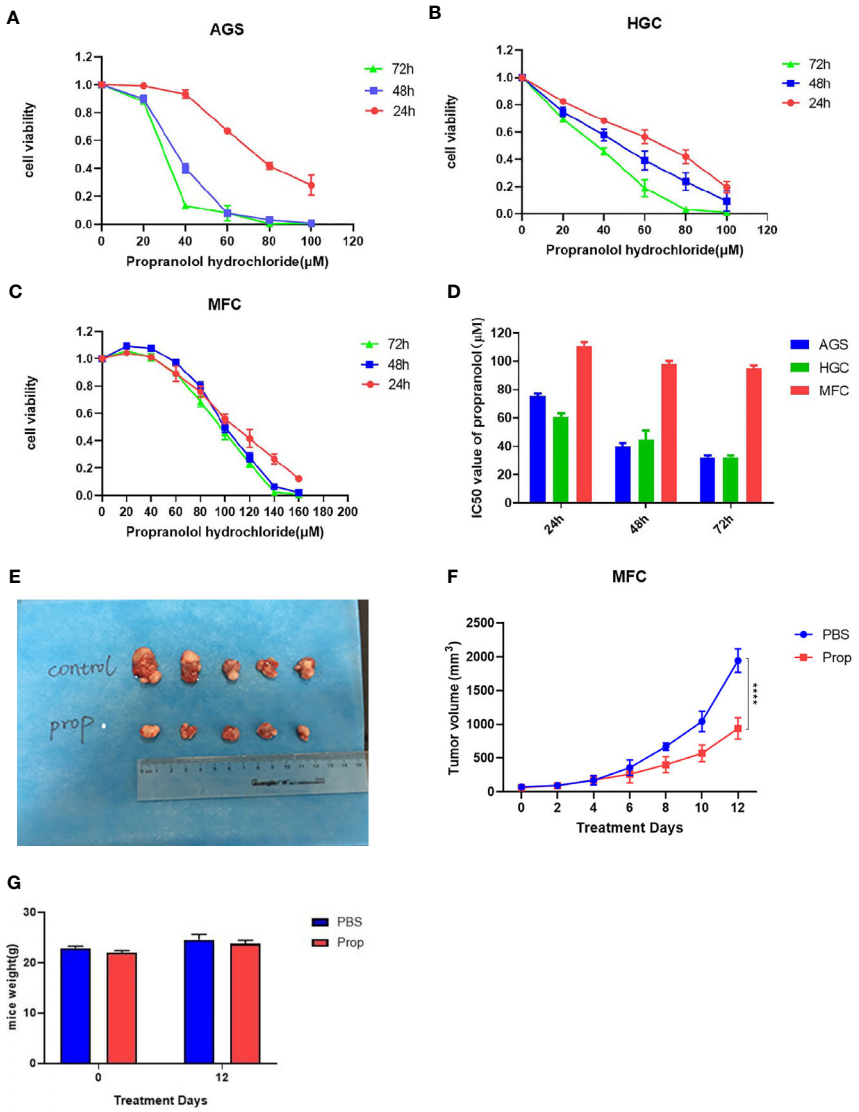

FIGURE 1 | Propranolol inhibits tumor growth in mice. **(A-C)** Cell viability was determined in following propranolol concentrations: 0, 20, 40, 60, 80, 100, 120, 140 μM for 24, 48, and 72 h by MTS assay. **(D)** IC50 of propranolol on gastric cancer cell lines. **(E)** Tumors excised from MFC tumor mice, untreated mice (PBS group) and mice treated with propranolol (propranolol group). **(F)** The tumor volume were measured, and the results are shown. **(G)** The body weight of mice before or after propranolol treatment. Cell viability experiments were repeated for at least three times independently. ****$P < 0.0001$, N = 5 per group.

TABLE 1 | IC50 of different gastric cell lines.

Cell	Gastric cancer cell lines	
	Time	IC-50 value
ASG	24h	75.43
	48h	39.43
	72h	32.29
HGC	24h	60.86
	48h	44.51
	72h	32.29
MFC	24h	110.87
	48h	98.24
	72h	95.35

TABLE 2 | Frequency of CD8+, CD4+ T cells and other cytokines in MFC spleen and tumor tissue.

Marker	MFC	
	Frequency%	*P*-value
CD8+ (spleen)	23.52 ± 0.99 *vs*. 22.00 ± 1.32	0.384
CD4+ (spleen)	63.40 ± 1.38 *vs*. 63.54 ± 1.88	0.954
CD8+ (tumor)	39.52 ± 2.28 *vs*. 34.86 ± 6.22	0.502
CD4+(tumor)	18.1 ± 1.08 *vs*. 22.80 ± 4.55	0.35
GrzmB	41.94 ± 4.19 *vs*. 50.06 ± 7.56	0.375
IFN-γ	3.95 ± 2.72 *vs*. 3.77 ± 1.20	0.911
T-bet	14.24 ± 1.73 *vs*. 16.58 ±3.79	0.59
FoxP3	48.46 ± 5.08 *vs*. 40.08 ± 6.90	0.357

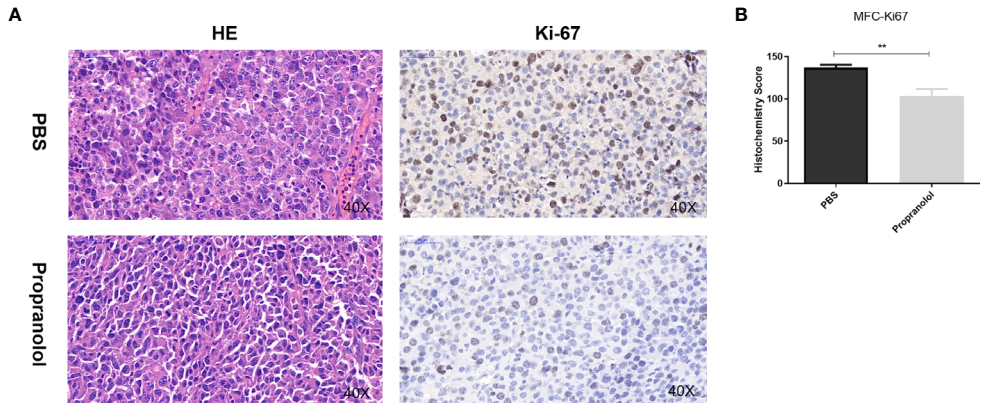

FIGURE 2 | Propranolol inhibited proliferation *in vivo*. **(A)** HE staining for cell morphology in propranolol and PBS group. Ki-67 was assessed by immunohistochemistry assay. The picture was enlarged 40 times. **(B)** Quantification of Ki-67 staining. Results are presented as mean ± SEM. All experiments were repeated for three times independently. $^{**}P < 0.01$, N = 5 per group.

BRAF, MEK1/2, and ERK1/2 (8). Liao et al. also found that propranolol inhibited colorectal cancer proliferation by regulating the AKT and MAPK pathways (7). Previous studies demonstrated that propranolol can down-regulate the expression of CyclinD1, leading to G1/S arrest (16, 17). Our results showed that propranolol decreased the expression of Ki-67 and the phosphorylation of AKT, MEK, and ERK which means that propranolol can inhibit the growth of gastric cancer. And our colleague found that propranolol can affect intracellular pH in bladder cancer cell lines, maybe this is a reason why propranolol can affect the AKT/MAPK signaling pathway.

Consistent with mouse tumor models, the expression of Ki-67 was significantly reduced in propranolol treated gastric cancer patients' samples; however, the phosphorylation of AKT and ERK was not. The length of propranolol treatment, which was only 1 week prior to surgery in patients, could be

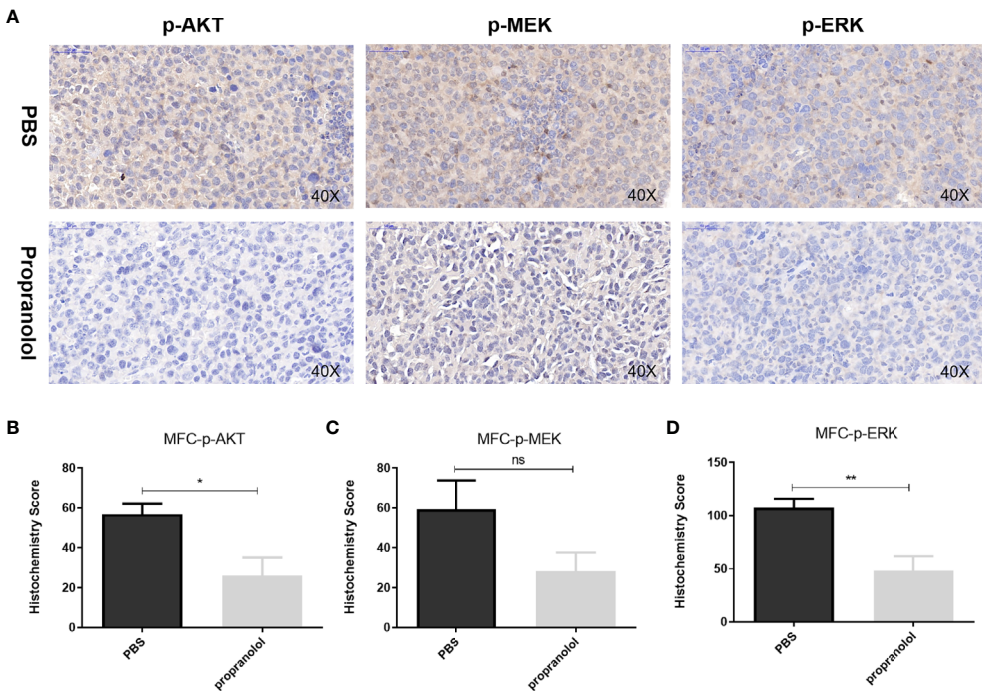

FIGURE 3 | Propranolol inhibited the AKT/MAPK pathway *in vivo*. **(A)** p-Akt, p-MEK, and p-ERK were assessed by immunohistochemistry assay in tumor tissue both in propranolol and PBS groups. **(B–D)** Quantification of p-Akt, p-MEK, and p-ERK staining. Results are presented as mean ± SEM. All experiments were repeated for at least three times independently. ns, no significance; $^{*}P < 0.05$, $^{**}P < 0.01$, N = 5 per group.

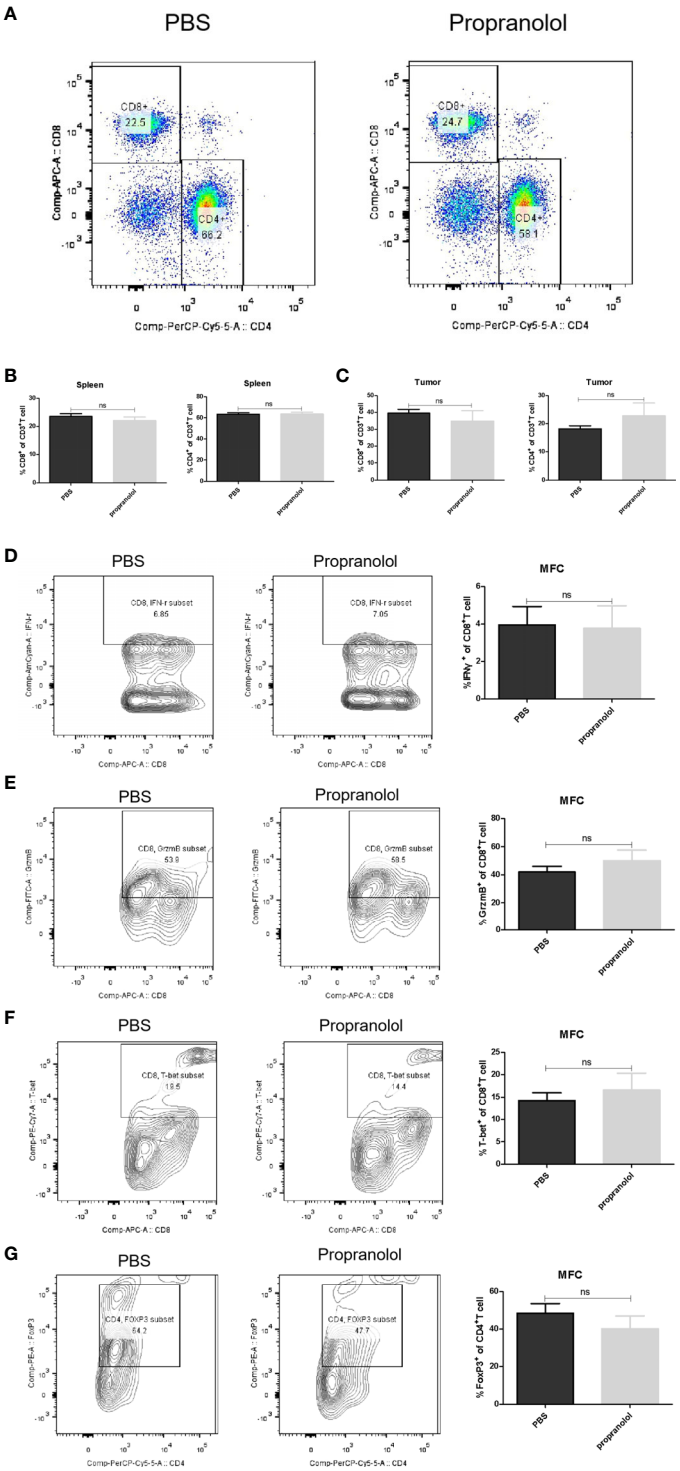

FIGURE 4 | Propranolol effect on the immune cells in MFC mice. **(A)** the flow plots picture of $CD8^+$, $CD4^+$ T cells of $CD3^+$ T cells in spleen of mice. **(B, C)** Quantification of $CD8^+$ and $CD4^+$ T cells in spleen and tumor tissue. **(D–G)** the contour plot and quantification of IFN-γ, GrzmB, T-bet of $CD8^+$ T cells and $CD4^+FoxP3^+$ cells. Results are presented as mean ± SEM. NS, no significance; N = 5 per group.

the major explanation for the lack of change for AKT/ERK phosphorylation. Longer treatment of propranolol could lead to more apparent differences in p-AKT and p-ERK in gastric cancer samples.

T cells expresses β-adrenergic receptors (AR) which could be activated by norepinephrine (NE) released from sympathetic nerve endings. Stimulation of β-ARs on T cells increases cAMP and PKA and inhibits T cell proliferation (18). Our group

TABLE 3 | The characteristics of gastric cancer patients.

	Gastric cancer (*n*)	
	Control	**Propranolol**
Age		
<60	9	4
≥60	11	5
Gender		
Female	8	2
Male	12	7
Tumor stage		
I	1	1
II	6	5
III	13	3

TABLE 4 | p-AKT, p-ERK, and p-MEK values in gastric cancer patient.

	Gastric cancer patient	
Protein	**H-Score**	***P*-value**
Ki-67	125.27±14.76 VS. 44.84±15.60	0.02
p-AKT	84.82 ± 10.42 *VS.* 89.45 ± 14.06	0.841
p-ERK	190.21 ± 4.47 *vs.* 176.26 ± 4.19	0.161
p-MEK	3.54 ± 1.36 *vs.* 4.70 ± 2.42	0.704

previously demonstrated that propranolol activated autologous $CD8^+$ T cells in both colorectal cancer mouse models and patients by blocking the activation of β-ARs. Inconsistent with this finding, the expression of GrzmB/IFN-γ/T-bet in the CD8+ T-cell population were not significantly altered in gastric cancer. It is known that T cells also express muscarinic and nicotinic acetylcholine (ACh) receptors which can be activated by Ach released from efferent cholinergic nerves (19), while stomach is mainly innervated by the vagus nerve (VN), which is comprised of both sensory and preganglionic parasympathetic fibers that release Ach in gastric tumors. Ach acting on α7 nicotinic receptors (nAChRs) inhibits cytokine production by T lymphocytes (20). Blocking β-ARs could relieve the inhibition on T lymphocytes by NE, however, Ach released by vagus nerve could still modulate T lymphocytes which indicated a more complex immune environment in gastric cancer.

In summary, these results revealed that propranolol could inhibit gastric cancer growth but failed to activate the $CD8^+$ T cell in mice and patients. In short, propranolol plays an important role in the treatment of tumors, opening a new chapter for this old drug. More clinical trials are needed to prove the anti-tumor effect of propranolol. Two clinical trials including one for recruiting gastric cancer patients in a single-

TABLE 5 | Expression of GrzmB, IFN-γ, PD-1, and T-bet on $CD8^+$ T cell.

	Gastric cancer patient	
Marker	**% of CD8+ T cells**	***P*-value**
GrzmB	5.90 ± 2.26 *vs.* 1.15 ± 0.38	0.331
IFN-γ	5.40 ± 2.72 *vs.* 0.70 ± 0.31	0.421
T-bet	4.98 ± 1.71 *vs.* 1.48 ± 0.63	0.344

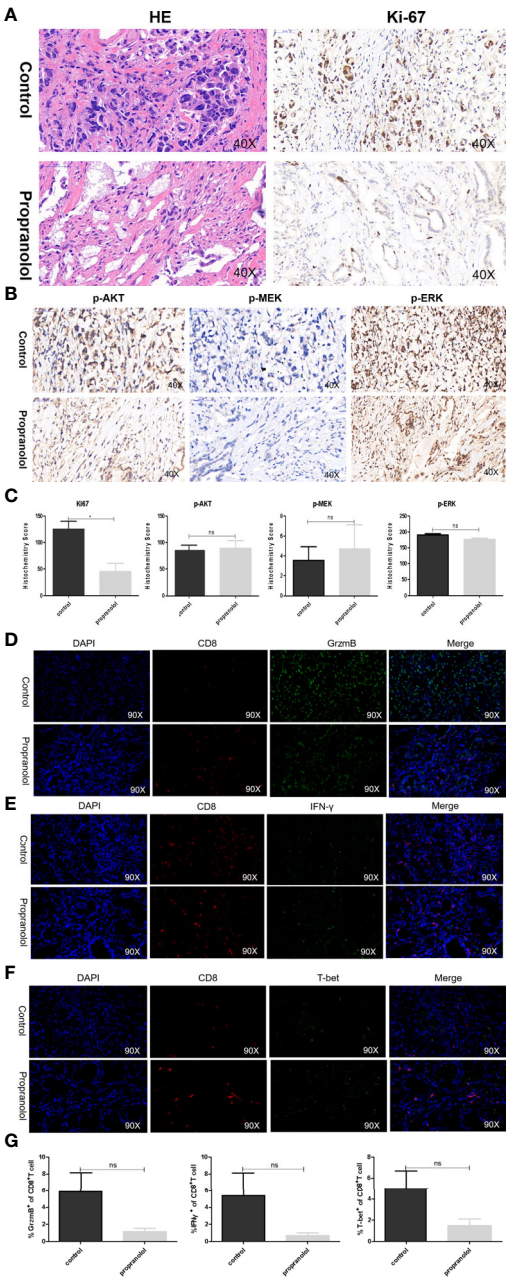

FIGURE 5 | Propranolol effects on the AKT/MAPK pathway and $CD8^+$ T cell in gastric cancer patients. **(A, B)** Ki-67, p-Akt, p-MEK, and p-ERK were assessed by immunohistochemistry assay in tumor tissue both in propranolol and PBS groups. **(C)** Quantification of Ki-67, p-Akt, p-MEK, and p-ERK staining. **(D–F)** Example pictures in tumor tissues using in the immunofluorescence panel, including GrzmB, IFN-γ, and T-bet in $CD8^+$ T cells. The first column shows the cell nucleus in blue by 4′,6-diamidino-2-phenylindole (DAPI); the next column shows the presence of $CD8^+$ T cells in red. The third column shows the factor of interest in green, and the final column shows the merged image of the three channels. **(G)** Quantification of the expression of GrzmB, IFN-γ, and T-bet in $CD8^+$ T cells populations. N = 17 in control group and N = 4 in propranolol group. Results are presented as mean ± SEM. ns, no significance; $^*P < 0.05$.

arm design (NCT04005365) and a randomized controlled clinical trial in bladder cancer patients (NCT04493489) were designed to further explore the anti-tumor effect of propranolol.

DATA AVAILABILITY STATEMENT

The original contributions presented in the study are included in the article/**Supplementary Material**. Further inquiries can be directed to the corresponding authors.

ETHICS STATEMENT

The patients/participants provided their written informed consent to participate in this study. The animal study was reviewed and approved by Animal Ethics Committee of Central South University.

AUTHOR CONTRIBUTIONS

QH and PL conceived and operated experiments, and wrote manuscripts. WL, JH, CC, YZ, and YW helped with the experiment. LC, KS, JL, WZ, and QL gave instructions for the experiment. HM and YH provided suggestions on experimental design, experimental process, experimental results and manuscript writing. All authors contributed to the article and approved the submitted version.

FUNDING

This study was supported by the National Natural Science Foundation of China (grants 81673517 and 81773821); Chinese National Major Project for New Drug Innovation (grant 2019ZX09201-002-006), the National Key Research and Development Program (2016YFC0905000), the research on precision colorectal surgery based on parallel AR auxiliary system Key R&D Program of Hunan Province (2018SK2129, China), the key project of health commission of Hunan Province (202113010141). Natural Science Foundation of Hunan Province, China (2019JJ40477).

SUPPLEMENTARY MATERIAL

The Supplementary Material for this article can be found online at: https://www.frontiersin.org/articles/10.3389/fonc.2021.628613/full#supplementary-material

REFERENCES

1. Storch CH, Hoeger PH. Propranolol for Infantile Haemangiomas: Insights Into the Molecular Mechanisms of Action. *Br J Dermatol* (2010) 163(2):269–74. doi: 10.1111/j.1365-2133.2010.09848.x
2. Gong L, Lei Y, Tan X, Dong Y, Luo Z, Zhang D, et al. Propranolol Selectively Inhibits Cervical Cancer Cell Growth by Suppressing the CGMP/PKG Pathway. *BioMed Pharmacother* (2019) 111:1243–8. doi: 10.1016/j.biopha.2019.01.027
3. Montoya A, Varela-Ramirez A, Dickerson E, Pasquier E, Torabi A, Aguilera R, et al. The Beta Adrenergic Receptor Antagonist Propranolol Alters Mitogenic and Apoptotic Signaling in Late Stage Breast Cancer. *BioMed J* (2019) 42(3):155–65. doi: 10.1016/j.bj.2019.02.003
4. Yao TH, Pataer P, Regmi KP, Gu XW, Li QY, Du JT, et al. Propranolol Induces Hemangioma Endothelial Cell Apoptosis Via a P53BAX Mediated Pathway. *Mol Med Rep* (2018) 18(1):684–94. doi: 10.3892/mmr.2018.9013
5. Pan WK, Li P, Guo ZT, Huang Q, Gao Y. Propranolol Induces Regression of Hemangioma Cells Via the Down-Regulation of the PI3K/Akt/eNOS/VEGF Pathway. *Pediatr Blood Cancer* (2015) 62(8):1414–20. doi: 10.1002/pbc.25453
6. Hiller JG, Cole SW, Crone EM, Byrne DJ, Shackleford DM, Pang JB, et al. Preoperative beta-Blockade With Propranolol Reduces Biomarkers of Metastasis in Breast Cancer: A Phase II Randomized Trial. *Clin Cancer Res* (2020) 26(8):1803–11. doi: 10.1158/1078-0432.CCR-19-2641
7. Liao P, Song K, Zhu Z, Liu Z, Zhang W, Li W, et al. Propranolol Suppresses the Growth of Colorectal Cancer Through Simultaneously Activating Autologous CD8(+) T Cells and Inhibiting Tumor AKT/MAPK Pathway. *Clin Pharmacol Ther* (2020). doi: 10.1002/cpt.1894
8. Zhou C, Chen X, Zeng W, Peng C, Huang G, Li X, et al. Propranolol Induced G0/G1/s Phase Arrest and Apoptosis in Melanoma Cells Via AKT/MAPK Pathway. *Oncotarget* (2016) 7(42):68314–27. doi: 10.18632/oncotarget.11599
9. Budwit-Novotny DA, McCarty KS, Cox EB, Soper JT, Mutch DG, Creasman WT, et al. Immunohistochemical Analyses of Estrogen Receptor in Endometrial Adenocarcinoma Using a Monoclonal Antibody. *Cancer Res* (1986) 46(10):5419–25.
10. Yeo W, Chan SL, Mo FK, Chu CM, Hui JW, Tong JH, et al. Phase I/II Study of Temsirolimus for Patients With Unresectable Hepatocellular Carcinoma (HCC)- a Correlative Study to Explore Potential Biomarkers for Response. *BMC Cancer* (2015) 15:395. doi: 10.1186/s12885-015-1334-6
11. Azim HAJr, Peccatori FA, Brohee S, Branstetter D, Loi S, Viale G, et al. RANK-ligand (RANKL) Expression in Young Breast Cancer Patients and During Pregnancy. *Breast Cancer Res* (2015) 17:24. doi: 10.1186/s13058-015-0538-7
12. Sanders VM, Baker RA, Ramer-Quinn DS, Kasprowicz DJ, Fuchs BA, Street NE. Differential Expression of the beta2-adrenergic Receptor by Th1 and Th2 Clones: Implications for Cytokine Production and B Cell Help. *J Immunol* (1997) 158(9):4200–10.
13. Ramer-Quinn DS, Baker RA, Sanders VM. Activated T Helper 1 and T Helper 2 Cells Differentially Express the beta-2-adrenergic Receptor: A Mechanism for Selective Modulation of T Helper 1 Cell Cytokine Production. *J Immunol* (1997) 159(10):4857–67.
14. Bishopric NH, Cohen HJ, Lefkowitz RJ. Beta Adrenergic Receptors in Lymphocyte Subpopulations. *J Allergy Clin Immunol* (1980) 65(1):29–33. doi: 10.1016/0091-6749(80)90173-6
15. Bucsek MJ, Qiao G, MacDonald CR, Giridharan T, Evans L, Niedzwecki B, et al. beta-Adrenergic Signaling in Mice Housed At Standard Temperatures Suppresses an Effector Phenotype in CD8(+) T Cells and Undermines Checkpoint Inhibitor Therapy. *Cancer Res* (2017) 77(20):5639–51. doi: 10.1158/0008-5472.CAN-17-0546
16. Liao X, Che X, Zhao W, Zhang D, Long H, Chaudhary P, et al. Effects of Propranolol in Combination With Radiation on Apoptosis and Survival of Gastric Cancer Cells in Vitro. *Radiat Oncol* (2010) 5:17–20. doi: 10.1186/1748-717X-5-98
17. Zhang X, Zhang Y, He Z, Yin K, Li B, Zhang L, et al. Chronic Stress Promotes Gastric Cancer Progression and Metastasis: An Essential Role for ADRB2. *Cell Death Dis* (2019) 10(11):12–3. doi: 10.1038/s41419-019-2030-2
18. Vischer TL. The Differential Effect of Cyclic AMP on Lymphocyte Stimulation by T- or B-Cell Mitogens. *Immunology* (1976) 30(5):735–9.

19. Mashimo M, Iwasaki Y, Inoue S, Saito S, Kawashima K, Fujii T. Acetylcholine Released From T Cells Regulates Intracellular Ca(2+), IL-2 Secretion and T Cell Proliferation Through Nicotinic Acetylcholine Receptor. *Life Sci* (2017) 172:13–8. doi: 10.1016/j.lfs.2016.12.015
20. Rosas-Ballina M, Olofsson PS, Ochani M, Valdes-Ferrer SI, Levine YA, Reardon C, et al. Acetylcholine-Synthesizing T Cells Relay Neural Signals in a Vagus Nerve Circuit. *Science* (2011) 334(6052):98–101. doi: 10.1126/science.1209985

Conflict of Interest: HM is on the board of directors for Cancer Genetics Inc and on a Speakers Bureau for Genentech. He is one of the founders of Interpares Biomedicine and Clariifi and a consultant to Pharmazam and eviCORE Health Solutions.

The remaining authors declare that the research was conducted in the absence of any commercial or financial relationships that could be construed as a potential conflict of interest.

frontiers in Oncology

REVIEW
published: 11 May 2021
doi: 10.3389/fonc.2021.617677

Mesenchymal Stem Cells in Gastric Cancer: Vicious but Hopeful

*Yuyi Li, Xingwei Zhong, Yunzhu Zhang and Xinliang Lu**

Department of Gastroenterology, The Second Affiliated Hospital, Zhejiang University School of Medicine, Hangzhou, China

Tumor progression depends on the collaborative interactions between tumor cells and the surrounding stroma. First-line therapies direct against cancer cells may not reach a satisfactory outcome, such as gastric cancer (GC), with high risk of recurrence and metastasis. Therefore, novel treatments and drugs target the effects of stroma components are to be promising alternatives. Mesenchymal stem cells (MSC) represent the decisive components of tumor stroma that are found to strongly affect GC development and progression. MSC from bone marrow or adjacent normal tissues express homing profiles in timely response to GC-related inflammation signals and anchor into tumor bulks. Then the newly recruited "naïve" MSC would achieve phenotype and functional alternations and adopt the greater tumor-supporting potential under the reprogramming of GC cells. Conversely, both new-comers and tumor-resident MSC are able to modulate the tumor biology *via* aberrant activation of oncogenic signals, metabolic reprogramming and epithelial-to-mesenchymal transition. And they also engage in remodeling the stroma better suited for tumor progression through immunosuppression, pro-angiogenesis, as well as extracellular matrix reshaping. On the account of tumor tropism, MSC could be engineered to assist earlier diagnosis of GC and deliver tumor-killing agents precisely to the tumor microenvironment. Meanwhile, intercepting and abrogating vicious signals derived from MSC are of certain significance for the combat of GC. In this review, we mainly summarize current advances concerning the reciprocal metabolic interactions between MSC and GC and their underlying therapeutic implications in the future.

Keywords: gastric cancer, mesenchymal stem cells, tumor tropism, reprogramming, tumor stroma, drug delivery, targeted therapy

OPEN ACCESS

Edited by:
Rui Liao,
First Affiliated Hospital of Chongqing Medical University, China

Reviewed by:
Mei Wang,
Jiangsu University, China
Fei Fei,
Peking University Third Hospital, China

***Correspondence:**
Xinliang Lu
lux@zju.edu.cn

Specialty section:
This article was submitted to Gastrointestinal Cancers, a section of the journal Frontiers in Oncology

Received: *15 October 2020*
Accepted: *22 April 2021*
Published: *11 May 2021*

Citation:
Li Y, Zhong X, Zhang Y and Lu X (2021) Mesenchymal Stem Cells in Gastric Cancer: Vicious but Hopeful. Front. Oncol. 11:617677. doi: 10.3389/fonc.2021.617677

INTRODUCTION

Gastric cancer (GC) is one of the most refractory malignancies with high morbidity and mortality. Updated statistics indicates that GC is the fifth frequently diagnosed cancer with over 1,000,000 new cases and the third leading cause of cancer-associated morbidity, an estimated 783,000 deaths worldwide (1). Helicobacter pylori (Hp) eradication, gastroscopy, and endoscopic treatment have reduced the risk of developing GC, as well as provided better long-term health-related quality of life for patients with early GC (2, 3). Regrettably, a larger population of people is already in the advanced stage at the first diagnosis for rarely present symptoms. Although a combination of surgical resection with adjuvant chemotherapy is the preferential option for advanced GC, the

survival outcome stays disappointing, dropping a median overall survival of 10-12 months (4, 5). Hence, searching for new strategies, such as immunotherapy, targeted therapy, and making clinical transformation remain urgently needed.

Of note, the occurrence and development of tumor cannot be isolated from the tumor microenvironment (TME). The surrounding microenvironment "soil" is to facilitate the survival and thriving of tumor cell "seed" *via* substantial reciprocal crosstalk between cell-cell or cell-non-cell components (6). TME is generally a complex network and largely composed of the stroma of tumor, covering mesenchymal stem cells (MSC), cancer-associated fibroblasts (CAF), endothelial cells (EC), pericytes, immune cells, vasculature together with the extracellular matrix (ECM) surrounding the cancerous tissue (7–9). Contrast to stroma under normal physiological conditions, which encompasses structural and supportive framework to maintain the stability of tissues and suppresses cancer proliferation, the tumor stroma is in an active state and has been documented to be firmly correlated with the aggressiveness and unfavorable clinical outcomes of a spread of malignancies including GC (10–12). A cohort study with 583 gastric adenocarcinomas demonstrated that stroma-rich patients tend to acquire a worse 5-year prognosis than stroma-poor ones, no matter in intestinal or diffuse histological phenotype (13). Other studies suggest tumor-stroma ratio a reliable prognostic indicator to optimize risk stratification in GC for the ability to quantify the effect of tumor-stroma interactions on tumor biology (14, 15). Such evidence sheds light on the important role of stroma for tumor development, which would arise novel anti-cancer strategies focusing not restrictive on cancer cells.

Among the stromal cells, MSC, a population of non-hematopoietic cells with self-renewal capacity, multi-differential potential, and immune-modulatory property, have received recent attention as a key contributor in directing tumor behavior and TME remodeling. MSC are spindle-shaped cells and capable of forming colonies when originally isolated from the hematopoietic microenvironment of bone marrow (BM), also named colony-forming unit-fibroblast (CFU-F) (16). Then the International Society for Cellular Therapy (ISCT) enacted the minimal criteria for better isolation of these cells: firstly, be plastic-adherent; secondly, highly express (>95%) surface molecules of CD73, CD90, CD105 and lack expression of (<2%) CD45, CD34, CD14, CD11b, CD79α, CD19 and HLA-DR; thirdly, hold the ability to differentiate into osteoblasts, adipocytes, and chondroblasts *ex vivo* (17). Over time, other surface antigens, like CD271, STRO-1, CD106 and CD146 come to be accepted and recognized for MSC identification (18, 19). MSC used to arouse excitement for regenerative medicine owing to they can quickly engraft to inflammatory cytokines or chemoattractant gradients produced by injured tissue and organs to exhibit their tissue healing functions, alone or in combination with other methods (20, 21). With the hypothesis "tumor equates wound that never heals" arises, the function of MSC in tumors has been realized to parallel the role of MSC in wound healing that actively promotes MSC from bone marrow or adjacent tissues to mobilize into the TME (22, 23). In a mouse model of hepatocellular carcinoma (HCC), MSC possess distinct homing profiles and contribute to a significant rapid depletion from circulation in cancerous condition (24). The result is consistent with findings in the patients with GC showing that an intensified peripheral trafficking of MSC in comparison to healthy individuals; and the egressed MSC are commonly aggregated in tumor bulks over adjacent normal tissues (25, 26). That throws the great interest to explore the possible roles of MSC in tumor progression and aggressiveness which previously may be neglected in GC-stroma interactions. In the following, we mainly cover recent advances in the interactions between MSC and GC, the role of MSC in rewiring the nearing cancer stroma, and potential underlying mechanisms. Furthermore, fresh boundaries regarding the potential application of MSC in GC are also within our discussion to inspire more preventive and therapeutic strategies.

THE RECRUITMENT AND REPROGRAMMING COURSE OF NAÏVE MSC INTO GC-MSC

The Tropism and Remodeling of Naïve MSC

GC as well as its progression niche is a reservoir of cytokines, chemokines, growth factors that specifically drive the tropism and motility of BM-derived cells including MSC. Under the co-culture system, the migratory ability of BM-MSC could be raised up to two- to threefold because of the high expression of CXC receptor 2 (CXCR2) in response to CXC ligand 1 (CXCL1), a chemokine stimulating factor released from cancer cells (26). Except for this, chemotactic signals derived from GC such as C-C chemokine ligand 19 (CCL19) and CXCL12 would also augment the migration potential of MSC to cancer in a dose-dependent manner, while the concrete mechanisms still to be further investigated (27). On the other hand, it is important to note that Hp infection would accelerate the trafficking of MSC into the stomach at the early stage of carcinogenesis. Hp-mediated chronic inflammation of gastric epithelial cells would significantly increase the secretion of tumor necrosis factor-alpha (TNF-α), an appreciable molecule in stimulating MSC migration in Nuclear Factor-kappa B (NF-κB)-dependent manner (28). Subsequently to being recruited, the naïve MSC [mainly refers to BM-MSC or MSC isolated from adjacent non-cancerous tissue (GCN-MSC)] were relentless to be educated by GC cells to become specialized ones equipped with the tumor-supporting capacity (29). Moreover, the immunomodulatory function of MSC could also be modified *via* the activation of the NF-κB signaling pathway, to strengthen their activation ability to immune cells (30). Intriguingly, a recent finding suggested that BM-MSC incorporated into metastatic lymph node microenvironment could be reprogrammed by cancer cells. Yes-associated protein (YAP) activation elicited by exosomal Wnt5a from lymph node-derived GC cells,

was verified pivotal for their reprogramming into cancer-associated MSC (31).

Characterization of GC-MSC

Evidence incline to depict that GC-MSC and naïve MSC share equivalent spindle-shaped morphology, similar surface antigens and stem cell-related gene expression. GC-MSC are positive for CD13, CD29, CD44, CD73, CD90 and CD105, but negative for CD14, CD31, CD34, CD38, CD45, CD71, CD133 and HLA-DR, among which the expression of CD105 was strongly associated with the poor prognosis of GC patients (12, 32–34). Another study denoted that the higher co-expression of CD29 and CD90 are more commonly seen in GC-MSC than GCN-MSC, and was correlated with more advanced pathological stage, worse disease-free survival and overall survival (35). In comparison with naïve MSC, GC-MSC seem to be on a less quiescent stage, ultrastructurally, phenotypically and functionally. GC-MSC typically feature greater number of cell organelles, such as mitochondria and endocytoplasmic reticulum, and higher expression of proliferation-related genes, all of which are coincide with their greater proliferative potential (32). Besides, GC-MSC display a stronger intensity of reactive stroma cell markers including fibroblast activation protein (FAP) and α-smooth muscle actin (α-SMA) (36). In virtue of the reprogramming by cancer cells, GC-MSC exhibit a higher secretion of inflammatory cytokines than naïve MSC, e.g., interleukin-6 (IL-6), IL-8, transforming growth factor β1 (TGF-β1), ect, which in turn display superior efficiency in facilitating cancer cell growth, invasion, migration and tumorigenesis *in vitro* and *in vivo* (36, 37).

MSC IMPACT ON GC CELLS

Aberrantly Activate Oncogenic Cell Signaling

MSC are capable of reprogramming GC cells to orchestrate the proliferation, invasion, migration and chemoresistance, *via* stimulation of oncogenic signaling pathways associated with aberrantly growth or transforming (**Figure 1**). The enhanced secretion of IL-8 from GC-MSC has been linked to cancer progression by inducing the activation of protein kinase B (AKT) and extracellular signal-regulated protein kinase (ERK) 1/2 signaling pathway (37). Moreover, GC-MSC could robustly express hepatocyte growth factor (HGF) as ligand of c-MET to trigger phosphorylation of its downstream signaling cascade in cancer cells, and aberrant HGF/c-MET axis has been well-established to be critical for GC progression (38). Recently, researches highlighted the crucial mediator of CXCR6 and signal transducer and activator of transcription 3 (STAT3) pathway, which suggest a prominent production of CXCL16 in MSC via the activation of Wnt5a/Ror2 signaling axis, in turn, activates its corresponding receptor CXCR6 to increase the expression of Ror1 via the activation of STAT3, eventually resulting in the promotion of proliferation and migration of GC cells (39, 40). In addition to these, emerging studies have uncovered the oncogenic potential of platelet-derived growth factor (PDGF)-DD/PDGFR-β axis (41) and YAP/β-catenin signaling (42) in the MSC-induced cancer initiation and progression, and blocking or interference of these signals has designated a certain positive significance for the treatment of GC.

Exosomes prove a kind of small lipid bilayer membrane vesicles delivering intercellular communication bioactive molecules, like

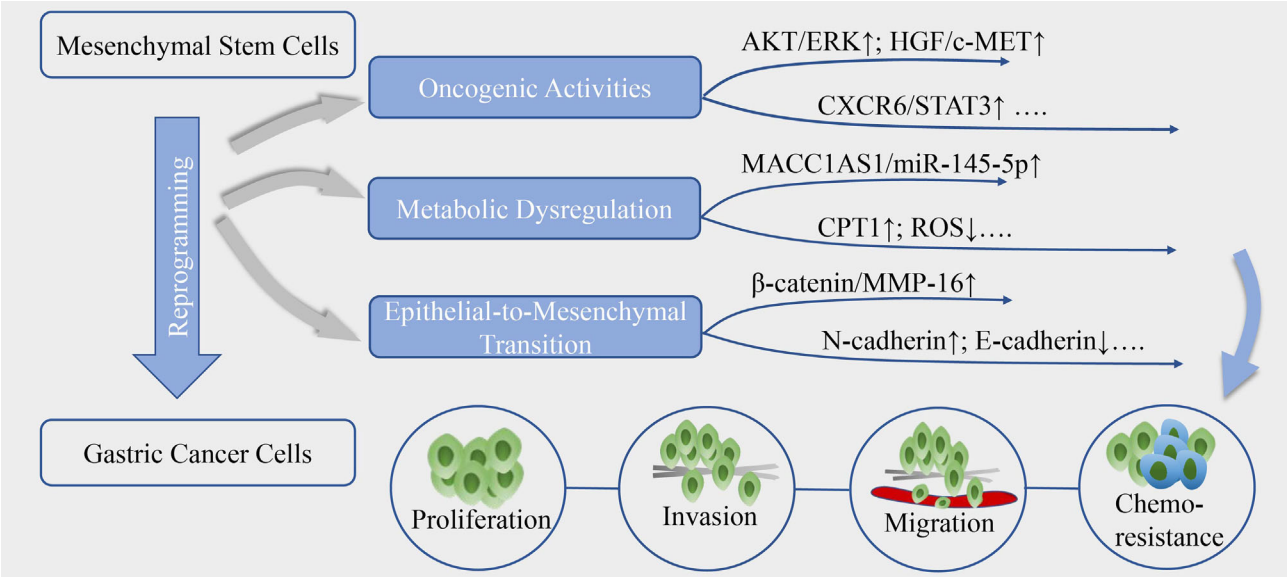

FIGURE 1 | The reprogramming of GC by MSC. MSC could reprogram the biological activities of gastric cancer cells, mainly through aberrantly activate oncogenic signals, metabolic reprogramming and epithelial-to-mesenchymal transition, contributing to cancer cells proliferation, invasion, migration and resistance to chemotherapy.

miRNAs, long non-coding RNAs (lncRNAs), and proteins to reshape the biological behavior of adjacent cells or remote targets of the body (43, 44). As research conducted by Ji et al. (45), the exosomes from MSC can trigger the calcium-dependent protein kinases (CaM-Ks) and its downstream RAF/MEK/ERK signaling cascade, elevating the expression of multi-drug resistant proteins in cancer cells to counteract 5-fluorouracil (5-FU) induced cell apoptosis, however, the exact molecules in exosomes that mediate this effect have yet been identified. Ubiquitin-protein ligase E3 component n-recognin 2 (UBR2) is a kind of protein that accounts for ubiquitination and degradation, was found to highly aggregate in exosomes of especially p53 deficient BM-MSC, could be internalized into GC cells and induce the activation of Wnt/β-catenin pathway to promote cell proliferation, migration and stemness maintenance (46). In addition, evidence has clarified that miRNAs are deregulated in exosomes of GC-MSC, to be transferred to transcriptionally modulate cancer aggressiveness, of which miR-221 deregulation has been linked with various tumorigenic pathways (47, 48).

Dysregulate Metabolic Plasticity

Metabolic reprogramming has been proposed as a new hallmark for cancer progression. Emerging discoveries highlight that MSC could dysregulate cell metabolism to confer GC cells stemness and tolerance to drug stress (**Figure 1**). He et al. (35) proposed that TGF-β1 secretion by MSC co-opt TGF-β receptors in GC cells could raise the expression level of lncRNA MACC1-AS1, which have sponge interaction with miR-145-5p to boost the expression of CPT1, the fatty acid oxidation (FAO) speed-limiting enzyme, subsequently decreasing reactive oxygen species (ROS) production and cell apoptosis under 5-FU and oxaliplatin. Mechanistically, MACC1-AS1 also is found to augment the expression of MACC1, an oncogene and a poor prognosis marker in GC, to elevate glutathione and nicotinamide adenine dinucleotide phosphate (NADPH) levels and sustain a lower ROS load under metabolic stress (49). In another study, MSC-induced lncRNA histocompatibility leukocyte antigen complex P5 (HCP5) in GC cells was demonstrated to serve as a miR-3619-5p sponge to facilitate FAO *via* the transactivation of CPT1, thereby alleviating the cell cycle arrest effect of cancer cells caused by chemotherapeutics (50). Besides, the antagonist of CPT-1 could remarkably reverse the MSC-induced tumor growth under FOLFOX regiment treatment *in vivo* (35), indicating that deregulated FAO could be a key regulator of MSC-mediated chemoresistance in GC and a potential target for anti-resistance interventions.

Elicit Epithelial-to-Mesenchymal Transition (EMT)

Phenotypic transition occurs in GC cells when close physical contact with MSC as well (**Figure 1**), they adopt mesenchymal phenotype including longitude ridging, ruffled membranes and finger-like extensions, concomitantly with increased level of α-SMA, N-cadherin, vimentin and Snail and repressed expression of cellular adhesion molecules especially E-cadherin (51–53). EMT is a dynamic process and the mesenchymal traits endow the malignant cells migratory and invasive capacities, and the susceptibility to cancer intravasation and metastasis. The paracrine signals of MSC also induce EMT to promote transendothelial migration, mechanistically, dependent on high expression of snail, twist, β-catenin and matrix metalloproteinase-16 (MMP-16) (52). Moreover, the activation of PI3K/AKT signaling pathway was shown to be linked with the process (51). Intriguingly, researchers found cell fusion maybe one of the underlying mechanisms in the MSC-primed EMT. Hybrids acquire the mesenchymal and stemness proteins, enhanced proliferation and migration potential during a physical fusion event with MSC (54). Notably, hybrids generated by MSC and immortalized non-tumorigenic human gastric epithelial cells also undergo EMT and are vulnerable to be malignant transformation, which makes a difference in cancer initiation (55).

MSC REMODELING THE GC STROMA

Immunosuppression Potential of MSC

Not only function directly back upon tumor cells to boost the growth and progression, but MSC are also involved in the continuous updating and transformation of stroma components, for the aim of enhancing their tumor-supporting roles and accommodating the rapid metabolic process of tumors (**Figure 2**). The immunomodulatory property of MSCs has been well exploited to prevent and treat severe graft-verse-host diseases (56). With the reprogramming of GC, MSC incorporation engraftment the TME could modulate the differentiation, polarization or anergy of immune cells thus offering local immune-suppressive milieu. GC-MSC, mainly by extracellular cytokines secretion, such as IL-15 contained in the conditioned medium (CM) could predispose peripheral blood mononuclear cells (PBMC) to skew their differentiation into regulatory T (Treg) population (57). The balance of Treg and Th17 subsets defines a key regulator for immune homeostasis for they exert the opposite immune-modulatory functions (58). Consistently, a study conducted by Wang et al. (59) revealed that by the joint activation of GC-MSC, the enhanced differentiation of Treg subsets and the suppressed Th17 cells proliferation can reverse the tumor-inhibitory effect of PBMC to significantly improve GC growth potential and facilitate liver metastases formation *in vivo*. Li and colleagues (60) have shown that GC-MSC also perform an intricate crosstalk with macrophages to drive the conversion of macrophages toward alternatively activated, immunosuppressive M2 phenotype, which exhibit a higher potential in promoting GC invasion and metastasis than that of GC-MSC. Importantly, the M2 phenotype has been manifested to play extensive roles in immune tolerance, neo-angiogenesis, pre-metastatic niche formation for GC advancement (61). Mirroring macrophages, the IL-6 enriched in the GC-MSC-CM can stimulate the phosphorylation of STAT3 and ERK1/2 in neutrophils, promoting their recruitment and activation into a pro-tumor phenotype that would finely cooperate with GC-MSC to synergistically prompt cancer migration and angiogenesis (34). Intriguingly, GC-MSC could induce the anergy and silence of immune potency through the secretion of IL-8 to upregulate the expression level of PD-LI in GC

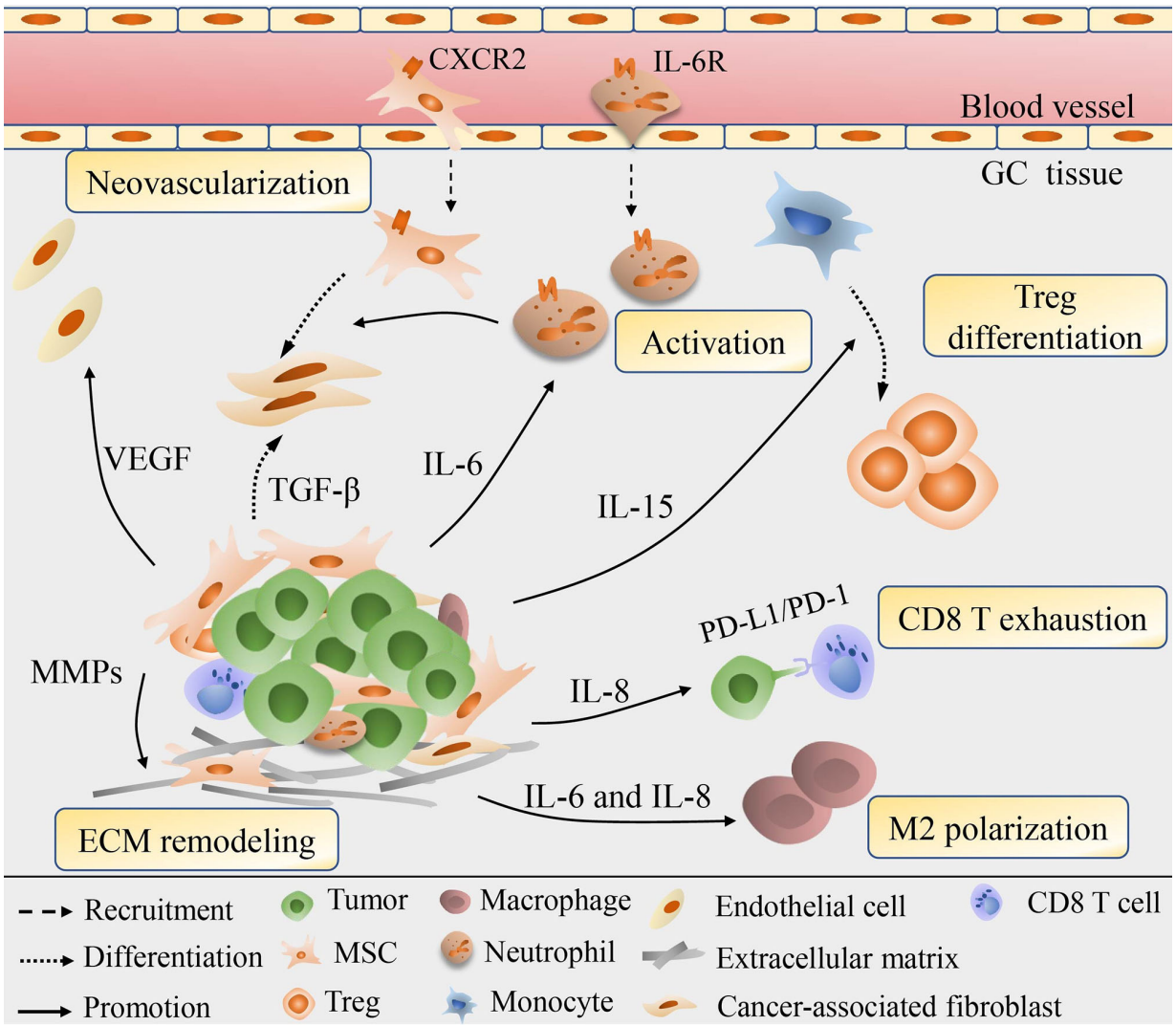

FIGURE 2 | Schematic diagram for the role of MSC in the remodeling of GC stroma. MSC could be recruited into cancer stroma and are involved in the continuous updating and transformation of stroma components. *Via* secretion of various cytokines, e.g., IL-6, IL-8, IL-15, MSC modulate the Treg differentiation, macrophage polarization, neutrophil recruitment and activation, exhaustion of CD8 T cells, thus offering local immune-suppressive milieu. MSC could also secret VEGF and MMPs to induce neovascularization and ECM degrading, or directly differentiate into CAF to exhibit synergistic effect in remodeling cancer cells and stroma.

cells that drive the exhaustion of CD8 T cells, resulting in immune resistance and contributing to GC progression (62). Emerging research spots that the immunophenotype of GC-MSC are also influenced by the CD4 T cells *via* the p-STAT3 signaling pathway to boost cancer growth rate-promoting role of GC-MSCs, highlighting that TME is a huge complicated signaling network in which tumor cells, immune cells, MSC and other components are in a multi-angle communication to facilitate cancer progression (63).

Vascularization and ECM Remodeling

Neovascularization provides favorable conditions for tumor invasion and metastasis and is therefore considered a marker of poor prognosis. Under the pretreatment of GC-CM *in vitro*, MSC would elevate the expression of vascular endothelial growth factor (VEGF), macrophage inflammatory protein-2 (MIP-2), TGF-β1, IL-6, and IL-8, among them VEGF being highly angiogenic works prominently in vascular development (37). Consistent with the prior finding, Feng et al. (64) proposed that VEGF production, in collaboration with NF-κB signaling in GC-MSC, could induce angiogenesis through driving the human umbilical vein endothelial cells (HUVEC) tube formation, suggesting the active involvement of GC-MSC in tumor neovascularization, while the inherent regulation mechanisms in VEGF/NF-κB signaling remains unquestioned. MSC are observed to trans-differentiation into EC with the induction of basic fibroblast growth factor (bFGF) or VEGF, and RNA chip result indicates the intrinsic epigenetic

modifications of MSC affect their differentiation into multiple cell lineages including EC that reshape the surrounding pathological GC stroma, hence MSC probably directly give rise to EC to contribute to GC vascular network (65–67). Additionally, experimental evidence shows that MSC are able to give rise to CAF with the activation of TGF-β derived from GC-exosomes (68). CAF are well-demonstrated stromal cells and are often coordinated and overlapping with GC-MSC in reprogramming tumor itself and the stroma vicinity to contribute to cancer invasion and migration, acquired chemoresistance and EMT (69–71). Hp infection in GC cells would therefore enhance the expression of hepatoma-derived growth factor (HDGF) which also accelerates the transition of MSC into CAF and amplify their synergistic effects (72). Former studies stressed the role of CAF in ECM remodeling that control the aggressiveness and metastasis of cancer cells (73, 74). However, newly data indicate that secretion of MMP-2, MMP-7, MMP-9 and MMP-14, matrix metalloproteinases needed for ECM degradation are also increased in MSC to destruct external barriers to facilitate GC invasion and migration (75).

THE PROSPECTS OF MSC IN TARGETED THERAPY

MSC Act as Drug Delivery Vehicles

With their inherent advantages, like tumor and metastases tropism, easy isolation, low immunogenicity, MSC are ideal vehicles for tumor-directed therapy to raise efficacy (**Table 1**). Recently, a novel polymer AHP-OA-FA has been employed to infuse with MSC that enhance the tropism into GC with increased drug concentration and aggregation in local tumor lesions than pure MSC, and the polymer exerts no impact on the surface marker, proliferative capacity and motility of MSC, thus could be serving as more potent carriers for targeted therapy (84). Prerequisites for application of MSC are that the therapeutic agents they transported can be released after reaching the tumor site and exhibit strong toxicity only to tumor tissues. Cai and coworkers (76) established immuneapoptotin-armored MSC which continually secrete immuneapoptotin e23sFv-Fdt-tBid and exhibit significantly killing effect to GC cells expressing HER2 *in vitro* study. Importantly, after being intravenously administered in HER2 reconstituted syngeneic mouse models, these primed MSC exhibit persistent localization at tumor areas, display markedly stronger immunoapoptotin staining and better anti-tumor effect in comparison with direct delivery of the purified immunoapoptotin or delivery by Jurkat cells, indicating that MSC mobility can be well extended for the specific killing of HER-2 overexpressed GC. Besides, MSC expressing a transgene encoding NK4, the antagonist of HGF receptors, were observed to migrate and accumulate in tumor tissue, and effectively inhibit GC growth *via* suppressing tumor angiogenesis as well as triggering tumor cell apoptosis (77). In much the same way, umbilical cord blood (UCB)-MSC being infected with lentivirus vectors carrying LIGHT (TNF receptor superfamily) genes are also reported to induce severer apoptosis of GC cells (78). These trails illustrate that MSC as vectors possess a large scope of complexity, including apoptosis-inducing genes, oncolytic viruses, cytotoxic agents and anti-angiogenic agents. To our interest, a recent study demonstrated that MSC could also be modified to carry hemoglobin genes and supply oxygen to GC cells to reverse the hypoxic microenvironment and reduce the resistance to cisplatin and 5-FU (79). However, there are still lacking in evidence to ensure that the engineered MSC do not cause tumor progression or recurrence after long periods of infiltrating in cancer stroma. The first prospective, uncontrolled, single-arm phase I/II study on MSC-based therapy using autologous genetically modified MSCs in advanced gastrointestinal adenocarcinoma (TREAT-ME1) has been finished and suggested that MSC_apceth_101 cells (a total dose of

TABLE 1 | Summary of applications of MSC in targeted therapy of GC.

Mechanism of action	Source of MSC	Anti-tumor compound	Effects	References
MSC as anti-tumor drug vectors	BM-MSC	Immunoapoptotin e23sFv-Fdt-tBid	Tumor growth↓	(76)
	BM-MSC	NK4: antagonist of hepatocyte growth factor receptors (Met)	Tumor necrosis↑; microvessel formation↓	(77)
	UCB-MSC	LIGHT(TNFSF14):TNF receptor	Tumor apoptosis↑	(78)
	BM-MSC	Hemoglobin genes (HBA2 and HBB)	Chemotherapeutic effect↑	(79)
Target the MSC recruitment	BM-MSC	AMD3100: inhibitor of CXCL12/CXCR4 signaling axis	Tumor growth↓; gastric dysplasia↓	(80)
	BM-MSC	SB225002: CXCR2 inhibitor	Tumor necrosis↑; growth↓; lymph node metastasis↓	(26)
Target the MSC-GC interactions	GC-MSC	Resveratrol	EMT↓; metastasis↓	(81)
	BM-MSC	Anti-IL-6 antibody Anti-IL-8 antibody Anti-CCL-5 antibody 17β- estradiol	Tumor invasiveness↓	(82–84)
	BM-MSC	Etomoxir (ETX): inhibitor of FAO	Cancer stemness↓; chemo-resistance↓	(35)
	GC-MSC	YAP shRNA	Tumor migration↓; invasion↓; pro-angiogenic ability↓	(41)
	GC-MSC	PDGF-DD siRNA or su16f	Tumor proliferation↓;migration↓	(42)
	GC-MSC	Curcumin	Tumor angiogenesis↓	(64)

3.0×10^6 cells/kg) expressing herpes simplex virus tyrosine kinase (HSV-TK) combined with ganciclovir was safe and could be well tolerated (85, 86). While it is a small study with 10 patients and no GC cases included, thus future multicenter investigations with larger samples are warranted to realize the safe and effective transformation of MSC-based therapy into GC settings.

Target the Recruitment Course of MSC and the Downstream Vicious Signals

In most circumstances, the active recruitment of MSC commonly occurs ahead of GC initiation, especially in Hp-related carcinogenesis. Hp induced inflammation milieu is abundant in functional molecules such as TNF-α, TGF-β, CXCL12 and interferon γ that conducive to MSC recruitment for their tissue healing functions (28, 87–89). Corresponding to this point, Ruan et al. (27) labeled MSC with amino-modified FMNP that keep stable fluorescent signal and magnetic properties with 14 days to display out the early gastric cancer (EGC) area, not only being with the potential of imaging EGC, these MSC also could inhibit tumor growth markedly under alternating magnetic field irradiation. MSC aggregating at inflamed stomach further prompts gastric carcinogenesis mainly through EMT once they fail to repair (55, 90). Hence earlier Hp eradication or intercepting MSC recruitment would make a difference to suspend carcinogenesis and progression (**Table 1**). Prior study has manifested that the AMD3100, an inhibitor of the CXCL12/CXCR4 signaling axis, could block the transformation of MSC into α-SMA+ myofibroblasts and the recruitment of MSC, inhibiting tumor growth and the development of gastric dysplasia (80). Similarly, the administration of antagonists of the CXCL1/CXCR2 axis was found to block the MSC recruitment in the GC mice model, decreasing the size of tumors as well as the number of lymph node metastases (26). On the other hand, directly disrupt inter-communication between MSC and GC also offer novel insights for GC treatment (**Table 1**). Such as resveratrol, which could suppress and revert the pro-metastatic effect of GC-MSC *via* counteracting GC-MSC-mediated Wnt/β-catenin signaling of GC cells (81). Curcumin is a bioactive compound and found to abrogate the NF-κB signaling and VEGF production to attenuate the GC-MSC-triggered tumor angiogenesis (64). In addition to these, several researchers have successfully adopted specific neutralizing antibodies of IL-8, IL-6, and CCL-5 to inhibit MSC-mediated GC invasive motility, and 17β- estradiol also impair the functions of IL-8, IL-6, and CCL-5 under the same context *via* ceasing the activation of their downstream Src/Cas/Paxillin signaling pathway, thus hormonal therapy might be anticipated based on MSC activity (82, 83, 91).

CONCLUSIONS

MSC, with their multi-lineage differentiation and immune privilege nature, have shared great popularity in regenerative medicine and allogeneic transplantation. As the stromal progenitor cells, their role in tumor progression and TME is being put under the spotlight of tumor researches. Most studies have confirmed the tumor-contributing role of MSC, while the anti-tumor effect of MSC gradually unveils in several cancer types such as melanoma; glioma; HCC (92–94). Also, there are opposite results clarifying that MSC from human adipose tissue and the umbilical cord could inhibit GC progression and induce apoptosis of cancer cells (95, 96). One convincing explanation of the discrepancy attaches importance on the process of reprogramming of tumor cells that convert naïve MSC, which often exert a divergent effect on tumor progression, into pro-tumorigenic educated tumor-associated MSC. However, other factors, like the differences among tumor models, the heterogeneity of MSC, the timing and dose of the MSC injected are also accepted to influence the process of MSC-cancer interactions and lead to inconsistent results [reviewed in (97, 98)].

This review stresses the reciprocal crosstalk of malignant cells and MSC in the progression of GC, which can partly account for the complexity and heterogeneity of tumor-stroma connections. GC and the secret mediators in the niche would induce MSC recruitment and educate them into cancer-associated MSC with stronger tumor-promoting potential. In response, through cell physical contact or secretomes, MSC could aberrantly motivate oncogenic signals, deregulate metabolic plasticity and elicit EMT in GC cells to promote proliferation, invasion, migration and chemoresistance. Indirectly, reprogrammed MSC can deliver their signals horizontally to non-tumor cells in the TME to boost their pro-tumor functions with the repression of local immune response, stimulation of tumor angiogenesis and ECM remodeling. Given that MSC homing occurs early in the precancerous stage, they can be used for the detection of EGC. And they are also ideal carriers to deliver anti-cancer agents to tumor lesions with their low immunogenicity and well-accommodation, an increased concentration and lethality of drugs in target tissues would be expected. While further researches are warranted to identify whether the tumor-promoting role of MSC would override the inhibiting effect from drugs they delivered. In addition, the reciprocal reprogramming of MSC and GC as well as their domino effect spread to the TME prove beneficial for tumor growth and progression, strategies intercepting these vicious signaling connections represent a hopeful prospect in GC treatment. Taken together, the reciprocal reprogramming of GC and MSC triggers more active tumor-supporting signals that sustain tumor progression and remodel the surrounding pathological stroma. The tumor tropism nature of MSC and their extensive roles in GC deserve more in-depth investigation as they earn promising targets for cutting-edge cancer treatments.

AUTHOR CONTRIBUTIONS

YL wrote the review. XZ and YZ were responsible for figure and legend and final editing. XL contributed to conceiving the concept, analyzing the article and preparing for submission. All authors contributed to the article and approved the submitted version.

FUNDING

This study was supported by research grants from Zhejiang Provincial National Science Foundation of China (Grant no.LY16H160031).

REFERENCES

1. Bray F, Ferlay J, Soerjomataram I, Siegel RL, Torre LA, Jemal A. Global Cancer Statistics 2018: GLOBOCAN Estimates of Incidence and Mortality Worldwide for 36 Cancers in 185 Countries. *Ca-a Cancer J Clin* (2018) 68 (6):394–424. doi: 10.3322/caac.21492
2. Digklia A, Wagner AD. Advanced Gastric Cancer: Current Treatment Landscape and Future Perspectives. *World J Gastroenterol* (2016) 22 (8):2403–14. doi: 10.3748/wjg.v22.i8.2403
3. Kim YI, Kim YA, Kim CG, Ryu KW, Kim YW, Sim JA, et al. Serial Intermediate-Term Quality of Life Comparison After Endoscopic Submucosal Dissection Versus Surgery in Early Gastric Cancer Patients. *Surg Endoscopy* (2018) 32(4):2114–22. doi: 10.1007/s00464-017-5909-y
4. Malfertheiner P, Megraud F, O'Morain CA, Gisbert JP, Kuipers EJ, Axon AT, et al. Management of Helicobacter Pylori Infection-the Maastricht V/Florence Consensus Report. *Gut* (2017) 66(1):6–30. doi: 10.1136/gutjnl-2016-312288
5. Nelen SD, van Putten M, Lemmens V, Bosscha K, de Wilt JHW, Verhoeven RHA. Effect of Age on Rates of Palliative Surgery and Chemotherapy Use in Patients With Locally Advanced or Metastatic Gastric Cancer. *Br J Surg* (2017) 104(13):1837–46. doi: 10.1002/bjs.10621
6. Fidler IJ. The Pathogenesis of Cancer Metastasis: The 'Seed and Soil' Hypothesis Revisited. *Nat Rev Cancer* (2003) 3(6):453–8. doi: 10.1038/nrc1098
7. Atiya H, Frisbie L, Pressimone C, Coffman L. Mesenchymal Stem Cells in the Tumor Microenvironment. *Adv Exp Med Biol* (2020) 1234:31–42. doi: 10.1007/978-3-030-37184-5_3
8. Valkenburg KC, de Groot AE, Pienta KJ. Targeting the Tumour Stroma to Improve Cancer Therapy. *Nat Rev Clin Oncol* (2018) 15(6):366–81. doi: 10.1038/s41571-018-0007-1
9. Kucerova L, Skolekova S. Tumor Microenvironment and the Role of Mesenchymal Stromal Cells. *Neoplasma* (2013) 60(1):1–10. doi: 10.4149/neo_2013_001
10. Li J, Pu T, Yin L, Li Q, Liao CP, Wu BJ. MAOA-Mediated Reprogramming of Stromal Fibroblasts Promotes Prostate Tumorigenesis and Cancer Stemness. *Oncogene* (2020) 39(16):3305–21. doi: 10.1038/s41388-020-1217-4
11. Dourado MR, Miwa KYM, Hamada GB, Paranaíba LMR, Sawazaki-Calone Í, Domingueti CB, et al. Prognostication for Oral Squamous Cell Carcinoma Patients Based on the Tumour-Stroma Ratio and Tumour Budding. *Histopathology* (2020) 76(6):906–18. doi: 10.1111/his.14070
12. Numakura S, Uozaki H, Kikuchi Y, Watabe S, Togashi A, Watanabe M. Mesenchymal Stem Cell Marker Expression in Gastric Cancer Stroma. *Anticancer Res* (2019) 39(1):387–93. doi: 10.21873/anticanres.13124
13. Kemi N, Eskuri M, Herva A, Leppänen J, Huhta H, Helminen O, et al. Tumour-Stroma Ratio and Prognosis in Gastric Adenocarcinoma. *Br J Cancer* (2018) 119(4):435–9. doi: 10.1038/s41416-018-0202-y
14. Kemi N, Eskuri M, Kauppila JH. Tumour-Stroma Ratio and 5-Year Mortality in Gastric Adenocarcinoma: A Systematic Review and Meta-Analysis. *Sci Rep* (2019) 9(1):16018. doi: 10.1038/s41598-019-52606-7
15. Peng C, Liu J, Yang G, Li Y. The Tumor-Stromal Ratio as a Strong Prognosticator for Advanced Gastric Cancer Patients: Proposal of a New TSNM Staging System. *J Gastroenterol* (2018) 53(5):606–17. doi: 10.1007/s00535-017-1379-1
16. Friedenstein AJ, Chailakhjan RK, Lalykina KS. The Development of Fibroblast Colonies in Monolayer Cultures of Guinea-Pig Bone Marrow and Spleen Cells. *Cell Tissue Kinetics* (1970) 3(4):393–403. doi: 10.1111/j.1365-2184.1970.tb00347.x
17. Dominici M, Le Blanc K, Mueller I, Slaper-Cortenbach I, Marini F, Krause D, et al. Minimal Criteria for Defining Multipotent Mesenchymal Stromal Cells. The International Society for Cellular Therapy Position Statement. *Cytotherapy* (2006) 8(4):315–7. doi: 10.1080/14653240600855905
18. Álvarez-Viejo M, Menéndez-Menéndez Y, Otero-Hernández J. CD271 as a Marker to Identify Mesenchymal Stem Cells From Diverse Sources Before Culture. *World J Stem Cells* (2015) 7(2):470–6. doi: 10.4252/wjsc.v7.i2.470
19. Lv FJ, Tuan RS, Cheung KM, Leung VY. Concise Review: The Surface Markers and Identity of Human Mesenchymal Stem Cells. *Stem Cells (Dayton Ohio)* (2014) 32(6):1408–19. doi: 10.1002/stem.1681
20. Sarveazad A, Babahajian A, Yari A, Rayner CK, Mokhtare M, Babaei-Ghazani A, et al. Combination of Laser and Human Adipose-Derived Stem Cells in Repair of Rabbit Anal Sphincter Injury: A New Therapeutic Approach. *Stem Cell Res Ther* (2019) 10(1):367. doi: 10.1186/s13287-019-1477-5
21. Chetty SS, Praneetha S, Govarthanan K, Verma RS, Vadivel Murugan A. Noninvasive Tracking and Regenerative Capabilities of Transplanted Human Umbilical Cord-Derived Mesenchymal Stem Cells Labeled With I-III-IV Semiconducting Nanocrystals in Liver-Injured Living Mice. *ACS Appl Mater Interfaces* (2019) 11(9):8763–78. doi: 10.1021/acsami.8b19953
22. Kidd S, Spaeth E, Dembinski JL, Dietrich M, Watson K, Klopp A, et al. Direct Evidence of Mesenchymal Stem Cell Tropism for Tumor and Wounding Microenvironments Using. *Vivo Biolumin Imaging Stem Cells (Dayton Ohio)* (2009) 27(10):2614–23. doi: 10.1002/stem.187
23. Dvorak HF. Tumors: Wounds That do Not Heal. Similarities Between Tumor Stroma Generation and Wound Healing. *New Engl J Med* (1986) 315 (26):1650–9. doi: 10.1056/nejm198612253152606
24. Xie C, Yang Z, Suo Y, Chen Q, Wei D, Weng X, et al. Systemically Infused Mesenchymal Stem Cells Show Different Homing Profiles in Healthy and Tumor Mouse Models. *Stem Cells Trans Med* (2017) 6(4):1120–31. doi: 10.1002/sctm.16-0204
25. Błogowski W, Zuba-Surma E, Sałata D, Budkowska M, Dołęgowska B, Starzyńska T. Peripheral Trafficking of Bone-Marrow-Derived Stem Cells in Patients With Different Types of Gastric Neoplasms. *Oncoimmunology* (2016) 5(4):e1099798. doi: 10.1080/2162402x.2015.1099798
26. Kasashima H, Yashiro M, Nakamae H, Kitayama K, Masuda G, Kinoshita H, et al. Cxcl1-Chemokine (C-X-C Motif) Receptor 2 Signaling Stimulates the Recruitment of Bone Marrow-Derived Mesenchymal Cells Into Diffuse-Type Gastric Cancer Stroma. *Am J Pathol* (2016) 186(11):3028–39. doi: 10.1016/j.ajpath.2016.07.024
27. Ruan J, Ji J, Song H, Qian Q, Wang K, Wang C, et al. Fluorescent Magnetic Nanoparticle-Labeled Mesenchymal Stem Cells for Targeted Imaging and Hyperthermia Therapy of. *Vivo Gastric Cancer Nanoscale Res Lett* (2012) 7 (1):309. doi: 10.1186/1556-276x-7-309
28. Ferrand J, Lehours P, Schmid-Alliana A, Mégraud F, Varon C. Helicobacter Pylori Infection of Gastrointestinal Epithelial Cells *in vitro* induces mesenchymal stem cell migration through an NF-κB-dependent pathway. *PloS One* (2011) 6(12):e29007. doi: 10.1371/journal.pone.0029007
29. Shamai Y, Alperovich DC, Yakhini Z, Skorecki K, Tzukerman M. Reciprocal Reprogramming of Cancer Cells and Associated Mesenchymal Stem Cells in Gastric Cancer. *Stem Cells (Dayton Ohio)* (2019) 37(2):176–89. doi: 10.1002/stem.2942
30. Shen Y, Xue C, Li X, Ba L, Gu J, Sun Z, et al. Effects of Gastric Cancer Cell-Derived Exosomes on the Immune Regulation of Mesenchymal Stem Cells by the NF-kB Signaling Pathway. *Stem Cells Dev* (2019) 28(7):464–76. doi: 10.1089/scd.2018.0125
31. Wang M, Zhao X, Qiu R, Gong Z, Huang F, Yu W, et al. Lymph Node Metastasis-Derived Gastric Cancer Cells Educate Bone Marrow-Derived Mesenchymal Stem Cells *via* YAP signaling activation by exosomal Wnt5a. *Oncogene* (2021) 40(12):2296–308. doi: 10.1038/s41388-021-01722-8
32. Cao H, Xu W, Qian H, Zhu W, Yan Y, Zhou H, et al. Mesenchymal Stem Cell-Like Cells Derived From Human Gastric Cancer Tissues. *Cancer Lett* (2009) 274(1):61–71. doi: 10.1016/j.canlet.2008.08.036
33. Xu X, Zhang X, Wang S, Qian H, Zhu W, Cao H, et al. Isolation and Comparison of Mesenchymal Stem-Like Cells From Human Gastric Cancer and Adjacent non-Cancerous Tissues. *J Cancer Res Clin Oncol* (2011) 137 (3):495–504. doi: 10.1007/s00432-010-0908-6
34. Zhu Q, Zhang X, Zhang L, Li W, Wu H, Yuan X, et al. The IL-6-STAT3 Axis Mediates a Reciprocal Crosstalk Between Cancer-Derived Mesenchymal Stem Cells and Neutrophils to Synergistically Prompt Gastric Cancer Progression. *Cell Death Dis* (2014) 5(6):e1295. doi: 10.1038/cddis.2014.263
35. He W, Liang B, Wang C, Li S, Zhao Y, Huang Q, et al. MSC-Regulated Lncrna MACC1-AS1 Promotes Stemness and Chemoresistance Through Fatty Acid Oxidation in Gastric Cancer. *Oncogene* (2019) 38(23):4637–54. doi: 10.1038/s41388-019-0747-0
36. Zhu M, Wang M, Yang F, Tian Y, Cai J, Yang H, et al. miR-155-5p Inhibition Promotes the Transition of Bone Marrow Mesenchymal Stem Cells to Gastric Cancer Tissue Derived MSC-like Cells *via* NF-κB p65 activation. *Oncotarget* (2016) 7(13):16567–80. doi: 10.18632/oncotarget.7767
37. Li W, Zhou Y, Yang J, Zhang X, Zhang H, Zhang T, et al. Gastric Cancer-Derived Mesenchymal Stem Cells Prompt Gastric Cancer Progression

Through Secretion of Interleukin-8. *J Exp Clin Cancer Res: CR* (2015) 34 (1):52. doi: 10.1186/s13046-015-0172-3
38. Berger L, Shamai Y, Skorecki KL, Tzukerman M. Tumor Specific Recruitment and Reprogramming of Mesenchymal Stem Cells in Tumorigenesis. *Stem Cells (Dayton Ohio)* (2016) 34(4):1011–26. doi: 10.1002/stem.2269
39. Takiguchi G, Nishita M, Kurita K, Kakeji Y, Minami Y. Wnt5a-Ror2 Signaling in Mesenchymal Stem Cells Promotes Proliferation of Gastric Cancer Cells by Activating CXCL16-CXCR6 Axis. *Cancer Sci* (2016) 107(3):290–7. doi: 10.1111/cas.12871
40. Ikeda T, Nishita M, Hoshi K, Honda T, Kakeji Y, Minami Y. Mesenchymal Stem Cell-Derived CXCL16 Promotes Progression of Gastric Cancer Cells by STAT3-mediated Expression of Ror1. *Cancer Sci* (2020) 111(4):1254–65. doi: 10.1111/cas.14339
41. Pan Z, Tian Y, Zhang B, Zhang X, Shi H, Liang Z, et al. YAP Signaling in Gastric Cancer-Derived Mesenchymal Stem Cells is Critical for its Promoting Role in Cancer Progression. *Int J Oncol* (2017) 51(4):1055–66. doi: 10.3892/ijo.2017.4101
42. Huang F, Wang M, Yang T, Cai J, Zhang Q, Sun Z, et al. Gastric Cancer-Derived MSC-secreted Pdgf-DD Promotes Gastric Cancer Progression. *J Cancer Res Clin Oncol* (2014) 140(11):1835–48. doi: 10.1007/s00432-014-1723-2
43. Zhang X, Yuan X, Shi H, Wu L, Qian H, Xu W. Exosomes in Cancer: Small Particle, Big Player. *J Hematol Oncol* (2015) 8:83. doi: 10.1186/s13045-015-0181-x
44. Lou G, Chen Z, Zheng M, Liu Y. Mesenchymal Stem Cell-Derived Exosomes as a New Therapeutic Strategy for Liver Diseases. *Exp Mol Med* (2017) 49(6): e346. doi: 10.1038/emm.2017.63
45. Ji R, Zhang B, Zhang X, Xue J, Yuan X, Yan Y, et al. Exosomes Derived From Human Mesenchymal Stem Cells Confer Drug Resistance in Gastric Cancer. *Cell Cycle (Georgetown Tex)* (2015) 14(15):2473–83. doi: 10.1080/15384101.2015.1005530
46. Mao J, Liang Z, Zhang B, Yang H, Li X, Fu H, et al. Ubr2 Enriched in P53 Deficient Mouse Bone Marrow Mesenchymal Stem Cell-Exosome Promoted Gastric Cancer Progression *via* Wnt/β-Catenin Pathway. *Stem Cells (Dayton Ohio)* (2017) 35(11):2267–79. doi: 10.1002/stem.2702
47. Wang M, Zhao C, Shi H, Zhang B, Zhang L, Zhang X, et al. Deregulated microRNAs in Gastric Cancer Tissue-Derived Mesenchymal Stem Cells: Novel Biomarkers and a Mechanism for Gastric Cancer. *Br J Cancer* (2014) 110(5):1199–210. doi: 10.1038/bjc.2014.14
48. Ma M, Chen S, Liu Z, Xie H, Deng H, Shang S, et al. miRNA-221 of Exosomes Originating From Bone Marrow Mesenchymal Stem Cells Promotes Oncogenic Activity in Gastric Cancer. *OncoTargets Ther* (2017) 10:4161–71. doi: 10.2147/ott.S143315
49. Zhao Y, Liu Y, Lin L, Huang Q, He W, Zhang S, et al. The Lncrna MACC1-AS1 Promotes Gastric Cancer Cell Metabolic Plasticity *via* AMPK/Lin28 mediated mRNA stability of MACC1. *Mol Cancer* (2018) 17(1):69. doi: 10.1186/s12943-018-0820-2
50. Wu H, Liu B, Chen Z, Li G, Zhang Z. MSC-Induced Lncrna HCP5 Drove Fatty Acid Oxidation Through Mir-3619-5p/AMPK/PGC1α/CEBPB Axis to Promote Stemness and Chemo-Resistance of Gastric Cancer. *Cell Death Dis* (2020) 11(4):233. doi: 10.1038/s41419-020-2426-z
51. Gu H, Ji R, Zhang X, Wang M, Zhu W, Qian H, et al. Exosomes Derived From Human Mesenchymal Stem Cells Promote Gastric Cancer Cell Growth and Migration *via* the activation of the Akt pathway. *Mol Med Rep* (2016) 14 (4):3452–8. doi: 10.3892/mmr.2016.5625
52. Xue Z, Wu X, Chen X, Liu Y, Wang X, Wu K, et al. Mesenchymal Stem Cells Promote Epithelial to Mesenchymal Transition and Metastasis in Gastric Cancer Though Paracrine Cues and Close Physical Contact. *J Cell Biochem* (2015) 116(4):618–27. doi: 10.1002/jcb.25013
53. Nishimura K, Semba S, Aoyagi K, Sasaki H, Yokozaki H. Mesenchymal Stem Cells Provide an Advantageous Tumor Microenvironment for the Restoration of Cancer Stem Cells. *Pathobiol: J Immunopathol Mol Cell Biol* (2012) 79 (6):290–306. doi: 10.1159/000337296
54. Xue J, Zhu Y, Sun Z, Ji R, Zhang X, Xu W, et al. Tumorigenic Hybrids Between Mesenchymal Stem Cells and Gastric Cancer Cells Enhanced Cancer Proliferation, Migration and Stemness. *BMC Cancer* (2015) 15:793. doi: 10.1186/s12885-015-1780-1
55. He X, Li B, Shao Y, Zhao N, Hsu Y, Zhang Z, et al. Cell Fusion Between Gastric Epithelial Cells and Mesenchymal Stem Cells Results in Epithelial-to-Mesenchymal Transition and Malignant Transformation. *BMC Cancer* (2015) 15:24. doi: 10.1186/s12885-015-1027-1
56. Bonig H, Kuçi Z, Kuçi S, Bakhtiar S, Basu O, Bug G, et al. Children and Adults With Refractory Acute Graft-versus-Host Disease Respond to Treatment With the Mesenchymal Stromal Cell Preparation "Msc-Ffm"-Outcome Report of 92 Patients. *Cells* (2019) 8(12):1577. doi: 10.3390/cells8121577
57. Sun L, Wang Q, Chen B, Zhao Y, Shen B, Wang X, et al. Human Gastric Cancer Mesenchymal Stem Cell-Derived Il15 Contributes to Tumor Cell Epithelial-Mesenchymal Transition*via* Upregulation Tregs Ratio and PD-1 Expression in CD4(+)T Cell. *Stem Cells Dev* (2018) 27(17):1203–14. doi: 10.1089/scd.2018.0043
58. Knochelmann HM, Dwyer CJ, Bailey SR, Amaya SM, Elston DM, Mazza-McCrann JM, et al. When Worlds Collide: Th17 and Treg Cells in Cancer and Autoimmunity. *Cell Mol Immunol* (2018) 15(5):458–69. doi: 10.1038/s41423-018-0004-4
59. Wang M, Chen B, Sun XX, Zhao XD, Zhao YY, Sun L, et al. Gastric Cancer Tissue-Derived Mesenchymal Stem Cells Impact Peripheral Blood Mononuclear Cells *via* disruption of Treg/Th17 balance to promote gastric cancer progression. *Exp Cell Res* (2017) 361(1):19–29. doi: 10.1016/j.yexcr.2017.09.036
60. Li W, Zhang X, Wu F, Zhou Y, Bao Z, Li H, et al. Gastric Cancer-Derived Mesenchymal Stromal Cells Trigger M2 Macrophage Polarization That Promotes Metastasis and EMT in Gastric Cancer. *Cell Death Dis* (2019) 10 (12):918. doi: 10.1038/s41419-019-2131-y
61. Gambardella V, Castillo J, Tarazona N, Gimeno-Valiente F, Martínez-Ciarpaglini C, Cabeza-Segura M, et al. The Role of Tumor-Associated Macrophages in Gastric Cancer Development and Their Potential as a Therapeutic Target. *Cancer Treat Rev* (2020) 86:102015. doi: 10.1016/j.ctrv.2020.102015
62. Sun L, Wang Q, Chen B, Zhao Y, Shen B, Wang H, et al. Gastric Cancer Mesenchymal Stem Cells Derived IL-8 Induces PD-L1 Expression in Gastric Cancer Cells *via* STAT3/mTOR-c-Myc signal axis. *Cell Death Dis* (2018) 9 (9):928. doi: 10.1038/s41419-018-0988-9
63. Xu R, Zhao X, Zhao Y, Chen B, Sun L, Xu C, et al. Enhanced Gastric Cancer Growth Potential of Mesenchymal Stem Cells Derived From Gastric Cancer Tissues Educated by CD4(+) T Cells. *Cell Prolif* (2018) 51(2):e12399. doi: 10.1111/cpr.12399
64. Huang F, Yao Y, Wu J, Liu Q, Zhang J, Pu X, et al. Curcumin Inhibits Gastric Cancer-Derived Mesenchymal Stem Cells Mediated Angiogenesis by Regulating NF-κb/VEGF Signaling. *Am J Trans Res* (2017) 9(12):5538–47.
65. Xu Y, Fu M, Li Z, Fan Z, Li X, Liu Y, et al. A Prosurvival and Proangiogenic Stem Cell Delivery System to Promote Ischemic Limb Regeneration. *Acta Biomater* (2016) 31:99–113. doi: 10.1016/j.actbio.2015.12.021
66. Tancharoen W, Aungsuchawan S, Pothacharoen P, Markmee R, Narakornsak S, Kieodee J, et al. Differentiation of Mesenchymal Stem Cells From Human Amniotic Fluid to Vascular Endothelial Cells. *Acta Histochem* (2017) 119 (2):113–21. doi: 10.1016/j.acthis.2016.11.009
67. Kalamohan K, Periasamy J, Bhaskar Rao D, Barnabas GD, Ponnaiyan S, Ganesan K. Transcriptional Coexpression Network Reveals the Involvement of Varying Stem Cell Features With Different Dysregulations in Different Gastric Cancer Subtypes. *Mol Oncol* (2014) 8(7):1306–25. doi: 10.1016/j.molonc.2014.04.005
68. Gu J, Qian H, Shen L, Zhang X, Zhu W, Huang L, et al. Gastric Cancer Exosomes Trigger Differentiation of Umbilical Cord Derived Mesenchymal Stem Cells to Carcinoma-Associated Fibroblasts Through TGF-β/Smad Pathway. *PloS One* (2012) 7(12):e52465. doi: 10.1371/journal.pone.0052465
69. Zhang H, Deng T, Liu R, Ning T, Yang H, Liu D, et al. CAF Secreted miR-522 Suppresses Ferroptosis and Promotes Acquired Chemo-Resistance in Gastric Cancer. *Mol Cancer* (2020) 19(1):43. doi: 10.1186/s12943-020-01168-8
70. Chong Y, Tang D, Xiong Q, Jiang X, Xu C, Huang Y, et al. Galectin-1 From Cancer-Associated Fibroblasts Induces Epithelial-Mesenchymal Transition Through β1 Integrin-Mediated Upregulation of Gli1 in Gastric Cancer. *J Exp Clin Cancer Res: CR* (2016) 35(1):175. doi: 10.1186/s13046-016-0449-1
71. Kurashige J, Mima K, Sawada G, Takahashi Y, Eguchi H, Sugimachi K, et al. Epigenetic Modulation and Repression of miR-200b by Cancer-Associated Fibroblasts Contribute to Cancer Invasion and Peritoneal Dissemination in Gastric Cancer. *Carcinogenesis* (2015) 36(1):133–41. doi: 10.1093/carcin/bgu232

72. Liu CJ, Wang YK, Kuo FC, Hsu WH, Yu FJ, Hsieh S, et al. Helicobacter Pylori Infection-Induced Hepatoma-Derived Growth Factor Regulates the Differentiation of Human Mesenchymal Stem Cells to Myofibroblast-Like Cells. *Cancers* (2018) 10(12):479. doi: 10.3390/cancers10120479
73. Kaukonen R, Mai A, Georgiadou M, Saari M, De Franceschi N, Betz T, et al. Normal Stroma Suppresses Cancer Cell Proliferation *via* mechanosensitive regulation of JMJD1a-mediated transcription. *Nat Commun* (2016) 7:12237. doi: 10.1038/ncomms12237
74. Jang M, Koh I, Lee JE, Lim JY, Cheong JH, Kim P. Increased Extracellular Matrix Density Disrupts E-Cadherin/β-Catenin Complex in Gastric Cancer Cells. *Biomater Sci* (2018) 6(10):2704–13. doi: 10.1039/c8bm00843d
75. Song L, Zhou X, Jia HJ, Du M, Zhang JL, Li L. Effect of hGC-MSCs From Human Gastric Cancer Tissue on Cell Proliferation, Invasion and Epithelial-Mesenchymal Transition in Tumor Tissue of Gastric Cancer Tumor-Bearing Mice. *Asian Pacific J Trop Med* (2016) 9(8):796–800. doi: 10.1016/j.apjtm.2016.06.004
76. Cai Y, Xi Y, Cao Z, Xiang G, Ni Q, Zhang R, et al. Dual Targeting and Enhanced Cytotoxicity to HER2-overexpressing Tumors by Immunoapoptotin-Armored Mesenchymal Stem Cells. *Cancer Lett* (2016) 381(1):104–12. doi: 10.1016/j.canlet.2016.07.027
77. Zhu Y, Cheng M, Yang Z, Zeng CY, Chen J, Xie Y, et al. Mesenchymal Stem Cell-Based NK4 Gene Therapy in Nude Mice Bearing Gastric Cancer Xenografts. *Drug Des Dev Ther* (2014) 8:2449–62. doi: 10.2147/dddt.S71466
78. Zhu X, Su D, Xuan S, Ma G, Dai Z, Liu T, et al. Gene Therapy of Gastric Cancer Using LIGHT-secreting Human Umbilical Cord Blood-Derived Mesenchymal Stem Cells. *Gastric Cancer* (2013) 16(2):155–66. doi: 10.1007/s10120-012-0166-1
79. Zhou YL, Li YM, He WT. Oxygen-Laden Mesenchymal Stem Cells Enhance the Effect of Gastric Cancer Chemotherapy. *Vitro Oncol Lett* (2019) 17 (1):1245–52. doi: 10.3892/ol.2018.9670
80. Quante M, Tu SP, Tomita H, Gonda T, Wang SS, Takashi S, et al. Bone Marrow-Derived Myofibroblasts Contribute to the Mesenchymal Stem Cell Niche and Promote Tumor Growth. *Cancer Cell* (2011) 19(2):257–72. doi: 10.1016/j.ccr.2011.01.020
81. Yin L, Zhang R, Hu Y, Li W, Wang M, Liang Z, et al. Gastric-Cancer-Derived Mesenchymal Stem Cells: A Promising Target for Resveratrol in the Suppression of Gastric Cancer Metastasis. *Hum Cell* (2020) 33(3):652–62. doi: 10.1007/s13577-020-00339-5
82. Liu CJ, Kuo FC, Wang CL, Kuo CH, Wang SS, Chen CY, et al. Suppression of IL-8-Src Signalling Axis by 17β-Estradiol Inhibits Human Mesenchymal Stem Cells-Mediated Gastric Cancer Invasion. *J Cell Mol Med* (2016) 20(5):962–72. doi: 10.1111/jcmm.12786
83. Kuo CH, Liu CJ, Lu CY, Hu HM, Kuo FC, Liou YS, et al. 17β-Estradiol Inhibits Mesenchymal Stem Cells-Induced Human AGS Gastric Cancer Cell Mobility *via* suppression of CCL5- Src/Cas/Paxillin signaling pathway. *Int J Med Sci* (2014) 11(1):7–16. doi: 10.7150/ijms.6851
84. Zhang S, Liu Y, Derakhshanfar S, He W, Huang Q, Dong S, et al. Polymer Self-Assembled Bmscs With Cancer Tropism and Programmed Homing. *Adv Healthcare Mater* (2018) 7(23):e1800118. doi: 10.1002/adhm.201800118
85. Niess H, von Einem JC, Thomas MN, Michl M, Angele MK, Huss R, et al. Treatment of Advanced Gastrointestinal Tumors With Genetically Modified Autologous Mesenchymal Stromal Cells (TREAT-ME1): Study Protocol of a Phase I/II Clinical Trial. *BMC Cancer* (2015) 15:237. doi: 10.1186/s12885-015-1241-x
86. von Einem JC, Guenther C, Volk HD, Grütz G, Hirsch D, Salat C, et al. Treatment of Advanced Gastrointestinal Cancer With Genetically Modified Autologous Mesenchymal Stem Cells: Results From the Phase 1/2 TREAT-ME-1 Trial. *Int J Cancer* (2019) 145(6):1538–46. doi: 10.1002/ijc.32230
87. Fakhari S, Kalantar E, Nikzaban M, Hakhamneshi MS, Fathi F, Nikkhoo B, et al. Effect of Helicobacter Pylori Infection on Stromal-Derived factor-1/CXCR4 Axis in Bone Marrow-Derived Mesenchymal Stem Cells. *Adv Biomed Res* (2014) 3:19. doi: 10.4103/2277-9175.124650
88. Donnelly JM, Engevik AC, Engevik M, Schumacher MA, Xiao C, Yang L, et al. Gastritis Promotes an Activated Bone Marrow-Derived Mesenchymal Stem Cell With a Phenotype Reminiscent of a Cancer-Promoting Cell. *Dig Dis Sci* (2014) 59(3):569–82. doi: 10.1007/s10620-013-2927-z
89. Donnelly JM, Chawla A, Houghton J, Zavros Y. Sonic Hedgehog Mediates the Proliferation and Recruitment of Transformed Mesenchymal Stem Cells to the Stomach. *PloS One* (2013) 8(9):e75225. doi: 10.1371/journal.pone.0075225
90. Choi YJ, Kim N, Chang H, Lee HS, Park SM, Park JH, et al. Helicobacter Pylori-Induced Epithelial-Mesenchymal Transition, a Potential Role of Gastric Cancer Initiation and an Emergence of Stem Cells. *Carcinogenesis* (2015) 36(5):553–63. doi: 10.1093/carcin/bgv022
91. Liu CJ, Kuo FC, Hu HM, Chen CY, Huang YB, Cheng KH, et al. 17β-Estradiol Inhibition of IL-6-Src and Cas and Paxillin Pathway Suppresses Human Mesenchymal Stem Cells-Mediated Gastric Cancer Cell Motility. *Trans Res: J Lab Clin Med* (2014) 164(3):232–43. doi: 10.1016/j.trsl.2014.04.009
92. Wu Z, Liu W, Wang Z, Zeng B, Peng G, Niu H, et al. Mesenchymal Stem Cells Derived From iPSCs Expressing interleukin-24 Inhibit the Growth of Melanoma in the Tumor-Bearing Mouse Model. *Cancer Cell Int* (2020) 20:33. doi: 10.1186/s12935-020-1112-7
93. Lu L, Chen G, Yang J, Ma Z, Yang Y, Hu Y, et al. Bone Marrow Mesenchymal Stem Cells Suppress Growth and Promote the Apoptosis of Glioma U251 Cells Through Downregulation of the PI3K/AKT Signaling Pathway. *Biomed Pharmacother = Biomed Pharmacother* (2019) 112:108625. doi: 10.1016/j.biopha.2019.108625
94. Serhal R, Saliba N, Hilal G, Moussa M, Hassan GS, El Atat O, et al. Effect of Adipose-Derived Mesenchymal Stem Cells on Hepatocellular Carcinoma: In Vitro Inhibition of Carcinogenesis. *World J Gastroenterol* (2019) 25(5):567–83. doi: 10.3748/wjg.v25.i5.567
95. Zhao J, Zhang Z, Cui Q, Zhao L, Hu Y, Zhao S. Human Adipose-Derived Mesenchymal Stem Cells Inhibit Proliferation and Induce Apoptosis of Human Gastric Cancer HGC-27 Cells. *3 Biotech* (2020) 10(3):129. doi: 10.1007/s13205-020-2090-0
96. Meng MY, Li L, Wang WJ, Liu FF, Song J, Yang SL, et al. Assessment of Tumor Promoting Effects of Amniotic and Umbilical Cord Mesenchymal Stem Cells *in vitro* and *in vivo*. *J Cancer Res Clin Oncol* (2019) 145(5):1133–46. doi: 10.1007/s00432-019-02859-6
97. Rahmatizadeh F, Gholizadeh-Ghaleh Aziz S, Khodadadi K, Lale Ataei M, Ebrahimie E, Soleimani Rad J, et al. Bidirectional and Opposite Effects of Naïve Mesenchymal Stem Cells on Tumor Growth and Progression. *Adv Pharm Bull* (2019) 9(4):539–58. doi: 10.15171/apb.2019.063
98. Sun Z, Wang S, Zhao RC. The Roles of Mesenchymal Stem Cells in Tumor Inflammatory Microenvironment. *J Hematol Oncol* (2014) 7:14. doi: 10.1186/1756-8722-7-14

Conflict of Interest: The authors declare that the research was conducted in the absence of any commercial or financial relationships that could be construed as a potential conflict of interest.

frontiers in Oncology

ORIGINAL RESEARCH
published: 14 May 2021
doi: 10.3389/fonc.2021.666847

Identification of Mutator-Derived Alternative Splicing Signatures of Genomic Instability for Improving the Clinical Outcome of Cholangiocarcinoma

Zijing Lin[1], Jianping Gong[2], Guochao Zhong[2], Jiejun Hu[2], Dong Cai[2], Lei Zhao[3] and Zhibo Zhao[2]**

[1] Department of Breast and Thyroid Surgery, the Second Affiliated Hospital of Chongqing Medical University, Chongqing, China, [2] Department of Hepatobiliary Surgery, The Second Affiliated Hospital, Chongqing Medical University, Chongqing, China, [3] Department of Hepatobiliary Surgery, The Second Affiliated Hospital & Centre for Lipid Research & Key Laboratory of Molecular Biology for Infectious Diseases (Ministry of Education), Chongqing Medical University, Chongqing, China

OPEN ACCESS

Edited by:
Yujun Shi, Sichuan University, China

Reviewed by:
Fei Wu Long, Sichuan University, China
Michele Ghidini, IRCCS Foundation Ca 'Granda Ospedale Maggiore Policlinico, Italy

***Correspondence:**
Zhibo Zhao
zhaozhibo@stu.cqmu.edu.cn
Lei Zhao
zhaolei@cqmu.edu.cn

Specialty section:
This article was submitted to Gastrointestinal Cancers, a section of the journal Frontiers in Oncology

Received: *11 February 2021*
Accepted: *26 April 2021*
Published: *14 May 2021*

Citation:
Lin Z, Gong J, Zhong G, Hu J, Cai D, Zhao L and Zhao Z (2021) Identification of Mutator-Derived Alternative Splicing Signatures of Genomic Instability for Improving the Clinical Outcome of Cholangiocarcinoma. Front. Oncol. 11:666847. doi: 10.3389/fonc.2021.666847

Background: Cholangiocarcinoma is an aggressive carcinoma with increasing incidence and poor outcomes worldwide. Genomic instability and alternative splicing (AS) events are hallmarks of carcinoma development and progression. The relationship between genomic instability, AS events, and tumor immune microenvironment remain unclear.

Methods: The splicing profiles of patients with cholangiocarcinoma were obtained from The Cancer Genome Atlas (TCGA) spliceSeq database. The transcriptomics, simple nucleotide variation (SNP) and clinical data of patients with cholangiocarcinoma were obtained from TCGA database. Patients were divided into genomic unstable (GU-like) and genomic stable (GS-like) groups according to their somatic mutations. Survival-related differential AS events were identified through integrated analysis of splicing profiling and clinical data. Kyoto Encyclopedia of Genes and Genomes enrichment analysis was used to identify AS events occurring in genes enriched in cancer pathways. Pearson correlation was applied to analyze the splicing factors regulating AS events. CIBERSORT was used identify differentially infiltrating immune cells.

Results: A prognostic signature was constructed with six AS events. Using this signature, the hazard ratio of risk score for overall survival is 2.362. For TCGA patients with cholangiocarcinoma, the area under the receiver operating characteristic curve is 0.981. CDK11A is a negative regulator of survival associated AS events. Additionally, the CD8+ T cell proportion and PD-L1 expression are upregulated in patients with cholangiocarcinoma and high splicing signatures.

Conclusion: We provide a prognostic signature for cholangiocarcinoma overall survival. The CDK11A splicing factor and SLC46A1-39899-ES and IARS-86836-ES AS events may be potential targets for cholangiocarcinoma therapy. Patients with high AS risk score may be more sensitive to anti-PD-L1/PD1 immunotherapy.

Keywords: cholangiocarcinoma, genomic instability, alternative splicing, immunotherapy, overall survival

INTRODUCTION

Cholangiocarcinoma describes a group of carcinomas that occur in the biliary tree. Cholangiocarcinoma accounts for approximately 15% of all primary liver tumors and 3% of gastrointestinal cancers and the incidence of cholangiocarcinoma is increasing globally (1). In early stages cholangiocarcinoma is asymptomatic, leading to diagnosis in advanced stages and poor patient prognosis (2). The 5-year survival rate for patients with cholangiocarcinoma is 7–20% and tumor recurrence rates after resection remain disappointing (3). Therefore, there is an urgent need to find new biomarkers for cholangiocarcinoma diagnosis and prognosis.

Genomic instability is a driving factor of caner (4), and is associated with poor outcome in patients with cholangiocarcinoma (5, 6). To date, the molecular mechanisms of genomic instability in cholangiocarcinoma remain unclear. Recently, some microRNA (miRNA) 48 and long non-coding RNA (lncRNA) signatures associated with genomic instability have been identified. These signatures have efficiently predicted the outcome of ovarian cancer and breast carcinoma (7). However, whether alternative splicing (AS) events are associated with genomic instability remains unclear. However, whether genomic instability-related alternative splicing events predicted the outcome of cholangiocarcinoma remains unclear.

AS is a process through which exons within the same gene are expressed in different combinations, allowing a single gene to produce different proteins at different times and in different environments (8). The unbalanced expression of different isoforms of a single gene is recognized as contributing to the tumorigenesis and progression of numerous carcinomas (9). CD44v8-10 isoforms are upregulated in cholangiocarcinoma, and promote the proliferation of cholangiocarcinoma cells (10). Similarly, AS alternative events in WISP1v, Nek2B, ΔEX2TFF2, Foxp3Δ3, Δ133p53, PKM2, EP3−4, and AGR2vH are associated with the proliferation, migration, and invasion of cholangiocarcinoma cells (11).

In addition to affecting tumor cells, AS affects immune cells in the tumor microenvironment. Unbalanced ESRI1 isoforms are linked with infiltrating lymphocyte activity and patient survival (12). Similarly, AS events have been evaluated as predictive biomarkers for tumor immunotherapy in gastric cancer and squamous cell carcinoma (13, 14). Therefore, dysregulated AS events may serve as prognosis indicators and as potential therapy targets.

In this study, we describe a new prognostic signature model based on genomic instability derived AS events. Additionally, we explore the splicing factors that regulate the alternative splicing events recruited in our model. Furthermore, we analyzed the infiltrating immune cells correlated with this prognostic signature.

METHODS

Data Collection

Transcriptomics, simple nucleotide variation, and clinical phenotype data of patients with cholangiocarcinoma (n = 36) were downloaded from The Cancer Genome Atlas (TCGA) database (https://tcga-data.nci.nih.gov/). AS data of patients with cholangiocarcinoma (n = 36) were downloaded from the TCGAspliceSeq database (http://bioinformatics.mdanderson.org). Percent splicing index values for AS events were applied to reflect the likelihood of each AS event.

Identification of Genomic Instability Associated AS Events

To identify genomic instability associated AS events, a mutator hypothesis-derived tumor genome computational framework combining Percent Spliced In (PSI) values of AS events and somatic mutation profiles was developed (**Figure 1**). This framework involved calculating the cumulative quantity of somatic mutations for each patient, and ranking patients in descending order of somatic mutation quantity. Then, the top 25% (n = 9) and the last 25% (n = 9) of patients were defined as genomic unstable (GU-like) and genomic stable (GS-like) group respectively. PSI values of AS events were compared between GU-like and GS-like groups with significance analysis of microarrays method. Differential AS events were defined as $p < 0.05$.

Identification of Survival Associated AS Events and Construction AS Related Prognostic Signature

The AS events were visualized by Upset plot using UpSetR package (R version 4.0.3). Survival associated AS events were identified by univariate Cox regression using R software. AS events with $P < 0.05$ were used in further research. Lasso regression was performed to remove AS events having high correlation with each other. Multivariate Cox regression was performed to determine the prognostic value of each AS event. Finally, the prognostic signature model was constructed: $Risksc\,ore = \Sigma_i^n PSIi * \beta i$ (β represents the regression coefficient of each event).

Prognostic Signature Validation

Based on risk score, patients with cholangiocarcinoma were divided into two groups (high/low risk). K-M survival curve and Log-Rank tests were applied to compare overall survival (OS) between high and low risk groups. The ROC curve was applied to validate the predictive effect of the prognostic signature by calculating 5-year survival in R 4.0.3. Univariate

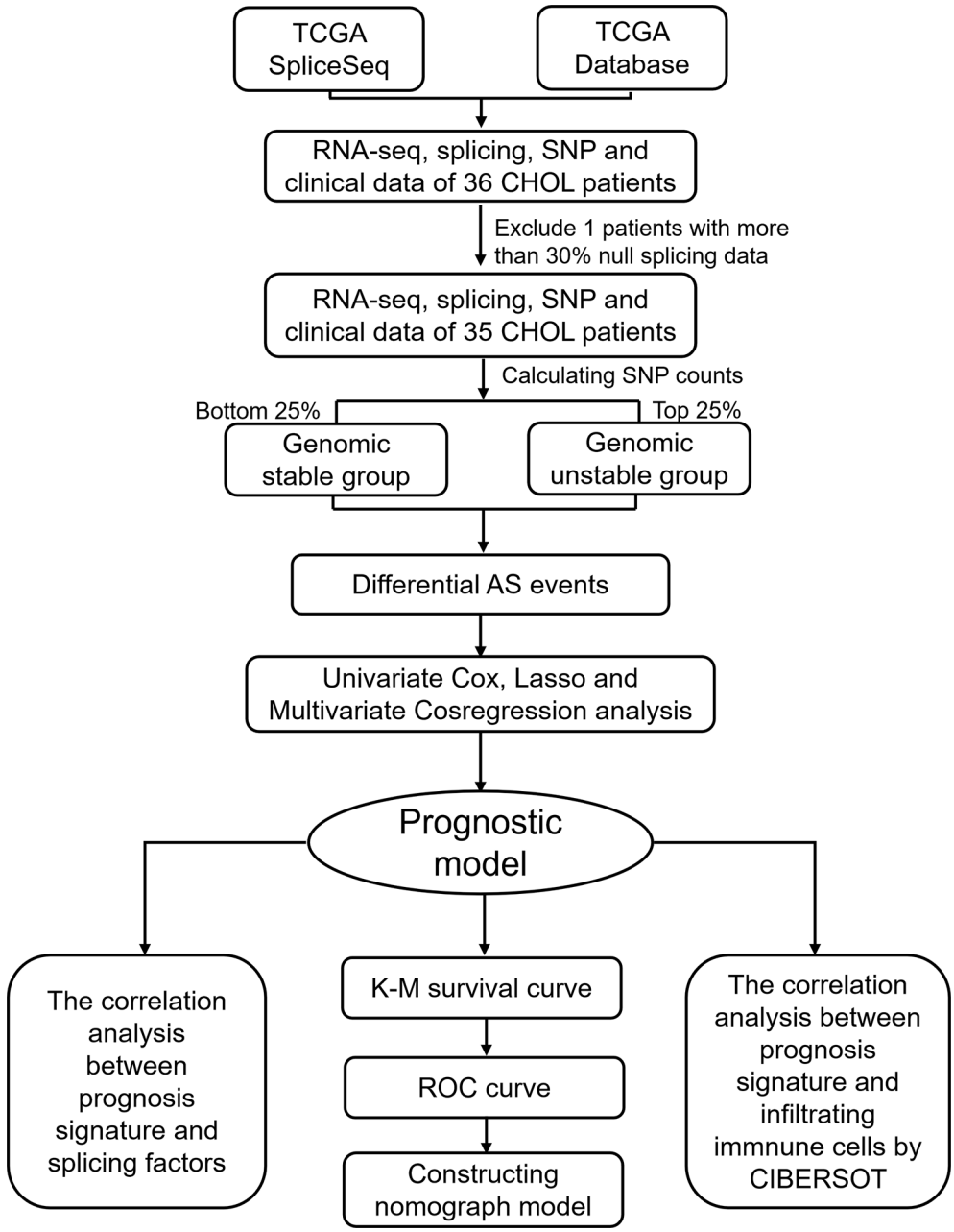

FIGURE 1 | Flow diagram of the approach used in this study.

Cox regression and Multivariate Cox regression were applied to calculate the hazard ratio (HR) of the high-risk score in OS.

Correlation Between Splicing Factors and Survival Associated AS Events

Information about 404 splicing factors was obtained from a previous study (15). The expression of splicing factors was obtained from TCGA database. Pearson correlation analysis was performed to assess the relationship between splicing factor expression and the PSI value of AS events. Splicing factors and AS events with $P < 0.05$ and correlation coefficient > 0.7 were selected for building correlation plots with Cytoscape 3.7.2.

Immune Cell Infiltration Analysis

CIBERSORT algorithm (http://cibersort.stanford.edu/), a computational framework providing immune cell type information from RNA profiles (16), was used to analyze the

infiltering immune cells in cholangiocarcinoma tissue. Twelve cases with CIBERSORT P values were selected for the further analysis. These cases were divided into high-risk (n = 4) and low-risk (n = 8) groups based on their risk scores. The differential immune cell types between high- and low-risk groups were identified using the vioplot package of R 4.0.3.

RESULTS

Clinical Characteristics and Integrated AS Events in Patients With Cholangiocarcinoma

The workflow of this study is shown in **Figure 1**. In total, 36 patients with cholangiocarcinoma were enrolled in this study from TCGA. The baseline characteristics of enrolled patients are listed in **Table 1**. We identified 2146 alternate acceptor (AA) events in 1639 genes, 1846 alternate donor (AD) events in 1406 genes, 4877 alternate promoter (AP) events in 2700 genes, 5204 alternate termination (AT) events in 2965 genes, 9480 exon skipping (ES) events in 4768 genes, 105 mutually exclusive exon (ME) events in 103 genes, and 1856 retained intron (RI) in 1303 genes (**Figure 2A**).

Identification of Genomic Instability Related AS Events in Patients With Cholangiocarcinoma

To identify genomic instability related AS events, the cumulative quantities of somatic mutations in each patient were calculated and sorted in descending order. The top 25% (n = 9) and bottom 25% (n = 9) of patients were assigned to GU-like and GS-like groups, respectively. Then the AS events in patients in GU-like and GS-like groups were compared to identify differential AS events. In total, 644 differential AS events, with P values < 0.05, were identified. A heat map of the top 40 differential AS events was constructed (**Figure 2B**). Genes involved in the differential AS events were enriched 10 Gene Ontology (GO) and 25 KEGG pathways (**Figures 2C, D**).

TABLE 1 | Characteristics of patients with cholangiocarcinoma from TCGA database.

Characteristics	No. of patients	%
Age		100.00
≥70	15	41.67
<70	21	58.33
Sex		100.00
Female	20	57.14
Male	26	74.29
Stage		100.00
I	19	54.29
II	9	25.71
III	1	2.86
IV	7	20.00
T category		100.00
T1	19	54.29
T2	12	34.29
T3	5	14.29
N category		100.00
N0	26	74.29
N1	5	14.29
unknown	5	14.29
M category		100.00
M0	28	80.00
M1	5	14.29
unknown	3	8.57

Construction of Survival-Associated AS Prognostic Model

Univariate cox regression analysis with P < 0.05 identified 26 AS events associated with cholangiocarcinoma progression (**Figures 3A, B**). Lasso regression analysis was performed on the 26 OS-related AS events to identify the events highly associated with cholangiocarcinoma (**Figures 3C, D**). Multivariate cox regression was applied to identify independent prognostic AS events. Finally, six AS events, SLC38A10-44114-AT, IL18BP-17488-RI, NBPF10-5531-ES, THNSL2-54469-ME, FAM3A-90629-ES, and KIAA1432-85794-AT, were identified as independent risk factors for OS in cholangiocarcinoma (**Figure 3E**). The risk score of each AS event was calculated (**Table 2**).

Validation of the Prognostic Signature in Patients With Cholangiocarcinoma

We validated the predictive capability and efficiency of the prognostic signature. The risk score distribution curve showed that patients with cholangiocarcinoma and higher risk score have shorter survival time (**Figures 4A, B**). K-M survival curve analysis verified that patients with higher risk scores had poorer OS, P < 0.05 (**Figure 4C**). ROC curve (AUC = 0.981) analysis was performed to validate the efficiency of the risk score in OS prediction (**Figure 4D**) and the univariate and multivariate Cox regression HR values for OS were 2.026 and 2.362, respectively (**Figures 5A, B**). Collectively, these data demonstrate that the risk score of cancer related AS can be used to predict OS in patients with cholangiocarcinoma. In addition, we constructed a nomograph model predicting 1-, 3-, and 5-year survival of patients with cholangiocarcinoma (**Figure 6**).

The Splicing Factors Regulating the Prognostic AS Events

Four AS events and 18 splicing factors were identified using a Pearson's correlation R value of > 0.7 and univariate cox regression P value of < 0.05 (**Figure 7**). Among these, SLC46A1-39899-ES, IARS-86836-ES, and ALDH1A3-32741-AT are upregulated AS events. The remained CDK10-38118-ES is a downregulated event.

HNRNPC is a core splicing factor that is positively correlated with down-regulated AS events. CCDC12, CLASRP, CLK4, RBM5, SEC31B, SRSF5, CIRBP, SNRNP70, ZRSR2, PPWD1, CLK1, CDK11A, NOSIP, U2AF1L4, RBM26, HNRNPC, HSPA1B, and CELF2 are core splicing factors that are negatively correlated with up regulated AS. We examined the

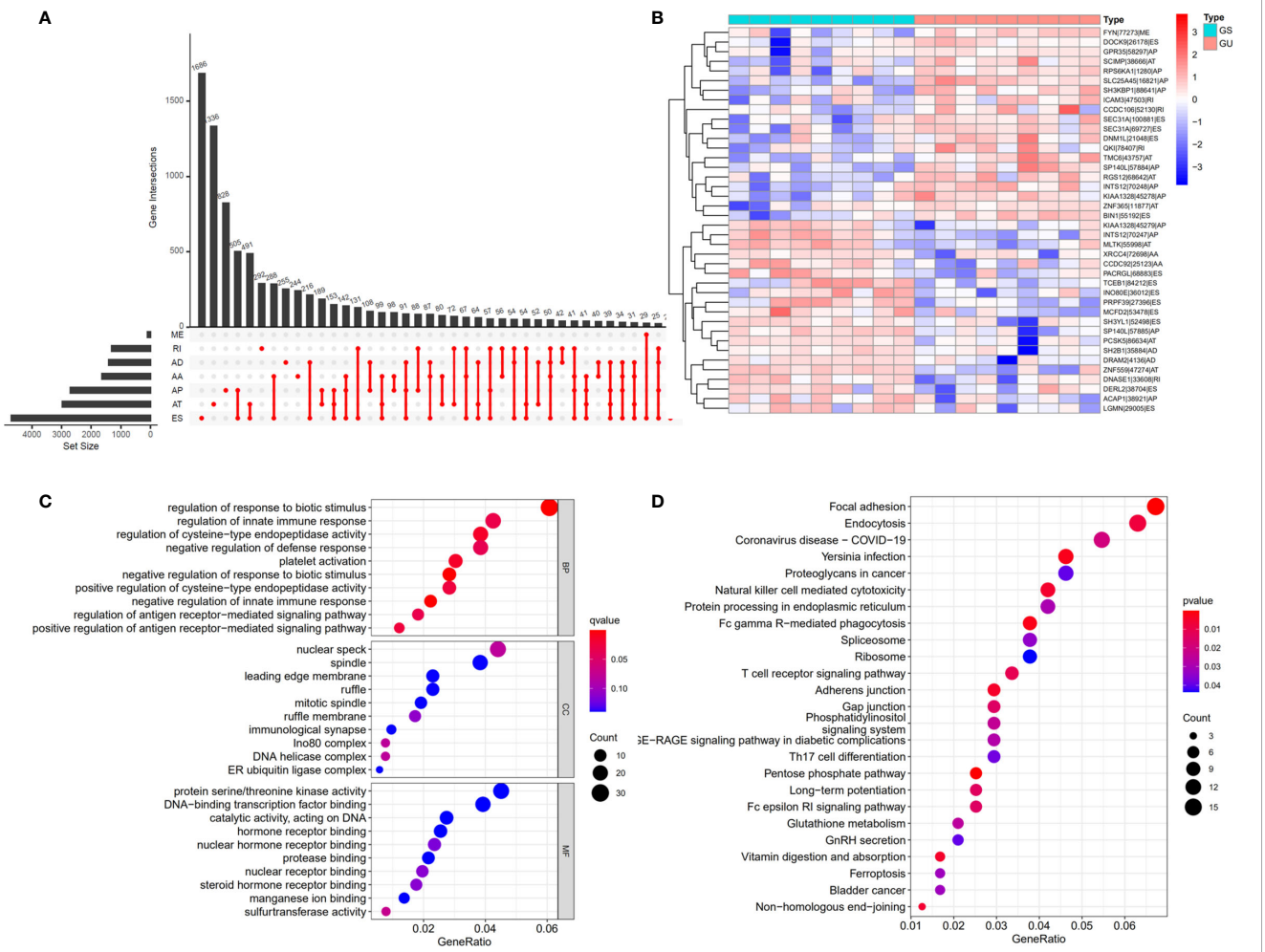

FIGURE 2 | Differential alternative splicing (AS) events between genomic stable (GS-like) and unstable (GU-like) patients. **(A)** AS events and related genes in cholangiocarcinoma patients. **(B)** Differential AS events between GU-like and GS-like groups. **(C)** Bubble graph showing GO analysis of differential AS events. **(D)** Bubble graph showing KEGG analysis of AS events.

relationship between these splicing factors and prognosis in patients with cholangiocarcinoma. Patients with higher CDK11A expression levels had higher disease-free survival rates (P = 0.023) than did patients with lower CDK11A expression levels. Patients with higher CIRBP expression levels had higher OS, but the associated P value is approaching insignificance (P=0.095, **Figure 8**).

Revealing the Relationship Between Prognostic Signature and Tumor-Infiltrating Immune Cells in Tumor Microenvironment

The tumor-infiltrating immune cells were identified with CIBERSORT. 12 patients were enrolled in this study with the P value of CIBERSORT < 0.05. The infiltrated immunes cells in cholangiocarcinoma are shown in **Figure 9A**. Among 22 kinds of immune cells, M2 macrophage are the main cell types that infiltrate in the cholangiocarcinoma tissue. Compared with low prognostic signature patients, high prognostic signature patients exhibited higher proportion of CD8+ T cells (**Figures 9B, C**). Additionally, the expression of PD-L1 is upregulated in patients with high AS risk score (**Figure 9D**).

DISCUSSION

The increasing incidence and poor outcomes for cholangiocarcinoma mean that biomarkers for diagnosis and therapy are urgently required. To the best of our knowledge, the biomarkers widely used in the clinic, including carcinoembryonic antigens (CEAs), CA-199, CA-242, and CA-

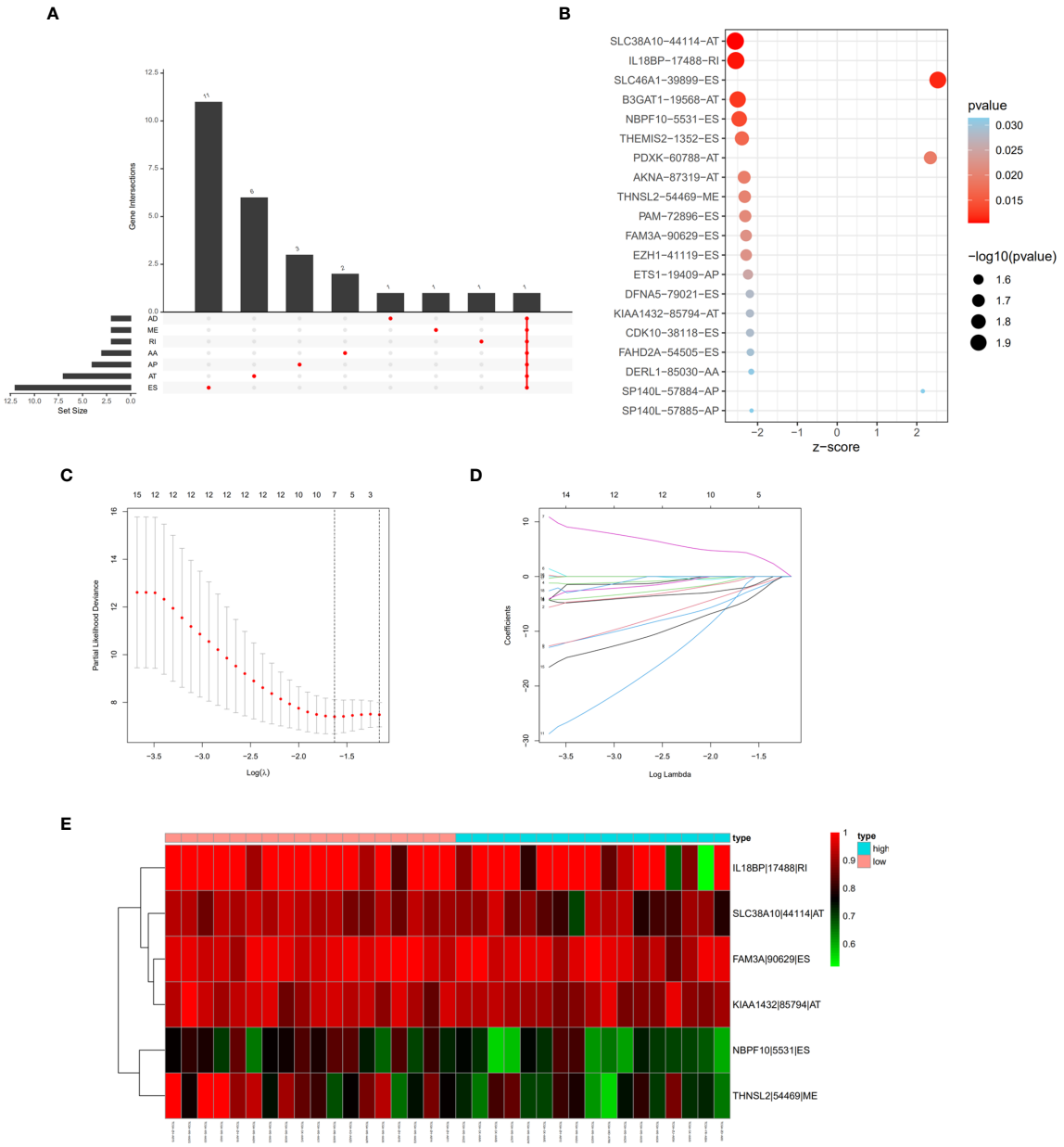

FIGURE 3 | Prognostic signature construction based on differential alternative splicing (AS) events between genomic stable (GS-like) and unstable (GU-like) groups. **(A)** Overall survival related AS events in patients with cholangiocarcinoma distinguished by alternate acceptor (AA), alternate donor (AD), alternate promoter (AP), alternate termination (AT), exon skipping (ES), mutually exclusive exon (ME), and retained intron (RI) splicing mode. **(B)** Bubble graph of overall survival related AS events in cholangiocarcinoma with P values and z-scores. **(C, D)** cvFit and lambda graph of the lasso regression model. **(E)** Heat map showed the expression of AS events enrolled in our prognosis model.

TABLE 2 | Multivariate cox model.

id	coef	HR	HR.95L	HR.95H	pvalue
SLC38A10-44114-AT	-15.32	2.23E-07	1.61E-12	0.031	0.011
IL18BP-17488-RI	-6.09	0.002	1.23E-05	0.422	0.022
NBPF10-5531-ES	-17.24	3.24E-08	2.23E-12	0	<0.001
THNSL2-54469-ME	-15.04	2.95E-07	3.19E-11	0.003	0.001
FAM3A-90629-ES	-33.3	3.47E-15	3.14E-24	0	0.002
KIAA1432-85794-AT	-29.78	1.16E-13	2.78E-23	0	0.008

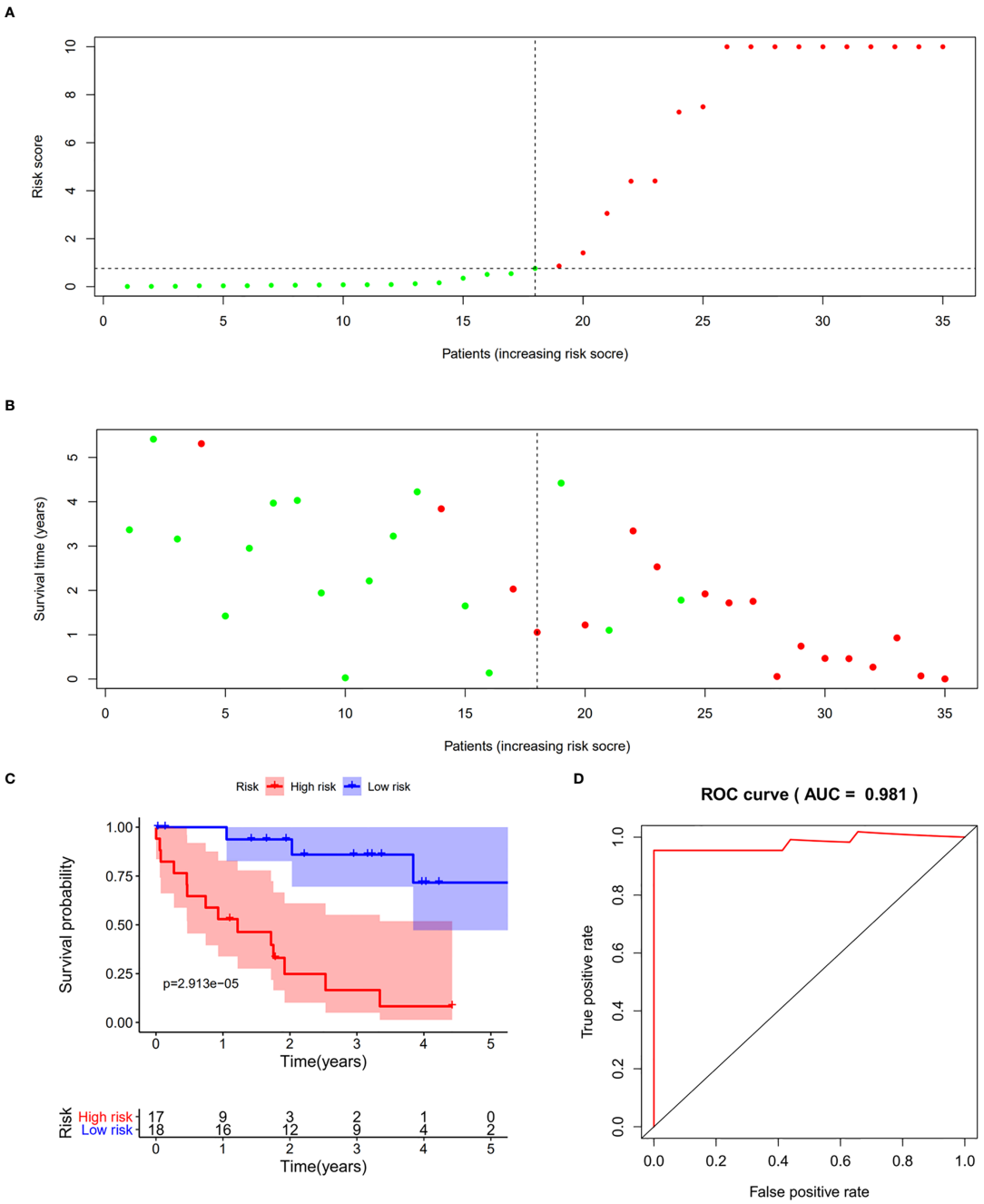

FIGURE 4 | Prognostic model validation. **(A, B)** Survival time and survival status of patients with different risk scores. **(C)** Survival curve of patients with high and low risk scores. **(D)** Receiver operating characteristic curve of the prognostic model.

50, have limited cholangiocarcinoma diagnostic and prognostic sensitivity and specify. The technical developments in sequencing techniques, have led to the wide clinical application of genetic diagnosis. Recently, transcriptome signatures have been applied to predict the outcome of cholangiocarcinoma. Wada Y and colleagues constructed a model based on 8 gene expression (BIRC5, CDC20, CDH2, CENPW, JPH1, MAD2L1, NEIL3, and POC1A), which predicts the recurrence of cholangiocarcinoma with AUC of ROC=0.92 (17). Xiaozai Xie and colleagues constructed a model predicting the overall survival of cholangiocarcinoma (AUC of ROC= 0.938) based on 5 lncRNA expression (18). In this study, we additionally provide an effective model based on genomic instability-related AS events for predicting OS with AUC of ROC curve of 0.981.

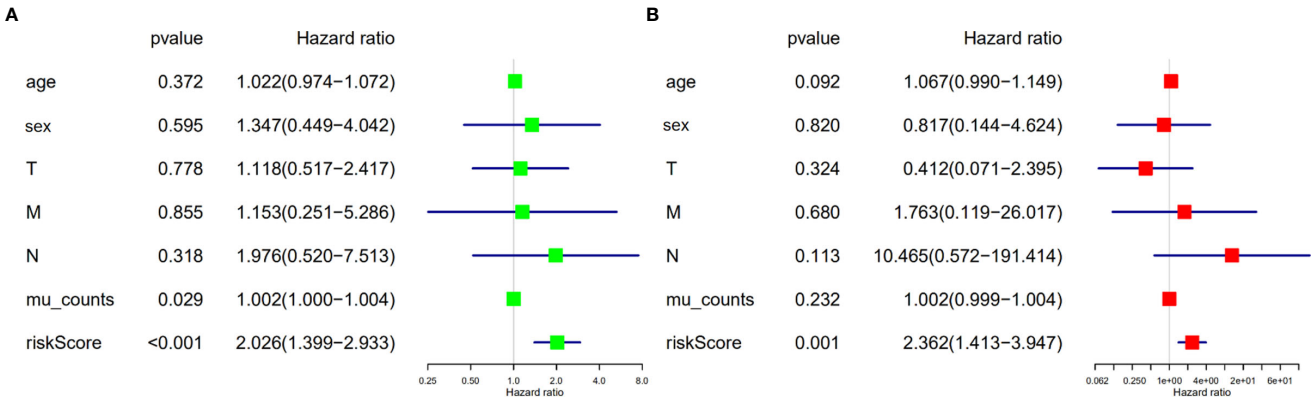

FIGURE 5 | Risk score is an independent risk factor for overall survival in patients with cholangiocarcinoma. **(A)** Forest plot of univariate cox regression. **(B)** Forest plot of multivariate cox regression.

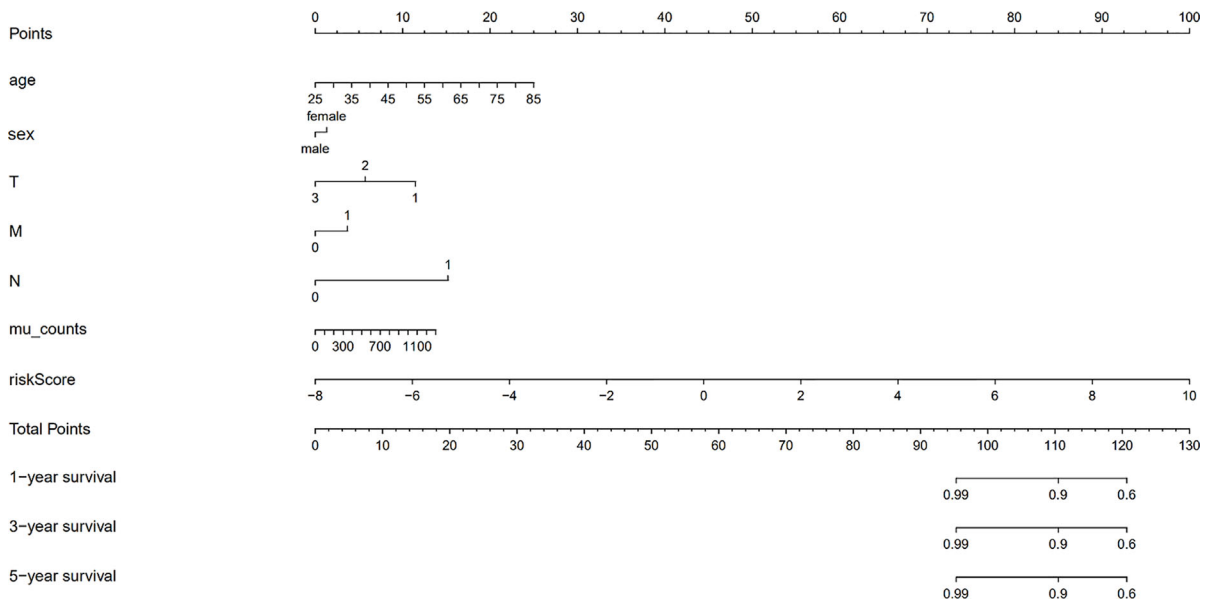

FIGURE 6 | The nomograph model predicting 1-, 3-, and 5-year survival in patients with cholangiocarcinoma based on age, sex, TMN stage, mutation counts, and risk score.

Genomic instability has been recognized a hallmark of carcinoma genesis. Recent studies have paid attentions to the role of genomic instability in the progression and recurrence indicating that the degree of genomic instability has prognostic implication. Although the molecular mechanisms of genomic instability remain unclear, previous studies have revealed that alternative splicing (AS) are associated with genomic instability (19). Some formula based on alternative splicing signature have been applied to quantify genomic instability degree (20). Recent studies have focused on the AS network, leading to the construction of prognostic signature models based on comprehensive AS events which suitable levels of predictivity and efficiency for carcinoma prognosis (21–23). Whether genomic instability-related AS events could effectively predict prognosis of cholangiocarcinoma remains unclear.

In the present study, we obtained single nucleotide polymorphism data of patients with cholangiocarcinoma from TCGA data sets. We identified differential AS events by comparing patients with genomic stability and those with genomic instability. Then, Univariate Cox regression analysis

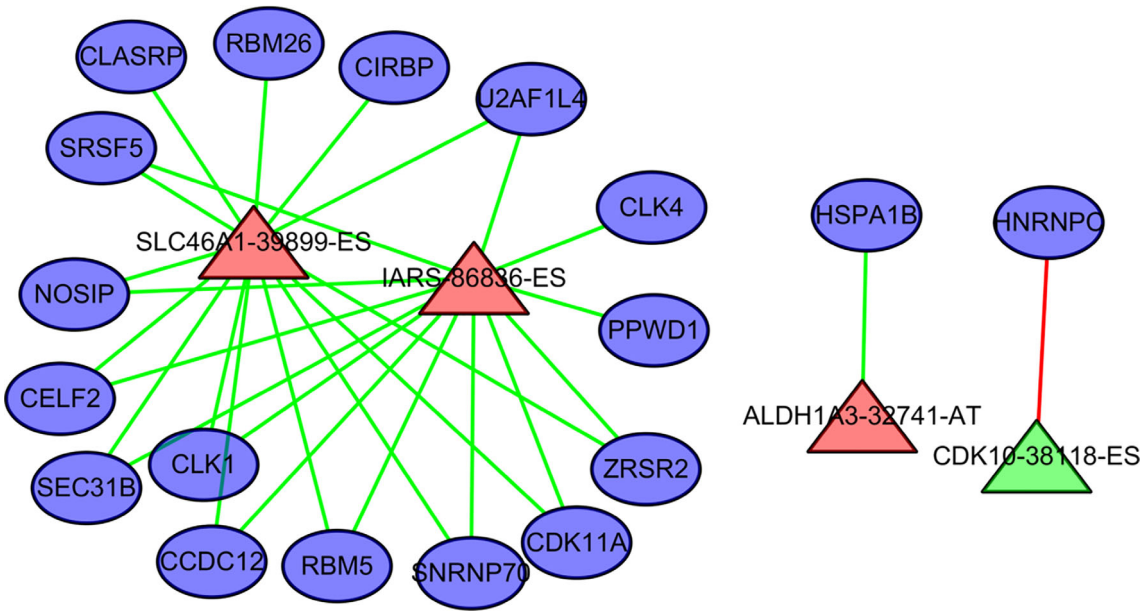

FIGURE 7 | The regulation relationship between alternative splicing (AS) events and splicing factors. The ovals represent splicing factors. The red triangles represent AS events associated with poor outcome in cholangiocarcinoma. Green triangles represent AS events negatively associated with poor outcome in cholangiocarcinoma. The lines between AS events and splicing factors represent the relationship between them. Red lines represent upregulation. Green lines represent downregulation.

revealed 26 differential AS events that were associated with the OS in cholangiocarcinoma. K-M survival and ROC analyses showed that this model has robust sensitivity and specify for predicting OS in patients with cholangiocarcinoma. However, a study using a larger cohort is needed to verify the efficiency of our model.

In our prognostic model, we identified the key roles of SLC46A1 and IARS AS in predicting the OS in patients with cholangiocarcinoma. SLC46A1 belongs to solute carrier family and participates in the import of heme folate. Previous studies show that SLC46A1 is abundant in the liver and is responsible for iron metabolism (24). Consistent with our results, Hlavac and colleagues found that SLC46A1 variants are associated with ERBB2/HER2 status and disease-free survival in hormonally treated patients with breast carcinoma (25). The underlying mechanism by which SLC46A1 variants affect cholangiocarcinoma prognosis requires further research.

Isoleucine-tRNA synthetase (IARS) is responsible for aminoacyl tRNA biosynthesis, which plays an essential role in protein translation. Recently, the IARS deficiency has been associated with human disease (26, 27). Hsu and colleagues found that IARS expression is upregulated in oral cavity squamous cell carcinoma (28). Additionally, our results show that IARS-86836-ES variants are associated with poor OS in patients with cholangiocarcinoma. The mechanism underlying this may be associated with insufficient aminoacylation activity to meet translational demand in tumor cells (29).

We then tried to explore the upstream regulators of prognosis associated AS events. Differential expression and hotspot mutations of splicing factor genes have recently been reported in numerous malignancies, suggesting the importance of splicing factors in cancer development and progression. Pearson correlation analysis revealed that CCDC12, CLASRP, CLK4, RBM5, SEC31B, SRSF5, CIRBP, SNRNP70, ZRSR2, PPWD1, CLK1, CDK11A, NOSIP, U2AF1L4, RBM26, HNRNPC, HSPA1B, and CELF2 negatively regulate prognosis associated AS events. Additionally, patients with cholangiocarcinoma were divided into high- and low-expression groups based on splicing factor expression. K-M survival curve analysis revealed that patients with high CDK11A expression levels had higher disease-free survival rates. Consistently, previously studies have reported the tumor-promoting anti-cancer effects of CDK11A (30, 31). Liu and colleagues also found that CDK11A upregulation suppresses cellular proliferation by inducing cell cycle arrest (32).

Recently, immune therapy has emerged as a promising treatment strategy for solid tumors. We summarized previous reported transcriptome signatures related to the change of immune microenvironment in cholangiocarcinoma (**Supplement Table 1**). Michele Ghidini and colleagues have revealed the characterization of the immune-related transcriptome in cholangiocarcinoma (33). They found that high CTLA4 expression, representing the enrichment of Treg cells, in adjacent tissue is associated with the poor recurrence free survival of cholangiocarcinoma. In addition to their study, we analyzed difference of infiltrated immune cells in patients with different alternative splicing signature. We found that the proportion of CD8+ T cells is upregulated in carcinoma tissue of

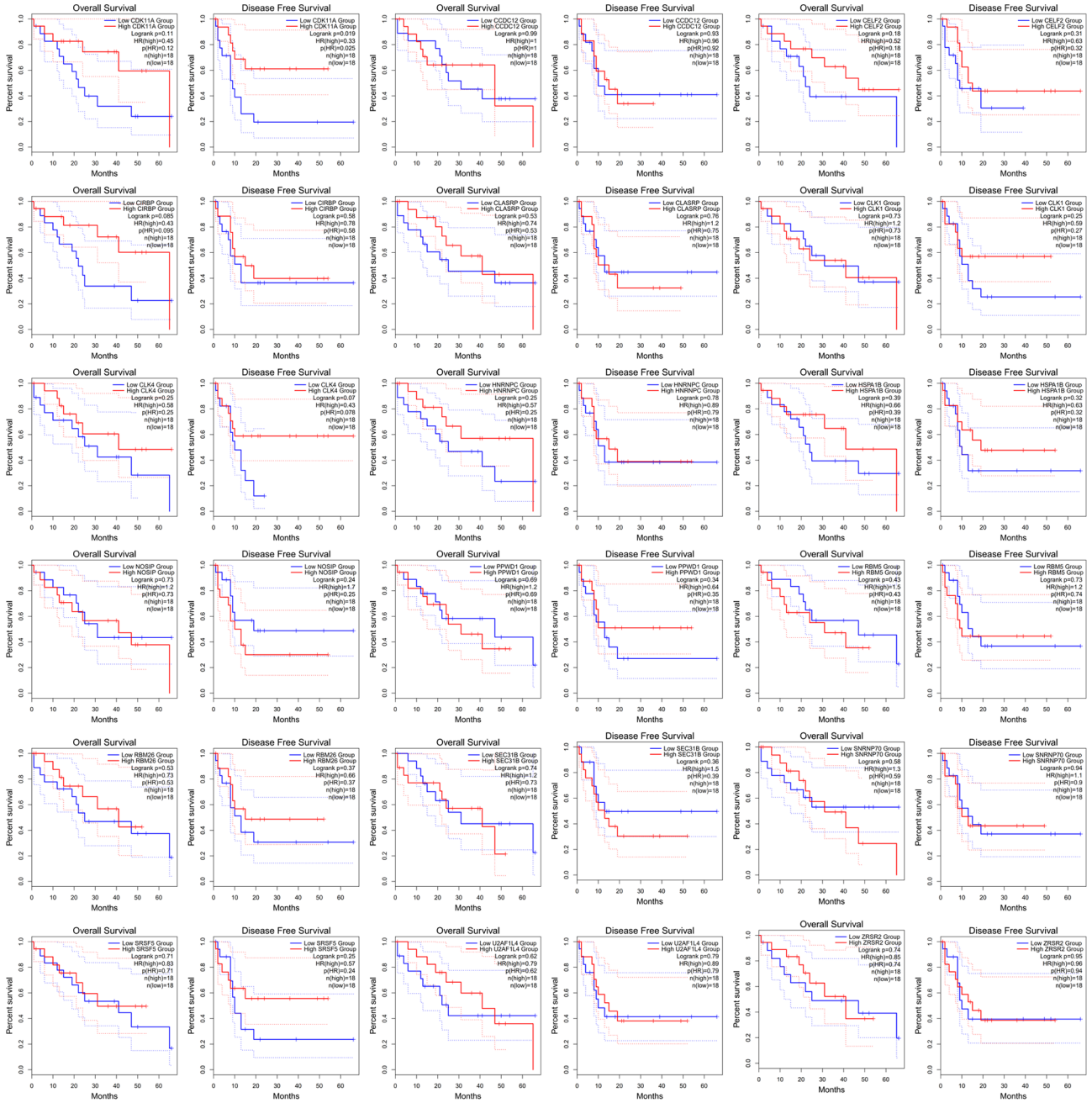

FIGURE 8 | The receiver operating characteristic curve of alternative splicing (AS) signature related splicing factors in overall survival and disease-free survival in patients with cholangiocarcinoma.

patients with higher splicing signature scores. Ying Zhu and colleagues found that INF-γ secretion by CD8+ T cells may increase cancer cell PD-L1 expression (34). Upregulated PD-L1 on cancer cells has been recognized as a marker of immune escape and poor outcome in patients with cholangiocarcinoma (35). Consistent with this, we found higher levels of PD-L1 expression in the high-risk group. Therefore, the high-risk group may more effectively respond to anti-PD-L1/PD-1 therapy. Finally, we also produced a nomograph model for predicting 1-, 3-, and 5-year survival in patients with cholangiocarcinoma based on age, sex, TMN stage, mutation counts, and risk score.

In conclusion, we have developed a prognostic signature for OS in patients with cholangiocarcinoma based on cancer

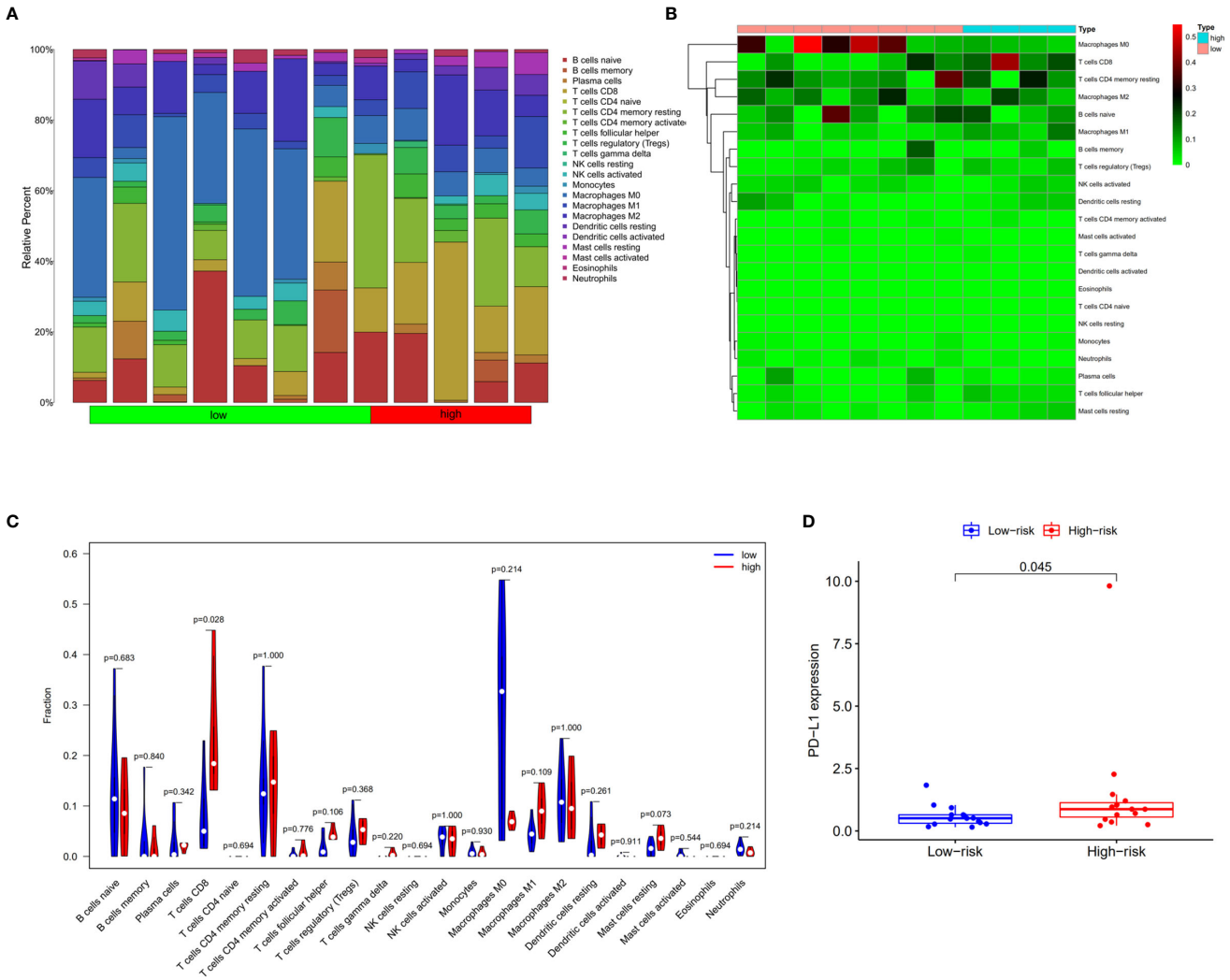

FIGURE 9 | Infiltrating immune cells in cholangiocarcinoma. **(A)** Bar plot showing the proportion of 22 kinds of immune cells in patients with CIBERSORT value < 0.05. **(B)** Heat map showing the proportion of 22 types of immune cells in high- and low-risk groups. **(C)** Violoplot showing the compression of each immune cell type between high- and low-risk groups. **(D)** Bar plot of PD-L1 expression in high- and low-risk groups.

pathway-related AS events. Additionally, AS events SLC46A1-39899-ES, IARS-86836-ES, and the CDK11A splicing factor may be therapeutic targets for cholangiocarcinoma. Anti-PD-L1/PD-1 immunotherapy may be a promising therapeutic strategy for patients with cholangiocarcinoma and high-risk scores. However, the small sample size used in this study means that our results require further external examination.

DATA AVAILABILITY STATEMENT

The datasets presented in this study can be found in online repositories. The names of the repository/repositories and accession number(s) can be found in the article/supplementary material.

AUTHOR CONTRIBUTIONS

ZZ designed the study and wrote the manuscript. ZL collected data and completed the data analysis. GZ and JH wrote the R script. JG and LZ guided the study and checked the data. All authors contributed to the article and approved the submitted version.

FUNDING

This study was funded by the National Natural Science Foundation of China (Grant NO.81970510), Talent Project of Chongqing (CQYC2019050790), and the Graduate Student Innovation Project of Chongqing (Grant number: CYB20153).

ACKNOWLEDGMENTS

We acknowledge the TCGA and TCGAspliceSeq for the transcriptomics, simple nucleotide variation, clinical phenotype, and splicing data. We acknowledge Chan Qiu for his assistance in writing the R script.

SUPPLEMENTARY MATERIAL

The Supplementary Material for this article can be found online at: https://www.frontiersin.org/articles/10.3389/fonc.2021.666847/full#supplementary-material

REFERENCES

1. Munoz-Garrido P, Rodrigues PM. The Jigsaw of Dual Hepatocellular-Intrahepatic Cholangiocarcinoma Tumours. *Nat Rev Gastroenterol Hepatol* (2019) 16(11):653–5. doi: 10.1038/s41575-019-0185-z
2. Banales JM, Marin JJG, Lamarca A, Rodrigues PM, Khan SA, Roberts LR, et al. Cholangiocarcinoma 2020: The Next Horizon in Mechanisms and Management. *Nat Rev Gastroenterol Hepatol* (2020) 17(9):557–88. doi: 10.1038/s41575-020-0310-z
3. Bertuccio P, Malvezzi M, Carioli G, Hashim D, Boffetta P, El-Serag HB, et al. Global Trends in Mortality From Intrahepatic and Extrahepatic Cholangiocarcinoma. *J Hepatol* (2019) 71(1):104–14. doi: 10.1016/j.jhep.2019.03.013
4. Negrini S, Gorgoulis VG, Halazonetis TD. Genomic Instability–an Evolving Hallmark of Cancer. *Nat Rev Mol Cell Biol* (2010) 11(3):220–8. doi: 10.1038/nrm2858
5. Suzuki K, Ohnami S, Tanabe C, Sasaki H, Yasuda J, Katai H, et al. The Genomic Damage Estimated by Arbitrarily Primed PCR DNA Fingerprinting is Useful for the Prognosis of Gastric Cancer. *Gastroenterol* (2003) 125 (5):1330–40. doi: 10.1016/j.gastro.2003.07.006
6. Wang Y, Hong Y, Li M, Long J, Zhao YP, Zhang JX, et al. Mutation Inactivation of Nijmegen Breakage Syndrome Gene (NBS1) in Hepatocellular Carcinoma and Intrahepatic Cholangiocarcinoma. *PloS One* (2013) 8(12):e82426. doi: 10.1371/journal.pone.0082426
7. Bao S, Zhao H, Yuan J, Fan D, Zhang Z, Su J, et al. Computational Identification of Mutator-Derived lncRNA Signatures of Genome Instability for Improving the Clinical Outcome of Cancers: A Case Study in Breast Cancer. *Briefings Bioinf* (2020) 21(5):1742–55. doi: 10.1093/bib/bbz118
8. Blencowe BJ. Alternative Splicing: New Insights From Global Analyses. *Cell* (2006) 126(1):37–47. doi: 10.1016/j.cell.2006.06.023
9. Sebestyen E, Zawisza M, Eyras E. Detection of Recurrent Alternative Splicing Switches in Tumor Samples Reveals Novel Signatures of Cancer. *Nucleic Acids Res* (2015) 43(3):1345–56. doi: 10.1093/nar/gku1392
10. Thanee M, Loilome W, Techasen A, Sugihara E, Okazaki S, Abe S, et al. CD44 Variant-Dependent Redox Status Regulation in Liver Fluke-Associated Cholangiocarcinoma: A Target for Cholangiocarcinoma Treatment. *Cancer Sci* (2016) 107(7):991–1000. doi: 10.1111/cas.12967
11. Yosudjai J, Wongkham S, Jirawatnotai S, Kaewkong W. Aberrant mRNA Splicing Generates Oncogenic RNA Isoforms and Contributes to the Development and Progression of Cholangiocarcinoma. *Biomed Rep* (2019) 10(3):147–55. doi: 10.3892/br.2019.1188
12. Yao J, Caballero OL, Huang Y, Lin C, Rimoldi D, Behren A, et al. Altered Expression and Splicing of ESRP1 in Malignant Melanoma Correlates With Epithelial-Mesenchymal Status and Tumor-Associated Immune Cytolytic Activity. *Cancer Immunol Res* (2016) 4(6):552–61. doi: 10.1158/2326-6066.CIR-15-0255
13. Kim EK, Yoon SO, Jung WY, Lee H, Kang Y, Jang YJ, et al. Implications of NOVA1 Suppression Within the Microenvironment of Gastric Cancer: Association With Immune Cell Dysregulation. *Gastric Cancer Off J Int Gastric Cancer Assoc Japanese Gastric Cancer Assoc* (2017) 20(3):438–47. doi: 10.1007/s10120-016-0623-3
14. Tan DSW, Chong FT, Leong HS, Toh SY, Lau DP, Kwang XL, et al. Long Noncoding RNA Egfr-AS1 Mediates Epidermal Growth Factor Receptor Addiction and Modulates Treatment Response in Squamous Cell Carcinoma. *Nat Med* (2017) 23(10):1167–75. doi: 10.1038/nm.4401
15. Seiler M, Peng S, Agrawal AA, Palacino J, Teng T, Zhu P, et al. Somatic Mutational Landscape of Splicing Factor Genes and Their Functional Consequences Across 33 Cancer Types. *Cell Rep* (2018) 23(1):282–96.e4. doi: 10.1016/j.celrep.2018.01.088
16. Newman AM, Liu CL, Green MR, Gentles AJ, Feng W, Xu Y, et al. Robust Enumeration of Cell Subsets From Tissue Expression Profiles. *Nat Methods* (2015) 12(5):453–7. doi: 10.1038/nmeth.3337
17. Wada Y, Shimada M, Yamamura K, Toshima T, Banwait JK, Morine Y, et al. A Transcriptomic Signature for Risk-Stratification and Recurrence Prediction in Intrahepatic Cholangiocarcinoma. *Hepatol* (2021). doi: 10.1002/hep.31803
18. Xie X, Wang Y, Zhang S, Li J, Yu Z, Ding X, et al. A Novel five-lncRNA Signature Panel Improves High-Risk Survival Prediction in Patients With Cholangiocarcinoma. *Aging* (2021) 13(2):2959–81. doi: 10.18632/aging.202446
19. Shkreta L, Chabot B. The RNA Splicing Response to DNA Damage. *Biomolecules* (2015) 5(4):2935–77. doi: 10.3390/biom5042935
20. Cahill K. Alternative Splicing and Genomic Stability. *Phys Biol* (2004) 1(1-2): C1–4. doi: 10.1088/1478-3967/1/2/C01
21. Liu Y, Jia W, Li J, Zhu H, Yu J. Identification of Survival-Associated Alternative Splicing Signatures in Lung Squamous Cell Carcinoma. *Front Oncol* (2020) 10:587343. doi: 10.3389/fonc.2020.587343
22. Suh YS, Na D, Lee JS, Chae J, Kim E, Jang G, et al. Comprehensive Molecular Characterization of Adenocarcinoma of the Gastroesophageal Junction Between Esophageal and Gastric Adenocarcinomas. *Ann Surg* (2020). doi: 10.1097/SLA.0000000000004303
23. Zhao Z, Li GZ, Liu YQ, Huang RY, Wang KY, Jiang HY, et al. Characterization and Prognostic Significance of Alternative Splicing Events in Lower-Grade Diffuse Gliomas. *J Cell Mol Med* (2020) 24(22):13171–80. doi: 10.1111/jcmm.15924
24. Li H, Wang D, Wu H, Shen H, Lv D, Zhang Y, et al. SLC46A1 Contributes to Hepatic Iron Metabolism by Importing Heme in Hepatocytes. *Metabolism: Clin Exp* (2020) 110:154306. doi: 10.1016/j.metabol.2020.154306
25. Hlavac V, Vaclavikova R, Brynychova V, Dvorak P, Elsnerova K, Kozevnikovova R, et al. Slc46a1 Haplotype With Predicted Functional Impact has Prognostic Value in Breast Carcinoma. *Mol diagnosis Ther* (2021) 25:99–110. doi: 10.1007/s40291-020-00506-2
26. Orenstein N, Weiss K, Oprescu S, Shapira R, Kidron D, Vanagaite-Basel L, et al. Bi-Allelic IARS Mutations in a Child With Intra-Uterine Growth Retardation, Neonatal Cholestasis, and Mild Developmental Delay. *Clin Genet* (2017) 91(6):913–7. doi: 10.1111/cge.12930
27. Kopajtich R, Murayama K, Janecke A, Haack T, Breuer M, Knisely A, et al. Biallelic IARS Mutations Cause Growth Retardation With Prenatal Onset, Intellectual Disability, Muscular Hypotonia, and Infantile Hepatopathy. *Am J Hum Genet* (2016) 99(2):414–22. doi: 10.1016/j.ajhg.2016.05.027
28. Hsu C, Chang K, Huang Y, Liu H, Hsueh P, Gu P, et al. Proteomic Profiling of Paired Interstitial Fluids Reveals Dysregulated Pathways and Salivary NID1 as a Biomarker of Oral Cavity Squamous Cell Carcinoma. *Mol Cell Proteomics MCP* (2019) 18(10):1939–49. doi: 10.1074/mcp.RA119.001654
29. Fuchs S, Schene I, Kok G, Jansen J, Nikkels P, van Gassen K, et al. Aminoacyl-tRNA Synthetase Deficiencies in Search of Common Themes. *Genet Med Off J Am Coll Med Genet* (2019) 21(2):319–30. doi: 10.1038/s41436-018-0048-y
30. Sotgia F, Fiorillo M, Lisanti MP. Hallmarks of the Cancer Cell of Origin: Comparisons With "Energetic" Cancer Stem Cells (E-Cscs). *Aging* (2019) 11 (3):1065–8. doi: 10.18632/aging.101822
31. Zhou QH, Deng CZ, Li ZS, Chen JP, Yao K, Huang KB, et al. Molecular Characterization and Integrative Genomic Analysis of a Panel of Newly Established Penile Cancer Cell Lines. *Cell Death Dis* (2018) 9(6):684. doi: 10.1038/s41419-018-0736-1
32. Liu T, Wu Y, Dong X, Pan C, Du G, Yang J, et al. Identification and Characterization of the BmCyclin L1-BmCDK11A/B Complex in Relation to Cell Cycle Regulation. *Cell Cycle (Georgetown Tex)* (2017) 16(9):861–8. doi: 10.1080/15384101.2017.1304339
33. Ghidini M, Cascione L, Carotenuto P, Lampis A, Trevisani F, Previdi MC, et al. Characterisation of the Immune-Related Transcriptome in Resected Biliary Tract Cancers. *Eur J Cancer* (2017) 86:158–65. doi: 10.1016/j.ejca.2017.09.005
34. Zhu Y, Wang X, Zhang Y, Xu D, Dong J, Zhang Z, et al. Programmed Death Ligand 1 Expression in Human Intrahepatic Cholangiocarcinoma and its Association With Prognosis and CD8 T-Cell Immune Responses. *Cancer Manage Res* (2018) 10:4113–23. doi: 10.2147/cmar.s172719

35. Wu H, Wei Y, Jian M, Lu H, Song Q, Hao L, et al. Clinicopathological and Prognostic Significance of Immunoscore and PD-L1 in Intrahepatic Cholangiocarcinoma. *OncoTargets Ther* (2021) 14:39–51. doi: 10.2147/ott.s288982

Conflict of Interest: The authors declare that the research was conducted in the absence of any commercial or financial relationships that could be construed as a potential conflict of interest.

frontiers in Oncology

ORIGINAL RESEARCH
published: 28 May 2021
doi: 10.3389/fonc.2021.625720

Metastasis Patterns and Prognosis of Elderly Patients With Esophageal Adenocarcinoma in Stage IVB: A Population-Based Study

Guanghao Qiu[†], *Hanlu Zhang*[†], *Fuqiang Wang*, *Yu Zheng*, *Zihao Wang* and *Yun Wang*[*]

Department of Thoracic Surgery, West China Hospital, Sichuan University, Chengdu, China

Background: Esophageal adenocarcinoma (EAC) is the most common kind of esophageal cancer. Age at diagnosis of advanced EAC is greater. Studies about practice patterns for elderly EAC patients with distant metastasis (DM) in stage IVB are limited. This retrospective, population-based study was conducted using data from the Surveillance, Epidemiology, and End Results (SEER) to evaluate 855 elderly EAC patients with DM in stage IVB from 2010 to 2015.

Methods: 855 elderly EAC patients with DM in stage IVB between 2010 and 2015 were included in this study. Univariate and multivariate Cox-regression and Kaplan-Meier analyses were used to assess prognosis. These patients were classified to bone-only, brain-only, lung-only, liver-only, and multiple (patients with two or more organs in metastasis)-site group according to the site of metastasis. Overall survival (OS), cancer-specific survival (CSS), median survival time (MST), and survival rate (SR) were evaluated to analyze the survival outcomes.

Results: The most common metastasis site was the liver among the single-organ metastasis population, followed by lung, bone, and brain. Compared with the bone-only group, the multiple-site group was associated with worst OS (HR: 1.037, 95% CI: 0.811–1.327, $p = 0.770$) and CSS (HR: 1.052, 95% CI: 0.816–1.357, $p = 0.695$). The multiple-site group also had the lowest MST in the population (MST: 2 months in OS and 3 months in CSS) and SR (6-month SR: 27.1% in OS, 29.9% in CSS, 1-year SR: 10.7% in OS, 12.0% in CSS, 3-year SR: 2.5% in OS, 2.8% in CSS). Compared to untreated patients (N) in the total population, other patients who were treated with surgery (S), radiotherapy (R), and chemotherapy (C) are beneficial for the prognosis (OS and CSS: $p < 0.001$).

Conclusion: This population-based study was conducted to ascertain metastasis patterns and survival outcomes of EAC patients with DM in stage IVB. Elderly patients with multiple-site metastasis exhibited the worst OS and CSS among all the populations, and patients with bone-only metastasis had the worst OS and CSS among single-organ metastasis populations. Active treatment is beneficial for elderly EAC patients with DM in stage IVB, especially chemotherapy. This study also shows that more than one third of the patients had not received any therapy.

Keywords: esophageal adenocarcinoma, elderly patients, treatment, metastasis, prognosis, chemotherapy, radiotherapy, surgery

OPEN ACCESS

Edited by:
Rui Liao,
First Affiliated Hospital of Chongqing Medical University, China

Reviewed by:
Xiangning Meng,
Harbin Medical University, China
Signe Friesland,
Karolinska University Hospital, Sweden

***Correspondence:**
Yun Wang
yunwwang@yeah.net

[†]*These authors have contributed equally to this work*

Specialty section:
This article was submitted to Gastrointestinal Cancers, a section of the journal Frontiers in Oncology

Received: *08 December 2020*
Accepted: *30 April 2021*
Published: *28 May 2021*

Citation:
Qiu G, Zhang H, Wang F, Zheng Y, Wang Z and Wang Y (2021) Metastasis Patterns and Prognosis of Elderly Patients With Esophageal Adenocarcinoma in Stage IVB: A Population-Based Study. Front. Oncol. 11:625720. doi: 10.3389/fonc.2021.625720

INTRODUCTION

Esophageal cancer (EC) is the seventh leading cause of cancer-related mortality in America, the sixth leading cause of cancer-related mortality worldwide, and its incidence continues to increase (1, 2). According to the incidence data of EC extracted from 12 countries, the number of EAC cases is expected to increase rapidly from 2005 to 2030, while the incidence of esophageal squamous cell carcinoma (ESCC) will continue to decline (3). The GBD 2017 Esophageal Cancer Collaborators estimated that there were approximately 473,000 new cases of EC all over the world in 2017 (age-standardized incidence of EC was 5.9 per 100,000 population) and 436,000 deaths (age-standardized mortality of EC was 5.5 per 100,000 population) (4).

With the extension of human life expectancy, the number of elderly EC patients will increase significantly in the future. According to the website of Cancer Research UK, more than 57% of EC patients were over 70 years old (5). Yuan Zeng et al. showed that, among people suffering from EC, compared with patients under 70 years of age, patients over 70 had distinctive clinical characteristics and inferior survival rate (6). There were also many studies of EC patients over 70, which proved that age alone was not a contraindication for surgery and neo-adjuvant chemo-radiotherapy made sense in treating EC patients over 70 (7, 8); however, there are no relevant studies on elderly EC patients with distant metastasis (DM) in stage IVB. Many causes can lead to death in patients with EC, including nutritional disorders, cachexia, local invasion of large blood vessels, *etc.*, but clinical studies indicated that DM was the most common cause of death (9): because the prognosis of patients with EC is poor and more than 50% of patients have lymph node or distant organ metastasis at first diagnosis, it is important to understand the metastasis pattern and prognosis of elderly EC patients with DM (9, 10).

To analyze DM patterns and prognosis of different metastasis groups in a large cohort of the elderly EAC population, we undertook this study by using the SEER database. As many studies on elderly patients use 70 years as the age threshold to define the elderly cohort (11–16), based on site of metastasis, patients were divided into bone-only group, brain-only group, lung-only group, liver-only group, and a multiple-site group. We compared both OS and CSS of these groups with metastasis to different single organs or a combination of multiple organs. Other clinicopathological parameters such as gender, race, grade, T stage, N stage, site of EAC, and treatment were included.

MATERIALS AND METHODS

Data Collection

The SEER 18-Registry custom data (with additional treatment fields, 1975 to 2016, data set submitted in November 2018) of the NCI were analyzed. The eligibility criteria included the following: (1) age ≥ 70 years; (2) Histology codes 8140-8211, 8255-8490, and 8574 were used to define EAC; (3) The primary site codes C15.0 (cervical esophagus) and C15.3 (upper third of the esophagus), C15.4 (middle third of the esophagus), C15.2 (abdominal esophagus), and C15.5 (lower third of the esophagus) were defined as the upper esophagus, middle esophagus, and lower esophagus, respectively. (4) Patients in stage IVB (since the SEER program included data pertaining to four site-specific distant metastases. Exclusion criteria included the following: (1) the values "histologically confirmed positive" were selected to exclude those without histological diagnosis; (2) the values "complete dates are available and there are 0 days of survival" and "complete dates are available and there are more than 0 days of survival" were selected to exclude those without survival data; (3) the values "active follow-up" were selected to exclude those without follow-up data. The flowchart demonstrates the patient selection from SEER database (**Figure 1**).

Statistical Analysis

Based on site of metastasis, patients were divided into bone-only, brain-only, lung-only, liver-only, and a multiple-site group. Clinical and demographic characteristics were compared for patients of different metastasis groups using Pearson's chi-squared test statistics for categorical variables. We did the Kaplan-Meier survival curves by the log-rank test, which was used to analyze the differences between the curves. Univariate and multivariate Cox regression analyses were applied to evaluate the prognostic effects of the overall survival (OS) and esophageal cancer-specific survival (CSS). SPSS 25 (IBM Corp., Armonk, NY, USA) and GraphPad Prism 8.0 (GraphPad Software, San Diego, CA, USA) were used in later statistical analysis. Two-tailed *P* values less than 0.05 were deemed statistically significant.

RESULTS

Demographics

According to the eligibility criteria, 855 elderly EAC patients with DM in stage IVB diagnosed between 2010 and 2015 were included, as the SEER database did not record the information about site-specific metastasis before 2010. The baseline characteristics are displayed in **Table 1**. **Table 1** summarizes the demographic and characteristics of the 855 patients, among which, 733 (85.7%) patients were male; 808 (94.5%) patients were Caucasian. The scales of patients with different patterns of metastasis are summarized in **Table 1**. The most common metastasis site was the liver (40.9%), followed by lung (12.7%), bone (12.0%), and brain (2.8%). The group with multiple metastatic sites had 269 (31.5%) patients. 793 (92.7%) patients had the original tumor located in the lower third of the esophagus. 246 (28.8%) patients had chemotherapy alone, followed by surgery (S) and/or radiotherapy (R) + chemotherapy (C) 189 (22.1%) and surgery and/or radiotherapy 113 (13.2%). Surprisingly, 307 (35.9%) patients (the "N" group in **Tables 1**–**3**) had not received any treatment.

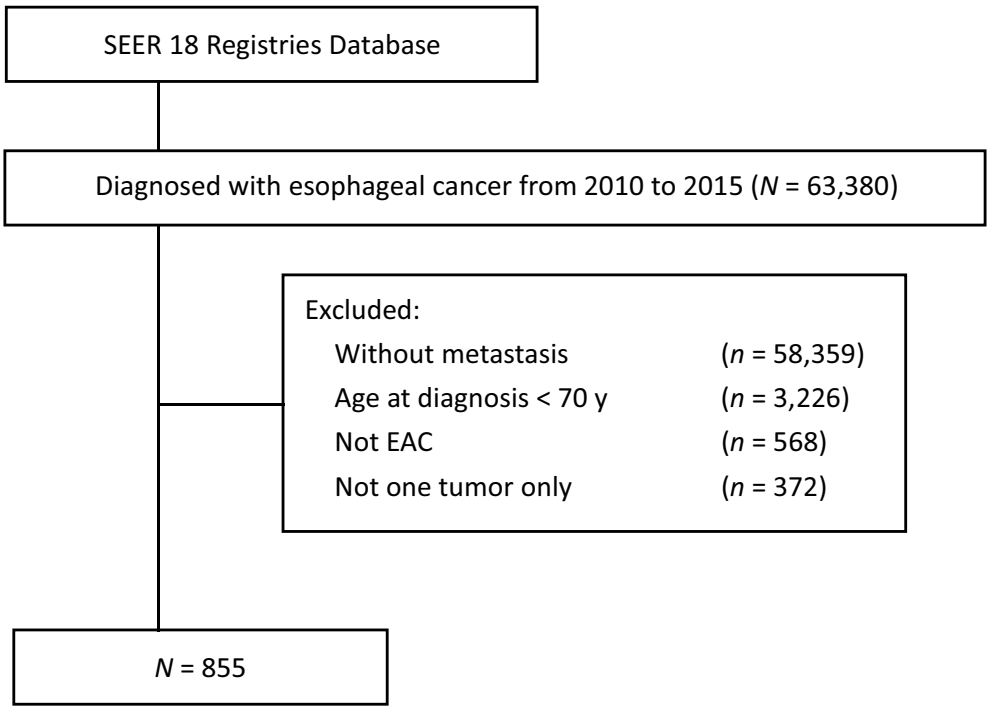

FIGURE 1 | Flowchart of patient selection from SEER database (2010–2015). SEER, surveillance, epidemiology and end results; EAC, esophageal adenocarcinoma.

Risks Examined for Association With Different Metastasis Sites and Treatments

Multivariate analysis of EAC patients with different DM indicated that the treatment can be the only independent prognostic factor affecting OS and CSS (**Tables 2**, **3**).

As shown in **Table 2**, treatment was associated with OS and CSS. Compared to the S and/or R+C group, the S and/or R group had the poorer OS (HR: 2.232, 95% CI: 1.730–2.880, $p < 0.001$) and the N group showed the worst OS (HR: 4.308, 95% CI: 3.500–5.301, $p < 0.001$). The results of C group and S and/or R+C group were not statistically significant in OS (HR: 1.014, 95% CI: 0.810–1.268, $p = 0.907$). Compared to the bone-only group, liver-only group (HR: 0.746, 95% CI: 0.583–0.954, $p < 0.05$), and lung-only group (HR: 0.730, 95% CI: 0.543–0.981, $p < 0.05$) had better OS. Multiple-site group (HR: 1.037, 95% CI: 0811–1.327, $p = 0.770$) had the worst OS. The similar results were found for CSS. The data in **Table 2** also show that the bone-only group had the worst OS and CSS among the single-organ metastasis population. The multiple-site group had the worst OS and CSS across the population.

As shown in **Table 3**, due to the lack of patients in the brain-only group (only 24 patients), we were unable to draw statistically significant results, so we did not consider this group; however, we found similar results in the other four groups (across the population). The results showed that compared to S and/or R+C group, the S and/or R group had the worse OS and CSS, and the N group showed the worst OS and CSS. The results of C group and S and/or R+C group were not statistically significant in OS and CSS.

In **Table 4**, data show that the MST in OS were 3, 5, 4, 3, and 2 months and the MST values in CSS were 4, 6, 4, 4, and 3 months in the bone-only, brain-only, lung-only, liver-only, and multiple-site groups, respectively. The 6-month survival rate (SR), 1-year SR, and 3-year SR were lowest in the multiple-site group than the other groups (6-month SR: 27.1% in OS, 29.9% in CSS, 1-year SR: 10.7% in OS, 12.0% in CSS, 3-year SR: 2.5% in OS, 2.8% in CSS). These results show that patients with multiple-site metastases had the lowest 6-month SR and 1-year SR among all populations, and patients with bone-only metastasis had the worst 6-month SR and 1-year SR among those with single-organ metastasis.

To elucidate the relationship about these treatment modalities for prognosis, a Kaplan-Meier survival analysis was undertaken (**Figure 2**). In **Figures 2A, B**, in the elderly patient population, the prognosis of different treatment modalities for elderly patients varied greatly. Regardless of whether the patient was treated with surgery or radiotherapy, the prognosis of elderly patients treated with chemotherapy was better than that of treatment without chemotherapy ($p < 0.001$). The prognosis of surgery and/or radiotherapy was better than that of untreated patients (OS and CSS: $p < 0.001$). However, the prognosis of surgery and/or radiotherapy + chemotherapy was not statistically different from chemotherapy alone (OS: $p = 0.812$, CSS: $p = 0.900$). The similar results were also found in bone-only, liver-only, and multiple-site groups (**Figures 2C–F, I, J**). In **Figures 2G, H**, the prognosis results of surgery and/or

TABLE 1 | Characteristics of elderly EAC patients with DM.

Characteristics	≥70
Sex	
Male	733 (85.7%)
Female	122 (14.3%)
Ethnicity	
White	808 (94.5%)
Black	17 (2.0%)
Other	30 (3.5%)
Grade	
I	26 (3.0%)
II	253 (29.6%)
III	423 (49.5%)
IV	10 (1.2%)
Unknown	143 (16.7%)
T stage	
T1	168 (19.6%)
T2	40 (4.7%)
T3	128 (15.0%)
T4	89 (10.4%)
Unknown	430 (50.3%)
N stage	
N0	208 (24.3%)
N1	331 (38.7%)
N2	49 (5.7%)
N3	36 (4.2%)
Unknown	231 (27.0%)
Site of EAC	
Upper	8 (0.9%)
Middle	54 (6.3%)
Lower	793 (92.7%)
Metastasis	
Bone only	103 (12.0%)
Brain only	24 (2.8%)
Liver only	350 (40.9%)
Lung only	109 (12.7%)
Multiple	269 (31.5%)
Treatment	
S or/and R+C	189 (22.1%)
C	246 (28.8%)
S or/and R	113 (13.2%)
N	307 (35.9%)

N, no treatment; S, surgery; R, radiotherapy; C, chemotherapy.

radiotherapy + chemotherapy, surgery and/or radiotherapy, and chemotherapy alone were not statistically significant in the lung-only group.

DISCUSSION

In our present study, the metastasis patterns and prognosis of EAC elderly patients with DM in stage IVB were investigated. Our results indicated that the most common site of metastasis was liver, followed by lung, bone, and brain among the single-organ metastasis population. In addition, treatment was an independent prognostic factor affecting OS and CSS; because the treatment of multiple-site metastasis was limited, the prognosis of patients with multiple-site metastasis was even worse. Chemotherapy played an essential role in EAC elderly patients with DM in stage IVB. Regardless of whether the patient was treated with surgery or radiotherapy, the prognosis of elderly patients who were treated with chemotherapy was better than that without.

According to autopsy results, the lung and liver were the most common metastatic organs in patients with EC, with 31% and 23% of patients therein, respectively (17). Some studies have shown that the liver and lung were the most common metastatic organs in patients with EC (18). Bone was also a common organ for DM (19, 20). Bone metastasis was the third most common site of metastasis in patients with EC (18, 21). Other studies have reported that the most common site for metastasis was the liver, followed by lung, bone, and brain (22–25). Moreover, there are limited studies on the effect of the DM on survival in metastatic EC. San-Gang Wu et al. found that the site of metastasis showed an effect on survival in metastatic EC and bone metastasis had the poorest OS, which was greatest for distant lymph node metastases (26). The study by Jin Zhang et al. included EC patients with bone metastasis and showed the prognostic factors for bone metastases patient survival in EC (27). However, Tanaka et al. found that there was no significant difference in median survival among different sites of DM, which included bone, liver, and lung (28). The mechanisms of bone metastasis leading to lower survival rate of metastatic EC than other sites remain unclear. Overproduced parathyroid hormone-related peptide (PTHrP) is usually caused by osteolytic bone metastasis (29). Hypercalcemia and leukocytosis are associated with bone metastasis in EC, which may induce rapid disease progression (30–32).

EC is often manifest as transmural invasion with far advanced and early metastatic spread at diagnosis. EC patients with distant organ metastasis are classified as stage IVB in the TNM classification and have not been treated with curative intent (in general). These patients often have been considered as candidates for palliative therapy, such as photodynamic therapy, stent placement, and palliative chemotherapy or radiotherapy (33–37). Thus, the prognosis of these patients relies on the degree of spread and is, in general, extremely poor, usually with an MST of less than 6 months.

In a sense, radiotherapy and chemotherapy and surgery are in fact palliative treatments for EAC patients with DM, but our results have shown the prognosis of no treatment < surgery and/or radiotherapy < surgery and/or radiotherapy + chemotherapy (**Figure 2**). Furthermore, chemotherapy had shown obvious benefits to the prognosis: according to our results, whether elderly patients received chemotherapy, radiotherapy, or surgery had an important effect on the prognosis. Since there were only 27 patients who had undergone surgery, thus, the results were mainly about the effects of radiotherapy and chemotherapy on the prognosis of EAC elderly patients with DM. Our results suggested that active treatment can significantly improve the prognosis of patients, and chemotherapy had played a more important role. This study proved that radiotherapy (such as stereotactic body radiotherapy and radio-frequency ablation) and chemotherapy (very necessary to treat DM patients) can help extend the survival time. The results in the lung-

TABLE 2 | Results of Univariate and Multivariate analysis using the COX proportional hazards model of the study population.

	Univariate analysis (OS)		Multivariate analysis (OS)		Univariate analysis (CSS)		Multivariate analysis (CSS)	
	HR (95% CI)	P value	HR (95% CI)	P value	HR (95% CI)	P value	HR (95% CI)	P value
Sex								
Male	1	1	1	1	1	1	1	1
Female	1.023 (0.833–1.357)	0.828	0.984 (0.797–1.215)	0.881	1.059 (0.859–1.307)	0.590	1.015 (0.818–1.260)	0.893
Ethnicity								
White	1	1	1	1	1	1	1	1
Black	1.009 (0.594–1.713)	0.973	1.058 (0.619–1.808)	0.837	0.997 (0.576–1.727)	0.992	1.044 (0.599–1.820)	0.879
Other	1.010 (0.678–1.505)	0.962	1.032 (0.689–1.546)	0.879	0.950 (0.621–1.453)	0.812	0.963 (0.627–1.481)	0.865
Grade								
I	1	1	1	1	1	1	1	1
II	1.223 (0.774–1.933)	0.388	1.155 (0.726–1.839)	0.543	1.145 (0.724–1.812)	0.562	1.071 (0.672–1.708)	0.773
III	1.546 (0.985–2.426)	0.058	1.454 (0.917–2.306)	0.112	1.410 (0.898–2.215)	0.136	1.307 (0.822–2.077)	0.258
IV	1.501 (0.702–3.207)	0.295	1.771 (0.805–3.898)	0.155	1.499 (0.702–3.204)	0.296	1.739 (0.789–3.834)	0.170
Unknown	1.215 (0.756–1.954)	0.420	1.068 (0.658–1.734)	0.789	1.180 (0.733–1.899)	0.496	1.020 (0.628–1.658)	0.936
T stage								
T1	1	1	1	1	1	1	1	1
T2	0.570 (0.393–0.826)	0.003	0.557 (0.379–0.820)	0.003	0.574 (0.391–0.841)	0.004	0.549 (0.368–0.818)	0.003
T3	0.663 (0.522–0.843)	0.001	0.831 (0.642–1.077)	0.162	0.652 (0.509–0.836)	0.001	0.798 (0.611–1.043)	0.099
T4	0.870 (0.669–1.133)	0.301	0.989 (0.752–1.301)	0.939	0.898 (0.686–1.176)	0.436	1.004 (0.758–1.328)	0.980
Unknown	0.965 (0.800–1.164)	0.708	0.967 (0.791–1.181)	0.740	0.954 (0.786–1.157)	0.631	0.948 (0.771–1.166)	0.615
N stage								
N0	1	1	1	1	1	1	1	1
N1	0.922 (0.771–1.101)	0.368	1.123 (0.928–1.359)	0.235	0.946 (0.786–1.139)	0.560	1.166 (0.956–1.423)	0.129
N2	0.630 (0.452–0.880)	0.007	0.798 (0.560–1.138)	0.213	0.662 (0.470–0.933)	0.018	0.845 (0.587–1.218)	0.368
N3	0.977 (0.676–1.413)	0.902	1.181 (0.803–1.738)	0.398	1.076 (0.742–1.560)	0.700	1.313 (0.889–1.939)	0.172
Unknown	0.926 (0.750–1.143)	0.472	1.053 (0.842–1.318)	0.650	0.963 (0.774–1.198)	0.736	1.105 (0.876–1.393)	0.399
Site of EAC								
Upper	1	1	1	1	1	1	1	1
Middle	1.312 (0.562–3.064)	0.530	1.375 (0.581–3.250)	0.469	1.235 (0.527–2.892)	0.627	1.334 (0.562–3.167)	0.513
Lower	1.165 (0.521–2.602)	0.710	1.594 (0.705–3.606)	0.263	1.091 (0.488–2.437)	0.833	1.510 (0.667–3.420)	0.323
Site-of metastasis								
Bone only	1	1	1	1	1	1	1	1
Brain only	0.813 (0.501–1.318)	0.400	0.928 (0.565–1.526)	0.770	0.739 (0.439–1.244)	0.255	0.853 (0.501–1.455)	0.561
Liver only	0.920 (0.728–1.162)	0.483	0.746 (0.583–0.954)	0.020	0.932 (0.732–1.187)	0.567	0.769 (0.597–0.992)	0.043
Lung only	0.820 (0.614–1.096)	0.180	0.730 (0.543–0.981)	0.037	0.794 (0.587–1.074)	0.135	0.719 (0.528–0.979)	0.036
Multiple	1.190 (0.936–1.512)	0.156	1.037 (0.811–1.327)	0.770	1.194 (0.932–1.530)	0.160	1.052 (0.816–1.357)	0.695
Treatment								
S or/and R+C	1	1	1	1	1	1	1	1
C	0.990 (0.799–1.228)	0.930	1.014 (0.810–1.268)	0.907	1.032 (0.825–1.290)	0.784	1.036 (0.821–1.306)	0.768
S or/and R	2.123 (1.653–2.728)	0.000	2.232 (1.730–2.880)	0.000	2.235 (1.726–2.894)	0.000	2.345 (1.803–3.050)	0.000
N	4.308 (3.500–5.301)	0.000	4.782 (3.821–5.984)	0.000	4.358 (3.509–5.411)	0.000	4.750 (3.762–5.998)	0.000

N, no treatment; S, surgery; R, radiotherapy; C, chemotherapy.

only group were not statistically significant in terms of difference between surgery and/or radiotherapy + chemotherapy, chemotherapy alone and surgery and/or radiotherapy. However, the prognosis of no treatment < surgery and/or radiotherapy < surgery or/and radiotherapy + chemotherapy was similar in other groups.

Although multimodal therapy has been considered as an effective treatment in locally advanced primary EC patients, its role in treating patients with DM remains poorly defined (9, 33). There is little research into the application of multimodal therapy in patients with DM (38–41). In our study, there was no difference in survival between patients treated with surgery or/and radiotherapy + chemotherapy and those treated with chemotherapy alone. Surgery and radiotherapy are not considered beneficial as the treatment modality for these patients with chemotherapy: chemotherapy can be deemed to be the primary mode of treatment.

Although all treatment modalities are considered as palliative treatment for patients with DM, chemotherapy is a systemic approach, which can treat other metastatic organs of EC patients, compared to radiotherapy, the local therapy modality and the results reflected this finding.

Our results showed that 307 (35.9%) patients did not have any treatment. The low percentage of active treatment limited the OS and CSS of elderly patients. The study by Basile Njei et al. showed that no surgery and no radiotherapy were independent negative prognostic factors that affect the prognosis of patients with EC (42).

We think the reasons for the poor prognosis of EAC elderly patients with DM in stage IVB were also mainly determined by

TABLE 3 | Results of Multivariate analysis using the COX proportional hazards model of the different populations.

Site-of metastasis n (%)	Treatment	OS		CSS	
		HR (95% CI)	P value	HR (95% CI)	P value
Bone 103 (12.0%)	S or/and R+C	1	1	1	1
	C	1.503 (0.774–3.036)	0.256	1.557 (0.757–3.205)	0.229
	S or/and R	3.322 (1.601–6.894)	0.001	3.328 (1.579–7.016)	0.002
	N	24.587 (10.183–59.361)	0.000	23.970 (9.760–58.873)	0.000
Brain 24 (2.8%)	S or/and R+C	1	1	1	1
	C				
	S or/and R	123.423 (5.256–2898.474)	0.003	1.000 (0.104–9.586)	1.000
	N	97.716 (0.983–9716.474)	0.051	1.000 (0.007–144.826)	1.000
Liver 350 (40.9%)	S or/and R+C	1	1	1	1
	C	1.099 (0.737–1.639)	0.643	1.074 (0.714–1.614)	0.733
	S or/and R	2.787 (1.700–4.567)	0.000	2.891 (1.755–4.763)	0.000
	N	4.040 (2.734–5.971)	0.000	3.916 (2.629–5.833)	0.000
Lung 109 (12.7%)	S or/and R+C	1	1	1	1
	C	1.111 (0.571–2.160)	0.758	1.116 (0.541–2.300)	0.766
	S or/and R	3.318 (1.342–8.204)	0.009	4.065 (1.582–10.447)	0.004
	N	6.378 (3.138–12.963)	0.000	7.215 (3.365–15.472)	0.000
Multiple 269 (31.5%)	S or/and R+C	1	1	1	1
	C	0.764 (0.514–1.137)	0.185	0.816 (0.543–1.228)	0.330
	S or/and R	2.082 (1.320–3.284)	0.002	2.122 (1.324–3.401)	0.002
	N	5.354 (3.556–8.060)	0.000	5.376 (3.512–8.227)	0.000

OS, overall survival; CSS, cancer-specific survival; N, no treatment; S, surgery; R, radiotherapy; C, chemotherapy.

TABLE 4 | Prognostic analysis in different population.

Site of Metastasis		OS	CSS
Bone	MST (month)	3	4
	6-month SR (%)	35.6	38.2
	1-year SR (%)	20.0	21.5
	3-year SR (%)	1.9	2.7
Brain	MST (month)	5	6
	6-month SR (%)	36.4	40.6
	1-year SR (%)	27.3	30.4
	3-year SR (%)	0	0
Liver	MST (month)	4	4
	6-month SR (%)	36.5	38.6
	1-year SR (%)	21.1	23.6
	3-year SR (%)	2.1	2.5
Lung	MST (month)	3	4
	6-month SR (%)	43.5	45.6
	1-year SR (%)	23.9	28.2
	3-year SR (%)	4.9	8.4
Multiple	MST (month)	2	3
	6-month SR (%)	27.1	29.9
	1-year SR (%)	10.7	12.0
	3-year SR (%)	2.5	2.8
Total	MST (month)	3	4
	6-month SR (%)	34.3	36.8
	1-year SR (%)	18.1	20.5
	3-year SR (%)	2.4	3.2

OS, overall survival; CSS, cancer-specific survival; MST, median survival time; yrs, years; SR, survival rate.

low percentage of active treatment. The reasons for that include the doctors' opinions and patient-related factors.

1. Doctor's point of view. Due to the presence of more complications in elderly patients, strict surgical indications limit surgical opportunities for elderly patients. Considering age-related health conditions, operative adverse events, and mortality, doctors tend to treat conservatively. Safe implementation of beneficial treatments at standard doses to improve survival and whether treatment-related side effects may influence the quality of life of patients become two conflicting aspects that clinicians need to consider.
2. Factors related to patients. Elderly patients are more likely to consider not taking active treatment. There are also many

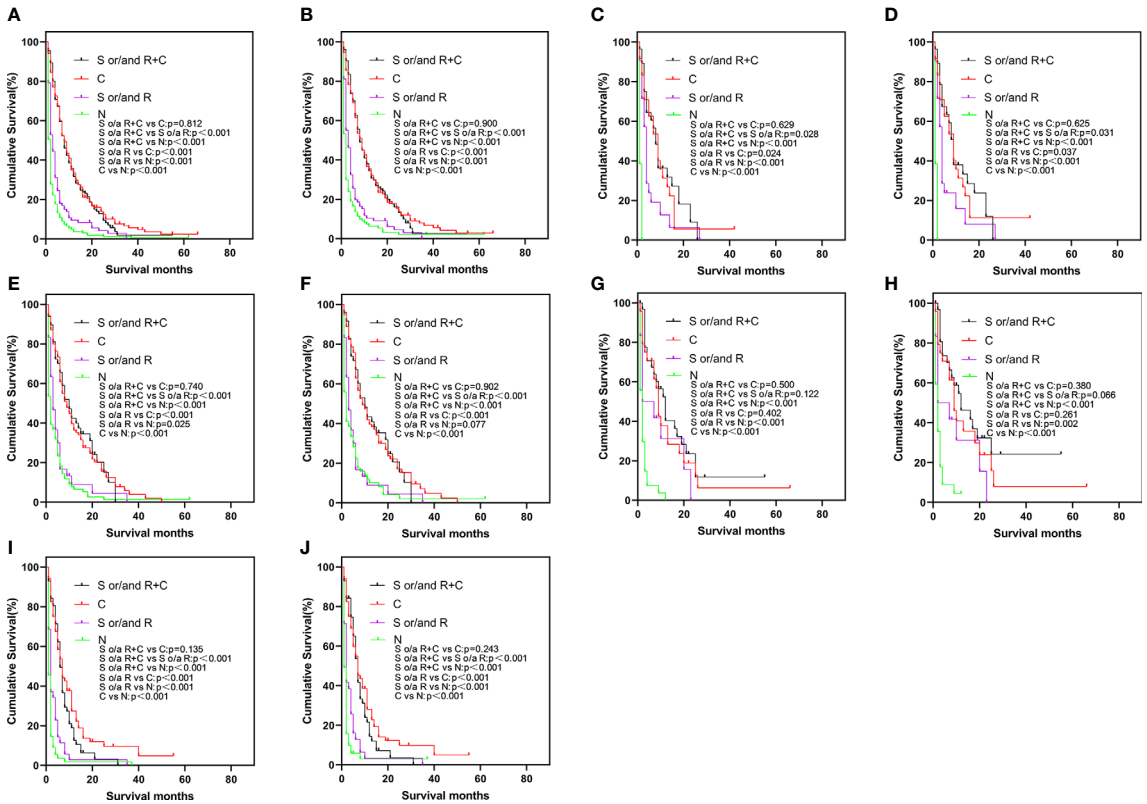

FIGURE 2 | Kaplan-Meier curve of OS **(A)** and CSS **(B)** by different treatments in the total study population, OS **(C)** and CSS **(D)** in bone-only group, OS **(E)** and CSS **(F)** in liver-only group, OS **(G)** and CSS **(H)** in lung-only group, OS **(I)** and CSS **(J)** in the multiple-site group. OS, overall survival; CSS, cancer-specific survival.

studies on malignant tumors that the reasons for patients' refusal to be treated may be associated with increased delivery of suboptimal therapy, decreased referral to specialists and increased patient refusal of therapy (43–46). The reasons that lead elderly patients to be treated conservatively also include the existence of comorbidities that affect the patients' drug absorption and/or metabolism (46, 47).

In addition, senescent cells can also secrete many growth factors to promote the growth of tumor cells. Age, the number of complications, the presence of tumors, and deep vein thrombosis associated with aging can significantly increase the risk of death (48, 49).

About 65% of cancer patients are over 65 years of age, with the increase in life expectancy, this may rise to 70% in the future (50), however, among those patients who participated in cancer-related clinical trials, only 40% were over 65 years of age, and no more than 10% were over 75 (51), therefore, clinical trials of cancer treatments need to focus on elderly patients.

The study has certain limitations: this is a retrospective study and many factors contributing to the possible poor prognosis for this patient group are missing. The study is generalized to the American population, but lacked inclusion of cases among ethnic minorities, thus the results can not represent the global population. Compared with the most common sites, such as liver, lung, and bone, brain metastasis is rare, which makes the survival results of patients with brain metastasis subject to statistical bias. Different patterns of multiple metastatic sites were not differentiated, such as bone + brain, bone + liver, bone + lung, bone + brain + liver, etc. Immunotherapy and targeted therapy were not taken into consideration. Due to the flaws in the database, we cannot know the detailed information of the treatment modalities such as surgery, radiotherapy, and chemotherapy, which may affect the results of the study. On the other hand, there are no relevant reports on elderly EC patients with DM, thus, the study on metastasis and prognosis of such patients shows an important significance.

In conclusion, metastasis patterns and survival outcomes of EAC patients with DM in stage IVB were studied in elderly patients. Elderly patients with multiple-site metastasis had the worst OS and CSS. Patients with bone-only metastasis had the worst OS and CSS among single-organ metastasis populations. Patients with active treatments had better CSS and OS. Chemotherapy was beneficial to these patients, however, over 35.9% patients more than 70 years of age did not take any anti-cancer treatment. These elderly patients had highest rate of cancer-specific deaths among the study population.

DATA AVAILABILITY STATEMENT

The raw data supporting the conclusions of this article will be made available by the authors, without undue reservation.

ETHICS STATEMENT

The studies involving human participants were reviewed and approved by the ethics committee of the West China Hospital. Written informed consent for participation was not required for this study in accordance with the national legislation and the institutional requirements.

AUTHOR CONTRIBUTIONS

GQ contributed the idea. HZ contributed the design of the study. FW contributed the calculation. YZ contributed the proofread. ZW contributed error correction. YW contributed the idea. All authors contributed to the article and approved the submitted version.

FUNDING

This study was supported by the National Key Research Project Fund of China (grant no. 2017YFC0113502) and the Key Research Project of Sichuan Province (grant no. 2020YFS0249).

REFERENCES

1. Thrift AP, Whiteman DC. The Incidence of Esophageal Adenocarcinoma Continues to Rise: Analysis of Period and Birth Cohort Effects on Recent Trends. *Ann Oncol* (2012) 23:3155–62. doi: 10.1093/annonc/mds181
2. Torre LA, Bray F, Siegel RL, Ferlay J, Lortet-Tieulent J, Jemal A. Global Cancer Statistics, 2012. *Ca-a Cancer J Clin* (2015) 65:87–108. doi: 10.3322/caac.21262
3. Arnold M, Laversanne M, Brown LM, Devesa SS, Bray F. Predicting the Future Burden of Esophageal Cancer by Histological Subtype: International Trends in Incidence Up to 2030. *Am J Gastroenterol* (2017) 112:1247–55. doi: 10.1038/ajg.2017.155
4. Collaborators GBDOC. The Global, Regional, and National Burden of Oesophageal Cancer and its Attributable Risk Factors in 195 Countries and Territories, 1990-2017: A Systematic Analysis for the Global Burden of Disease Study 2017. *Lancet Gastroenterol Hepatol* (2020) 5:582–97. doi: 10.1016/S2468-1253(20)30007-8
5. UK CR. *Oesophageal cancer incidence by age*. Available at: https://www.cancerresearchuk.org/health-professional/cancer-statistics/statistics-by-cancer-type/oesophageal-cancer/incidence#heading-One. UK: Cancer Research
6. Zeng Y, Liang W, Liu J, He J, Ng CSH, Liu CC, et al. Esophageal Cancer in Elderly Patients: A Population-Based Study. *J Thorac Dis* (2018) 10:448–57. doi: 10.21037/jtd.2018.01.89
7. Furlong H, Bass G, Breathnach O, O'Neill B, Leen E, Walsh TN. Targeting Therapy for Esophageal Cancer in Patients Aged 70 and Over. *J Geriatr Oncol* (2013) 4:107–13. doi: 10.1016/j.jgo.2012.12.006
8. Nienhueser H, Kunzmann R, Sisic L, Blank S, Strowitzk MJ, Bruckner T, et al. Surgery of Gastric Cancer and Esophageal Cancer: Does Age Matter? *J Surg Oncol* (2015) 112:387–95. doi: 10.1002/jso.24004
9. Enzinger PC, Mayer RJ. Esophageal Cancer. *N Engl J Med* (2003) 349:2241–52. doi: 10.1056/NEJMra035010
10. Horner MJ, Ries LAG, Krapcho M, Neyman N, Aminou R, Howlader N, et al. *SEER Cancer Statistics Review, 1975–2006*. Bethesda, MD: National Cancer Institute. Available at: http://seer.cancer.gov/csr/1975_2006/ (Accessed May 10, 2017).
11. Cijs TM, Verhoef C, Steyerberg EW, Koppert LB, Tran TC, Wijnhoven BP, et al. Outcome of Esophagectomy for Cancer in Elderly Patients. *Ann Thorac Surg* (2010) 90:900–7. doi: 10.1016/j.athoracsur.2010.05.039
12. Karl RC, Smith SK, Fabri PJ. Validity of Major Cancer Operations in Elderly Patients. *Ann Surg Oncol* (1995) 2:107–13. doi: 10.1007/BF02303624
13. Kinugasa S, Tachibana M, Yoshimura H, Dhar DK, Shibakita M, Ohno S, et al. Esophageal Resection in Elderly Esophageal Carcinoma Patients: Improvement in Postoperative Complications. *Ann Thoracic Surg* (2001) 71:414–8. doi: 10.1016/S0003-4975(00)02333-X
14. Markar SR, Karthikesalingam A, Thrumurthy S, Ho A, Muallem G, Low DE. Systematic Review and Pooled Analysis Assessing the Association Between Elderly Age and Outcome Following Surgical Resection of Esophageal Malignancy. *Dis Esophagus* (2013) 26:250–62. doi: 10.1111/j.1442-2050.2012.01353.x
15. Ruol A, Portale G, Zaninotto G, Cagol M, Cavallin F, Castoro C, et al. Results of Esophagectomy for Esophageal Cancer in Elderly Patients: Age has Little Influence on Outcome and Survival. *J Thoracic Cardiovasc Surg* (2007) 133:1186–92. doi: 10.1016/j.jtcvs.2006.12.040
16. Yang HX, Ling L, Zhang X, Lin P, Rong TH, Fu JH. Outcome of Elderly Patients With Oesophageal Squamous Cell Carcinoma After Surgery. *Br J Surg* (2010) 97:862–7. doi: 10.1002/bjs.7005
17. Mandard AM, Chasle J, Marnay J, Villedieu B, Bianco C, Roussel A, et al. Autopsy Findings in 111 Cases of Esophageal Cancer. *Cancer* (1981) 48:329–35. doi: 10.1002/1097-0142(19810715)48:2<329::AID-CNCR2820480219>3.0.CO;2-V
18. Ai D, Zhu H, Ren W, Chen Y, Liu Q, Deng J, et al. Patterns of Distant Organ Metastases in Esophageal Cancer: A Population-Based Study. *J Thorac Dis* (2017) 9:3023–30. doi: 10.21037/jtd.2017.08.72
19. Guo Q, Zhang C, Guo X, Tao F, Xu Y, Feng G, et al. Incidence of Bone Metastasis and Factors Contributing to its Development and Prognosis in Newly Diagnosed Renal Cell Carcinoma: A Population-Based Study. *Cancer Manag Res* (2018) 10:2935–44. doi: 10.2147/CMAR.S170083
20. Guo X, Zhang C, Ma W, Tian F, Xu G, Han X, et al. Patterns of Bone Metastases in Newly Diagnosed Colorectal Cancer: A Real-World Analysis in the SEER Database. *Int J Colorectal Dis* (2019) 34:533–43. doi: 10.1007/s00384-018-3213-5
21. Wu SG, Zhang WW, Sun JY, Li FY, Lin Q, He ZY. Patterns of Distant Metastasis Between Histological Types in Esophageal Cancer. *Front Oncol* (2018) 8. doi: 10.3389/fonc.2018.00302
22. Bosch A, Frias Z, Caldwell WL, Jaeschke WH. Autopsy Findings in Carcinoma of the Esophagus. *Acta Radiol Oncol Radiat Phys Biol* (1979) 18:103–12. doi: 10.3109/02841867909128196
23. Chen MQ, Xu BH, Zhang YY. Analysis of Prognostic Factors for Esophageal Squamous Cell Carcinoma With Distant Organ Metastasis at Initial Diagnosis. *J Chin Med Assoc* (2014) 77:562–6. doi: 10.1016/j.jcma.2014.05.014
24. Mariette C, Balon JM, Piessen G, Fabre S, Van Seuningen I, Triboulet JP. Pattern of Recurrence Following Complete Resection of Esophageal Carcinoma and Factors Predictive of Recurrent Disease. *Cancer* (2003) 97:1616–23. doi: 10.1002/cncr.11228
25. Tustumi F, Kimura CM, Takeda FR, Sallum RA, Ribeiro-Junior U, Cecconello I. Evaluation of Lymphatic Spread, Visceral Metastasis and Tumoral Local Invasion in Esophageal Carcinomas. *Arq Bras Cir Dig* (2016) 29:215–7. doi: 10.1590/0102-6720201600040001
26. Wu SG, Zhang WW, He ZY, Sun JY, Chen YX, Guo L. Sites of Metastasis and Overall Survival in Esophageal Cancer: A Population-Based Study. *Cancer Manage Res* (2017) 9:781–8. doi: 10.2147/CMAR.S150350
27. Zhang J, Ma W, Wu H, Wang J, Lin Y, Wang X, et al. Analysis of Homogeneous and Heterogeneous Factors for Bone Metastasis in Esophageal Cancer. *Med Sci Monit* (2019) 25:9416–25. doi: 10.12659/MSM.920483
28. Tanaka T, Fujita H, Matono S, Nagano T, Nishimura K, Murata K, et al. Outcomes of Multimodality Therapy for Stage IVB Esophageal Cancer With Distant Organ Metastasis (M1-Org). *Dis Esophagus* (2010) 23:646–51. doi: 10.1111/j.1442-2050.2010.01069.x

29. Langley RR, Fidler IJ. Tumor Cell-Organ Microenvironment Interactions in the Pathogenesis of Cancer Metastasis. *Endocr Rev* (2007) 28:297–321. doi: 10.1210/er.2006-0027
30. Watanabe HA, Matsushita H, Matsui H, Komatsu T, Taguchi S, Sata H, et al. Esophageal Carcinoma With High Serum Parathyroid Hormone-Related Protein (PthrP) Level. *J Gastroenterol* (1999) 34:510–5. doi: 10.1007/s005350050305
31. Deans C, Wigmore S, Paterson-Brown S, Black J, Ross J, Fearon KCH. Serum Parathyroid Hormone-Related Peptide is Associated With Systemic Inflammation and Adverse Prognosis in Gastroesophageal Carcinoma. *Cancer* (2005) 103:1810–8. doi: 10.1002/cncr.20972
32. Tachimori Y, Watanabe H, Kato H, Yamaguchi H, Nagasaki K, Honda S, et al. Hypercalcemia in Patients With Esophageal-Carcinoma - the Pathophysiologic Role of Parathyroid Hormone-Related Protein. *Cancer* (1991) 68:2625–9. doi: 10.1002/1097-0142(19911215)68:12<2625::AID-CNCR2820681219>3.0.CO;2-T
33. Mariette C, Piessen G, Triboulet JP. Therapeutic Strategies in Oesophageal Carcinoma: Role of Surgery and Other Modalities. *Lancet Oncol* (2007) 8:545–53. doi: 10.1016/S1470-2045(07)70172-9
34. Homs MY, Kuipers EJ, Siersema PD. Palliative Therapy. *J Surg Oncol* (2005) 92:246–56. doi: 10.1002/jso.20366
35. Lightdale CJ. Esophageal Cancer. American College of Gastroenterology. *Am J Gastroenterol* (1999) 94:20–9. doi: 10.1111/j.1572-0241.1999.00767.x
36. Homs MY, Steyerberg EW, Eijkenboom WM, Tilanus HW, Stalpers LJ, Bartelsman JF, et al. Single-Dose Brachytherapy Versus Metal Stent Placement for the Palliation of Dysphagia From Oesophageal Cancer: Multicentre Randomised Trial. *Lancet* (2004) 364:1497–504. doi: 10.1016/S0140-6736(04)17272-3
37. Luketich JD, Christie NA, Buenaventura PO, Weigel TL, Keenan RJ, Nguyen NT. Endoscopic Photodynamic Therapy for Obstructing Esophageal Cancer: 77 Cases Over a 2-Year Period. *Surg Endosc* (2000) 14:653–7. doi: 10.1007/s004640000144
38. Iwase H, Shimada M, Nakamura M, Nakarai K, Iyo T, Kaida S, et al. Concurrent Chemoradiotherapy for Locally Advanced and Metastatic Esophageal Cancer: Longterm Results of a Phase II Study of UFT/CDDP With Radiotherapy. *Int J Clin Oncol* (2003) 8:305–11. doi: 10.1007/s10147-003-0344-6
39. Kosugi SI, Kanda T, Nishimaki T, Nakagawa S, Yajima K, Ohashi M, et al. Successful Treatment for Esophageal Carcinoma With Lung Metastasis by Induction Chemotherapy Followed by Salvage Esophagectomy: Report of a Case. *World J Gastroenterol* (2006) 12:4101–3. doi: 10.3748/wjg.v12.i25.4101
40. Yamamoto T, Tachibana M, Kinugasa S, Yoshimura H, Nagasue N. Esophagectomy and Hepatic Arterial Chemotherapy Following Hepatic Resection for Esophageal Cancer With Liver Metastasis. *J Gastroenterol* (2001) 36:560–3. doi: 10.1007/s005350170060
41. Yoshizumi Y, Morisaki Y, Koike H, Shibata H, Yanagawa R, Sugiura Y, et al. Successful Combined Resection of Carcinoma of the Esophagus and Adrenal Metastasis: Report of a Case. *Surg Today* (1997) 27:330–3. doi: 10.1007/BF00941807
42. Njei B, McCarty TR, Birk JW. Trends in Esophageal Cancer Survival in United States Adults From 1973 to 2009: A SEER Database Analysis. *J Gastroenterol Hepatol* (2016) 31:1141–6. doi: 10.1111/jgh.13289
43. Bouchardy C, Rapiti E, Blagojevic S, Vlastos AT, Vlastos G. Older Female Cancer Patients: Importance, Causes, and Consequences of Undertreatment. *J Clin Oncol* (2007) 25:1858–69. doi: 10.1200/JCO.2006.10.4208
44. Dale DC. Poor Prognosis in Elderly Patients With Cancer: The Role of Bias and Undertreatment. *J Support Oncol* (2003) 1:11–7.
45. Liu CY, Chen WT, Kung PT, Chiu CF, Wang YH, Shieh SH, et al. Characteristics, Survival, and Related Factors of Newly Diagnosed Colorectal Cancer Patients Refusing Cancer Treatments Under a Universal Health Insurance Program. *BMC Cancer* (2014) 14:446. doi: 10.1186/1471-2407-14-446
46. Steyerberg EW, Neville B, Weeks JC, Earle CC. Referral Patterns, Treatment Choices, and Outcomes in Locoregional Esophageal Cancer: A Population-Based Analysis of Elderly Patients. *J Clin Oncol* (2007) 25:2389–96. doi: 10.1200/JCO.2006.09.7931
47. Smith GL, Smith BD, Buchholz TA, Liao Z, Jeter M, Swisher SG, et al. Patterns of Care and Locoregional Treatment Outcomes in Older Esophageal Cancer Patients: The Seer-Medicare Cohort. *Int J Radiat Oncol Biol Phys* (2009) 74:482–9. doi: 10.1016/j.ijrobp.2008.08.046
48. Lin J, Li C, Li A, Liu A, Wang R, Chen C, et al. Encephalitis With Antibodies Against the GABAB Receptor: High Mortality and Risk Factors. *Front Neurol* (2019) 10:1030. doi: 10.3389/fneur.2019.01030
49. Parrinello S, Coppe JP, Krtolica A, Campisi J. Stromal-Epithelial Interactions in Aging and Cancer: Senescent Fibroblasts Alter Epithelial Cell Differentiation. *J Cell Sci* (2005) 118:485–96. doi: 10.1242/jcs.01635
50. Daste A, Chakiba C, Domblides C, Gross-Gupil M, Quivy A, Ravaud A, et al. Targeted Therapy and Elderly People: A Review. *Eur J Cancer* (2016) 69:199–215. doi: 10.1016/j.ejca.2016.10.005
51. Singh H, Kanapuru B, Smith C, Fashoyin-Aje LA, Myers A, Kim G, et al. FDA Analysis of Enrollment of Older Adults in Clinical Trials for Cancer Drug Registration: A 10-Year Experience by the US Food and Drug Administration. *J Clin Oncol* (2017) 35(15_suppl):10009–10009. doi: 10.1200/JCO.2017.35.15_suppl.10009

Conflict of Interest: The authors declare that the research was conducted in the absence of any commercial or financial relationships that could be construed as a potential conflict of interest.

frontiers in Oncology

REVIEW
published: 12 July 2021
doi: 10.3389/fonc.2021.672500

Early and Next-Generation KIT/PDGFRA Kinase Inhibitors and the Future of Treatment for Advanced Gastrointestinal Stromal Tumor

Sebastian Bauer[1]*, *Suzanne George*[2], *Margaret von Mehren*[3] and *Michael C. Heinrich*[4]*

[1] Department of Medical Oncology, West German Cancer Center, Essen University Hospital, University of Duisburg-Essen, Essen, Germany, [2] Department of Medical Oncology, Dana-Farber Cancer Institute, Boston, MA, United States, [3] Department of Hematology and Medical Oncology, Fox Chase Cancer Center, Philadelphia, PA, United States, [4] Department of Medicine, Portland VA Health Care System and OHSU Knight Cancer Institute, Oregon Health and Science University, Portland, OR, United States

OPEN ACCESS

Edited by:
Yujun Shi,
Sichuan University, China

Reviewed by:
César Serrano,
Vall d'Hebron Institute of Oncology (VHIO), Spain
Ciara Kelly,
Memorial Sloan Kettering Cancer Center, United States

***Correspondence:**
Sebastian Bauer
sebastian.bauer@uk-essen.de
Michael C. Heinrich
heinrich@ohsu.edu

Specialty section:
This article was submitted to Gastrointestinal Cancers, a section of the journal Frontiers in Oncology

Received: 25 February 2021
Accepted: 22 June 2021
Published: 12 July 2021

Citation:
Bauer S, George S, von Mehren M and Heinrich MC (2021) Early and Next-Generation KIT/PDGFRA Kinase Inhibitors and the Future of Treatment for Advanced Gastrointestinal Stromal Tumor. Front. Oncol. 11:672500. doi: 10.3389/fonc.2021.672500

The majority of gastrointestinal stromal tumors (GIST) harbor an activating mutation in either the KIT or PDGFRA receptor tyrosine kinases. Approval of imatinib, a KIT/PDGFRA tyrosine kinase inhibitor (TKI), meaningfully improved the treatment of advanced GIST. Other TKIs subsequently gained approval: sunitinib as a second-line therapy and regorafenib as a third-line therapy. However, resistance to each agent occurs in almost all patients over time, typically due to secondary kinase mutations. A major limitation of these 3 approved therapies is that they target the inactive conformation of KIT/PDGFRA; thus, their efficacy is blunted against secondary mutations in the kinase activation loop. Neither sunitinib nor regorafenib inhibit the full spectrum of KIT resistance mutations, and resistance is further complicated by extensive clonal heterogeneity, even within single patients. To combat these limitations, next-generation TKIs were developed and clinically tested, leading to 2 new USA FDA drug approvals in 2020. Ripretinib, a broad-spectrum KIT/PDGFRA inhibitor, was recently approved for the treatment of adult patients with advanced GIST who have received prior treatment with 3 or more kinase inhibitors, including imatinib. Avapritinib, a type I kinase inhibitor that targets active conformation, was approved for the treatment of adults with unresectable or metastatic GIST harboring a PDGFRA exon 18 mutation, including PDGFRA D842V mutations. In this review, we will discuss how resistance mutations have driven the need for newer treatment options for GIST and compare the original GIST TKIs with the next-generation KIT/PDGFRA kinase inhibitors, ripretinib and avapritinib, with a focus on their mechanisms of action.

Keywords: gastrointestinal stromal tumor (GIST), KIT, PDGFRA, ripretinib, avapritinib

Abbreviations: GIST, gastrointestinal stromal tumor; PDGFRA, platelet-derived growth factor receptor α; RTK, receptor tyrosine kinase; VEGFR, vascular endothelial growth factor receptor.

INTRODUCTION

Gastrointestinal stromal tumors (GISTs) arise from the interstitial cells of Cajal (1, 2); they occur primarily within the stomach (~56%) and small intestine (~32%) but can arise anywhere in the gastrointestinal (GI) tract (3). Although rare, GISTs are the most common sarcoma of the GI tract (3), with reported incidences between 10 and 15 cases per million annually (3). GISTs are best categorized by molecular subtype, which have differing clinical characteristics and treatment response (4). The majority of GISTs harbor activating mutations in 1 of 2 receptor tyrosine kinases (RTKs): KIT (approximately 69%–83%) (4),or platelet-derived growth factor receptor α (PDGFRA; approximately 5%–10%) (5, 6). The 10%–15% of GISTs without *KIT/PDGFRA* mutations are a heterogeneous group, historically referred to as "wild-type", (4, 7) before disease-defining genomic events were identified. "Wild-type" or preferably non-*KIT/PDGFRA*-mutant GISTs may have a succinate dehydrogenase complex deficiency (8), or harbor other mutations, such as activating mutations of *BRAF* or loss-of-function of *NF1*, that lead to activation of the PI3K/mTOR and/or the RAS/RAF/MAPK pathways (7, 9, 10).

The identification of RTK mutations in GIST led to the use of the tyrosine kinase inhibitors (TKI) for the treatment of advanced GIST (11). While the use of TKIs significantly improves progression-free survival (PFS) and overall survival (OS) in patients with advanced GIST (10), the inevitable development of TKI resistance remains an ongoing challenge (12). Recently, next-generation TKIs with novel mechanisms of action (MOA) have been developed to specifically address these challenges (13, 14). In this review, we will discuss how specific classes of mutations have driven the need for newer treatments for GIST and compare historical and next-generation KIT/PDGFRA kinase inhibitors with a focus on their MOA.

GIST IS COMMONLY A KIT- OR PDGFRA-ONCOGENE DRIVEN DISEASE

Most GISTs are driven by oncogenic *KIT*- or *PDGFRA*-activating mutations (10). Both KIT and PDGFRA are members of the class III tyrosine kinase family (15). Gain of function mutations in either the KIT or PDGFRA receptor leads to constitutive, ligand-independent activation, which alters cell proliferation, differentiation, apoptosis, and survival by regulating downstream signaling pathways (4).

KIT Mutations

Expression of KIT is important for cellular survival and proliferation, particularly in hematopoietic cells, melanocytes, mast cells, and interstitial cells of Cajal (11, 16). The *KIT* proto-oncogene maps to 4q12-13 and encodes a 145-kDA transmembrane RTK, KIT (aka CD117) (11, 17). KIT is activated through binding of its cognate ligand, stem cell factor, to its extracellular domain, inducing receptor homodimerization and activation of the intracellular kinase domain (18). Kinase activation initializes downstream signaling pathways, such as the JAK–STAT3, PI3K–Akt–mTOR, and RAS–MAPK pathways, which are important in regulating cellular functions such as cell proliferation, differentiation, and apoptosis (4). Gain of function mutations in *KIT* are a key oncogenic driver in approximately 80% of GISTs (4), and result in ligand-independent kinase activation (4). Primary mutations in *KIT* affect exons encoding the functional domains of the RTK (exons 8, 9, 11, 13, 17) (11). The majority of mutations occur in exon 11 (70%–80%), which encodes the juxtamembrane domain, leading to disruption in auto-inhibitory function and resulting in increased auto-activation of the kinase (17, 19). Approximately 10% of mutations occur in exon 9, which encodes a portion of the extracellular domain, and mostly consist of a typical duplication mutation of codons 502 and 503 (20). Primary mutations are also found in exon 13 (which encodes the ATP-binding region) and exon 17 (which encodes the activation loop), with an occurrence of about 1% each and less frequently in exon 8, encoding part of the extracellular domain (4, 17, 19).

PDGFRA Mutations

PDGFRA is the second most commonly mutated oncogene in GIST. PDGFRA and KIT are highly homologous, activating similar downstream signal transduction pathways (21). Primary *PDGFRA* mutations occur mainly in exons 18 and 12 and more rarely in exon 14 (6). Exon 18 encodes the activation loop and is the most frequent site for *PDGFRA* mutation (~6%) (5, 6, 22). A single mutation, D842V, is the most common exon 18 mutation and detected in 62.6% of *PDGFRA*-mutated tumors (5, 6). Mutations affecting exon 12 (encoding the juxtamembrane domain) and exon 14 (encoding the ATP-binding domain) are rare, identified in approximately 1%–2% and <0.1% of GISTs, respectively (5, 6, 22).

EARLY TARGETED TREATMENTS TO INACTIVATE MUTATED KIT/PDGFRA

KIT/PDGFRA are logical therapeutic targets as the key oncogenic drivers expressed in the majority (85%–90%) of GIST, especially given the minimal activity of conventional treatments such as chemotherapy or radiation for the treatment of advanced GIST. The first early targeted therapies for advanced GIST include the type II kinase inhibitors (which bind the inactive confirmation) (23) imatinib, sunitinib, and regorafenib, which are approved for first-, second-, and third-line treatment, respectively (24–26).

Imatinib

Imatinib (formerly STI571) is an oral, small-molecule TKI that was originally developed for the treatment of Philadelphia-chromosome-positive chronic myeloid leukemia (27, 28). Imatinib is a competitive inhibitor of the ATP-binding site of

certain RTKs including KIT, PDGFRA, ABL kinase, and the chimeric BCR-ABL fusion oncoprotein of chronic myeloid leukemia (29). When KIT is in the inactive conformation, imatinib can occupy the ATP-binding site and prevent substrate phosphorylation and inhibit downstream signal transduction (29).

Multiple clinical trials demonstrated the efficacy of imatinib in treating advanced GIST, leading to its approval for first-line treatment in 2001 (27). The first report of imatinib efficacy was a case report of imatinib (400 mg daily) resulting in a complete metabolic response in a patient with metastatic GIST who had failed to respond to conventional sarcoma therapies (30). After establishing safety and initial efficacy of imatinib in phase 1 testing in advanced GIST (31), an open-label randomized phase 2 trial randomized patients to receive either imatinib 400 or 600 mg once daily. Overall, 53.7% of patients had a partial response and 27.9% had stable disease (32). Imatinib was generally well tolerated, though most patients experienced mild to moderate adverse events (AEs) (32). Common AEs included edema (74.1%), nausea (52.4%), diarrhea (44.9%), myalgia or musculoskeletal pain (39.5%), fatigue (34.7%), dermatitis or rash (30.6%), headache (25.9%), and abdominal pain (25.9%) (32). Two large phase 3 trials compared treatment with imatinib 400 mg once daily to 400 mg twice daily in patients with unresectable or metastatic GIST. In the imatinib 400 mg daily group of the first trial, 5% had a complete response, 45% had a partial response, and 32% had stable disease. In the higher dose group (400 mg twice daily), 6% had a complete response, 48% had a partial response, and 32% had stable disease (33). A second large phase 3 trial, S0033, showed similar antitumor results in advanced GIST, with a median PFS (mPFS) of 18 months and 20 months and an OS of 55 months and 51 months on imatinib 400 mg once daily and twice daily, respectively (34). These results were dramatically improved compared to cytotoxic chemotherapy for advanced/metastatic GIST, which had minimal responses rates (0% –5%) and very short PFS, indicating the futility of standard sarcoma regimens for the treatment of GIST (32).

Despite the high response rates with front-line imatinib, disease progression still occurs in the majority of patients (35). Disease progression as the initial response to imatinib (i.e., during the first 6 months of treatment) is considered primary resistance, while disease progression that occurs after an initial response or stable disease is considered secondary resistance (11). Imatinib primary resistance was first reported by Demetri et al., who noted that 5% of patients had primary resistance to imatinib within 2 months (32). Overall, approximately 10% of GISTs have primary resistance to imatinib (35), which is correlated with the KIT/PDGFRA mutational status. A few other primary mutations are associated with resistance, such as *PDGFRA* exon 18 RD841-842KI or the primary *KIT* exon 17 N822K mutation (5, 36). Tumors that harbor *PDGFRA* D842V mutations confer unequivocal resistance regardless of imatinib dose (35). Relative primary resistance has also been observed in patients with exon 9 mutations (37); however, a higher dose of imatinib (400 mg twice daily) improves the response rate and PFS of this GIST genotype (38).

In most cases, KIT-mutant GISTs develop secondary resistance to imatinib as a result of the emergence of subclones harboring secondary KIT mutations (39). Secondary mutations most commonly occur in KIT exons 13 and 14 (encoding the ATP/drug-binding site) or exons 17 and 18 (encoding the activation loop) (11). Secondary mutations within the ATP-binding domain and activation loop cause resistance by different mechanisms (36). Mutations in the ATP-binding domain are thought to directly inhibit imatinib binding, whereas activation loop mutations are thought to stabilize the kinase in the active formation to which imatinib cannot bind (35). In 31 patients treated with imatinib and undergoing surgical resection, 15 tumors showed secondary resistance (40). Secondary mutations were identified in tumors from 7 (46%) of these patients; the majority had *KIT* exon 17 mutations, but *KIT* exons 13 and 14 mutations were also identified (40). In a separate study, 79 samples from 43 patients with advanced GIST were examined pre- and post-imatinib treatment. Of 33 patients with secondary resistance, 22 (67%) had 1 or more secondary mutations that included *KIT* exon 17 (15 patients), *KIT* exon 13 (7 patients), and exon 14 (1 patient) (41). Many of these samples were from tumor biopsy specimens and likely underestimate the true frequency of secondary mutations in patients with clinical imatinib resistance. In addition, substantial intra- and inter tumor mutational heterogeneity has been noted using sensitive sequencing technologies (12).

Sunitinib

Sunitinib (formerly SU11248), a small-molecule, multitarget TKI, was approved in 2006 as second-line treatment for advanced GIST after imatinib failure. Originally developed as a treatment for acute myeloid leukemia and advanced renal cell carcinoma, sunitinib is a potent competitive inhibitor of the ATP-binding sites of vascular endothelial growth factor receptor (VEGFR)-1, VEGFR-2, FMS-like tyrosine kinase-3, KIT, and PDGFRs (42–45).

In preclinical *in vivo* models, sunitinib exhibited dose-dependent antitumor activity (42, 44). In patients with advanced GIST who had progressed on imatinib, the safety and efficacy of sunitinib therapy was tested in an open-label, dosing-ranging phase 1/2 trial that enrolled 97 patients (46). The maximum tolerated dose was determined to be 50 mg daily, administered on a 4 weeks on/2 weeks off schedule, after 2 of 4 patients at 75 mg daily experienced dose-limiting toxicities (46). A clear clinical benefit was shown with sunitinib use at follow-up, with 7 (7%) of patients having a partial response and 45 (46%) stable disease (46). Overall, the mPFS was 7.8 months and the median OS was 19 months (46). Sunitinib had an acceptable safety profile with mostly mild to moderate treatment-emergent AEs (TEAEs). In a pivotal double-blind, placebo-controlled randomized phase 3 trial, the safety and efficacy of sunitinib as a second-line treatment in GIST was confirmed (47). Overall, the mPFS for patients on sunitinib was 5.6 months compared with 1.4 months for patients on placebo [hazard ratio (HR) 0.33; 95% confidence interval (CI) 0.24–240.47, p <0.0001] (47). A total of 14 (7%) patients had a partial response, and 120 (58%) had stable

disease with sunitinib therapy. In the placebo arm, none had a partial response and 50 (48%) had stable disease (47). Sunitinib showed an acceptable safety profile with most AEs being mild to moderate according to Common Terminology Criteria for Adverse Events. However, low-grade toxicities such as stomatitis and enteral mucositis impact quality of life to a greater degree than the grading would imply as present on a daily basis. In addition, serious treatment-related AEs were reported in 20% of sunitinib-treated patients (47) including hand-foot syndrome, hypertension, and diarrhea as well as hematological AEs (47).

Like imatinib, the efficacy of sunitinib correlates with both primary and secondary mutational status. In a retrospective study of 1124 patients with GIST who progressed on imatinib, those who received sunitinib and had tumors that carried exon 9 *KIT* mutations had significantly longer mPFS (12.3 months) than those with exon 11 mutations (7 months) (48). In the above referenced phase 1/2 trial of sunitinib, primary *KIT* mutations were identified in 83% of tumors (49). Clinical benefit and mPFS were better in patients with GIST exon 9 *KIT* mutations compared with exon 11 mutations (clinical benefit: 58% *vs* 34%; PFS: 19.4 *vs* 5.1 months, p = 0.0005) (49). Most secondary mutations occurred in *KIT* exons 13, 14, and 17 (49). Preclinical studies strongly suggest that sunitinib is highly potent against secondary mutations in exons 13 and 14, while mostly inactive against secondary mutations in exon 17 and 18 (50). Clinical evidence supports these findings in retrospective analyses. Patients with a detectable *KIT* exon 13/14 mutation had significantly longer mPFS compared with patients with a detectable exon 17/18 mutation (49).

Regorafenib

Regorafenib (formerly BAY 73-4506) is an oral, multitarget TKI that was originally developed for renal cancer with a focus on VEGFR inhibitory function (51). It is a competitive inhibitor of the ATP-binding site for KIT and several other targets, including VEGFR-2, TIE2, PDGFRβ, FGFR, RET, cRAF/RAF1, and BRAF (52). Regorafenib is approved for third-line treatment of advanced GIST after progression on imatinib and sunitinib (25).

In preclinical studies, regorafenib showed potent antitumor activity in multiple *in vivo* cancer models (52). In a phase 2 clinical trial as a third-line or higher in patients with advanced GIST (N = 34), of 33 eligible patients, regorafenib provided a mPFS of 10 months. Overall, 4 (12%) patients had a partial response and 22 (66.7%) had stable disease (53). Regorafenib has a safety profile similar to other TKIs with a comparable target spectrum; the most commonly observed AEs were mostly Grade 1 or 2 and consisted of hand-foot syndrome (85%), fatigue (79%), hypertension (67%), and diarrhea (61%) (53). A placebo-controlled, randomized, phase 3 trial (GRID), confirmed the efficacy of regorafenib as third-line or later treatment in patients with advanced GIST. Regorafenib treatment resulted in a mPFS of 4.8 months compared to 0.9 months on placebo (HR 0.27, 95% CI 0.19–0.39; p <0.0001) (54). In patients on regorafenib, a partial response was observed in 6 (4.5%) and 95 (71.4%) had stable disease *vs* 1 (1.5%) with a partial response and 22 (33.3%) with stable disease in the placebo arm (54). Drug-related AEs of any grade were reported in 98.5% of patients on regorafenib and in 68.2% of patients in the placebo arm (54). Grade 3 or higher AEs were reported in 61.4% of regorafenib-treated patients. Some of these AEs included hypertension (23.5%), hand-foot syndrome (19.7%), and diarrhea (5.3%) (54). Grade 3 events in the placebo arm were less frequent (13.6%): hand-foot syndrome (0), hypertension (3.0%), diarrhea (0) (54).

As with imatinib and sunitinib, tumor mutational status also affects regorafenib efficacy. In a phase 2 trial of patients with *KIT* exon 17 secondary mutations, treatment with third-line regorafenib provided significant clinical benefit, with a mPFS of 22.1 months (55). Using tumor samples obtained from the phase 2 trial and additional cell culture and GIST xenograft studies, the impact of different mutations on tumor response to drug was assessed (56). The results showed regorafenib has a complementary activity profile to sunitinib against secondary *KIT* mutations (56). While regorafenib is effective against many mutations, it has poor efficacy against the *KIT* exon 13 V654A mutation, a common secondary imatinib-resistant mutation. Regorafenib is effective for several exon 17 amino acid substitutions involving residue 816, but is resistant to D816V (56).

While these 3 early TKIs have improved the treatment of advanced GIST, treatment resistance remains a challenge as these drugs are not effective against all relevant GIST-associated mutations (**Figure 1**). Two issues are evident. First, all 3 TKIs are type II multikinase inhibitors, which bind to the ATP-pocket of KIT/PDGFRA only in the inactive formation. Secondary mutations in the activation loop induce a shift towards the active confirmation, reducing the ability of these drugs to bind to the kinase (13). Second, complex intra- and intertumor heterogeneity contribute to drug resistance, making global tumor control difficult. Early GIST TKIs inhibit certain mutations in KIT and PDGFRA, but they do not inhibit all mutations, and in particular, have limited activity against activation loop mutations. Two recently approved next-generation TKIs, avapritinib and ripretinib, were specifically developed to address these issues.

NEXT-GENERATION NOVEL TKIs RIPRETINIB AND AVAPRITINIB HAVE UNIQUE MOAs

Ripretinib (DCC-2618)

Ripretinib received FDA approval on May 15, 2020, for the treatment of adult patients with advanced GIST who have received prior treatment with 3 or more kinase inhibitors, including imatinib (57). Ripretinib is a novel type II switch control kinase inhibitor with a dual MOA, regulating both the kinase switch-pocket and activation loop (**Figure 2**) (14). Ripretinib functions by binding to the switch pocket, preventing access by the activation loop and thus blocking the kinase from adopting an active state. This results in the inhibition of downstream signal transduction (14). Ripretinib was designed as a broad-spectrum KIT and PDGFRA kinase

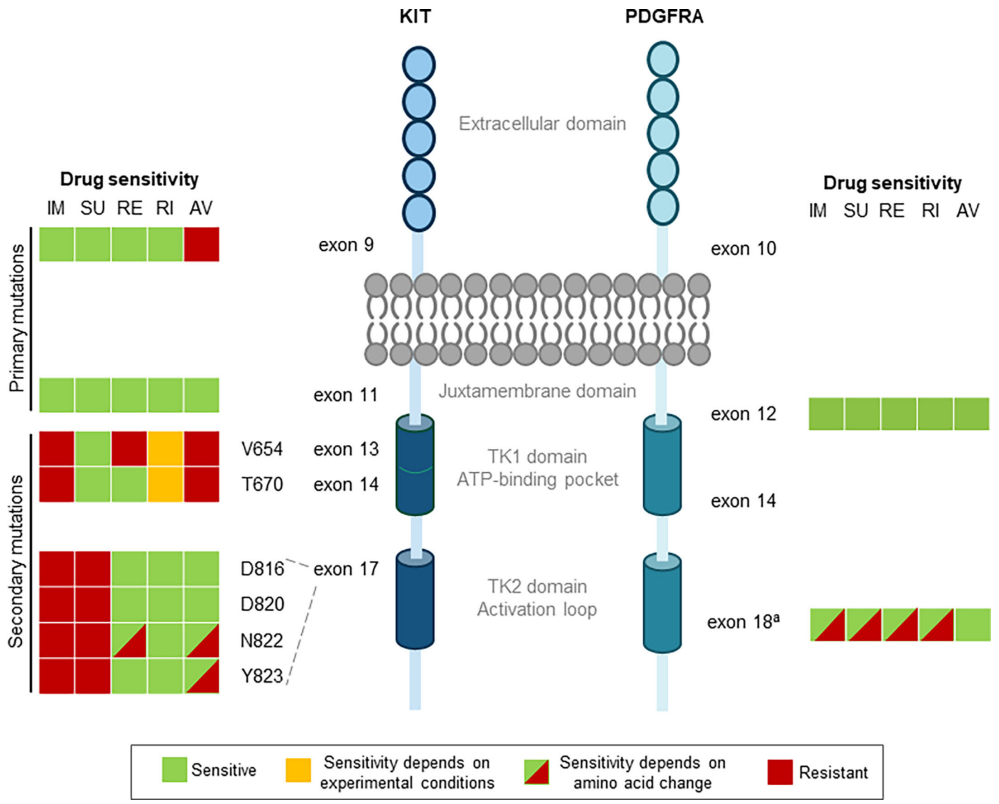

FIGURE 1 | Drug sensitivities for primary and secondary mutations in GIST. Colors denote drug sensitivity: green indicates sensitive, orange indicates sensitivity depends on experimental conditions, red indicates resistant, and red/green hatching indicates that the sensitivity is dependent on the amino acid change. [a]Approved TKIs are sensitive to non D842V, but only avapritinib and, to some degree, ripretinib are potent against the PDGFRA exon 18 D842V mutation. AV, avapritinib; GIST, gastrointestinal stromal tumors; IM, imatinib; PDGFRA, platelet-derived growth factorreceptor a; RE, regorafenib; RI, ripretinib; SU, sunitinib; TK1, tyrosine kinase domain 1; TK2, tyrosine kinase domain 2.

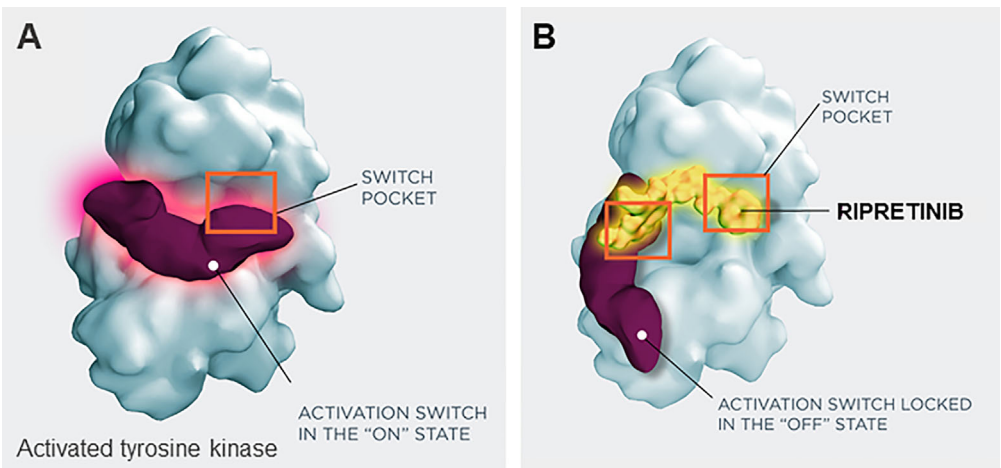

FIGURE 2 | Switch control inhibition by ripretinib. **(A)** Activated tyrosine kinase, **(B)** inactivated tryosine kinase, with ripretinib. Ripretinib uses a dual mechanism of action that secures the kinase into an inactive confirmation and prevents downstream signaling by binding both the switch-pocket region and the activation switch.

inhibitor that inhibits the full spectrum of primary and secondary drug resistance mutations, including activation loop mutations previously thought to be targeted only by type I inhibitors (14).

Preclinical studies of ripretinib showed significant antitumor activity in GIST and mastocytosis models, including inhibition of proliferation and induction of apoptosis (14, 58). In a preclinical study, ripretinib displayed a broader spectrum of inhibition and, compared with early TKIs, was a potent inhibitor of both wild-type and mutant KIT and PDGFRA kinases, including *PDGFRA* exon 18 D842V mutation (14).

The first human trial, a two-part (dose escalation and dose expansion) phase 1 study, assessed safety and tolerability of ripretinib in advanced GIST with KIT or PDGFRA mutations that had at least one prior line of therapy (59). No maximum tolerated dose was reached during the study, with less than 33% of patients at each dose level experiencing a dose-limiting toxicity (59). The recommended phase 2 dose was established at 150 mg once daily, based on preclinical pharmacology studies predicting 150 mg once daily to be an effective dose, as well as the initial pharmacokinetics analysis. Peak plasma concentration [mean C_{max} (coefficient of variation %)] following a single dose of 150 mg ripretinib on cycle 1 day 1 was determined to be 502 ng/mL (56.8%) and exposure ($AUC_{0\text{-}24h}$) was 6634 ng x h/mL (59.8%) (59). Overall, in the phase 1 trial, ripretinib had a favorable safety profile and was generally well tolerated; the most common TEAE was alopecia (62%) (59). In patients on second-line treatment, the mPFS was 10.7 months; as a third-line treatment, the mPFS was 8.3 months; for fourth-line, the mPFS was 5.5 months (59). Among patients receiving 150 mg once daily, upon disease progression, they had the option to dose escalate to 150 mg twice daily. Dose escalation demonstrated an additional PFS clinical benefit across all treatment lines with a safety profile similar to that observed at the once-daily dose (60).

The efficacy of ripretinib was further evaluated in the INVICTUS study (NCT03353753), a double-blind, randomized, placebo-controlled phase 3 trial assessing ripretinib in patients with advanced GIST who had progressed on at least imatinib, sunitinib, and regorafenib (61). As a fourth-line or later treatment, ripretinib significantly increased mPFS over placebo (6.3 months *vs* 1 month, respectively; HR 0.15, 95% CI 0.09–0.25; p <0.0001) (61). The median OS was 15.1 months in the ripretinib group compared to 6.6 months in the placebo group. For patients in the ripretinib arm, 8 (9%) had a partial response, 56 (66%) had stable disease at 6 weeks, and 40 (47%) had stable disease at 12 weeks, compared with patients in the placebo arm, which showed 0 patients with a partial response, 9 (20%) with stable disease at 6 weeks, and 2 (5%) with stable disease at 12 weeks (61). Patients in the INVICTUS study also had the option to dose escalate to 150 mg twice daily. Of the 43 patients in the ripretinib arm that dose escalated, mPFS before dose escalation was 4.6 months and after escalation mPFS was 3.7 months, providing further support for the potential of dose escalation with ripretinib following disease progression (62). A third clinical trial—the randomized, open-label, phase 3 INTRIGUE (NCT03673501) trial—completed accrual in December 2020, comparing the safety and efficacy of ripretinib to sunitinib in patients with advanced GIST who have progressed on imatinib (61, 63). This trial is poised to provide some important information on the efficacy of ripretinib on secondary mutations. In addition, effective salvage therapies may shift based upon the differential activity of ripretinib as compared with sunitinib, with the spectrum and distribution of resistance mutations likely differing between the 2 cohorts after treatment with ripretinib or sunitinib.

While ripretinib shows improved survival in GIST patients, even following treatment with all approved agents, and has a proposed broad-spectrum inhibition for primary and secondary mutations, patients continue to show disease progression. This disease progression may be due to yet unidentified resistance mechanisms; it has been speculated that potential resistance mechanisms in ripretinib could involve ATP-binding pocket resistance mutations (10). In addition, when strong KIT/PDGFRA inhibition is achieved, emergence of KIT-independent resistance mechanisms is likely to occur, potentially involving mutations of PI3K, RAS/RAF, TSC1 and 2, and NF1 (36). Alternatively, not all mutations may be maximally inhibited. A recent study has suggested that ripretinib may only have modest activity against exon 13 and 14 *KIT* mutations in an assay performed in the presence of physiological amounts of human serum albumin and alpha1-acid glycoprotein (64), which may explain why the PFS in the INVICTUS study was not longer. This is in contrast to what was reported in Smith et al. (14), which showed strong inhibition of these mutations. However, there were methodological differences between these two studies, including the amount and type of serum protein in the assay system.

Avapritinib (BLU285)

Avapritinib, a selective, small-molecule inhibitor of KIT and PDGFRA activation loop mutants, was approved in January 2020 by the FDA for treatment of GISTs that harbor a *PDGFRA* exon 18 mutation, including D842V mutations (65). Notably, it was the first TKI approved with efficacy for GIST with the *PDGFRA* D842V mutation and is more potent (~10 fold) against this mutation than ripretinib (14). Avapritinib is a competitive ATP-binding site inhibitor; however, it was designed to specifically interact with the active conformation (type I kinase inhibitor), unlike the early type II kinase inhibitors that only bind to the inactive conformation (13).

In both *in vitro* and *in vivo* preclinical testing, avapritinib demonstrated potency across a spectrum of primary and secondary mutations, including the difficult-to-treat *PDGFRA* D842V mutation (13, 66). In preclinical murine models with patient-derived GIST xenografts (UZLX-GIST9$^{KIT11+17}$; UZLX-GIST3^{KIT11}GIST3^{KIT11}; UZLX-GIST2B^{KIT9}GIST2B^{KIT9}), avapritinib reduced tumor volume and inhibited proliferation (66).

The safety and efficacy of avapritinib was evaluated in 2 clinical trials, NAVIGATOR and VOYAGER. The NAVIGATOR trial was an open-label, 2-part, dose escalation and dose expansion phase 1 trial of patients with advanced GIST (67). Part 1 of the study, dose escalation, included patients with advanced GIST who were refractive to imatinib and at least one other TKI. Part 2, dose expansion, had several cohorts, including one restricted to patients

with advanced GIST with the *PDGFRA* D842V mutation, regardless of prior therapy status (67). Part 1 enrolled 46 patients, of whom 20 had *PDGFRA* D842V mutant GIST; part 2 enrolled 36 patients with *PDGFRA* D842V mutant GIST (67). Overall, in the *PDGFRA* D842V mutant GIST population (56 patients), 5 (9%) had a complete response, 44 (79%) had a partial response, and 7 (13%) had stable disease; PFS was 81% at 12 months (67). Updated results of the *PDGFRA* D842V mutant GIST population report an overall response rate of 91% (51/56 patients), a median PFS of 34 months, and the median OS not yet reached (68). In this study, avapritinib had an acceptable safety profile, with AEs typically Grade 1 or 2. Two AEs of special interest were identified: cognitive effects (40%, including memory impairment, cognitive disorder, confusional state, and encephalopathy) and intracranial bleeding (2%) (67). The majority of cognitive effects were Grade 1 and led to discontinuation of treatment in 2 patients (67). For effective management of neurocognitive side effects greater than Grade 1, patients need immediate dose reductions or interruptions, which requires close monitoring, in order to allow long-term treatment in a GIST genotype for which no other treatment is available (65).

Very recently, mechanisms of secondary resistance to avapritinib in PDGFRA-mutant GIST have been described (69). They involve compound mutations of exons 13, 14, and 15 of *PDGFRA* that show cross-resistance to all other drugs that inhibit PDGFRA (69).

The VOYAGER trial (NCT03465722) was an open-label, randomized, phase 3 trial comparing avapritinib and regorafenib in patients with metastatic GIST previously treated with imatinib and 1 or 2 other TKIs (70). A press release from the study sponsor indicated that the VOYAGER trial did not meet its primary endpoint of increased PFS in patients treated with avapritinib compared to regorafenib. The reported PFS with avapritinib was 4.2 months, which was not significantly different from regorafenib at 5.6 months (70).

INTRA- AND INTERTUMORAL HETEROGENEITY AND CLONAL EVOLUTION COMPLICATES TREATMENT

Tumor heterogeneity is a major issue in cancer treatment because it contributes to the variable response between patients. As discussed above, exposure to imatinib exerts pressure on a tumor that can trigger the selection and expansion of clones with secondary mutations (71). In patients with GIST primary mutations, tumors harboring multiple secondary kinase mutations are reported in approximately 19% – 44% of patients; up to 70% of patients have GIST with ≥2 different mutations in separate metastases (12, 41, 72, 73). As TKIs have selective efficacy for different mutations, intra- and intertumoral heterogeneity result in mixed responses to treatment. This may explain why PFS is shorter with subsequent TKIs post-imatinib. Resistance to second-line and greater TKIs may result from pre-existing small clones or new mutations driven by selective pressure. Whole genome sequencing in TKI-resistant GIST has revealed a subset of patients who harbor mutations in intermediates of KIT-downstream signaling that are potentially involved with resistance (36).

Heterogeneity can be difficult to detect and is likely underestimated, as samples cannot be taken from every tumor. Currently, tissue biopsy is the gold standard for molecular characterization (74); however, it provides a static picture of one part of the tumor at a single point in time and repeated sampling is not feasible for these patients (74). Liquid biopsy combined with sequencing techniques, such as next-generation sequencing, is an emerging technology that has the potential to address these issues. Circulating tumor-associated molecules within the blood such as circulating tumor DNA (ctDNA) and circulating tumor cells can be captured and sequenced to monitor the evolution of GIST mutations and identify those associated with drug resistance (74). The majority of liquid biopsy studies in GIST have assessed ctDNA (for a detailed review, see Gómez-Peregrina et al.) (75). Patients with localized disease were less likely to have detectable ctDNA, whereas those with high-burden metastatic disease that was progressing showed the highest rate of ctDNA detection (76). Overall, it is difficult to make direct comparisons between studies, as they have different methodologies. The data suggests, however, that there is potential for the utility of liquid biopsy in GIST, and there is ongoing research to optimize this utility in this patient population (74, 75). In a recent study, next-generation sequencing of liquid biopsies of GIST from treated patients with high tumor burden confirmed that multiple resistance mutations can be simultaneously present and detected in ctDNA shed from tumors (77). Secondary mutations were diverse and determined to be spatially distributed in the tumors *via* detailed analysis of tissue from surgical resection (77). For one patient in the study, comprehensive analysis of repeated plasma samples over 53 weeks identified intratumor heterogeneity and polyclonal evolution that would not have been captured with tissue biopsy (77). In the INVICTUS trial, combining tumor and liquid biopsy increased the rate of detection for resistance mutations, allowing detection in 73% of patients (78). Plasma sequencing from these liquid biopsies revealed secondary resistance mutations in at least 1 exon in 70% of KIT/PDGFRA primary mutant GIST, and 24% of patients had 2 or more exons affected, with up to 4 exon mutations detected in 1 patient (78). These results highlight the heterogeneity of GIST tumors. Liquid biopsy has also been correlated with treatment response. The NAVIGATOR trial, which assessed avapritinib in patients with GIST, showed lower baseline ctDNA levels were associated with prolonged PFS (79). However, despite its potential, liquid biopsy is in the early stages of development for GIST and is not yet validated as a tool for clinical decision-making. Given the role of mutations in GIST, it is likely that the combined results from primary tumor genotyping, ctDNA, and tumor biopsies will be used in the future to guide treatment decisions for patients with TKI-resistant disease. Therefore, patients would benefit from treatment with a multidisciplinary team that routinely evaluates and uses such data in their clinical decision making.

TABLE 1 | Summary of approved treatments for advanced GIST.

	Imatinib	Sunitinib	Regorafenib	Ripretinib	Avapritinib
Indication for advanced GIST	1st line	2nd line	3rd line	4th line	PDGFRA Exon 18 mutant (including D842V)
MOA	Type II[a] Competitive ATP-binding site inhibitor	Type II[a] Competitive ATP-binding site inhibitor	Type II[a] Competitive ATP-binding site inhibitor	Type II[a] Switch-pocket inhibitor	Type I[b] Competitive ATP-binding site inhibitor
Efficacy					
mPFS (mo)	18	5.6	4.8	6.3	34 [c]
ORR (%)	50	7	4.5	9.4	91[c]

[a]*Binds the inactive confirmation.*
[b]*Binds the active confirmation.*
[c]*D842V patients only.*
GIST, gastrointestinal stromal tumor; mo, months; MOA, mechanism of action; mPFS, median progression-free survival; ORR, overall response rate; PDGFRA, platelet-derived growth factor receptor a.

SUMMARY OF ADVANCED GIST TREATMENTS AND FUTURE STEPS

KIT/PDGFRA inhibition remains the backbone of therapy for metastatic GIST due to the underlying oncogenic drivers of this disease. Despite providing significant clinical benefit, resistance and disease progression limit patient survival, with secondary KIT mutations as the major driver of resistance. In 2020, two new TKIs, avapritinib and ripretinib, were approved for advanced GIST (57, 65). Both have unique MOAs and were designed to address known mechanisms of resistance to early TKIs. Ripretinib, as a switch-pocket inhibitor may inhibit a broader range of mutations, while avapritinib, a type 1 kinase inhibitor, clearly provides benefit for the previously treatment-resistant PDGFRA D842V mutation. **Table 1** presents a summary of the key differences between the available treatments.

Future of Advanced GIST Treatment

A major challenge in GIST treatment is polyclonal resistance, whereby a single drug is insufficient to target all resistant KIT mutations, thus resulting in tumor progression. While ripretinib has a broad spectrum of inhibition compared to early TKIs, disease progression still occurs. In an attempt to address the need for multiple TKIs to cover the heterogeneity of the tumors, clinical trials have investigated TKI treatments with rapid alternation for tumors with polyclonal secondary mutations. In the SURE study (NCT02164240), a phase 1/2, open-label trial, rapid alternation of sunitinib and regorafenib was used to treat advanced GIST that was refractory to imatinib (80). Sunitinib and regorafenib were chosen because of their complementary inhibition profiles for KIT mutations (80). Patients experienced 3 days of sunitinib followed by 4 days of regorafenib (80). Of 13 enrolled patients, 4 had stable disease, and the mPFS for all patients was 1.9 months, which is similar to rechallenge with imatinib (80). All 13 patients experienced treatment-related AEs, the majority of which were Grade 1 or 2. The most common AEs were fatigue (92%), weight loss (62%), hand-foot syndrome (54%), anorexia (38%), hypertension (38%), and hoarseness (38%) (80). Rapid alteration with other TKIs may represent a viable strategy in the future for the treatment of advanced GIST. The possibility of using the new generation TKIs with more favorable safety profiles, like ripretinib, in such a scenario is an appealing possibility. Another combination of 2 drugs with complementary activity that showed promise is PLX9486 (a selective TKI now known as CGT9486) with sunitinib, yielding a mPFS of 12 months in the initial study report (81). Other future strategies to overcome polyclonal resistance using currently approved drugs may include combination treatment. For example, preliminary results of the combination of imatinib and binimetinib for first-line treatment of advanced GIST has shown promise; of 38 patients, 26 had a partial response (82). Additional future strategies may include more complex scheduling or brief periods of using a triple combination of anti-cancer therapies.

Additionally, other targets are in development, including heat-shock protein 90 (HSP90) inhibitors. HSP90 inhibitors can induce KIT degradation and thus represent a potential therapy for GIST (83). Early HSP90 inhibitors had issues with hepatotoxicity and neurological toxicities (83). However, newer HSP90 inhibitors such as TAS-116 are showing promise in both preclinical and clinical trials for antitumor activity and more manageable AEs with intermittent dosing (83–85). Finally, reports showing adaptive and innate immune cells in the GIST tumor microenvironment also suggest immunotherapy may be a potential future treatment for GIST (86). Anti-human CD117 chimeric antigen receptor T-cells were recently shown to eliminate healthy and malignant CD117-expressing hematopoietic cells (87); these cells may have potential for malignant CD117-expressing cells in GIST as well, but more research is needed.

In conclusion, KIT and PDGFRA, as the oncogenic drivers of GIST, are still viable targets for therapy as demonstrated by the approval of ripretinib and avapritinib. Their unique MOAs have helped address some of the limitations of early TKI treatments. Despite improved outcomes, polyclonal resistance and tumor heterogeneity still lead to disease progression, and continued research to overcome these challenges is necessary.

AUTHOR CONTRIBUTIONS

SB and MCH devised the main conceptual ideas and outline. All authors contributed to the article and approved the submitted version.

FUNDING

The authors received no financial support for the research, authorship, and/or publication of this article. Funding for editorial support was provided by Deciphera Pharmaceuticals, LLC. Medical writing and editorial support were provided by Helen Rodgers, PhD, of AlphaBioCom, LLC, King of Prussia, PA, USA, and funded by Deciphera Pharmaceuticals, LLC, Waltham, MA, USA. MCH received partial salary support from Veterans Affairs Merit Review Grants (2I01BX000338-05 and 1I01BX005358).

REFERENCES

1. Robinson TL, Sircar K, Hewlett BR, Chorneyko K, Riddell RH, Huizinga JD. Gastrointestinal Stromal Tumors may Originate From a Subset of CD34-Positive Interstitial Cells of Cajal. *Am J Pathol* (2000) 156(4):1157–63. doi: 10.1016/S0002-9440(10)64984-X
2. Sircar K, Hewlett BR, Huizinga JD, Chorneyko K, Berezin I, Riddell RH. Interstitial Cells of Cajal as Precursors of Gastrointestinal Stromal Tumors. *Am J Surg Pathol* (1999) 23(4):377–89. doi: 10.1097/00000478-199904000-00002
3. Soreide K, Sandvik OM, Soreide JA, Giljaca V, Jureckova A, Bulusu VR. Global Epidemiology of Gastrointestinal Stromal Tumours (GIST): A Systematic Review of Population-Based Cohort Studies. *Cancer Epidemiol* (2016) 40:39–46. doi: 10.1016/j.canep.2015.10.031
4. Szucs Z, Thway K, Fisher C, Bulusu R, Constantinidou A, Benson C, et al. Molecular Subtypes of Gastrointestinal Stromal Tumors and Their Prognostic and Therapeutic Implications. *Future Oncol* (2017) 13(1):93–107. doi: 10.2217/fon-2016-0192
5. Corless CL, Schroeder A, Griffith D, Town A, McGreevey L, Harrell P, et al. PDGFRA Mutations in Gastrointestinal Stromal Tumors: Frequency, Spectrum and *In Vitro* Sensitivity to Imatinib. *J Clin Oncol* (2005) 23 (23):5357–64. doi: 10.1200/JCO.2005.14.068
6. Martin-Broto J, Martinez-Marin V, Serrano C, Hindi N, Lopez-Guerrero JA, Bisculoa M, et al. Gastrointestinal Stromal Tumors (GISTs): SEAP-SEOM Consensus on Pathologic and Molecular Diagnosis. *Clin Transl Oncol* (2017) 19(5):536–45. doi: 10.1007/s12094-016-1581-2
7. Hostein I, Faur N, Primois C, Boury F, Denard J, Emile JF, et al. BRAF Mutation Status in Gastrointestinal Stromal Tumors. *Am J Clin Pathol* (2010) 133(1):141–8. doi: 10.1309/AJCPPCKGA2QGBJ1R
8. Belinsky MG, Rink L, von Mehren M. Succinate Dehydrogenase Deficiency in Pediatric and Adult Gastrointestinal Stromal Tumors. *Front Oncol* (2013) 3:117. doi: 10.3389/fonc.2013.00117
9. George S, Heinrich MC, Zalcberg J, Bauer S, Gelderblom H, Schoffski P, et al. Safety Profile of Ripretinib, Including Impact of Alopecia and Palmar-Plantar Erythrodyesthesia Syndrome (PPES) on Patient Reported Outcomes (PROs) in ≥4th-Line Advanced Gastrointestinal Stromal Tumors (GISTs): Analyses From INVICTUS. *J Clin Oncol* (2020) 38(suppl):Abstract 11539. doi: 10.1200/JCO.2020.38.15_suppl.11539
10. Serrano C, George S. Gastrointestinal Stromal Tumor: Challenges and Opportunities for a New Decade. *Clin Cancer Res* (2020) 26(19):5078–85. doi: 10.1158/1078-0432.CCR-20-1706
11. Li GZ, Raut CP. Targeted Therapy and Personalized Medicine in Gastrointestinal Stromal Tumors: Drug Resistance, Mechanisms, and Treatment Strategies. *Onco Targets Ther* (2019) 12:5123–33. doi: 10.2147/OTT.S180763
12. Liegl B, Kepten I, Le C, Zhu M, Demetri GD, Heinrich MC, et al. Heterogeneity of Kinase Inhibitor Resistance Mechanisms in GIST. *J Pathol* (2008) 216(1):64–74. doi: 10.1002/path.2382
13. Evans EK, Gardino AK, Kim JL, Hodous BL, Shutes A, Davis A, et al. A Precision Therapy Against Cancers Driven by KIT/PDGFRA Mutations. *Sci Transl Med* (2017) 9(414):1–12. doi: 10.1126/scitranslmed.aao1690
14. Smith BD, Kaufman MD, Lu WP, Gupta A, Leary CB, Wise SC, et al. Ripretinib (DCC-2618) Is a Switch Control Kinase Inhibitor of a Broad Spectrum of Oncogenic and Drug-Resistant KIT and PDGFRA Variants. *Cancer Cell* (2019) 35(5):738–51.e9. doi: 10.1016/j.ccell.2019.04.006
15. Klug LR, Kent JD, Heinrich MC. Structural and Clinical Consequences of Activation Loop Mutations in Class III Receptor Tyrosine Kinases. *Pharmacol Ther* (2018) 191:123–34. doi: 10.1016/j.pharmthera.2018.06.016
16. Cruse G, Metcalfe DD, Olivera A. Functional Deregulation of KIT: Link to Mast Cell Proliferative Diseases and Other Neoplasms. *Immunol Allergy Clin North Am* (2014) 34(2):219–37. doi: 10.1016/j.iac.2014.01.002
17. Ding H, Yu X, Yu Y, Lao X, Hang C, Gao K, et al. Clinical Significance of the Molecular Heterogeneity of Gastrointestinal Stromal Tumors and Related Research: A Systematic Review. *Oncol Rep* (2020) 43(3):751–64. doi: 10.3892/or.2020.7470
18. Corless CL, Barnett CM, Heinrich MC. Gastrointestinal Stromal Tumours: Origin and Molecular Oncology. *Nat Rev Cancer* (2011) 11(12):865–78. doi: 10.1038/nrc3143
19. Rubin BP, Singer S, Tsao C, Duensing A, Lux ML, Ruiz R, et al. KIT Activation Is a Ubiquitous Feature of Gastrointestinal Stromal Tumors. *Cancer Res* (2001) 61(22):8118–21.
20. Lasota J, Miettinen M. KIT and PDGFRA Mutations in Gastrointestinal Stromal Tumors (GIST). *Semin Diagn Pathol* (2006) 23(2):91–102. doi: 10.1053/j.semdp.2006.08.006
21. Heinrich MC, Corless CL, Duensing A, McGreevey L, Chen CJ, Joseph N, et al. PDGFRA Activating Mutations in Gastrointestinal Stromal Tumors. *Science* (2003) 299(5607):708–10. doi: 10.1126/science.1079666
22. Corless CL. Gastrointestinal Stromal Tumors: What do We Know Now? *Mod Pathol* (2014) 27(Suppl 1):S1–16. doi: 10.1038/modpathol.2013.173
23. Kufareva I, Abagyan R. Type-II Kinase Inhibitor Docking, Screening, and Profiling Using Modified Structures of Active Kinase States. *J Med Chem* (2008) 51(24):7921–32. doi: 10.1021/jm8010299
24. Gleevec. *Prescribing Information*. East Hanover, NJ: Novartis Pharmaceuticals Corporation (2020).
25. Stivarga. *Prescribing Information*. Whippany, NJ: Bayer HealthCare Pharmaceuticals Inc (2020).
26. Sutent. *Prescribing Information*. New York, NY: Pfizer Labs (2020).
27. Dagher R, Cohen M, Williams G, Rothmann M, Gobburu J, Robbie G, et al. Approval Summary: Imatinib Mesylate in the Treatment of Metastatic and/or Unresectable Malignant Gastrointestinal Stromal Tumors. *Clin Cancer Res* (2002) 8(10):3034–8.
28. Peng B, Lloyd P, Schran H. Clinical Pharmacokinetics of Imatinib. *Clin Pharmacokinet* (2005) 44(9):879–94. doi: 10.2165/00003088-200544090-00001
29. Iqbal N, Iqbal N. Imatinib: A Breakthrough of Targeted Therapy in Cancer. *Chemother Res Pract* (2014) 2014:357027. doi: 10.1155/2014/357027
30. Joensuu H, Roberts PJ, Sarlomo-Rikala M, Andersson LC, Tervahartiala P, Tuveson D, et al. Effect of the Tyrosine Kinase Inhibitor STI571 in a Patient With a Metastatic Gastrointestinal Stromal Tumor. *N Engl J Med* (2001) 344 (14):1052–6. doi: 10.1056/NEJM200104053441404
31. van Oosterom AT, Judson I, Verweij J, Stroobants S, Donato di Paola E, Dimitrijevic S, et al. Safety and Efficacy of Imatinib (STI571) in Metastatic Gastrointestinal Stromal Tumours: A Phase I Study. *Lancet* (2001) 358 (9291):1421–3. doi: 10.1016/S0140-6736(01)06535-7
32. Demetri GD, von Mehren M, Blanke CD, Van den Abbeele AD, Eisenberg B, Roberts PJ, et al. Efficacy and Safety of Imatinib Mesylate in Advanced Gastrointestinal Stromal Tumors. *N Engl J Med* (2002) 347(7):472–80. doi: 10.1056/NEJMoa020461
33. Verweij J, Casali PG, Zalcberg J, LeCesne A, Reichardt P, Blay JY, et al. Progression-Free Survival in Gastrointestinal Stromal Tumours With High-Dose Imatinib: Randomised Trial. *Lancet* (2004) 364(9440):1127–34. doi: 10.1016/S0140-6736(04)17098-0
34. Blanke CD, Rankin C, Demetri GD, Ryan CW, von Mehren M, Benjamin RS, et al. Phase III Randomized, Intergroup Trial Assessing Imatinib Mesylate at Two Dose Levels in Patients With Unresectable or Metastatic Gastrointestinal Stromal Tumors Expressing the Kit Receptor Tyrosine Kinase: S0033. *J Clin Oncol* (2008) 26(4):626–32. doi: 10.1200/JCO.2007.13.4452
35. Gramza AW, Corless CL, Heinrich MC. Resistance to Tyrosine Kinase Inhibitors in Gastrointestinal Stromal Tumors. *Clin Cancer Res* (2009) 15 (24):7510–8. doi: 10.1158/1078-0432.CCR-09-0190
36. Muhlenberg T, Ketzer J, Heinrich MC, Grunewald S, Marino-Enriquez A, Trautmann M, et al. KIT-Dependent and KIT-Independent Genomic

Heterogeneity of Resistance in Gastrointestinal Stromal Tumors - TORC1/2 Inhibition as Salvage Strategy. *Mol Cancer Ther* (2019) 18(11):1985–96. doi: 10.1158/1535-7163.MCT-18-1224
37. Heinrich MC, Corless CL, Demetri GD, Blanke CD, von Mehren M, Joensuu H, et al. Kinase Mutations and Imatinib Response in Patients With Metastatic Gastrointestinal Stromal Tumor. *J Clin Oncol* (2003) 21(23):4342–9. doi: 10.1200/JCO.2003.04.190
38. Debiec-Rychter M, Sciot R, Le Cesne A, Schlemmer M, Hohenberger P, van Oosterom AT, et al. KIT Mutations and Dose Selection for Imatinib in Patients With Advanced Gastrointestinal Stromal Tumours. *Eur J Cancer* (2006) 42(8):1093–103. doi: 10.1016/j.ejca.2006.01.030
39. Napolitano A, Vincenzi B. Secondary KIT Mutations: The GIST of Drug Resistance and Sensitivity. *Br J Cancer* (2019) 120(6):577–8. doi: 10.1038/s41416-019-0388-7
40. Antonescu CR, Besmer P, Guo T, Arkun K, Hom G, Koryotowski B, et al. Acquired Resistance to Imatinib in Gastrointestinal Stromal Tumor Occurs Through Secondary Gene Mutation. *Clin Cancer Res* (2005) 11(11):4182–90. doi: 10.1158/1078-0432.CCR-04-2245
41. Heinrich MC, Corless CL, Blanke CD, Demetri GD, Joensuu H, Roberts PJ, et al. Molecular Correlates of Imatinib Resistance in Gastrointestinal Stromal Tumors. *J Clin Oncol* (2006) 24(29):4764–74. doi: 10.1200/JCO.2006.06.2265
42. Abrams TJ, Lee LB, Murray LJ, Pryer NK, Cherrington JM. SU11248 Inhibits KIT and Platelet-Derived Growth Factor Receptor Beta in Preclinical Models of Human Small Cell Lung Cancer. *Mol Cancer Ther* (2003) 2(5):471–8.
43. Christensen JG. A Preclinical Review of Sunitinib, a Multitargeted Receptor Tyrosine Kinase Inhibitor With Anti-Angiogenic and Antitumour Activities. *Ann Oncol* (2007) 18(Suppl 10):x3–10. doi: 10.1093/annonc/mdm408
44. Mendel DB, Laird AD, Xin X, Louie SG, Christensen JG, Li G, et al. *In Vivo* Antitumor Activity of SU11248, a Novel Tyrosine Kinase Inhibitor Targeting Vascular Endothelial Growth Factor and Platelet-Derived Growth Factor Receptors: Determination of a Pharmacokinetic/Pharmacodynamic Relationship. *Clin Cancer Res* (2003) 9(1):327–37.
45. O'Farrell AM, Foran JM, Fiedler W, Serve H, Paquette RL, Cooper MA, et al. An Innovative Phase I Clinical Study Demonstrates Inhibition of FLT3 Phosphorylation by SU11248 in Acute Myeloid Leukemia Patients. *Clin Cancer Res* (2003) 9(15):5465–76.
46. Demetri GD, Heinrich MC, Fletcher JA, Fletcher CD, Van den Abbeele AD, Corless CL, et al. Molecular Target Modulation, Imaging, and Clinical Evaluation of Gastrointestinal Stromal Tumor Patients Treated With Sunitinib Malate After Imatinib Failure. *Clin Cancer Res* (2009) 15(18):5902–9. doi: 10.1158/1078-0432.CCR-09-0482
47. Demetri GD, van Oosterom AT, Garrett CR, Blackstein ME, Shah MH, Verweij J, et al. Efficacy and Safety of Sunitinib in Patients With Advanced Gastrointestinal Stromal Tumour After Failure of Imatinib: A Randomised Controlled Trial. *Lancet* (2006) 368(9544):1329–38. doi: 10.1016/S0140-6736(06)69446-4
48. Reichardt P, Demetri GD, Gelderblom H, Rutkowski P, Im SA, Gupta S, et al. Correlation of KIT and PDGFRA Mutational Status With Clinical Benefit in Patients With Gastrointestinal Stromal Tumor Treated With Sunitinib in a Worldwide Treatment-Use Trial. *BMC Cancer* (2016) 16:22. doi: 10.1186/s12885-016-2051-5
49. Heinrich MC, Maki RG, Corless CL, Antonescu CR, Harlow A, Griffith D, et al. Primary and Secondary Kinase Genotypes Correlate With the Biological and Clinical Activity of Sunitinib in Imatinib-Resistant Gastrointestinal Stromal Tumor. *J Clin Oncol* (2008) 26(33):5352–9. doi: 10.1200/JCO.2007.15.7461
50. Garner AP, Gozgit JM, Anjum R, Vodala S, Schrock A, Zhou T, et al. Ponatinib Inhibits Polyclonal Drug-Resistant KIT Oncoproteins and Shows Therapeutic Potential in Heavily Pretreated Gastrointestinal Stromal Tumor (GIST) Patients. *Clin Cancer Res* (2014) 20(22):5745–55. doi: 10.1158/1078-0432.CCR-14-1397
51. Zopf D, Heinig R, Thierauch K, Hirth-dietrich C, Hafner F, Christensen O, et al. Regorafenib (BAY 73-4506): Preclinical Pharmacology and Clinical Identification and Quantification of its Major Metabolites. *Cancer Res* (2010) 70:abstract 1666. doi: 10.1158/1538-7445.AM10-1666
52. Wilhelm SM, Dumas J, Adnane L, Lynch M, Carter CA, Schutz G, et al. Regorafenib (BAY 73-4506): A New Oral Multikinase Inhibitor of Angiogenic, Stromal and Oncogenic Receptor Tyrosine Kinases With Potent Preclinical Antitumor Activity. *Int J Cancer* (2011) 129(1):245–55. doi: 10.1002/ijc.25864
53. George S, Wang Q, Heinrich MC, Corless CL, Zhu M, Butrynski JE, et al. Efficacy and Safety of Regorafenib in Patients With Metastatic and/or Unresectable GI Stromal Tumor After Failure of Imatinib and Sunitinib: A Multicenter Phase II Trial. *J Clin Oncol* (2012) 30(19):2401–7. doi: 10.1200/JCO.2011.39.9394
54. Demetri GD, Reichardt P, Kang YK, Blay JY, Rutkowski P, Gelderblom H, et al. Efficacy and Safety of Regorafenib for Advanced Gastrointestinal Stromal Tumours After Failure of Imatinib and Sunitinib (GRID): An International, Multicentre, Randomised, Placebo-Controlled, Phase 3 Trial. *Lancet* (2013) 381(9863):295–302. doi: 10.1016/S0140-6736(12)61857-1
55. Yeh CN, Chen MH, Chen YY, Yang CY, Yen CC, Tzen CY, et al. A Phase II Trial of Regorafenib in Patients With Metastatic and/or a Unresectable Gastrointestinal Stromal Tumor Harboring Secondary Mutations of Exon 17. *Oncotarget* (2017) 8(27):44121–30. doi: 10.18632/oncotarget.17310
56. Serrano C, Marino-Enriquez A, Tao DL, Ketzer J, Eilers G, Zhu M, et al. Complementary Activity of Tyrosine Kinase Inhibitors Against Secondary Kit Mutations in Imatinib-Resistant Gastrointestinal Stromal Tumours. *Br J Cancer* (2019) 120(6):612–20. doi: 10.1038/s41416-019-0389-6
57. Qinlock. *Prescribing Information*. Waltham, MA: Deciphera Pharmaceuticals, LLC (2020).
58. Schneeweiss M, Peter B, Bibi S, Eisenwort G, Smiljkovic D, Blatt K, et al. The KIT and PDGFRA Switch-Control Inhibitor DCC-2618 Blocks Growth and Survival of Multiple Neoplastic Cell Types in Advanced Mastocytosis. *Haematologica* (2018) 103(5):799–809. doi: 10.3324/haematol.2017.179895
59. Janku F, Abdul Razak AR, Chi P, Heinrich MC, von Mehren M, Jones RL, et al. Switch Control Inhibition of KIT and PDGFRA in Patients With Advanced Gastrointestinal Stromal Tumor: A Phase I Study of Ripretinib. *J Clin Oncol* (2020) 38:3294–303. doi: 10.1200/JCO.20.00522
60. Janku F, Chi P, Heinrich MC, von Mehren M, Jones RL, Ganjoo K, et al. Ripretinib Intra-Patient Dose Escalation (IPDE) Following Disease Progression Provides Clinically Meaningful Progression-Free Survival (PFS) in Gastrointestinal Stromal Tumor (GIST) in Phase I Study. *Ann Oncol* (2020) 31:S974–S5. doi: 10.1016/j.annonc.2020.08.1849
61. Blay JY, Serrano C, Heinrich MC, Zalcberg J, Bauer S, Gelderblom H, et al. Ripretinib in Patients With Advanced Gastrointestinal Stromal Tumours (INVICTUS): A Double-Blind, Randomised, Placebo-Controlled, Phase 3 Trial. *Lancet Oncol* (2020) 21(7):923–34. doi: 10.1016/S1470-2045(20)30168-6
62. Zalcberg J, Heinrich MC, George S, Bauer S, Schoffski P, Serrano C, et al. (2021). Intra-Patient Dose Escalation of Ripretinib After Disease Progression in Patients With Advanced Gastrointestinal Stromal Tumor: Analyses From the Phase 3 INVICTUS Study Presented at the American Society of Clinical Oncology annual meeting.
63. Deciphera Pharmaceuticals, LLC. *Deciphera Pharmaceuticals Completes Target Enrollment in the INTRIGUE Phase 3 Clinical Study of QINLOCK® (Ripretinib) in Patients With Second-Line Gastrointestinal Stromal Tumor* (2020). Available at: https://investors.deciphera.com/news-releases/news-release-details/deciphera-pharmaceuticals-completes-target-enrollment-intrigue.
64. Rivera V, Huang W-S, Lu M, Pritchard J, Dalgarno DC, Shakespeare W. Preclinical Characterization of THE-630, a Next-Generation Inhibitor for KIT-Mutant Gastrointestinal Stromal Tumors (GIST). Presented at the American Association for Cancer Research (AACR). (2021).
65. Ayvakit. *Prescribing Information*. Cambridge, MA: Blueprint Medicines Corporation (2020).
66. Gebreyohannes YK, Wozniak A, Zhai ME, Wellens J, Cornillie J, Vanleeuw U, et al. Robust Activity of Avapritinib, Potent and Highly Selective Inhibitor of Mutated KITIn Patient-Derived Xenograft Models of Gastrointestinal Stromal Tumors. *Clin Cancer Res* (2019) 25(2):609–18. doi: 10.1158/1078-0432.CCR-18-1858
67. Heinrich MC, Jones RL, von Mehren M, Schoffski P, Serrano C, Kang YK, et al. Avapritinib in Advanced PDGFRA D842V-Mutant Gastrointestinal Stromal Tumour (NAVIGATOR): A Multicentre, Open-Label, Phase 1 Trial. *Lancet Oncol* (2020) 21(7):935–46. doi: 10.1016/S1470-2045(20)30269-2
68. Jones RL, Serrano C, von Mehren M, George S, Heinrich MC, Kang YK, et al. Avapritinib in Unresectable or Metastatic PDGFRA D842V-Mutant Gastrointestinal Stromal Tumours: Long-Term Efficacy and Safety Data From the NAVIGATOR Phase I Trial. *Eur J Cancer* (2021) 145:132–42. doi: 10.1016/j.ejca.2020.12.008

69. Grunewald S, Klug LR, Muhlenberg T, Lategahn J, Falkenhorst J, Town A, et al. Resistance to Avapritinib in PDGFRA-Driven GIST Is Caused by Secondary Mutations in the PDGFRA Kinase Domain. *Cancer Discov* (2020) 11:108–25. doi: 10.1158/2159-8290.CD-20-0487
70. Blueprint Medicines Corporation. *Blueprint Medicines Announces Top-Line Results From Phase 3 VOYAGER Trial of Avapritinib Versus Regorafenib in Patients With Advanced Gastrointestinal Stromal Tumor*. (2020).
71. Desai J, Shankar S, Heinrich MC, Fletcher JA, Fletcher CD, Manola J, et al. Clonal Evolution of Resistance to Imatinib in Patients With Metastatic Gastrointestinal Stromal Tumors. *Clin Cancer Res* (2007) 13(18 Pt 1):5398–405. doi: 10.1158/1078-0432.CCR-06-0858
72. Wardelmann E, Merkelbach-Bruse S, Pauls K, Thomas N, Schildhaus HU, Heinicke T, et al. Polyclonal Evolution of Multiple Secondary KIT Mutations in Gastrointestinal Stromal Tumors Under Treatment With Imatinib Mesylate. *Clin Cancer Res* (2006) 12(6):1743–9. doi: 10.1158/1078-0432.CCR-05-1211
73. Wardelmann E, Thomas N, Merkelbach-Bruse S, Pauls K, Speidel N, Buttner R, et al. Acquired Resistance to Imatinib in Gastrointestinal Stromal Tumours Caused by Multiple KIT Mutations. *Lancet Oncol* (2005) 6(4):249–51. doi: 10.1016/S1470-2045(05)70097-8
74. Ravegnini G, Sammarini G, Serrano C, Nannini M, Pantaleo MA, Hrelia P, et al. Clinical Relevance of Circulating Molecules in Cancer: Focus on Gastrointestinal Stromal Tumors. *Ther Adv Med Oncol* (2019) 11:1–19. doi: 10.1177/1758835919831902
75. Gomez-Peregrina D, Garcia-Valverde A, Pilco-Janeta D, Serrano C. Liquid Biopsy in Gastrointestinal Stromal Tumors: Ready for Prime Time? *Curr Treat Options Oncol* (2021) 22(4):32. doi: 10.1007/s11864-021-00832-5
76. Arshad J, Roberts A, Ahmed J, Cotta J, Pico BA, Kwon D, et al. Utility of Circulating Tumor DNA in the Management of Patients With GI Stromal Tumor: Analysis of 243 Patients. *JCO Precis Oncol* (2020) 4:66–73. doi: 10.1200/PO.19.00253
77. Namlos HM, Boye K, Mishkin SJ, Baroy T, Lorenz S, Bjerkehagen B, et al. Noninvasive Detection of ctDNA Reveals Intratumor Heterogeneity and Is Associated With Tumor Burden in Gastrointestinal Stromal Tumor. *Mol Cancer Ther* (2018) 17(11):2473–80. doi: 10.1158/1535-7163.MCT-18-0174
78. Bauer S, Schoffski P, Heinrich MC, George S, Zalcberg J, Gelderblom H, et al. Characterization of the Extensive Heterogeneity of KIT/PDGFRA Mutations in Patients With Fourth-Line Advanced Gastrointestinal Stromal Tumor: Genomic Analysis of the Phase 3 INVICTUS Study. Presented at the Connective Tissue Oncology Society Virtual Annual Meeting. (2020)
79. George S, Bauer S, Jones RL, Serrano C, von Mehren M, Kang YK, et al. Correlation of ctDNA and Response in Patients (Pts) With PDGFRα D842 GIST Treated With Avapritinib. *Ann Oncol* (2018) 29:VIII582. doi: 10.1093/annonc/mdy299.021
80. Serrano C, Leal A, Kuang Y, Morgan JA, Barysauskas CM, Phallen J, et al. Phase I Study of Rapid Alternation of Sunitinib and Regorafenib for the Treatment of Tyrosine Kinase Inhibitor Refractory Gastrointestinal Stromal Tumors. *Clin Cancer Res* (2019) 25(24):7287–93. doi: 10.1158/1078-0432.CCR-19-2150
81. Trent J, Chugh R, Tinoco G, Tsiatis A, Severson P, Inokuchi K, et al. The Potent and Selective KIT Inhibitor PLX9486 Dosed in Combination With Sunitinib Deomonstrates Promising Progression Free Survival (PFS) in Patients With Advanced Gastrointestinal Stromal Tumor (GIST): Final Results of a Phase 1/2 Study. Presented at the Connective Tissue Oncology Society (CTOS) annual meeting. (2020).
82. Chi P, Qin L-X, Kelly C, D'Angelo S, Dickson M, Gounder M, et al. A Phase II Study of MEK162 (Binimetinib [BINI]) in Combination With Imatinib in Patients With Untreated Advanced Gastrointestinal Stromal Tumor (GIST). *J Clin Oncol* (2020) 38:11508. doi: 10.1200/JCO.2020.38.15_suppl.11508
83. Saito Y, Takahashi T, Obata Y, Nishida T, Ohkubo S, Nakagawa F, et al. TAS-116 Inhibits Oncogenic KIT Signalling on the Golgi in Both Imatinib-Naive and Imatinib-Resistant Gastrointestinal Stromal Tumours. *Br J Cancer* (2020) 122(5):658–67. doi: 10.1038/s41416-019-0688-y
84. Shimomura A, Yamamoto N, Kondo S, Fujiwara Y, Suzuki S, Yanagitani N, et al. First-In-Human Phase I Study of an Oral HSP90 Inhibitor, TAS-116, in Patients With Advanced Solid Tumors. *Mol Cancer Ther* (2019) 18(3):531–40. doi: 10.1158/1535-7163.MCT-18-0831
85. Honma Y, Kurokawa Y, Sawaki A, Naito Y, Iwagami S, Baba H, et al. Randomized, Double-Blind, Placebo (PL)-Controlled, Phase III Trial of Pimitespib (TAS-116), an Oral Inhibitor of Heat Shock Protein 90(HSP90), in Patients (Pts) With Advanced Gastrointestinal Stromal Tumor (GIST) Refractory to Imatinib (IM), Sunitinib (SU) and Regorafenib (REG). *J Clin Oncol* (2021) 39(15):11524. doi: 10.1200/JCO.2021.39.15_suppl.11524
86. Pantaleo MA, Tarantino G, Agostinelli C, Urbini M, Nannini M, Saponara M, et al. Immune Microenvironment Profiling of Gastrointestinal Stromal Tumors (GIST) Shows Gene Expression Patterns Associated to Immune Checkpoint Inhibitors Response. *Oncoimmunology* (2019) 8(9):e1617588. doi: 10.1080/2162402X.2019.1617588
87. Myburgh R, Kiefer JD, Russkamp NF, Magnani CF, Nunez N, Simonis A, et al. Anti-Human CD117 CAR T-Cells Efficiently Eliminate Healthy and Malignant CD117-Expressing Hematopoietic Cells. *Leukemia* (2020) 34 (10):2688–703. doi: 10.1038/s41375-020-0818-9

Conflict of Interest: SB has received honoraria from Bayer, Eli Lilly, Novartis, Pfizer, and PharmaMar, serves in an advisory/consultancy role for ADC Therapeutics, Bayer, Blueprint Medicines, Daiichi Sankyo, Deciphera Pharmaceuticals, Eli Lilly, Exelixis, Janssen-Cilag, Nanobiotix, Novartis, PharmaMar, Plexxikon, and Roche, receives research funding from Novartis, and serves as a member of the External Advisory Board of the Federal Ministry of Health for "Off-label use in oncology." SG serves in an advisory/consultancy role for AstraZeneca, Bayer, Blueprint Medicines, Daiichi Sankyo, Deciphera Pharmaceuticals, Eli Lilly, and Exelixis, has a leadership role in Alliance Foundation, receives licensing royalties from Wolters Kluwer Health, is a shareholder/stockholder of Abbott Labs and Allergan, and her institution receives research support from Bayer, Blueprint Medicines, Deciphera Pharmaceuticals, Novartis, and Pfizer. MVM serves in an advisory/consultancy role for Deciphera Pharmaceuticals, Blueprint, Exelexis, has received travel/accommodation expenses from Deciphera Pharmaceuticals, and NCCN and her institution has received funding from Arog, ASCO, Blueprint, Deciphera Pharmaceuticals, Garadalis, GenMab, Novartis, and Solarius. MCH serves in a consultancy role for Blueprint, Deciphera Pharmaceuticals, and Novartis, receives royalties from Novartis, receives grant funding from Blueprint, and Deciphera Pharmaceuticals, and has received travel, accommodations, expenses from Blueprint, and Deciphera Pharmaceuticals.

The reviewer CS declared a past co-authorship with the authors to the handling Editor.

frontiers in Oncology

SYSTEMATIC REVIEW
published: 31 January 2022
doi: 10.3389/fonc.2022.667736

Association Between Cholecystectomy and Gastric Cancer Risk: A Systematic Review and Meta-Analysis

*Ying Yang, Ming-Hua Liu and Yan Li**

Department of Gastroenterology, Shengjing Hospital of China Medical University, Shenyang, China

OPEN ACCESS

Edited by:
Rui Liao,
First Affiliated Hospital of Chongqing Medical University, China

Reviewed by:
Jie Yang,
Stony Brook University, United States
Jill Koshiol,
National Cancer Institute (NCI), United States

***Correspondence:**
Yan Li
yanli0227@126.com

Specialty section:
This article was submitted to Gastrointestinal Cancers, a section of the journal Frontiers in Oncology

Received: *14 February 2021*
Accepted: *05 January 2022*
Published: *31 January 2022*

Citation:
Yang Y, Liu M-H and Li Y (2022) Association Between Cholecystectomy and Gastric Cancer Risk: A Systematic Review and Meta-Analysis. Front. Oncol. 12:667736. doi: 10.3389/fonc.2022.667736

Objectives: Although several epidemiological studies have attempted to evaluate the relationship between cholecystectomy and gastric cancer risk, the findings have been controversial. This study aimed to carry out a systematic review and meta-analysis following the reporting guidelines to comprehensively analyze and quantify the evidence of the aforementioned association.

Methods: Studies were identified by searching the Medline (PubMed), Embase, and Web of Science from inception to November 30, 2020, with only studies published in English being considered. Summary relative risks (RRs) and 95% confidence intervals (CIs) were calculated by random-effects models.

Results: Eight studies (five cohort studies and three case–control studies) with a total of 26,063 gastric cancer patients and 848,081 participants were included. The summarized RR of the relationship between cholecystectomy and gastric cancer risk was 1.11 (95%CI: 1.03–1.20), with low heterogeneity (P = 0.117, I^2 = 37.8%). These positive findings were consistent in most subgroup analyses like region in Asia, number of cases ≥200, cohort study design, sex in male, low risk of bias, exposure collection by database, and adjustments made for age, gender, calendar year. Of note, we also observed positive association between cholecystectomy and non-cardia of gastric cancer risk (RR = 1.17, 95%CI: 1.04–1.33). No publication bias was present.

Conclusions: The aforementioned evidence suggested that a history of cholecystectomy was associated with a slightly elevated risk of gastric cancer. Results of most subgroup analyses also supported the main findings. More prospective studies are warranted to further validate these findings.

Keywords: cholecystectomy, gastric cancer, meta-analysis, observational study, systematic review

INTRODUCTION

Gastric cancer (GC) is one of the most common cancers in the world. Although the incidence of GC is decreasing, it is still the sixth most common malignancy and the third leading cause of cancer-related deaths. The incidence of GC is significantly elevated in East Asia, while that in North America, northern Europe, and the entire African region is generally lower (1, 2). GC is a multifactorial disease with several risk factors, such as *Helicobacter pylori* infection, consumption of foods preserved by salting, low intake of fruits, alcohol consumption, and active tobacco smoking (3–5).

Cholelithiasis (i.e., the presence of gallstones) is the most common gastrointestinal disease. An estimated 10% of Europeans and Americans and 5–10% of Asians are carriers of gallbladder stones (6, 7). The incidence of cholelithiasis is still on the rise, with the improvement in living standards and the extension of life expectancy. Cholecystectomy, especially laparoscopic cholecystectomy, is the standard therapy for uncomplicated gallstone disease (8). Although cholecystectomy can improve inflammation, it may also increase duodenal gastric reflux (9), which has been proposed to increase the risk of several types of cancers in digestive system organs, such as liver cancer, colorectal cancer, and pancreatic cancer (10–12). Recent epidemiological evidence investigating the relationship between cholecystectomy and GC risk has been reported. In 2012, Ge and colleagues (13) carried out a systematic review and meta-analysis that suggested that cholecystectomy did not increase the overall risk of GC. However, some later published studies with a larger sample size generated different findings, which were different from the previous meta-analysis. For example, Chen et al. conducted a cohort study with 202 GC patients and 77,725 participants and observed that cholecystectomy was significantly associated with the risk of GC throughout the follow-up periods (14). Of note, the results of these published cohort studies have been conflicting, which might be attributed to the differences in the number of participants and the years of follow-up (14–17).

Considering that the previous meta-analysis is out of date and does not include research from the past decade, and given the conflicting conclusions of current research, this study aimed to carry out an updated systematic review and meta-analysis of observational studies to evaluate the association between cholecystectomy and the risk of GC.

MATERIALS AND METHODS

The reporting standards of the Meta-Analysis of Observational Studies in Epidemiology group (18) and Preferred Reporting Items for Systemic Reviews and Meta-Analyses (PRISMA) (**Supplementary Table Sl**) guidelines (19) for systematic reviews and meta-analyses of non-randomized controlled trials were followed in the present study.

Search Strategy

Two independent individuals (YY and M-HL) comprehensively searched the Medline (PubMed), Embase, and Web of Science from inception to November 30, 2020, with only studies published in English being considered. Details of the full search strategy are provided in the **Supplementary Table S2**. Furthermore, the reference lists of all included studies and pertinent reviews and meta-analyses were manually examined to identify additional eligible studies.

Study Selection

A study was eligible for inclusion if it (1) utilized an observational study design; (2) evaluated the relationship between cholecystectomy and GC risk; and (3) demonstrated estimates of odds ratios (ORs), relative risks (RRs), or hazard ratios (HRs) with 95% confidence intervals (CIs) or extractable data necessary to calculate these parameters. However, publications meeting any of the following criteria were excluded: (1) clinical trials, letters, editorials, case reports, reviews, meta-analyses, and meeting abstracts; (2) lack of sufficient risk estimates or related data to calculate risk estimates; and (3) not published in English. The selection and exclusion of studies were reviewed by two investigators (YY and M-HL). Disagreements were resolved by consensus with a third author (YL).

Data Abstraction and Quality Assessment

Data were extracted in duplicate using standardized forms. Disagreements were resolved by consensus. The following information was collected: last name of the first author, publication year, geographical location, study design, number of cases, number of controls/cohorts, and characteristics of exposure and covariates matched in the study design or adjusted in the statistical analysis.

Quality assessment was performed using the Newcastle–Ottawa Scale (NOS), which consisted of eight items grouped into three domains (selection, comparability, and exposure/outcome) to assess the methodological quality of case–control or cohort studies (20). Studies that achieved a full rating in at least two categories of the three assessments were considered to have a low risk of bias (21).

Statistical Analysis

The risk estimates were extracted from the original studies, namely, standardized incidence ratio, HR, OR, and RR. As the absolute risk of GC was low, the other risk estimates were considered similar estimates to RR (22). The random-effects model, which considers both within- and between-study variations, was used to summarize RR with their 95%CI of each study (23). Heterogeneity among studies was assessed with I^2 statistics. I^2; estimates the proportion of variability in the meta-analysis caused by differences between studies instead of sampling error (24). The larger I^2 indicated the greater heterogeneity of the studies included in the meta-analysis. Meanwhile, *P*-values are generated according to the degree of heterogeneity in Forest plot (24). Cutoff points ≤25%, ≤50%, ≤75%, and >75% indicated no, low, moderate, and significant heterogeneities, respectively (24). Subgroup analyses were conducted to probe into heterogeneous sources by using pre-

specified variables like region, anatomic subsite of GC, number of cases, study design, sex, risk of bias, exposure collection, and adjustments made for potential confounders, namely, age, sex, and calendar year. Associations that resulted from studies with small study biases (e.g., publication bias) were evaluated by visual inspection of funnel plot and formal testing using Egger's test and Begg's test (25, 26). Sensitivity analysis was conducted in which the summarized risk estimates were recalculated by omitting one study at a time so as to assess the effect of individual studies on the estimated RR (27). All statistical analyses were performed using Stata 12.0 software (Stata LLC, TX, USA).

RESULTS

Summary of the Selection Process

The search yielded 4,763 studies from three electronic biographic databases using a predefined search strategy. Two more studies (28, 29) were identified for full review by checking references. After removing 1,542 duplicates, 3,221 studies were screened based on title and abstract for further reading and 15 studies were eligible for further assessment by studying the full text. Eight studies met the inclusion and exclusion criteria and were selected for this systematic review and meta-analysis (**Figure 1**). The list of excluded studies was appended (**Supplementary Table S3**).

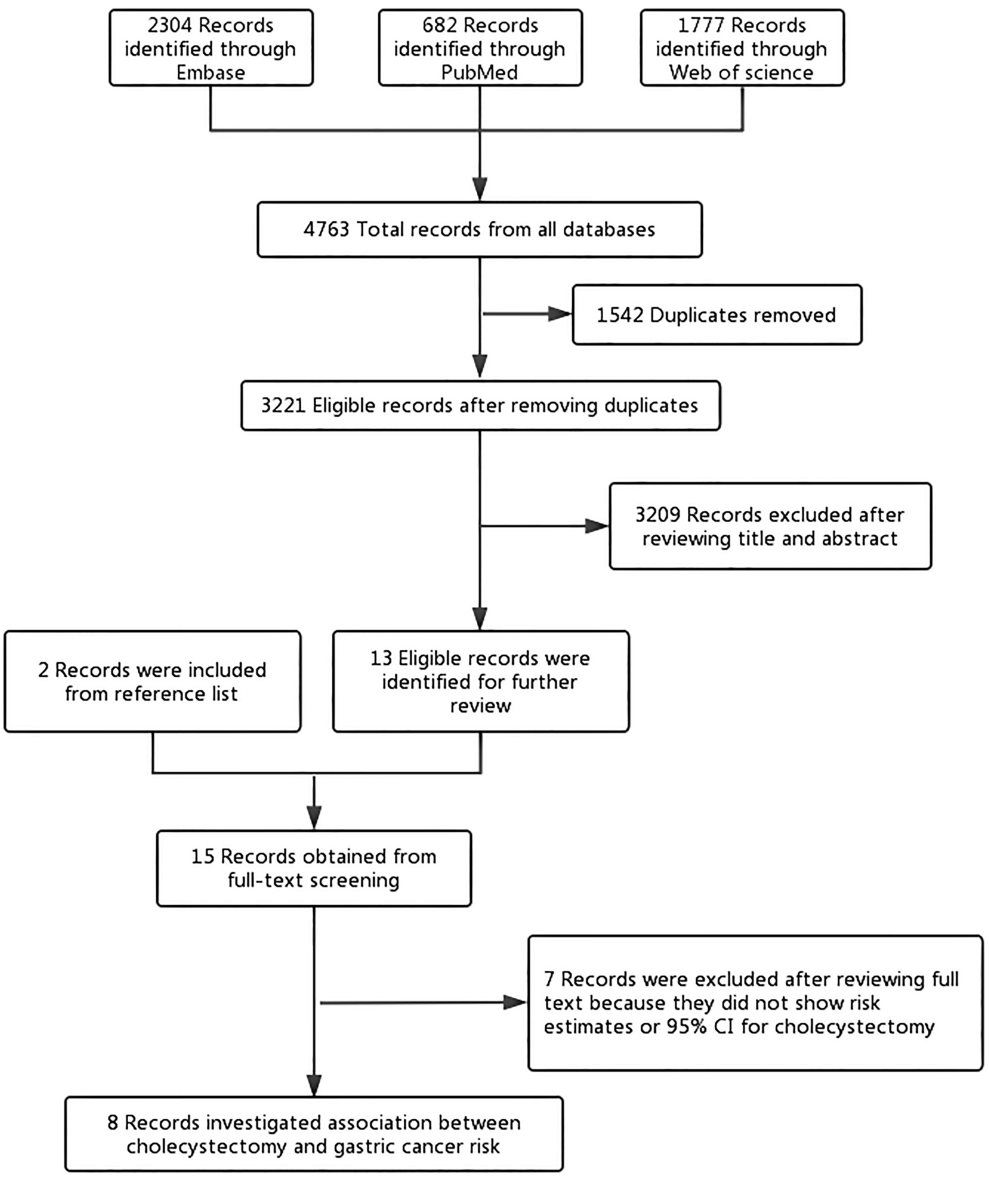

FIGURE 1 | Flowchart of the study selection. The flowchart shows the process used to select studies for our meta-analyses focusing on the association between cholecystectomy and gastric cancer risk.

Study Characteristics

The characteristics of the eight included studies are summarized in **Table 1**. These studies were published between 1984 and 2020 and included 26,063 GC patients with a range of 14–22,860 patients in individual studies. Of these eight studies, three (30, 32, 33) were case–control studies and five (14–17, 31) were cohort studies. Five (16, 17, 31–33) of these studies were conducted in Europe, two (14, 15) in Asia, and one (30) in the United States. Most studies collected the exposure through medical records or government databases. Furthermore, all studies required an objective GC diagnosis. All studies, except for one, were adjusted for age and sex ($n = 6$). Fewer studies were adjusted for the calendar year ($n = 3$). Specifically, one study was adjusted for more than five potential confounders in the primary analysis.

Risk of Bias Within Studies

Supplementary Tables S4 and **S5** provide details of the study quality assessment as reflected by NOS scoring. Two studies were graded as high risk (15, 17). For the cohort study, three (15–17) studies that did not illustrate the source of cohort were not given a star for the selection of the unexposed cohort; two (15, 17) study failing to adjust any confounder was not given a star for comparability; two studies (14, 15) were not assigned a star for insufficient duration of follow-up. For the case–control study, one (33) study that included hospital-based controls was not given a star for the selection of control subjects; two (30, 33) case–control studies were not given a star for the definition of cases by the International Classification of Diseases code.

RR of Cholecystectomy-Associated GC

Figure 2 shows the study-specific and summarized RRs and 95% CIs of GC for ever having cholecystectomy versus no history of cholecystectomy. Based on the eight studies, the summarized RR was 1.11 (95%CI: 1.03–1.20), with low heterogeneity among studies (I^2 = 37.8%). No publication bias was present (P for Begg's test = 0.754, P for Egger's test = 0.683) (**Supplementary Figure S1**).

The estimates by subgroups together with the results of the heterogeneity tests are given in **Table 2**. In subgroup analysis by study design, a significant result was observed after summarizing five cohort studies (14–17, 31) (RR = 1.12, 95%CI: 1.01–1.24), which was similar to the main finding, but not in case–control studies (30, 32, 33). In addition, similar situation was observed after summarizing six studies (14, 16, 30–33) with low risk (RR = 1.12, 95%CI: 1.02–1.23) instead of high risk (15, 17), two studies (14, 15) conducted in Asia (RR = 1.55, 95%CI: 1.06–2.26) instead of conducted in Europe (16, 17, 31–33), five studies (14, 16, 17, 30, 31) collecting exposure information on the basis of government database (RR = 1.12, 95%CI: 1.04–1.21) instead of other collecting exposure information methods (15, 32, 33), five studies (14, 16, 30–32) with more than 200 GC patients (RR = 1.12, 95%CI: 1.02–1.23) instead of less than 200 GC patients (15, 17, 33), six studies (14, 16, 30–33) adjusted for age or sex (RR = 1.12, 95%CI: 1.02–1.23), and three studies (16, 30, 31) adjusted for calendar year (RR = 1.13, 95%CI: 1.06–1.20). Of note, after summarizing these results of subgroup analyses by sex and anatomic subsite of GC in their primary analyses, significant results were only observed in male and non-cardia GC (**Table 2**).

Additionally, no influential study was found in the sensitivity analyses, in which one study was omitted at a time and a summarized RR was calculated for the remainder of the studies. The estimated RR in this sensitivity analysis ranged from 1.09 (95%CI: 0.98–1.22, I^2 = 43.5%) to 1.13 (95%CI: 1.05–1.22, I^2 = 32.9%) (**Supplementary Figure S2**).

TABLE 1 | Characteristics of studies included in the meta-analysis of the association between cholecystectomy and gastric cancer risk.

First author, ref, year	Location	Study design	No. of cases	No. of controls/ cohorts	Exposure source	Risk estimate	Adjustments
Kim et al. (15), 2020	Korea	Cohort study	14	3,588	Medical record	SIR	N/A
Chen et al. (14), 2014	Taiwan	Cohort study	202	77,725	Database	HR	Age, sex, and comorbidities
Nogueira et al. (30), 2014	USA	Case-control study	22,860	100,000	Database	OR	Age, sex, and calendar year of selection, duration of Medicare benefits coverage
Fall et al. (16), 2007	Sweden	Cohort study	948	251,672	Database	SIR	Age, sex, and calendar year
Goldacre et al. (31), 2005	UK	Cohort study	15,31	374,067	Database	RR	Age, sex, calendar year, and district of residence
Freedman et al. (32), 2000	Sweden	Case-control study	2,62	820	Questionnaire	OR	Age, sex, tobacco use, alcohol use, body mass index, educational level, intake of fruit and vegetables, meal size, and physical activity
Sarli et al. (33), 1986	Italy	Case-control study	1,57	157	Medical record	OR	Age, sex, and geographic area of origin and dietary habits
Gustavsson et al. (17), 1984	Sweden	Cohort study	89	16,773	Database	RR	None

HR, hazard ratio; N/A, not available; OR, odds ratio; RR, relative risk; SIR, standardized incidence ratio.

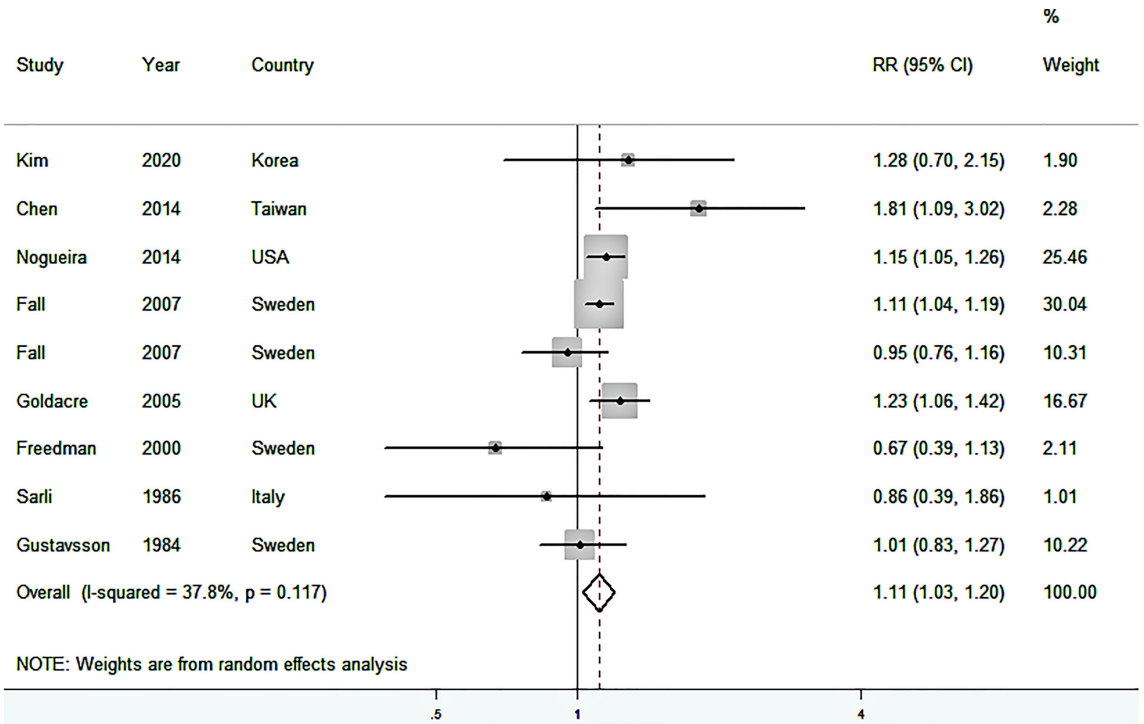

FIGURE 2 | Forest plot (random-effects model) of the association between cholecystectomy and gastric cancer risk. Squares indicate study-specific relative risk (RR), where the size of the square reflects the study-specific statistical weight; horizontal lines indicate the 95% confidence interval (CI); diamonds denote the summary RR with 95% CI.

DISCUSSION

The current systematic review and meta-analyses included three case–control and five cohort studies involving 26,063 patients and 848,081 participants. The studies focused on cholecystectomy and GC risk. The findings revealed that cholecystectomy was associated with 11% increased risk of GC, with low heterogeneity among studies. This association was also significantly observed in cohort studies and studies with a low risk of bias. In subgroup analysis by anatomic subsite of GC, this effect was more pronounced in non-cardia GC compared with cardia GC. However, no evidence of the relationship between the duration of the follow-up period after cholecystectomy and GC risk was found.

One previous meta-analysis of observational studies was reported, but with inconsistent findings. In 2012, based on a meta-analysis of two case–control and three cohort studies, with 2,073 GC patients, Ge et al. (13) observed a non-significant excess risk of GC related to prior cholecystectomy (RR = 1.03, 95%CI: 0.93–1.13). Moreover, they also found a null association between cholecystectomy and risk of gastric cardia cancer (RR = 0.87, 95%CI: 0.65–1.17). However, the study had some limitations. First, the methodological quality of the included studies was not evaluated, and only a few subgroup analyses were made. Second, generalization of the results of previous meta-analysis in other countries was difficult because the included studies were conducted only in Western countries.

In the subgroup analysis layered by anatomic subsite of GC, we found that the positive association between cholecystectomy and non-cardia of GC risk. However, due to limited studies included in this subgroup analysis (n = 2), the probability of chance findings could not be ruled out. Additionally, although the two included studies both supported the aforementioned positive correlation results, Fall et al. (16) conducted the cohort study which had the limitations of small sample size and fewer confounding factors adjustment. Therefore, further studies are needed to explore the relationship between cholecystectomy and non-cardia of GC risk.

The underlying exact mechanisms of these contradictory links between cholecystectomy and GC risk have been unclear; however, some potential plausible mechanisms have been proposed to explain these findings. After cholecystectomy, bile flow changes, increasing the bile exposure of the stomach, changing bile salts, and subsequently changing the levels of metabolic hormone (34). Increased bile flow can cause bile to return to the stomach and esophagus, increasing the risk of GC (17). In addition, the presence of bile could cause another type of inflammation known as reactive gastritis (35). Moreover, clinical and epidemiological evidence have supported the functional relationship between chronic inflammation and cancer (36, 37). Furthermore, evidence suggests that one of these bile acids might be a weak mutagen, causing DNA damage, inducing frequent apoptosis, and ultimately increasing cancer incidence (38, 39).

TABLE 2 | Risk estimates for cholecystectomy associated with gastric cancer in subgroup analysis.

	No. of studies	RR (95%CI)	I^2 (%)	P*
Region				
Asia	2	1.55 (1.06–2.26)	0	0.370
Europe	5	1.07 (0.97–1.19)	41.2	0.131
USA	1	1.15 (1.05–1.26)	N/A	N/A
Anatomic subsite of gastric cancer				
Cardia	3	0.89 (0.78–1.02)	0	0.479
Non-cardia	2	1.17 (1.04–1.33)	74.1	0.050
Number of cases				
<200	3	1.03 (0.85–1.25)	0	0.666
≥200	5	1.12 (1.02–1.23)	55.6	0.047
Study design				
Cohort study	5	1.12 (1.01–1.24)	41.1	0.131
Case-control study	3	0.95 (0.66–1.38)	53.7	0.115
Gender				
Male	3	1.15 (1.00–1.32)	17.4	0.304
Female	3	0.99 (0.90–1.09)	0	0.827
Risk of bias				
Low risk	6	1.12 (1.02–1.23)	48.8	0.069
High risk	2	1.04 (0.85–1.27)	0	0.439
Exposure collection				
Database	5	1.12 (1.04–1.21)	41.8	0.126
Questionnaire	1	0.67 (0.39–1.14)	N/A	N/A
Medical record	2	1.04 (0.85–1.27)	0	0.439
Adjustment for potential confounders				
Age				
Yes	6	1.12 (1.02–1.23)	48.8	0.069
No	2	1.04 (0.85–1.27)	0	0.439
Gender				
Yes	6	1.12 (1.02–1.23)	48.8	0.069
No	2	1.04 (0.85-1.27)	0	0.439
Calendar year				
Yes	3	1.13 (1.06–1.20)	29.6	0.234
No	5	1.07 (0.79–1.45)	49.9	0.092

CI, confidence interval; N/A, not available; RR, relative risk.
**P-value for heterogeneity within each subgroup.*

To our knowledge, the present study is the most comprehensive meta-analysis of cholecystectomy and GC risk so far. The strengths of this study include the following: First, this meta-analysis involved a large sample size (26,063 patients and 848,081 participants) to evaluate the effect of cholecystectomy and GC risk, which increased the statistical power to detect the association. Second, numerous subgroup analyses were performed to analyze the study characteristics that might affect results, and sensitivity analyses were further performed to explore the heterogeneity in this study. Third, this present meta-analysis had no publication bias and low heterogeneity, and most of the included studies had a low risk of bias. All these strengths make the results of this study more convincing.

However, the study also had several limitations. First, a significant excess risk of GC related to cholecystectomy was observed in cohort studies, but not in case–control studies. Furthermore, the subgroup analysis of case–control studies represented moderate heterogeneity, which was higher than the subgroup of cohort studies. The case–control studies were prone to generate selection and recall bias, and the quality of the cohort studies was inconsistent, which might explain the observed heterogeneity in the study. Second, the different exposure rates of cholecystectomy varied among the included studies, which might be an important issue. Most included studies were conducted in European countries, and only a few were conducted in other countries. The exposure rate of cholecystectomy was observed to be 20% of the total participants in Taiwan but 10% of that in the United Kingdom (14, 31). Third, potential confounders that were not adjusted in individual studies could not be controlled. Although eight studies were included, the number of studies in each subgroup analysis was relatively small, leading to the need for further verification of some subgroup analysis results. In addition, only subgroup analyses for region, age, sex, exposure collection, and calendar year were conducted. The positive association between cholecystectomy and risk of GC persisted when the analysis of studies that adjusted for these confounders was restricted. Further studies should also consider whether the important risk factors of GC, such as *H. pylori* infection (4) and diet intake, affected the association of cholecystectomy and GC risk (3, 5). Fourth, only three included studies evaluated the association between cholecystectomy and different anatomic sites of stomach; therefore, inconsistent results were obtained for different anatomic sites with high heterogeneity. As cardia GC and non-cardia GC could have differences in the possibility of exposure to reflux bile, and data for further analysis were lacking, more studies are warranted to better elucidate this issue in the future. Fifthly, the cohort studies included in our meta-

analysis differed in the evaluation of follow-up time, so it is difficult to summarize the RR and 95%CI of comparing longest vs shortest duration of the follow-up period. Future large cohort studies with longer follow-up time need to further explore the effect of cholecystectomy on gastric cancer risk. Additionally, the reasons for cholecystectomy in these included original studies were different or unknown. For example, Fall et al. identified participants through the Swedish National Inpatient Register, who had undergone cholecystectomy without illustrating the reason for the cholecystectomy (16). The patients who underwent cholecystectomy for symptomatic cholelithiasis or its complications, gallbladder polyp, or acalculous cholecystitis were included in the Kim et al. study (15). Therefore, further studies are needed to consider this in the future. Finally, only published studies were searched and included, while the gray literature and unpublished studies were ignored.

CONCLUSIONS

The present systematic review and meta-analysis indicated that cholecystectomy had an increased risk of developing GC. Meanwhile, most subgroup analyses also supported the main findings. More large-scale prospective cohort studies are needed to validate these findings worldwide to gain further insights.

DATA AVAILABILITY STATEMENT

The data that support the findings of this study are available from the corresponding author upon reasonable request. Requests to access the datasets should be directed to yanli0227@126.com.

AUTHOR CONTRIBUTIONS

YL: conceived and designed the study. YY and M-HL: literature search, data curation and formal analysis, writing the original draft. All authors contributed to the article and approved the submitted version.

SUPPLEMENTARY MATERIAL

The Supplementary Material for this article can be found online at: https://www.frontiersin.org/articles/10.3389/fonc.2022.667736/full#supplementary-material

REFERENCES

1. Ferlay J, Colombet M, Soerjomataram I, Mathers C, Parkin DM, Pineros M, et al. Estimating the Global Cancer Incidence and Mortality in 2018: GLOBOCAN Sources and Methods. *Int J Cancer* (2019) 144:1941–53. doi: 10.1002/ijc.31937
2. Bray F, Ferlay J, Soerjomataram I, Siegel RL, Torre LA, Jemal A. Global Cancer Statistics 2018: GLOBOCAN Estimates of Incidence and Mortality Worldwide for 36 Cancers in 185 Countries. *CA Cancer J Clin* (2018) 68:394–424. doi: 10.3322/caac.21492
3. Buckland G, Travier N, Huerta JM, Bueno-de-Mesquita HB, Siersema PD, Skeie G, et al. Healthy Lifestyle Index and Risk of Gastric Adenocarcinoma in the EPIC Cohort Study. *Int J Cancer* (2015) 137:598–606. doi: 10.1002/ijc.29411
4. Plummer M, Franceschi S, Vignat J, Forman D, de Martel C. Global Burden of Gastric Cancer Attributable to Helicobacter Pylori. *Int J Cancer* (2015) 136:487–90. doi: 10.1002/ijc.28999
5. Lin SH, Li YH, Leung K, Huang CY, Wang XR. Salt Processed Food and Gastric Cancer in a Chinese Population. *Asian Pac J Cancer Prev* (2014) 15:5293–8. doi: 10.7314/apjcp.2014.15.13.5293
6. Huang J, Chang CH, Wang JL, Kuo HK, Lin JW, Shau WY, et al. Nationwide Epidemiological Study of Severe Gallstone Disease in Taiwan. *BMC Gastroenterol* (2009) 9:63. doi: 10.1186/1471-230X-9-63
7. Kratzer W, Mason RA, Kachele V. Prevalence of Gallstones in Sonographic Surveys Worldwide. *J Clin Ultrasound* (1999) 27:1–7. doi: 10.1002/(sici)1097-0096(199901)27:1<1::aid-jcu1>3.0.co;2-h
8. Zang J, Yuan Y, Zhang C, Gao J. Elective Laparoscopic Cholecystectomy Without Intraoperative Cholangiography: Role of Preoperative Magnetic Resonance Cholangiopancreatography - A Retrospective Cohort Study. *BMC Surg* (2016) 16:45. doi: 10.1186/s12893-016-0159-9
9. Mahid SS, Jafri NS, Brangers BC, Minor KS, Hornung CA, Galandiuk S. Meta-Analysis of Cholecystectomy in Symptomatic Patients With Positive Hepatobiliary Iminodiacetic Acid Scan Results Without Gallstones. *Arch Surg* (2009) 144:180–7. doi: 10.1001/archsurg.2008.543
10. Zhang Y, Liu H, Li L, Ai M, Gong Z, He Y, et al. Cholecystectomy can Increase the Risk of Colorectal Cancer: A Meta-Analysis of 10 Cohort Studies. *PloS One* (2017) 12:e0181852. doi: 10.1371/journal.pone.0181852
11. Liu Y, He Y, Li T, Xie L, Wang J, Qin X, et al. Risk of Primary Liver Cancer Associated With Gallstones and Cholecystectomy: A Meta-Analysis. *PloS One* (2014) 9:e109733. doi: 10.1371/journal.pone.0109733
12. Fan Y, Hu J, Feng B, Wang W, Yao G, Zhai J, et al. Increased Risk of Pancreatic Cancer Related to Gallstones and Cholecystectomy: A Systematic Review and Meta-Analysis. *Pancreas* (2016) 45:503–9. doi: 10.1097/MPA.0000000000000502
13. Ge Z, Zhao C, Wang Y, Qian J. Cholecystectomy and the Risk of Esophageal and Gastric Cancer. *Saudi Med J* (2012) 33:1073–9.
14. Chen YK, Yeh JH, Lin CL, Peng CL, Sung FC, Hwang IM, et al. Cancer Risk in Patients With Cholelithiasis and After Cholecystectomy: A Nationwide Cohort Study. *J Gastroenterol* (2014) 49:923–31. doi: 10.1007/s00535-013-0846-6
15. Kim SB, Kim KO, Kim TN. Prevalence and Risk Factors of Gastric and Colorectal Cancer After Cholecystectomy. *J Korean Med Sci* (2020) 35:e354. doi: 10.3346/jkms.2020.35.e354
16. Fall K, Ye W, Nyren O. Risk for Gastric Cancer After Cholecystectomy. *Am J Gastroenterol* (2007) 102:1180–4. doi: 10.1111/j.1572-0241.2007.01169.x
17. Gustavsson S, Adami HO, Meirik O, Nyren O, Krusemo UB. Cholecystectomy as a Risk Factor for Gastric Cancer. A Cohort Study. *Dig Dis Sci* (1984) 29:116–20. doi: 10.1007/BF01317051
18. Stroup DF, Berlin JA, Morton SC, Olkin I, Williamson GD, Rennie D, et al. Meta-Analysis of Observational Studies in Epidemiology: A Proposal for Reporting. Meta-Analysis of Observational Studies in Epidemiology (MOOSE) Group. *JAMA* (2000) 283:2008–12. doi: 10.1001/jama.283.15.2008
19. Moher D, Liberati A, Tetzlaff J, Altman DG. Preferred Reporting Items for Systematic Reviews and Meta-Analyses: The PRISMA Statement. *PloS Med* (2009) 6:e1000097. doi: 10.1371/journal.pmed.1000097
20. Wells GA, Shea B, O'Connell D, Peterson J, Welch V, Losos M, et al. *The Newcastle-Ottawa Scale (NOS) for Assessing the Quality of Nonrandomised Studies in Meta-Analyses* (2013). Available at: http://www.ohri.ca/programs/clinical_epidemiology/oxford.asp (Accessed on May 2020).
21. Odutayo A, Wong CX, Hsiao AJ, Hopewell S, Altman DG, Emdin CA. Atrial Fibrillation and Risks of Cardiovascular Disease, Renal Disease, and Death: Systematic Review and Meta-Analysis. *BMJ* (2016) 354:i4482. doi: 10.1136/bmj.i4482
22. Siristatidis C, Sergentanis TN, Kanavidis P, Trivella M, Sotiraki M, Mavromatis I, et al. Controlled Ovarian Hyperstimulation for IVF: Impact

on Ovarian, Endometrial and Cervical Cancer–a Systematic Review and Meta-Analysis. *Hum Reprod Update* (2013) 19:105–23. doi: 10.1093/humupd/dms051
23. Ades AE, Lu G, Higgins JP. The Interpretation of Random-Effects Meta-Analysis in Decision Models. *Med Decis Making* (2005) 25:646–54. doi: 10.1177/0272989X05282643
24. Higgins JP, Thompson SG. Quantifying Heterogeneity in a Meta-Analysis. *Stat Med* (2002) 21:1539–58. doi: 10.1002/sim.1186
25. Egger M, Davey SG, Schneider M, Minder C. Bias in Meta-Analysis Detected by a Simple, Graphical Test. *BMJ* (1997) 315:629–34. doi: 10.1136/bmj.315.7109.629
26. Begg CB, Mazumdar M. Operating Characteristics of a Rank Correlation Test for Publication Bias. *Biometrics* (1994) 50:1088–101. doi: 10.2307/2533446
27. Wu QJ, Wu L, Zheng LQ, Xu X, Ji C, Gong TT. Consumption of Fruit and Vegetables Reduces Risk of Pancreatic Cancer: Evidence From Epidemiological Studies. *Eur J Cancer Prev* (2016) 25:196–205. doi: 10.1097/CEJ.0000000000000171
28. Johansen C, Chow WH, Jorgensen T, Mellemkjaer L, Engholm G, Olsen JH. Risk of Colorectal Cancer and Other Cancers in Patients With Gall Stones. *Gut* (1996) 39:439–43. doi: 10.1136/gut.39.3.439
29. Maringhini A, Moreau JA, Melton LR, Hench VS, Zinsmeister AR, DiMagno EP. Gallstones, Gallbladder Cancer, and Other Gastrointestinal Malignancies. An Epidemiologic Study in Rochester, Minnesota. *Ann Intern Med* (1987) 107:30–5. doi: 10.7326/0003-4819-107-1-30
30. Nogueira L, Freedman ND, Engels EA, Warren JL, Castro F, Koshiol J. Gallstones, Cholecystectomy, and Risk of Digestive System Cancers. *Am J Epidemiol* (2014) 179:731–9. doi: 10.1093/aje/kwt322
31. Goldacre MJ, Abisgold JD, Seagroatt V, Yeates D. Cancer After Cholecystectomy: Record-Linkage Cohort Study. *Br J Cancer* (2005) 92:1307–9. doi: 10.1038/sj.bjc.6602392
32. Freedman J, Lagergren J, Bergstrom R, Naslund E, Nyren O. Cholecystectomy, Peptic Ulcer Disease and the Risk of Adenocarcinoma of the Oesophagus and Gastric Cardia. *Br J Surg* (2000) 87:1087–93. doi: 10.1046/j.1365-2168.2000.01459.x
33. Sarli L, Gafa M, Lupi M, Sansebastiano G, Longinotti E, Peracchia A. Gallstones and Gastric Cancer: A Matched Case-Control Study. *World J Surg* (1986) 10:884–91. doi: 10.1007/BF01655266
34. Kang SH, Kim YH, Roh YH, Kim KW, Choi CJ, Kim MC, et al. Gallstone, Cholecystectomy and Risk of Gastric Cancer. *Ann Hepatobiliary Pancreat Surg* (2017) 21:131–7. doi: 10.14701/ahbps.2017.21.3.131
35. Dixon MF, Genta RM, Yardley JH, Correa P. Classification and Grading of Gastritis. The Updated Sydney System. International Workshop on the Histopathology of Gastritis, Houston 1994. *Am J Surg Pathol* (1996) 20:1161–81. doi: 10.1097/00000478-199610000-00001
36. Mantovani A, Allavena P, Sica A, Balkwill F. Cancer-Related Inflammation. *Nature* (2008) 454:436–44. doi: 10.1038/nature07205
37. Grivennikov SI, Greten FR, Karin M. Immunity, Inflammation, and Cancer. *Cell* (2010) 140:883–99. doi: 10.1016/j.cell.2010.01.025
38. Atak I, Ozdil K, Yucel M, Caliskan M, Kilic A, Erdem H, et al. The Effect of Laparoscopic Cholecystectomy on the Development of Alkaline Reflux Gastritis and Intestinal Metaplasia. *Hepatogastroenterology* (2012) 59:59–61. doi: 10.5754/hge11244
39. Kunsch S, Neesse A, Huth J, Steinkamp M, Klaus J, Adler G, et al. Increased Duodeno-Gastro-Esophageal Reflux (DGER) in Symptomatic GERD Patients With a History of Cholecystectomy. *Z Gastroenterol* (2009) 47:744–8. doi: 10.1055/s-0028-110917

Conflict of Interest: The authors declare that the research was conducted in the absence of any commercial or financial relationships that could be construed as a potential conflict of interest.

Publisher's Note: All claims expressed in this article are solely those of the authors and do not necessarily represent those of their affiliated organizations, or those of the publisher, the editors and the reviewers. Any product that may be evaluated in this article, or claim that may be made by its manufacturer, is not guaranteed or endorsed by the publisher.

Advantages of publishing in Frontiers

OPEN ACCESS
Articles are free to read for greatest visibility and readership

FAST PUBLICATION
Around 90 days from submission to decision

HIGH QUALITY PEER-REVIEW
Rigorous, collaborative, and constructive peer-review

TRANSPARENT PEER-REVIEW
Editors and reviewers acknowledged by name on published articles

Frontiers
Avenue du Tribunal-Fédéral 34
1005 Lausanne | Switzerland

Visit us: www.frontiersin.org
Contact us: frontiersin.org/about/contact

REPRODUCIBILITY OF RESEARCH
Support open data and methods to enhance research reproducibility

DIGITAL PUBLISHING
Articles designed for optimal readership across devices

FOLLOW US
@frontiersin

IMPACT METRICS
Advanced article metrics track visibility across digital media

EXTENSIVE PROMOTION
Marketing and promotion of impactful research

LOOP RESEARCH NETWORK
Our network increases your article's readership